UNIVERSITÉ LAVAL

Charting PARP-1 dependent mechanisms for DNA double-strand break resection

Thèse

Julia O'Sullivan

Doctorat en biologie cellulaire et moléculaire
Philosophiæ doctor (Ph. D.)

Québec, Canada

Charting PARP-1 dependent mechanisms for DNA double-strand break resection

Thèse

Julia O'Sullivan, B.Sc., MRes

Doctorat en Biologie cellulaire et moléculaire

Philosophiæ Doctor (Ph.D.)

Québec, Canada

Principal Supervisors: Guy Poirier & Jean-Yves Masson

Résumé

L'intégrité de l'ADN génomique humain est maintenue par des systèmes de réparation de l'ADN qui protègent les cellules des dommages causés par des agents environnementaux ou des lésions spontanées de l'ADN. Chaque cellule peut subir jusqu'à 10^5 lésions par jour, y compris les cassures double-brin de l'ADN (CDB). La poly(ADP-ribosyl)ation (PARylation) est l'un des premiers événements de signalisation moléculaire survenant aux CDBs. Il est catalysé par les poly(ADP-ribose)polymérases (PARP) qui sont directement activées par ces lésions d'ADN. Le fait de ne pas générer de poly(ADP)ribosyl (pADPr) en réponse à des dommages à l'ADN par une inhibition chimique ou par l'absence de PARP-1 augmente la sensibilité cellulaire au stress génotoxique, indiquant que la pADPr elle-même est une molécule clé de signalisation des dommages à l'ADN. L'inhibition de l'enzyme de signalisation des dommages à l'ADN, la poly(ADP-ribose) polymérase-1 (PARP-1) est l'une des nouvelles thérapies les plus prometteuses contre le cancer. Les inhibiteurs de PARP sensibilisent les cellules cancéreuses aux agents endommageant l'ADN et tuent efficacement les cellules cancéreuses du sein, des ovaires et du pancréas déficientes en BRCA1 (Breast Cancer gene 1) et BRCA2 (Breast Cancer gene 2), ce qui suggère que les cellules déficientes en réparation des CDBs sont extrêmement sensibles à l'inhibition de PARP. Pourtant, les mécanismes sous-jacents à cette létalité synthétique entre le déficit de réparation du CDB et l'inhibition de PARP restent mal définis. Il y a un débat considérable sur le mécanisme par lequel l'inhibition de PARP tue les cellules déficientes en réparation de l'ADN, et le plein potentiel des inhibiteurs de PARP dans le traitement du cancer ne peut être obtenu que par une compréhension claire des voies de réponse aux dommages de l'ADN (DDR) aux CDB et comment ils sont affectés par les inhibiteurs de PARP.

L'objectif général de ma thèse est d'étudier le rôle de PARP-1 dans la réparation DSB et d'identifier les interacteurs de PARP-1 qui jouent également un rôle dans ce processus. Les cellules eucaryotes réparent les CDBs par deux voies principales, la jonction d'extrémité non homologue (NHEJ) et la recombinaison homologue (HR). La HR est initiée par la liaison des CDBs par BRCA1 et le complexe MRE11-RAD50-NBS1

et des nucléases EXO1/DNA2 pour générer de l'ADN simple-brin, qui est ensuite utilisé par la recombinase RAD51 et le complexe BRCA1-PALB2-BRCA2. Une question clé dans notre domaine concerne les facteurs critiques pour réguler le choix de la voie CDB. HR est initiée à partir d'extrémités DSB hautement résectées, tandis que dans le NHEJ, la résection est empêchée par des facteurs de réparation clés incluant RIF1 et 53BP1. En utilisant des cellules déficientes en PARP-1, nous avons observé que deux inhibiteurs de la résection de l'ADN et des régulateurs de choix de voie, RIF1 et 53BP1, la formation de foyers induits par des dommages à l'ADN sont fortement altérés. Cela confirme notre hypothèse selon laquelle PARP-1 participe à la réparation du DSB en influençant la résection de l'ADN.

Afin de mieux comprendre le mécanisme de résection et le rôle que PARP-1 y joue, nous avons identifié d'autres protéines qui interagissent avec PARP-1 et modulent ce processus. Pour ce faire, nous avons utilisé des données sur les protéines de liaison au pADPr générées à la fois dans notre laboratoire et celui de notre collaborateur Ted Dawson de Johns Hopkins. Les candidats sélectionnés à partir de ces listes ont été criblés pour identifier une seule cible qui démontrerait un phénotype similaire à la perte de PARP-1. Deux cibles initiales ont été explorées et finalement une seule protéine à doigt de zinc a été choisie comme cible principale. Nous devons relever la fonction de ce doigt de zinc en HR, dans l'espoir qu'il permettra de découvrir davantage les mécanismes de PARP-1 en résection.

En résumé, cette thèse élucide le rôle de PARP-1 dans la résection de l'ADN et identifie une protéine à doigt de zinc non étudiée auparavant qui interagit avec PARP-1 et partage une fonction similaire à PARP-1 dans la résection de l'ADN.

Abstract

The integrity of human genomic DNA is maintained by DNA repair systems that will protect cells from damage by environmental agents or spontaneous DNA lesions. Each cell can experience up to 10^5 lesions daily, including DNA double-strand breaks (DSB)s. Poly(ADP-ribosyl)ation (PARylation) is one of the earliest molecular signalling events occurring at DNA DSBs. It is catalysed by poly(ADP-ribose) polymerases (PARPs) that are directly activated by those DNA lesions. Failure to generate pADPr in response to DNA damage by either chemical inhibition or absence of PARP-1 increases the cellular sensitivity to genotoxic stress, indicating that pADPr itself is a key DNA damage signalling molecule. Inhibition of the DNA damage signalling enzyme poly(ADP-ribose) polymerase-1 (PARP-1) is among the most promising new therapies in cancer. PARP inhibitors sensitize cancer cells to DNA damaging agents and efficiently kill BRCA1- and BRCA2-deficient breast, ovarian and pancreatic cancer cells, suggesting that cells deficient in DSB repair are exquisitely sensitive to PARP inhibition. Yet, the mechanisms underlying this synthetic lethality between DSB repair deficiency and PARP inhibition remain poorly defined. There is considerable debate about the mechanism through which PARP inhibition kills DNA repair-deficient cells, and the full benefit of PARP inhibitors in cancer therapy can only be achieved by a clear understanding of the DNA damage response (DDR) pathways to DSBs and how these are affected by PARP inhibitors.

The overall aim of my PhD is to investigate the role of PARP-1 in DSB repair and identify interactors of PARP-1 which also play a role in this process**.** Eukaryotic cells repair DSBs by two major pathways, non-homologous end-joining (NHEJ) and homologous recombination (HR). HR is initiated by the binding of DSB by BRCA1 and the end resection of the DSB by MRE11 (and the associated NBS1, RAD50, CtIP, and EXO1) to generate single-stranded DNA, which is further processed by RAD51 and BRCA1-PALB2-BRCA2. A key question in our field regards which factors are critical for regulating the DSB pathway choice. HR is initiated from highly resected DSB ends, whereas in NHEJ, resection is prevented by key repair factors that include RIF1 and 53BP1. Using PARP-1-deficient cells, we have observed that two inhibitors of DNA resection and regulators of pathway choice, RIF1 and 53BP1, are strongly impaired in

forming DNA damage-induced foci. This supports our hypothesis that PARP-1 participates in DSB repair by influencing DNA resection.

In order to further understand the mechanism of resection and the role that PARP-1 plays in it we also aim to identify other proteins which interact with PARP-1 and modulate this process. To accomplish this, we made use of data on PAR binding proteins generated both in our lab and that of our collaborator Ted Dawson. The candidates selected from these lists were screened to identify a single target that would demonstrate a similar phenotype to PARP-1 loss. Two initial targets were further explored and finally a single zinc finger protein was selected as our primary target. We aim to characterize the function of this zinc finger in HR, in the hopes that it will further uncover the mechanisms of PARP-1 in resection.

In summary this thesis elucidates the role of PARP-1 in DNA resection and identifies a previously unstudied zinc finger protein which interacts with PARP-1 and shares a similar function to PARP-1 in DNA resection.

Contents

Figures

Tables

Abbreviations

ABC	ATP Binding Cassette
ABCB1	ATP Binding Cassette Subfamily B Member 1
4-OHT	4-hydroxytamoxifen
ACF1	Bromodomain Adjacent to Zinc Finger Domain 1A
ADN	Acide désoxyribonucléique
ADP	Adenosine diphosphate
ADPR	ADP-ribose
AIF	Apoptosis-Inducing Factor
AMP	Adenosine Monophosphate
AMPK	AMP-activated protein kinase
ANK	Ankyrin
APE-1	Apurinic/apyrimidinic endonuclease
APLF	Aprataxin and PNK-like factor
APTX	Aprataxin
ARE	ADP-ribosylating exotoxins
ARH	ADP-ribose hydrolase
ARH1	ADP-ribose hydrolase 1
ARH2	ADP-ribose hydrolase 2
ARH3	ADP-ribose hydrolase 3
ARN	Acide ribonucléique
ART	ADP-ribosyltransferases
ARTD	ADP-ribosyl transferases diphtheria
ARTD1	ADP-ribosyl transferases diphtheria 1
ARTD10	ADP-ribosyl transferases diphtheria 10
ARTD2	ADP-ribosyl transferases diphtheria 2
ATM	Ataxia-Telangiectasia Mutated
ATP	Adenosine triphosphate
ATP5F1A	ATP synthase subunit alpha, mitochondrial
ATP5F1B	ATP synthase subunit beta, mitochondrial
ATR	Ataxia Telangiectasia and Rad3-related
ATRIP	ATR-interacting protein
ATRX	Alpha Thalassemia/Mental Retardation Syndrome X-Linked
BACH1	BTB Domain and CNC Homolog 1
BARD1	BRCA1-associated RING domain protein 1
BAZ1A	Bromodomain Adjacent to Zinc Finger Domain 1A
BER	Base Excision Repair
BLM	Bloom syndrome protein
BRCA	Breast Cancer gene
BRCA1	Breast cancer type 1 susceptibility protein
BRCA2	Breast cancer type 2 susceptibility protein
BRCT	BRCA1 C-terminal
BSA	Bovine serum albumin

BTB	Broad-Complex, Tramtrack and Bric-a-brac
CDB	Cassure Double-Brin
CDC25A	Cell Division Cycle 25A
CDK	Cyclin-dependent kinases
CDK2	Cyclin-dependent kinase 2
CDK4	Cyclin-dependent kinase 4
CDT	Cytolethal distending toxin subunit A
CHD1L	Chromodomain-helicase-DNA-binding protein 1-like
CHFR	Checkpoint With Forkhead and Ring Finger Domain
CHK1	Checkpoint Kinase 1
CHK2	Checkpoint Kinase 2
CHO	Chinese hamster ovary
CO2	Carbon Dioxide
CRIP1	Cysteine-rich intestinal protein 1
CRISPR	Clustered Regularly Interspaced Short Palindromic Repeats
CTC1	CST Telomere Replication Complex Component 1
CTCF	CCCTC-binding factor
CYREN	Cell Cycle Regulator Of NHEJ
DAPI	4′,6-diamidino-2-phenylindole
DCK	Deoxycytidine Kinase
DDR	DNA Damage Response
DDX21	Nucleolar RNA helicase 2
DHX9	ATP-dependent RNA helicase A
DMC1	DNA Meiotic Recombinase 1
DMEM	Dulbecco's Modified Eagle Medium
DMSO	Dimethyl sulfoxide
DNA	Deoxyribonucleic acid
DNA2	DNA replication ATP-dependent helicase/nuclease DNA2
DPC	DNA-protein cross-links
DS	Double-strand
DSB	Double-strand Break
DSS1	Exoribonuclease II
DTT	Dithiothreitol
DYNLL1	Dynein light chain 1
EDTA	Ethylenediaminetetraacetic acid
EGTA	Egtazic acid
ENPP1	Ectonucleotide Pyrophosphatase/Phosphodiesterase 1
EXO1	Exonuclease 1
FACS	Fluorescence-activated cell sorting
FANCD2	FA Complementation Group D2
FBS	Fetal Bovine Serum
FDA	Food and Drug Administration
FOXA1	Forkhead box A1
GAPDH	Glyceraldehyde 3-phosphate dehydrogenase

GFP	Green Fluorescent Protein
GST	Glutathione S-transferases
H2A	Histone H2 A
H2AC18	Histone H2A type 2-A
H2AX	H2A histone family member X
H2B	Histone 2 B
H2BC12	Histone H2B type 1-K
H2BC14	Histone H2B type 1-M
H2BC21	Histone H2B type 2-E
H2O2	Hydrogen peroxide
H3	Histone H3
H3C15	Histone H3.2
H3K36me2	Histone H3 Lysine 36 Demethylation
H3K9	Histone H3 lysine 9
H3K4me3	Demethylating H3 lysine 4 trimethyl
H4C1	Histone H4
H6PD	Hexose-6-phosphate Dehydrogenase
HCL	Hydrochloric acid
HD	Helical subdomain
HDR	Homologous Driven repair
HELB	DNA Helicase B
HEPES	4-(2-hydroxyethyl)-1-piperazineethanesulfonic acid
HERC2	HECT And RLD Domain Containing E3 Ubiquitin Protein Ligase 2
HNRNPM	Heterogeneous nuclear ribonucleoprotein M
HNRNPU	Heterogeneous nuclear ribonucleoprotein U
HP1	Heterochromatin Protein 1
HPF1	Histone PARylation factor 1
HR	Homologous Recombination
HSPA8	Heat shock cognate 71 kDa protein
IARS1	Isoleucine--tRNA ligase, cytoplasmic
ICL	Intra- and inter-strand cross-links
IF	Immunofluorescence
IGF2BP1	Insulin-like growth factor 2 mRNA-binding protein 1
IP	Immunoprecipitation
IR	Irradiation
iTRAQ	Isobaric tags for relative and absolute quantitation
KAP1	Transcription intermediary factor 1-beta
KBM	Ku-binding-motif
KD	Knock Down
KDM2A	Lysine-specific demethylase 2A
KDM4D	Lysine-specific demethylase 4D
KDM5A	Lysine-specific demethylase 5A
KDM5B	Lysine-specific demethylase 5B
KIF20B	Kinesin-like protein KIF20B

KIF2C	Kinesin-like protein KIF2C
KO	Knock Out
KRAB	Krüppel-associated box
L3MBTL2	Lethal Malignant Brain Tumour-like 2
LIG3	Ligase 3
LIG4	Ligase 4
LMNA	Lamin A
MAR	Mono (ADP-ribose)
MART	MAR transferases
MDC1	Mediator of DNA damage checkpoint 1
MEF	Mouse Embryonic Fibroblast
MMC	Mitomycin C
MMR	Mismatch Repair
MMS	Methyl Methane Sulfonate
MNNG	N-methyl-N'-nitro-N-nitrosoguanidine
MNU	N-methyl-N-nitrosourea
MOPS	3-(N-morpholino) propane sulfonic acid
MRE11	Meiotic Recombination 11
MRN	Mre11–Rad50–Nbs1 complex
MS	Mass Spectrometry
mTOR	Mechanistic Target of Rapamycin
MTS	Mitochondrial Targeting Sequence
NAD	Nicotinamide Adenine Dinucleotide
NBS1	Nibrin
NCL	Nucleolin
NCS	Neocarzinostatin
NER	Nucleotide Excision Repair
NES	Nuclear Export Signals
NHEJ	Non-Homologous End Joining
NLS	Nuclear Localisation Signal
NMN	Nicotinamide mononucleotide
NONO	Non-POU Domain Containing Octamer Binding
NPM1	Nucleophosmin
NTR	N-terminal region
NUDIX	Nucleoside Diphosphate-linked moiety-X
NUDIX5	Nudix (Nucleoside Diphosphate Linked Moiety X)-Type Motif 5
NUDT16	Nudix (Nucleoside Diphosphate Linked Moiety X)-Type Motif 16
NUDT9	Nudix (Nucleoside Diphosphate Linked Moiety X)-Type Motif 9
OB	Oligonucleotide/Oligosaccharide-Binding
OGG1	8-Oxoguanine glycosylase
ORF	Open Reading Frame
PALB2	Partner and Localizer of BRCA2
PAR	Poly (ADP-Ribose)
PARG	Poly (ADP-ribose) glycohydrolase

PARP	Poly (ADP-ribose) polymerase
PARP1	Poly (ADP-ribose) polymerase-1
PARP2	Poly (ADP-ribose) polymerase-2
PARP3	Poly (ADP-ribose) polymerase-3
PBM	PAR Binding Motif
PBS	Phosphate-buffered saline
PBZ	PAR-binding zinc-finger
PCNA	Proliferating cell nuclear antigen
PCR	Polymerase chain reaction
PDE	phosphodiesterase
PFA	Paraformaldehyde
PHB2	Prohibitin-2
PHD	Plant Homeodomain
PIKK	Phosphatidylinositol 3-kinase-like protein kinases
PIP	PCNA-interacting protein
PIPES	Piperazine-N, N′-bis (2-ethanesulfonic acid)
PNK	Polynucleotide kinase
POP1	Ribonucleases P/MRP protein subunit POP1
POZ	Poxvirus and Zinc Finger
PRPF38A	Pre RNA-Processing Factor 38 A
PTM	Post Translational Modification
RAD18	E3 ubiquitin-protein ligase RAD18
RAD50	DNA repair protein RAD50
RAD51	DNA repair protein RAD51
RAD51C	RAD51 Paralog C
RAD51D	RAD51 Paralog D
RBM14	RNA-binding protein 14
RBPI	Rhodamine-based PARG inhibitors
RIF1	Rap1-Interacting Factor 1
RNA	Ribonucleic acid
RNF113A	E3 ubiquitin-protein ligase RNF113A
RNF126	E3 ubiquitin-protein ligase RNF126
RNF138	E3 ubiquitin-protein ligase RNF138
RNF168	E3 ubiquitin-protein ligase RNF168
RNF2	E3 ubiquitin-protein ligase RING2
RNF68	Polycomb group RING finger protein 1
RNF8	E3 ubiquitin-protein ligase RNF8
RPA	Replication protein A
RPA1	Replication protein A 1
RPA2	Replication protein A 2
RPA3	Replication protein A 3
RPA70	Replication protein A 70
RPM	Revolutions per minute
RPN1	Ribophorin 1

RRM	RNA recognition motif
RS	Regulatory Segment
SAM68	SRC associated in mitosis of 68
SAP	SAF/Acinus/PIAS
SCAN	SRE-ZBP, CTfin51, AW-1 and Number 18 cDNA
SCE	Sister-Chromatid Exchanges
SDS	Sodium Dodecyl Sulphate
SEM	Standard Error of the Mean
SETDB1	SET Domain Bifurcated Histone Lysine Methyltransferase 1
SF9	*Spodoptera frugiperda* Sf9 insect cells
SHLD1	Shieldin complex subunit 1
SHLD2	Shieldin complex subunit 2
SILAC	Stable Isotope Labelling by/with Amino acids in Cell culture
SLC25A5	ADP/ATP translocase 2
SMART	Single Molecule Analysis of Resection Tracts
SPR	Surface plasmon resonance
SS	Single-Strand
SSA	Single-Strand Annealing
SSB	Single-Strand Break
SSBER	Single-strand base excision repair
SSBR	Single strand break repair
SUMO	Small Ub-related Modifier Proteins
TARG1	Terminal ADP-ribose protein glycohydrolase 1
TBE	Tris/Borate/EDTA
TBS	Tris-buffered saline
TE	Tris-EDTA
TIRM28	Tripartite Motif Containing 28
TLC	Thin-layer chromatography
TNBC	Triple Negative Breast Cancer
TRF1	Telomeric repeat-binding factor 1
TTN	Titin
TUBA1B	Tubulin alpha-1B chain
TUBB	Tubulin beta chain
UV	Ultraviolet
VDAC1	Voltage-dependent anion-selective channel protein 1
WB	Western Blot
WGR	Tryptophan-glycine-arginine-rich
WT	Wild Type
WWE	Tryptophan and glutamate
WWP2	NEDD4-like E3 ubiquitin-protein ligase WWP2
XRCC1	X-Ray Repair Cross Complementing 1
XRCC4	X-Ray Repair Cross Complementing 4
YAP1	Yes-associated protein 1
ZBTB24	Zinc Finger and BTB Domain Containing 24

ZEB1	Zinc Finger E-Box Binding Homeobox 1
ZNF	Zinc Finger

Acknowledgements

When I started this journey nearly 5 years ago, I certainly did not anticipate finishing my PhD during a global pandemic, sometimes I'm not sure which required more mental fortitude. I would not be here, submitting my PhD thesis, if it wasn't for the incredible opportunity I was presented by Dr Jean-Yves Masson and Dr Guy Poirier. I can honestly say that I am leaving this PhD a different person, with an entire vault of new techniques and skills at my disposal. They have encouraged and supported my growth as a scientist during my time under their watchful eyes. It is due to them that I will be leaving my PhD with several impactful articles added to my C.V., something I will always be grateful for. They have helped me grow as person and determine what I want for my future, what is important and what I am not willing to compromise on for my life. I am very thankful to both my supervisors for giving me several opportunities to present my work in both national and international conferences, particularly the NAD^+ conference back home in Dublin. These conferences were an excellent place to exchange and develop new ideas for my project with both leading-researchers and other students working on similar topics to myself.

The first person I need to thank is Marie-Christine the other resident of the PARP island in the lab, who took me under her wing to teach me the ropes of lab and has been a source of support and collaboration throughout my time here. Of course, I can't forget Yan and Amé the other pillars which support the lab and without whom there would be chaos. To Jean-Philippe who is Guy's right-hand man and the core of the lab at the CHUL your help and advice has been invaluable.

Let's not forget my siblings in arms; Laura and Daryl, both who joined the lab shortly after me and with whom I have shared each and every trial that is found in the PhD together. I'm sure that one day we will find a robot in a rowboat, I think back fondly on our time together. Daryl, you have become like another brother to me, and I will miss you desperately when we separate, thank you for putting up with my nonsense and getting a ton of my references and jokes that don't make sense unless you lived in Ireland or the UK. Laura your company and listening skills have been invaluable, I will miss our cell culture discussions. At same time we have our Rockstar postdoc Laure, who swept into

the lab like a hurricane of enthusiasm and forgetfulness. When thinking about Laure you can't forget Yuandi, who joined as a baby intern only to return to do a PhD in the lab. There is no one as innocent and adorable as Yuandi. This hardworking and frantic duo were followed by the most relaxed person I have ever met, Thibaut. Whose calm demeanour has been almost unshakeable and so very reliable in the chaotic atmosphere that is a PhD student office. Then came Adèle, who quickly became a close friend, who I would spend many evenings and weekends with, the cheesy club wouldn't be the same without you. Next came Gemma and Larissa who have been forced to endure my company all throughout the pandemic when we would trade off shifts. There are no bonds like those forged in a global pandemic. Louis my replacement as a codirection student binding both labs together, what fun times we have shared annoying Adèle. Last, we have Sofiane who I need to thank for working with me on the JoVe methods paper and always providing interesting scientific discussions, sometimes even when I just wanted to go home to sleep after the night shift together.

For the last chapter of my PhD, I can't let it pass without acknowledging Larissa, who not only struggled with me to generate a CRISPR KO line but has also been by my side, step by step as I fought to conquer ZNF432. Without her guidance and unyielding support, I don't know that my progress in shedding light on ZNF432 would be close to where it is now. From every ugly blot to beautiful graph, she has been there to commiserate and celebrate each result and always suggesting new things to try in order to progress. Outside of acting as a pillar in the lab she has also become a great friend who has put up with all my nonsense.

To all the other members of both labs who I have met throughout my tenure here, thank you for the time we shared, the things you have taught me and the fun we have had. A huge thank you to everyone in the centre who has been a part of my life, particularly Justine and Salar. No matter where we end Justine you will always be my budding yeast, which means Salar you will have to put up with me. Both of you helped make Québec feel a little bit like home and I know that you will both go on to do incredible and impressive things in the future that cannot wait to hear about.

I wish to also thank the CHU de Québec, the Centre de Recherche sur le Cancer, the Harley Owners Group and the FRQS for their generous scholarships which have

funded a great deal of my PhD. I would like to thank my jury, Dr. Amélie Fradet-Turcotte, Dr. Michel Lebel and Dr. Michael Cohen for agreeing to read and evaluate my doctoral work and joining me on this final stage of my PhD.

Finally, I would like to thank my parents and brother; Cathal, Catherine and Tadhg who have heard plenty of my complaints when experiments failed and nodded along as if they understood. Who have stood by me no matter how down I was feeling and always telling me I could do it. To my father especially who took the time to read through much of thesis as I was writing it, even if he didn't really understand what I was writing about. To my extended family who have been nothing but supportive, constantly asking parents when I will finish, when I will be home and is she a doctor yet. Without them I wouldn't who I am today and certainly wouldn't have had the determination or confidence to move halfway across the world alone to fight through a PhD.

Preface

The scientific work presented in this thesis is the product of nearly five years of work as a doctoral student in the laboratories of the Drs Jean-Yves Masson and Guy G. Poirier. Throughout this time, I have contributed as co-first author to two manuscripts.

The first is a review on the current knowledge surrounding PAR erasers **—"Emerging roles of eraser enzymes in the dynamic reversal of protein mono- and poly(ADP-ribosylation)"** (Julia O'Sullivan (=), Maria Tedim Ferreira (=), Jean-Philippe Gagné, Ajit Sharma, Michael J. Hendzel, Jean-Yves Masson, and Guy G. Poirier) I wrote the manuscript and designed the figures in conjunction with Dr Maria Tedim Ferreira, but would not have succeeded without contribution and critical discussion with the co-authors mentioned on the manuscript. (**Chapter 1**)

I had the privilege of contributing to the manuscript: **—Poly(ADP-ribose) polymerase-1 antagonizes DNA resection at double-strand breaks**" (Marie-Christine Caron[=] Ajit K. Sharma[=], Julia O'Sullivan, Logan R. Myler, Maria Tedim Ferreira, Amélie Rodrigue, Yan Coulombe, Chantal Ethier, Jean-Philippe Gagné, Marie-France Langelier, John M. Pascal, Ilya J. Finkelstein, Michael J. Hendzel, Guy G. Poirier & Jean-Yves Masson). The manuscript was published in Nature Communications in July 2019. My contributions were in several of the figures, some under the supervision of the first author Marie-Christine at the very beginning of my PhD, others done independently. Notably I was responsible for the optimisation of the SMART technique, a previously unused technique in our lab. The publication is fundamental for the comprehension of my thesis and acted as the background for the continuation of my project, I have added it as **Chapter 2**.

Thirdly, I had the opportunity to share a technique that was essential in both the previously mentioned article and my continued work, in the Journal of Video Editing: **— Assessment of global DNA double-strand end resection using a coupled BrdU-DNA labeling with cell cycle discrimination imaging method**" (Julia O'Sullivan=, Sofiane Y. Mersaoui1=, Guy Poirier and Jean-Yves Masson). I have performed the experiments and made the figures; the writing was done in conjunction with Dr. Sofiane Y. Mersaoui (**Chapter 3**).

My last chapter contains currently unpublished data for which I have fully generated the figures and written the manuscript **— Zinc-Fingers? A new candidate for PARP-1 dependent DNA repair through Homologous Recombination**. (Julia O'Sullivan, Marie-Christine Caron, Jean-Philippe Gagné, Larissa Milano de Souza, Ted Dawson, Guy G. Poirier and Jean-Yves Masson). Though I would like to particularly thank Marie-Christine Caron in the help producing the purified protein and Dr Larissa Milano de Souza for her help in attempting to generate a CRISPR KO cell line. Furthermore, the project would not have advanced to this stage without the critical input of Drs Ted Dawson, Jean-Philippe Gagné, Jean-Yves Masson and Guy Poirier (**Chapter 4**).

I have also had the great privilege to participate as a co-author in the seminal work Dr Suryasree Subramania which was published in Nucleic Acids Research February 2019. **SAM68 interaction with U1A modulates U1 snRNP recruitment and regulates *mTor* pre-mRNA splicing.** Suryasree Subramania, Laurence M Gagné, Sébastien Campagne, Victoire Fort, Julia O'Sullivan, Karel Mocaer, Miki Feldmüller, Jean-Yves Masson, Frédéric HT Allain, Samer M Hussein, Marc-Étienne Huot. *Nucleic Acids Research*, Volume 47, Issue 8, May 2019, Pages 4181–4197 **(Annex)**

Introduction

Increased levels of genomic instability can promote or exacerbate carcinogenesis and ageing. Due to this, accurate repair of DNA damage is essential for prolonged health and increased resistance to diseases such as cancer. Poly(ADP-ribose) polymerase-1 (PARP-1) is a key member of the DNA damage response which plays roles in multiple DNA repair pathways. Furthermore, compounds which inhibit PARP-1 promote the accumulation of DNA double-strand breaks to kill cancer cells. The specific function of PARP-1 in the repair of DNA double-strand breaks has not been fully elucidated, nor has the full complement of its partners been uncovered. This is the core topic of my thesis and will be introduced throughout.

The DNA damage response to DSBs is a multi-layered process

Cells continuously experience challenges as a result of both endogenous and exogenous DNA damaging agents, which may result in DNA lesions. The sources of DNA damage are varied and result in different types of lesions. It is predicted that on a daily basis cells suffer from 10^4 to 10^6 DNA damaging events, which require repair[1]. This inevitable sequence of damage and repair is discussed in the following section.

Sources and types of DNA Damage

DNA damage may result from either endogenous processes or exogenous sources and is one of the major causes for genomic instability (Figure 0.1A). Cells suffer from thousands of DNA lesions per day and for this reason have developed a multitude of ways of repairing these damages efficiently. Different sources of DNA damage can result in different types of DNA lesions, such as single-strand breaks (SSB), double-strand breaks (DSB), intra- and inter-strand cross-links (ICL) and DNA-protein cross-links (DPC)[2]. Each of these require different repair pathways (Figure 0.1B).

Exogenous sources leading to DNA damage include ionizing radiation (IR), ultraviolet radiation (UV) and anti-cancer chemotherapeutic drugs. Each damage type has a preference as to what type of lesion it will form. Natural UV radiation can cause pyrimidine-dimers and 6-4-photoproducts in the DNA helix that interfere with proper transcription and replication[1, 3]. IR damage, which can be caused by exposure to cosmic radiation or clinical radiation such as x-rays, causes both single- and double-strand breaks with approximately ten times more single-strand than double-strand breaks. Though fewer in number, these DSBs are some of the most severe lesions as that can lead to chromosomal translocations and cell death if they are not repaired. Endogenous DNA damage sources include processes such as hydrolysis, oxidation, and alkylation of nucleotides, as well as the mismatch and loss of DNA bases by deamination and depurination, and replication faults[4-8].

In this work while we are focused on the repair of double-strand breaks, it is still important to have a basic understanding of some of the other DNA damage lesions and how they are repaired (Figure 0.1B). There are several different pathways which repair specific types of lesions; Nucleotide Excision Repair (NER) which repairs bulky adducts and intra-strand cross-links, Mismatch Repair (MMR) which targets A-G and T-C mismatch, insertions and deletions, and Base Excision Repair (BER) which repairs damaged DNA bases and single-strand breaks, which can also be repaired by Single-Strand break Repair (SSBR)[9]. Depending on the source of the damage and the resulting lesion, one of these pathways is then selected to repair the damaged DNA (Figure 0.1C).

This is particularly important when considering cancer treatments, as cancer cells unlike non-cancerous cells proliferate regardless of DNA damage[10]. For this reason, cancer therapy is often based on the induction of DNA DSBs in order to induce cell death. To study the repair pathways which are activated upon DNA damage, whose disfunction can either propagate cancer or be used to target cancers, chemical agents have been developed and employed to mimic these damages. In order to mimic the effect of IR, neocarzinostatin (NCS) and other radiomimetic drugs have been used. NCS, for example, has been used in the treatment of lung cancer[11, 12]. Intra- and inter-strand crosslinking can be induced through the use of cross-linking agents like mitomycin C (MMC), cisplatin or nitrogen mustard. Cisplatin is a platinum based cross-linking agent which has been used as a cancer treatment[13, 14]. In order to induce the attachment of alkyl groups,

alkylating agents such as methyl methanesulfonate (MMS), N-methyl-N'-nitro-N-nitrosoguanidine (MNNG) can be used. These create DNA adducts through primarily N7- and N3-alkyl purines[15]. Furthermore, inhibition of the enzymes topoisomerase I or II by camptothecin and etoposide respectively, has also been used to induce SSBs or DSBs. These represent some of the most commonly used DNA damaging agents when studying DNA repair.

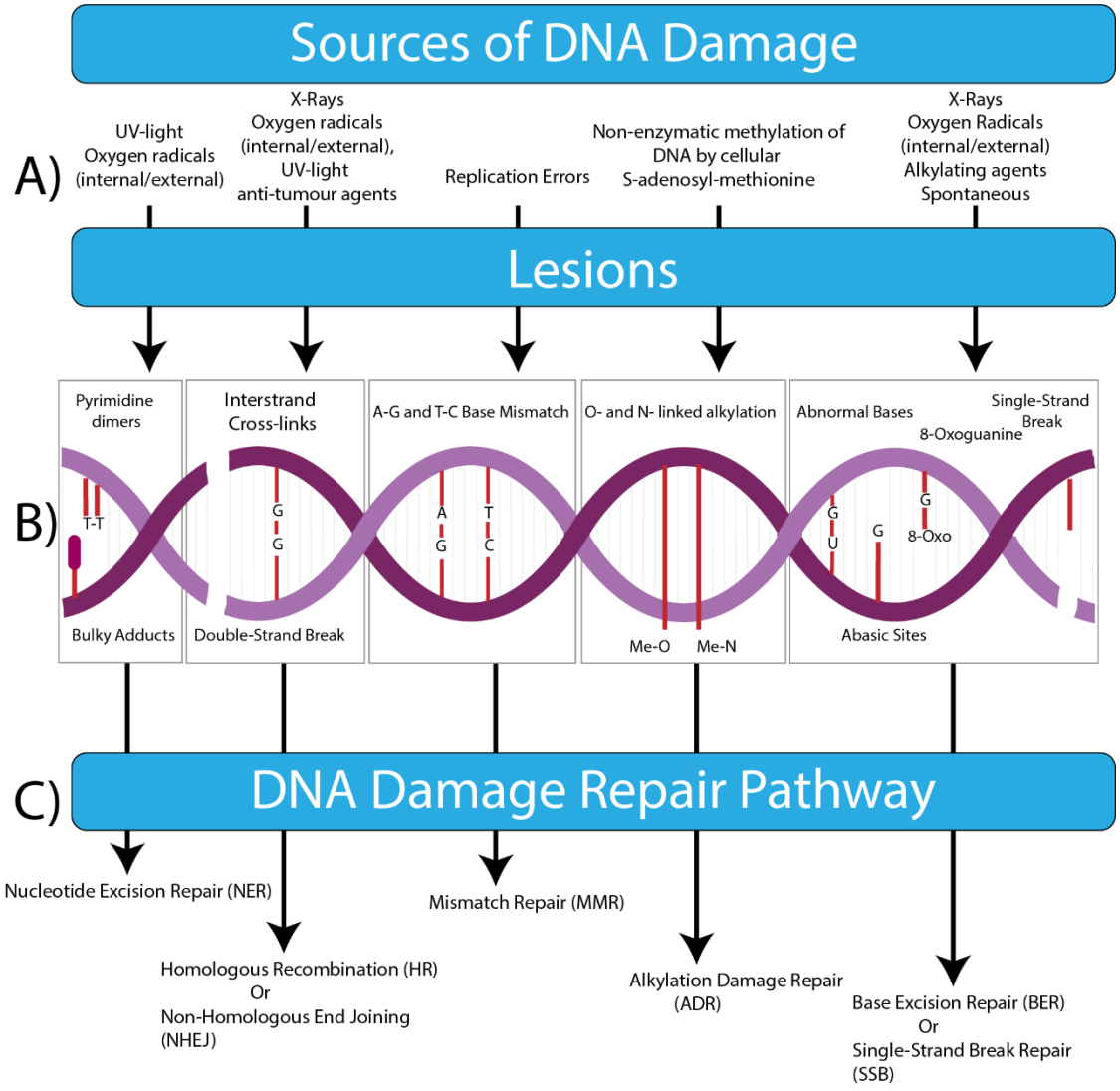

Figure 0.1: Potential sources of DNA damage, the resulting lesions, and their associated DNA repair pathways.

A) Endogenous and exogenous sources of DNA damage. These summarise a selection of potential damaging events which commonly cause DNA lesions. B) The resulting DNA lesions caused by the endogenous/exogenous sources shown in A. The different types of lesions are represented. C) Repair pathways for the different lesion types.

DSB Sensing, Signalling, and Checkpoint Control

The complex DNA Damage Response (DDR) to cellular DNA double-strand breaks is not simply comprised of the many proteins required for the repair itself but is in fact a signalling cascade made up of many elements. This signalling cascade is comprised of DNA damage sensors, mediators and effectors proteins, as depicted in Figure 0.2[16]. The DDR is principally mediated by the phosphatidylinositol 3-kinase-like protein kinases (PIKKs), ATM (ataxia-telangiectasia mutated), ATR (ATM and Rad3 related) and DNA-PK (DNA-dependent Protein Kinase)[17]. The activation of ATM and ATR by DSBs leads to the phosphorylation mediator proteins such as p53 (Tumor Protein p53) and BRCA1 (Breast Cancer type 1 susceptibility protein). These have been linked to the phosphorylation of some ATM substrates, amplifying the DNA damage response. Effector proteins are directly phosphorylated by either ATM or ATR. ATM is primarily activated in response to DSBs whereas ATR is primarily activated in response to tracts of single-stranded DNA[18-21]. The sequence of signalling events will be described further below. Defects in this signalling pathway can have severe consequences for genomic integrity, resulting in poorly coordinated repair or loss of repair thus leading to an accumulation of mutations or DNA breaks. In an attempt to avoid such consequences, mechanisms have evolved to appropriately recruit the necessary enzymes in the right order and location.

The initial step following the formation of a double-strand break is the transmission of the signal to stop the cell from cycling to prevent replication errors on top of the existing break. Double-strand breaks are sensed by proteins which are rapidly recruited to the break site to control the complicated flow of information and actions required to repair the DNA. Some of the first responders to the double-strand breaks are PARP-1 and MRE11/RAD50/NBS1 (MRN)[22]. PARP-1 arrives on scene within milliseconds of the break formation and facilitates the rapid recruitment of both MRE11 within 40 seconds and NBS1 within 117 seconds post damage [23, 24]. PARP-1 binds to the free ends of the DNA, activating then generating the poly(ADP-ribose) polymer (PAR). This acts as a scaffold for many other repair proteins. PARP-1 and MRN recruit and activate ATM, DNA-PK and ATR, though ATR is primarily involved in the initiation of the repairs for stalled replication forks.

ATM, ATR and DNA-PK have various targets which are involved in the repair of DNA damage. It is within a very short time period; minutes of the formation of the double-strand break, that activated ATM and ATR phosphorylate other essential DNA damage response proteins. This is an essential post-translational modification (PTM) for the successful repair of DSBs. One such element to be phosphorylated at the beginning of the repair sequence is the histone variant H2AX located at either side of the break[25]. The phosphorylated version of this histone is referred to as γ-H2AX[26, 27]. This subsequently recruits other proteins and initiates the essential chromatin-remodelling process needed for the repair of the DNA[28].

γ-H2AX is bound by MDC1 (mediator of DNA damage checkpoint 1), that along with ATM and NBS1 spreads the phosphorylation of H2AX up to megabases from the damage site, thus creating a positive feedback loop of signalling[29-31]. MDC1 itself is phosphorylated by ATM, resulting in the recruitment of RNF8 to the break-site. RNF8 binds to phosphorylated MDC1 promoting RNF168 recruitment. RNF8 and RNF168 conjugate ubiquitin chains on H2A inducing chromatin remodelling and the recruitment of 53BP1 and BRCA1[32-39].

Other targets for ATM and ATR include CHK1 and CHK2 respectively, the phosphorylation of these proteins is necessary for the induction of CDC25A phosphorylation, leading to its proteosomal degradation[40]. Loss of the CDC25A results in the G1/S arrest thus preventing the cell from proliferating. Furthermore, activated ATM, ATR, DNA-PK, CHK2 and CHK1 help in the phosphorylation and activation of p53, a key player in DNA-damage checkpoints[41, 42]. Activated p53 induces cell-cycle arrest, apoptosis and senescence in response to DNA damage by regulating the cyclin-dependent kinase (CDK) inhibitor p21, which inhibits two G1/S-promoting CDKs, CDK2 and CDK4. This leads to G1 arrest, thus halting replication of the damaged DNA. The transition from S to G2 phase has been linked through the decline in ATR activity mediated by a CDK1-pFOXM1 switch, providing an intrinsic S/G2 checkpoint[43].

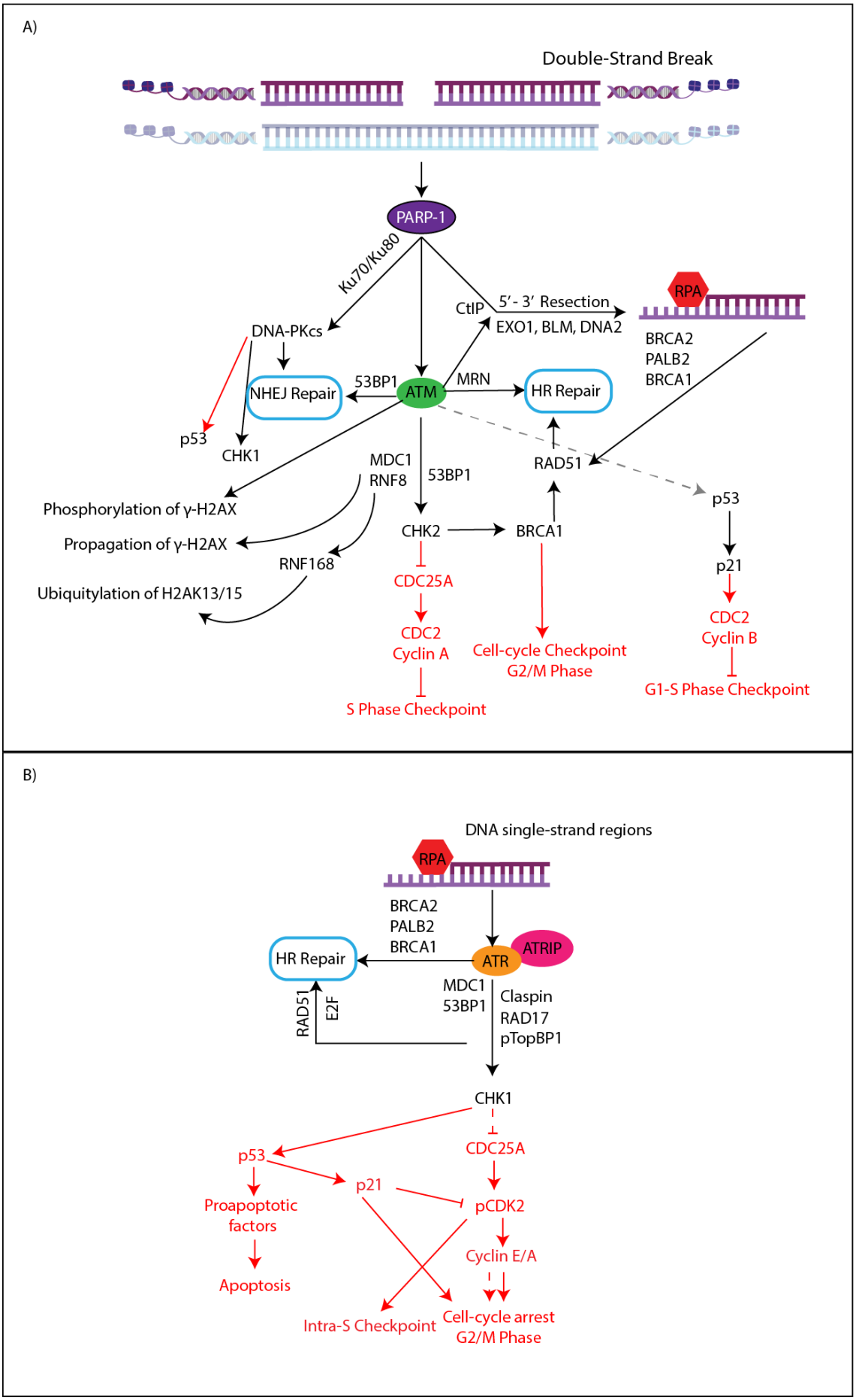
A)
Double-Strand Break
PARP-1
Ku70/Ku80
DNA-PKcs
CtIP
5′- 3′ Resection
EXO1, BLM, DNA2
RPA
BRCA2
PALB2
BRCA1
NHEJ Repair
53BP1
ATM
MRN
HR Repair
p53
CHK1
MDC1
RNF8
53BP1
RAD51
Phosphorylation of γ-H2AX
Propagation of γ-H2AX
RNF168
Ubiquitylation of H2AK13/15
CHK2
BRCA1
p53
p21
CDC25A
CDC2
Cyclin A
Cell-cycle Checkpoint
G2/M Phase
CDC2
Cyclin B
S Phase Checkpoint
G1-S Phase Checkpoint
B)
DNA single-strand regions
RPA
BRCA2
PALB2
BRCA1
HR Repair
ATR
ATRIP
MDC1
53BP1
Claspin
RAD17
pTopBP1
RAD51
E2F
CHK1
p53
CDC25A
p21
pCDK2
Proapoptotic
factors
Cyclin E/A
Apoptosis
Intra-S Checkpoint
Cell-cycle arrest
G2/M Phase

Figure 0.2: Schematic representation of the DNA damage signalling cascade.

A) Upon DNA damage PARP-1 is recruited, recruiting either MRN or the Ku heterodimer. If Ku binds, then DNA-PKcs will be recruited and repair through NHEJ will take place. If MRN is recruited, it then recruits ATM which mediates the phosphorylation of H2AX to γ-H2AX, this acts as a beacon for DDR factors. This activates the downstream effector kinase CHK2, which is phosphorylated by ATM. CHK2 is then thought to dissociate from the site of damage and disperse as monomer to affect processes of cell cycle progression. ATM also targets other DDR proteins such as NBS1, BRCA1, MDC1 and p53BP1. B) ATR and ATRIP are activated following the binding of RPA which coats the ssDNA post resection, ATR-CHK1 signalling is activated most strongly following replication errors. The text in red is the negative loop of the signalling cascade, which will result in cell-cycle arrest and apoptosis. The dashed lines represent the results of stalled replication. Activated ATM/ATR mediate the phosphorylation and activation of CHK2 and CHK1, this is necessary for the phosphorylation of CDC25A which is a marker for proteasomal degradation. Additionally, ATM/ATR, DNA-PK, CHK1, and CHK2 all aid in the phosphorylation and activation of p53, which leads to sustained G1 arrest. Another substrate of CHK2 is E2F1 which is involved in cell the G1/S transition. CHK2 phosphorylation of E2F1 results cell cycle arrest and induces apoptosis, conversely E2F1 is also recruited to the sites of damage where it interacts with NBS1 and is thought to further promote the recruitment of other DDR proteins. Depletion of E2F1 affects RAD51 an essential factor in HR repair[44, 45]. Adapted from Waterman, D.P., J.E. Haber, and M.B. Smolka, *Checkpoint Responses to DNA Double-Strand Breaks.* Annual Review of Biochemistry, 2020 [46]

DNA Double-Strand Break Repair Mechanisms

DSBs can be repaired through two main pathways depending on the cell cycle stage. The first pathway is Non-Homologous End Joining (NHEJ), which can take place at any time during the cell cycle and can be further subdivided into its Canonical and Alternative forms (C-NHEJ and Alt-NHEJ)[47]. Secondly, Homologous Driven repair (HDR) which is primarily exemplified by Homologous Recombination (HR). This requires the presence of the sister chromatid and therefore can only take place during the S/G2 phase of the cell cycle. Single-Strand Annealing (SSA) is the other homologous

driven repair pathway which also takes place in the S/G2 cell cycle as it is suppressed in G1 phase[48]. A basic illustration of these pathways is shown in Figure 0.3. With a variety of repair mechanisms available for the repair of double-strand breaks, a choice is required. One of the ways this choice can be facilitated depends on whether the process of DNA end resection is undertaken, this process can be promoted or inhibited by certain proteins[49, 50]. DNA end resection is the process by which one strand of the duplex on either side of the double-strand break is digested to produce single-stranded DNA. The size of the resected DNA is key for pathway choice. In the case of canonical NHEJ (C-NHEJ), little to no sequence homology is needed thus no resection is required[51]. Conversely for Homologous Recombination a 3' single-strand DNA overhang is needed, meaning a substantial amount of resection is required. Alternative NHEJ (Alt-NHEJ) requires short stretches of microhomology and thus needs only minimal resection. Finally, Single-Strand Annealing requires the longest stretch of resection often resulting in deletions between DNA repeats[52].

In C-NHEJ, DSBs are first recognized by the Ku70-Ku80 (Ku) heterodimer. Recruitment of the Ku70-Ku80 heterodimer improves the subsequent binding of DNA polymerases, nuclease, and ligation complexes[53-55]. DNA-dependent protein kinase catalytic subunits (DNA-PKcs) have a high affinity for Ku-DNA ends. Acting with Ku as a bridge between the broken ends[56]. DNA-PKcs are recruited in a complex with Artemis when DNA resection is required to produce microhomologies or clean DNA ends[57]. They undergo autophosphorylation and subsequently activate Artemis, which then has the capability to cut DNA substrates at the edges of the breaks. This is through its endonuclease activity. However, it has been shown that Artemis can undergo 5' – 3' exonuclease activity independently of DNA-PKcs[58]. In addition, polynucleotide kinase (PNK), APLF (Aprataxin and PNPK Like Factor) nuclease and terminal deoxynucleotidyl transferase (TdT) polymerase have all been found to be involved in the removal of damaged nucleotides[59-61].

After the nucleolytic action of Artemis, polymerases insert nucleotides to prepare the broken ends for ligation. This is accomplished by the polymerases from the POLX family, λ and μ, which have been shown to bind the Ku-DNA complexes through their BRCT domains[62-64]. The final step in this repair process is the ligation of the DNA ends. This involves the X4L4 (XRCC4, DNA ligase IV and XLF) ligation complex. The

X4L4 complex is proposed to form a sleeve-like structure which surrounds the DNA duplex[60, 65]. This is thought to stabilize the positioning of the DNA ends before they are covalently ligated.

Alt-NHEJ is believed to be a backup pathway for C-NHEJ or HR, when certain repair factors are mutated or deficient, such as the Ku complex. Repair by Alt-NHEJ is suppressed by Ku, indicating competition for the same DNA repair factors in both Alt-NHEJ and C-NHEJ. Alt-NHEJ is DNA-PKcs independent, and it is believed that PARP-1 has a similar function in this pathway as the DNA-PKcs in C-NHEJ[66]. It is also likely that PARP-1 acts as a scaffold for either directly or indirectly recruiting Alt-NEHJ proteins. Though the exact role for PARP-1 in Alt-NHEJ is still unclear. As this is a Lig4 independent pathway, other enzymes are needed to catalyse strand ligation. DNA ligase III and its cofactor XRCC1 have both been strongly implicated to take over this role[67]. Based on the size of the deletion it is thought that Alt-NHEJ uses limited resection before joining the DNA ends. This resection shares the initial mechanism with HR, using the MRE11 nuclease and CtIP, which is comprehensively described in section 1.1.4[57].

Single-Strand Annealing (SSA) is another pathway available to repair DSBs. Like HR this takes place during the primarily in the S/G2 phase of the cell cycle. In SSA, extensive 5’ – 3’ resection takes place in order to expose single-strand complementary sequences of greater than 30 nucleotides[52, 68]. These complementary sequences anneal creating a DNA duplex with non-complementary 3’ DNA tails. These tails get removed and gap filling synthesis and ligation take place to repair the break. This form of repair often generates large intra chromosomal deletions.

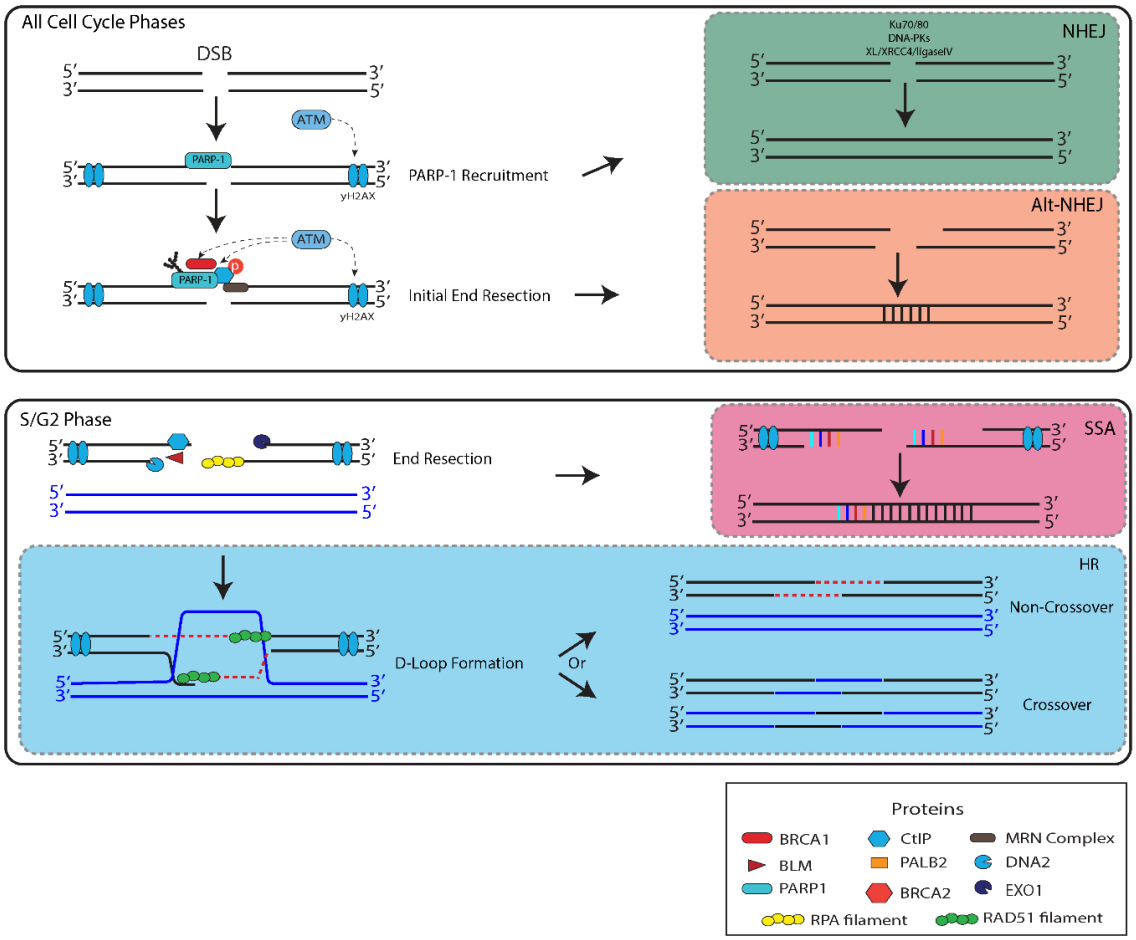

Figure 0.3: The DNA double-strand break repair pathways in the context of the cell cycle.

Several different pathways are available to repair double-strand breaks. Due to the different requirements for each repair pathway, some are limited to specific cell cycle phases. C-NHEJ and Alt-NHEJ do not require the sister chromatid and as such can take place at any time during the cell cycle. By contrast, SSA and HR are Homology Driven Repair (HDR) pathways which require homologous sequences from either the opposite strand in the case of SSA or the sister chromatid for HR, these two pathways are limited to the S/G2 phase of the cell cycle.

A basic understanding of the available DSB repair pathways is essential for my thesis. I have summarized the current understanding surrounding these pathways. The work in my thesis centres around the Homologous Recombination pathway and the key step of DNA Resection, which are described in detail in the following section.

Homologous Recombination and Resection

One of the crucial steps in the HR pathway is the resection of DNA ends. This has proven to be a very complex process that relies on several different vital proteins. This process is summarized as the digestion of the broken DNA ends, leaving behind 3'-OH single-stranded DNA ends[69]. Here, we will further explore the known components and processes involved in this essential step of repair. Figure 0.4 illustrates the general steps of the HR pathway. The MRN complex, one of the first responders to DNA damage, is comprised of two subunits of each MRE11, RAD50 and NBS1. These subunits form a flexible scaffold that allows for its many functions[24]. The complex, facilitated by the endonuclease activity of MRE11, creates an initial nick opening the way for EXO1 and DNA2 nucleases to process the DNA[70]. These nucleases process long tracts of DNA in a 5' to 3' direction on either side of the break, generating the necessary 3' overhangs[71]. In order to improve the effectiveness of resection, the DNA is unwound by the BLM helicase. DNA2 has also shown to have helicase activity which improves the resulting resection[56, 71]. The single-strand DNA is then coated by RPA to protect it from further degradation.

Another essential protein is CtIP, which stimulates the endonuclease activity of MRE11[72]. CtIP is a protein that is known to interact with BRCA1 early in the repair process. Due to this, it has long been assumed that BRCA1 plays a role in resection. While this is true indirectly, through the recruitment of CtIP, BRCA1 has not been shown to play a direct role in the resection process[73, 74]. Furthermore, it has been seen that this BRCA-CtIP cooperation is not essential for resection though it can modulate the overall speed at which resection occurs[75]. The newly resected DNA is rapidly coated by RPA molecules in order to protect it from further processing. BRCA2 mediates the ATP-dependent RAD51 recruitment to the RPA coated single-strand DNA. The N-terminal domain of RAD51 then interacts with the RPA70 subunit facilitating the displacement of RPA and thus allowing for the exchange of an RPA coated filament to a RAD51 coated single-strand DNA filament[76-78]. Once fully coated by RAD51, the newly formed helical nucleofilament, will seek out the sister chromatid in search for a homologous sequence to use as a template for repair. This process is mediated by the BRCA1-PALB2-BRCA2 complex. It is presumed that BRCA1 promotes the recruitment of BRCA2 and PALB2. These act as mediators in assisting the exchange of RPA and RAD51. BRCA2

and PALB2 stimulate D-loop (Displacement loop) formation and further assist RAD51 in the strand invasion[79, 80]. The D-loop is the paired double-strand DNA intermediate that is generated as a result of successful strand invasion of the sister chromatid. The invading strand is the 3' single-strand DNA coated in RAD51 moieties, which forms a new set paired DNA strands with the sister chromatid. Leaving the non-homologous strand to form the D of the D-loop[81, 82].

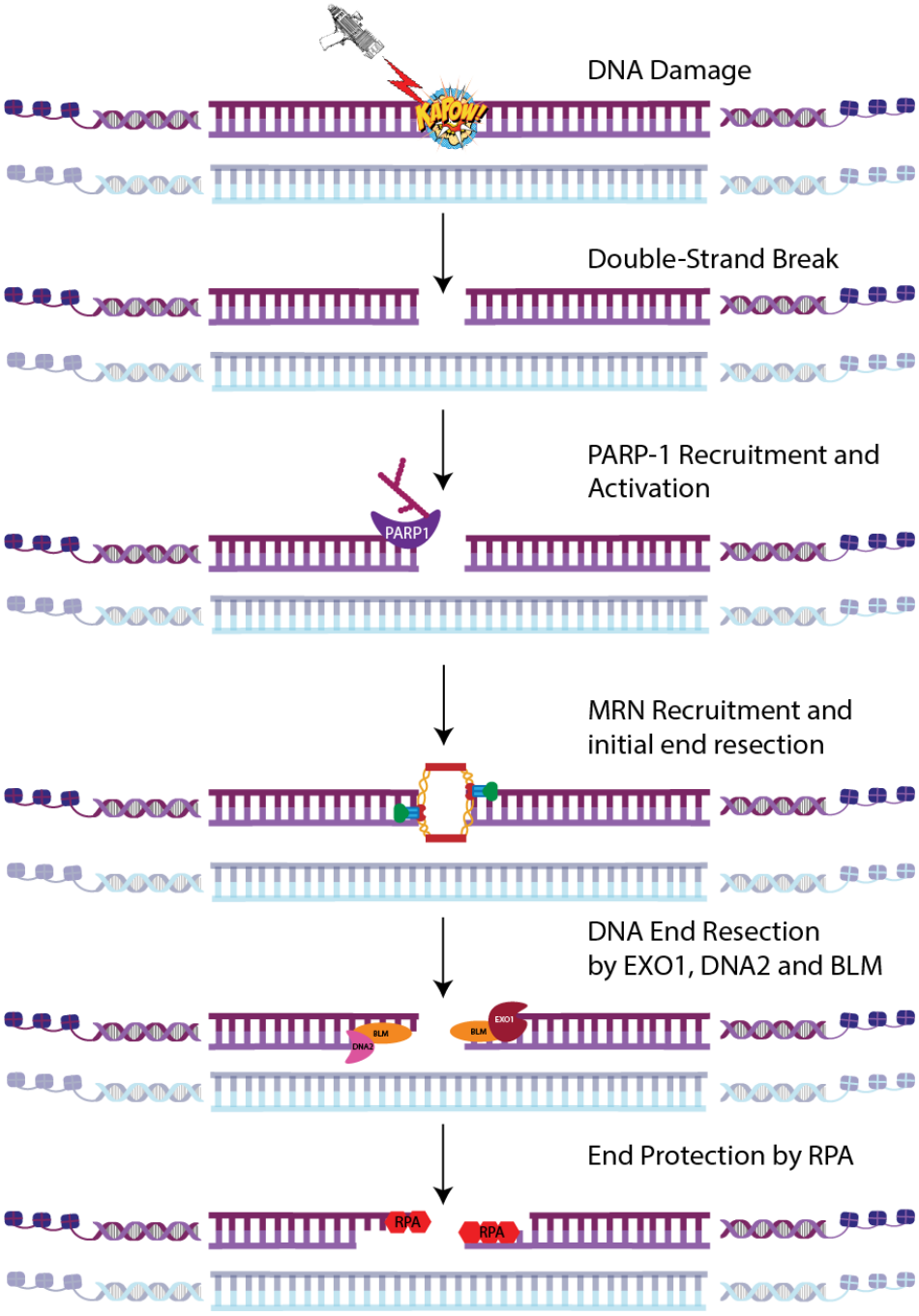

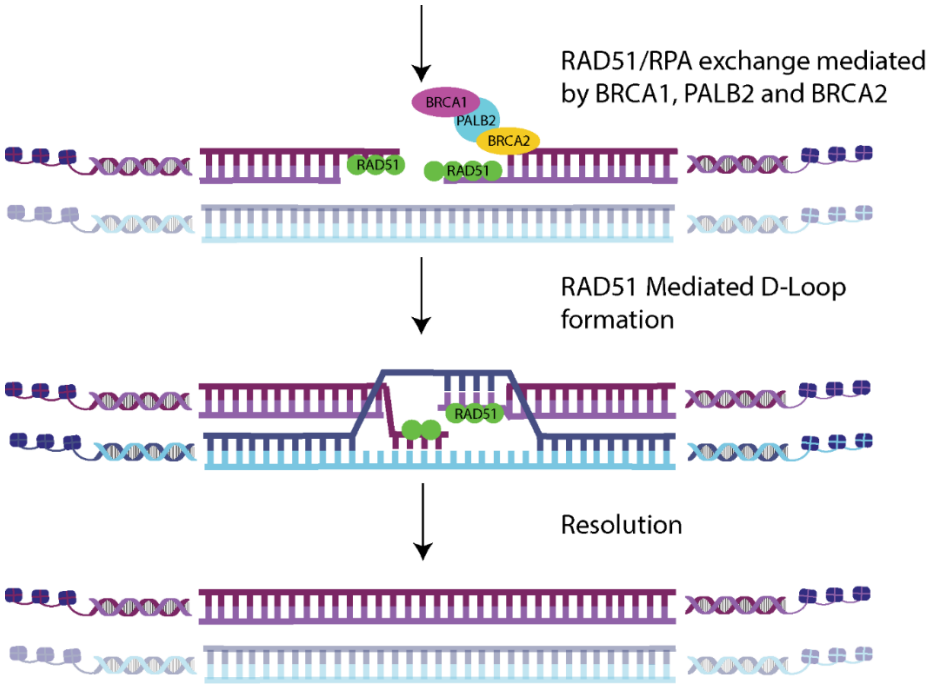

Figure 0.4: A schematic representation of the Homologous Recombination Pathway. This schematic represents a basic view of the HR repair pathway steps. PARP-1 is rapidly recruited to newly formed DSBs. Upon DNA binding, PARP-1 activates to form the PAR chain which is involved in both the signalling and modification of other repair proteins. Shortly after the MRN complex is recruited to undergo the initial 5' to 3' end resection. This is a nick mediated by the MRE11 endonuclease activity. This nick is expanded by the helicases BLM and DNA2 and the endonuclease EXO1. The resulting 3' overhang strand is encased in RPA molecules to protect it from degradation. RPA is then replaced with RAD51 with the help of BRCA1, BRCA2 and PALB2. RAD51 then mediates strand invasion of the sister chromatid, which is used as a template for repair, allowing for the faithful repair of DNA double-strand breaks.

Poly(ADP-ribose) polymerase

In the early 1960s Pierre Chambon made a ground-breaking discovery by uncovering a poly-adenine-nucleic acid structure, now commonly referred to as the PAR. The initial discovery was made while studying the synthesis of RNA by the RNA polymerases. What was found was that upon the addition of nicotinamide mononucleotide (NMN) a large increase in the uptake of ^{32}P was seen, this was initially referred to as polyA[83]. Further study quickly demonstrated that the product was not the classical

polyA as it contained the phosphate and ribose from the NMN, thus leading to the identification of the structure we now refer to as ADP-ribose. From there came the identification of both Mono(ADP-ribose) (MAR) and PAR transfer reactions[84, 85].

These polymers are the products of the members of the PARP family of proteins, which are the focus of the following section.

The PARP family of proteins

The PARP genes or PARP-like genes are conserved throughout evolution; however, they are absent in *Saccharomyces cerevisiae* and *Schizosaccharomyces pombe*. The PARP family is made up of 17 proteins who share a conserved catalytic domain containing a β-α-loop-β-α-NAD^+ binding pocket[86]. The members of this family have a multitude of functions from cell proliferation to cell death. This family is also referred as ADP-Ribosyltransferases (ARTs), as many members of the family do not have polymerase activity[86, 87]. The majority of the PARP proteins have the enzymatic ability to form the (ADP-ribose)-chains, which are associated with the family. These (ADP-ribose) chains can either be single units: MAR; or multiple units: PAR. The conserved catalytic domain is located in the C-terminal of the proteins except for PARP-4 (Figure 0.5).

In the PARP family, while having the conserved NAD^+ binding pocket, there are other domains which are commonly found. These include the WGR (tryptophan-glycine-arginine-rich), RRM (RNA recognition motif), Macro domains, BRCT (BRCA1 carboxy terminal), WWE (tryptophan and glutamate), SAM (sterile alpha motif), HD (helical subdomain) and ANK (Ankyrin) repeats. Each domain has a different function which may influences the activity of the different family members. The zinc finger domains present in some members of this family can be either $CX_2CX_{28-30}HX_2C$-type DNA binding or $CX_{7-11}CX_{3-9}CX_3$-H-type putative RNA binding domain. It is only with PARP-1 that these zinc-finger domains are involved in the DNA dependant enzymatic activation. These different domains can be known for their structure or function; the WGR domain is a tryptophan, glycine, and arginine rich motif, whereas the RRM is an RNA binding motif, and the Macro domains bind to (ADP-ribose) chains in some proteins[88-90]. The BRCT (BRCA1 C-terminus) domain promotes protein-protein interactions, and the WWE

domain is a putative *iso*-ADP-ribose-binding domain. Finally, the SAM domain is a protein or RNA interaction domain, the HD domain is involved in the stability of the CAT domain and the ANK repeats mediate protein-protein interaction. Regarding the repair of DNA damage, it is PARP-1, PARP-2 and PARP-3 which have been most studied. This thesis, however, will focus on PARP-1.

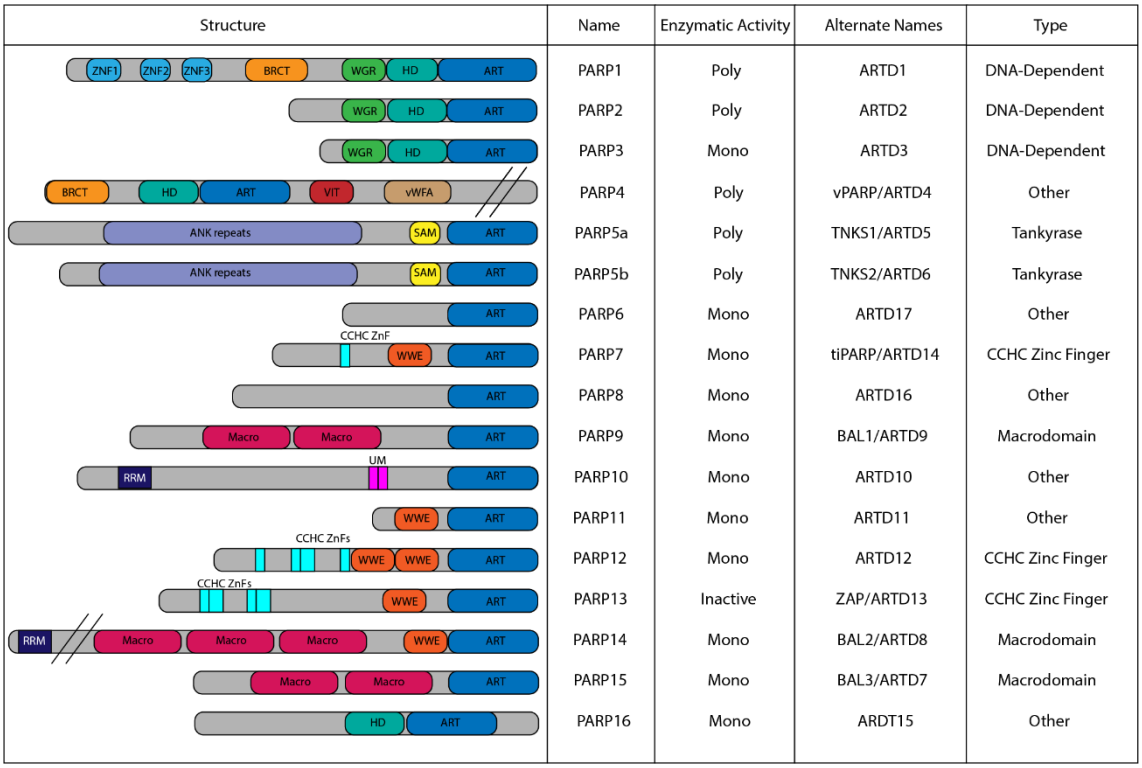

Figure 0.5: Structure and domains of the PARP family of proteins.

Schematic representation of the members of the PARP family of proteins. Enzymatic activity refers to the formation of ADP-ribose chains; Mono being a single ADP-ribose unit and Poly referring to multiple ADP-ribose units in a chain. Inactive PARP members do not synthesize ADP-ribose chains. Also provided are the alternative names used for these proteins and type of protein they are. This figure has been adapted from Daugherty M.D., et al. PLOS Genetics (2014)[91].

PARP-1, the star member of the PARP family is a 116 kDa protein made up of three zinc finger domains, a BRCT domain, a WGR domain and the characteristic PARP or ART (ADP-ribosyltransferase) catalytic motif containing an NAD^+ binding pocket, Figure 0.6 [92, 93]. The NAD^+ binding pocket is the highly conserved glutamate 988 residue in the centre of the catalytic domain on which the polymer modification is

reliant[94]. The PAR chains that are formed as a result of PARP-1 activity make up more than 80% of the nuclear PAR in the cell and are an essential element to both the signalling and the mechanism of DSB repair. This polymer chain is both DNA and NAD^+ dependent, as accessibility of the NAD^+ binding pocket is dependent on the conformational change exhibited upon binding DNA and the NAD^+ itself acts as the base material to form these chains[94].

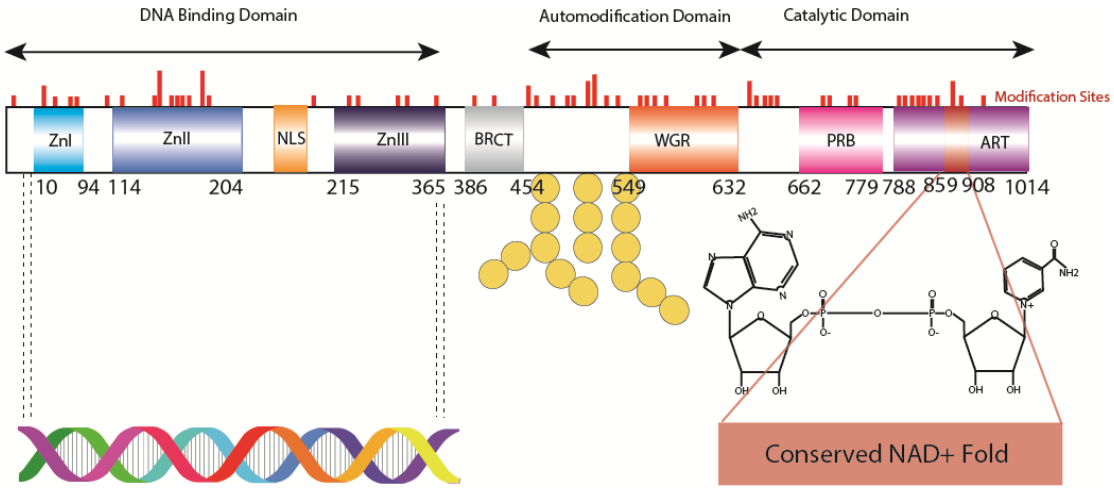

Figure 0.6: PARP-1 structure. Individual domains are identified by different coloured boxes.

The N-terminal region which contains the three zinc finger domains (blue) is the DNA binding region. Also found in the N-terminus is the NLS (light orange). The BRCT (grey) and WGR (orange) domains are in the auto modification domain, the region which is modified most heavily by the formation of PAR. The catalytic domain contains a PRB (pink) and ART (purple) domain along with the conserved NAD^+ binding pocket (red). This NAD^+ binding pocket is made accessible upon DNA binding. The red lines of the top of the structure represent the possible PAR modification sites within the protein. The figure was adapted from David K.K. et al. Frontiers in Biosciences (2009)[95] and Gagné JP. et al. DNA repair (2015)[96].

PARP-1 is activated by DNA damage

Upon DNA damage, PARP-1 is recruited and binds to the DNA. This causes a conformational change to the protein allowing for the NAD^+ binding pocket to become accessible to NAD^+. This then allows for the formation of the (ADP-ribose) chains which are important both as a signalling event and as a scaffold to other repair proteins. The

activation of PARP-1 following binding the DNA results in the local chromatin relaxation and histone displacement. This activation is dependent on the ability of the zinc finger domains binding to the DNA[87, 97]. This process is depicted in Figure 0.7.

These three zinc finger domains (ZnFI, ZnFII, ZnFIII), are located in the N-terminus of the protein. Two of these zinc fingers, ZnfI and ZnfII are homologous CCHC type ZnFs (CysCysHisCys), located within close proximity of each other. Of the three, the ZnfIII is unique[98, 99]. They recognize specific DNA-structures irrespective of the sequence. PARP-1 uses these zinc fingers to detect DNA damage sites with exposed nucleotide bases. When presented with single-stranded DNA, the ZnFII will load itself onto the 3' end via its hydrophobic platform. It will then form a dimer with ZnFI creating an opening which accommodates the undamaged nucleotide[97]. In regard to DSBs, the ZnFI recognises the terminal base pair while the ZnFIII and WGR domains contact each other around the DNA helix backbone, binding to the major and minor grooves in order to stabilize this structure[87, 100]. This results in a series of interdomain contacts that transmits the detection of the DNA damage to the catalytic domain, allowing for its activation in exposing the NAD^+ binding pocket[87, 93, 100, 101].

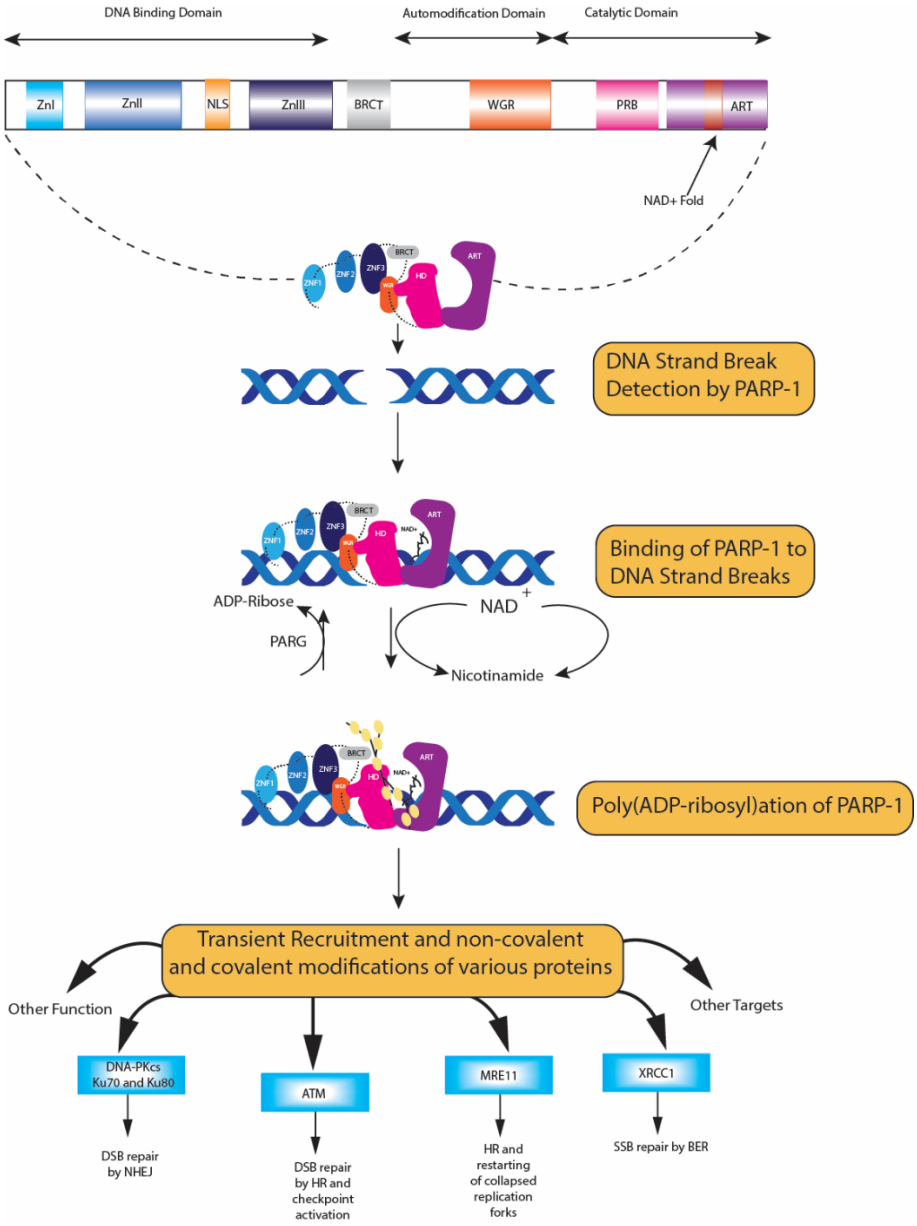

Figure 0.7: PARP-1 Activation upon DNA Binding.

Upon DNA damage, PARP-1 binds to the DNA causing a conformational change which allows for access to the NAD^+ binding pocket. This allows for the formation of PAR, as previously described. This binding and activation has been seen to be involved in the recruitment of many different proteins and their modification by PAR. A prime example shown in the above diagram is MRE11, whose recruitment time is affected by the presence or loss of PARP-1[24]. Another protein whose recruitment is affect is XRCC1, a coordinator of SSB repair by BER. The figure was adapted from Rouleau M., et al. Nature Reviews Cancer (2010)[102].

PARP-2

The second member of the PARP family that is also located in the nucleus is PARP-2, a 62 kDa protein that along with PARP-1 is capable of generating PAR. There are eleven PARP-2 transcripts generated through alternative splicing, some of which do encode for PARP-2 isoforms; however, the significance of these isoforms is unknown. The protein is comprised of an N-terminal region (NTR), a central WGR domain and the C-terminal catalytic domain[103-106]. This domain is made up of the HD and the PARP subdomains[106]. The PARP-2 NTR is natively unstructured, though it shares homology with the SAF/Acinus/PIAS(SAP) DNA binding domain of other DNA repair proteins, such as Ku70 and APE-1[86, 106, 107]. It also contains a bipartite nuclear localisation signal (NLS) and a nucleolar localisation signal (NoLS). This NTR domain has been shown to non-specifically interact with DNA[104, 108, 109]. It is required for nuclear localisation but not DNA-binding, however, deletion of the NTR lowers DNA-binding affinity[106]. RNA binding activity has been reported for the NTR also [110].

The DNA binding activity of PARP-2 is not regulated by its autoPARylation unlike PARP-1 [111]. However the recruitment of PARP-2 appears to be dependent on PARP-1 and PARylation [112]. PARP-2 binds to specific DNA structures; DNA with 5'phosphate, DNA without 5'phosphate and DNA with a 5'-nucleotide overhang that has a 5' phosphate, with a preference for SSBs over DSBs or undamaged DNA [103, 104, 113]. PARP-2 has shown high activity levels when bound to DNA with a 5'phosphorylated end [103, 104, 106]. Interestingly PARP-2 can bring two DNA ends together shielding the nick with its WGR domain *in vitro* [105]. Without DNA damage the interaction between PARP-2 and DNA is mainly facilitated by the disordered N-terminus [103-105].

Mice lacking PARP-1 or PARP-2 are viable but they are more sensitive to genotoxic agents. The double knock-out of PARP-1 and PARP-2, however, leads to early embryonic lethality in mice[114-119]. PARP-2 interacts with the BER/single-strand base excision (SSBER) factors XRCC1, DNA polymerase β and DNA ligase IIIα, indicating a role for PARP-2 in these repair pathways. This is demonstrated with PARP-2-/- MEFs that show slower repair of MNU(N-methyl-N-nitrosourea)-induced DNA single-strand breaks, which are repaired primarily through BER [120]. A reduction in the initial SSB

repair rate was seen in A549 PARP-2 depleted cells after hydrogen peroxide treatment, further indicating the importance of PARP-2 in SSB repair[121]. While the involvement of PARP-2 in SSB repair has been widely accepted, its role in DSB repair has only recently been demonstrated. PARP-2 depletion shows a decrease in HR and Alt-NHEJ efficiency and an increase in C-NHEJ efficiency, suggesting a role for PARP-2 in HR. A decrease in RAD51 mobilization post-bleomycin treatment suggests a role for PARP-2 in the promotion of DNA end resection [122].

PARylation

As previously mentioned, one of the key functions of the PARP proteins is the formation of either Mono(ADP-ribose) or Poly(ADP-ribose) chains. Mono(ADP-ribose) modifications are referred to as MARylation and Poly(ADP-ribose) modifications are referred to as PARylation. PARylation is the transfer of ADP-ribose units from NAD^+ to form long and branched chains of negatively charged PAR on specific amino acids residues, such as arginine, serine, lysine, glutamate and aspartate on PARP-1 and other acceptor proteins[101, 123, 124]. It is important to note that PARylation of target proteins changes their physio-chemical characteristic due to the highly negative charge of PAR. This can influence the resulting protein-protein or protein-DNA/RNA-interactions.

The first ADP-ribose moiety of a chain is bound by an ester bond, most commonly to a glutamate or aspartate residue, though lysine, cysteine and serine have been identified as targets as well. The next ADP-ribose unit will bind to the first via a 2'1"-O-glycosidic bond, this is repeated all along the chain, Figure 0.8. These chains can be linear, i.e., one ADP-ribose after another or they can be branched chains, whereby a secondary chain extends from the main chain like the branches of a tree. They can grow as long as 200 units, with branching opportunities every 20-50 residues[125].

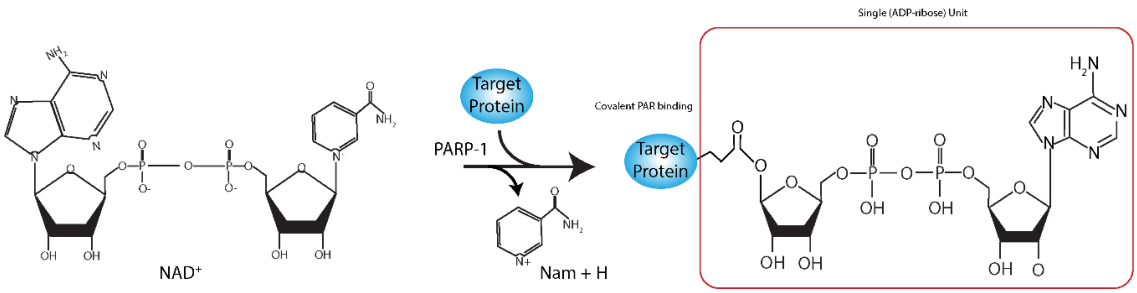

Figure 0.8: Representation of ADP-ribose and the chains it can form.

A schematic representation of the conversion of NAD^+ into an (ADP-ribose) unit covalently bound to the target protein by PARP-1. PARP-1 cleaves the glycosidic bond between the Nicotinamide and the ribose of NAD^+, then covalently binds them to the target protein. Further (ADP-ribose) units are attached at the 2'1''-O'glycosidic bond. The process of building the (ADP-ribose) chain results in the production of Nicotinamide (Nam), which can be processed to produce more NAD^+. Illustration inspired by *Liu, C., et al., Nucleic Acids Res, 2017* [126].

PARP-1 influences DNA repair, chromatin structure and transcription

It has been shown that PARP-1 has many protein interactors that are not isolated to DNA repair, but also include proteins which 1) regulate transcription, 2) methylate DNA and 3) modulate chromatin structure[127]. PARP-1 is considered a chromatin modulator due to histones being one of the major targets for PARylation. Recently the protein HPF1 (Histone PARylation Factor 1) has been determined to be essential for the function of PARP-1 in the PARylation of histones[128]. While loss of HPF1 does not alter the association of PARP-1 and undamaged histones, it does however, prevent it from PARylating histones. Furthermore, while not affecting the recruitment of PARP-1 it does increase the time PARP-1 remains at DNA lesions, resulting in DNA damage-induced PARP-1 hyper-automodification. The resulting negative charge causes the relaxation of the chromatin[129]. It has been further shown that the macro-domain containing histone macro-H2A1.1 can sense PAR being generated at the damage site through its macrodomain. This results in a compaction of the local chromatin and reduced Ku recruitment[130].

Continuing with PARP-1's non-DNA repair functions, it has been identified at the site of promoters of actively transcribed areas[131]. This localisation correlates with the binding of Polymerase II and the presence of the lysine 4 trimethylation modification of Histone 3, a marker for active gene expression. It has also been shown that PARP-1 can further modify the chromatin by PARylating KDM5B, thus preventing its binding to the chromatin and demethylating H3 lysine 4 trimethyl (H3Kme3)[127].

The readers of PARylation

Aside from covalently modifying proteins through the formation of these chains it is also possible for proteins to bind non-covalently to PAR. This is accomplished through distinct PAR-binding motifs. The most studied PAR-binding motifs are the PAR-binding zinc finger (PBZ), PAR-binding motif (PBM) and the macrodomains. The table below shows the known domains and their structure.

PAR-binding Motif	Motif Structure
PBZ	C_2H_2 Type $CX_5CX_6HX_5H$
PBM	[HKR]1 × 2 × 3 [AIQVY]4 [KR]5 [KR]6 [AILV]7 [FILPV]8
Macrodomain	Globular α/β/α sandwich β-α-β-α-α-β-β-α-β-α-β
PbR	C_2H_2 Type $CX_8CX_6HX_8H$
RING	C_3HC_4 Type $CX_2CX_{9-39}CX_{1-3}HX_{2-3}CX_2CX_{4-48}CX_2C$
WWE	β2-β1-β6-β5-β4-β3 and/or β2-β1-β5-β3-β4
PIN-domain	Compact structure β1-α1-β2-α2-β3-α3-β4-α4-β5
FHA domain	Two β sheets with Greek key topology β2-β1-β11-β10-β7-β8 and β4-β3-β5-β6-β9
BRCT	β-α-β-β-α-β-α
OB-fold	Antiparallel β-barrel β1-β2-β3-β5-β4-β1
KR-rich domains, SR repeats, RG/RGG repeats	KR-, SR- or RG/RGG-rich repeats
RRM	[RK]1G2 [FY]3 [GA]4 [FY]5V6 × 7 [FY]8–Xn–[LI]1 [FY]2 [VI]3 × 4 [NG]5L6 β-α-β-β-α-β

Table 0.1: List of PAR-binding motifs.

Above is a table listing the different known PAR-binding domains and their structural motif. Taken from *Kamaletdinova T. et al 2019.*

I will briefly describe some of the PAR binding motifs. The PBM motif binds to the structure between the second phosphate of the first ADP-ribose residue and the first phosphate of the second residue. Macrodomains completely bind the terminal ADP-ribose of the PAR chain. The OB-fold motif is a single-strand DNA or RNA binding motif that binds to PAR during DNA damage repair. One well known DNA repair protein containing an OB-fold is BRCA2, Figure 0.9.

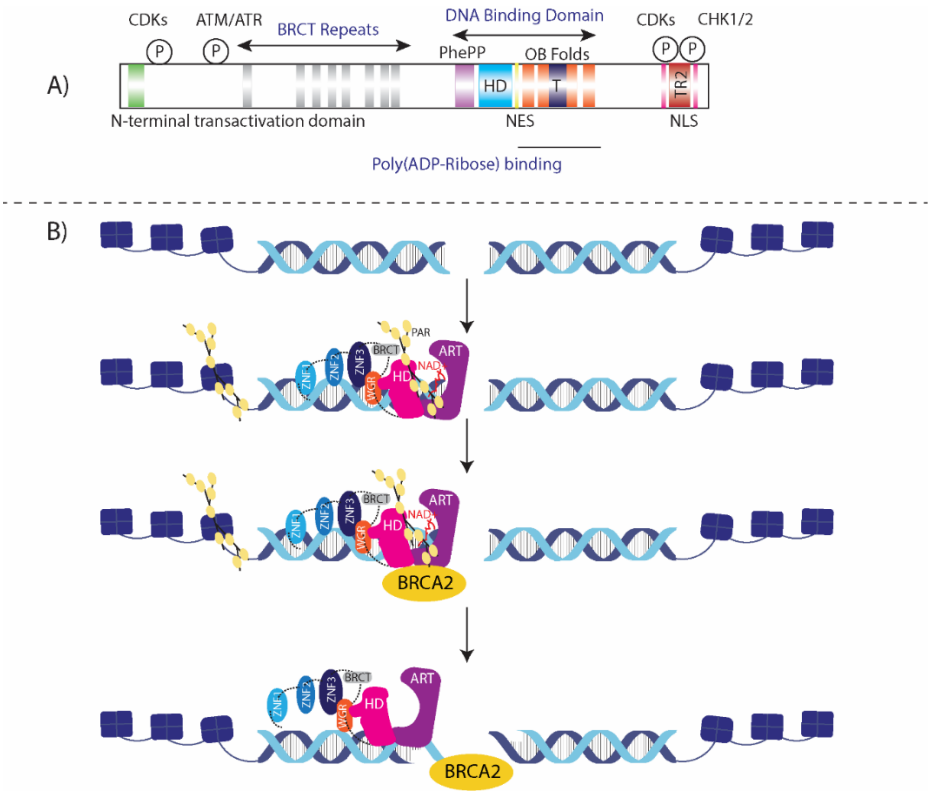

Figure 0.9: OB-Folds containing BRCA2 protein.

A) Schematic of the BRCA2 protein. BRCA2. There is an N-terminal transactivation domain where PALB2 binding occurs (green). Eight BRCT repeats (grey) that are involved in protein-protein interactions, primarily with RAD51 though interaction has also been seen with APRIN and Polη. Finally, a phenylalanine-proline-proline (PhePP) motif domain involved in the interaction with DMC1. The DNA-binding domain is made up of a helical domain (HD) (light blue), a Tower domain (T) (dark blue) and three OB-Folds (orange). The OB-folds promote the association with DSS1, and BRCA2 binding to single-stranded DNA. The C-terminal of BRCA2 is made up of a TR2 (red) domain which interacts with RAD51 nucleofilaments, and two distinct nuclear localization signals (NLSs) (pink). **B)** After a DSB is formed PARP-1 is recruited and activated, PARylating the nearby histone and itself. Subsequently BRCA2 is recruited and interacts

with PAR through its OB-folds. Once PAR is degraded, and PARP-1 disassociates following resection, BRCA2 binds to the single-stranded DNA again through its OB-fold.

Many PAR readers play a role in the DNA damage response. As such the function of PAR-binding readers can be subdivided into several categories: (1) fast and efficient recruitment to the damage site, (2) DNA damage signal transduction, (3) apoptosis initiation and (4) protein degradation. An example of the role of these PAR-binding motifs is the recruitment of BRCA2, which as mentioned above contains three OB-folds[132]. It has been shown that the recruitment of BRCA2 is delayed in the presence of the PARP inhibitor Olaparib, suggesting that PAR plays a role in either the signalling for BRCA2 or is directly involved in the recruitment. EXO1 is another repair protein which binds the PAR chain. This time due to the presence of the PIN domain, which is an evolutionarily conserved single-stranded DNA and RNA recognition domain[133].

The PBZ domain is another PAR binding motif, centring on zinc fingers. Two examples of DDR proteins which contain this domain are APLF (Aprataxin and PNKP Like Factor) and CHFR (Checkpoint with Forkhead and Ring Finger). PAR-binding proteins also play a role in the regulation of cell cycle progression, genome maintenance and transcriptional regulation. PARP-1 is activated at stalled replication forks, forming PAR chains and causing S-phase checkpoint activation. CHK1, the S-phase checkpoint kinase has been shown to bind directly to PAR through its PbR motif independently of ATR and its activity[134]. More information on zinc finger proteins in DNA repair and PAR binding is discussed later in this chapter (section 1.4). Furthermore, free PAR chains have the ability to bind non-covalently to other proteins. In fact, after non-covalent interaction between PAR and 53BP1, the ability for 53BP1 to bind to DNA is reduced[135]. Further demonstrating the essential role of both PARP-1 and PARylation in DNA damage repair.

Erasing PARylation by PAR-degrading enzymes

PAR concentrations within the cell are carefully maintained, meaning that once the desired response is achieved the PAR chain is quickly degraded and the ADP-ribose can be recycled. This is accomplished by PAR erasers, primarily Poly(ADP-ribose)

glycohydrolase (PARG), however it is not the only protein which is capable of degrading the PAR chains[31].

PARG, the other erasers and the mechanisms responsible for degrading PAR are discussed in depth in Chapter 1.

Inhibition of PARylation as a therapeutic strategy for cancer treatment

PARP inhibition has become a standard treatment in cancer therapy for a variety of different types of cancer, such as prostate cancer and particularly in homologous recombination-deficient cancers such as breast/ovarian cancer[102, 136]. This functions under the principle of synthetic lethality. This occurs when synthetic compounds or genetic ablation are used to block a secondary pathway that would normally act as a backup DNA repair pathway. In regards to homologous recombination-deficient cancers, one repair pathway has already been knocked-out through mutation (for example, the loss of BRCA1 and thus the loss of HR) and the secondary backup pathway is then knocked-out through pharmaceutical means, for example PARP inhibition to inhibit repair by c-NHEJ dysregulation[137, 138]. This is one of the proposed mechanisms of action for PARP inhibition. Without the addition of the PARP inhibitor in this case the cell would survive and repair its DNA using NHEJ. However, by adding the PARP inhibitor the cell can no longer repair the DNA and will eventually succumb to death. This is an effective strategy as normal cells in the system which are not homologous deficient will survive, as they can still repair using HR, as is illustrated in Figure 0.10.

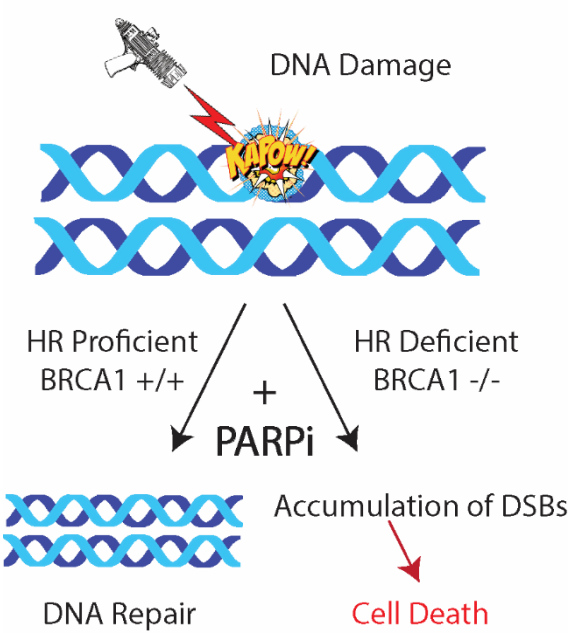

Figure 0.10: Schematic representation of synthetic lethality through PARP inhibition.

Following DNA damage cells with a deficit in homologous recombination will be dependent on DNA repair from other pathways, such as NHEJ or BER. The addition of PARP inhibitors halts the repair through these other pathways leading to an accumulation of DSBs and eventual cell death. Those cells that do not have a homologous repair deficit will survive as they will be able to continue repairing through the HR pathway.

Currently there are two main methods of inhibiting PARP proteins, both of which target PARP-1 and PARP-2 primarily. The first method is by providing nicotinamide analogues which compete with NAD^+ for the binding pocket and ART domain thus preventing the formation of PAR chains. In this case the PARP inhibitors form hydrogen bonds with the Gly863, Ser904 and Glu988; and hydrophobic stacking interactions with the two Tyr residues (896 and 907) within the NAD^+ binding pocket, docking the inhibitor into the catalytic site (Figure 0.11)[139]. The second method is PARP trapping, this is where in addition to the catalytic inhibition the molecule binds PARP to the DNA, the binding of the inhibitor causes an allosteric change that enhances the DNA binding affinity of PARP[140]. As long as the inhibitor is bound to the active site it is not possible to use NAD^+ to auto-PARylate and results in delayed dissociated from the DNA[141]. Certain PARPi destabilize the HD subdomain which in turn increases PARP-1's affinity

to DNA and increases PARP-1 retention at DNA breaks[142]. The cytotoxicity of these PARP inhibitors is linked to the strength of its trapping ability.

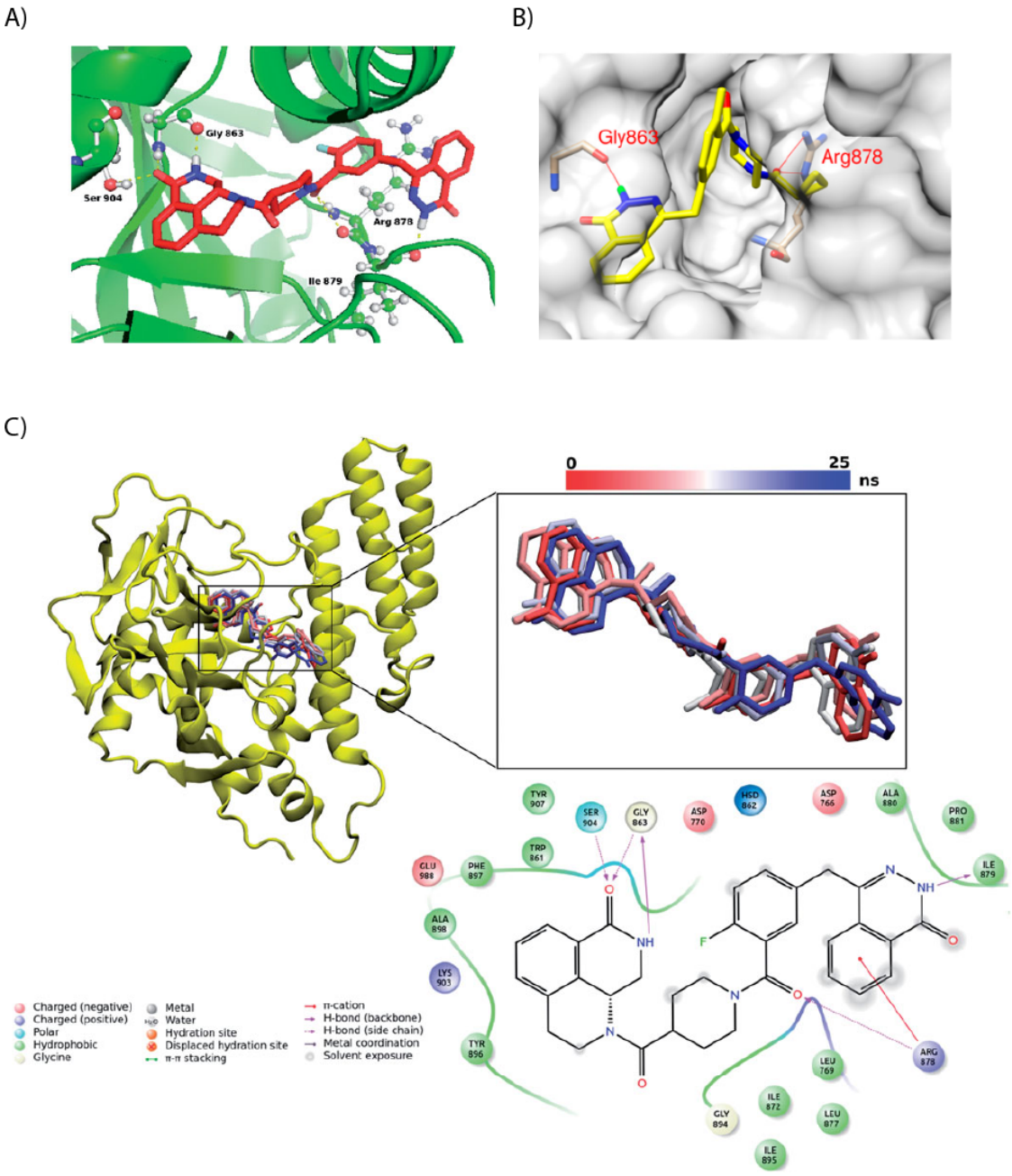

Figure 0.11 PARP inhibitor binding

A) The equilibrated inhibitor position and its interactions with active site residues[143]. B) Binding modes of Olaparib towards PARP-1 at the binding site[144]. C) Mainly observed conformations of inhibitors in the binding pocket throughout 25ns MD simulations. 2D ligand interaction diagram for the representative complex structure has also been shown in the figure[143]. Images taken from Li *et al* International Journal of

Molecular Science 2016 and Salmas *et al* Journal of Enzyme inhibition and Medicinal Chemistry 2017

Currently there are four FDA approved PARP inhibitors; olaparib, rucaparib, niraparib and talazoparib. Veliparib is currently still in trials though it is showing promising results. Aside from the trapping ability of some PARP inhibitors, the specificity of the inhibitor for PARP-1/PARP-2 is also a defining characteristic. talazoparib is the most efficient PARP trapper and veliparib is the least[145]. Incidentally talazoparib is also the largest of the inhibitors, possessing a rigid structure whereas veliparib is the smallest. While size may play a role in its trapping ability the mechanism of PARP trapping is not well understood[146]. Veliparib has shown to have the highest level of specificity to PARP-1/PARP-2. Rucaparib is the least specific, binding to PARP-1, PARP-2, PARP-3, PARP-4, PARP-5a, PARP-5b, PARP-10, PARP-15 and PARP-16[147, 148]. Furthermore, both rucaparib and niraparib have also demonstrated lower efficiency binding to hexose-6-phosphate dehydrogenase (H6PD) and deoxycytidine kinase (DCK) respectively[149].

PARP inhibitors are often used in combination with DNA damaging agents such as radiotherapy, chemotherapy, and DNA-alkylating agents. These enhance the effectiveness of the inhibitors by increasing the level of unrepaired DNA breaks[150, 151]. While an extremely useful therapy, PARP inhibitor resistance is a genuine issue in cancer treatment and there are a few posited mechanisms for resistance to these compounds[152]. One such mechanism is where the drugs are pumped out of the cell directly. In this case the compounds are no longer readily available to compete with NAD^+ for the binding pocket and thus do not prevent (ADP-ribose) formation. This is accomplished through the overexpression of ABC transporters such as the P-glycoprotein (PgP) efflux pump, which enhance the extracellular trafficking of many compounds[153, 154]. Another mechanism is through the reactivation of BRCA1, BRCA2, RAD51C, RAD51D or PALB2 functions through secondary mutations. Thus, restoring repair by homologous recombination[14, 155-164]. In the case of BRCA1, hypomorphic variants have been seen to be expressed[13, 165]. Inactivation of different NHEJ-promoting factors which inhibit resection can also lead to a partial restoration of HR in BRCA-1 deficient cells. These factors include 53BP1, RIF1, PTIP, Artemis, the Shieldin complex (SHLD1-3 and REV7) and the CTC1-STN1-TEN1 (CST) complex[49, 58, 166-175].

Promotion of end resection and restoration of the HR pathway can also be accomplished through inactivation of DYNLL1 and the HELB helicase independently of 53BP1 also resulting in PARPi resistance[176-178]. In the context of inactivation of the NHEJ-promoting factors restoration the HR pathway becomes dependent on BRCA2[179].

PARP inhibition has presented itself as an exceptional tool in the fight against cancer, however a better understanding of the role of PARP-1 in DNA repair is needed to maximize the efficiency of these exceptional drugs. Our latest contribution to the trove of PARP-1 knowledge can be found in chapter 2.

Mass spectrometry-based proteomics as an approach to analyse the PAR-interactome

The catalytic activity of PARP-1 resulting in PARylation is an initiating event in DNA damage sensing and signalling. Crucial elements of the DDR are recruited to the sites of damage in a PAR-dependent manner. Due to PAR's function as a scaffold facilitating repair, it is of great interest to identify PAR-interacting proteins. Mass spectrometry (MS)-based proteomics is an ever-advancing technology that allows for the identification of protein interactions. This technically challenging approach has been used exhaustively in our laboratory and others to identify the PARylome (PAR-binding interactome) in the response to DNA damage.

A very brief description of the principles of peptide sequencing which is important for the interpretation of proteomics data as presented in my thesis is given in the following section. This is the basis for chapter 4.

The principle of peptide sequencing

Mass spectrometry (MS) is an analytical tool which measures the mass-to-charge ratio of one or more molecules in a sample in order to detect, identify and quantify molecules. It surrounds biomolecules which are ionized with or without fragmentations and, following their specific trajectories in a vacuum system, measures their mass and abundance. Biological samples must be initially processed before they can be submitted to the spectrometer for analysis, this step can have a great impact on the returned results

through the quality of the sample extraction and preparation. There is no standard protocol for preparing protein samples due to the complexity of the proteome and the individuality of protein structure and function. Aside from different preparations required for different proteins there is also the sample itself which may require different preparations.

While there are many different protocols there are common steps among them. First the sample must be lysed to extract the cellular contents, following this the sample goes through specific depletion and enrichment processes, for example fractionation and immunoprecipitation. Next the sample is often dialysed and desalted to remove ions such as sodium and potassium which can interfere in the MS measurement of the charged ions. The sample will then be denatured through digestion. This can be done through two different methods: in-solution or in-gel digestion. In-solution digestion is useful when the sample size is small, in-gel digestion can result in peptide loss and is not ideal for limited samples. With in-solution digestion, proteins are denatured with strong chaotropic agents, for example urea or thiourea. This denaturing is usually followed by or combined with disulphide reduction with a reducing agent such as dithiothreitol (DTT). After digestion, enrichment is often used when studying post-translational modifications, as they are in low abundance. Following this the salts and buffers are removed through the use of either graphite or C-18 tips or columns. Detergents can be removed with affinity columns or detergent-precipitating agents. The now purified peptides are ready for MS analysis at this point.

The PAR interactome as revealed by MS

In order to further understand the role and importance of ADP-ribosylation, extensive work has taken place in the MS field to study this modification. Due to the heterogeneity of PARylation, its study through MS has proven to be complicated[180]. Currently two main strategies are employed to analyse PARylation by MS. The first method is based on the depolymerization and degradation of PAR to mono-ADP-ribose. This is accomplished through *in vitro* treatment with PARG resulting in proteins with a single ADP-ribose moiety attached[181]. Alternatively, it is possible to use snake venom phosphodiesterase or NUDIX to hydrolyse PAR into a simpler phospho-ribose[182, 183]. The second strategy makes use of chemical hydrolysis to convert mono- and poly-ADP-ribose into simple and unique spectral signatures. This is done primarily through the use

of hydroxylamine, which converts ADP-ribose modifications to hydroxamic acid adducts[184-186]. However, it has recently been demonstrated that the use of hydrofluoric acid is also possible. This is accomplished through the cleavage of the phosphodiester bonds resulting in a unique 132 Da signature[187].

A large-scale proteomics approach was conducted in our laboratory in 2008 which confirmed previously identified PAR-binding proteins and uncovered an expansive new list of PAR-interacting proteins that are involved in the repair mechanisms. This proteome was identified following extensive alkylation-induced DNA damage and was comprised of proteins with roles in both DNA damage and chromatin regulation[188]. One notable member of this cohort was the RNA-binding protein NONO, which was the topic of study of a previous graduate from the laboratory Dr Jana Krietsch[189].

In 2012, this strategy was refined to focus on the dynamic interaction and protein assembly in response to alkylation-induced DNA damage. In this study the use of antibody-mediated and substrate trapping strategies provided a clearer overall picture of the PAR interactome[190]. This study used three complimentary methods to obtain the widest view of the PAR interactome possible. 1) GeLC-MS/MS which is a combination of 1DSDS-PAGE (one-dimensional sodium dodecyl sulphate-polyacrylamide gel electrophoresis) followed by RP LC-MS/MS (Reverse Phase LC-MS/MS). RP LC-MS/MS is where proteins are separated by molecular weight through electrophoresis, followed by an in-gel digestion[191]. The peptide extracts are then dried and processed for reversed-phased nanoscale capillary LC-MS and analysed by electrospray MS. 2) High precision quantitative proteomics through iTRAQ[192]. This involved the use of isobaric tagging of immunoprecipitated proteins and 3) SILAC which is the incorporation of stable isotopically labelled amino acids during cell culture[193].

These two studies are just a couple of examples of the valuable contributions our laboratory has provided to solving the puzzle of the PAR interactome as a response to DNA damage. A driving force behind the study of the PAR interactome has been the development of PARPi as a cancer treatment. This is to further understand this incredible tool and also to help identify biomarkers for favourable outcomes following PARPi or new targets which can be inhibited in combination or as an alternative to PARPi. One limiting factor of the studies which have been previously performed by our laboratory is

that they use primarily MNNG, an alkylating agent, as opposed to IR which induces both single- and double-strand breaks. Furthermore, they were done in asynchronous cells as opposed to synchronised cells which would allow for the targeting for specific repair pathways. This is limiting as PARPi is often used in combination with radiation or chemotherapy and is primarily used in HR deficient tumour environments.

Considering this we have since conducted a proteomic approach to identify the protein-dynamics of the whole nuclear proteome of PAR interactions following irradiation induced DNA damage during the replication phase of the cell cycle. This is described further in Chapter 4 and led to our interest in proteins containing zinc-finger domains. The literature on this family of proteins is explored below.

Zinc Finger proteins and their role in DNA repair

According to the ADPriboDB 2.0, hundreds of zinc finger (ZnF) proteins have been identified in different ADP(ribose) targeting MS screens, though the functions of these is rarely known[194, 195]. Zinc finger domain-containing proteins encode for almost 5% of all human genes and are the largest class of DNA-binding proteins[196]. ZnF domains are small peptide domains with a secondary structure comprised of cysteine and histidine residues which coordinate zinc binding. Aside from DNA binding, recent work has shown that zinc finger motifs have the ability to interact with RNA, proteins and lipids[197-202]. ZnFs have been seen to mediate protein-protein interaction and even bind to other modified proteins including post-translation modification such as SUMO, ubiquitin, methylated histones and PAR[201-203].

These zinc finger containing proteins can be subdivided into eight different classes based on the motifs present. These include the Cys2His2 (C2H2) like, Gag knuckle, Treble clef, Zinc ribbon, Zn2/Cys6, TAZ2 domain like, Zinc binding loops and Metallothionein (Figure 0.12 A) [204]. These different motifs result in different biological functions for these proteins. Several of these ZnF domains have been found in DNA repair proteins and serve roles for both DNA binding and protein-protein interactions (Table 0.2). Furthermore, some of the ZnF domains are also PAR binding domains, a prime example of this is in the protein APLF which contains the two PBZ zinc-finger domains, a domain also recognized by PAR. Interestingly in the case of APLF

the two domains are auto-MARylated by PARP-3 at sites of damage. APLF also contains a Ku-binding-motif (KBM) which is needed for its recruitment to damage sites[205]. Mutations in the PBZ and KBM domains of APLF abolishes its recruitment and impairs XRCC4 loading leading to compromised efficiency and accuracy of NHEJ[59-61, 206]. Thus, corroborating the potential of ZnF proteins in DNA repair.

Domain Name	Number of Genes	Genes Implicated in Genome Stability	Binding specificities	Examples	References
3CxxC	7	0			
A20	7	1	Ubiquitin	A20/TNFAIP3	[207]
AD-type	1	0			
ADD	4	1	DNA, modified histones	ATRX	[208, 209]
AN-1	8	0	DNA, RNA, Protein, Lipid		
B-Box	75	5	DNA	PML, TRIM28 (KAP1)	[210-212]
BED	6	0	DNA		
BTB/POZ	139	6	DNA, Protein	ZBTB7A, YY1, BACH1	[213-217]
C1_4	1	0			
C2C2	6	1	DNA	TCEA	[218]
C2H2	759	13	DNA, RNA, Protein, Lipid, Methylated DNA	ZBTB24, ZNF281, PHF11, ZNF830, APTX, RNF138, ZATT	[217, 219-223]
C2HC	6	3	DNA	RNF138, TOP3A[224]	[50]
C2CH	13	0	DNA		
C3H1	59	2	RNA	ZC3H11A, RNF113A	[218]
C3HC	2	0			
C4	56	2	DNA	ESR2, NR1H4	[218]
C5HC2	24	3	Modified histones	KDM4D, KDM2A, KDM5A	[225-227]
C2HC5	1	0			
CXXC	12	2	DNA	KDM2A	[226, 228]
CCHC	38	0	DNA, RNA		
CCHHC	7	0	DNA		
CHHC	4	0	RNA		
CTCHY	1	1		PIRH2	[229]
CW	7	1	Modified histones	MORC2	[230]
DBF	3	0	DNA, Protein		
DNA-Directed DNA Polymerase, Family B, Alpha	1	1		POLA1	[231]
ePHD	23	1	Modified histones	PHF11	[221]

FCS	5	2	RNA	L3MBTL2	[232]
FYVE	32	0	Lipid, methylated DNA	ZFYVE26(SPG15)	[233]
FLYWCH	1	0			
GATA	15	3	DNA	MTA2	[218]
HIT	6	0	Protein, DNA	INO80B (ZNHIT4)	[234]
KRAB	362	1	DNA, Ubiquitin	ZNF829	[218]
LIM	71	0	Protein	CRIP1	[235]
MATRIN	8	1	RNA	ZMAT1	[218]
MIZ (SP-RING)	7	3	SUMO	PIAS1 and PIAS4	[236, 237]
MYM	6	1	SUMO	ZMYM3	[238]
MYND	21	2	Protein	ZMYND8, SMYD3	[239, 240]
PARP	2	2	DNA	PARP1, LIG3	[67, 241]
PBZ	2	2	Poly(ADP)ribose	APLF, CHFR	[59, 205, 242]
PHD	71	27	Modified histones	PHF6, ACF1, KDM2A, KDM5A, TRIM28, BAZ1A	[211, 226, 227, 243-245]
RAD18 (UBZ4)	8	3	Ubiquitin	RAD18, SPRTN, POLK, SNM1A	[246-249]
RBZ (RANBP2)	23	4	Ubiquitin	RYBP, NEIL3, ZRANB3	[250-252]
RING	282	28	Protein, Ubiquitin	RNF8, RNF126, BARD1, RNF138, FRUCC, RNF168, TRIM28	[33-36, 50, 54, 55, 211, 253-257]
Sec23/Sec24 ZNF	6	0			
SCA7	6	0	Protein		
SWIM	9	1	DNA, Protein	ZSWIM7	[258] [259]
TAZ	2	2	Protein, DNA	CBP/p300	[260]
TFIIB	3	0	DNA		
TFIIS	6	1	DNA, RNA, Protein	TCEA1	[218]
TRAF	23	0	Ubiquitin, Protein	TRAF6	[261]
UBP	14	4	Ubiquitin	USP44, USP51, USP3, USP16	[222, 262-265]
ZBR	2	0	Protein		
ZZ	18	3	Protein	CBP/p300, HERC2	[260, 266, 267]

Table 0.2 Overview of Zinc finger domains, with a focus on DSB repair.

List of ZnF domains and their known binding affinity and involvement in DDR. Adapted from Singh J.K, Elsevier 2020 and Vilas C.K, Trends in Genetics 2018[268, 269].

The C2H2 family makes up the largest faction of Zinc finger proteins and is often referred as the “classical zinc finger protein”. The two cysteine and histidine residues fold into a finger-like structure of a double-stranded antiparallel β-sheet and an α-helix after

interaction with zinc ions[203, 270]. This motif is comprised of an Cx2CX3FX5LX2HC3H epitope. It has been seen that two to three successive C2H2 motifs are optimal for DNA binding. Furthermore GC-rich or GT-rich sequence act as C2H2 cis-regulatory elements [203, 270]. The C2H2 type ZnFs can be further divided into four classes; single-fingered, triple-fingered, separated-paired-fingered, and multiple adjacent fingered (Figure 0.12 B). These types may help to identify the potential function of a ZnF containing protein.

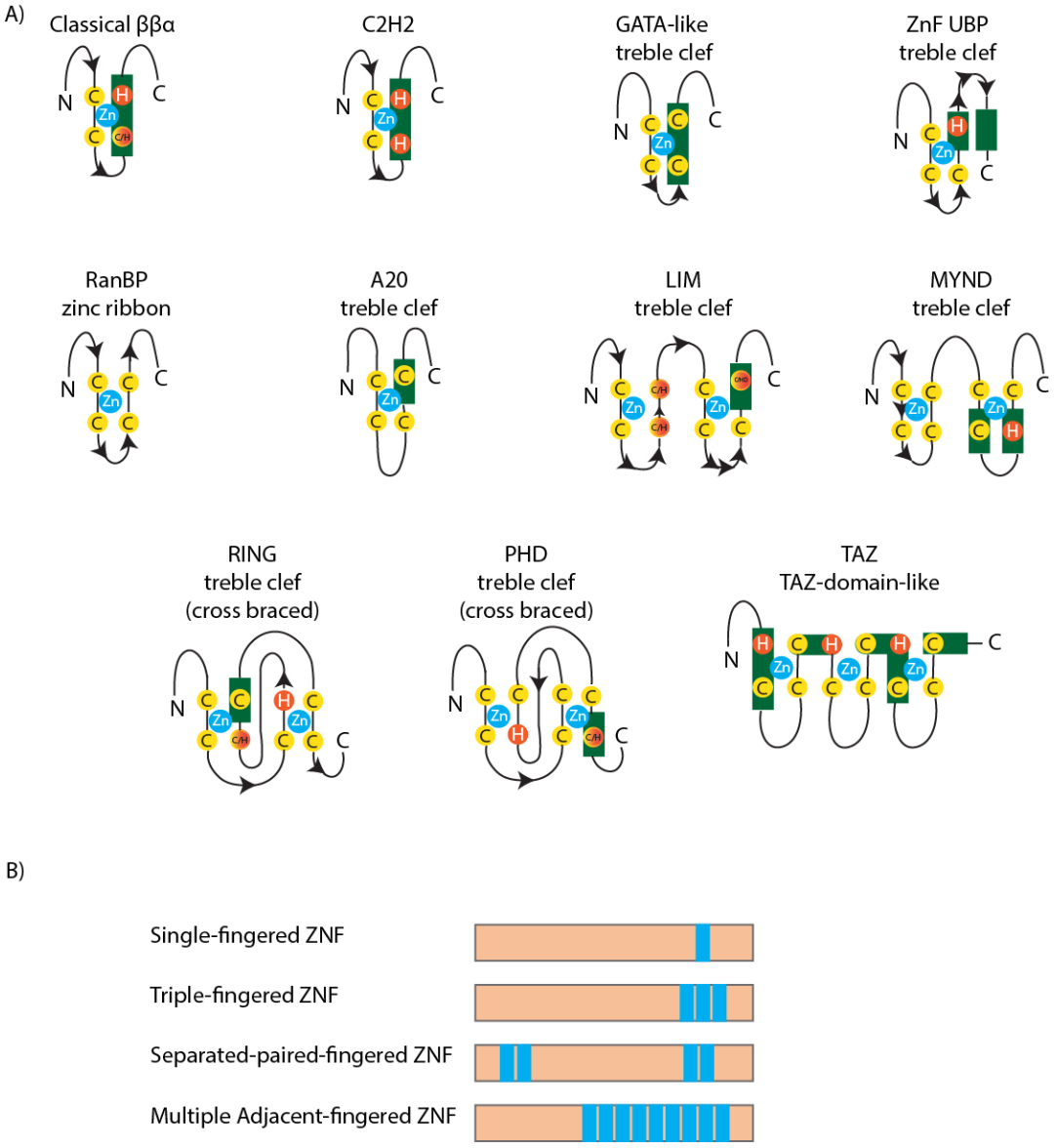

Figure 0.12 Zinc finger motifs

A) Schematic representation the topology and structures of ZnF domains. B) C2H2 zinc finger motif types. Adapted from Gamsjaeger R, Liew C.K. *et al* 2007 and Mackeh R, *et al* 2018 [271, 272]

In addition to the successive C2H2 motifs, these ZnF also contain functional domains primarily located in the N-terminal. These include BTB/POZ (Broad-Complex, Tramtrack and Bric-a-brac)/(poxvirus and zinc finger), the Krüppel-associated box (KRAB) and SCAN (SRE-ZBP, CTfin51, AW-1 and Number 18 cDNA) domain, which may play a role in the subcellular localisation of the ZnFs[273, 274]. However, approximately sixty-seven percent of human C2H2 ZnFs have only ZnF motifs and no secondary domain and are thus referred to as poly-ZNFs[275].

As a result of the diversity seen within the ZnF family it is understandable that they carry out many different functions with different partners, even at times eliciting opposing actions depending on the partner. For example, ZEB1 which is a transcription repressor becomes a co-activator of transcription when it interacts with YAP and frequently leads to aggressive cancer phenotypes[276]. In the case of the C2H2 ZnF proteins, they make up the largest class of putative transcription factors[275]. However, it is important to remember that many of the more than 700 proteins containing this motif have not been studied in depth and so it is not possible to claim that all C2H2 ZnFs are transcription factors.

Interestingly, a large-scale DNA damage recruitment screen identified transcriptions factors including ZnFs as a large class of DNA damage response factors. This screen showed that the recruitment of these proteins was dependant on PARP activity. When treated with a PARP inhibitor the recruitment was lost, providing a link between PARP activity in the response to DNA damage and ZnF proteins[218]. It is possible of course that the recruitment of these proteins is simply a result of the decompaction of the chromatin to allow for repair rather than through interaction with PARP-1 and DNA repair. However, it is just as possible that these proteins are previously unknown DNA repair factors or that they locate to the sites to regulate chromatin and transcription in order to facilitate DNA damage repair.

Further evidence supporting the importance of ZnFs in DNA repair can be found in the form of ZBTB24 and ZNF281, two ZnF proteins containing C2H2 structures. Both of these proteins have been implicated in NHEJ repair. Additionally, domain-mapping revealed in the case of ZBTB24 that the C2H2 domain has PAR-binding affinity and mediates its interaction with PAR chains, which is important for ZBTB24 recruitment to

DNA breaks. The C2H2 domain of ZBTB24 protects the PAR-chains and is essential for the LIG4-XRCC4 complex assembly[219]. Similarly, it's the C2H2 domain of ZNF281 that is required for its recruitment to damage in a PARP-1 dependent manner[218, 220]. It has not been determined whether the recruitment is dependent on the C2H2 binding to the PARP-1 generated PAR chains or the exposed DNA. Other proteins involved in NHEJ which contain ZnF domains are RNF8 and RNF126, which are involved in the proteasomal degradation of Ku80 and the ubiquitination of Ku80 to trigger its release from DNA break sites respectively[54, 55, 272]. Both RNF8 and RNF126 promote cNHEJ through the regulation of Ku70/Ku80 release, though it is not clear if they work cooperatively or redundantly of each other.

PARP-1 itself is a ZnF domain protein which is involved in both NHEJ and HR[93, 98]. KDM2A another example of a ZnF protein in HR, interacts and is phosphorylated by ATM through its PHD domain. This phosphorylation reduces KDM2A's binding to damaged chromatin and subsequently enhances the H3K36me2 levels at DSB sites. This H3K36me2 acts as a platform for the recruitment of MRE11 through its binding partner NBS1 which binds to the histone mark through its BRCT domain, thus facilitating HR by encouraging MRE11-dependent DNA end resection[226]. Moreover, proteomic approaches have identified a CXXC-dependent KDM2A-53BP1 interaction, which is required for the KDM2A-mediated ubiquitination and recruitment of 53BP1[228]. Another C2H2 ZnF; CTCF has been identified again through proteomic approaches as a DNA damage dependant binding-partner for MRE11 and CtIP. It was found to facilitate the recruitment of CtIP[277]. It has also been observed to interact with and recruit RAD51 and BRCA2 to the sites of damage[278, 279]. This data suggests a strong role for ZnF proteins in all facets of repair. Additionally, there has been clear links between ZnF proteins/PAR and DNA repair, though a study exclusively on ZnF containing PAR binders has not been attempted.

The role of zinc finger proteins in DNA repair is a newly emerging field of study, one which will be explored further in chapter 4 of my thesis.

Objectives

As described above, PARP-1 recruitment and its catalytic activation are one of the first steps in the DSB DNA damage response. The formation of PAR as a result of DNA damage is essential for the recruitment of other important DNA damage repair proteins. PAR is also important in modification of proteins for their proper function in DNA repair. The identified PARylome through mass spectrometry by our laboratory has previously identified DNA repair factors. Since then, however, mass spectrometry techniques have advanced tremendously in the study of PAR and PAR-binding proteins. As such new candidates have been identified, whether they are directly modified by PAR or indirectly interact with PAR is in question. Furthermore, whether these proteins truly play a role in the DNA damage response and if so, what that role is has not yet been defined. And while PARP-1 has been extensively studied, much of the specifics of its function are as yet unknown. Particularly the exact mechanism by which PARPi and irradiation induced DNA damage results in cell death is still in question. As such the focus of my thesis encompasses the following questions:

- According to the literature, how is PAR erased and regulated? (**Chapter 1**)

- What is the role of PARP-1 in the key step of DNA resection in Homologous Recombination repair following irradiation? (**Chapter 2**)

- Can we improve upon a method to explore the effects of resection by selecting for the cell cycle *in cellulo*? (**Chapter 3**)

- Is the PARylome a viable source for the identification of proteins involved in Homologous Recombination repair of double-strand breaks? (**Chapter 4**)

- Articles in the **Annex**:
    - A collaboration with Dr. Suryasree Subramania from the lab of Dr. Marc-Étienne Huot entitled “SAM68 interaction with U1A modulates U1 snRNP recruitment and regulates *mTor* pre-mRNA splicing”. Suryasree Subramania, Laurence M Gagné, Sébastien Campagne, Victoire Fort, Julia O’Sullivan, Karel Mocaer, Miki Feldmüller, Jean-Yves Masson, Frédéric

HT Allain, Samer M Hussein, Marc-Étienne Huot. *Nucleic Acids Research*, Volume 47, Issue 8, May 2019, Pages 4181–4197

- **Julia O'Sullivan**(=), Maria Tedim Ferreira(=), Jean-Philippe Gagné, Ajit Sharma, Michael Hendzel, Jean-Yves Masson and Guy G. Poirier - Emerging roles of eraser enzymes in dynamic reversal of protein mono- and poly(ADP-ribosylation) **(= Equal participants)** (Nature Communications –2019, 10(1), 1182) (Chapter 2)

- Marie-Christine Caron(=), Adjit Sharma(=), **Julia O'Sullivan**, Logan Myler, Jean-Philippe Gagné, Chantal Ethier, Maria Tedim Feirrera, John Pascal, Ilya Finkelstein, Michael Hendzel, Guy G. Poirier, and Jean-Yves Masson – PARP-1 is a key regulator of DNA end resection (Nature Communications, 2019,10(1),2954) **(= Equal participants)** (Chapter 3)

- **Julia O'Sullivan**(=), Sofiane Y. Mersaoui(=), Guy G. Poirier, Jean-Yves Masson - Assessment of global DNA double-strand end resection using a coupled BrdU-DNA labeling with cell cycle discrimination imaging method. **(**= Equal participants) Journal of Visualized Experiments: Jove, 28 Apr 2021, (170) (Chapter 4)

Chapter 1 **Emerging roles of eraser enzymes in dynamic reversal of protein mono- and poly(ADP-ribosylation)**

Julia O'Sullivan[1,2], Maria Tedim Ferreira[1,2,3], Jean-Philippe Gagné[2,3], Ajit K. Sharma[4], Michael J. Hendzel [4,5], Jean-Yves Masson[1,2,6] & Guy G. Poirier[2,3,6]

[1]Genome Stability Laboratory, Centre de Recherche du Centre Hospitalier Universitaire de Québec-Université Laval, HDQ Pavilion, Oncology Division, Québec G1R 2J6, Canada.

[2]Département de Biologie Moléculaire, Biochimie Médicale et Pathologie, Faculté de Médecine, Université Laval, Québec G1V0A6, Canada.

[3]Centre de Recherche du Centre Hospitalier Universitaire de Québec-Université Laval, CHUL Pavilion, Oncology division, Québec G1V 4G2, Canada.

[4]Department of Oncology, Faculty of Medicine and Dentistry, University of Alberta, Edmonton T6G 1Z2, Canada. 5Department of Cell Biology, Faculty of Medicine and Dentistry, University of Alberta, Edmonton T6G 2H7, Canada.

[6]Centre de Recherche sur le Cancer de l'Université Laval, Québec G1R3S3, Canada. These authors contributed equally: Julia O'Sullivan, Maria Tedim Ferreira.

Preface

During the second year of my PhD Dr Guy G. Poirier and Dr Jean-Yves Masson were invited to write a review covering the topic of PAR erasers in Nature communications. I was therefore very grateful to take the opportunity to summarise the current literature on this subject with the help of the other co-first author Dr Maria Tedim Ferreira. This review entitled **"Emerging roles of eraser enzymes in the dynamic reversal of protein mono- and poly(ADP-ribosylation)"** (Julia O'Sullivan (=), Maria Tedim Ferreira (=), Jean-Philippe Gagné, Ajit Sharma, Michael J. Hendzel, Jean-Yves Masson, and Guy G. Poirier), focuses primarily on PARG and its role in erasing PAR, though it does touch on the other PAR and MAR erasers in the resolution of the PARP DNA damage response.

The importance of understanding PAR modifiers is often underestimated, however as modulation of PARP-1 function is currently on the frontline of cancer treatment. It is vitally important to also consider the biological controls already set in place to regulate PAR modifications. These modifiers act as a counterbalance to the formation of PAR. As such they represent another direction for modulation of PARP activity as a cancer treatment. Writing this review article helped to expand my personal knowledge on the topic while also providing a single comprehensive source for information on PAR erasers. Since its publication not only has it been cited multiple times in other articles demonstrating the importance and value of such a review, but I have the immense pleasure of seeing the figures used in presentations at large international conferences. Validating not only the need for such a review but also the quality of content that the group as a whole was able to produce. A copy of the PDF of this article can be found in the Annex.

Résumé

L’ADP-ribosylation des protéines est essentielle pour la régulation de plusieurs voies cellulaires, permettant des réponses dynamiques sous diverses conditions physiopathologiques. Elle est modulée par une interaction dynamique entre les lecteurs ADP-ribose, les graveurs et les effaceurs de cette modification. Alors que la synthèse de l'ADP-ribose a été étudiée et revue de manière approfondie, le retrait des groupements ADP-ribose par des d'enzymes a reçu moins d'attention. Cependant, des progrès majeurs dans l'identification par spectrométrie de masse des résidus ADP-ribosylés et la caractérisation biochimique des effaceurs ADP-ribose ont considérablement élargi nos connaissances de la dynamique de l'ADP-ribosylation. Ici, nous décrivons des informations récentes sur la biologie des effaceurs ADP-ribose et discutons des processus cellulaires orchestrés de manière complexe pour désactiver les mécanismes dépendants de l'ADP-ribose.

Abstract

Protein ADP-ribosylation is essential for the regulation of several cellular pathways, enabling dynamic responses to diverse pathophysiological conditions. It is modulated through a dynamic interplay between ADP-ribose readers, writers and erasers. While ADP-ribose synthesis has been studied and reviewed extensively, ADP-ribose processing by erasing enzymes has received comparably less attention. However, major progress in the mass spectrometric identification of ADP-ribosylated residues and the biochemical characterization of ADP-ribose erasers has substantially expanded our knowledge of ADP-ribosylation dynamics. Herein, we describe recent insights into the biology of ADP-ribose erasers and discuss the intricately orchestrated cellular processes to switch off ADP-ribose-dependent mechanisms.

1.1 Introduction

Reversible post-translational modifications (PTMs) contribute to the dynamic regulation of the proteome through a diversified repertoire of functions. Protein ADP-ribosylation has emerged as a complex, dynamic, and reversible PTM system within which fundamental components work antagonistically to fine tune and tightly regulate protein behavior[280]. Similar to other transient biological processes, the ADP-ribosylation turnover relies on synthesis and degradation mechanisms[281, 282]. The enzymes that perform these functions can essentially be described as writers and erasers, a nomenclature borrowed from the classification of proteins involved in epigenetic regulation. ADP-ribose writers are collectively referred to as ADP-ribose transferases (ARTs), a family of proteins with mono- or poly(ADP-ribose) transferase activities. These enzymes, especially the promising drug target poly(ADP-ribose) polymerase-1 (PARP-1), have been intensely studied by the ADP-ribosylation community for many years. More recently, attention has shifted towards the biological roles of ADP-ribose erasers, stimulated by the identification of a variety of ADP-ribose degrading enzymes with different substrate specificities. These recent findings have profoundly changed the prevailing view that ADP-ribose erasing depends almost solely on poly(ADP-ribose) glycohydrolase (PARG) activity.

ADP-ribosylation—in its strictest sense—refers to the enzymatic addition of an ADP-ribose molecule to a target substrate. The transferrable ADP-ribosyl units are typically derived from NAD^+ through the cleavage of the nicotinamide-ribosyl bond. Therefore, ADP-ribosylation reactions generally depend on NADase activity. A fundamental distinction exists between mono-ADP-ribosylation (MARylation), i.e., the transfer of a single ADP-ribose monomer, and poly(ADP-ribosylation) (PARylation), which involves the biosynthesis of elongated ADP-ribose polymers (Fig. 1.1). PAR polymers form nucleic acid-like polyanion structures that can serve as a docking site for a variety of reader domains (reviewed in ref. [283]). MARylation can impact protein activity, stability, substrate specificity, folding, or localization. For instance, substrates of the bacterial MAR transferases can undergo substantial structural rearrangements that profoundly modify host cell physiology and promote cellular intoxication[284]. The functional divergence between MARylating and PARylating enzymes is consistent with a biological system that involves multiple layers of antagonizing activities. This concept

is supported by a rapidly expanding repertoire of ADP-ribose-degrading enzymes, suggesting that MAR and PAR modifications are continuously transferred to, and removed from, substrates by an antagonizing set of enzymes.

This review will first focus on PARG and the more recently characterized enzymes that can reverse ADP-ribosylation. Subsequently, we will discuss the biochemical methods used to detect ADP-ribosylation turnover, and expand on the regulation of ADP-ribosylation through combinatorial selective erasing mechanisms. We will conclude by discussing the therapeutic target potential of ADP-ribose erasers, focusing on the use of PARG inhibitors in synthetic lethal approaches against cancer.

1.2 Enzymes involved in the removal of ADP-ribosylation

Recent advances in defining ADP-ribose metabolism suggest that the balance between ADP-ribose writers and erasers is crucial for the coordination of multiple cellular response pathways[285]. This view is supported by the identification of a growing number of proteins implicated in writing, reading, and erasing the ADP-ribosylation modifications. Although a synthesis and degradation duality is inherent to transient PTMs, specialized erasers might occupy different catalytic niches to provide a functional and temporal reversibility of the reaction and for the recycling of ADP-ribosylated substrates. The inability of PARG—the main dePARylating enzyme—to remove MARylation marks[146, 286] , and its limited processivity on short PAR polymers, leaves room for the involvement of other erasers (Table 1.2). A complete reversal of MARylation is performed in human cells by amino-acid-specific ADP-ribose-acceptor hydrolases, such as the macrodomain-containing proteins MacroD1 and MacroD2, the terminal ADP-ribose protein glycohydrolase 1 (TARG1), and the ADP-ribose hydrolase (ARH) family members ARH1 and ARH3. Moreover, several phosphodiesterases have been shown to possess ADP-ribose processing activity. In this section, we provide an overview of these different ADP-ribose erasing enzymes.

1.2.1 Poly(ADP-ribose) glycohydrolase (PARG)

Although a role of MARylation in response to genotoxic stress has become better established recently (reviewed in ref. [287]), only PARylation occurs in conjunction with a substantial decrease of intracellular NAD^+ concentrations when extensive DNA damage is encountered. Globally, PARylation processes account for a large proportion of the ART activity in cells. Therefore, dePARylation can be viewed as the predominant erasing activity. PARG is the major dePARylating enzyme, and is primarily responsible for hydrolyzing the glycosidic linkages between ADP-ribose units of PAR polymers to generate free ADP-ribose monomers. Only a single PARG gene has been identified in mammals and its sequence is highly conserved[288]. PARG homologs are detected in a wide range of eukaryotes with the exception of budding yeast. The human PARG gene encodes for multiple variants produced by alternative splicing of a unique mRNA[289, 290]. The characterization of PARG expression products and the apparent molecular weight heterogeneity of PARG have been reviewed elsewhere[291]. PARG is a modular protein with a four domain architecture[288] (Fig. 1.2). Domain A spans exons 1–3 and forms a predicted N-terminal intrinsically disordered regulatory domain[292]. Domain B (exons 4–8) connects the N-terminal region to the catalytic domain through a hinge region[289] and contains a regulatory segment[293]. Domain C (exons 9–14) contains the catalytic active site and the PARG signature motif[294]. Domains C and the C-terminal domain D (exons 15–18) form the PARG macrodomain[146, 295]. A number of nuclear export signals (NES) and nuclear localization signals (NLS) are distributed throughout the PARG sequence.

The expression of a variety of *PARG* splice variants with different localizations enables functional specialization[289, 296]. In human cells, major isoforms include a full length 111 kDa PARG enzyme and splice variants that generate proteins of 102 and 99 kDa (Fig. 1.2). While full length PARG is mostly nuclear and accounts for a minor fraction of global cellular activity, the smaller isoforms localize primarily to the cytoplasm with a perinuclear distribution, and seem to be responsible for most of the PAR processing activity[297]. Therefore, nuclear and cytoplasmic compartmentalization, and the shuttling of PARG isoforms between the nucleus and cytoplasm have been proposed as a mechanism to regulate cellular PAR levels[296, 298]. PARG mRNA also undergoes additional alternative splicing that generates small isoforms of 55 and 60 kDa. Both hPARG55 and hPARG60 isoforms have been found to be catalytically inactive due to the

absence of exon 5-encoded amino-acids[299] (Fig. 1.2). Therefore, these small human PARG isoforms are not involved in general PAR turnover in cells.

Human PARG is a constitutively active, low abundance enzyme that possesses both exoglycosidase and endoglycosidase activities. PARG mainly functions as an exoglycosidase, sequentially digesting glycosidic linkages from the protein-distal end of the polymer similar to carbohydrate glycosyl hydrolases[300]. This processivity improves the catalytic activity of PARG but is strongly chain-length dependent[301]. On the other hand, it has been estimated that ~20% of PARG depolymerization activity can be accounted for by in-chain endoglycosidic degradation[302]. The fact that PARG has two mechanisms of action with different degradation kinetic parameters and PAR structure-affinity might be an overlooked characteristic in the complex and intricate interplay between ADP-ribose readers and erasers, as will be discussed further below.

The importance of the catalytic activity of PARG became clear with the observation that *PARG*$^{-/-}$ mice were embryonic lethal[303] and that PARG-depleted cells are hypersensitive to genotoxic insults[304, 305]. This is accompanied by PAR accumulation and early apoptosis, suggesting that efficient PARG-mediated PAR turnover is required for the recovery from DNA damage. PARG has also been shown to be necessary to prevent massive PAR production upon prolonged replicative stress[306]. Schreiber and colleagues demonstrated that PARG deficiency delays cellular recovery from persistent replication stress, triggered by prolonged hydroxyurea treatment[306]. These blocked cells display high PAR levels, which negatively impacts RPA foci formation and its association with single-stranded DNA (ssDNA). The prevention of RPA loading eventually leads to increasing areas of uncovered ssDNA, which then transform into DNA double-strand breaks (DSBs), resulting in the formation of more PAR. Ultimately, this amplification loop promotes apoptosis and/or necrotic cell death in proliferating cell populations. These observations are in agreement with the finding that PARG localizes to replication foci throughout S-phase and interacts with the replication protein PCNA[307, 308]. Furthermore, they complement an earlier report that PARG-deficient cells treated with DNA alkylating agents have an increase in S-phase arrest together with high levels of the DSB marker γH2AX[309]. Correspondingly, the Lopes group showed that PARG inactivation affects the progression of all replication forks and alters the molecular architecture of a significant fraction of replication

intermediates[310]. These results provided mechanistic insight into the essential role of PARG in cell growth and development, in line with the observed embryonic lethality of *PARG*$^{-/-}$ mice[311].

Another important role of PARG during the DNA damage response is to maintain stable levels of PAR and to recycle highly automodified PARP-1. The stabilization of PAR levels is crucial for protecting the cell against parthanatos, a caspase-independent PAR-mediated type of cell death[312]. Parthanatos is triggered by the release of the apoptosis-inducing factor (AIF) from the mitochondria to the nucleus[313, 314]. Once translocated to the chromatin environment, AIF leads to large-scale DNA fragmentation and chromatin condensation, which is followed by cell death[315]. Depletion of PARG has been shown to be protective against oxidative stress-induced parthanatos by preventing the release of AIF from the mitochondria[316].

Lastly, PARG has also been implicated in telomere maintenance. PARG is capable of negatively regulating the access to telomeric DNA by reversing ADP-ribosylation of the telomeric-specific protein TRF1, contributing to the regulation of telomere repair and replication[317, 318]. Overall, these examples show that the dynamic equilibria established between PARP-1 and PARG activities, and therefore PAR levels, are key for controlling cell fate, suggesting that PAR erasers are as important as PAR writers for cellular homeostasis.

1.2.2 ADP-ribose hydrolases (ARHs)

ADP-ribose conjugation was first described as a PTM catalyzed by bacterial ADP-ribosylating exotoxins (bAREs)[319]. Bacterial MAR transferases (MARTs) have related genes in humans whose extracellular expression makes them irrelevant or inoperative with respect to intracellular ADP-ribose-mediated pathways[320]. In human cells, intracellular protein MARylation is performed by members of the ADP-ribosyl transferases diphtheria toxin-like proteins (ARTDs). Formerly classified as PARPs[89], the 17 members of the ARTD family in human were renamed according to a systematic nomenclature that better reflects their structural features and catalytic properties[86]. There are currently 11 members of the human ARTD family characterized as MARTs,

typically renamed after the type of ADP-ribose molecule (i.e., MAR) they transfer onto themselves or target substrates[90, 321].

The ADP-ribose hydrolase (ARH) family consists of three related proteins[322]. While ARH2 substrates are yet to be discovered, ARH1 is a highly active ADP-ribosyl-arginine hydrolase[323] and ARH3 is an ADP-ribosyl-serine hydrolase[324] (Table 1.1 and Fig. 1.3). Mice that lack ARH1 are more sensitive to cholera toxin[325] and tumor-prone, having increased incidences of adenocarcinoma, lymphoma, and metastases[326]. ARH3-deficient mouse embryonic fibroblasts show increased steady-state abundance of serine-ADP-ribosylation *in vivo*[327] and DNA damage-induced serine-ADP-ribosylation is efficiently reversed by ARH3[324]. In contrast to ARH1, ARH3 also possesses activity toward the O-glycosidic bond of PAR, similar to the exoglycosidic activity of PARG[320]. However, ARH3 does not rescue *Drosophila* or mouse genetic knockouts of PARG from cell death or PAR accumulation[303, 328] , suggesting that it cannot compensate for the loss of PARG. Owing to its abundance in the cytoplasm, ARH3 participates in a second stage of PAR hydrolysis following the release of free PAR polymer branches by other erasers. This may help lower the cytoplasmic PAR levels, ultimately preventing mitochondria-dependant apoptotic pathways such as parthanatos[329].

While ARHs only erase arginine- and serine-MARylation and macrodomain-containing enzymes specifically target aspartate- and glutamate-MARylation (see next section), ARTDs have been shown to mediate ADP-ribosylation on a wide range of amino-acid residues[330, 331] This apparent discrepancy will be discussed later on in this article.

1.2.3 Macrodomain-containing ADP-ribose erasers

The macrodomain fold is an evolutionarily conserved, compact globular-shaped structure of ~25 kDa present throughout all of the biological kingdoms[332]. It can be found as a stand-alone module or integrated into multi-domain proteins. The macrodomain was the first characterized ADP-ribose-binding module. It can bind terminal ADP-ribose structures with nanomolar affinity[88]. There is functional diversity related to structural variation in the macrodomain protein family. A subgroup of

macrodomains lacks the ability to bind ADP-ribose while others acquired glycosidic activity involved in ADP-ribosylation reversal[283]. There are ten human macrodomain-coding genes: the histone H2A variants Macro H2A.1 and Macro H2A.2; MacroD1, D2, and D3; TARG1; the chromodomain-helicase-DNA-binding protein 1-like (CHD1L) and the macrodomain-containing ARTDs 7-8-9 (formerly named PARPs 15-14-9). Among these, MacroD1, MacroD2, and TARG1 were classified as ADP-ribose erasers because of their ADP-ribose hydrolase activities. MacroD1 and MacroD2 cleave the chemical link between MAR and an acceptor protein while TARG1 presents the unique capability of cleaving both MARylated and PARylated side chains of aspartate and glutamate residues[333] (Fig. 1.3).

The role of TARG1 in PAR turnover remains elusive but a PARylation-dependent relocation of TARG1 to the nucleoplasm has been observed[334] in addition to its recruitment to DNA lesions in a PAR-dependent fashion[333]. The catalytic domain of TARG1 is different from PARG but resembles the OGG1 DNA glycosylase[333] and directly targets the carboxyl ester ADP-ribose linkages to remove the modification from its substrate. The ability of TARG1 to remove whole PAR chains from the substrate most proximal attachment point is unique among the known erasers, adding another putative regulatory layer to PAR cellular functions. For years, only PARG was known to generate protein-free ADP-ribose polymers as a consequence of its endoglycosidic activity[301] (Fig. 1.3), which becomes the major mode of action when robust PARP activation (i.e., strong genotoxic insults) leads to the synthesis of large and branched PAR[335]. Although this idea has not been fully evaluated, TARG1-mediated production of protein-free PAR might be involved in parthanatos[333].

Similarly to TARG1, the mono-ADP-ribose hydrolase activities of MacroD1 and MacroD2 are also selectively directed toward ester bonds established by ADP-ribosylated aspartate and glutamate residues, although with different catalytic modes (reviewed in ref. [336]). Current experimental data suggest that ester-type ADP-ribose bonds in protein substrates are specific targets of the macrodomain erasers. This activity could play a regulatory role *in vivo* as MacroD2, for example, has been implicated in the recycling of automodified PARP-1[337]. The removal of the autoinhibitory MAR moieties from PARP-1 by MacroD2 has been suggested to explain the accumulation of MARylated PARP-1 in the context of MacroD2 gene deletion in human colorectal cancer cells[338].

The underlying MacroD2-dependent PARP-1 recycling model proposed by Sakthianandeswaren et al. involves a biphasic erasing of PARP-1 automodification, which implicates PARG as the primary PAR trimming enzyme responsible for the generation of MAR adducts that can subsequently be targeted by MacroD2[338].

As mentioned above, PARG is a member of the macrodomain eraser family, although there is no similarity between the amino-acid sequence of PARG and other macrodomain-containing proteins. However, there is a close structural and evolutionary relationship between macrodomains and PARG[295], and its catalytic center is essentially a macrodomain fold[146, 295].

1.2.4 Phosphodiester ADP-ribose hydrolases

Homopolymers of PAR are composed of successive ADP-ribose moieties linked together by alternating phosphodiester and O-glycosidic linkages (Fig. 1.3). The phosphodiester bond is also central to the ADP-ribose monomer itself as it links the adenosine structure to the ribose. The activity of snake venom phosphodiesterases was instrumental in the elucidation of PAR structure in the early studies of PARylation, as it was used to determine chain length and PAR branching frequency[339]. Only recently, a role of phosphodiesterases in the reversal of ADP-ribosylation has been proposed, following the discovery of a group of ADP-ribose processing phosphodiesterases that includes NUDIX (nucleoside diphosphates linked to moiety-X) superfamily members NUDT9 and NUDT16 as well as ectonucleotide pyrophosphatase/phosphodiesterase 1 (ENPP1)[340-342]. These erasers target the phosphodiester bound in ADP-ribose moieties. Therefore, their activity is independent of the type of ADP-ribose linkage established with the substrate protein. However, these enzymes should be classified as partial erasers since they leave a phosphoribose remnant attached to the target protein (Fig. 1.3 and Table 1.1). It is still unclear whether these phosphoribose remnants are correlated with specific biological outcomes but a pathological accumulation of phosphoribose on glutamate residues has been described[343]. Furthermore, the phosphodiesterase-catalyzed removal of the distal adenine in PAR ploymers through cleavage of the terminal AMP likely prevents digestion by PARG, as it was observed with etheno-PAR, a derivatized PAR with modified adenine moieties[344].

In vivo, NUDIX hydrolases seem to fulfil 'housekeeping' functions, facilitating the detoxification of potentially deleterious endogenous metabolites[345]. Furthermore, they have been proposed to be involved in replenishing the cellular AMP pool from ADP-ribose monomer products of PARG/ARH3-mediated PAR depolymerization. This metabolic response is consistent with the AMP-dependent mitochondrial energy failure observed following DNA damage and PARP-1 activation[346]. The accumulation of PAR-derived AMP has also been implicated in the modulation of mTOR signalling through AMPK activation[347]. These examples show that ADP-ribose erasing reactions can have diverse effects on metabolism by generating free ADP-ribose monomers and related molecules such as AMP.

Interestingly, the hydrolase activity of a third NUDIX, NUDT5, diverges from the other ADP-ribose-processing NUDIX hydrolases because it cannot hydrolyze protein-conjugated ADP-ribose. However, NUDT5 generates ATP from free ADP-ribose and pyrophosphate in a recycling-like process to quickly replenish nuclear ATP levels[348]. While NUDT5 cannot be classified as an ADP-ribose eraser per se because of its inability to remove protein ADP-ribosylation, it certainly deserves attention as it can influence the level of energetic substrates following PAR catabolism.

The extracellular ENPP1 phosphodiesterase, which lacks a NUDIX and a macrodomain, is yet to be characterized regarding its involvement in ADP-ribose processing. ENPP1 shows considerable phosphodiesterase activity *in vitro* against MAR and PAR, exceeding that observed for NUDT16 in a cell-free system[342]. The high conversion rate of ADP-ribosylation modifications to phosphoribose adducts by ENPP1 has been suggested as a key feature for the generation of phosphoribose signatures for analysis by liquid chromatography-mass spectrometry (LC-MS)[342].

1.3 **Detection and evaluation of MAR and PAR erasing activities**

The emergence of a variety of new players that modulate ADP-ribose catabolism underscore the urgent need for methods capable of rapidly measuring erasing activities. Historically, most assays were developed to measure the disappearance of PAR as a

consequence of PARG glycosidic activity. Usually based on residual PAR precipitation assays, these methods give rise to inconsistencies when monitoring PARG activity[349]. Based on this observation, a thin-layer chromatography (TLC)-based strategy coupled to a radiolabed PAR substrate was developed to monitor ADP-ribose accumulation rather than substrate disappearance[349]. This TLC method has been used successfully to measure PARG activity in cell extracts and tissues[350], characterize site-directed mutants[351] and to evaluate the inhibitory strength of small molecules[352, 353]. Later, the conversion of the reaction product, the monomeric ADP-ribose, into a quantifiable fluorophore has been reported as a nonradiometric and high-throughput assay for PARG activity[354].

TLC assays are inadequate to demonstrate the contribution of individual PARG isoforms or additional PAR-degrading enzymes to global PAR erasing activity in cells. In this respect, PAR zymograms were developed to detect alternative catabolic activity against PAR in complex samples. Zymograms are essentially composed of radiolabeled automodified PARP-1 co-polymerized with a polyacrylamide gel. Following renaturation, digested regions can be visualized on the autoradiogram. Although protein renaturation and in-gel activity constraints the applicability of this strategy, zymography proved to be an effective and sensitive method to detect PAR hydrolysis by PARG[349]. However, no significant additional PAR erasing activity has been detected in most cell extracts using this approach, contributing to the long-held belief that PARG was solely responsible for mediating PAR degradation in cells.

Consistent measurements of PARG activity under standardized conditions are hindered by the absence of a well-defined substrate (i.e., of defined length and branching frequency). Additionally, none of the above-mentioned methods is sufficiently accurate to discriminate between the exo- and endoglycosidic activities of PARG. A number of assays have been designed to specifically monitor the endoglycosidic activity of PARG in protein-bound and protein-free polymer populations, but the most widely used methods are based on the analysis of PAR reaction products on high-resolution DNA sequencing gels[302] and by HPLC[303, 355]. Despite being experimentally challenging, HPLC analysis of PARG degradation products following digestion with snake venom phosphodiesterase (svPDE) remains the method of choice to determine the relative contribution of both PARG glycosidic activities to PAR erasing. In this assay, the

exoglycosidic activity allows PARG to attack PAR polymers at the protein-distal chain end to release ADP-ribose units, which are subsequently converted to AMP by cleaving the phophodiester bond with snake venom phosphodiesterase. The endoglycosidic actvity of PARG generates additional chain termini that release supplementary AMP upon double digestion with svPDE, which can be measured to estimate the relative endo/exo activities[301].

A more recently developed alternative to measure PARG endoglycosidic activity is based on the detection of ADP-ribose oligomers by LC-MS[335]. In this approach, PAR termini are protected with an inactive bacterial $PARG^{E115Q}$ mutant that blocks exoglycosidic cleavage. When human PARG is added to the blocked PAR substrate, only endoglycosidic cleavage can occur. The accumulation of PAR fragments (ADP-ribose oligomers) is detected by LC-MS in the form of specific mass-to-charge ratios and correlated to the endoglycosidic activity of PARG[335]. Although exo- and endoglycosidic mechanisms are essential for efficient dePARylation, it is common to reflect PARG activity in a single value that integrates both activities based on commercially available chemiluminescence- and colorimetric-based detection systems. These assays are suitable for high-throughput screening of PARG inhibitors in addition to antibody-based detection methods[356]. However, immunological detection of PAR is prone to underestimating the presence of residual ADP-ribose oligomers for which the antibodies generally possess low affinity[357]. The recent development of antibody-like MAR- and PAR-binding reagents should prove beneficial to the evaluation of PARG inhibition in cells[358].

Given the increasingly important role of MAR erasers, a number of approaches have also been developed to facilitate the detection of MAR hydrolase activities. One of the most effective approaches is to use the auto-MARylated $PARP\text{-}1^{E988Q}$ mutant as a substrate for MARylation erasers. This PARP-1 mutant is significantly more active than other MARTs and thus represents a robust approach to generate a MARylated substrate. *Bona fide* MARTs such as PARP-10/ARTD10 also have been used as MARylated substrates[324, 333, 341, 342, 359]. Furthermore, the oligo(ADP-ribosyl)ated PARP of *H. aurantiacus* was employed as an intermediate length substrate for ADP-ribose erasing assays[340]. Reaction products are generally resolved by SDS-PAGE or TLC. These approaches provide valuable substrate models for ADP-

ribosylation erasing studies but may not reflect the diversity and wide range of ADP-ribose polymer species, which could explain the persisting confusion regarding the linkage selectivity of MAR hydrolases. While some MARTs such as PARP-10/ARTD10 appear to be MARylated exclusively on acidic residues[359], it is less clear which types of ADP-ribose–protein linkages exist in other MARTs and PARP-1^{E988Q}. A panel of linkage-specific substrates would be necessary to assess the diversity of MARylation reversal. For example, ADP-ribosylated actin by the arginine-specific ADP-ribosyltransferase CDTa provides a defined substrate for arginine-mediated ADP-ribosylation studies while the threonine-specific transferase TccC3 mono-ADP-ribosylates threonine residues of the same substrate[359].

It should be kept in mind that the amino-acid sequence surrounding the ADP-ribosylation site is unknown in these substrates and might influence the recognition by the eraser. Similarly, MARylated substrates, such as histones, may carry additional PTM decorations that could also tune the binding affinity of the erasing enzyme. The development of synthetic peptides with site-specific ADP-ribosylations will be particularly useful for dissecting the substrate specificity of ADP-ribose erasers[360]. *Trans*-ADP-ribosylation of synthetic peptides with PARP-1^{E988Q} has been demonstrated by MS analysis but the actual yield of peptide MARylation is probably too low for subsequent biochemical analysis, even after affinity purification[99]. Alternatively, peptide microarrays containing several ADP-ribosylated residues in a variety of sequence contexts may allow profiling of the recognition and processing specificity of MARylation erasers.

1.4 **ADP-ribose linkage selectivity of erasers**

An intrinsic characteristic of ADP-ribosylation is the molecular heterogeneity and complexity of the reaction product transferred to target substrates. Therefore, ADP-ribosylation needs to be viewed in a length- and site-dependent manner. The site-specific length of PAR polymers is difficult to test experimentally and further studies are needed to characterize the length diversity of PARylated substrates. More progress has been made with regard to determining ADP-ribosylation sites within proteins. The site-specific localization of ADP-ribosylation modifications could be mapped in a system-wide

manner in several recent MS-based proteomics studies. Notably, these methods are significantly more challenging and difficult to implement than standard MS-based approaches that only aim for protein identification[331, 361-365].

A survey of the current literature indicates that all chemically reactive amino acids (i.e., excluding those with hydrophobic side chains) may be targeted by ADP-ribosylation under physiological conditions[321, 366]. The biological significance of differential ADP-ribosylation site usage is unknown but ADP-ribose–protein linkages appear to be processed by erasers with rigid selectivity (Table 1.1). For instance, ARH1 hydrolyzes N-linked MARylated arginines[320], the macrodomain-containing proteins are specific for the carboxyl ester bond formed with the side chains of aspartate and glutamate residues[359] while ARH3 hydrolyzes O-linked MARylated serines[327]. Although only limited information is available, a modulation of ADP-ribose recognition has been reported for MAR erasers, suggesting that the local amino acid sequence environment influences ADP-ribosylation erasability[327, 367].

The different susceptibility of each type of ADP-ribosylation to degradation by the erasers suggests that the stability of ADP-ribosylation in cells may vary depending on the type of linkages. For example, the absence of a specific enzyme to erase ketoamine-linked ADP-ribose from lysine residues has been hypothesized to be involved in the long-term maintenance of histone epigenetic marks[368]. Furthermore, PAR polymer populations with different half-lives, depending on their length and complexity, have been reported[301, 369]. This suggests that recognition and processing of multi-site and multi-structural ADP-ribosylation involves complex coordination of the erasers. However, current atlases of ADP-ribosylation signatures, notwithstanding their importance, from human cancer cells provide little information regarding the occupancy rate of different ADP-ribosylation modifications. At the moment, it is unclear how multiple ADP-ribosylation linkages can be read and transformed into meaningful signalling information.

The termini of a DNA strand break can also be reversibly modified by covalent PARylation *in vitro*[370-373] , and the ADP-ribose ester bonds of MARylated, phosphorylated double-stranded DNA can be hydrolyzed by MacroD1[374]. PARP-3-mediated MARylation of DNA can also be erased by MacroD2, TARG1, PARG, and ARH3[372]. For DNA MARylation reversal, MacroD1, MacroD2, and TARG1 target the

same type of ester bonds (Table 1.1), while ARH3 activity likely targets the O-glycosidic ribose-ribose bond. Moreover, PARG can efficiently remove MAR moieties attached to DNA phosphate residues - in contrast to its activity on protein substrates[371, 372]. This observation emphasizes the importance of exploring the substrate specificity of erasers, which might not be as rigid as initially thought. The role of DNA ADP-ribosylation in the repair mechanisms that maintain the integrity of genomic DNA remains elusive but represents a new dimension in ADP-ribosylation dynamics.

The identification of ADP-ribosylated substrates is undergoing rapid expansion owing to the development of high-sensitivity mass spectrometers. The functional significance of most ADP-ribosylation that occurs on a variety of amino-acid targets is not yet understood. Some of these modifications might be generated nonenzymatically when a biomolecule encounters a reactive metabolite such as ADP-ribose. The formation of ketoamine glycation conjugates on histones lysine and arginine amino acids, in the presence of ADP-ribose, has been documented[375]. This phenomenon might be explained by the local accumulation of ADP-ribose, as a result of PAR hydrolysis by PARG *in vitro* during sample preparation for MS analysis[331]. However, artefactual glycation by free ADP-ribose released by PARG on lysine and arginine residues was not observed in cell extracts supplemented with free PAR chains and PARG[376]. Alternatively, the accumulation of free ADP-ribose within a confined area might arise from a side reaction based on PARP-1's abortive NADase activity[377]. Following PARP-1 automodification, NAD^+ hydrolysis becomes a major component of PARP-1 activity, which releases ADP-ribose that can react with glycation-prone amino groups of proteins or other biomolecules. Therefore, caution is recommended in interpreting results based on the identification of rare, low abundant or atypical ADP-ribosylation modifications.

1.5 **A model for cellular PARylation dynamics**

The existence of a continuum of ADP-ribose polymer lengths in cells coupled to a variety of amino acid linkages suggests that various erasing modes act together to drive the ADP-ribosylation cycle. PARG possesses the highest level of PAR chain degradation activity. However, its inability to remove the proximal ADP-ribose moiety from proteins

illustrates that a complete reversal of ADP-ribosylation likely requires an orchestrated cellular response involving both MAR and PAR erasers[335]. Substrates that would have undergone fast, but partial, trimming of their PARylation modifications by PARG could then be processed by a group of specialized erasers. The rapid initial degradation process likely depends on the synergistic endo/exo dePARylation activity of PARG, considering that endoglycosidic PARG activity also releases protein-bound PAR polymers and predominates in the earliest phases of the degradation process[302].

At the same time, the interplay between ADP-ribosylation writers and erasers could regulate the temporal order of the signalling response to PARP-1 activation. For example, the dynamics of ADP-ribosylation reversal strongly depend on the type of PAR polymer synthesized. Large and complex polymers generated during the DNA damage response are short-lived and transient with half-lives of few seconds while the constitutive fraction of PAR is degradation-resistant for hours[369]. Collectively, these observations suggest that ADP-ribosylation erasing may be described as a multistep processing cascade with specific kinetics depending on the physiological context (Fig. 1.4).

Our understanding of ADP-ribosylation has been substantially advanced by the identification of histone PARylation factor 1 (HPF1) as a regulator of both histone ADP-ribosylation and PARP-1 automodification. This finding demonstrated that a PARP-1-interacting factor can modulate PARP-1's PARylation activity, switching it to O-linked ADP-ribosylation[128]. In contrast, most previous reports showed that PARP-1 activity is modulated by a variety of DNA lesions[378], post-translational modifications[379] or NAD^+ availability[380]. The observed HPF1-dependent serine-ADP-ribosylation of PARP-1, histones and chromatin-interacting factors as well as accumulating evidence that serine residues are the preferred ADP-ribosylation targets upon DNA damage induction[381-385] suggest that serine-ADP-ribosylation predominates. This challenges the current model, in which protein ADP-ribosylation is primarily localized to aspartate, glutamate, lysine and arginine residues with cell type- and tissue context-dependent stoichiometries. However, it would be premature to conclude that DNA-dependent PARPs are uniquely engaged in O-glycosidic linkages with serine and, as recently demonstrated, tyrosine residues[386] in all HPF1-expressing cells and that all other amino acid linkages are *in vitro* artifacts. For instance, large-scale proteomics studies

provided convincing and robust evidence of site-specific glutamate and aspartate ADP-ribosylation[185, 186, 361].

As discussed above, HPF1 appears to switch PARP-1 ADP-ribosyltransferase activity toward O-linked ADP-ribosylation. This observation implies that PARP-1-interacting proteins can have profound impact on the PARP-1 enzymatic mechanism. In the case of HPF1, the switch from a carboxyl ester ADP-ribosylation chemistry on acidic glutamate and aspartate amino acids to O-linked ADP-ribosylation of neutral serine residues may be explained by an HPF1-dependent reconfiguration of PARP-1 active site[382, 387]. HPF1 accumulates at DNA lesions in a PARP-1-dependent but PAR-independent manner[128]. Considering that PARP-1 relocation to DNA damage sites precedes HPF1 recruitment, PARP-1 could be involved in the glutamate and aspartate ADP-ribosylation of the nucleosomal surface[388] before switching its catalytic activity toward serine residues as HPF1 accumulates locally. This may indicate a regulatory mechanism with several overlapping waves of linkage-specific ADP-ribosylation (Fig. 1.4).

The modulation of PARP-1 activity can also be observed in polymer turnover systems that recapitulate PAR metabolism. In these systems, the addition of PARG shifts the ADP-ribose transferase activity of PARP-1 from automodification to histone modification[301, 389-391]. Similarly, HPF1 promotes histone ADP-ribosylation and limits PARP-1 hyper-automodification[128]. These results motivate the identification of additional modulators of PARP-1 activity. They also suggest that PARP-1 intramolecular conformational changes may be transmitted via protein-protein interactions. This mechanism is exploited to provide an alternative to common PARP-1 inhibition by antagonizing NAD^+ binding at the catalytic site[392]. Besides, a network of allosteric communications is known to connect damage recognition to catalytic domain remodelling in order to activate PARP-1[87, 94, 100, 393, 394]. The fact that PARP-1 activity depends on protein conformational flexibility is illustrated by the identification of a PARP-1 inhibitor that promotes the formation of a complex specifically through PARP-1 BRCT domain[392]. Although the BRCT domain itself is dispensable for PARP-1 activity[87], the rigidity of the cross-linked PARP-1 BRCT/small-molecule inhibitor product presumably blocks allosteric communications and the propagation of the activation signal to the active site. We can only speculate how additional effectors might rearrange the

PARP-1 active site pocket to enable the formation of alternative ADP-ribosylation linkages. Notwithstanding, different PARP-1 ADP-ribosylation activities within the same pathway further support the notion that cells must produce diverse, specialized erasers.

Non-covalent interactions are thought to play an important regulatory role in ADP-ribose catabolism. For example, a marked inhibition of PARG activity is observed when free PAR is associated with histones or nuclear matrix proteins, most likely through protection of ADP-ribose polymers from PARG-mediated degradation[395]. Alternatively, ADP-ribose polymers that are non-covalently bound to different acceptor proteins may be differentially accessible to PARG[369, 396]. Such competition between PAR and MAR-binding proteins (i.e., readers) and erasers adds an additional layer of complexity as PAR readers might influence the kinetics of degradation of polymers and MAR production.

The regulatory model of sequential erasing waves shown in Fig. 1.4 can be illustrated by the bimodal recruitment kinetics of MacroD2 to sites of laser-induced DNA damage[397]. Following a rapid relocation of MacroD2 in a PARP-1-dependent initial phase, a second slower phase is observed, presumably as a consequence of the accumulation of MARylated species generated through PARG activity. This two-step mechanism reveals that ADP-ribosylation reversal provides a temporal ordering to orchestrate MAR/PAR-regulated pathways. More generally, the different states of ADP-ribosylation and the proteins responding to them may help to sequence and coordinate related reactions and eventually decide cell fate (Fig. 1.4). Since the loss of the eraser can have consequences other than removing the writer, it is likely that the ADP-ribsolyation intermediates are exploited to activate reactions rather than to simply terminate the actions of the writers.

1.6 **Synthetic lethal strategies with PARG inhibitors**

Fuelled by the success of PARP inhibition (PARPi) as a therapeutic strategy for the treatment of many cancers, the field is now exploring the therapeutic potential of PARG inhibition (PARGi). Probably inspired by the postulated nucleic acid-like helical conformation of PAR[398], Tavassoli and colleagues reported that DNA intercalators can form a complex with PAR and protect it from PARG hydrolysis[399]. These

homopolynucleotide intercalators (e.g., ethacridine) were the first class of compounds used to inhibit PARG. However, the influence of DNA intercalators on PARG activity is primarily indirect by restricting access of substrates rather than through direct interaction with PARG. Later, naturally occurring polyphenolic compounds such as the tannins were found to inhibit PARG activity[400]. In particular, Gallotannin[401] was shown to inhibit PARG and to be synthetic lethal to BRCA2-deficient tumors[402]. However, the utility of this compound was subsequently called into question as it exhibits nonspecific effects and is essentially cell membrane impermeable[353].

Despite its lack of cell permeability, one of the most widely used and best characterized PARG inhibitors is adenosine diphosphate hydroxymethyl pyrrolidinediol (ADP-HPD)[403, 404]. Photoincorporation studies with analogues of ADP-HPD showed that the high molecular weight and branched PAR bind PARG at a different sites than short, linear polymers and ADP-HPD[405]. This is consistent with the identification of a secondary substrate binding site on PARG, hypothesized to be involved in its processive behavior[351]. These results indicate that small-molecule inhibitors of PARG might have different effects on PAR processing by modulating its ratio of exo/endoglycosidic activities.

To overcome cellular permeability issues with PARG inhibitors, a new generation of compounds was developed by Hergenrother and colleagues[352]. Rhodamine-based PARG inhibitors (RBPIs) proved to be potent and selective PARG inhibitors since they do not inhibit ARH3 as does ADP-HPD[352]. However, these compounds exhibited only low micromolar inhibitory activity against PARG. Other non-tannin inhibitors such as the GPI 1552 were reported to protect against neuronal damage[406] and potentiate temolozomide anti-metastatic activity in brain tumours[407]. A careful reexamination of the actual evidence for PARG inhibition leads to the conclusion that GPI 1552 was inadequate for a pharmacological evaluation of PARG[353].

More recently, using the cell permeable PARGi PDD00017273[408], Bryant and colleagues demonstrated that PARGi treatment selectively kills BRCA1-, BRCA2-, PALB2-, FAM175A/ABRAXAS-, and BARD1-depleted cells in the absence of any exogenous DNA damaging agents. The underlying mechanism for this synthetic lethality is that PARGi provokes replication forks stalling and a reduction of DNA double-strand

break repair via homologous recombination (HR). An alternative explanation is that inhibition of PARG might cause irreversible PAR association with several proteins needed to complete HR[409]. Importantly, PARGi does not phenocopy PARPi. PARGi induces a rapid increase in IR-induced activation of DNA-PK and impairs normal mitotic progression. This suggests that PARG has different effects on activation of DNA damage repair pathways following ionizing radiation, consistent with the notion that blocking PAR removal has a different consequence to inhibiting PAR addition[410].

Genetic studies have suggested PARG inhibitors as chemosensitizing agents. PARG-deficient cells display centrosome amplification and accumulate aberrant mitotic figures, which induced either polyploidy or cell death by mitotic catastrophe[411]. ES cells derived from knock-out PARG mice showed enhanced sensitivity towards γ-irradiation and other forms of ionizing radiation[412]. More recently it was shown that PARG suppression potentiates the toxicity of radiation therapy in BRCA-deficient cells[409] and that PDD00017273 radiosensitizes MCF-7 cells[410].

PARG protein expression can be regulated by the stabilization of its mRNA by the RNA-binding protein HuR[413]. In pancreatic ductal adenocarcinomas (PDA) cells, genetic deletion of HuR enhances PARPi sensitivity. In this context, the PARPi-induced toxicity is attributable to downregulation of PARG expression. The inhibition of HuR can also re-sensitize PDA cells to PARPi, suggesting that the loss of PARG activity could enhance the clinical effectiveness of PARP inhibitors[413]. In contrast, Gogola and colleagues have shown that PARPi-resistance can be mediated by PARG downregulation[414]. The loss of PARG activity in BRCA2-deficient tumours treated with potent PARP-1 inhibitors is sufficient to restore PAR formation and rescue PARP-1 downstream signaling. PARG depletion indeed occurs in triple-negative breast cancers and serous ovarian cancers. When treatment-naive TNBC biopsies from women eligible for PARPi treatment were analyzed for PARG expression, lack of PARG occurred in some areas of the tumours[413]. This suggests that these tumour sections can become de facto resistant to PARPi treatment. Further studies are needed to clarify the role of PARG and the accumulation of PAR polymers that survived erasing in a dynamic system that has undergone profound alterations. Differences in genetic backgrounds can certainly account for contradictory results (e.g., DNA damage response-proficient vs -deficient cells) but the nature of PAR itself (either free or protein-bound) might also be an

important and significant clue to interpret these results. Although there is a bright future for PARG inhibitors, so far they are only effective at relatively high doses in contrast to PARP-1 inhibitors characterized with half maximal inhibitory concentration in the low nanomolar range. In addition, the fact that PARG activity can be regulated at multiple levels with respect to PAR length and branching patterns poses a particular challenge.

1.7 Concluding remarks and future challenges

In this review, we have provided an overview of the dynamic and reversible processes that regulate ADP-ribosylation. Determining the contribution of each regulator in this delicate equilibrium represents a daunting challenge. Experimental dissection of these processes are complicated by the heterogeneous nature of ADP-ribosylation, which needs to be addressed by the development of specialized analytical methods.

Substantial progress has been made to understand the mechanisms that contribute to ADP-ribosylation reversal, yet several obstacles need to be overcome: (1) Sensitive and reproducible methods to monitor physiological MAR and PAR levels in cells are difficult to implement; (2) better methods are needed to evaluate site-specific PAR chain length distribution in ADP-ribosylated substrates; (3) measuring kinetics and performance of erasers are precluded by the lack of standardized and defined substrates; (4) the ADP-ribosylation conjugation chemistry and linkage selectivity of erasers need to be further clarified; (5) enzyme-specific targets and interactors, especially for the MARTs and ARHs, remain largely unknown; (6) the modulatory effect of many ADP-ribose readers, which have multiple binding sites for the same ligand is largely unresolved; (7) the biological relevance of site-specific ADP-ribosylation events is often difficult to determine.

Despite these obstacles and intricacies, the machinery responsible for the processing of ADP-ribose is now beginning to be revealed. A more detailed understanding of the interplay between ADP-ribosylation writers, readers and erasers, at a molecular level, will be required to correlate these dynamics with cellular responses and translate them into clinical applications.

1.8 **Figures and Legends**

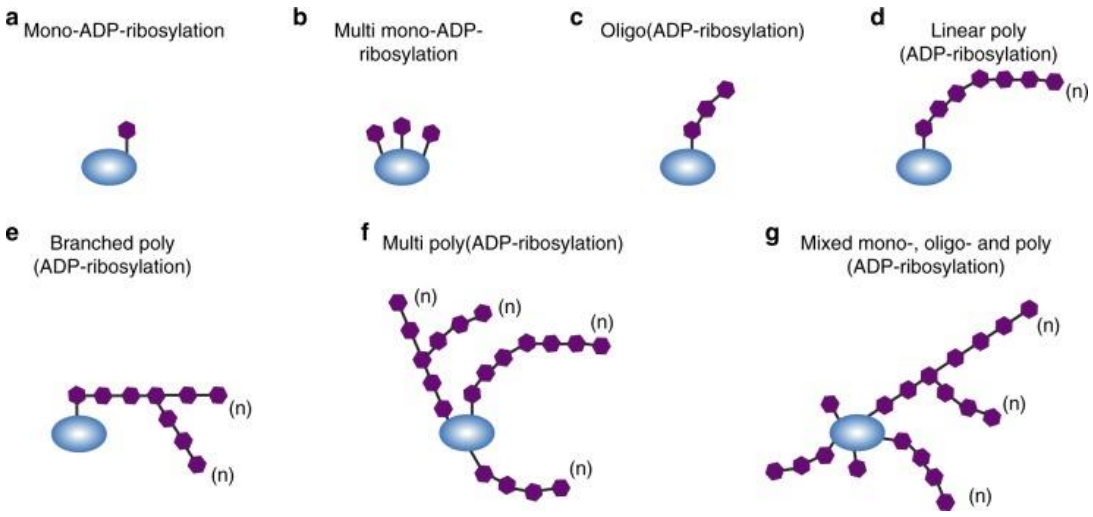

Figure 1.1 Possible patterns of ADP-ribosylation on target proteins.

a) Mono-ADP-ribosylation; a single ADP-ribose molecule is attached to the protein. **b)** Multi mono-ADP-ribosylation; multiple single ADP-ribose units are bound along the protein. **c)** Oligo(ADP-ribosylation); short linear chains of ADP-ribose are transferred to the protein. **d)** Linear poly(ADP-ribosylation); ADP-ribose moieties forming a long linear chain up to 200 units in length. **e)** Branched poly(ADP-ribosylation); complex molecules composed of large and branched polymers of ADP-ribose. **f)** Multi poly(ADP-ribosylation); multiple PAR chains either linear or branched on the same protein. **g)** Mixed ADP-ribosylation; a mixture of the previously described ADP-ribose patterns on the same protein, generated either by the combined action of MAR- and PAR transferases or by the degradative action of erasers.

Table 1.1: Human ADP-ribose Erasers

Table 1 Human ADP-ribose erasers							
Eraser	**Classification**	**Substrate**	**Targeted bond**	**ADP-ribosylation reversal**	**Protein adducts**	**Amino acid selectivity**	**References**
PARG	Macrodomain	PAR	O-glycosidic	Partial	ADP-ribose	Linkage-independent	139, 154
MacroD1	Macrodomain	MAR	Carboxyl ester	Complete	None	D/E	199
MacroD2	Macrodomain	MAR	Carboxyl ester	Complete	None	D/E	199
TARG1	Macrodomain	MAR/PAR	Carboxyl ester	Complete	None	D/E	173
ARH1	ARH fold	MAR	N-glycosidic	Complete	None	R	163
ARH3	ARH fold	MAR/PAR	O-glycosidic	Complete	None	S	161,163
NUDT9	NUDIX	PAR	Phosphodiester	Partial	Phosphoribose	Linkage-independent	180
NUDT16	NUDIX	MAR/PAR	Phosphodiester	Partial	Phosphoribose	Linkage-independent	180,181
ENPP1	ENPP (PDNP)	MAR/PAR	Phosphodiester	Partial	Phosphoribose	Linkage-independent	182

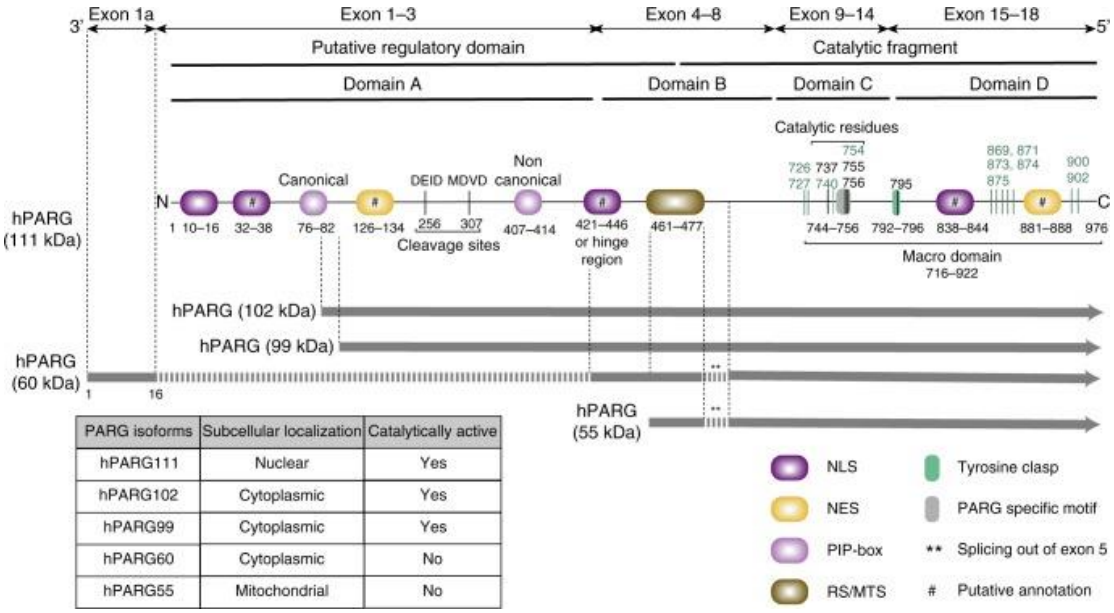

PARG isoforms	Subcellular localization	Catalytically active
hPARG111	Nuclear	Yes
hPARG102	Cytoplasmic	Yes
hPARG99	Cytoplasmic	Yes
hPARG60	Cytoplasmic	No
hPARG55	Mitochondrial	No

Figure 1.2: Schematic representation of human PARG and its isoforms.

Human PARG originates from a 3198 bp mRNA sequence with a single 2931 bp open reading frame (ORF). The ORF contains 18 exons and encodes a protein of 976 amino acids with a molecular weight of 111.1 kDa. This mRNA undergoes alternative splicing to produce different PARG isoforms. Five human PARG transcripts have been identified. Full-length human PARG (hPARG111) contains an N-terminal regulatory domain and a C-terminal catalytic domain that is essentially a macrodomain fold. hPARG102 and hPARG99 are translated from the start codons located in exon 2 and exon 3, respectively. hPARG60 results from alternative splicing that connects exon 1a, exon 4, and exons 6–18. Because of the usage of a facultative exon (exon 1a), hPARG60 has an alternative N-terminal protein sequence of 16 amino acids that is unique to this isoform. hPARG55 is produced from the initiation of translation at the start codon located in exon 4. Exon 5 is

spliced out in both hPARG60 and hPARG55 isoforms. PARG can be sub-classified into four different domains. Domain A, which includes exons 1–3, forms the majority of the putative regulatory domain. This region contains two caspase-3 cleavage sites at amino acid position 256 (DEID) and 307 (MDVD). An uncharacterized nuclear localization signal (NLS) overlaps with a hinge region between the putative regulatory domain and the catalytic fragment. Furthermore, PARG comprises domain B (exons 4–8), domain C (exons 9–15) and domain D (exons 15–18). The latter two domains form the base of the macrodomain fold and contain the catalytic pocket and ligand binding sites. The catalytic residues (Asp737, Glu755, and Glu756) and Tyr795, which interacts with PARG inhibitor ADP-HPD are indicated as black lines. Residues colored in green have been implicated in the binding of ADP-ribose. Furthermore, colored boxes denote PARG-specific motif (GGG-X6–8-QEE), regulatory segment/mitochondrial targeting sequence (RS/MTS), Tyrosine Clasp structural motif, PCNA-interacting protein (PIP) motif, and nuclear export signal (NES).

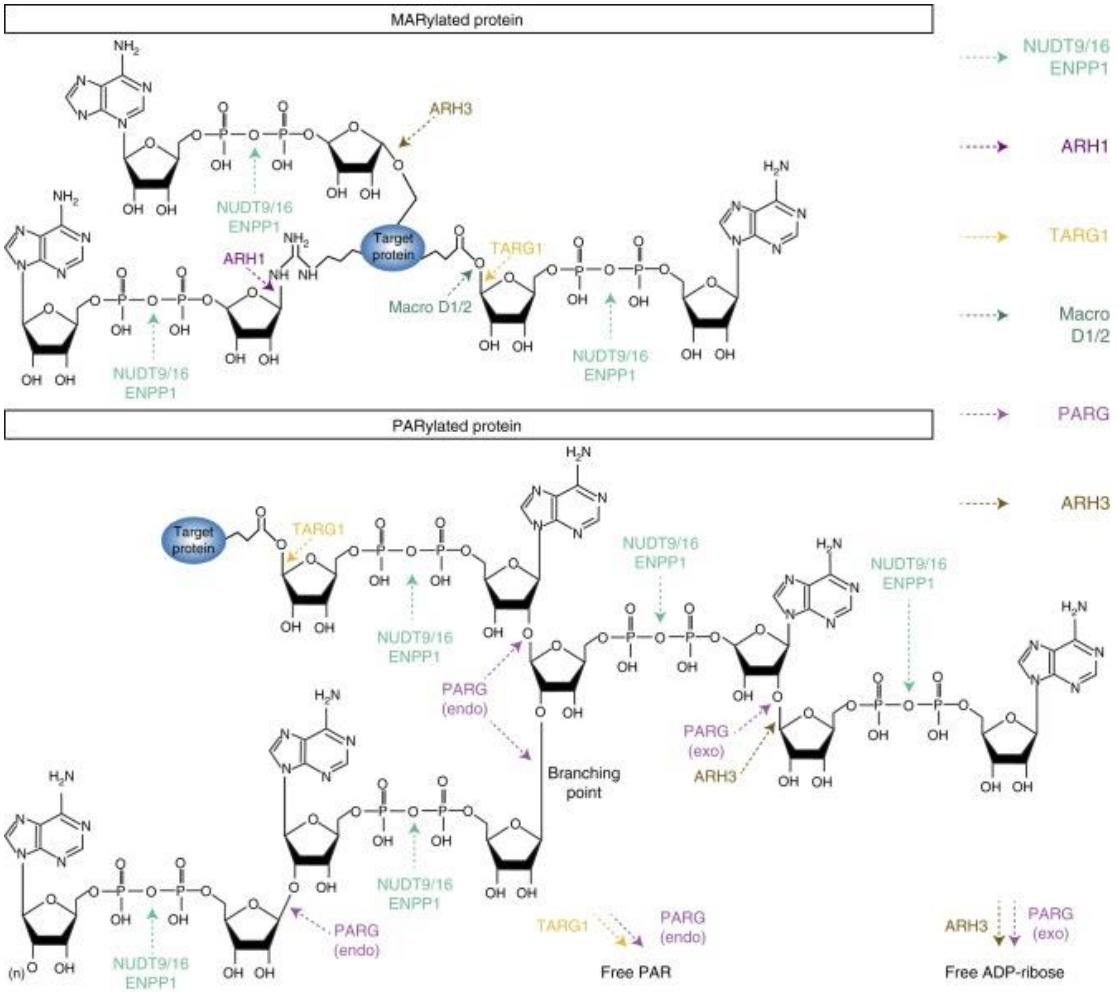

Figure 1.3: Reversal of protein ADP-ribosylation by MAR and PAR erasers.

The diagrams represent MARylated (upper panel) and PARylated proteins (lower panel) with bond-specific chemical cleavage sites for each eraser. A subgroup of erasers that comprises MacroD1, MacroD2, and ARH1 are MAR-specific erasers involved in the removal of single ADP-ribose adducts. MacroD1 and MacroD2 are macrodomain-containing enzymes that release ADP-ribose from ADP-ribosylated acidic residues (aspartate and glutamate). ARH1 is currently the only known MAR hydrolase that specifically removes MAR from arginine residues. A second subgroup that includes TARG1, ARH3, NUDT9, NUDT16, and ENPP1 can target both MAR and PAR modifications. The TARG1 macroprotein hydrolyzes glutamate-ADP-ribose bonds and releases ADP-ribose from MARylated proteins. TARG1 has also the unique ability to remove entire PAR chains from acidic residues of PARylated proteins. ARH3 is limited to exoglycosidic activity toward PAR chains and releases free ADP-ribose. In addition, it possesses MAR hydrolase activity specifically targeting the O-linked ADP-ribosylation. NUDT9 and NUDT16 have nucleoside diphosphate-linked moiety-X (NUDIX) domains, which cleave pyrophosphate bonds and release phospho-ribosyl-AMP from PAR chains or AMP from MARylated proteins as major reaction products. ENPP1 is a pyrophosphatase lacking a NUDIX domain but with the capability of digesting PAR and MAR modifications similar to NUDIX enzymes. PARG is the main PAR-degrading enzyme but shows no activity towards MARylated proteins. Human PARG is unable to cleave the proximal ADP-ribose groups from a modified protein but possesses exo- and endoglycosidic activities to hydrolyze the glycosidic bonds between ribose units of PAR. The exoglycosidic activity of PARG generates free ADP-ribose from the processive degradation of PAR from the distal to the proximal end while its in-chain cleavage activity (endoglycosidic) produces protein-free PAR. The endoglycosidic degradation of PAR by of PARG is also responsible for the hydrolysis of the branching points formed when non-adenine riboses are linked together (branching point).

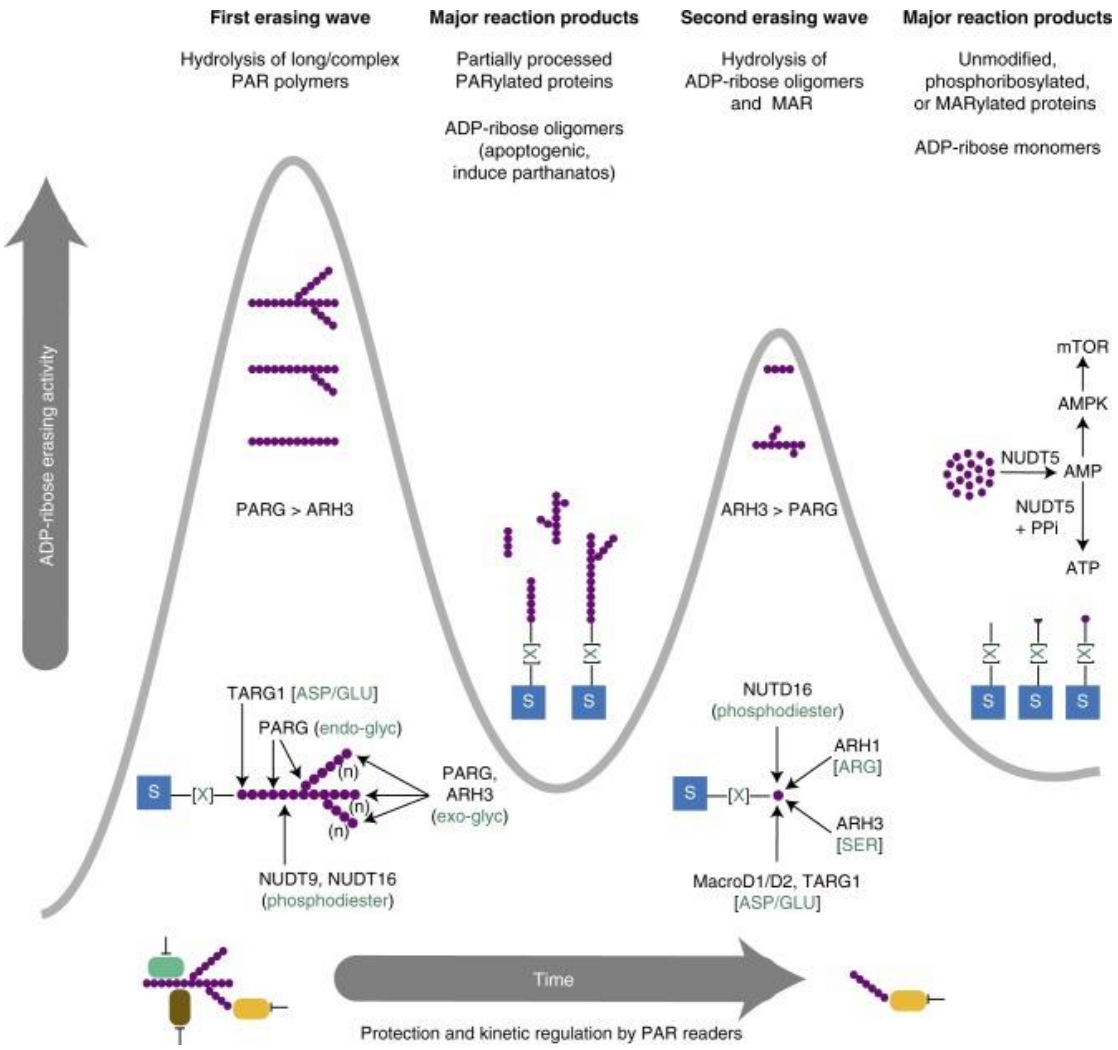

Figure 1.4: The dynamic mechanism of ADP-ribosylation reversal.

ARTDs consume NAD^+ and transfer ADP-ribose moieties onto target substrates (blue boxes) on different amino acids side chains (green [X]). These proteins can have a variety of different ADP-ribosylation modification patterns, as described in Fig. 1. In the context of severe genotoxic insult, complex PAR polymers composed of large and branched molecules are synthesized by ARTD1 and ARTD2 (PARP-1 and PARP-2). These polymers are rapidly recognized and processed by a variety of erasers in a biphasic mode. At the same time, a variety of PAR readers can bind PAR and regulate the kinetics of the erasing process. In the first phase of the ADP-ribosylation reversal, PARG activity predominates and presumably exceeds ARH3 activity since PARG possesses high affinity for complex polymers and a very rapid and processive exoglycosidic activity toward ribose-ribose linkages. The dePARylation process is enhanced by the unique ability of PARG to cleave in-chain ribose-ribose linkages and branching points owing to its

endoglycosidic activity. In addition, TARG1 can contribute to protein dePARylation by detaching entire PAR chains through cleavage of the proximal protein−ribose linkage. As PAR polymers are rapidly shortened by the combined endo- and exoglycosidic activities of PARG, the dePARylation activity drops and partially trimmed apoptogenic ADP-ribose oligomers accumulate. These small PAR fragments induce a second erasing wave in which rate and processivity of PARG is markedly decreased while ARH3 activity becomes dominant. The residual PARG activity and ARH3-catalyzed PAR hydrolysis generate MARylated proteins, which are further degraded by amino acid-specific MAR hydrolases and NUDIX phosphodiesterases. These waves of ADP-ribosylation erasing generate unmodified, phosphoribosylated, and MARylated proteins as well as free ADP-ribose. The latter might be deleterious for the cells and thus recycled by NUDT5 to quickly replenish ATP levels or converted to AMP which activates the AMP kinase (AMPK) and the mTOR signalling pathway.

Chapter 2 Poly(ADP-ribose) polymerase-1 antagonizes DNA resection at double-strand breaks

Marie-Christine Caron[1,2,7], Ajit K. Sharma[3,7], **Julia O'Sullivan**[1,2], Logan R. Myler[4], Maria Tedim Ferreira[2,5], Amélie Rodrigue[1,2], Yan Coulombe[1,2], Chantal Ethier[2,5], Jean-Philippe Gagné[2,5], Marie-France Langelier[6], John M. Pascal[6], Ilya J. Finkelstein [4], Michael J. Hendzel[3], Guy G. Poirier[2,5] & Jean-Yves Masson[1,2]

[1]Genome Stability Laboratory, CHU de Québec Research Center, HDQ Pavilion, Oncology Division, 9 McMahon, Québec City, QC G1R 3S3, Canada.

[2]Department of Molecular Biology, Medical Biochemistry and Pathology, Laval University Cancer Research Center, Québec City, QC G1V 0A6, Canada.

[3]Department of Oncology, Faculty of Medicine and Dentistry, University of Alberta, 11560 University Avenue, Edmonton, AL T6G 1Z2, Canada.

[4]Department of Molecular Biosciences, University of Texas at Austin, Austin, TX 78712, USA.

[5] CHU de Québec Research Center, CHUL Pavilion, Oncology Division, 2705 Boulevard Laurier, Québec City, QC G1V 4G2, Canada.

[6]Biochemistry and Molecular Medicine, Université de Montréal, 2900 Boulevard Edouard-Montpetit, Pavillon Roger-Gaudry, Montréal, QC H3T 1J4, Canada.

[7]These authors contributed equally: Marie-Christine Caron, Ajit Sharma.

Preface

When I joined the lab, I was fortunate enough that this incredible project characterizing the role of PARP-1 in HR was already underway. It is through this project I was able to learn many of the techniques used in the lab while also contributing to what would be an excellent trove of PARP-1 knowledge for the field. PARP-1 is such an abundant protein that has been linked to so many different processes in the cell that identifying its function has been a complicated and time-consuming affair. Our article published in Nature Communications in 2019, entitled "**Poly(ADP-ribose) polymerase-1 antagonizes DNA resection at double-strand breaks**" (Marie-Christine Caron= Ajit K. Sharma=, Julia O'Sullivan, Logan R. Myler, Maria Tedim Ferreira, Amélie Rodrigue, Yan Coulombe, Chantal Ethier, Jean-Philippe Gagné, Marie-France Langelier, John M. Pascal, Ilya J. Finkelstein, Michael J. Hendzel, Guy G. Poirier & Jean-Yves Masson) is the accumulation of our work exploring the role of PARP-1 in DNA resection.

This paper represents a collaborative effort from several laboratories, chiefly the laboratories of my co-supervisors Dr Jean-Yves Masson and Dr Guy Poirier and their close collaborated Dr Michael Hendzel. I started in the laboratory under the supervision of Marie-Christine Caron while working on this project, learning many of the techniques in the laboratory from protein purification, *in vitro* resection to immunofluorescence. I contributed directly to figures 2.4 and 2.7 and the supplemental figures 2.6, 2.8 and 2.9. Not only did this give me the opportunity to learn what was already established in the laboratory, but it also allowed me to explore a new technique which was not part of the laboratory repertoire in the form of the SMART DNA resection assay. For me this perfectly represents our laboratory, in that not only do we make good use of the standard techniques we have but we are always growing our technical know-how in order to best explore the world of DNA repair. A copy of the PDF of this article can be found in the annexe.

Résumé

PARP-1 est rapidement recrutée et activée aux cassures double-brin de l'ADN (DSB). Lors de son activation, PARP-1 synthétise un polymère structurellement complexe composé d'unités ADP-ribose qui facilite la relaxation locale de la chromatine et le recrutement de facteurs de réparation de l'ADN. Ici, nous identifions une fonction pour PARP-1 dans la résection de l'ADN aux DSB. De manière remarquable, l'inhibition de PARP-1 conduit à l'ADN hyper-résecté. Nous démontrons que la perte de PARP-1 et l'hyper-résection sont associées à la perte des inhibiteurs de résection Ku, 53BP1 et RIF1 aux sites de cassures. L'analyse par *DNA curtains* montre que la résection médiée par EXO1 est bloquée par PARP-1. En outre, l'abrogation de PARP-1 conduit à une augmentation des de la résection de l'ADN et à une augmentation de la recombinaison homologue *in cellulo*. Nos résultats placent donc l'activation de PARP-1 comme événement critique précoce pour l'activation de la réparation des DSB de l'ADN et la régulation de la résection. Par conséquent, nos travaux ont des implications directes pour l'utilisation clinique et l'efficacité de l'inhibition de PARP, qui est prescrite pour le traitement de diverses tumeurs malignes.

Abstract

PARP-1 is rapidly recruited and activated by DNA double-strand breaks (DSBs). Upon activation, PARP-1 synthesizes a structurally complex polymer composed of ADP-ribose units that facilitates local chromatin relaxation and the recruitment of DNA repair factors. Here, we identify a function for PARP-1 in DNA DSB resection. Remarkably, inhibition of PARP-1 leads to hyperresected DNA DSBs. We show that loss of PARP-1 and hyperresection are associated with loss of Ku, 53BP1 and RIF1 resection inhibitors from the break site. DNA curtains analysis show that EXO1-mediated resection is blocked by PARP-1. Furthermore, PARP-1 abrogation leads to increased DNA resection tracks and an increase of homologous recombination *in cellulo*. Our results, therefore, place PARP-1 activation as a critical early event for DNA DSB repair activation and regulation of resection. Hence, our work has direct implications for the clinical use and effectiveness of PARP inhibition, which is prescribed for the treatment of various malignancies.

2.1 **Introduction**

Each day, the eukaryotic genome is confronted with up to 50 endogenous DNA double-strand breaks (DSBs)[415]. These are extremely hazardous for a cell, because if left unrepaired, DSBs can have pathological consequences, such as cell death, or drive cells to genomic instability and tumor development. The cellular response to DNA damage involves an intricate network of enzymes responsible for sensing, signaling, and repairing damaged DNA, as well as the regulation of cell cycle checkpoints that collectively maintain genomic integrity[16].

Poly(ADP-ribose) polymerase-1 (PARP-1) is an abundant and ubiquitous nuclear protein that uses NAD^+ to synthesize a multibranched polyanion composed of ADP-ribose moieties, giving rise to poly(ADP-ribose) (PAR), onto itself or a variety of target proteins. Protein ADP-ribosylation permits the transfer of the ADP-ribose moiety from NAD^+ to the side chain of several amino acids[96, 186, 416]. Predominant biological processes targeted by PARylation include RNA splicing, processing, and maturation, DNA replication, and transcription as well as the DNA damage response (DDR)[184, 190, 416]. PARP-1 acts as a highly sensitive sensor for DNA damage and rapidly produces PAR at newly generated DNA DSBs. This promotes local chromatin relaxation due to its negative charge[417] and histone displacement[418], as well as facilitating the recruitment of repair factors, such as MRE11[24]. Several PAR-binding modules orchestrate the relocation of DDR-associated factors in addition to the accumulation of intrinsically disordered proteins through an intracellular liquid demixing mechanism[135, 419]. PARP-1 is responsible for 80–90% of the global PAR synthesis following DNA strand breakage[420]. The dynamic turnover of PAR within seconds to minutes is executed by poly(ADP-ribose) glycohydrolase, the main PAR-degrading enzyme, which possesses both endoglycosidic and exoglycosidic activities, thereby enabling a new round of DNA damage signaling[146]. More recently, it has been shown that PARP-1 inhibition increases the speed of fork elongation and does not cause fork stalling, which is in contrast to the accepted model in which inhibitors of PARP induce fork stalling and collapse[421]. It was also recently shown that PARP-1 is a sensor of unligated Okazaki fragments during DNA replication[422] and cells deficient in ribonucleotide excision repair are sensitized to PARP inhibition[423].

PARP-1 is the best-characterized member of the diphtheria toxin-like ADP-ribosyl transferases (ARTDs) family of proteins. Among the 17 ARTDs members, only PARP-1, PARP-2, and PARP-3 are activated by DNA strand breaks[61, 89, 241]. De Murcia and colleagues provided the first evidence implicating PARP-1 in DNA repair by demonstrating that PARP-1-deficient mice are highly sensitive to γ-irradiation[114]. PARP-1 plays a critical role in DSB sensing and we have shown that PARP-1 recruitment and activation occur within 100 ms after introduction of DSBs. This makes PARP-1 activation one of the earliest and most critical events in the sensing of DSBs. Consistent with this, PARP-1 activity increases the rate of recruitment of the MRE11-RAD50-NBS1 (MRN) complex[24] and stimulates Ku binding in Dictyostelium[424]. Structural analyses of PARP-1 have shown that PARP-1 binds DSBs. It does so through interactions with its zinc fingers and a WGR domain[93, 94, 425].

In mammalian cells, most DSBs are repaired using long homologous sequences (homologous recombination (HR)), microhomology-mediated end joining, or no homology end joining (NHEJ). A key event that controls the DSB repair pathway choice is DNA end resection, which is characterized by 5′ to 3′ degradation of one strand at each side of the break. HR is initiated by CtBP-interacting protein (CtIP), a key molecular switch that controls DNA end resection and interacts with BRCA1. Although BRCA1 is a CtIP-interacting protein, there are conflicting reports on the roles of BRCA1 in DNA resection. While an early report found that disrupting the CtIP–BRCA1 interaction in DT40 cells diminished DNA-end resection[73], a later report showed that CtIP mutated at Ser332, which is required for interaction with BRCA1, is competent for RPA and Rad51 assembly, indicating that resection is proficient in this background[74]. More recently, the CtIP–BRCA1 complex was found not to be essential for DNA end resection but rather modulated its speed[75]. The resection process is controlled by two core resection machineries in human cells: BLM–DNA2–RPA–MRN and EXO1–BLM–RPA–MRN[71]. DNA resection is also negatively regulated by the HELB helicase in an RPA-dependent manner[176] and by 53BP1 and RIF1 proteins[49, 426].

Many years ago, we demonstrated that MRE11 and NBS1, which are core components of the early DSB sensing complex MRN, are recruited in a PARP-1-dependent manner to laser-induced DNA damage tracks. MRE11 was further shown to interact non-covalently with PAR via its intrinsically disordered glycine- and arginine-

rich region, an interaction that modulates the resection functions of MRE11[24]. We have previously shown that PARP-1 can interact with Ku70 and Ku80[427] and PARP-1 activity is necessary for Ku binding in Dictyostelium through PAR binding by Ku70[424]. Importantly, PARP-1 activation precedes the recruitment of both the MRN and the Ku complex, previously recognized as the primary DSB sensors that recruit signaling proteins at DSB sites. Because the Ku complex and MRN bind PAR, PARylation may serve to guide and concentrate the Ku and MRN complexes at DSBs to facilitate their loading. As MRN is the initiator of DNA resection while the Ku complex inhibits end resection, we set out to determine whether PARP-1 could affect DNA resection.

The hypersensitivity of HR-deficient cancers to PARP inhibitors (PARPi) provided a conceptual basis for synthetic lethality. PARPi are currently being tested in over 200 clinical studies, with at least 50 trials in phase III (www.clinicaltrials.gov). Because of their specific mechanism of action, PARPi show a low toxicity profile[428]. PARPi has proven to be of significant clinical benefit, even for patients without HR deficiencies. Defining how PARP-1-dependent DNA processing functions mechanistically will help identify genetic markers of sensitivity and resistance to guide PARPi therapy by identifying patients most likely to respond to either single agent or combination therapy through cytotoxic or radiation chemopotentiation[429]. Here, we identify PARP-1 as a critical regulator of DNA end resection of DSBs. We show that PARP-1 recruitment protects DNA ends from nucleolytic degradation and inhibition of PARP-1 leads to hyper-resected DNA double-strand breaks. Our data provide an alternative mechanism by which PARPi function in the presence of irradiation (IR).

2.2 **Results**

2.2.1 Recruitment of PARP-1 and PARP-2 at laser-induced DNA breaks

We initially scrutinized the recruitment kinetics of PARP-1 to laser-induced DNA damage. Consistent with previous findings[112, 430] , we observed that PARP-1 is recruited rapidly to laser-induced DNA damage tracks within milliseconds

(Supplementary Fig. 1). The dynamics of PARP-1 recruitment under normal conditions was compared with the dynamics observed under PARP inhibition with BMN 673 (Talazoparib). The initial rapid accumulation of PARP-1 at sites of damage was followed by a steady reduction over the next 10 min, while in the presence of BMN 673, PARP-1 is lost from the damage site more slowly, possibly due to trapping at DSBs[140]. Similar to PARP-1, PARP-2 retention at laser-induced DNA lesions is normally transient, with a slow decline after an initial maxima at approximately 2 min post damage. However, in cells exposed to BMN 673, an initial rapid accumulation is observed, but rather than decline, there persists a slowly increasing accumulation of PARP-2 over the 10 min experiment (Supplementary Fig. 2). Because the ultrafast recruitment of PARP-1 at DNA lesions precedes and primes the accumulation of other DNA damage repair factors, including the MRN complex, and because PARylation is a determining factor for their local accumulation, we reasoned that PARylation-dependent events might also affect DSB repair pathway choice through DNA end resection.

2.2.2 Effect of PARPi on DNA end resection

We used two different methods to determine whether PARP-1 itself or its catalytic activation influences DNA resection. First, we used a bromodeoxyuridine (BrdU)-based assay for visualizing the single-stranded DNA (ssDNA) product of resection. Second, we measured the accumulation of replication protein A (RPA). RPA is an essential trimeric protein complex that binds to ssDNA in eukaryotic cells. It is recruited to sites of DNA damage when regions of ssDNA are exposed. Hence, it serves as a readout for resection and for ongoing HR. Thus the amount of RPA that accumulates at each site should reflect the amount of ssDNA. Remarkably, both PARP-1 inhibition by BMN 673 or small interfering RNA (siRNA)-mediated PARP-1 silencing led to a substantial increase in the generation of ssDNA as measured by BrdU intensity in U2OS or HeLa cells (Fig. 2.1a, c). This was further confirmed using CRISPR/Cas9-mediated knockout of PARP-1 in 293T cells (Supplementary Fig. 2a, b). We quantified this data by measuring the total amount of BrdU (or RPA) in each focus. The summed intensity values for each individual focus reveals a greater than two-fold increase in the average amount of ssDNA generated per DSB (focus) when PARP-1 is inhibited by BMN 673 or silenced by siRNA. Consistent with an accumulation of RPA foci following pharmacological inhibition of

PARP-1 or PARP-1 knockdown (Fig. 2.1d, b, Supplementary Fig. 3C), we observed an overall increase of chromatin-bound and phosphorylated RPA (Fig. 2.1e). Microirradiation experiments also showed enhanced recruitment of GFP-RPA1, GFP-RPA2, or GFP-RPA3 in S-phase cells following pharmacological inhibition of PARP-1 (Fig. 2.1f, Supplementary Fig. 3E, F). It is well known that the activation of the ATR kinase following perturbations in S-phase relies on a complex mechanism involving ATR recruitment to RPA-coated ssDNA. Consistent with an increase in RPA recruitment in PARP-1 knockdown cells, the activation of ATR was enhanced as judged by using anti-ATR Thr-1989 as a proximal marker of ATR activation[431] (Supplementary Fig. 3G).

To rule out the possibility that PARP-1 plays an indirect role that promotes the accumulation of ssDNA, we repeated the BrdU-based assay with a knockdown of CtIP, which is expected to suppress DNA resection at DSBs[432]. The simultaneous knockdown of PARP-1 and CtIP completely suppressed the accumulation of ssDNA, implying that knockdown of PARP-1 affects the DSB resection process and does not promote a resection-independent accumulation of ssDNA (Fig.2.1g, Supplementary Fig. 4A, B). CtIP foci formation was also increased in PARP-1 knockdown cells (Supplementary Fig. 4C, D). The accumulation of ssDNA was not observed in DNA Ligase IV knockdown cells, suggesting that cells compromised in later stages of NHEJ do not share this phenotype (Supplementary Fig. 4E). Since we are monitoring DNA resection products 3 h after IR, we ascertained that the above results were not a consequence of an accumulation of cells in S/G2 (Supplementary Fig. 5A, B). In addition to the intensity, the number of BrdU or RPA foci per nucleus were increased in BMN 673-treated U2OS cells or PARP-1-silenced HeLa cells compared to controls (Supplementary Fig. 5C–F). Treatment with another PARPi, Veliparib, caused also an enhancement of BrdU or RPA intensity per nucleus (Supplementary Fig. 6A, B).

To quantify ssDNA at the sites of DSBs, we used the ER-*Asi*SI system in which the restriction enzyme *Asi*SI is fused to the estrogen receptor hormone-binding domain. Upon treatment with 4-hydroxytamoxifen (4-OHT), the *Asi*SI nuclease translocates to the nucleus and generates up to 150 DSBs at sequence-specific sites[26, 433]. In this system, the presence of DSB resection will lead to the generation of ssDNA that cannot be cleaved by the duplex DNA-specific endonuclease *Bsr*GI before PCR. In the absence of DNA resection, the remaining double-stranded DNA (dsDNA) will be cleaved, therefore

yielding no PCR products (Fig. 2.2a). Thus the system can be used to distinguish between ssDNA and dsDNA. Interestingly, PARP-1 depletion or inhibition by BMN 673 (Fig. 2.2b) led to a ~30% increase in DNA resection compared to the control at two different sites (Fig. 2.2c). Similarly, PARP-1 inhibition led to a ~3–6-fold increase in bound RPA2 to processed DSBs (Fig. 2.2d). Altogether, these results show that PARP-1 limits DNA processing *in cellulo*.

2.2.3 PARP-1 knockdown cells show decreased 53BP1 and RIF1 foci

The mechanism underlying PARP-1-regulated DNA resection was investigated further. We monitored the accumulation of the resection inhibitors 53BP1 and RIF1 in G1 cells (Fig. 2.3a, b) depleted of PARP-1. Interestingly, PARP-1 inhibition led to a decrease of 53BP1 and RIF1 foci following etoposide treatment (average number of foci = 46 in the control and 28 in PARP-1 knockdown for 53BP1, and average number of foci = 27 in the control and 11 in PARP-1 knockdown for RIF1). These results were corroborated by chromatin immunoprecipitation (ChIP) analysis using cells stably expressing mCherry-*Lac*I-*Fok*I at an integrated reporter transgene (U2OS-DSB-reporter system (Fig. 2.3c)), which showed a drastic reduction of 53BP1 (Fig. 2.3d) or RIF1 accumulation (Fig. 2.3e) on two different DSBs in PARP-1 knockdown or BMN 673-treated cells.

2.2.4 PARP-1 blocks DNA resection by MRN-RPA-BLM-EXO1-DNA2

The above data suggest that PARP-1 may be able to directly suppress the activity of DNA resection enzymes. We further examined whether purified PARP proteins (Fig. 2.4a) could block DNA resection *in vitro*. We monitored DNA resection of a 3′-end-labeled dsDNA (2.7 kb) via the two main DNA resection machineries MRN-RPA-BLM-EXO1 or MRN-RPA-BLM-DNA2. In the absence of PARPs, the MRN-RPA-BLM-EXO1 assembly resected ~75% of the 2.7 kb substrate (Fig. 2.4b). When the reaction was supplemented with PARP-1, a concentration-dependent inhibition was observed. At 50 nM PARP-1, only 10% of the DNA could be resected within the 60 min incubation time, without NAD or at a NAD concentration that still supports DNA binding. As

specificity controls, we also performed similar reactions with PARP-2 and PARP-3. Importantly, PARP-2 and PARP-3 enzymes did not inhibit MRN-RPA-BLM-EXO1-mediated DNA degradation. PARP-1 also blocked the MRN-RPA-BLM-DNA2 complex and PARP-1-mediated inhibition was retained with the catalytic mutant E988K but abolished when a PARP-1 fragment devoid of its zinc fingers (PARP-1 216-1014) was used (Fig. 2.4c, Supplementary Fig. 6C). PARP-1 216-1014 has been reported to have a severely decreased affinity (250-fold less) for DNA lesions compared to wild-type (WT) PARP-1[93]. PARP-1 blocked the resection complexes at 5 and 30 μM concentration of NAD^+, where PARP-1 undergoes only moderate PAR automodification (Supplementary Fig. 6D, E) and remains bound to DNA (Fig. 2.4b–d, Supplementary Fig. 6F, G). In contrast, the higher NAD^+ concentration of 250 μM NAD^+, where PAR automodification releases PARP-1 from DNA, prevented PARP-1 inhibition of resection (Fig. 2.4e, Supplementary Fig. 6F, G). Since even low levels of PAR alone could sequester protein components of the resection reaction leading to suppression of DNA resection, we performed reactions with protein-free PAR (Fig. 2.4f). This failed to inhibit DNA resection. These results show that PARP-1 but not PARP-2, PARP-3, or PAR can robustly inhibit DNA resection through a direct DNA-binding mechanism.

We used a high-throughput single-molecule DNA curtain assay to directly observe how PARP-1 inhibits EXO1 processing of substrate DNA. Arrays of DNA molecules (48.5 kb, derived from λ-phage) were assembled on the surface of a microfluidic flowcell coated with a surface-passivating fluid lipid bilayer[434]. The DNA substrate was linked to the bilayer via a biotin–streptavidin linkage. Fluorescently labeled PARP-1 was injected into the flowcell and visualized using total internal reflection fluorescence microscopy on thousands of DNA molecules for high-throughput data collection and analysis (Fig. 2.5a). Nearly all PARP-1 molecules were bound to the end of the DNA. This conclusion is based on the observation that turning off buffer flow led to the coordinated retraction of both the DNA and associated PARP-1 molecules to the diffusion barrier (Fig. 2.5b, c). Most PARP-1 molecules localized to the DNA end via binding internally and sliding along the DNA in the direction of buffer flow (88% of PARP-1 molecules, $N = 109/124$). This indicates that PARP-1 is able to diffuse along the DNA and one-dimensional (1D) diffusion may represent a mechanism by which PARP-1 quickly associates with DNA ends or other DNA lesions. In conditions where PARP-1 was pre-bound to the end of DNA molecules (Fig. 2.5d, magenta in right panel), a second

PARP-1 molecule (Fig. 2.5d, green in right panel) bound upstream and slid along the DNA to co-localize at the DNA end. Consequently, the red and green traces can be seen to merge in the kymograph (Fig. 2.5d). Pre-bound PARP-1 blocked DNA resection by preventing EXO1 loading onto the DNA end (Fig. 2.5e–g). This suggests that PARP-1 may physically occlude the end of DNA. In contrast, end-bound PARP-2 did not block EXO1 loading and DNA resection. Consistent with this, microirradiation experiments showed enhanced accumulation of GFP-EXO1 in PARP-1-deficient cells at laser-induced DNA damage sites (Fig. 2.5h) and phosphorylated EXO1 accumulated more in the absence of PARP-1 (Supplementary Fig. 7A). Altogether, our results show that PARP-1 counteracts DNA resection *in vitro*, likely by occluding the free DNA ends from the EXO1 or DNA2 resection machineries.

2.2.5 PARP-1 is required for efficient loading of the Ku complex

Another mechanism whereby PARP-1 could inhibit end resection is through regulation of the association of the Ku complex with DNA ends. Consequently, we performed laser microirradiation experiments to determine whether Ku80-GFP recruitment to sites of DNA damage is sensitive to PARPis (Fig. 2.6a, b). We found that the recruitment of Ku80-GFP was almost completely inhibited in cells treated with PARPi but robustly recruited in control cells. We next tested PARP-1-deficient cells and found that they also fail to efficiently recruit Ku80-GFP to sites of DNA damage (Fig. 2.6c, d). In order to determine the influence of PARP activity on the association of Ku80 with DNA ends, we performed ChIP experiments in the presence or absence of PARP-1 or PARPi (Fig. 2.6e) and in the presence of RNAse to avoid indirect binding through RNA. We find that Ku association with the DSB is dependent on both PARP-1 and PARP-1 activity. Consequently, in addition to acting as a direct inhibitor of DNA end resection, PARP-1 also inhibits end resection by promoting Ku loading onto the DSB. To assess this further on other NHEJ components, we monitored phospho-DNA-PKcs foci formation in PARP-1 U2OS CRISPR/Cas9-mediated knockout cells. Consistent with our previous studies showing a decrease of NHEJ *in cellulo* following ABT-888 treatment[189], a decrease of phosphorylated DNA-PKcs foci was observed (Supplementary Fig. 7B). A Ku80 knockdown in HEK 293T cells leads to enhanced

EXO1 recruitment (Supplementary Fig. 7C), suggesting that the recruitment of Ku80 by PARP-1 is a critical event for regulating EXO1-mediated DNA resection.

2.2.6 Increased resection tracks and HR in PARP-1-deficient cells

Next, we measured DNA resection *in cellulo* using a high-resolution technique to see whether PARP-1 inhibition would lead to increased resection in different genetic contexts. The single-molecule analysis of resection tracks (SMART) assays is a very sensitive technique that can detect DNA resection upon IR, while almost no fibers can be detected without DNA damage[75]. It has been reported that BRCA1 is important to control the speed of DNA resection[75] and that inhibition of 53BP1 in BRCA1-deficient cells rescue these cells through enhanced DNA resection[166]. Hence, our data predict that the DSB-induced over-resection phenotype would not appear in BRCA1-deficient cells when challenged with the PARP-1 inhibitor BMN 673. However, the DNA resection machinery is intact in BRCA2-deficient cells, because BRCA2 acts later in HR, and we should observe this over-resection phenotype under the same conditions. First, SMART assays revealed that PARP-1-deficient cells have longer resection tracks after IR treatment (Fig. 2.7a) and are IR sensitive in survival assays (Fig. 2.7b). When cells were treated with BMN 673 and IR, BRCA1 knockdown led to a decrease of BrdU accumulation, which could be partially rescued by 53BP1 knockdown (Supplementary Fig. 8A, B, D). SMART assays also recapitulated these results (Supplementary Figs. 8C, D and 9A). Conversely, BRCA2 knockdown or DLD1 BRCA2 (−/−) cells showed a similar increase of BrdU staining (Supplementary Fig. 8A, B) or DSB resection tracks following treatment with BMN 673 (Fig. 2.7c) compared to the controls. These results show that PARP-1 inhibition-mediated over-resection of DSBs is achieved when cells have an effective DNA resection machinery.

Based on these results, we hypothesize that PARP-1 plays an important regulatory role in the DNA damage response by influencing DNA resection and consequently DNA repair. HR depends heavily on the extent of DNA resection. To address whether PARP-1 influences HR, we monitored RAD51 foci formation following γ-irradiation (Fig. 2.7d). In agreement with previous findings with an older generation of PARP-1 inhibitors[435], we observed that the percentage of cells harboring >10 RAD51 foci was increased in

HEK 293T cells subjected to CRISPR/Cas9-mediated knockout of PARP-1 (Supplementary Fig. 9B, C) or in cells treated with a siRNA targeting PARP-1 or exposed to PARP-1 inhibition (Fig. 2.7d). In addition, using a doxycycline (Dox)-inducible I-*Sce*I/DRGFP cell line, HR was increased with PARP-1 knockdown (Fig. 2.7e), BMN 673, or ABT 888-treated cells (Supplementary Fig. 9D). Collectively, these results show that PARP-1 negatively regulates HR *in cellulo*.

2.3 **Discussion**

In this study, we show evidence that PARP-1 antagonizes the activity of the MRN-RPA-BLM-EXO1 and MRN-RPA-BLM-DNA2 machineries for DNA DSB repair. Interestingly, PARP-1 mediates this effect through DNA end binding and promoting Ku80 loading. Furthermore, loss of PARP-1 leads to a decrease in the accumulation of HR suppressors 53BP1 and RIF1 at DSBs, which in turn increases the DNA accessibility to EXO1 resulting in excessive degradation of DNA lesions. Such an effect can be obtained with either PARP-1 knockdown or pharmacological inhibition of PARP-1 activity. Thus mammalian cells have evolved several distinct regulatory systems that limit ssDNA overhang formation. First, a PARP-1-dependent mechanism influencing the Ku heterodimer and the 53BP1 pathway, and second, HELB that limits end resection in an RPA-dependent manner[176]. Recent studies have shown that DYNLL1[177] and the Shieldin complex[174, 436, 437] can also counteract DNA resection.

PARP-1 is an abundant nuclear chromatin-associated protein, well characterized for its high DNA damage-sensing ability. Once encountering free DNA ends, PARP-1 is catalytically activated and generates large amounts of PAR, which can function as a scaffold for the recruitment of a variety of DNA repair proteins[135]. It has been proposed that the local accumulation of PAR at DNA damage sites promotes liquid demixing, a phase separation event leading to compartmentalization of repair foci[135]. PAR polymers not only provide a loading platform for DDR-associated proteins and repair factors but also reprograms their functions through spatial and temporal interactions with their PAR reading motifs[135, 189]. We envision that PARP-1 activation orchestrates the initial steps of DNA resection, granting access to the resection machineries. PARP-1 interacts with DNA-PKcs/Ku70/Ku80[438] and mediates this effect through DNA end

binding and recruitment of the Ku complex to DNA ends. Although Ku and PARP-1 have been found to compete for binding to DNA end *in vitro*[53], temporally, PARP-1 precedes Ku loading and its activity is required to load Ku onto DSB ends. This correlates well with the timing of PARP-1-mediated displacement of histones[418], suggesting that PARP-1 activity is necessary to prepare chromatin for loading of Ku onto broken DSB ends. When PARP-1 is absent, neither PARP-1 nor Ku assemble to protect the DNA ends when analyzed by ChIP at nuclease-induced DSBs. Consequently, EXO1 has higher access to DSBs, and with a concomitant decrease of RIF1 and 53BP1, this leads to excessive DNA processing. In line with this observation, using the ER-*Asi*SI system, the group of Tanya Paull has shown that siKu86 or Ku86 conditional HCT116 cells show increased DNA resection[433]. This enhanced DNA resection has been observed in PARP-1 knockdown and PARP-1 knockout using SMART analysis, RPA staining as a surrogate marker of ssDNA accumulation, and native anti-BrdU staining. It is important to note that this excess of ssDNA is dependent on CtIP thereby confirming that the ssDNA detected is generated by DNA end resection. In a similar manner, we also observed excessive DSB processing in Veliparib- or BMN 673-treated cells. Initially, BMN 673 delays the displacement of PARP-1 on DSBs but does not prevent displacement, which reaches completion over a 10 min time frame following laser-induced DNA damage. At that point, it will no longer protect DSB ends, leading to a similar phenotype as a complete deletion of PARP-1 (Model in Fig. 2.8).

Using purified proteins, we also show that PARP-1 directly blocks both the EXO1 and DNA2 end resection machineries. Specifically, PARP-1 is able to slide to the end of DNA. This suggests a search mode employing 1D diffusion, which should stimulate the rate of recognition of newly formed DNA ends relative to three-dimensional diffusion mechanisms. Using single-molecule microscopy, we determined that PARP-1, but not PARP-2, prevents the binding of EXO1 to DNA ends. The structural differences that allow PARP-1 but not PARP-2 or PARP-3 to inhibit end resection would be interesting to determine, given that PARP-1 physically occludes DNA ends from recognition by EXO1. The regulatory zinc finger domains that are unique to PARP-1 are likely to be key to this specificity of function. Our data suggest that, even prior to Ku loading, which strongly prevents the loading of EXO1, PARP-1 acts to block the end resection machinery. This observation fits into a model where both PARP-1 and Ku limit end resection, possibly by controlling the accumulation of the MRN complex[439] and CtIP

and that loss of either PARP-1 or Ku binding results in over-resection. We propose that this mechanism is conserved in pluricellular organisms, as the Iliakis group report that Chinese hamster ovary (CHO) Hamster cells treated with BMN 673 also have elevated DNA processing as measured by RPA foci[440]. PARP-2 has recently been shown to promote DNA resection[122], but since BMN 673 inhibits PARP-2[441], it might not contribute to the over-resection phenotype observed in BMN673-inhibited cells.

Our work provides a conceptual framework to explain many observations reported in previous studies detailing the effects of PARP inhibition in a variety of contexts involving DNA recombination transactions. Since the early 1980s, PARP-1 has been proposed to carry out an antirecombinogenic function. The group of Oikawa et al. first described a positive correlation between PARPis (benzamide and *m*-aminobenzamide) and induction of sister-chromatid exchanges (SCEs) in CHO-K1 cells[442]. Hori demonstrated that reduced NAD as well as inhibition of PARP-1 (using 3-aminobenzamide) lead to a significant increase in SCEs in CHO cells[443]. Morrison et al. using PARP-$1^{-/-}$ mice, provided evidence of PARP-1 functions in maintaining genomic stability by demonstrating that PARP-1 is an anti-recombinogenic factor that inhibits ligation between the DNA termini exposed during (V(D)J) recombination[444]. More recently, it was shown that PARP-1 PARylates BRCA1, and short- and long-track gene conversions, as well as chromosome aberrations after DNA damage, were increased by a BRCA1 PARylation mutant. In addition, treatment with olaparib also led to an enhancement of both types of HR frequencies[445]. Altogether, our data suggest that loss of PARP-1 facilitates HR, through enhanced DNA resection accounting for the (i) increase of sister chromatid exchanges[442]; (ii) anti-recombinogenic function of PARP-1[444]; and (iii) increased HR repair by a BRCA1 PARylation mutant[445]. PARP-1 inhibition-induced HR is in accordance with our previous findings with another PARPi, ABT-888, which remained unexplained at the time[189]. It also mimics the effect of a HELB knockdown, another DNA resection inhibitor[176].

One of the first models proposed to explain the antitumor effects of PARPis in HR-deficient cells was based on the functions of PARP-1 in BER. This model postulated that catalytic inhibition of PARP-1 results in the accumulation of single-strand breaks that could not be repaired in HR-deficient cells. Two observations challenged this model. First, it was not possible to demonstrate increased single-strand breaks after PARP

inhibition[446], and synthetic lethality was not achieved when XRCC1, a key BER protein, was downregulated in BRCA2-deficient cells[447]. Hence, these observations raised the possibility that the effects of PARPis may be mediated through a mechanism distinct from BER. Consistent with this, Patel et al. have shown that deregulated NHEJ plays a major role in generating the genomic instability and cytotoxicity in HR-deficient cells treated with PARPis[447].

We suggest that the observed synthetic lethality and cytotoxicity in different genetic contexts can be related to aberrant DNA resection as consequence of PARP-1 inhibition and DNA damage. Under these conditions, this phenotype will only be attained if DSBs are created and the DNA resection machinery is functional. This conclusion is highlighted by SMART analysis or BrdU staining of BRCA1- and BRCA2-deficient cells. Recent phase III studies have shown that PARPi activity extends beyond BRCA-related cancers for ovarian cancers devoid of known *BRCA* mutations, especially when platinum sensitivity and high-grade serous histology are present[448]. We propose that this effect could be due to misregulation of DNA resection. There are several ongoing clinical trials combining PARP-1 inhibitors with radiation therapy for which our study provides mechanistic insights into the tumor-killing activity observed in the clinic. Collectively, our results highlight that the functionality of DNA resection enzymes in response to DNA damage may be an important criterion to consider for the cell's ability to survive BMN 673 in the presence of DNA damage during clinical interventions in breast/ovarian cancer and other solid tumors.

2.4 Methods

2.4.1 Cell lines, cell culture, drugs, and DNA constructs

Mouse embryonic fibroblasts proficient for PARP-1 (WT), or deficient for PARP-1 (PARP-1 (−/−)) were cultured in Dulbecco's modified Eagle's medium (DMEM) supplemented with 10% fetal bovine serum (FBS) (Hyclone-ThermoFisher Scientific, Ottawa, Canada). U2OS, HeLa, and HeLa PARP-1 SilenciX control (Tebu-bio) were cultured in DMEM with 10% FBS. PARP-1 HeLa SilenciX is a cell line engineered to stably knock down PARP-1 via RNA interference. Cells were maintained under hygromycin B selection (250 μg/mL; Invitrogen). U2OS-PARP-1 (−/−) cells were

cultured in DMEM supplemented with 10% FBS and 2 μg/mL puromycin. U2OS cells stably expressing GFP-RPA2 were maintained in DMEM through continuous G418 selection (500 μg/mL; Invitrogen). The ER-*Asi*SI U2OS cell line was maintained in phenol red-free DMEM media supplemented with 10% charcoal-stripped FBS (Sigma) and 1 μg/mL puromycin. In order to induce DNA damage, AsiS1 U2OS cells were treated with 300 nM 4-OHT for 3 h. U2OS cells stably expressing an mCherry-LacI-FokI construct containing an integrated reporter transgene were maintained in DMEM by puromycin (2 μg/mL) and hygromycin B (100 μg/mL) selection. To induce DNA DSBs, cell lines were treated with both 0.5 mM Shield-1 and 1 mM 4-OHT for 1 h. Human embryonic kidney 293 cells (HEK 293), HEK 293T, or HEK 293T-PARP-1 (−/−) cells were cultured in DMEM supplemented with 10% FBS.

2.4.2 Generation of PARP-1 CRISPR/Cas9

U2OS cells were transfected with the appropriate guide RNA against PARP-1, cloned in a pSpCas9(BB)-2A-Puro (PX459) V2.0. The sgDNA sequence (5′-CGATGCCTATTACTGCACTG -3′) was cloned at the *Bbs*I site into pSpCas9(BB)-2A-Puro (PX459) V2.0 (Addgene plasmid ID: 62988). The positive clone was confirmed by restriction enzyme digestion (*Bbs*I and *Age*I) of purified plasmids to check for insertion and further confirmed by Sanger sequencing. Twenty-four hours later, the transfected cells were selected in medium containing 2 μg/mL puromycin and then subcloned into 96-well plates. Once at sufficient cell density, the subclones were analyzed for the presence of the target protein by western blotting (PARP-1).

2.4.3 Cell fractionation

Cell fractionation was carried out as described in ref. [449] with slight modifications. Briefly, 3×10^6 HEK293T or CRISPR PARP-1 (−/−) cells per condition were collected and resuspended in 200 μL of buffer A (10 mM HEPES pH 8.0, 10 mM KCl, 1.5 mM $MgCl_2$, 0.34 M sucrose, 10 % glycerol, 1 mM dithiothreitol (DTT), 1 mM phenylmethanesulfonylfluoride (PMSF), 0.1 % Triton-X-100, 10 mM NaF, 1 mM Na_3VO_4, supplemented with protease inhibitors) and kept for 5 min on ice. The soluble cytoplasmic fraction (S1) was separated from the nuclei (P2) by centrifugation for 4 min at 1300 × *g* at 4 °C. The nuclear fraction P2 was washed twice with 300 μL buffer A, then

resuspended in 200 µL buffer B (3 mM EDTA, 0.2 mM EGTA, 1 mM DTT, 1 mM PMSF, 10 mM NaF, 1 mM Na_3VO_4, and protease inhibitors) and kept for 30 min on ice. The insoluble chromatin fraction (P3) was separated from nuclear soluble proteins (S3) by centrifugation for 4 min at 1700 × *g* at 4 °C and washed three times with solution B. S1 was cleared of insoluble proteins by centrifugation at 14,000 × *g* for 15 min at 4 °C and the supernatant (S2) was kept for analysis. Cell fractions were subsequently analyzed by western blotting.

2.4.4 Antibodies, reagents, resources, and siRNAs

The antibodies used in this study as well as the working dilutions are listed in Supplementary Table 2.1. Key reagents or resources are listed in Supplementary Table 2.2. siRNAs are listed in Supplementary Table 2.3.

2.4.5 Western blot analysis

Total cell lysates were prepared by lysing cells in RIPA buffer (25 mM Tris–HCl, 125 mM NaCl, 1% Nonidet-P-40, 0.5% sodium deoxycholate, 0.1% sodium dodecyl sulfate (SDS), and a complete protease inhibitor cocktail (Roche)). Equal amounts of total protein were separated by SDS–polyacrylamide gel electrophoresis and then transferred to polyvinylidene difluoride membrane (BioRad) and immunoblotted with antibodies (Supplementary Table 2.1). When secondary antibodies conjugated with infrared-specific dyes (either Alexa Fluor 680 or Alexa Fluor 750) were used, fluorescence was imaged on the Odyssey Infrared Imaging system (LiCor Biosciences).

2.4.6 Transfection and siRNA

Transient siRNA transfections were carried out with Lipofectamine RNAiMax (Invitrogen) or Oligofectamine (Thermo Fisher Scientific) and analyses were performed 48–72 h after siRNA transfection. The siRNAs used in this study can be found in Supplementary Table 2.3.

2.4.7 Immunofluorescence staining

The effect of PARP-1 knockdown on IR-induced DNA end-resection was analyzed by immunofluorescence staining against RPA2 and BrdU. For RPA2 immunodetection, cells were pre-extracted with RPA buffer (25 mM HEPES pH 7.9, 300 mM sucrose, 50 mM NaCl, 1 mM EDTA, 3 mM $MgCl_2$, and 0.5% Triton X-100) for 5 min on ice before being fixed at the indicated incubation time points after IR. This method removes nucleoplasmic signal and helps in the detection of foci. Cells were washed two times with phosphate-buffered saline (PBS) followed by fixation with 4% paraformaldehyde (w/v) in PBS for 15 min at room temperature. After two washes with PBS, cells were permeabilized in 0.5% Triton X-100 in PBS for 5 min. Cells were co-stained with primary antibodies against γ-H2AX (Active motif) and RPA2 (Abcam) in PBS for 1 h at room temperature. After three washes with PBS, cells were stained with goat anti-rabbit Alexa Fluor 488 and anti-mouse Cy3 secondary antibody (Molecular Probes, 1:400) in PBS for 30 min at room temperature.

CtIP and Geminin immunofluorescence was performed as reported previously[450]. For RIF1, 53BP1, and cyclin A immunofluorescence staining, cells were either untreated or treated with 50 μM etoposide for 1 h and fixed with 4% paraformaldehyde in PBS for 15 min. Then cells were washed with TBS and fixed with cold methanol (−20 °C) for 5 min and permeabilized with PBS containing 0.2% Triton X-100 for 5 min and washed three times 5 min with TBS. The cells were quenched with 0.1% sodium borohydride for 5 min, washed once with TBS, blocked in PBS containing 10% goat serum and 1% bovine serum albumin (BSA) for 1 h, and incubated with the primary antibody diluted in PBS 1% BSA for 2 h at room temperature. Coverslips were washed three times for 10 min with TBS before 1-h incubation with the appropriate secondary antibody conjugated to a fluorophore. Cells were rinsed again three times for 10 min with TBS. Coverslips were mounted onto slides with ProLong Gold (Thermo Fisher Scientific) antifade mountant with 4’,6-diamidino-2-phenylindole (DAPI) (Life technologies).

For RAD51 and phosphoDNA-PKcs(S2056) immunostaining, cells were either untreated or treated with 5 Gy IR, released for 1 h, and fixed with 4% paraformaldehyde in PBS for 25 min. Next, cells were permeabilized with PBS containing 0.5% Triton X-100 (PBS-T) for 15 min and washed three times with PBS 1×. The cells were blocked in PBS containing 10% FBS for 1 h and incubated with the primary antibody (RAD51:

1:1000 or phosphoDNA-PKcs(S2056): 1:500) diluted in the blocking buffer for 2 h at room temperature. Coverslips were washed three times with PBS before 1-h incubation with the appropriate secondary antibody (1:1000) conjugated to a fluorophore again in blocking buffer. Cells were rinsed twice with PBS 1×, then incubated in (1:1000) PBS-DAPI solution for 5 min, and then washed twice with PBS 1×. Coverslips were mounted onto slides with ProLong Gold antifade mountant.

2.4.8 Recruitment of RPA and EXO1 to laser-induced DNA damage sites

The evaluation of the recruitment kinetics of RPA to DNA damage sites was performed essentially as described6 with the exception of the following modifications. After overnight transfections with Effectene reagent (Qiagen), unsynchronized HEK 293 cells expressing the indicated RPA subunit fused to green fluorescent protein (GFP) and mCherry-PCNA fusion protein were incubated with fresh medium containing 1 μg/mL of Hoechst 33342 for 15 min at 37 °C and treated with 5 μM of PARPi BMN 673 (20 mM stock solution prepared in dimethyl sulfoxide (DMSO), Selleckchem) 1 h prior to microirradiation and recruitment analysis. A 37 °C pre-heated stage with 5% CO_2 perfusion was used for time-lapse analysis on a Zeiss LSM-510 META NLO laser-scanning confocal microscope (×40 objective). Localized DNA damage was generated along a defined region across the nucleus of a single living cell by using a bi-photonic excitation of the Hoechst 33342 dye, generated with a near-infrared 750-nm titanium:sapphire laser line (Chameleon Ultra II, Coherent Inc.) The laser output was set to 1.5% with 5 iterations. For each cell, 30 images were collected with a 5 sec interval. A Multi-Time macro developed in-house for the AIM software v3.2 (Zeiss) was used for image acquisition. Background and photobleaching corrections were applied to each dataset as described[24]. The average accumulation ± s.e.m. of RPA was plotted using a minimum of ten recruitment kinetic profiles per each RPA construct from three independent experiments. Only S-phase-positive PCNA (proliferating cell nuclear antigen) cells were chosen for recruitment[451]. Recruitment of GFP-EXO1 to laser-induced DSBs was performed as reported previously[452].

2.4.9 Recruitment of Ku80 to laser-induced DNA damage sites

For Ku80 laser microirradiation experiments, a 1-μm diameter band of damage was introduced across the width of the nucleus. Background was determined based on measuring the fluorescence intensity outside of the cells (i.e., in regions containing only the growth medium). Fluorescence loss due to photobleaching that takes place during acquisition is removed by normalizing the total nuclear fluorescence to remain constant throughout the experiment. The fluorescence intensity of the damaged region was then monitored over time after correcting for background and fluorescence loss. The distribution of recruited protein can deviate from the initial band for two reasons. First, the distribution of chromatin determines whether or not the full width and full diameter of the band are sites of DNA damage. Second, as we have previously published, there is a decondensation of the damaged chromatin that causes the band to expand in width beyond the boundary of the original damaged area. Consequently, measurements restricted to the 1-μm wide band where the laser microirradiation took place will slightly underestimate the extent of recruitment and chromatin-bound proteins that are unaffected will commonly show a very slight decrease in fluorescence intensity within the region.

2.4.10 BrdU/ssDNA assays

Cells were pre-incubated in the presence of 10 μM BrdU (Sigma) for 16 h followed by a 3-h incubation after IR at 10 Gy. Cells were subjected to in situ fractionation on ice for 10 min using sequential extraction with two different buffers. Pre-extraction buffer 1 (10 mM PIPES, pH 7.0, 300 mM sucrose, 100 mM NaCl, 3 mM $MgCl_2$, and 0.5% Triton-X100) and followed by pre-extraction buffer 2 (10 mM Tris pH 7.5, 10 mM NaCl, 3 mM $MgCl_2$, 1% Nonidet P-40, and 0.5% sodium deoxycholate). Cells were washed three time with PBS followed by fixation with 4% paraformaldehyde (w/v) for 15 min at room temperature. Cells were washed with PBS and permeabilized in 0.5% Triton X-100 in PBS for 5 min. Cells were incubated overnight at 4 °C with anti-BrdU antibody under non-denaturing conditions. In these native conditions, the anti-BrdU antibody only has access to its epitope in ssDNA. Unbound primary antibody was removed by washing in PBS at room temperature followed by incubation with the anti-mouse Cy3 secondary antibody for 30 min at room temperature. Slides were then washed for four times in PBS before mounting with Vectashield mounting medium (Vector Laboratories) containing DAPI. BrdU foci were observed by using an upright fluorescence microscope (Zeiss AxioImager.Z1) with a Plan Neofluar 1.3 N.A. ×40 oil

immersion objective. Image analysis was carried out by the ImageJ software (version 1.51k). The integrated intensity of individual BrdU foci and RPA2 foci were quantified by using GDSC ImageJ Find Foci plugins[453].

2.4.11 ChIP assays

The effect of PARP-1 knockdown and PARP inhibition on RPA2, 53BP1, and RIF1 recruitment to a sequence-defined DSB site was determined quantitatively by ChIP followed by quantitative polymerase chain reaction (qPCR). Cells were crosslinked with 1% (v/v) formaldehyde for 10 min and then glycine was added to a final concentration of 125 mM for 5 min to stop the crosslinking reaction. Cells were lysed in lysis buffer (25 mM HEPES pH 7.9, 300 mM sucrose, 50 mM NaCl, 1 mM EDTA, 3 mM $MgCl_2$, and 0.5% Triton X-100) and nuclei were isolated. Nuclear fractions were resuspended in sonication buffer (50 mM HEPES pH 7.9, 140 mM NaCl, 1 mM EDTA, 1% Triton X-100, 0.1% sodium deoxycholate, 1% SDS, 1× protease inhibitor cocktail, and 1× phosphatase inhibitor cocktail (Roche)) for 10 min on ice and sonicated to obtain approximately 200–500-bp chromatin fragments using a Bioruptor (Diagenode). Chromatin fragments were precleared with magnetic Dynabeads protein G (Life Technologies) for 1 h and incubated with pre-bound antibody–Dynabeads protein G overnight at 4 °C. Beads were washed once in low-salt buffer (20 mM Tris, pH 8.1, 2 mM EDTA, 50 mM NaCl, 1% Triton X- 100, and 0.1% SDS), once in high-salt buffer (20 mM Tris, pH 8.1, 2 mM EDTA, 500 mM NaCl, 1% Triton X-100, and 0.1% SDS), once in LiCl buffer (10 mM Tris, pH 8.0, 1 mM EDTA, 0.25 mM LiCl, 1% Nonidet P-40, and 1% deoxycholic acid), and twice in TE buffer (10 mM Tris-HCl, pH 8.0, and 1 mM EDTA). Washed beads were eluted twice with 100 µL of elution buffer (1% SDS and 0.1 M $NaHCO_3$) and crosslinks were reversed by overnight incubation at 65 °C in 0.1 mg/mL RNase A, 0.3 M NaCl, and 0.2 mg/mL proteinase K. The DNA samples were purified with Qiaquick PCR columns (Qiagen). qPCR was carried out on an Applied Biosystem 7900 HT Fast instrument using the SYBR Green detection system. The results of the quantitative ChIP assays are the mean with s.e.m. of qPCR reactions from three independent experiments and primers used are listed in Supplementary Tables 2.4 and 2.5.

2.4.12 ER-AsiSI resection assay

The percentage of resection adjacent to a specific DSB1 (Chr 1: 89231183) was measured as described[433] with some modifications. The primer pairs for "DSB1" and "DSB2" are across *Bsr*G1 and *Bam*H1 restriction sites, respectively. Briefly, ER-*Asi*SI U2OS cells were treated with 300 nM of 4-OHT (Sigma) for 3 h to allow the nuclear translocation of *Asi*SI and the induction of DSBs. Cells were collected and genomic DNA was extracted and digested with *Bsr*GI or *Bam*H1 enzymes or mock digested overnight at 37 °C. Digested or mock-digested samples were used as a template for qPCR performed using SYBR Green master mix. Primers used are listed in Supplementary Table 2.6[433]. For each sample, a ΔCt was calculated by subtracting the Ct value of the mock-digested sample from the Ct value of the digested sample.

2.4.13 Protein purification

PARP-1, PARP-2, and PARP-3 were purified according to standard procedures[80, 92]. BLM was tagged at the N-terminus with GST and at the C-terminus with His_{10} and purified as described for PALB2[80]. MRE11-RAD50-NBS1 was purified according to an established protocol[454]. RPA was purified as described[455]. Human EXO1[176] or biotinylated EXO1 for single-molecule experiments was purified as described[456]. For recombinant DNA2 protein purification, Sf9 insect cells (1 L at 10^6 cells/mL) were infected with a GST-DNA2-FLAG baculovirus. At 48 h post-infection, cells were harvested by centrifugation and the pellet was frozen on dry ice. Cells were lysed in Buffer 1 (1× PBS containing 150 mM NaCl, 1 mM EDTA, 0.05% Triton X-100, 1 mM DTT, and protease inhibitors) and homogenized by 20 passes through a Dounce homogenizer (pestle A). The cell lysate was incubated with 1 mM $MgCl_2$ and 2.5 U/mL benzonase nuclease at 4 °C for 1 h followed by centrifugation at 93,753 × *g* for 1 h. The soluble cell lysate was incubated with 1 mL of GST-Sepharose beads for 90 min at 4 °C with gentle rotation. The beads were washed twice with buffer 1 followed by incubation with buffer 2 (Buffer 1 with 5 mM ATP, 15 mM $MgCl_2$) for 1 h at 4 °C. Sepharose GST beads were washed twice with buffer 1 supplemented with 200 mM NaCl and once with P5 buffer (50 mM $NaHPO_4$ pH 7.0, 500 mM NaCl, 10% glycerol, 0.05% Triton-X-100, 5 mM imidazole) followed by cleavage with PreScission protease (60 U/mL, GE Healthcare Life Sciences), overnight at 4 °C in P5 buffer. The

supernatant was then collected and completed to 10 mL with Flag-binding buffer (50 mM Tris–HCl pH 7.5, 150 mM NaCl, 1 mM EDTA, 10% glycerol, 0.025% Triton X-100) before incubation with 600 µL of M2 anti-Flag affinity gel (Invitrogen) for 1 h at 4 °C. The beads were washed twice with washing buffer (Flag-binding buffer supplemented with 100 mM NaCl). After two additional washes with Flag Elution buffer (50 mM Tris–HCl pH 7.5, 150 mM NaCl, 0.025% Triton X-100, and 10% glycerol), proteins were eluted twice in one volume of beads with Flag Elution buffer and 500 µg/mL of 3×-Flag peptide for 45 min at 4 °C. Proteins were then dialyzed in the storage buffer (20 mM Tris-HCl, pH 7.4, 200 mM NaCl, 10% glycerol, 1 mM DTT) and stored in aliquots at −80 °C.

2.4.14 DNA resection assays

Assays were performed with pUC19 DNA linearized with *Kpn*I and then 3′ labeled with [α-^{32}P] ATP and terminal deoxytransferase (NEB). For the DNA2 resection machinery, reactions were conducted using 50 nM of substrate in standard buffer (20 mM Na-HEPES pH 7.5, 0.1 mM DTT, 0.05% Triton X-100, 100 µg/mL BSA). Two millimolar ATP and 5 mM $MgCl_2$ were added to the reaction buffer immediately before reconstitution of the resection machineries. The reactions were initiated on ice by adding either NAD, PARP-1, PARP-2 or PARP-3 as indicated in the figure and transferred immediately to 37 °C. After 5 min, the order of addition and incubation of the respective protein components were: MRN (10 nM, 5 min), RPA (100 nM, 5 min), BLM (15 nM, 3 min) and DNA2 (15 nM, 45 min). For the EXO1 resection machinery, reactions were conducted using resection buffer (25 mM MOPS pH 7, 60 mM KCl, 1% Tween 20, 2 mM DTT, 5 mM MgCl2, 2 mM ATP) and the same proteins and time of incubation as mentioned above except for EXO1 at a concentration of 10 nM instead of DNA2. Reactions were followed by proteinase K treatment for 30 min at 37 °C. Products were analyzed on a 1% native agarose gel. Gels were dried on DE81 paper (Whatman) and signals were detected by autoradiography. Densitometric analyses were performed using the FLA-5100 phosphorimager (Fujifilm) and quantified using the Image Reader FLA-5000 v1.0 software.

2.4.15 DNA-binding assays

The DNA-binding reactions (10 μL) contained ^{32}P-labeled DNA oligonucleotides (100 nM) and the indicated concentrations of PARP-1 and NAD in resection buffer (20 mM Na-HEPES pH 7.5, 0.1 mM DTT, 0.05% Triton X-100, 100 μg/mL BSA, 5 mM $MgCl_2$, 2 mM ATP). Reaction mixtures were incubated at 37 °C for 10 min and then protein–DNA complexes were fixed with 0.2% (v/v) glutaraldehyde for 15 min. The reactions were subjected to electrophoresis on an 8% 1×-TBE-acrylamide gel and ^{32}P-labeled DNA was visualized by autoradiography. Sequences of the oligonucleotides are found in Supplementary Table 2.7.

2.4.16 Single-molecule imaging and DNA curtains

Single-molecule DNA curtain data were collected at 37 °C using a Nikon Ti-E microscope in a prism-TIRF configuration. Data were collected with a 200-ms exposure through a ×60 water-immersion objective (1.2 NA, Nikon), a 500-nm long-pass (Chroma), and a 638-nm dichroic beam splitter (Chroma) for two-channel detection through two EMCCD cameras (Andor iXon DU897, cooled to −80 °C). Histograms of PARP-1-binding preference on DNA were acquired by fitting a two-dimensional Gaussian to each individual molecule and finding the center of the fit relative to the barrier position using a custom-written FIJI script (available upon request). A Gaussian curve with a constant offset was fit to the largest peak of the histogram using a custom script written in MATLAB (available upon request). The constant offset in the fitting accounts for molecules that bind nonspecifically along the length of the DNA substrate. The center of the fit is reported in the corresponding figure panel.

For DNA curtains, microscope slides with microfabricated chromium barriers were encased in a microfluidic flowcell and passivated with a fluid lipid bilayer. DNA molecules (λ, 48.5 kb) with biotinylated ends were bound to a subset of the lipids via a biotin–streptavidin interaction. The flowcells were attached by nanoports to a syringe pump-controlled microfluidics system.

λ–DNA substrates for DNA curtains were purchased from NEB and annealed with two oligonucleotides: IF7: (5′-[p]AGG TCG CCG CCC[Biotin]- 3′) and LM3: (5′-[p]GGG CGG CGA CCT TTT TTT TTT TTT TTT TTT TTT TTT TTT TTT TTT

TTT TTT TTT TTT TTT TTT TTT TTT TTT TTT TTT TTT TTT TTT -3′). This generated a substrate that had a biotin for attaching to the flowcell surface on one side and a 78-nt 3′ overhang on the other side, which was suitable for Exo1 loading. For visualizing the DNA, YoYo-1 was injected into the flowcell with a glucose oxidase/catalase mixture.

To perform PARP-1 labeling, 300 nM mouse anti-6xHis antibody (Clontech) was pre-incubated with 400 nM anti-mouse secondary QDots (Invitrogen, 605 or 705 depending on labeling strategy) in a 5 µL volume for 10 min on ice. PARP-1 or PARP-2 were incubated with the antibody mixture for another 10 min on ice and diluted to a final volume of 200 µL (6.25 nM PARP, 7.5 nM anti-His antibody, 10 nM QDots; final concentrations). PARP-1 or PARP-2 were injected onto the microscope flowcell at 200 µL/min in loading buffer (40 mM Tris-HCl pH 8, 200 µg/mL BSA, 2 mM DTT, 2 mM $MgCl_2$). After binding, the flowcell was switched to EXO1 resection buffer (40 nM Tris-HCl pH 8, 60 mM NaCl, 200 µg/mL BSA, 2 mM DTT, 2 mM MgCl2, 1 mM ATP) for subsequent EXO1 loading.

EXO1 loading was performed by pre-incubating 100 nM Streptavidin QDots 605 with 80 nM EXO1-biotin in 10 µL EXO1 loading buffer (40 mM Tris-HCl pH 8, 60 mM NaCl, 200 µg/mL BSA, 2 mM DTT, 2 mM MgCl2, 1 mM ATP) on ice for 10 min. Then the mixture was diluted to a final volume of 200 µL in EXO1 loading buffer plus free biotin (4 nM EXO1, 5 nM QDots) and injected onto DNA curtains at 200 µL/min. To prevent dye-induced changes in protein–DNA interactions, YoYo-1 was omitted in experiments involving PARP-1/EXO1 and PARP-2/EXO1.

2.4.17 Single-molecule analysis of resection tracks

The indicated cell lines or siRNA transfected cells were incubated with 10 µM BrdU for 48 h. After 48 h, the cells were treated with 5 µM BMN 673 for 1 h before IR (10 Gy and released for 1 h). Cells were harvested and counted, 1×10^5 cells per condition were spun down, and resuspended in the resuspension buffer from the FiberPrep DNA Extraction Kit (Genomic Vision). Agarose plugs and DNA solutions were made according to the FiberPrep DNA extraction Kit. Using the FiberComb (Genomic Vision), the DNA was stretched onto a Combicoverslip. The cover slips were baked for 2 h at

60 °C, then incubated in primary antibody (1:100 anti-BrdU) in 5% PBS–BSA for 2 h at 37 °C. The coverslips were washed with PBS-T 3 times for 3 min with shaking and incubated for 1 h in the appropriate secondary antibody (1:200) conjugated to a fluorophore in a humidified chamber at 37 °C. The slides were washed with PBS-T 3 times for 3 min. If needed, YOYO™-1 Iodide staining (1:1000) was performed for 10 min. The slides were washed with ddH_2O for 1 min. The DNA is then dehydrated by submerging it for 1 min in 70%, 90%, and 100% ethanol sequentially and visualized on a DMI6000B microscope. Fiber length was evaluated by Image J analysis (version 1.51k).

2.4.18 Survival assays

Cells were seeded in triplicates into a Corning 3603 black-sided clear bottom 96-well microplate at a density of 2000 cells per well. Once attached, the media was changed to include the desired concentration of BMN 673. One hour after BMN 673 treatment, the plate was irradiated with 7.5 Gy. The plates were incubated for 120 h. The nuclei were stained with Hoechst 33342 (Invitrogen) at 10 μg/mL in media for 30 min at 37 °C. Images of entire wells were acquired at ×4 with a Cytation 5 Cell Imaging Multi-Mode Reader followed by quantification of Hoechst-stained nuclei with the Gen5 Data Analysis Software v3.03 (BioTek Instruments). Cell viability was expressed as the percentage of survival in BMN673-treated cells relative to vehicle (DMSO)-treated cells.

2.4.19 HR *in cellulo* reporter assays

Dox-inducible I-*Sce*I/DRGFP cell line (TRI-DR-U2OS) was treated without/with 10 μg/mL Dox and BMN 673 (1 μM) or ABT-888 (5 μM) and incubated for 48 h. HR efficiencies were analyzed by flow cytometry after 48-h incubation. HR efficiency was expressed as the percentage of GFP-positive cells. Samples were analyzed in triplicate. Values are expressed as mean and s.e.m.

2.4.20 Statistical analyses

All data are representative of three or more independent experiments. Prism ver 6.0 was used to do the statistical analyses.

2.5 **Figures and Legends**

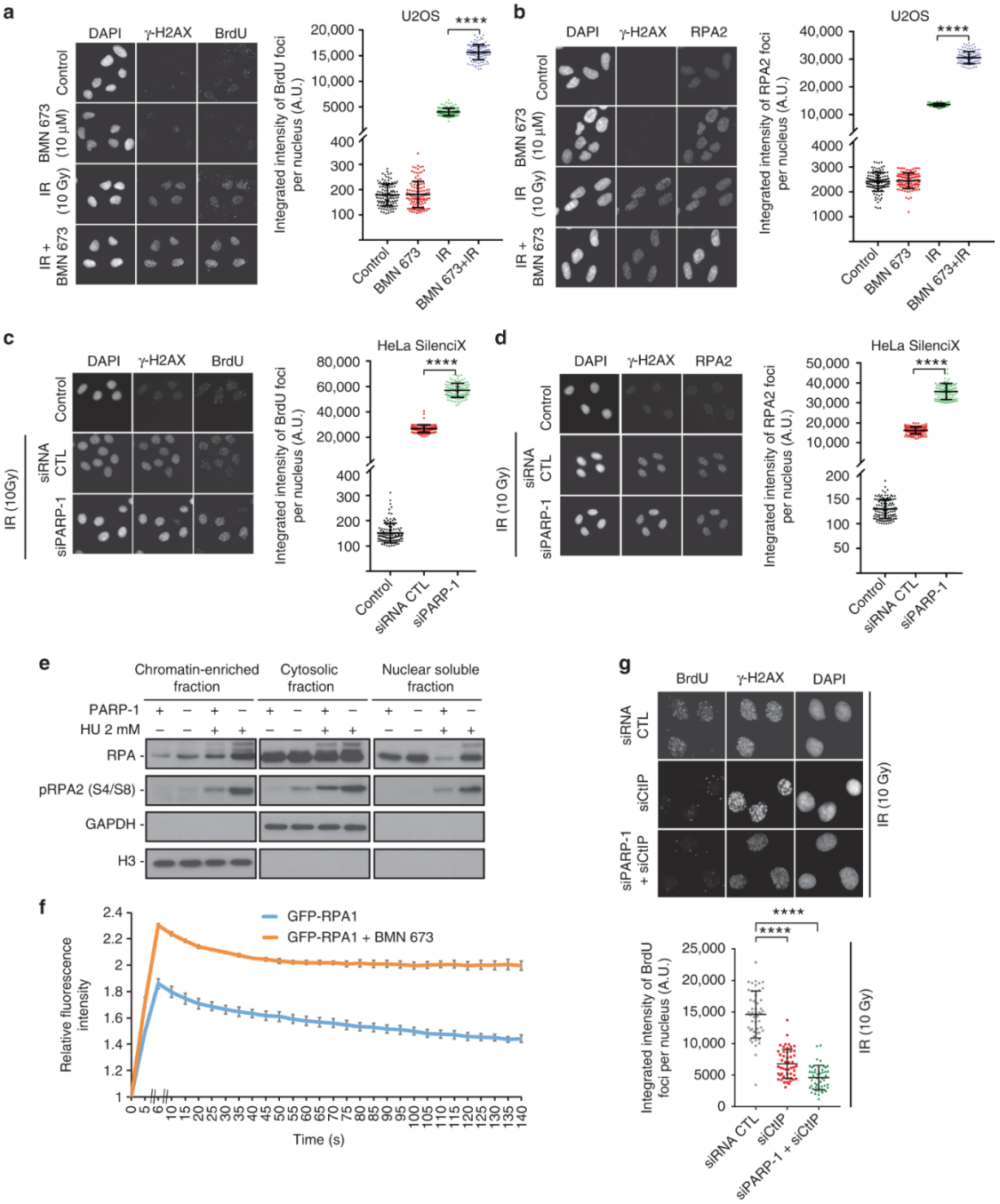

Figure 2.1: Poly(ADP-ribose) polymerase-1 (PARP-1) regulates DNA end resection and chromatin accumulation of replication protein A (RPA).

U2OS cells mock treated, treated with BMN 673, irradiated (10 Gy), or irradiated (10 Gy) in combination with BMN 673 were subjected to immunofluorescence against γ-H2AX, bromodeoxyuridine (BrdU) (**a**), or RPA2 foci formation (**b**). HeLa SilenciX cells underexpressing PARP-1 by siRNA-mediated gene knockdown were subjected to immunofluorescence against γ-H2AX, BrdU (**c**) or RPA2 foci formation after irradiation

(10 Gy, 3 h release) (**d**). In panels **a**–**d**, the data show the mean ± s.d. (Mann–Whitney *U* test). **e** HEK293T wild type or CRISPR-PARP-1 were treated with 2 mM hydroxyurea for 16 h, fractionated into chromatin enriched, nuclear soluble and cytoplasmic fractions. **f** GFP-RPA1 recruitment in the absence (blue line) or presence of BMN 673 (orange line). The peak of intensity was at 6 s. Data show the mean ± s.e.m. **g** knockdown of CtIP suppresses the accumulation of single-stranded DNA in HeLa SilenciX PARP-1 knockdown cells after irradiation (10 Gy, 3 h release). The data show the mean ± s.d. ****$p \leq 0.0001$ (Mann–Whitney *U* test). Source data are provided as a source data file.

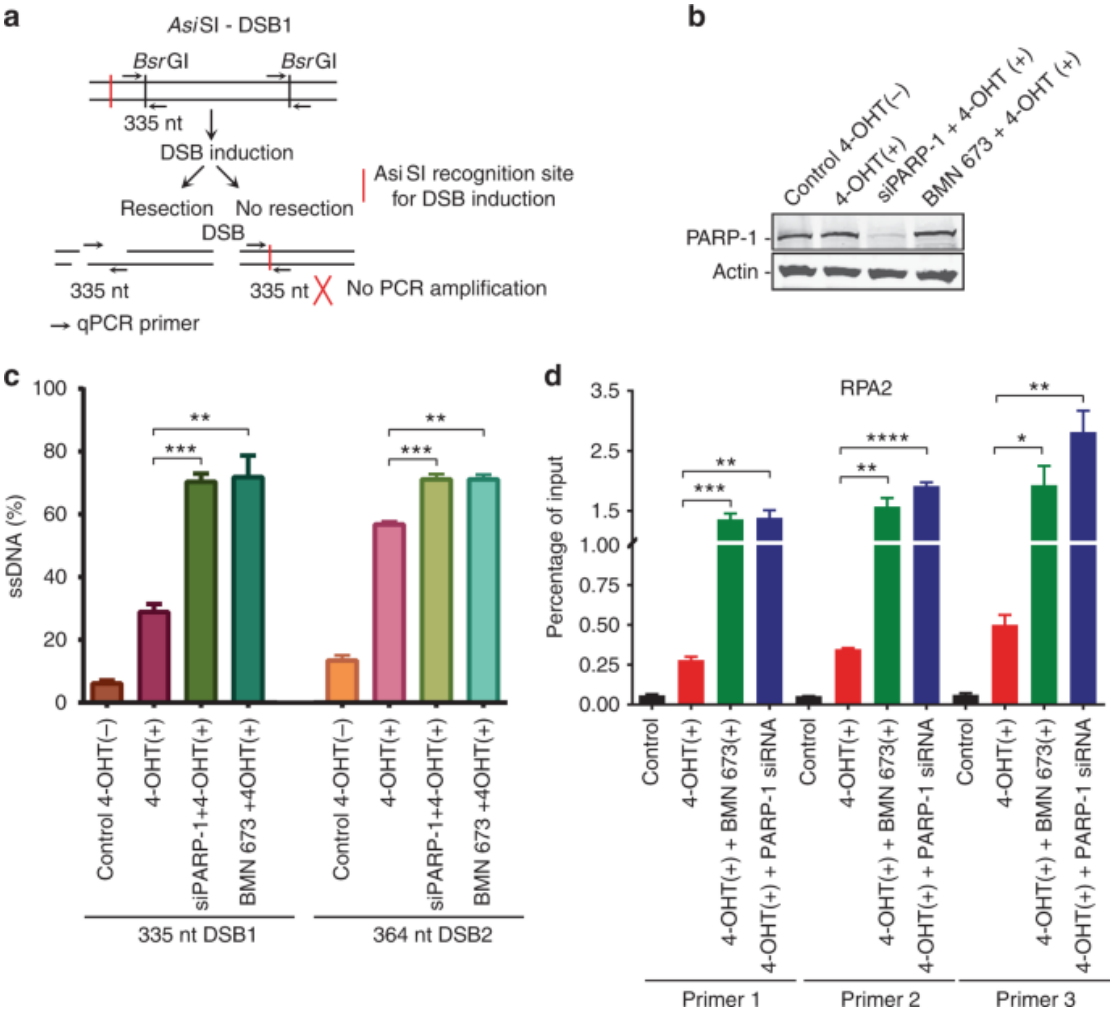

Figure 2.2: Measurement of double-strand break (DSB) resection in ER-AsiSI U2OS cells knocked down for poly(ADP-ribose) polymerase-1 (PARP-1) or treated with a PARP inhibitor.

a Quantitative polymerase chain reaction (qPCR) primers and probes for measurement of DSB resection at two *Asi*SI sites. **b** ER-*Asi*SI U2OS cells were knocked down for PARP-1 or treated with BMN 673 for 1 h, followed by induction with 300 nM 4-hydroxytamoxifen for 3 h. **c** Quantitation of the percentage of DNA resection. Error bars

represent mean ± s.e.m. $^{**}p \leq 0.01$, $^{***}p \leq 0.001$ (Mann–Whitney *U* test). **d** Chromatin immunoprecipitation–qPCR was performed with antibody against RPA2 in the ER-*Asi*SI U2OS cells. DSBs were induced at 48–72 h after siRNA transfection or after 1 h BMN 673 treatment. Immunoprecipitated chromatin samples were analyzed by qPCR using specific primer pairs located at Chr 1: chr1_89231183, Chr 6: chr6_90404906, and Chr 21: distal region of chr21_21292316. Error bars represent mean ± s.e.m. $^{*}p \leq 0.05$, $^{**}p \leq 0.01$, $^{***}p \leq 0.001$, $^{****}p \leq 0.0001$, (Mann–Whitney *U* test). Source data are provided as a source data file.

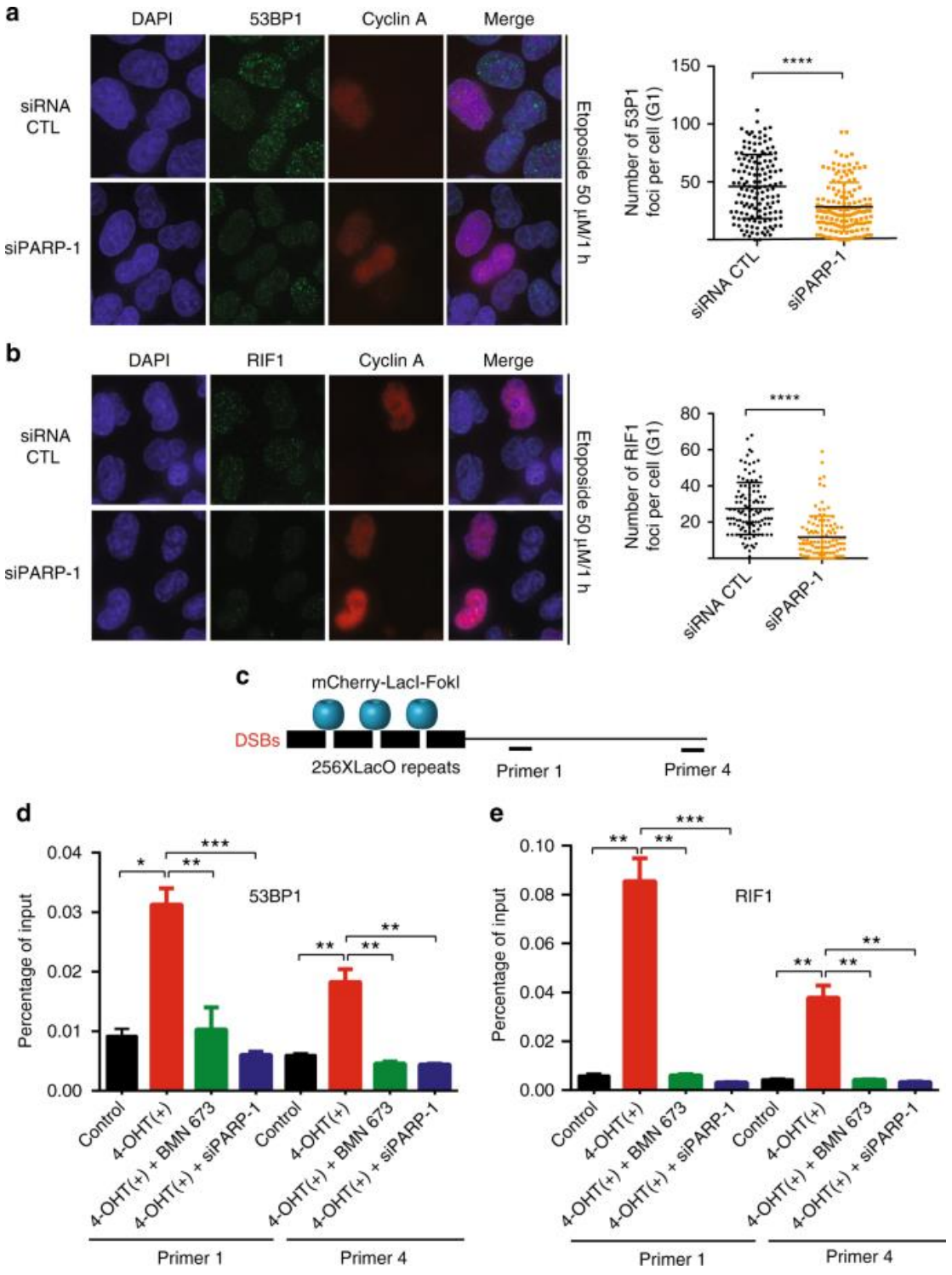

Figure 2.3: Poly(ADP-ribose) polymerase-1 (PARP-1) inhibition reduces the accumulation of 53BP1 and RIF1 foci.

a Etoposide-treated HeLa cells were either transfected with an small interfering RNA (siRNA) control or PARP-1 siRNA and subjected to immunofluorescence staining against 53BP1 or Cyclin A. The mean foci count was 46.05 for siRNA CTL and 28.42 for siPARP-1. Data show the mean ± s.d. ****$p \leq 0.0001$ (Mann–Whitney *U* test). **b** Etoposide-treated HeLa cells were either transfected with a control

siRNA or PARP-1 siRNA and subjected to immunofluorescence staining against RIF1 or Cyclin A. The mean foci count was 27.52 for siRNA CTL and 11.68 for siPARP-1. Data show the mean ± s.d. ****$p \leq 0.0001$ (Mann–Whitney *U* test). **c** Cartoon of the U2OS-DSB-reporter with inducible DSB generation by mCherry-*LacI*-*Fok*1. Chromatin immunoprecipitation (ChIP)–quantitative polymerase chain reaction (qPCR) primer sets are shown as p1–p4. ChIP of 53BP1 (**d**) or RIF1 (**e**) from the fixed chromatin of U2OS–DSB reporter cells stably expressing mCherry-*LacI*-*Fok*1 construct and treated with both 0.5 mM Shield-1 (1:500 dilution) and 1 mM 4-hydroxytamoxifen (4-OHT) for 1 h in order to generate DSBs. The ChIP–qPCR primer sets are labeled as primer 1 and primer 4. Data in **d**–**e** show the mean ± s.e.m. *$p \leq 0.05$, **$p \leq 0.01$, ***$p \leq 0.001$ (Mann–Whitney *U* test). Source data are provided as a source data file.

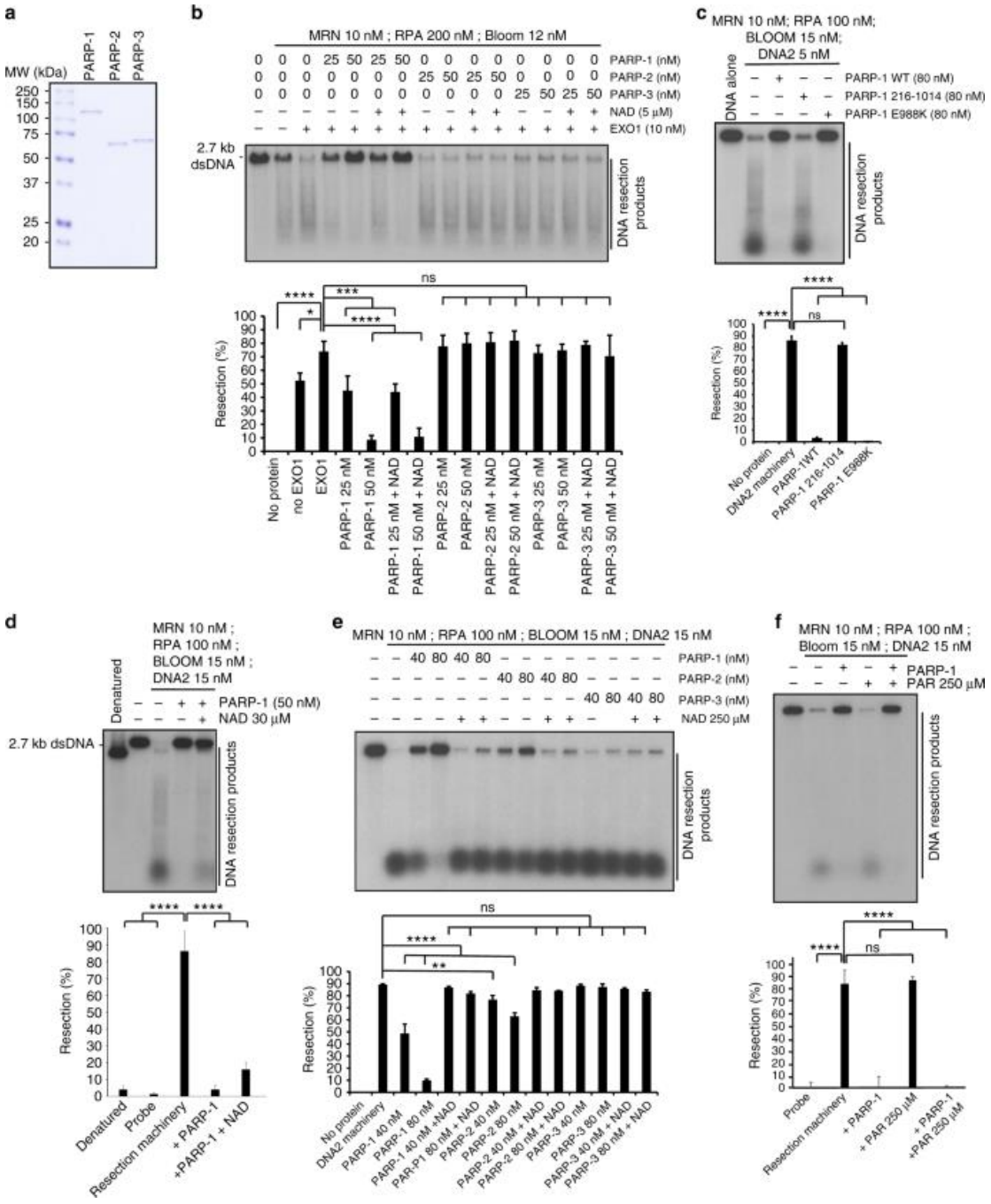

Figure 2.4: Poly(ADP-ribose) polymerase-1 (PARP-1) limits DNA end resection *in vitro*.

a Sodium dodecyl sulfate-polyacrylamide gel electrophoresis of purified human PARP-1, PARP-2, and PARP-3. **b** The indicated PARP proteins were incubated with the MRN-RPA-BLM-EXO1 machinery in the absence or presence of NAD (5 µM). The resection products were detected by autoradiography after agarose gel electrophoresis. Bottom: quantification of the results. **c** The PARP-1 DNA-binding mutant PARP-1 216-1014 fails to inhibit DNA resection. Bottom: quantification of the results. **d** DNA end resection by the MRN-RPA-BLM-DNA2 machinery is decreased in the absence or presence of NAD

(30 μM). **e** The indicated PARP proteins were incubated with the MRN-BLM-RPA-DNA2 machinery in the absence or presence of NAD (250 μM). **f** The addition of purified PAR (250 μM) alone does not block DNA resection by MRN-BLM-RPA-DNA2. PARP-1 was used at 87 nM. Error bars in **b**–**f** indicate s.d. from three independent experiments. *$p \leq 0.05$, **$p \leq 0.01$, ***$p \leq 0.001$, ****$p \leq 0.0001$ (ordinary one-way analysis of variance). Source data are provided as a source data file.

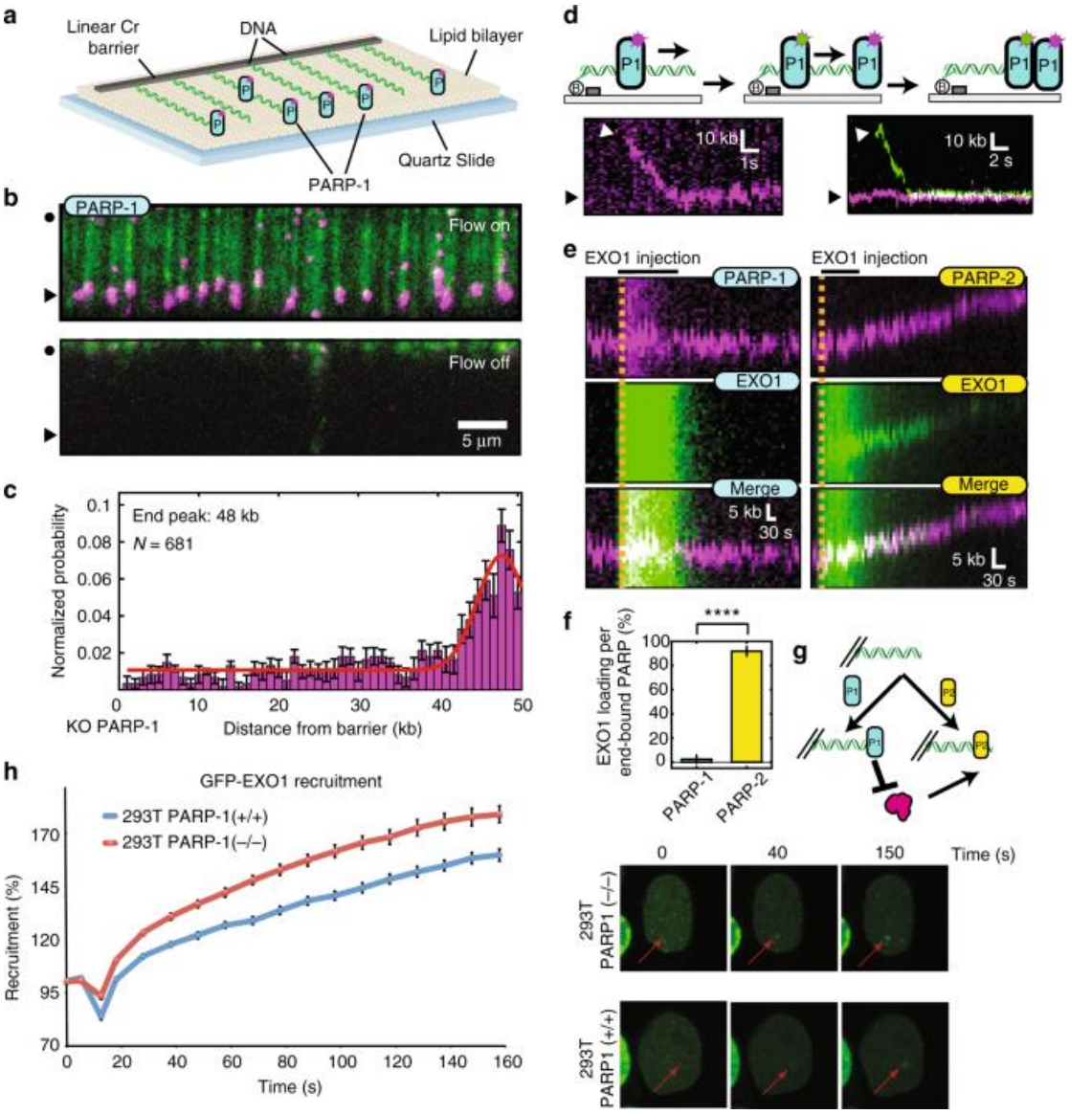

Figure 2.5: Poly(ADP-ribose) polymerase-1 (PARP-1) slides to accumulate at ends and prevent EXO1 binding.

a Illustration of the DNA curtain assay with fluorescent PARP-1 (blue ovals). **b** Fluorescent PARP-1 (magenta) binding to DNA curtains in the presence (top) or absence (bottom) of buffer flow. Black circles indicate the diffusion barrier and arrows

indicate the DNA ends. After PARP-1 was loaded, the DNA was stained with the fluorescent intercalating dye YoYo-1. **c** Histogram of the positions of 681 individual PARP-1 molecules along the length of the DNA substrate. Error bars were calculated by bootstrapping the data[457] and indicate a 70% confidence interval. **d** Illustration (top) and kymograph (bottom) of two differently labeled PARP-1 (P1) molecules binding to the DNA end. PARP-1 reached the end by buffer flow-assisted one-dimensional sliding 88% of the time ($N = 109/124$). **e** Representative kymographs of EXO1 resection of DNA pre-bound with PARP-1 (left) or PARP-2 (right). **f** Quantification of EXO1 loading events per DNA end bound by PARP-1 (left; $2.4 \pm 3.4\%$; $N = 42$ PARP-1 molecules) or PARP-2 (right; $91.8 \pm 4.1\%$; $N = 65$ PARP-2 molecules). Error bars represent mean ± s.e.m. ****$p \leq 0.0001$, (Student's t test). **g** Model for PARP-1 inhibition of EXO1. P2 refers to PARP-2. YoYo-1 was omitted from all experiments described in **c**–**f**. **h** Recruitment of GFP-EXO1 at laser-induced double-strand breaks in HEK293T wild-type or PARP-1−/− cells. Source data are provided as a source data file.

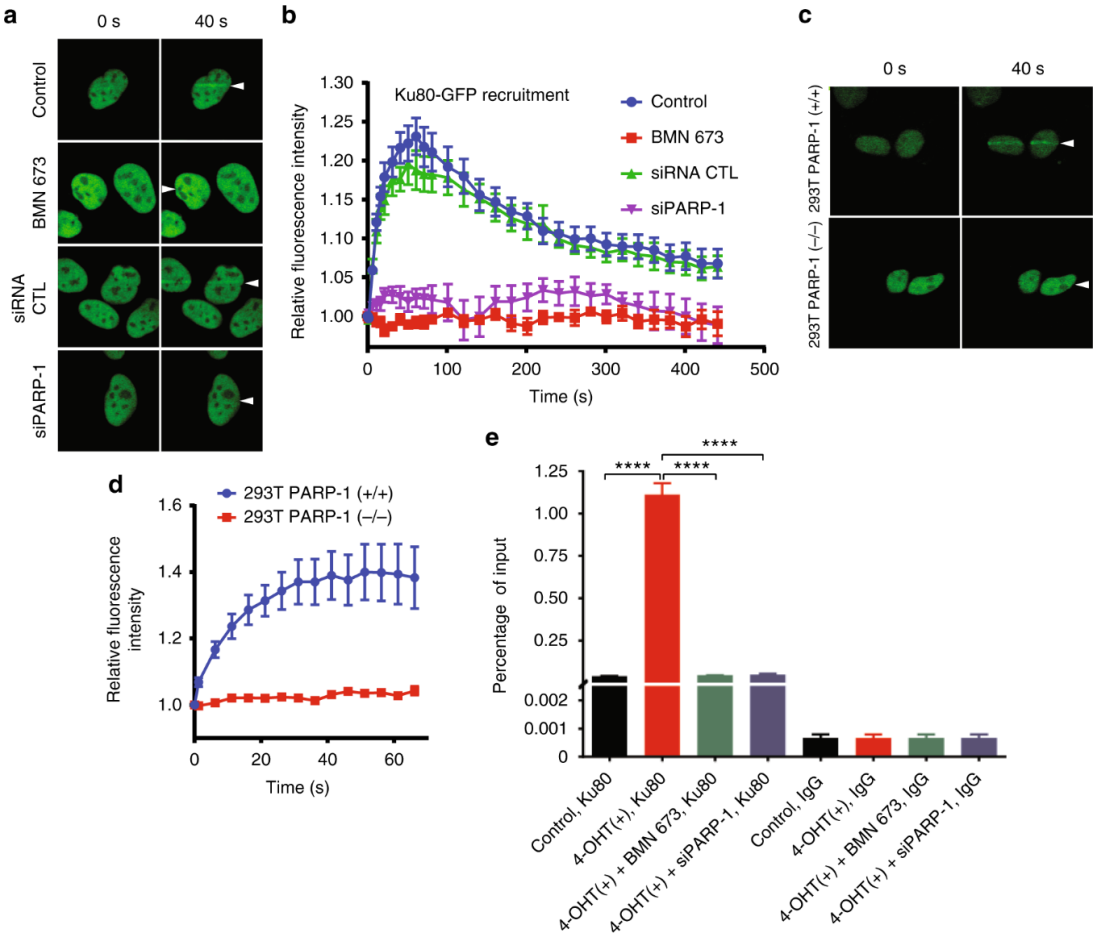

Figure 2.6: Poly(ADP-ribose) polymerase-1 (PARP-1) knockdown or pharmacological inhibitor affects Ku80 recruitment on double-strand breaks.

a U2OS cells stably expressing the Ku80-GFP were mock treated, treated with BMN 673, or silenced with PARP-1 siRNA and subjected to laser microirradiation-track studies. **b** Quantification of the relative fluorescence intensity of Ku80-GFP over time. Error bars represent mean with s.e.m. **c** Recruitment of Ku80-GFP in PARP-1-deficient CRISPR 293T cells is severely affected. **d** Quantification of the relative fluorescence intensity of Ku80-GFP over time. Error bars represent mean with s.e.m. **e** AsiS1-ER-U2OS reporter cells were cultured and treated with 4-hydroxytamoxifen (300 nM) for 1 h. Soluble chromatin fractions were prepared and subjected to immunoprecipitation against IgG control and Ku80-specific antibody. Immunoprecipitated chromatins fractions were analyzed by quantitative polymerase chain reaction using specific primer pairs: chr1_89231183. Error bars represent mean ± s.e.m. ****$p \leq 0.0001$ (Mann–Whitney *U* test). Source data are provided as a source data file.

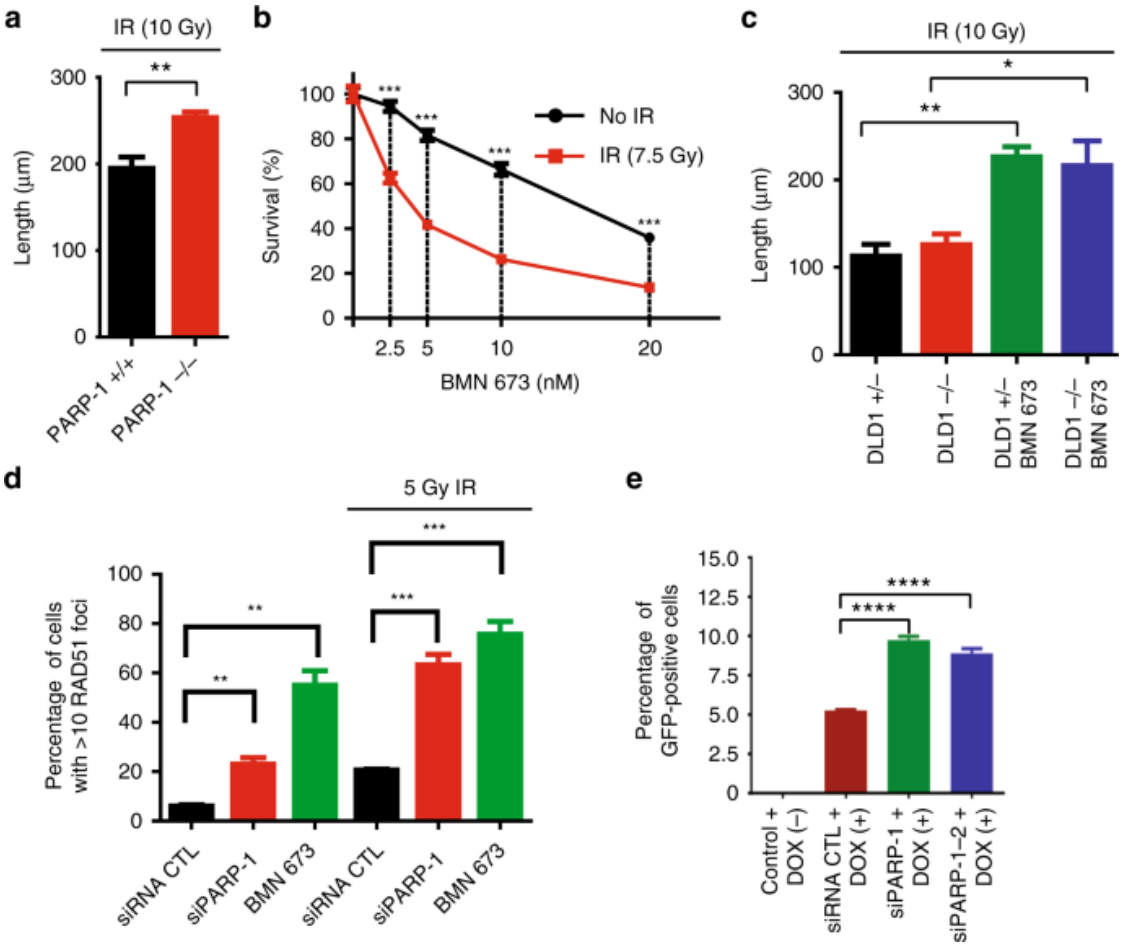

Figure 2.7: Single-molecule analysis of resection tracks (SMART) analysis and effect of poly(ADP-ribose) polymerase-1 (PARP-1) on homologous recombination.

a SMART of PARP-1-deficient mouse embryonic fibroblasts (MEFs). MEFs were treated with 10 Gy irradiation (IR). Error bars represent mean ± s.e.m. **b** Treatment of HeLa cells with BMN 673 results in IR sensitivity. Error bars represent mean with s.e.m. **c** SMART of BRCA2-proficient (DLD1 BRCA2 (+/−)) and BRCA2-deficient cells (DLD1 BRCA2 (−/−)) either mock treated of treated with BMN 673 (5 µM) were irradiated (10 Gy). Error bars represent Mean with s.e.m. **d** Attenuation of PARP-1 increases RAD51 foci *in cellulo*. Error bars represent mean ± s.e.m. **e** Homologous recombination is increased in PARP-1 knockdown cells. Error bar represents mean ± s.d. *$p \leq 0.05$, **$p \leq 0.01$, ***$p \leq 0.001$, ****$p \leq 0.0001$ (Mann–Whitney *U* test). Source data are provided as a source data file.

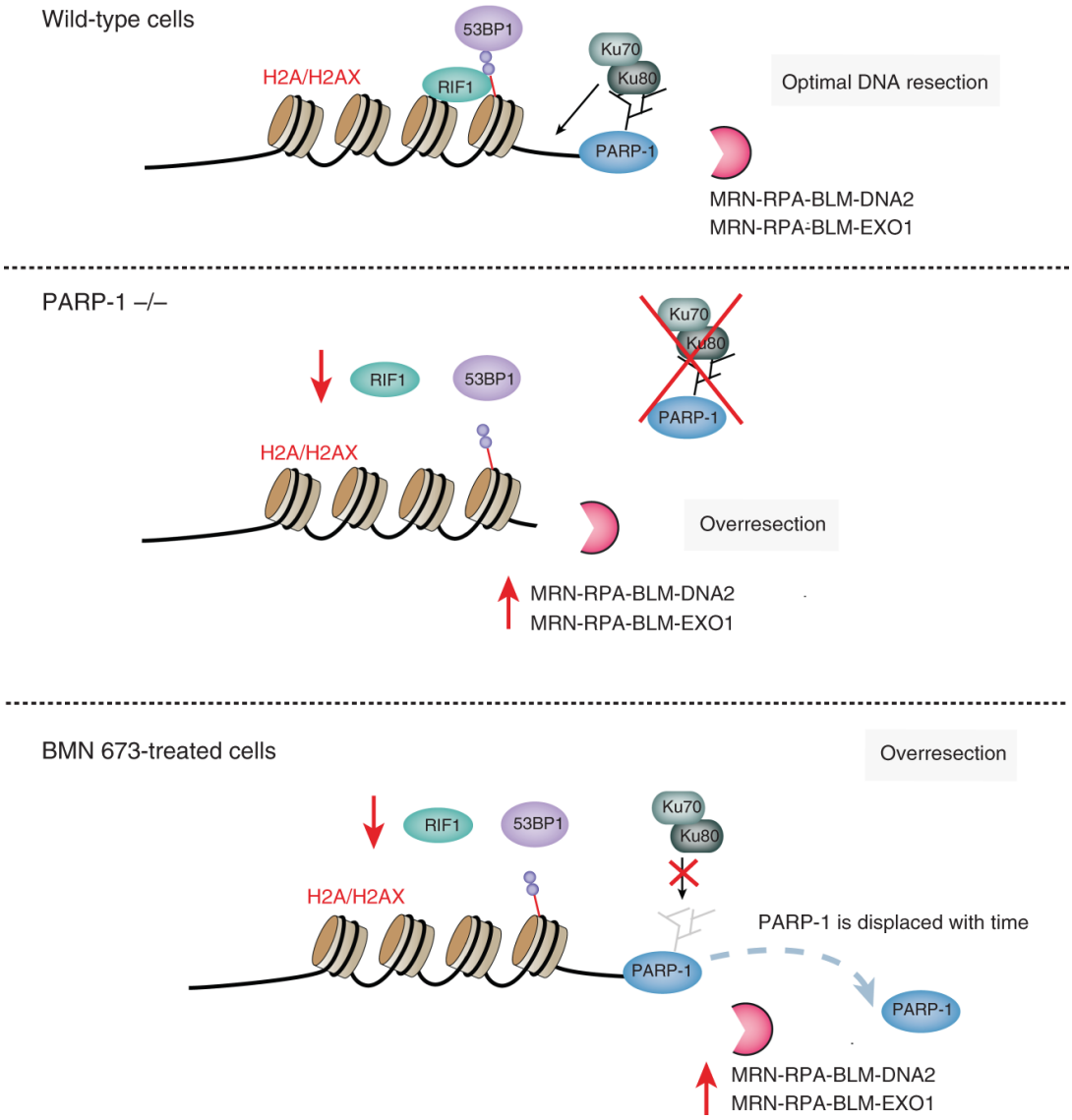

Figure 2.8: Model.

Following DNA damage, poly(ADP-ribose) polymerase-1 inhibition leads to a decrease of Ku80-end protection, RIF1 and 53BP1 foci formation, and increased DNA resection. Details are given in the text.

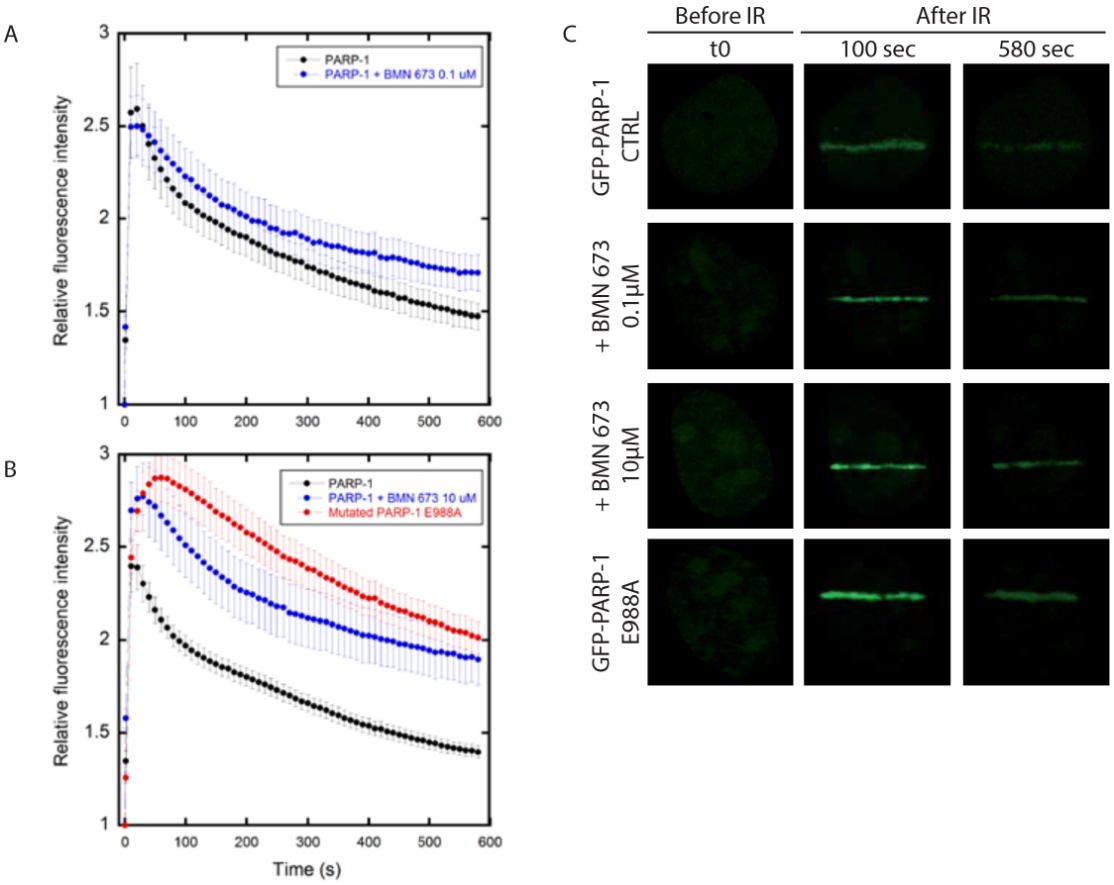

Figure 2.9 Supplementary Figure 1. Recruitment of PARP-1 at laser-induced DNA breaks.

The recruitment dynamics of PARP-1 under normal conditions was compared with the dynamics observed following PARP inhibition. The recruitment kinetics was obtained by plotting the relative fluorescence intensity of GFP-PARP-1 at the damage site as a function of time. (A) Accumulation of PARP-1 in normal conditions or in presence of 0.1µM BMN 673. (B) Accumulation of PARP-1 in normal conditions, in presence of 10µM BMN 673, and of polymerization mutant (E988A). (C) Representative images of local accumulation of GFP-PARP-1 at laser-induced DNA damage sites. Experiments were repeated three times and the average of at least 8 cells from a representative experiment was used to generate the graphs. Error bars represent the SEM. Two-way analysis of variance followed by Tukey pairwise comparisons shows no significant differences between PARP-1 and PARP-1 + BMN 673 0.1µM but significant differences in time between PARP-1 and PARP-1 + BMN 673 10µM ($P < 0.02$) and between PARP-1 and mutated PARP-1 E988A ($P < 0.01$) (from 20 to 580 seconds). Data show the mean ± s.d. (Mann-Whitney test U-test).

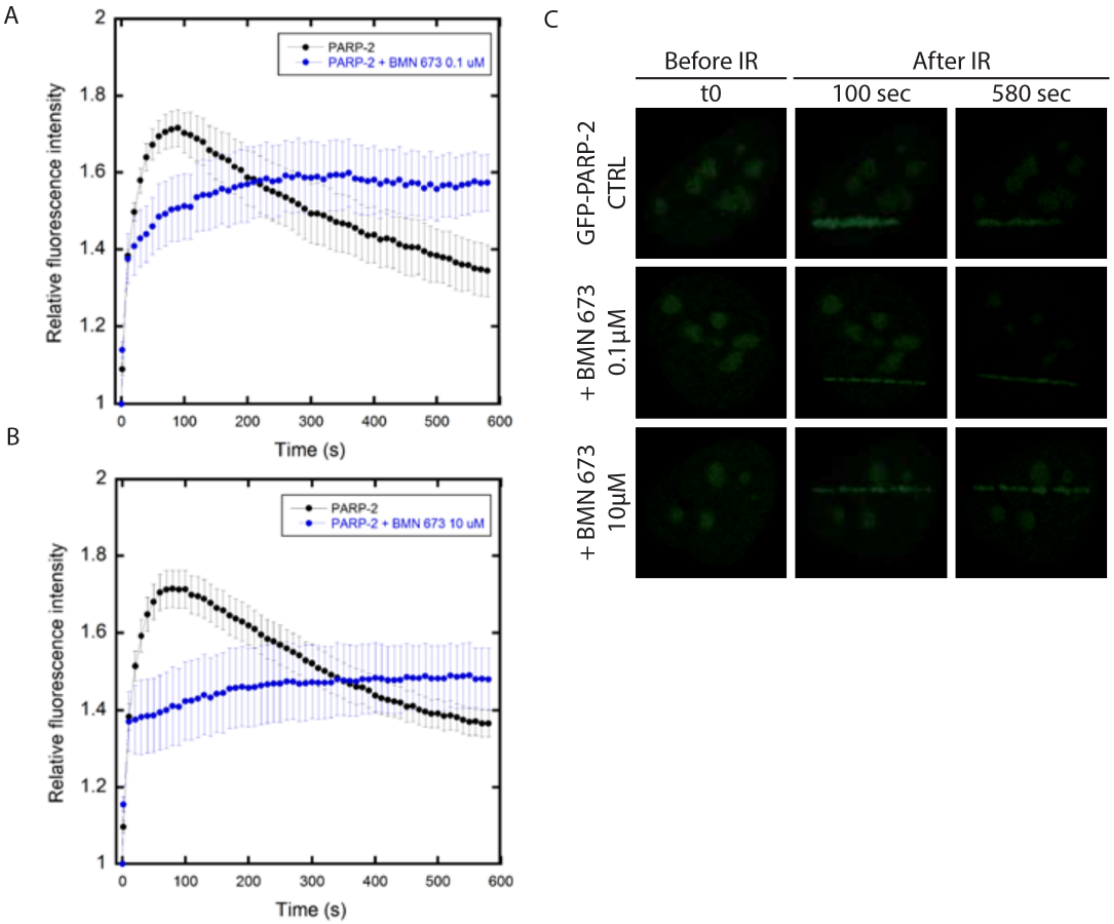

Figure 2.10: Supplementary Figure 2. Recruitment of PARP-2 at laser induced DNA breaks.

The recruitment dynamics of PARP-2 under normal conditions was compared with the dynamics observed following PARP inhibition. The recruitment kinetics was obtained by plotting the relative fluorescence intensity of GFP-PARP-2 at the damage site as a function of time. Accumulation of PARP-2 in normal conditions or in presence of (A) 0.1µM BMN 673 and (B) 10µM BMN 673. (C) Representative images of local accumulation of GFP-PARP-2 at laser-induced DNA damage sites. Experiments were repeated three times and the average of at least 8 cells from a representative experiment was used to generate the graphs. Error bars represent the SEM. By two-way ANOVA, we observed a significant difference between PARP-2 and PARP-2 + BMN 673 0.1µM ($P < 0.002$) and between PARP-2 and PARP-2 + BMN 673 10µM ($P < 0.001$) over time. Data show the mean ± s.d. (Mann-Whitney test U-test).

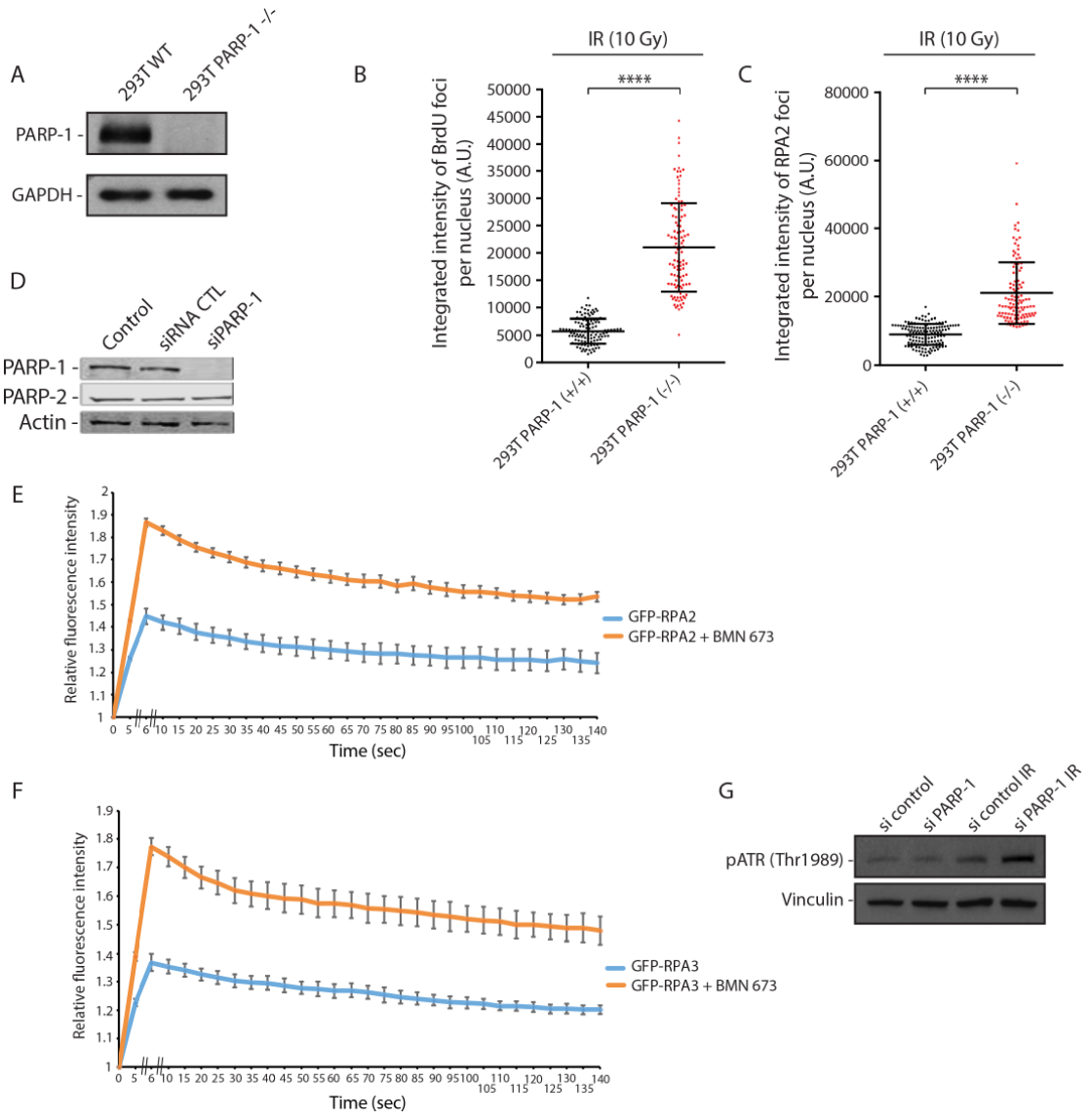

Figure 2.11: Supplementary Figure 3.

(A) Western blotting to validate the absence of PARP-1 in CRISPR 293T PARP-1 (-/-) compared to the 293T PARP-1 (+/+) control. CRISPR 293T PARP-1 (+/+) or 293T PARP-1 (-/-) cells were subjected to immunofluorescence against BrdU (B) or RPA2 (C) after irradiation (10Gy, 3 hrs release). Data show the mean ± s.d. (D) PARP-1 knockdown efficiency monitored by western blotting. The recruitment of GFP-RPA2 (E) or GFP-RPA3 (F) is accelerated by PARP inhibition at laser-induced DNA breaks. HEK293 cells were co-transfected with mCherry-PCNA and RPA subunit 2 or 3. Cells in S-phase, co expressing mCherry and GFP, were micro-irradiated using 750-nm two-photon laser beam, and the accumulation of RPA at the sites of DNA damage was monitored on a Zeiss LSM 510 NLO laser scanning confocal microscope. The peak of intensity was at 6

seconds. Data show the mean ± s.e.m. (G) ATR is over-activated in the PARP-1 knockdown cells (after 5Gy irradiation and 90 min release). **** $p \leq 0.0001$.

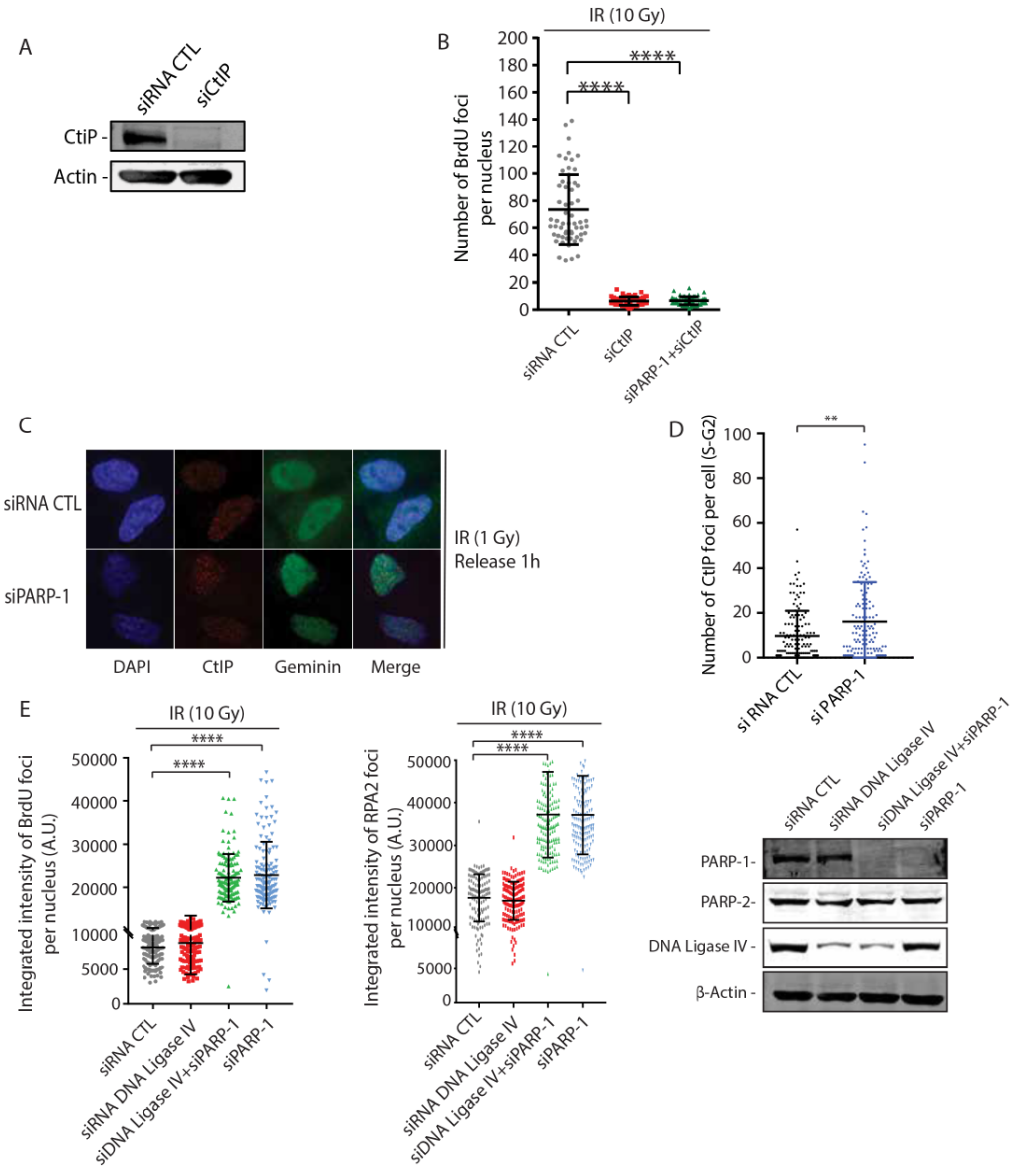

Figure 2.12: Supplementary Figure 4.

(A) Western blotting to monitor CtIP knockdown efficiency. (B) Quantification of the number of BrdU foci in the indicated knockdowns in HeLa SilenciX following irradiation (10 Gy 3hr release). (C) CtIP foci formation is increased in PARP-1 knockdown cells. (D) Quantification of the results. (E) The indicated knockdown in HeLa SilenciX control or PARP-1 HeLa SilenciX cells were subjected to immunofluorescence against BrdU (left panel) or RPA2 (middle panel) following irradiation (10 Gy, 3 hr release). (Right) . Data

show the mean ± s.d. Western blotting to validate siRNA knockdowns of DNA ligase IV or/and PARP-1. ** $p \leq 0.01$, **** $p \leq 0.0001$.

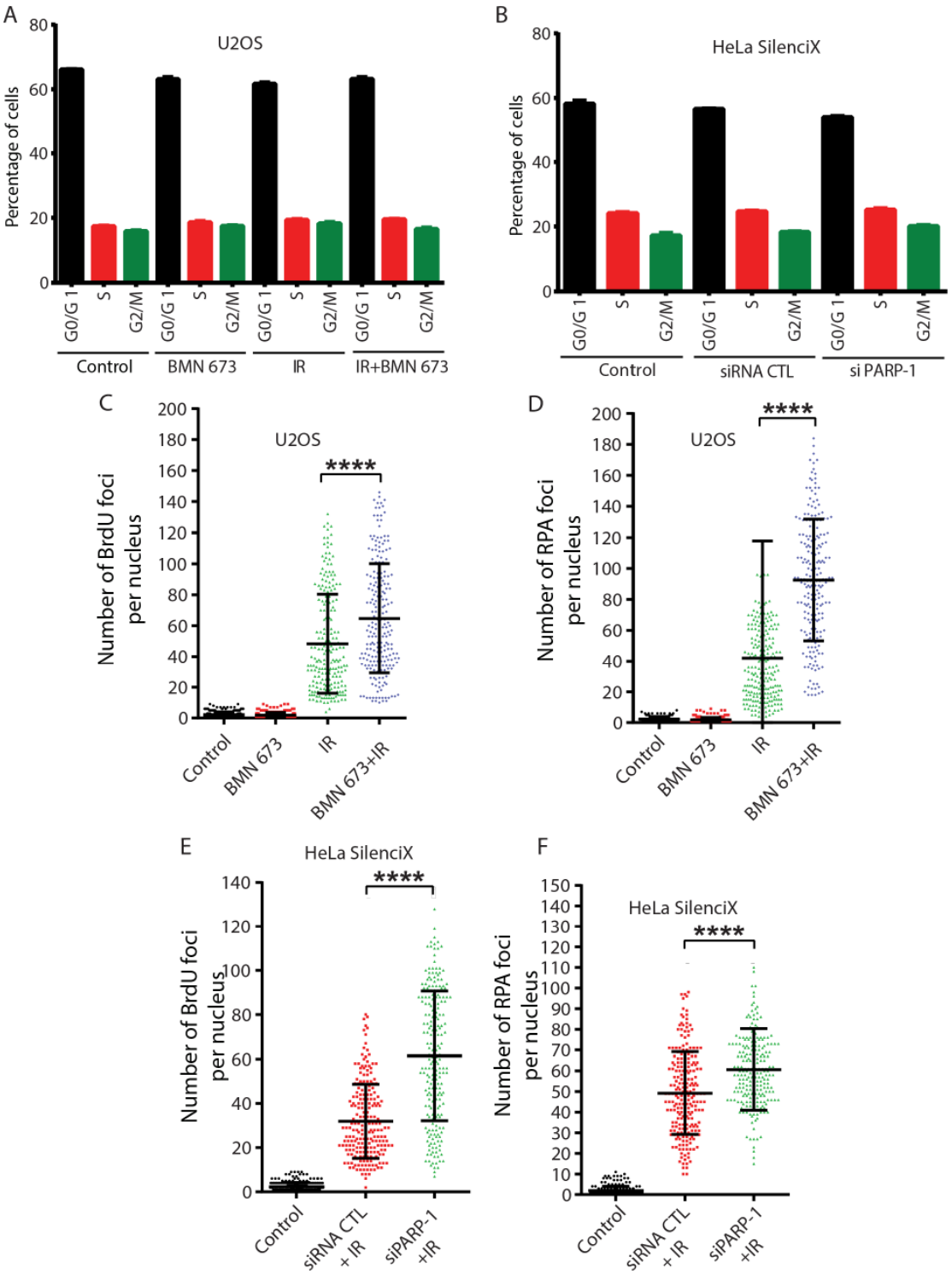

Figure 2.13: Supplementary Figure 5.

(A-B) FACS analysis to monitor the distribution of the indicated cells in each cell cycle phase for the BrdU/RPA analysis (3 hours release from the indicated treatments). Data show the Mean ± S.E.M. U2OS cells either mock treated, treated with BMN 673, irradiated (10 Gy), or irradiated (10 Gy) in combination with BMN 673, were subjected to immunofluorescence against BrdU (C) or RPA2 foci formation (D). The graph represent the number of BrdU/RPA focus per nucleus. HeLa SilenciX cells underexpressing PARP-1 by siRNA-mediated gene knockdown were subjected to immunofluorescence against BrdU (E) or RPA2 foci formation (F). The graph represent the number of BrdU/RPA focus per nucleus. **** $p \leq 0.0001$. Data show the mean ± s.d.

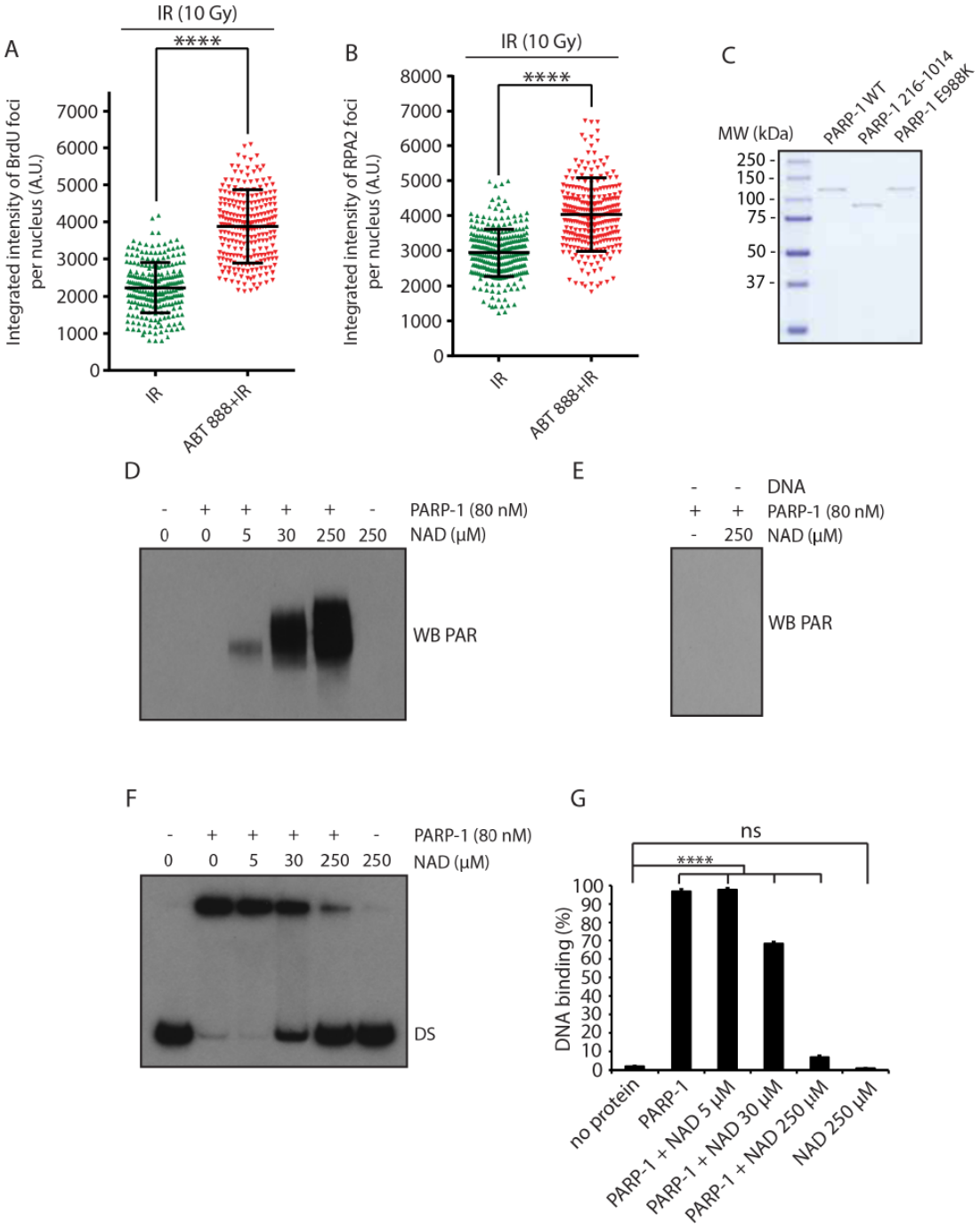

Figure 2.14: Supplementary Figure 6.

U2OS cells were either irradiated (10 Gy), or irradiated (10 Gy) in combination with Veliparib (5 μM), and subjected to immunofluorescence against BrdU (A) or RPA2 foci formation (B). The graph represents the intensity of BrdU/RPA focus per nucleus after 3 hrs recovery. Data show the Mean ± s.d. (C) SDS-PAGE of purified PARP-1 WT, PARP-1 DNA binding mutant 216-1014, and PARP-1 E988K. (D) PARP-1 was incubated in the resection buffer in the absence or presence of different concentrations of NAD and with

100 nM of dsDNA for 10 minutes at 37°C. PARP-1 activation was then visualized by western blotting using a pADPr antibody. (E) The same reactions were performed as mentioned in (D) without DNA. (F) DNA binding activity of PARP-1 to the dsDNA substrate in the presence or absence of different concentrations of NAD. (G) DNA binding quantifications. ****p<0.0001, Error bars indicate s.d.

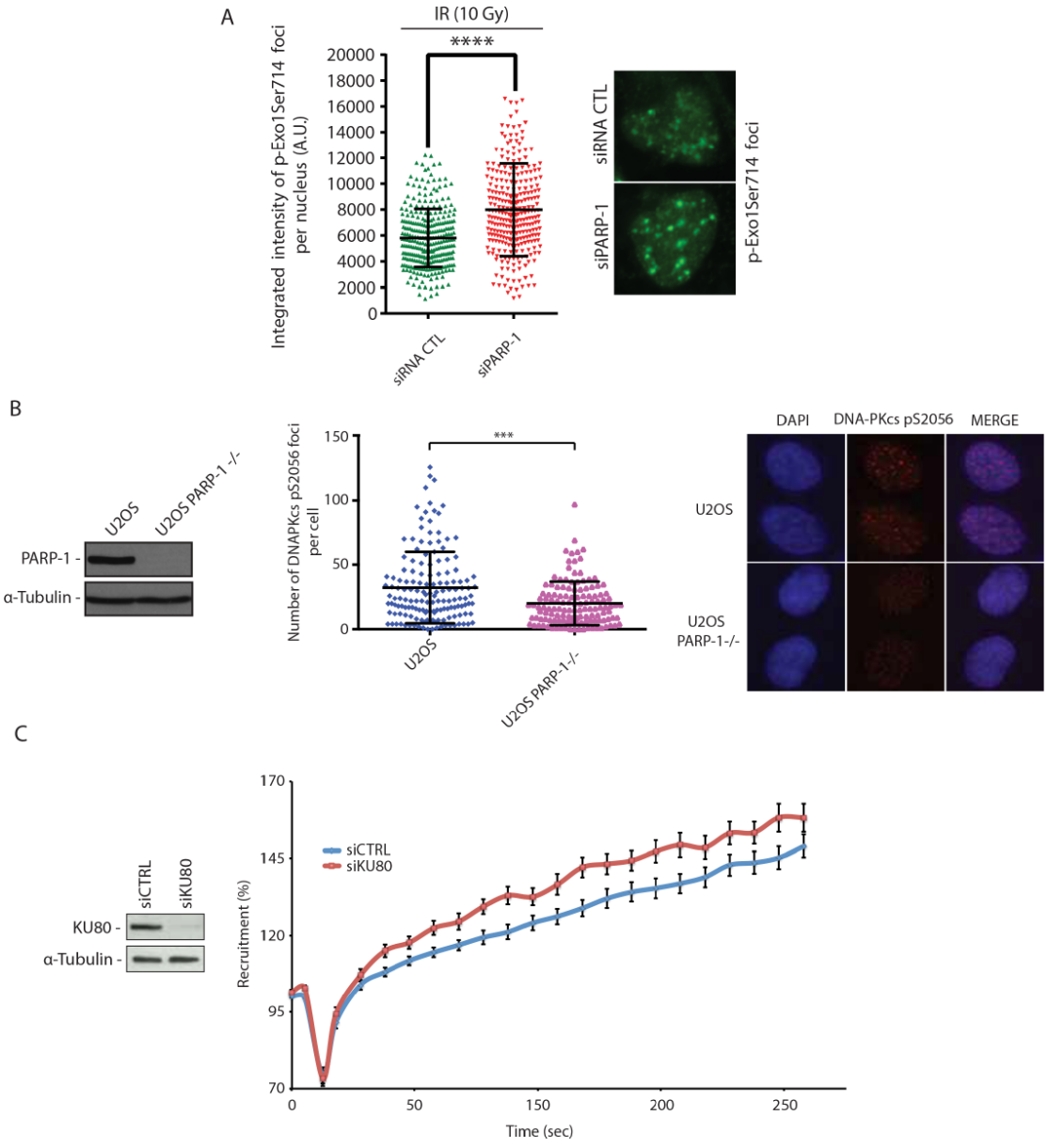

Figure 2.15: Supplementary Figure 7.

(A) Quantification of EXO1phospho-Ser 714 foci in U2OS cells knockdown for PARP-1 after irradiation (10Gy, 3 hours release). A representative immunofluorescence picture

is shown of the right. The graph represents the integrated intensity of EXO1phospho-Ser 714 foci per nucleus. Data show the Mean ± s.d. (B) Quantification of DNA-PKcs pS2056 foci in U2OS cells knockout for PARP-1 (left) after irradiation (5 Gy, 1 hour release). Data show the Mean ± s.d. A representative immunofluorescence picture is shown (right). (C) Left. Western blotting to monitor the knockdown efficiency of Ku80 in HeLa cells. Right. Recruitment of GFP-EXO1 in Ku80 knockdown cells. Data show the Mean ± S.E.M. *** $p \leq 0.001$, **** $p \leq 0.0001$.

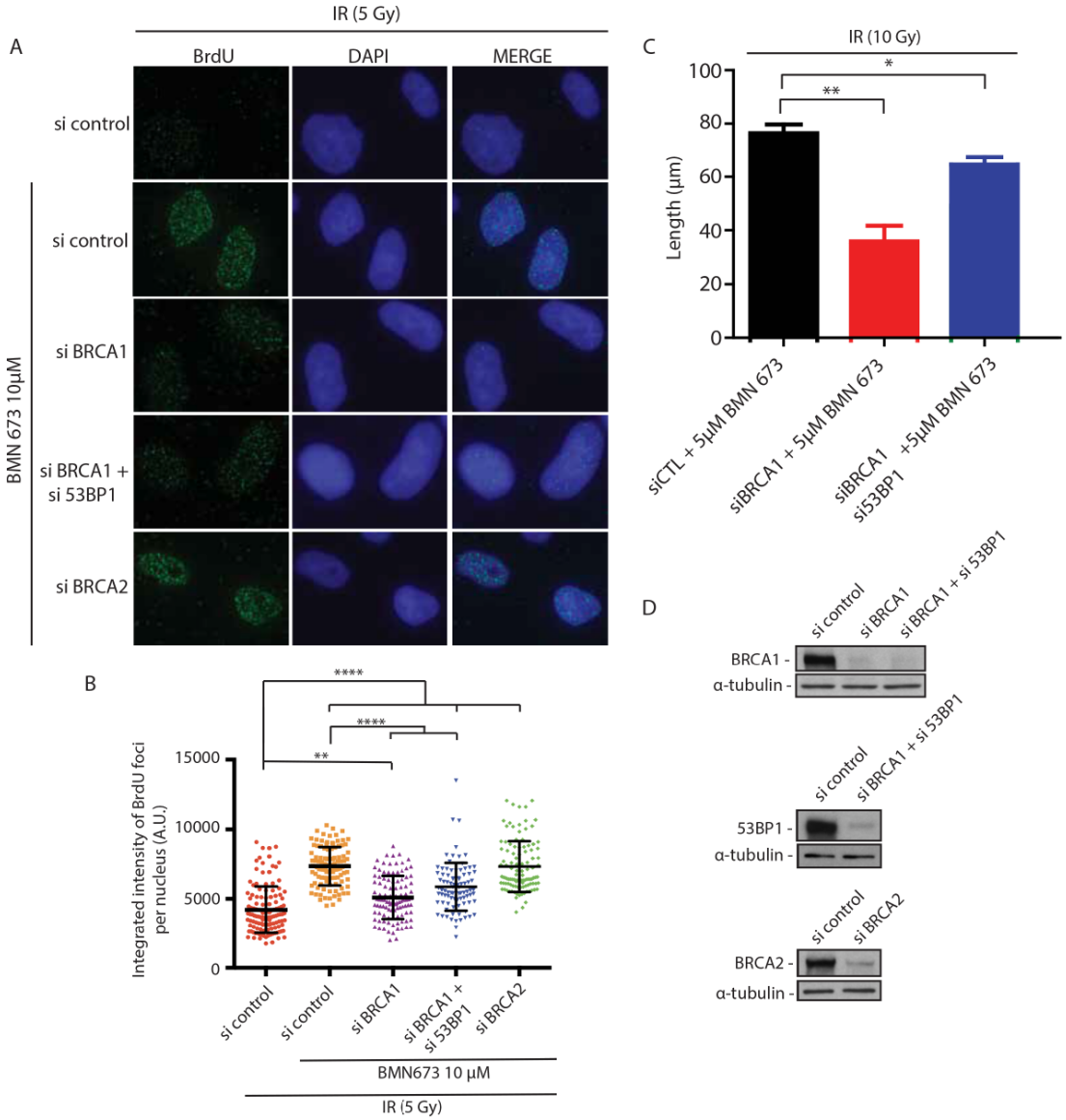

Figure 2.16: Supplementary Figure 8.

(A) In contrast to siRNA inhibition of BRCA2, BRCA1 knockdown decreases single-strand DNA accumulation after irradiation as detected by BrdU staining following

irradiation (5 Gy) and BMN 673 treatment. (B) Quantification of the results by integrated intensity of BrdU foci per nucleus. Data show the Mean ± s.d. In this panel, the statistical analysis was performed using Kruskal Wallis. (C) SMART assay. HeLa cells were transfected with the indicated siRNAs followed by irradiation (5 Gy) and treatment with BMN 673. 200 fibers were counted in triplicate. Data show the mean ± S.E.M. (D) Western blotting to monitor the knockdown efficiency of BRCA1, 53BP1, BRCA2 knockdown. * $p \leq 0.05$; ** $p \leq 0.01$, **** $p \leq 0.0001$.

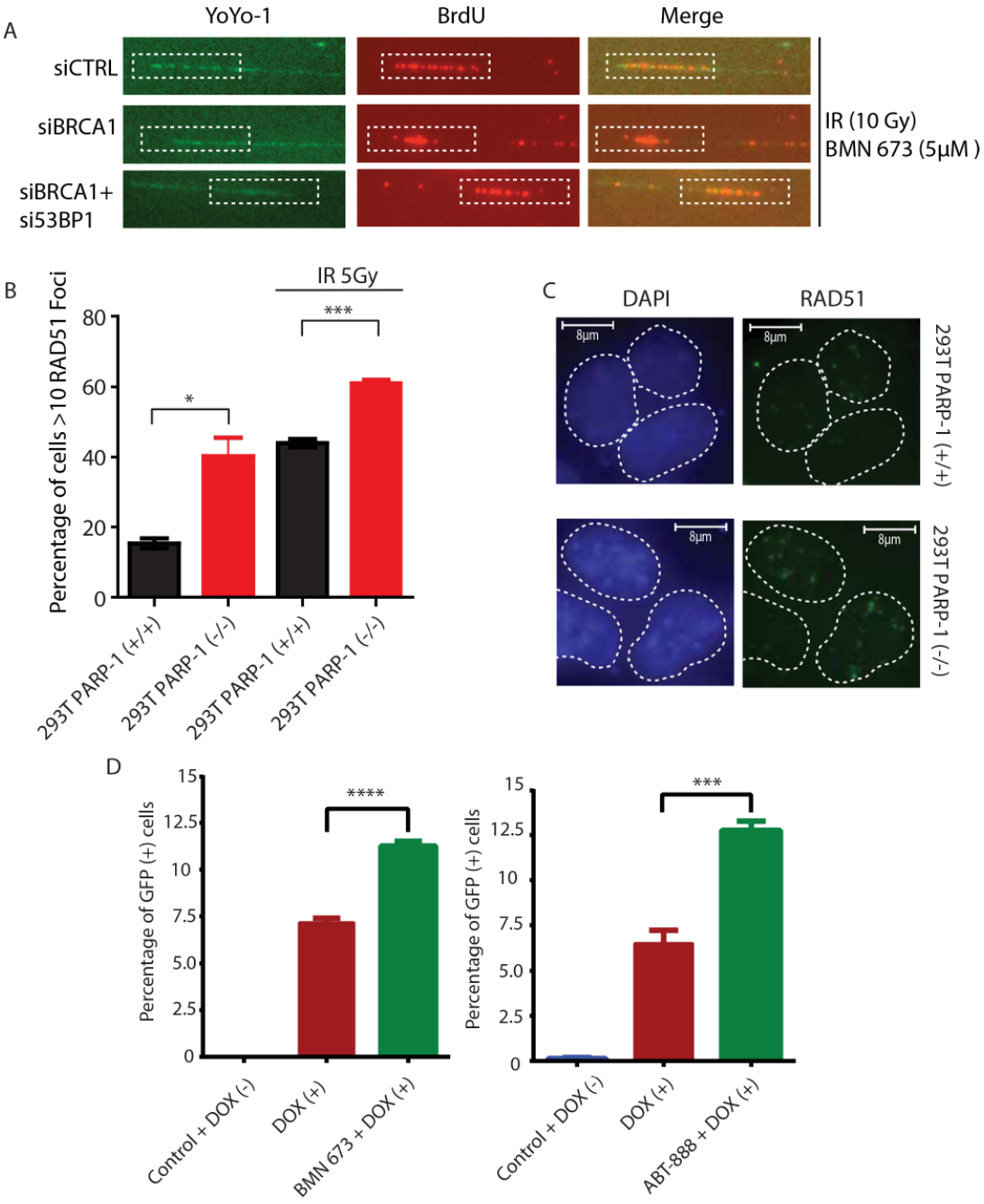

Figure 2.17: Supplementary Figure 9.

(A) Representative pictures of SMART assay samples. DNA tracks were stained with YoYo-1 and an anti-BrdU. The merge picture represent the overlay between the green and red channels. The BrdU signal could not be detected without irradiation. (B) RAD51 foci formation in CRISPR HEK293T cells proficient and deficient for PARP-1 without or with 5 Gy irradiation. The percentage of cells with more than 10 RAD51 foci were scored. (C) Typical example of RAD51 foci in both CRISPR HEK293T PARP-1 (+/+) and CRISPR HEK293T PARP-1 (-/-) after IR (5 Gy). (D) *In cellulo* homologous recombination is increased in BMN 673 (left) or ABT-888 (right) treated cells. Data show the mean ± S.E.M. ** $p \leq 0.01$, *** $p \leq 0.001$, **** $p \leq 0.0001$.

Supplementary Table 2.1 List of antibodies used in this study.

REAGENTS	SOURCE	DILUTION USED	IDENTIFIER
Antibodies			
PARP-1	Abcam	1:4000 (WB)	ab194586
PARP-1 (C2-10)	Homemade	1:5000 (WB)	This study
PARP-2	Abcam	1:4000 (WB)	ab176330
PARP-2	Enzo Life Sciences		ALX-804-639
β-Actin	Sigma	1:10000 (WB)	A5316
RIF1	Bethyl	3µl each sample (CHIP)	A300-569A
53BP1	Novus	3µl each sample (CHIP)	NB100-304
RPA2	Abcam	3µl each sample (CHIP)	ab76420
RPA2	Calbiochem	1:1000 (WB)	NA18
RPA2 S4/S8	Novus	1:1000 (WB)	NBP1-23017

BrdU	GE healthcare	1:750 (IF)	RPN202
Cyclin A	BD Biosciences	1:300 (IF)	611264
RPA2	Abcam	1:2000 (IF)	ab2175
γ-H2AX	Active motif	1:2000 (IF)	39117
BRCA1	Millipore	1:1000 (WB)	07-434
BRCA2	Millipore	1:250 (WB)	OP95
53BP1	Novus	1:2000 (WB)	NB100-304
53BP1	Novus	1:500 (IF)	NB100-304
Histone H3	Abcam	1:10 000 (WB)	Ab1791
GAPDH	Fitzgerald	1:20 000 (WB)	10R-G109A
Alpha-tubulin (DM1A)	Abcam	1:100 000 (WB)	Ab7291
RIF1	Bethyl	1:400 (IF)	A300-569A
CtIP	Active Motif	1:400 (IF)	61141
CtIP	Active Motif	1:3000 (WB)	61141
Geminin	Proteintech	1:300 (IF)	10802-1-AP
Alexa Fluor 488 goat anti-rabbit	Molecular probe	1:800 (IF)	A11008
Alexa Fluor 488 goat anti-mouse	Molecular probe	1:1000 (IF)	A11001
Alexa 568 goat anti-mouse	Molecular probe	1:800 (IF)	A11004

Alexa 568 goat anti-rabbit	Molecular probe	1:800 (IF)	A11011
Ku80	Cell Signalling	1:3000 (WB)	2180S
DNA Ligase IV	Abcam	1:3000 (WB)	ab193353
His tag	Clontech		631212
GFP	Abcam	1:8000 (WB)	Ab290
Alexa488 goat anti-rabbit	Life technology	1:400 (IF)	A11034
Mouse Cy3 goat anti-mouse	Jackson immuno	1:400 (IF)	115-165-146
RAD51	Cedarlane Labs	1:1000 (IF)	70-001
QDot 605 streptavidin conjugate	Thermo Fisher Scientific	5 nM (final working concentration)	Q10101MP
QDot 605 anti-mouse conjugate	Thermo Fisher Scientific	10 nM (final working concentration)	Q11001MP
QDot 705 anti-mouse conjugate	Thermo Fisher Scientific	10 nM (final working concentration)	Q11062MP
YOYO™-1 Iodide	Thermofisher	1 nM (final working concentration)	Y3601
Anti-BrdU	GE Healthcare	1:100 (SMART)	RPN202
Anti-YOYO	Invitrogen	1:1000 (SMART)	Y3601
DNA PKcs(phospho S2056)	Abcam	1:500 (WB)	Ab18192

pADPr (10H)	Tulip Biolabs	1:5000 (WB)	1020
pATR(Thr1989)	Genetex	1:1000 (WB)	GTX128145
Vinculin	Sigma	1:100 000 (WB)	V9131
Phospho-EXO1	Homemade	1:1000 (WB)	Kum Kum Khanna https://doi.org/10.1093/nar/gkp1164

Supplementary Table 2.2. Reagents or resources used in this study.

Chemicals, Peptides, and Recombinant Proteins		
Proteinase K	Sigma	P2308-100MG
Bromodeoxyuridine (BrdU)	Sigma	B5002
BMN 673	MedChem Express	HY-16106
Veliparib	MedChemExpress	HY-10129
Pre-stained Protein ladder	Frogga Bio	PM008-0500F
RNAiMAX	Invitrogen	13778-075
Oligofectamine	Thermo Fisher Scientific	12252011
Effectene	Qiagen	301425
BSA	Sigma	A7906

Fetal Bovine serum	Gibco	12483-020
Charcoal striped Serum	Sigma	F6765-100ML
Trypsin	Sigma	T4049-500ML
Hygromycin B	invitrogen	10687010
Shield1	TaKaRa	632189
Puromycin	Sigma	P9620-10ML
4-Hydroxytamoxifen (4-OHT)	Sigma	H7904-5MG
BsrG1	NEB	R0575S
BamH1-HF	NEB	R3136S
Bright Green 2x qPCR MasterMix-ROX	abm	MasterMix-R
DMEM high glucose	Fisher scientific	10063542
G418-Geneticin	Gibco	11811-031
Dynabeads Protein G	Invitrogen	10003D
Engraved Combicoverslips	Genomic Vision	COV-002-RUO
[α-32P] ATP	Perkin Elmer	NEG512H250UC
[γ-32P] ATP	Perkin Elmer	BLU002H250UC
NAD	Sigma	N0632
Terminal Transferase	NEB	M0315S
ProLong^{R} Gold Antifade Mountant	Invitrogen Life Technology	P-36930
Critical Commercial Assays		
FiberPrep^{R} (DNA Extraction Kit)	Genomic Vision	EXTR-001

Click-iT EdU Alexa Fluor™ 488 Imaging Kit	Thermo Fisher Scientific	C10337
Experimental Models: Cell Lines		
PARP-1 HeLa SilenciX	Tebu-bio	01-00019
Control Hela SilenciX	Tebu-bio	01-00001
U2OS	ATCC	HTB-96
U2OS CRISPR PARP-1(-/-)	This study	N/A
HeLa	ATCC	CCL-2
HEK 293T	ATCC	CRL-11268
HEK 293T CRISPR PARP-1 (-/-)	This study	N/A
ER-AsiSI U2OS	Gaëlle Legube	N/A
TRI-DR-U2OS	Philipp Oberdoerffer	N/A
DLD1 (BRCA2 +/-)	Scott Kern	N/A
DLD1 (BRCA2 -/-)	Scott Kern	N/A
HEK 293	ATCC	CRL-1573
U2OS-RPA2-GFP(stable)	This study	N/A
U2OS-DSB reporter cell line (Fok1 system)	Roger A Greenberg	N/A
Sf9	ThermoFisher	B82501
U2OS-Ku80-GFP(stable)	This study	N/A
MEFs PARP1 +/+	This study	N/A
MEFs PARP1-/-	This study	N/A

Oligonucleotides		
siRNA sequences	This paper	Table S1
qPCR primer sequences used in ER-*Asi*SI CHIP experiment	This paper	Table S2
qPCR primer sequences used in U2OS-DSB-reporter locus (FoK1) CHIP experiment.	This paper	Table S3
qPCR primer sequences used in ER-AsiSI resection assay	This paper	Table S4
Sequences of the oligonucleotides used for the bandshift assay	This paper	Table S5
Recombinant DNA		
Plasmid: pEGFP-C1-FLAG-Ku80	Addgene	Plasmid#46958
Plasmid: RPA1-GFP	This paper	N/A
Plasmid: RPA2-GFP	This paper	N/A
Plasmid: RPA3-GFP	This paper	N/A
Plasmid : GFP-EXO1	This paper	N/A
Plasmid : mCherry-PCNA	Schonenberger et al.	N/A
Software and Algorithms		
Prism	GraphPad	Ver-6
Image J	Image J	V1.51k
GDSC ImageJ (Find Foci plugins)	Herbert et al., 2014	http://www.sussex.ac.uk/gdsc/intranet/microscopy/imagej/gdsc_plugins.
Image Reader FLA-5000	FLA-5100 phosphorimager Software	V1.0

Gen5 Data Analysis Software v3.03	Gen5 Data Analysis Software	v3.03

Supplementary Table 2.3. List of siRNAs used in the study.

Target protein	**siRNA name**	**Sequence** 5'-3'
None	siRNA control	GGG AUA CCU AGA CGU UCU ATT dTdT
None	siRNA control	UUCGAACGUGUCACGUCAAdTdT
PARP-1	siPARP-1	AAG AUA GAG CGU GAA GGC GAA dTdT
PARP-1	siPARP-1-2	AAG AGC GAU GCC UAU UAC UGC dTdT
CtiP	CtiP	GGGAACAGCAGAAAGTCCTTCATGA
Ku80	siKu80	SASI_Hs01_00099411 (NM_021141, Sigma)
DNA Ligase IV	siDNA ligase IV	L-004254-00-0005 (Dharmacon)
53BP1	Si53BP1	GGACUCCAGUGUUGUCAUU dTdT
BRCA1	siBRCA1	CAGCAGUUUAUUACUCACUAA dTdT
BRCA2	siBRCA2	GAAGAAUGCAGGUUUAAUAUU dTdT
KU80	siKU80	GCGAGUAACCAGCUCAUAAUU

Supplementary Table 2.4: qPCR primer sequences used in ER-AsiSI CHIP experiment.

Name	Sequence 5'-3'

chr1_89231183: FW	GATTGGCTATGGGTGTGGAC
chr1_89231183: REV	CATCCTTGCAAACCAGTCCT
chr6_90404906: FW	TGCCGGTCTCCTAGAAGTTG
chr6_90404906: REV	GCGCTTGATTTCCCTGAGT
chr21_21292316:FW	TGGCTGGAACTGCTTTCTTT
chr21_21292316:REV	GGTGAGTGAATGAGCTGCAA

Supplementary Table 2.5: qPCR primer sequences used in U2OS-DSB-reporter locus (FoK1) CHIP experiment.

Name	Sequence 5'-3'
p1: FW	GGAAGATGTCCCTTGTATCACCAT
p1: Rev	TGGTTGTCAACAGAGTAGAAAGTGAA
p4: FW	CCACCTGACGTCTAAGAAACCAT
p4: REV	GATCCCTCGAGGACGAAAGG

Supplementary Table 2.6: qPCR primer sequences used in ER-AsiSI resection assay.

Name	Sequence 5'-3'
DSB-335 FW	GAATCGGATGTATGCGACTGATC'
DSB-335 REV	TTCCAAAGTTATTCCAACCCGAT

No DSB FW	ATTGGGTATCTGCGTCTAGTGAGG
No DSB Rev	GACTCAATTACATCCCTGCAGCT

Supplementary Table 2.7: Sequences of the oligonucleotides used for the EMSA assays.

Name	Sequence 5'-3'
JYM696	GGGCGAATTGGGCCCGACGTCGCATGCTCCTCTAGACTCGAGGAA TTCGGTACCCCGGGTTCGAAATCGATAAGCTTACAGTCTCCATTTAA AGGACAAG
JYM698	CTTGTCCTTTAAATGGAGACTGTAAGCTTATCGATTTCGAACCCGGG GTACCGAATTCCTCGAGTCTAGAGGAGCATGCGACGTCGGGCCCAA TTCGCCC

Chapter 3 **Assessment of global DNA double-strand end resection using a coupled BrdU-DNA labeling with cell cycle discrimination imaging method.**

Julia O'Sullivan[1],(*), Sofiane Y. Mersaoui[1],(*), Guy Poirier[2],[3] and Jean-Yves Masson[1],[5]

[1] Genome Stability Laboratory, CHU de Québec Research Center, HDQ Pavilion, Oncology Division, 9 McMahon, Québec City, QC, G1R 3S3, Canada.

[2] Department of Molecular Biology, Medical Biochemistry, and Pathology, Laval University Cancer Research Center, Québec City, QC, G1V 0A6, Canada.

[3] CHU de Québec Research Center, CHUL Pavilion, Oncology Division, 2705 Boulevard Laurier, Québec City, QC, G1V 4G2, Canada

(*) Equal contribution

Corresponding Authors:
Guy Poirier
Guy.Poirier@crchudequebec.ulaval.ca

Jean-Yves Masson
Jean-Yves.Masson@crchudequebec.ulaval.ca

Preface

In the final year of my PhD, we were contacted by the Journal of Video Editing (JoVE) and asked if we wished to contribute to a collection for methods of analysing the DNA damage response. I was very fortunate that Dr Jean-Yves Masson agreed to allow us to undertake this and share the specifics for the technique that has become central to my PhD work. The article entitled "**Assessment of global DNA double-strand end resection using a coupled BrdU-DNA labeling with cell cycle discrimination imaging method**" (Julia O'Sullivan[=], Sofiane Y. Mersaoui[=], Guy Poirier and Jean-Yves Masson) provides a step-by-step guide on how to perform the BrdU DNA resection immunofluorescence technique.

This technique allows for the analysis of effects on DNA end resection in HR through the use of immunofluorescence. In chapter 2, "Poly(ADP-ribose) polymerase-1 antagonizes DNA resection at double-strand breaks", we use this technique to explore the role of PARP-1 in resection, furthermore in chapter 4, "Zinc-Fingers? A new candidate for PARP-1 dependent DNA repair through Homologous Recombination" it is used as a screening tool in identifying a new candidate to study, making up the latter half of my PhD. This method for DNA resection analysis was one of the first techniques I was taught in the laboratory and has remained a core method for my PhD from start to finish. A copy of the PDF of this article can be found in the annexe.

Résumé

L'étude de la réponse aux dommages à l'ADN (DDR) est un domaine complexe et essentiel, qui n'a pris de l'importance que grâce à l'utilisation de médicaments ciblant la DDR pour le traitement du cancer. Ces cibles sont les poly (ADP-ribose) polymérases (PARP) qui initient diverses formes de réparation de l'ADN. L'inhibition de ces enzymes à l'aide d'inhibiteurs de PARP (PARPi) permet d'obtenir une létalité synthétique en conférant une vulnérabilité thérapeutique dans les cellules déficientes en recombinaison homologue (HR), en raison de mutations dans BRCA1, BRCA2 ou PALB2.

Les cellules traitées avec des PARPi accumulent des cassures double-brin de l'ADN. Ces cassures sont traitées par la machinerie de résection, conduisant à la formation d'ADN simple-brin et à la réparation ultérieure de l'ADN. Dans un contexte de déficience en BRCA1, rétablir la résection de l'ADN par des mutations dans les inhibiteurs de la résection tels que 53BP1 et DYNLL1 provoque une résistance aux PARPi. Par conséquent, être capable de surveiller la résection de l'ADN *in vivo* est essentiel pour une compréhension plus claire des voies de réparation de l'ADN et le développement de nouvelles stratégies afin de surmonter la résistance aux PARPi. Parmi les multiples méthodes, les techniques basées sur l'immunofluorescence (IF) permettent de détecter la résection globale de l'ADN après des dommages à l'ADN. Cette stratégie nécessite un marquage d'ADN génomique à impulsions longues avec du 5-bromo-2'-désoxyuridine (BrdU). Suite à des dommages à l'ADN et à la résection des extrémités de l'ADN, l'ADN simple-brin résultant est spécifiquement détecté par un anticorps anti-BrdU dans des conditions natives. De plus, la résection de l'ADN peut également être étudiée à l'aide de marqueurs du cycle cellulaire afin de différencier les différentes phases de celui-ci. Les cellules en phase S / G2 permettent l'étude de la résection finale lors de la recombinaison homologue, tandis que les cellules G1 peuvent être utilisées pour étudier la jonction d'extrémités non-homologues. Un protocole détaillé pour cette méthode d'IF couplée à la discrimination du cycle cellulaire est décrit dans cet article.

Abstract

The study of the DNA damage response (DDR) is a complex and essential field, which has only become more important due to the use of DDR-targeting drugs for cancer treatment. Such targets are poly(ADP-ribose) polymerases (PARP) which initiate various forms of DNA repair. Inhibiting these enzymes using PARP inhibitors (PARPi) achieves synthetic lethality by conferring a therapeutic vulnerability in homologous recombination (HR) deficient cells, due to mutations in BRCA1, BRCA2, or PALB2.

Cells treated with PARPi accumulate DNA double-strand breaks. These breaks are processed by the DNA end resection machinery leading to the formation of single-strand DNA and subsequent DNA repair. In a BRCA1 deficient context, reinvigorating DNA resection through mutations in DNA resection inhibitors such as 53BP1 and DYNLL1 causes PARPi resistance. Therefore, being able to monitor DNA resection *in vivo* is critical for a clearer understanding of the DNA repair pathways and the development of new strategies to overcome PARPi resistance. Among multiples methods, immunofluorescence (IF) based techniques allow for monitoring of global DNA resection after DNA damage. This strategy requires long pulse genomic DNA labeling with 5-bromo-2′-deoxyuridine (BrdU). Following DNA damage and DNA end resection, the resulting single-strand DNA is specifically detected by an anti-BrdU antibody under native conditions. Moreover, DNA resection can also be studied using cell cycle markers in order to differentiate between various phases of the cell cycle. Cells in the S/G2 phase allow the study of end resection within Homologous Recombination, whereas G1 cells can be used to study Non-Homologous End Joining. A detailed protocol for this IF method coupled to cell cycle discrimination is described in this paper.

3.1 **Introduction**

Modulation of DNA repair factors is an ever-evolving method for cancer therapy, particularly in DNA double-strand break (DSB) repair deficient tumour environments. The inhibition of specific repair factors is one of the ingenious strategies used to sensitize cancer cells to DNA damaging agents. Decades of research led to the identification of various mutations of DNA repair genes as biomarkers for therapeutic strategy choices[458]. Consequently, the DNA repair field has become a hub for drug development to insure a wide range of treatments, empowering the personalized medicine concept. DSBs are repaired by two main pathways: non-homologous end joining (NHEJ) and homologous recombination (HR)[459]. The NHEJ pathway is error-prone; rapidly ligating the two DNA ends with little to no DNA end-processing, involving the protein kinase (DNA-PKcs), the Ku70/80 complex, 53BP1 and RIF1 protein[460].

Alternatively, Homologous recombination (HR) is a faithful mechanism, initiated by BRCA1[461]. An essential step in HR repair is the DNA-end resection process, which is the degradation of the broken ends leading to single-stranded DNA with 3’-OH ends. BRCA1 facilitates the recruitment of the downstream proteins that form the resectosome MRE11/RPA/BLM/ DNA2/EXO1, which are involved in the 5' to 3' DNA resection (reviewed in ref [69]). The initial end-resection is accomplished through the endonuclease activity of MRE11, allowing for further processing by the DNA2 and EXO1 nucleases. The generated single-strand (ssDNA) overhangs are quickly coated by Replication Protein A (RPA) to protect them from further processing. Subsequently, BRCA2, PALB2 and BRCA1 engage mediating the displacement of RPA and the assembly of the RAD51 nucleofilament required for homology directed repair mechanism. A fine balance between the usage of NHEJ and HR is necessary for the optimal maintenance of genomic integrity. The pathway choice depends on the cell cycle phase. The HR is preferentially used during the S to G2 phases wherein DNA resection is at the highest level and the sister chromatids are available to unsure a proper repair.

Poly (ADP-ribose) polymerase 1 (PARP-1) is one of the earliest proteins recruited to the DSB, it regulates both resection activity and the assembly of downstream effectors involved in the NHEJ[69, 445]. PARP-1 is also required for DNA single-strand breaks

(SSB) repair during replication[462, 463]. Due to its important role in DNA repair, PARP inhibitors (PARPi) are used as cancer therapies. In several HR-deficient cancers PARPi treatment leads to a synthetic lethal response, due to the incapacity of HR-deficient cells to repair the accumulated damage with an alternative pathway[138, 464]. There are currently four FDA approved PARPi: Olaparib, Rucaparib, Niriparib and Talazoparib (also called BMN 673), which are used for various breast and ovarian cancer treatments[465]. However, PARP inhibitors resistance is common and one potential cause arises through the reacquisition of HR proficiency[466]. We recently reported that loss or inhibition of PARP-1 in the presence of irradiation missregulate the resectosome machinery leading to the accumulation longer ssDNA tracts[467]. Therefore, an in-depth study of DNA resection *in vivo* is critical for a clearer understanding of the DNA repair pathways and the subsequent development of new strategies to treat cancer and to overcome PARPi resistance.

Several methods have been developed to detect DNA Resection events[69]. One such method is the classical immunofluorescence-based technique allowing for an indirect staining and visualization of the resected DNA after stress-induced DSB through the use of an anti-RPA antibody. Given that RPA is also involved in DNA replication, the use of the labeling genomic DNA with 5-bromo-2′-deoxyuridine (BrdU) overcomes the false positive RPA foci due to the replication. Cells incubated with BrdU for a single cell cycle allows for BrdU to be incorporated into one strand of the replicating cellular DNA. After resection, immunofluorescent staining is performed in conditions where BrdU can only be detected in the single-stranded (ss)DNA with an anti-BrdU antibody, limiting the identification to only single-stranded DNA following resection. The resected DNA can be visualized by fluorescence microscopy as punctate BrdU/ssDNA “foci” whose nuclear intensity or number can serve as a metric to quantify resection in cells responding to DNA damage. Herein, we describe step-by-step this method, which does not involve sophisticated instrumentation and can be applied to most mammalian cell lines. This method should be of broad utility as a simple way of monitoring DNA end resection *in cellulo*, as a proof of concept.

3.2 **Protocol**

3.2.1 Cell culture, treatments, and coverslip preparation

NOTE: All cell plating, transfections, and treatments, aside from irradiation, should take place under a sterile cell-culture hood.

3.2.1.1 Day 1

1. In a 6-well plate, place a single coverslip in each well for as many conditions as needed. Plate ~150,000 Hela cells for transfection or drug treatment, as desired.

NOTE: If transfecting, it is recommended to do a reverse transfection at the time of plating, or it is possible to do a forward transfection several hours after plating to allow for adherence. A reverse transfection is accomplished by adding the transfection mix to the coverslip before the cells are added; thus, transfection begins before the cells start adhering. A forward transfection, by contrast, is the addition of the transfection mix post-adherence to the surface usually on the following day. However, it is possible to do this on the same day, provided enough time is given for the cells to adhere.

2. For this method, use 4 wells: Well 1: siRNA control (termed siCTRL); Well 2: siRNA against PARP-1 (siPARP-1); Well 3: untreated; Well 4: Cells to be treated with 5 µM BMN673 1 h prior to irradiation.

NOTE: In this protocol, all the tests were conducted under irradiated conditions (see section 1.3).

3. Incubate the cells at 37 °C in a 5% CO_2 humidified incubator overnight, although the transfection protocol allows for up to 3 days of incubation. The incubation time prior to BrdU treatment will depend on the siRNA transfection efficiency. If there is no transfection, incubation for 16 h is sufficient to allow for adherence to the coverslip and some cell growth.

NOTE: Incubator conditions can be changed according to the cell line used.

3.2.1.2 Day 2

1. Add BrdU at a final concentration of 10 µM in the appropriate culturing media, and incubate for 16 h (one cell cycle).

NOTE: The BrdU solution is prepared in dimethylsulfoxide; the stock solution used is 10 mM and is stored in aliquots at -20 °C.

3.2.1.3 Day 3

1. Irradiate the plates with a total dose of 5 Gy of X-ray irradiation (vary the dose of irradiation depending on the irradiator type, for example, small animal irradiators vs. benchtop irradiators). See the **Table of Materials** for the brand and model of irradiator used.

2. Return the plates to the incubator, and release the cells for 3 h.

3. During the 3 h incubation period, prepare the two buffers, A and B, and 4% paraformaldehyde (PFA) in 1x phosphate-buffered saline (PBS).

NOTE: Buffers A and B and the sucrose should be prepared fresh the day of fixation, using fresh sucrose solution to prevent contamination.

4. Prepare buffer A (Pre-Extraction Buffer), according to the order (30 mL) described in **Table 4.1**.

NOTE: The 1M sucrose should be prepared the day of use to prevent contamination.

5. Prepare buffer B (Cytoskeleton Stripping Buffer) according to the order described in **Table 4.1** (30 mL)

NOTE: Buffer B must be prepared in the cited order to prevent precipitation of Tween-20 and sodium deoxycholate solution.

6. Prepare 4% PFA, 2 mL per condition (10 mL), under a chemical hood (**Table 4.1**).

3.2.2 Pre-extraction and fixation

NOTE: All pre-extraction and fixation steps are performed with the coverslips remaining in the tissue culture plate on ice or at 4ºC; the coverslip is only lifted in the last step of mounting (see discussion).

1. Pre-extraction

1.1. Aspirate the medium, carefully wash the cells twice with 1x PBS, and remove the PBS. Add 2 mL of Pre-extraction Buffer A and immediately incubate at 4 °C for 10 min.

NOTE: It is important that incubation time in buffer A is not extended. Extended incubation in the pre-extraction buffers will result in an increased number of detached cells from the coverslip. Alternatively, instead of incubation at 4°C, incubation can be done on ice.

1.2. Remove Buffer A through aspiration.

NOTE: Do not wash the coverslips after removing buffer A. Proceed to the next step.

1.3. Add 2 mL of Cytoskeleton Stripping Buffer B and immediately incubate at 4 °C for 10 min. Carefully aspirate Buffer B, and carefully wash the cells once with 1x PBS. Carefully aspirate the 1x PBS.

2. Fixation

2.1. Fix the cells by adding 2 mL of 4% PFA under the chemical hood.

NOTE: PFA is toxic and must be manipulated under a chemical hood.

2.2. Incubate the cells at room temperature for 20 min. Wash the coverslips twice with 1x PBS, and aspirate the excess.

2.3. Cover the coverslips with 100% cold methanol, and incubate the coverslips at -20 °C for 5 min. Wash twice with 1x PBS.

NOTE: The protocol can be paused here. The coverslips can be stored at 4 °C in 1x PBS and the plate wrapped in aluminum foil if necessary. The cells should not be kept more than 5 days before continuing the IF protocol.

3. Permeabilization

3.1. Incubate the cells with 2 mL of 1x PBS containing 0.5% Triton X-100 at room temperature for 15 min. Wash the coverslips three times with 2 mL of 1x PBS.

4. Immunostaining

4.1. Blocking step

4.1.1. Prepare enough fresh blocking buffer (3% BSA in 1x PBS) to use 2 mL per coverslip.

NOTE: Prepare an extra 5mL of blocking buffer to make the antibody solutions.

4.1.2. Add 2 mL of blocking buffer to each well and incubate at room temperature for 1 h.

4.2. Primary antibody incubation

4.2.1. Prepare the primary antibody solution in fresh blocking buffer: BrdU RPN202 1:1000 and proliferating cell nuclear antigen (PCNA) 1:500, 100 µL per coverslip.

NOTE: To preserve the antibody, a smaller volume can be used, 75–100 µL for a 22 x 22 mm coverslip, 50–75 µL for an 18 x 18 mm coverslip.

4.2.2. On each coverslip, add 100 µL of primary antibody solution. Cover the coverslips with a square of parafilm using tweezers, and carefully position the parafilm to not create bubbles.

4.2.3. Cover the plate in aluminum foil and incubate the primary antibody overnight at 4 °C in a humidified chamber.

4.2.4. Remove the parafilm squares and wash the coverslips three times with 2 mL of sterile 1x PBS.

4.3. Secondary antibody incubation

4.3.1. Prepare enough secondary antibody solution in fresh blocking buffer: anti-mouse 488 fluorescent secondary A11011 (for BrdU) dilution 1:800 and anti-rabbit 568 fluorescent secondary A11011 (for PCNA) dilution 1:800.

NOTE: The colors used can be changed to suit the experimental needs. The specific brand used can be found in the **Table of Materials**.

4.3.2. Add on each coverslip 100 µL of secondary antibody solution, cover the coverslips with a square of parafilm using tweezers, and carefully position the parafilm without bubbles. Cover the plate in aluminum foil.

4.3.3. Incubate the secondary antibody at room temperature for 1 h.

4.3.4. Wash the coverslips three times with 2 mL of 1x PBS.

4.4. Nuclear staining

4.4.1. Prepare a volume of 2 mL per coverslip of 1x PBS containing 4',6-diamidino-2-

phenylindole (DAPI) at a final concentration of 1 µg/mL (1:1000).

4.4.2. Add on each coverslip 2 mL of the DAPI solution. Cover the plate in aluminum foil. Incubate the coverslips at room temperature for 10 min. Wash the coverslips twice with 1x PBS.

4.4.3. Cover the coverslips with 1x PBS, and use either a needle or fine tweezers to lift the coverslip from the bottom of the well. Carefully blot the off the excess liquid by tapping one edge gently on a paper towel.

NOTE: Be careful not to drop the slide or allow the flat surface with the adherent cells to touch the paper.

4.4.4. Mount the coverslips on slides using 10–20 µL of IF-specific mounting media.

5. Image acquisition and analysis

NOTE: Image acquisition can be done on several types of fluorescent microscopes. An epifluorescence microscope with a 63x oil objective was used; see the **Table of Materials** for the brand and model. Z-stacks are not required, although they may be of use depending on the cell line and level of mitochondrial staining.

5.1. Image analysis

5.1.1. For each image, create multiple tiff files; merge all planes, but keep the color channels separate. Import these files into Cell Profiler (The Broad Institute https://cellprofiler.org/home) and analyze using the Speckle Counting pipeline (**Supplemental Video 1**).

5.1.2. Upload the images (**Figure 3.3 Supplemental Figure S1A**).

5.1.3. To begin creating the project, load the speckle counting pipeline into the program and the images to be analyzed in the provided area.

5.1.4. Use the **NamesAndTypes** module to assign a meaningful name to each image by which other modules will refer to it—C01: Representing BrdU Channel; C02: Representing PCNA Channel; C03: Representing DAPI Channel.

NOTE: These identifiers will depend on the microscope; there should be an identifier in the file name to distinguish between the channels.

5.1.5. Identify which file will be used to identify the nuclei and name it (change this name as required) (see **Figure .3 Supplemental Figure S1B** and **Supplemental Figure S1C**).

5.1.6. Select the diameter of the object between 50 and 300 pixel units, which is the acceptable size range for nuclei, but change the value to fit the nuclei in the image.

NOTE: It may be that 50 is too large a value and prevents smaller nuclei from being identified; likewise, 300 may allow for large groupings of nuclei to be counted as 1.

5.1.7. Discard objects outside of the diameter range to ensure only those that match the criteria will be counted.

5.1.8. Discard objects touching borders to remove cells that may only be partially in the field.

5.1.9. Apply the threshold to fit the specific images. Note the following settings as an example. Change the thresholding correction factor based on how stringent the thresholding strategy will be. Other settings include threshold strategy: Global; thresholding method: Otsu; two class or three class thresholding: Two class; threshold smoothing scale: 1; threshold smoothing factor: 1; lower and upper bounds on threshold: 0.0 and 1.0; method to distinguish clumped objects: Shape; and method to draw dividing lines between clumped objects: Propagate.

NOTE: For each parameter, cell profiler provides complementary definitions and available possibility for the variable setting.

5.1.10. Identify the primary object to identify the foci (**Supplemental Figure S2A**).

5.1.11. Use the following settings: select the input image: Maskedgreen; named the primary object to be identified: BrdUFoci; typical diameter of the object: 1-15; discard the object outside the diameter range: Yes; discard the object touching the border of the image : No; threshold strategy: Adaptative; thresholding method: Otsu; two class or three class thresholding: Three class; threshold smoothing scale: 1; threshold smoothing factor: 3; and size of smoothing filter: 4.

5.1.12. Measure intensity (**Supplemental Figure S2B**).

5.1.13. Select the image to be measured: OrigGreen.

5.1.14. Click on **Add another image**. Select the image to be measured: PCNA. Select objects to measure: Nuclei.

NOTE: This will be used to measure the BrdU and PCNA intensity—the final data that will be graphed.

3.3 Representative Results

In this protocol, the bromodeoxyuridine (BrdU)-based assay was used to quantitatively measure the resection response of HeLa cells to irradiation-induced damage. The generated ssDNA tracks are visualized as distinct foci after immunofluorescence staining (**Figure 3.1A**). The identified foci were then quantified and expressed as the total integrated intensity of the BrdU staining in the nuclei (**Figure 3.1B**, **4.3 Supplemental Figure S1**, **3.4 Supplemental Figure S2**, and **3.5 Supplemental Figure S3**). It is possible to measure the foci number or mean foci intensity, although this can be less reliable than the total nuclear intensity, largely in part to the variable size of the BrdU foci.

To differentiate between the short-range resection as a result of NHEJ and the long-range resection of HR, co-staining was performed using an anti-PCNA antibody to identify cells going through S-phase (**Figure 3.1** and **3.6 Supplemental Figure S4**).

PCNA constitutes the DNA clamp that acts as a processivity factor for DNA polymerase and is essential for replication. PCNA is prominent in the nucleus and reaches maximal expression during the S-phase of the cell cycle. Hence, in early S-phase, the PCNA signal is low and has a granular distribution. In contrast, in late S-phase, the PCNA staining is quite strong (**Figure 3.1A**). When first analyzing the PCNA (S-phase) signal, the nuclei must be identified and the PCNA intensity measured.

The resulting values are then plotted as a scatter plot to best determine the cut-off intensity to discriminate between the PCNA-positive and PCNA-negative nuclei (**3.6 Supplemental Figure S4A**). The PCNA-negative results will then be removed from the data set to allow for the BrdU intensity-based analysis because of the low BrdU signal regardless of the condition (**3.6 Supplemental Figure S4B**). In these experimental conditions, the PCNA-negative nuclei harbor a basal integrated intensity of BrdU foci of 900 arbitrary units (A.U.). However, this value reaches 1800 A.U. in PCNA-positive nuclei (**Figure 3.1B**). This represents a 100% increase in the amount of the integrated signal of the BrdU foci. Increase in BrdU intensity can be then correlated to an increase in DNA resection, which is more pronounced and efficient when cells go through S and G2 phases and are irradiated.

In this protocol, to demonstrate an increase in DNA resection after irradiation (5 Gy), PARP-1 activity was modulated either through the loss of PARP-1 using an siRNA knockdown condition or after potent inhibition of PARP-1 using Talazoparib (BMN673) (**Figure 3.2** and **3.7 Supplemental Figure S5**). The amounts of resected DNA in each condition were then quantified after IF (**Figure 3.2B**). In unperturbed condition (siCTRL), the integrated intensity of BrdU foci per nucleus is approximately 1500 A.U. in the PCNA-positive nuclei (**Figure 3.2A, B**). After an efficient knockdown of PARP-1 using an siRNA (**Figure 3.2C**), a significant increase in the intensity of the BrdU foci to approximately 1900 A.U. was observed, which corresponds to 26% increase in intensity ($p < 0.0001$). Similarly, after inhibition of PARP-1 using BMN673 (5 µM final concentration), the intensity of foci increased from approximately 1750 to 2500 A.U. corresponding to 43% increase of the foci intensity ($p < 0.0001$). These corroborate that loss of PARP-1 misregulates DNA resection as reported previously[13]. It is important to remember that BMN-673 both inhibits the activity of PARP-1 and traps it to DNA, as such the effect of this treatment is much more detrimental to the cell, resulting in the

greater increase of BrdU intensity than in our siRNA treated cells. The slight difference in untreated and siCTRL intensities demonstrate how any treatment, such as siRNA transfection may affect the response and output of an assay. It can further demonstrate the importance of using the proper controls for each condition.

3.4 **Discussion**

We have described a method that makes use of immunofluorescent staining to measure variations in DNA resection *in cellulo*. The current standard for observing an effect on DNA resection is through RPA staining, this is, however an indirect method that may be influenced by DNA replication. Previously, another BrdU incorporation-based DNA resection IF has been described, the method for classifying the resulting intensities was in BrdU positive and negative cells, this allowed for cells which are not undergoing HR to be counted as positive due to background or mitochondrial staining which resulted in a high BrdU intensity[432, 468, 469]. The primary novelty of our method is the addition of the PCNA staining which allows for selectivity for S and G2 phases of the cell cycle, ensuring that the resulting BrdU signal is due resection and thus homology-directed repair.

The critical step in this protocol is the pre-extraction, without this, the BrdU foci will not be visible and if done incorrectly the cells will detach completely. Incorrectly prepared buffers will result in incomplete pre-extraction, such as partial cytoskeletal removal or increased background signal. It is very important to respect the incubation timing of the pre-extraction buffers, an increased time in the buffers can result in the cells detaching from the coverslip. Importantly if you are attempting this protocol with poorly adherent cells, pretreat the coverslips with polylysine to reduce cell detachment during pre-extraction. Subsequently, without methanol fixation, the PCNA signal will not be visible. Another important variable in this protocol is the blocking buffer, incompatible blocking buffers will result in loss of BrdU signal. 10%FBS in PBS 1X blocking buffer for example will function when not in combination with the methanol fixation, when combined with methanol fixation as required for the PCNA staining the BrdU signal is significantly reduced. It is possible other blocking will function with this protocol but in our experience, the 3% BSA in PBS 1X provides the best results.

A possible modification to the protocol is the PCNA antibody used; we have successfully tested two different PCNA antibodies, the one listed here and another with is no longer in production which was a rat monoclonal antibody (Bulldog Bio PCA16D10). Finally, while we suggest covering the coverslips with paraffin during antibody incubation. It is not strictly necessary, though a significantly larger volume of antibody solution would be required to cover the coverslip entirely without this. Another method for this is the place a sheet of paraffin surrounding a glass plate and placing drops of the antibody solution onto the paraffin and carefully placing the coverslip cell side down onto the drop of antibody solution. This glass plate can then be placed in a humid chamber at 4°C overnight for primary incubation and in the dark at room temperature for secondary incubation. This method is completely functional though does significantly increase the time handling the coverslips and as a result increases the probability of dropping or breaking the coverslip.

An alternative method to measure resection is through the use of the DNA combing SMART method, while this technique provides very clear results it is much more complicated, requires more time and is more expensive[470]. Requiring the extraction of the DNA without damaging it, followed by stretching this DNA onto coverslips to be followed by an IF. Our BrdU IF method by comparison is both simple and cost effective not requiring a greater investment than the cost of the antibody. As such this method provides an initial way to measure resection that is more accurate than simply measuring RPA foci formation, which as previously stated could include replication foci. This technique provides not only a method to determine if a protein is involved in resection but also to determine if cell death resulting from drug treatment is because of hypo/hyper-resection. This information will be key in better understanding not only DNA repair but also the biological mechanism behind the drug-induced cell death.

3.5 Acknowledgments

This work is supported by funding from Canadian Institutes of Health Research J.Y.M (CIHR FDN-388879). J.-Y.M. holds a Tier 1 Canada Research Chair in DNA Repair and Cancer Therapeutics. J.O'S is an FRQS PhD student fellow and S.Y.M is a FRQS postdoctoral fellow.

3.6 **Figure and table legends**

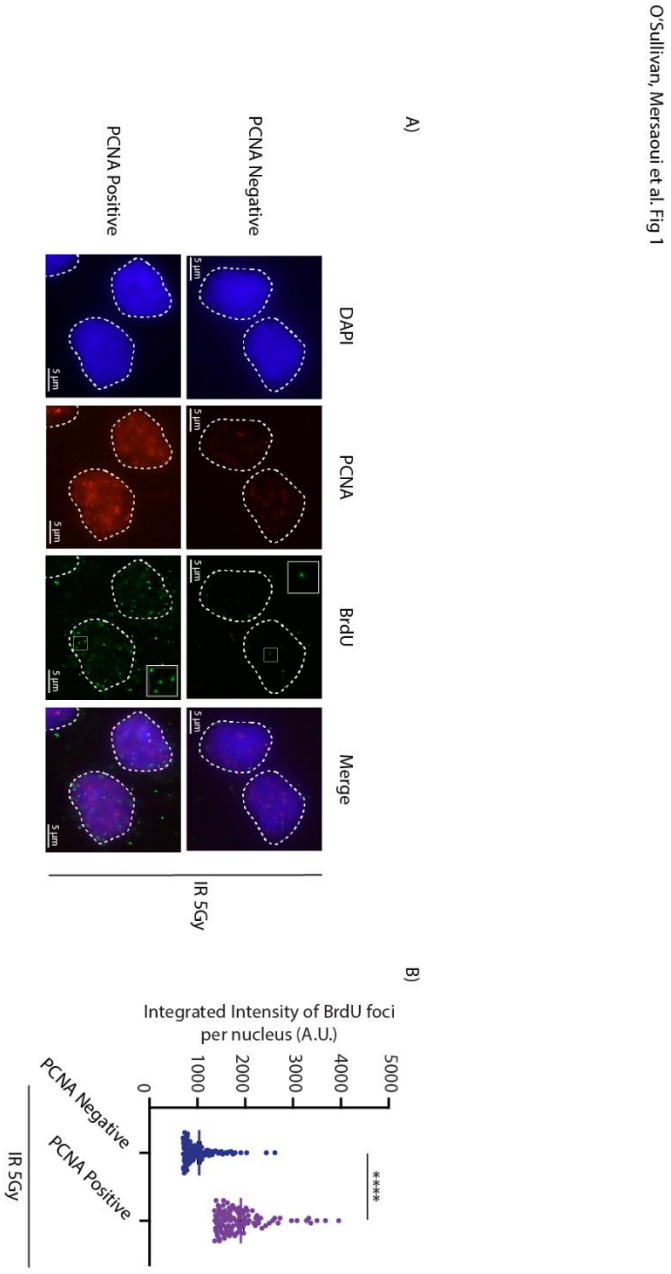

Figure 3.1: BrdU foci formation is more prone to occur in PCNA-positive cells than in replicating cells.

A) Representative images of BrdU foci formation and PCNA staining following 5 Gy irradiation and 3 h release. A zoomed-in square showing marked BrdU foci is present in the corner of each BrdU image. Scale bars = 5 µm. (B) Quantification of the BrdU nuclear intensity in untreated (without BMN-673) HeLa cells. The data show the mean ± s.e.m (Mann–Whitney U-test). Abbreviations: BrdU = 5-bromo-2′-deoxyuridine; PCNA =

proliferating cell nuclear antigen; IR = irradiation; DAPI = 4',6-diamidino-2-phenylindole; A.U. = arbitrary units; s.e.m. = standard error of the mean.

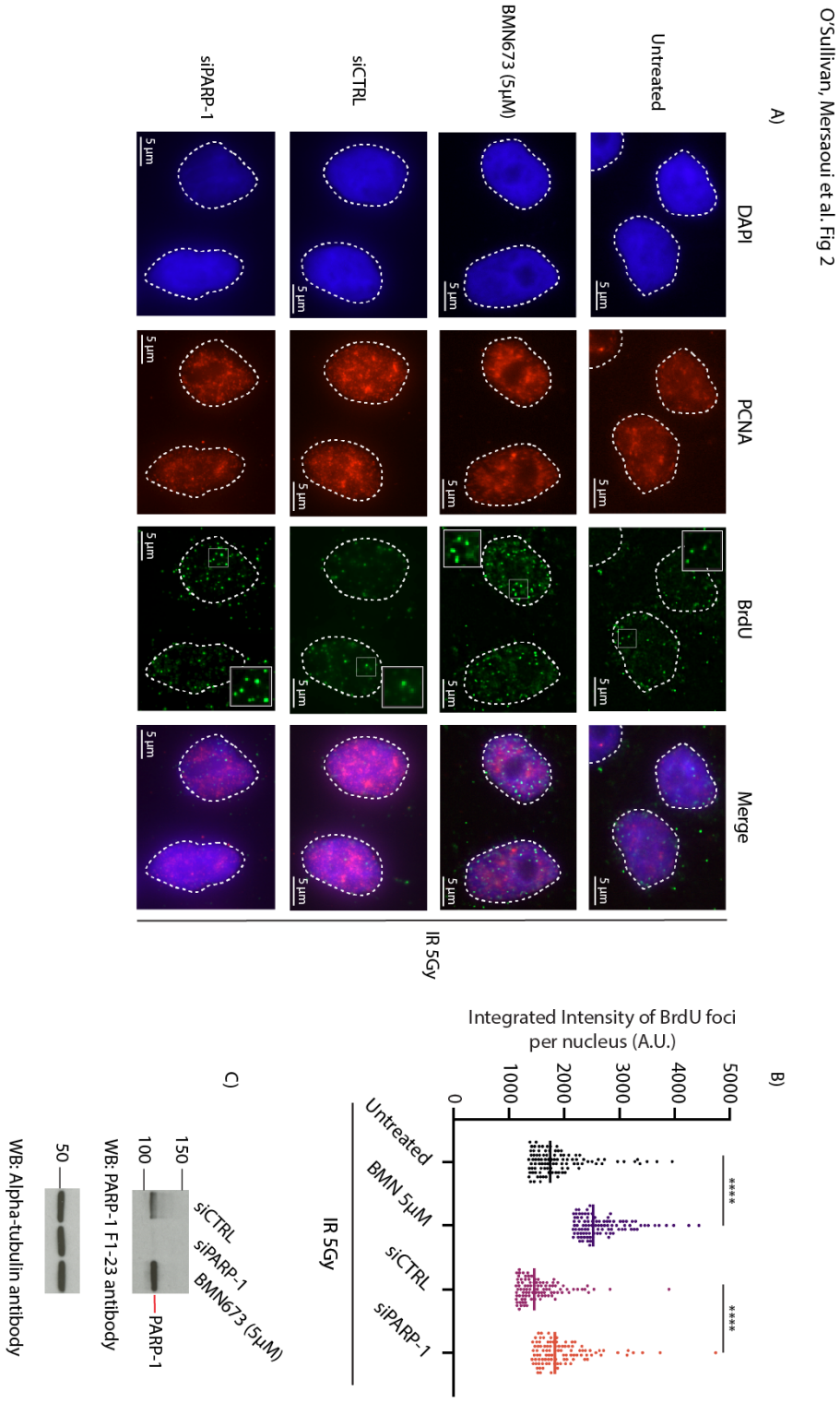

Figure 3.2: Poly(ADP-ribose) polymerase-1 knockdown or inhibition results in increased BrdU foci formation in replicating cells.

(**A**) Representative images of BrdU foci formation and PCNA staining in untreated HeLa cells, treated with 5 μM BMN-673, siCTRL, and siPARP-1, followed by 5 Gy irradiation and 3 h release. A zoomed-in square showing marked BrdU foci is present in the corner of each BrdU image. Scale bars = 5 μm. (**B**) Quantification of the BrdU nuclear intensity in untreated HeLa cells, treated with 5 μM BMN-673, siCTRL, and siPARP-1 followed by 5 Gy irradiation, the data show the mean ± s.e.m (Mann–Whitney *U*-test). (**C**) Western blot to validate the siRNA knockdown of *PARP-1*. The F1-23 PARP-1 antibody recognizes automodified PARP-1 resulting in the smeared appearance of the siCTRL band and the solid appearance of the catalytically inhibited PARP-1 in BMN-673-treated samples. Abbreviations: PARP-1 = poly(ADP-ribose) polymerase 1; BrdU = 5-bromo-2′-deoxyuridine; PCNA = proliferating cell nuclear antigen; IR = irradiation; DAPI = 4',6-diamidino-2-phenylindole; A.U. = arbitrary units; siCTRL = siRNA control; siPARP-1 = siRNA to knock down *PARP-1*; s.e.m. = standard error of the mean.

Figure 3.3 Supplemental S1: Visual representation of the Cell Profiler Software and Speckle counting pipeline part 1.

(**A**) Screenshot shows the window used to identify the different channel files of the images to be analyzed. These shots show the cell profiler interface. (**B**) Screenshot of the Identify Primary Objects menu to identify the Nuclei. The highlighted values are the

commonly altered values to best identify nuclei. Abbreviations: BrdU = 5-bromo-2′-deoxyuridine; DAPI = 4',6-diamidino-2-phenylindole.

A)

B)

7) The channel used to identify the foci is the processed BrdU channel.

8) The name that will be given to data resulting from this section of analysis, which can be changed without issue.

9)The threshold strategy to identify and differentiate individual foci.

10) The threshold level, this will be changed to increase or decrease the number of objects identified as foci.

11) How the foci are differentiated from each other by the program

12) The unprocessed channel whose intensity will be measured, in this instance the green BrdU channel.

13) The unprocessed channel whose intensity will be measured, in this instance the red PCNA channel.

14) The area that is to be measured, either nuclei or foci.

Figure 3.4 Supplemental S2: Visual representation of the Cell Profiler Software and Speckle counting pipeline part 2.

A) Screenshot of the Identify Primary Objects menu to identify the BrdU foci within the nuclei. (**B**) Screenshot of Measure Object Intensity menu to measure the BrdU and PCNA nuclear intensity. Abbreviations: BrdU = 5-bromo-2′-deoxyuridine; PCNA = proliferating cell nuclear antigen.

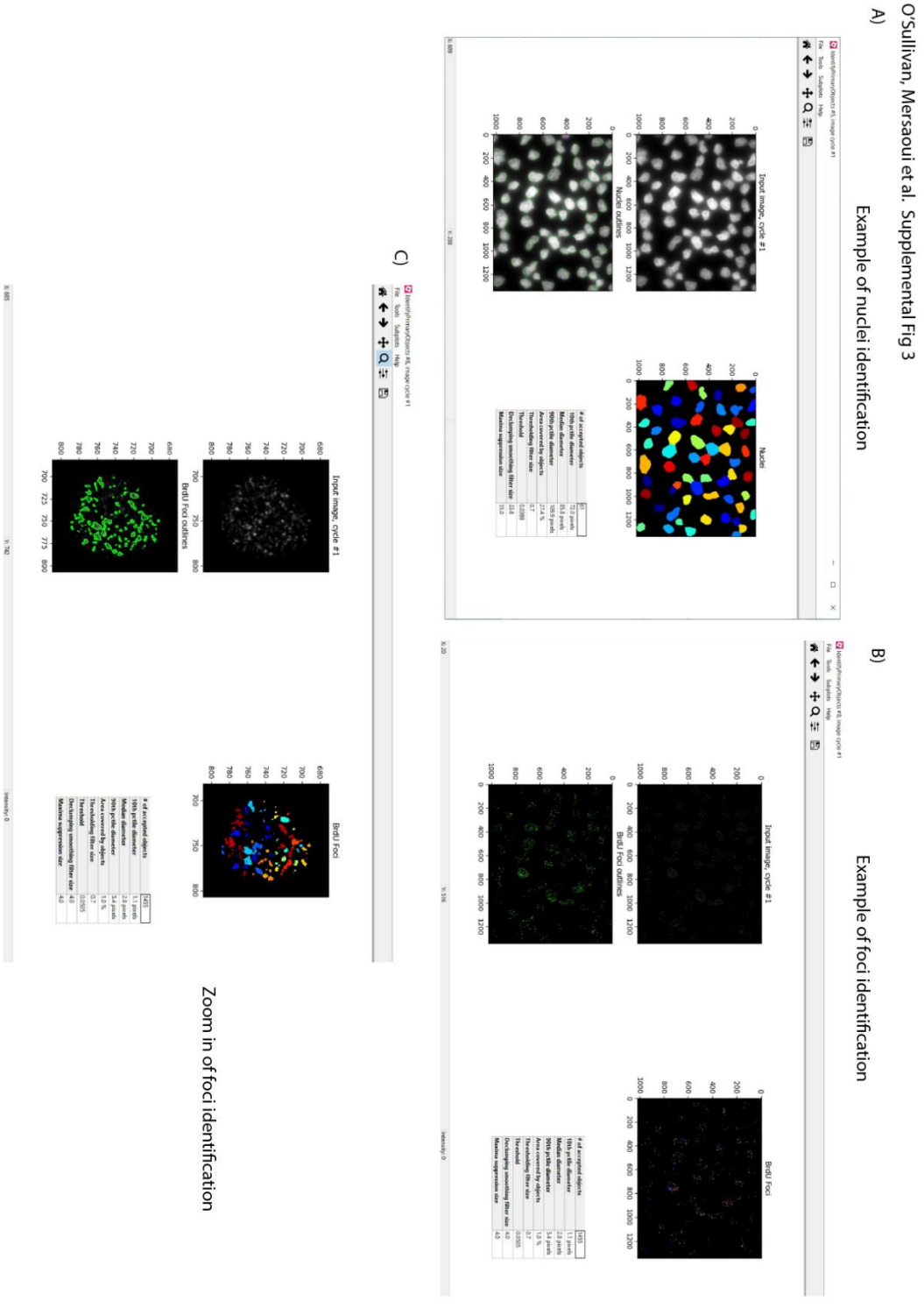

Figure 3.5 Supplemental S3: Visual representation of the Cell Profiler Software and Speckle counting pipeline part 3.

(A)Representation of the nuclei identification by cell profiler following optimization. (**B**) Representation of the BrdU foci identification. (**C**) Screenshot is a zoom-in on one cell within the initial window.

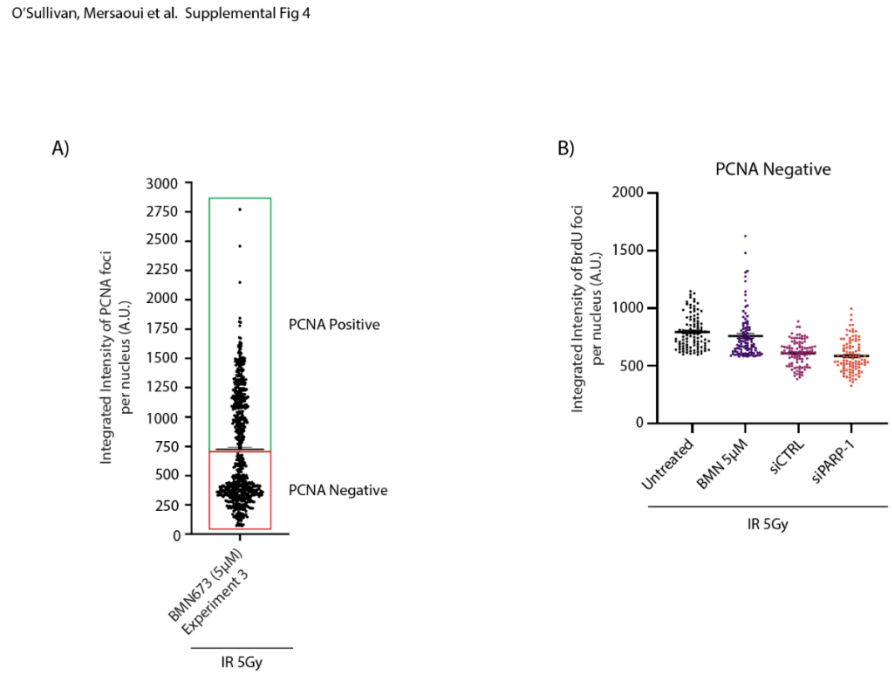

Figure 3.6 Supplemental 4: Scatter plot of PCNA positive and negative cells.

A) An example of a PCNA scatter plot used to distinguish PCNA-positive from PCNA-negative cells. The PCNA intensity from a single condition was plotted and the distinction between the two populations identified. The green highlights the PCNA-positive cells, the red represents the PCNA-negative cells. This is done for each individual experiment and condition. (**B**) Quantification of the BrdU nuclear intensity in PCNA-negative untreated HeLa cells, treated with 5 μM BMN-673, siCTRL, and siPARP-1; the data show the mean ± s.e.m (Mann–Whitney *U*-test). Abbreviations: PARP-1 = poly(ADP-ribose) polymerase 1; BrdU = 5-bromo-2′-deoxyuridine; IR = irradiation; PCNA = proliferating cell nuclear antigen; A.U. = arbitrary units; siCTRL = siRNA control; siPARP-1 = siRNA to knock down *PARP-1*; s.e.m. = standard error of the mean.

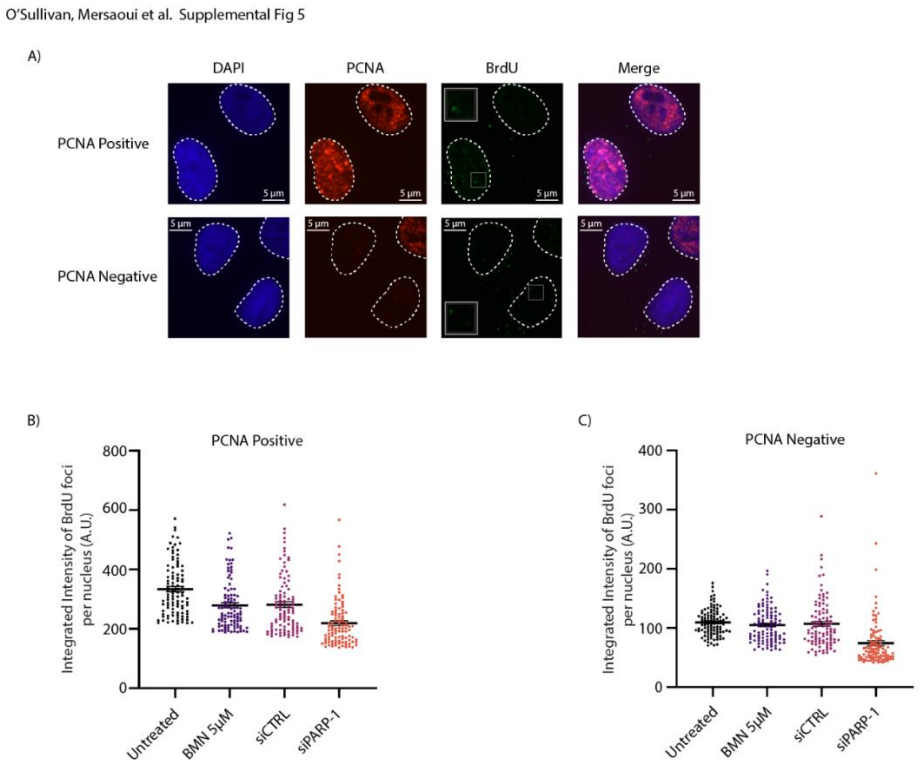

Figure 3.7 Supplemental Figure S5: BrdU signal without irradiation.

(**A**) Representative images of BrdU foci formation and PCNA staining without irradiation. Scale bars = 5 µm. A zoomed-in square showing marked BrdU foci is present in the corner of each BrdU image. (**B**) Quantification of the BrdU nuclear intensity in PCNA-positive untreated Hela cells, treated with 5 µM BMN-673, siCTRL, and siPARP-1; the data show the mean ± s.e.m (Mann–Whitney *U*-test). (**C**) Quantification of the BrdU nuclear intensity in PCNA-negative untreated HeLa cells, treated with 5 µM BMN-673, siCTRL, and siPARP-1; the data show the mean ± s.e.m (Mann–Whitney *U*-test). Abbreviations: PARP-1 = poly(ADP-ribose) polymerase 1; BrdU = 5-bromo-2′-deoxyuridine; PCNA = proliferating cell nuclear antigen; IR = irradiation; DAPI = 4',6-diamidino-2-phenylindole; A.U. = arbitrary units; siCTRL = siRNA control; siPARP-1 = siRNA to knock down *PARP-1*; s.e.m. = standard error of the mean.

Supplemental Video 1: Use of Cell Profiler and the Speckle Counting pipeline to analyze BrdU staining for the measurement of DNA resection. This video demonstrates the use of Cell Profiler and the Speckle counting pipeline. It shows how to import and analyze images with this tool specifically for this protocol. Abbreviation: BrdU = 5-bromo-2′-deoxyuridine.

Chapter 4 **Zinc-Fingers? A new candidate for PARP-1 dependent DNA repair through Homologous Recombination.**

Julia O'Sullivan[1,2]*; Marie-Christine Caron*[1]*, Jean-Philippe Gagné*[2]*, Larissa Milano de Souza*[1]*, Ted Dawson*[3]*, Guy G. Poirier*[2] *and Jean-Yves Masson*[1]

[1]Département de Biologie Moléculaire, Biochimie Médicale, et Pathologie et Centre de recherche sur le cancer de l'Université Laval et CRCHU de Québec (Oncology division).

[2]Centre de recherche du CHU de Québec, CHUL, Faculté de Médecine, Université Laval, Québec, Canada

[3]Department of Neurology, Johns Hopkins University School of Medicine, Baltimore, Maryland

Preface

During the second half of my PhD, continuing from our previous paper which identified PARP-1 as a regulator of resection, I endeavoured to further explore this key step of HR repair. To further this, I tried to identify PARP-1 interactors that play a role in DNA resection. The goal was to better understand the regulation of DNA resection and the role of PARP-1 in this essential process. The hope was that in uncovering new proteins that are also part of this mechanism we would be able to paint a clearer picture as to the function of PARP-1. This would help in understanding how PARPi works as a cancer therapy and potentially lead to explanations for PARPi resistance. Furthermore, we hoped that our discoveries could potentially pave the way for new drugs to be studied which could be used in conjunction with PARPi or as a replacement, reducing the detrimental PARPi resistance phenotype.

We identified two proteins which modulated HR, however only one showed an effect on resection and as such this was the protein I pursued. At the beginning of this undertaking, we had no concept of how daunting this task would become. At each corner we were met with a new set of complicated and frustrating challenges, from purification issues to difficulty in knock-down or knocking out the protein. However, the results have been extremely promising, hopefully indicating that this struggle will produce important knowledge for the future.

Résumé

La découverte que les cancers présentant des défauts dans les gènes de réparation de l'ADN sont particulièrement sensibles à l'inhibition des poly(ADP-ribose) polymérases (PARP) a alimenté le déploiement clinique de la dernière génération d'inhibiteurs de PARP (PARPi). Cependant, il y a un débat considérable sur le mécanisme par lequel l'inhibition de PARP tue les cellules déficientes pour les gènes de réparation de l'ADN. Par conséquent, le plein bénéfice des PARPi dans le traitement du cancer ne peut être obtenu que par une compréhension claire de la façon dont la réponse aux dommages à l'ADN est affectée par l'inhibition de PARP. La poly(ADP-ribosylation) des protéines est une modification post-traductionnelle catalysée principalement par les PARP qui sont dépendants de l'ADN, au début du DDR. Lors de l'activation, PARP-1 synthétise un polymère complexe composé d'unités d'ADP-ribose qui facilite la relaxation locale de la chromatine. Nous avons pu étudier en profondeur l'interaction du poly (ADP-ribose) (PAR) et la dynamique du réseau protéique. Des études antérieures ont établi que PARP-1 affecte une étape spécifique de la recombinaison homologue pendant la résection de l'ADN en phase S. L'inhibition de PARP-1 conduit à des cassures double-brin d'ADN hyper-résectées.

Nous visons à identifier de nouveaux interacteurs de PARP-1 ou des protéines liant PARP qui peuvent jouer un rôle direct dans la réparation des DSB, devenant potentiellement des cibles létales synthétiques elles-mêmes. En étudiant les protéines liant PAR, nous espérons clarifier davantage le rôle de PARP-1 dans la réparation des DSB et ainsi améliorer l'application clinique des PARPi. Notre étude a identifié deux candidats potentiels : un facteur de traitement pré-ARN et une protéine à doigt de zinc extrêmement prometteuse qui pourrait jouer un rôle important dans la HR. Nos tests initiaux ont déterminé que les deux ont un effet sur la HR, mais la protéine à doigt de zinc affecte spécifiquement la résection de l'ADN. En tant que telle, notre étude explore plus en détails cette protéine à doigts de zinc pour mieux élucider cette étape critique de résection.

Abstract

The discovery that cancers with defects in DNA repair genes are particularly sensitive to poly(ADP-ribose)polymerase (PARP) inhibition has fuelled the clinical development of the latest generation of PARP inhibitors (PARPi). However, there is considerable debate about the mechanism through which PARP inhibition kills DNA repair-deficient cells. Therefore, the full benefit of PARP inhibitors in cancer therapy can only be achieved by a clear understanding of how the DNA damage response (DDR) is affected by PARP inhibition. Protein poly(ADP-ribosylation) (PARylation), is a post-translational modification catalysed primarily by DNA-dependent PARPs at the start of the DDR. Upon activation, PARP-1 synthesizes a complex polymer composed of ADP-ribose units which facilitates local chromatin relaxation. We have been able to extensively study the poly(ADP-ribose)(PAR)-interacting and binding protein network dynamics. Previous studies have established that PARP-1 affects a specific step of homologous recombination (HR), DNA resection. Inhibition of PARP-1 leads to hyper-resected DNA double-strand breaks.

We aimed to identify new PARP-1 interactors or PAR binding proteins which may play a direct role in DSB repair, potentially becoming synthetic lethal targets themselves. By studying PAR-binders we hope to further clarify the role of PARP-1 in DSB repair and thus improve the clinical application of PARPi. Our study identified two potential candidates for study, a pre-RNA processing factor and an extremely promising Zinc-finger protein which may play an important role in HR. Our initial tests have determined that both proteins have an effect on HR, but the zinc-finger protein specifically affects DNA resection. As such our study further explores this zinc-finger protein to better elucidate this critical resection step.

4.1 Introduction

Cells suffer from DNA damage as a result of both endogenous and exogenous sources. This leads to the formation of many DNA breaks on a daily basis [1]. One of the most severe type of DNA damage is the double-strand break (DSB). If repaired incorrectly these can have detrimental effects on the cell, from cell death, or much worse, genomic instability which can cause an accumulation of mutations and potentially lead to tumour development[1, 471]. Due to the severity of unrepaired breaks, the complicated process of repairing them is essential to cell survival. These repair mechanisms are controlled by a complex web of proteins which play roles in sensing, signalling, and finally repairing the damaged DNA [16, 17]. Furthermore, enzymes which regulate the cell cycle checkpoints play a pivotal role in the choice of the repair pathway and the eventual maintenance of genomic stability.

There are two main pathways which are used to repair DSBs, Non-Homologous End Joining (NHEJ) and Homologous Recombination (HR)[472]. NHEJ can take place during any phase of the cell cycle and requires no homology or microhomology to fuse the DNA ends together, which can lead to "error-prone" repair [460]. The HR pathway is "error-free" but is limited to the S/G2 phase of cell because of the need for the sister chromatid as a template for DNA repair[472, 473]. HR requires long stretches of homology to successfully repair the break. The process of DNA end resection is a critical step in DSB repair and acts as another modulator for pathway choice. DNA end resection can be defined as the 5' to 3' degradation of a single DNA strand. This process is the regulated digestion of a single-strand on either side of the broken DNA leaving behind single-strand 3'-OH DNA ends. In human cells, this is driven by the Bloom syndrome protein (BLM) – DNA replication helicase/nuclease 2 (DNA2) – Replication Protein A (RPA) –MRE11/NBS1/RAD50 (MRN) and Exonuclease 1 (EXO1) [71].

One of the initial sensors of these breaks is poly(ADP-ribose) polymerase-1 (PARP-1), which is recruited within 100 milliseconds of the formation of the DSB[24, 89, 474]. The NAD^+ binding pocket of PARP-1 is exposed upon binding of its zinc-fingers to DNA, this allows for the NAD^+ dependant formation of Poly(ADP-Ribose) (PAR) chains[85]. These PAR chains promote chromatin relaxation and histone rearrangement as a result of their negative charge[129]. This scaffolding system has also

been linked to the recruitment of other DNA damage repair proteins, notably MRE11, which is a member of the MRN complex[24]. This complex, which is made up of MRE11, NBS1 and RAD50, creates an initial nick through the endonuclease activity of MRE11 and its interaction with the (C-terminal binding protein) CtBP-interacting protein (CtIP) [72, 475]. CtIP is known to interact with BRCA1 early in the repair process and this BRCA-CtIP cooperation can modulate the overall speed at which the resection occurs[73-75, 426, 432]. This initial nick opens a path for the EXO1 and DNA2 nucleases. These nucleases process the long tracts of DNA in a 5' to 3' direction on either side of the break, generating the 3' overhangs necessary for the downstream repair process[71, 456]. The BLM helicase unwinds the DNA improving the overall effectiveness of the resection. The newly generated single-strand DNA is coated in trimeric RPA to protect it from further degradation. A BRCA1-PALB2-BRCA2 complex will facilitate the exchange of RPA for RAD51 on the single-strand[79, 166, 179, 476]. The RAD51-DNA filament can then seek out the sister chromatid to faithfully repair the damage. DNA resection is negatively regulated by the HELB helicase in an RPA-dependent manner[176] and by 53BP1 and RIF1[49, 426].

PARP-1, the most studied member of the PARP family of proteins, is an abundant nuclear protein that has been linked to many different processes in the cell, but its activity in the DNA damage response has been the source of much research[241, 477]. The interest in the role of PARP-1 and PAR in DSB repair has developed largely due to the use of PARP inhibitors (PARPi) as a therapeutic in HR deficient cancers[150, 465, 478]. These PARPi are thought to function in a synthetic lethal fashion in HR deficient cancers, however the exact mechanism for this lethality has not yet been determined. This has led to a fervent desire to fully understand the role of PARP-1 in DNA repair. More and more PARPi are being approved for use as both monotherapies and combination therapies. They are being used in a growing range of cancers, such as breast, ovarian and prostate cancer. A Phase 1b trial has demonstrated encouraging data in the use of PARP inhibition in combination with chemical HR deficiencies in previously HR proficient cells[479]. This further increases the potential cancer types which could be treated with PARPi.

While an excellent therapy option PARPi are not without their drawbacks. A significant one being the development of PARPi resistance[480, 481]. PARPi resistance can be classified into 3 categories: 1) the cellular availability of the inhibitor, 2) impact

on the activity and abundance of PAR chains and 3) reactivation for HR. Overexpression of drug-efflux transporter genes such as ABCB1 has been observed in chemotherapy-treated ovarian and breast cancers and in a PARPi-resistant ovarian cancer cell line. This overexpression could account for reduced cellular availability of the PARPi[482]. Studies have found that PARP inhibition results in greater cytotoxicity than RNAi mediated depletion, possibly as a result of the "trapping" mechanism of PARPi. This mechanism decreases the speed at which PARP-1 disengages from the DNA. Mutations in PARP-1 which diminish this "trapping" effect have been shown to induce PARPi resistance[483], loss of PARG has also been seen to result in PARPi resistance[414]. Reversion mutations in BRCA1/2 have been observed in tumours allowing them to overcome the PARPi sensitivity[14, 159, 484]. These various methods for accomplishing PARPi resistance should indicate the importance of PARP-1 activity and the lengths that will be gone to in order to avoid cell death.

Aside from desiring a clearer understanding of the function of PARP-1 in DSB repair and how the PARPi treatment mechanism works, fully understanding the role of PARP-1 would help to determine the efficacy of these inhibitors and help uncover methods or alternatives to overcome PARPi resistance. In pursuit of this understanding, our group previously focused on the resection step of HR. PARP-1 has been observed to interact with the NHEJ proteins Ku70 and Ku80 which inhibit resection by protecting the DNA ends[485]. However, as mentioned above it is also involved in the recruitment of MRE11, which is indicative of a role as a regulator for DNA resection. This was elucidated in our work Caron. M.C, Sharma A.K, *et al* Nature Communications (2019)[467].

Our previous work identified PARP-1 as a key regulator for DNA end resection. We were able to show that activated PARP-1 inhibits the EXO1 and DNA2 resection machinery *in vitro*. Furthermore, we demonstrated that loss of PARP-1 results in a decrease of the HR suppressors 53BP1 and RIFI at DSBs. Consequently, this enhances the accessibility of the DNA for EXO1, leading to hyper-resection of the DNA. This hyper-resection phenotype was observed *in cellulo* through the use of both the BrdU immunofluorescence (BrdU) assay and the Single Molecule Analysis of Resection Tracts (SMART) assay, in PARPi, PARP-1 knock-down and knock-out conditions[467].

To further understand the mechanism by which PARP-1 regulates DNA end resection we sought to identify new PARP-1 and PAR interactors that also play a role in this process. This was accomplished using two different techniques IP:MS and a PAR-binding microarray. This identified a new PARP-1 interactor involved in resection: ZNF432. ZNF432, a previously unstudied zinc-finger protein whose knock-down displays a similar phenotype to that of the loss of PARP-1. The ensuing work demonstrates the identification process and the subsequent exploration of ZNF432 in regards to its interaction with PARP-1 and its role in HR.

4.2 Results

4.2.1 PAR interactors a source of modulators of HR DSB repair.

Initially, in our quest to understand the role of PARP-1 as a regulator for DNA resection we were determined to search for interactors of the protein which also played a role in this key step of HR. To achieve this goal, we made use of two different methods of identifying PAR binders, which were performed in two different laboratories. As previously stated, PAR is generated by PARP-1 following DNA damage and has been identified to act as a scaffold for DNA repair proteins and involved in their recruitment. As PAR is a PTM which can bind to several different structures it provides a wide range of potential interactors, more so than when looking for interactors of an individual protein. The first method we attempted was to immunoprecipitate (IP) PAR from shPARG Hela cells using the 10H antibody. We determined that the best damage source for PAR formation was irradiation and confirmed the lack of PARG activity through western blot (Figure 4.1. A &B). From this, we decided to treat with either BMN-673 or 5Gy of irradiation (Figure 4.1D) for our experimental conditions. In an attempt to limit our pool of results to HR, we blocked the cells in S-phase using a double thymidine block (Figure 4.1F) before the irradiation treatment. One hour post irradiation, the peak time for RAD51 foci formation in the shPARG cells (Figure 4.1 C), the cells were harvested to be used for the 10H IP (Figure 4.1 E). This was then sent for MS analysis and resulted in a massive list of over 500 proteins. From this list, two candidates were selected from the literature: PRPF38A and DHX9. I will only present results on PRPF38A as DHX9 was studied by another student.

For our second approach, we were provided with a list of 375 proteins which the Dawson laboratory of Johns Hopkins had found to have PAR binding capabilities. This was done by placing 17,000 individual human proteins onto a protein microarray and then adding purified PAR polymer. Following washes, a PAR specific antibody was applied allowing for the detection of these 375 PAR binding proteins (Fig 4.2C). An illustrative representation of this process is shown in Figure 4.2 A and a photo representation of the microarray is shown Figure 4.2 B. Obviously as this was done *in vitro*, thus it is not a final and complete list. It does however provide a more than adequate pool of candidates to start from. Upon receiving this list, we chose to narrow down the candidates based on the available literature, domains, expression in cancer and any known interactions with DNA repair proteins. The 30 shortlisted proteins were then initially screened for an effect on RAD51 foci formation (Figure 4.2 D) following small interfering RNA (siRNA)-mediated knock down. Our data was reviewed following the first round of IFs and it was decided that the proteins from the ZnF family all showed an effect and thus would be our target group. A second round of RAD51 foci formation IFs was done for these 7 ZnF proteins, while in parallel they were also being screened for an effect on BrdU foci formation in order to identify those which would modulate resection (Figure 4.2 E). From this double screening our final target was identified, the ZnF protein ZNF432.

There has been very little research done on this particular ZnF. It has appeared in multiple screens for drug responses to asthma, and more recently is appearing in large-scale MS screens also in regards primarily to lung disorders[486-495]. Interestingly one of these large-scale MS screened identified ZNF432 as an interactor of the transcriptional regulator and potential DDR protein TRIM28[218]. ZNF432 is located on chromosome 19q13.41. Structurally it is comprised of an N-terminal KRAB domain and 16 zinc-finger domains and is 652 amino acids in length.

4.2.2 ZNF432 and PRPF38A an in-depth exploration of their effects on HR

We used multiple IF techniques to explore the importance of ZNF432 and PRPF38A on DNA repair in S/G2 phase following siRNA knock down in Hela cells. We selected for S/G2-phase cells to better limit our data to HR and thus help in further elucidating the role of PARP-1 and PARP-1 interactors in resection. For PRPF38A we determined the knock-down efficiency via QPCR at 99% and for ZNF432 we checked

the siRNA efficiency by western blot (Figure 4.14 Supplemental Figure 1 A) with a maximum knock-down estimated at 50%. For all the IFs, a cell cycle marker was used to select for S-phase or S/G2-phase. First, we looked at RAD51 foci formation to confirm an effect on HR repair. For both proteins we see a significant increase in the percentage of cells with more than 10 RAD51 foci following 5Gy irradiation (Figure 4.3 A & 4.4 A). For siPRPF38A there is no increase in non-irradiated cell, though there is a significant increase in the irradiated conditions with ~1.7 fold increase in siPRPF38A (74%) compared to siCTRL(43%). In the case of the siZNF432 knock-down cells there is a significant increase in foci formation both with and without irradiation. Following irradiation there is a ~1.8 fold increase in the siZNF432 (51%) condition compared to the siCTRL (28%). This is indicative of an increase of repair by HR. Furthermore, phosphorylated DNA-PK, a marker for NHEJ was reduced in the siZNF432 condition compared to siCTRL (Figure 4.15 Supplemental Figure 2). For this we used an antibody specific for the phosphorylation of DNA-PK at the Ser2056.

To begin our exploration into resection, we measured the accumulation of RPA. RPA is a trimeric protein complex that binds to ssDNA to protect it from degradation in eukaryotic cells. When regions of ssDNA are exposed by DNA damage or replication, RPA is recruited. Hence, it can serve as a readout for resection and for ongoing HR following treatment with a DNA damaging agent. Thus, the amount of RPA that accumulates at each site should reflect the amount of ssDNA. Interestingly, the knock down of ZNF432 led to an increase in the generation of ssDNA as measured by RPA foci (Figure 4.4B) and knockdown of PRPF38A resulted in a decrease of ssDNA as measured by RPA foci (Figure 4.3 B). For RPA foci formation the cells were fixed 1 hour post irradiation. Following the interesting results of the RPA foci formation, we observed the integrated intensity of nuclear BrdU foci following irradiation. Unfortunately, here we found that PRPF38A did not play a role in resection, as there was no effect on the nuclear intensity of the BrdU foci (Figure 4.3 C). Fortunately, a knock down of ZNF432 did cause a significant increase in nuclear BrdU foci (figure 4.4 C). Providing a similar phenotype to that of siPARP-1, suggesting a role for ZNF432 in the regulation of resection alongside PARP-1. BrdU foci formation is measured 3-hour post irradiation. For all the IFs the cells were selected for S/G2 phase thus removing any bias that could occur due to the timing difference or cell cycle abrogation.

4.2.3 ZNF432 knockdown reduces 53BP1 and RIF1 accumulation post DNA damage and alters the cell cycle.

The mechanism underlying ZNF432-regulated DNA resection was investigated further. 53BP1 and RIF1 are both negative regulators for resection which promote NHEJ. We monitored the accumulation of the resection inhibitors 53BP1 and RIF1 in S/G2 phase cells (Figure 4.5 A- D) depleted of ZNF432. Interestingly, ZNF432 depletion led to a significant decrease of 53BP1 and RIF1 foci following 5Gy irradiation treatment (average number of foci = 64 in the control and 58 in ZNF432 knockdown for 53BP1 (Figure 4.5 A & B), and average number of foci = 59 in the control and 47 in ZNF432 knockdown for RIF1 (Figure 4.5 C& D)). This combined with the reduced accumulation of 53BP1 and RIF1 foci supports the increase in resection seen by the BrdU and RPA IF experiments. Furthermore, depletion of ZNF432 results in alterations in the cell cycle. FACS analysis revealed a significant increase of cell in G2 phase and a significant decrease in G1 phase of the cell cycle (Figure 4.5 E&F). As mentioned before, HR can only take place during the S/G2 phase of the cell cycle and requires resection. Suggestion a preference for HR repair in siZNF432 cells.

4.2.4 ZNF432 Recruited to the site of DNA damage.

We initially scrutinized the recruitment kinetics of ZNF432 to DNA damage in live cells through both laser-tract and UV-blast. We observed that ZNF432 is recruited to laser-induced DNA damage tracks within 2 minutes in 293T cells (Figure 4.6 A & B) and to UV-blast within 30 seconds in U2OS cells (Figure 4.16 Supplementary Figure 3 A &B). The initial rapid accumulation of ZNF432 at sites of damage was followed by a gradual reduction over the next 10 min when treated with the two-photon laser-tract damage. The dynamics of ZNF432 recruitment under normal conditions was compared with the dynamics observed under PARP inhibition with BMN-673 (Talazoparib) and in PARP-1 KO cells. ZNF432 recruitment was lost in the PARP-1 KO cells, indicating a role for PARP-1 in its recruitment (Figure 4.6 C & D, 4.16 Supplementary Figure 3 B & C). Interestingly, recruitment was maintained when treated with BMN-673 (Figure 4.6 E & F, 4.16 Supplementary Figure 3 D & E) though the dynamics of recruitment appeared to be affected. While in the presence of BMN-673, PARP-1 is still recruited to sites of damage but displays a delayed displacement, possibly due to trapping at DSBs. The

recruitment of ZNF432 as following the two-photon laser-tract in 293T cells was delayed and presented as a more granular pattern, this was not observed in the UV-blasted U2OS cells. It is possible that the different sources of damage or the cell lines are what causes this difference. Though in either case the recruitment still occurs following BMN-673 treatment[141]. This indicates that the ZNF432 recruitment to DNA damage is done in a PARP-1 dependent manner that is not fully reliant on the PARylation activity. These results suggest the possibility of a direct interaction between PARP-1 and ZNF432, this does not rule out a role for PARylation in ZNF432 function.

4.2.5 ZNF342 binds DNA

These observations suggested that ZNF432 may have the capacity to directly bind DNA. To test this hypothesis, we purified recombinant full-length ZNF432 from Sf9 insect cells (Figure 4.14 Supplemental Figure 1 B) and monitored its capacity to bind *in vitro* single-stranded (SS), double-stranded (DS), 5' prime and 3' prime overhang radiolabelled DNA probes. Interestingly, we found that ZNF432 is proficient in binding all four substrates *in vitro* (Figure 4.7 A-D). Furthermore, we observed that when presented with a competition either between SS and DS (Figure 4.8 A) there is preference for the SS probe, and we see a dramatic decrease in the binding of ZNF432 to DS compared to the binding with just the DS probe alone. In the SS and 3' prime (Figure 4.8 B) competition, ZNF432 bound SS preferentially though we see an increase in the binding of ZNF432 to the 3' prime compared to the 3' prime alone suggesting that ZNF432 binds preferentially resected DNA.

4.2.6 ZNF432 a direct inhibitor of resection and interactor of PARP-1

The above data suggest that ZNF432 may be able to directly suppress the activity of DNA resection. We further examined whether purified ZNF432 (Figure 4.14 Supplemental Figure 1 B) could block DNA resection *in vitro*. We monitored DNA resection of a 3′-radiolabelled dsDNA (2.7 kb) probe by one of the main DNA resection enzymes: EXO1. In the absence of ZNF432, the purified 6.5nM EXO1 resected ~100% of the 2.7 kb substrate (Fig. 4.9 A). When the reaction was supplemented with ZNF432,

a concentration-dependent inhibition was observed. With 10 nM ZNF432, only 15% of the DNA could be resected compared to 86% at 40nM, within the 30 min incubation time. To determine if PAR would affect the inhibitory function of ZNF432, we performed reactions with protein-free 250nM PAR followed by 20nM ZNF432 (Figure 4.9 B). This failed to change the inhibitory effect ZNF432 has on EXO1 resection. These results show that ZNF432 can robustly inhibit the DNA resection ability of EXO1, likely through a direct DNA-binding mechanism. Though we did not see an effect on ZNF432 inhibition with purified PAR this does not exclude the possibility for natively generated PAR to have an effect. Considering this we were curious if there may be an interaction between ZNF432 and PARP-1 due to the previously shown recruitment dependence on PARP-1. To explore this, we used GFP-beads to pulldown GFP-ZNF432 from transfected Hela cells and blotted against PARP-1. Subsequently confirming an interaction *in cellulo* between ZNF432 and PARP-1, both with and without damage (Figure 4.9 C). This interaction was confirmed via Mass Spectrometry (Table 4.1 & 4.2), Another interactor which had previously been identified in the screen by the Elledge laboratory was KAP1/TRIM28 was also confirmed in this MS experiment[218]. This interaction is something that will be studied further in the future.

4.2.7 ZNF432 knock down leads to resistance to BMN-673 and overexpression leads to sensitivity.

We attempted to generate a CRISPR KO cell line for ZNF432, unfortunately we were unable to and thus reached out to a company: Ubigene. They were able to produce two U20S clones which were genomically edited, however they did not produce a protein knock out (Figure 4.14 Supplemental Figure 1). The clones were knock down, one having very low levels of ZNF432 visible by western, clone C5. As such we tested if there would be an effect on cell viability when treated with varying concentrations of BMN-673 (Figure 4.10). We found that the C5 clone showed resistance to BMN-673 compared to the U20S wild type cells (Figure 4.10 C & D). The F1 clone, which had a greater level of ZNF432 expression shared the same viability as the wild type (Figure 4.10 B, D & F). Furthermore, overexpression of ZNF432 in the wild type resulted in increased sensitivity to BMN-673 (Figure 4.10 A & E), the F1 clone shared this sensitivity to a lesser extent than the wild type (Figure 4.10 B, E & F) and in the C5 clone overexpression also caused sensitivity bringing the viability percentage to that of the non-transfected wild type cells

(Figure 4.10 C, E & G). This effect was confirmed to be as a result of ZNF432 overexpression as in the GFP-CTRL transfected cells we did not see the same effects (Figure 4.16 Supplemental Figure 3). These results suggest that not only does ZNF432 function in the same pathway as PARP-1, but that low levels of ZNF432 can be sufficient to allow for cell survival. Considering the results seen in the resection assay, it is possible that the sensitivity seen from the overexpression is as a result of inhibition of the resection step of HR.

4.3 **Discussion**

Over the last several decades huge strides have been made in uncovering the mysteries of DSB repair. It is clear the eukaryotic cells have developed multiple mechanisms for DSB repair. These are highly regulated in order to optimise genome stability. One particularly important mechanism which regulates this repair is the switch between the NHEJ and HR pathways, which antagonise each other. Both pathways repair optimally under different conditions, such as cell cycle and chromatin structures, factors which are involved in this regulation. Another regulator in the repair choice is the process of DNA resection, a mechanism that is highly regulated and dependent on several key repair proteins. In addition to furthering our knowledge on DNA repair, study in this field can have a direct clinical relevance, particularly in regards to the development of cancer therapeutics, biomarkers and potentially a clearer understanding for the best contexts to use the available therapeutics or a possible explanation for resistance to these therapies. PARP inhibitors are one such therapy that has proven to be largely effective, though it is not fool proof. Resistance to PARPi remains an important clinical issue that is under scrutiny. However, one possible way to overcome this resistance could be through combination therapies, combining PARPi and other drugs, or the development of completely alternative targets that have similar phenotypes. The role of PARP-1 in DSB repair has been somewhat contentious but our group previously demonstrated its importance as an antagonistic regulator for resection thus providing a context to search for PARP-1/PAR interactors which in the future could be used as alternative therapeutics to PARPi or in conjunction with them.

In this study, we show that PARP-1/PAR interactors are a rich source for identifying new DNA repair regulators. We uncovered two proteins of interest the pre-

RNA processing factor PRPF38A and a zinc finger protein ZNF432. While both showed positive effects on RAD51 foci formation, a marker for HR, only ZNF432 showed an effect on resection as measured by integrated BrdU nuclear intensity, which is a measure for DNA end resection *in cellulo*. As our goal was to further explore the mechanism for regulating resection, we focused our attentions on ZNF432. ZNF432 is a 75kDa zinc-finger protein, comprised of a KRAB domain and 16 zinc-fingers. Very little is known about this protein, as it has not been widely studied. According to cBioPortal analysis of the TCGA Research Network: https://www.cancer.gov/tcga, it has not been well studied but has been found to be altered in many cancers, and that this alteration coincides with a reduced survival (Figure 4.12 A-C)[496, 497]. Aside from this, the only information on ZNF432, comes from several cDNA screens and screens linked to lung disorders, such as asthma. No focused study has as yet been published on ZNF432.

As mentioned, we observed an increase in BrdU and RPA foci when ZNF432 was knocked-down, indicative of its role in resection. Upon successful purification of this protein, a task made more complex due to the 16 zinc-finger domains, we observed binding capabilities to double- and single-strand and 3' and 5' overhang substrates. Interestingly, in our competition assay it demonstrated a preference for single-strand DNA. In the competition assay between single-strand and double-strand DNA the presence of single-strand DNA dramatically reduced the binding to double-strand compared to the binding with just the double-strand probe. Conversely in the competition between the single-strand and 3' prime we see an increase in the binding of ZNF432 to the 3' prime compared the binding of ZNF432 to the 3' prime alone suggesting that ZNF432 binds preferentially resected DNAs. Following this confirmation of DNA binding we showed evidence that ZNF432 has the ability to halt EXO1 resection *in vitro*. This supports the *in cellulo* data that ZNF432 is an inhibitor of DNA end resection. While identified from a PAR-binding data set, the presence of purified free PAR had no effect on the inhibition of EXO1 resection. This was also seen with PARP-1 and free PAR contrasting to PARP-1 activated by NAD^+ *in vitro* [467]. As such, this does not remove the possibility that PAR may have an effect ZNF432's inhibition of EXO 1 *in vivo*.

Confirming the role of ZNF432 as a DNA repair protein we observed negative effects on 53BP1 and RIF1 foci formation, both of which are HR suppressor. We also observed a reduction in phosphorylated DNA-PK foci, a marker for NHEJ. The antibody

used recognises the phosphorylation of the Ser2056 of DNA-PK, this particular phosphorylation is inhibited when BRCA1's BRCT domains binds DNA-PK preventing NHEJ in S and G2 phase of the cell cycle. This, in tandem with cell cycle analysis, suggests a preference for HR when ZNF432 is reduced. It is unclear if there is a block following G2 or if the progression through G1 is accelerated and G2 delayed. Continuing, we found that ZNF432 is recruited to sites of damage by laser-tracks or UV-blast and that it is done in a PARP-1 dependent manner, as it is lost in our 293t PARP-1 KO and U2OS PARP-1 KO cells. Curiously, this recruitment was not lost by PARP inhibition by BMN-673. This is likely as the recruitment of PARP-1 is not stopped by BMN-673 treatment, though it does affect the dissociation from the DNA[141]. This indicates that PAR is may not be required for recruitment of ZNF432 to the sites of damage, though it may play a role in the kinetics of ZNF432 recruitment. Regardless, this does not mean that PARylation is not involved in the proper activity of ZNF432. Using GFP-binding beads we were able to confirm the interaction between ZNF432 and PARP-1 *in cellulo*. GFP-ZNF432 was capable of pulling down PARP-1 from whole cell extracts with and without irradiation damage.

As our knock-down efficiency was not very high, we attempted to generate a CRIPR-KO cell line. Unfortunately, we were unable to create a successful KO. We tested multiple cell lines with varying degrees of knock-out efficiency, according to the synthego (https://www.synthego.com/) ICE analysis software. Yet following clone isolation only a small number of knock downs were identified and no KOs. In a desire to pursue this we engaged a company: Ubigene (https://www.ubigene.us/), to generate the KO for us, only for them to struggle also. Finally, 2 U2OS clones were provided, which were determined to be acceptably edited from QPCR analysis. Unfortunately. upon receiving them and testing via western blot we quickly determined that they were not in fact KO on a protein level though they did demonstrate a better knockdown than the siRNA transfection. It is possible that ZNF432 is a carefully regulated protein, whose total knock out is lethal to the cells or it could be that the current CRISPR strategies are not optimised for the KO of this protein.

Using these CRISPR knock down cells we were able to test the viability of ZNF432 treated with BMN-673. We found that the more severe knock down found in the C5 clone resulted in resistance to BMN-673, one that was rescued with the transfection of GFP-

ZNF432. Interestingly the overexpression of ZNF432 in the wild type cells resulted in increased sensitivity to BMN-673, potentially as a result of increased inhibition of resection, something that will be explored in the future. This finding does propose ZNF432 as a marker for the efficacy of PARPi, more testing in animal models would be needed but if the phenotype of PARPi resistance is shared when ZNF432 is depleted it would serve as an excellent indicator to use another form of treatment.

Our current model (Figure 4.11) is that following DSB formation PARP-1 is rapidly recruited. It then recruits ZNF432 and together they regulate the resection which takes place. Loss of PARP-1 will result in loss of ZNF432 recruitment and thus hyper-resection. Similarly, loss of ZNF432 also results in hyper-resection. As of yet we have not uncovered the exact mechanism by which this occurs, we intend to continue our study to hopefully unravel this mechanism. Intriguingly, one of the few known interactors of ZNF432 is the transcriptional co-regulator TRIM28/KAP1 (Figure 4.13)[487, 498], which is involved in the containment of flexible nucleosomes during DNA repair. We were able to validate this interaction and that of PARP-1/ZNF432 through GFP IP/MS (Table 4.1 & 4.2). It is possible that the interaction between PARP-1/ZNF432 and TRIM28 will uncover the regulation mechanism for resection, an avenue of study that we shall pursue. Regardless of its specific mechanism of action, ZNF432 clearly represents an interest target for the study of DSB repair and if it is possible to inhibit, may become a target for cancer therapeutics as an alternative to PARPi. This however is something that will need much more study.

More and more ZnF proteins are being identified as DDR proteins, additionally there is a growing link between ZnF proteins and PARP-1/PARylation. This is visible in the ADPriboDB 2.0 where hundreds of zinc finger (ZnF) proteins have been identified in different MS screens[194, 195] or the DNA-damage recruitment screen performed by the Elledge laboratory in 2015 which identified 25 previously unknown PAR dependant ZnF proteins[218]. While these did not directly implicate the identified proteins as DDR modulators, it does support the hypothesis that there is a vast network of unknow ZnF proteins which are DDR modulators. These proteins may become the key in clarifying many repair mechanisms and thus expand the possibilities for DDR targeted therapeutics, not simply in connection to PARPi or cancer but a multitude of different disorders and target pathways.

4.4 Materials and Methods

4.4.1 S-phase synchronization

Prior to immunoprecipitation and mass spectrometry, shPARG cells were synchronized to S-phase through the double thymidine block method. The cells were treated with 2mM thymidine once at 40-50% confluency for 19 hours. Following this the plates were washed 3 times with PBS and released for 9 hours. The second block is achieved by treating the cells with 2mM thymidine for 16 hours, allowing the cells to accumulate in the G1/S cell cycle boundary. This is followed by 3 PBS washes and a release for 4 hours to allow for the transition into S-Phase.

4.4.2 FACS analysis of cell cycle

Cell cycle analysis was performed through flow cytometry with propidium iodide (PI) DNA staining. Cells were trypsinized, centrifuged and washed with PBS. The cells were centrifuged again and resuspended in 300µl of PBS and fixed with 100% ethanol (EtOH) overnight. Prior to the flow cytometry the cells are stained with a mixture of PI and RNAse for 30 minutes in the dark on ice. The cell cycle distribution was performed on a BD FACSCanto II flow cytometer (BD Biosciences) and analysed using FACSDIva software v.6.1.3 (BD Biosciences).

4.4.3 Cellular fractionation

Cellular fractionation was preformed using the Qproteome® Cell Compartment kit from QIAGEN according to the manufacturer's instructions. The PARG inhibitor (ADP-HPD 1µM) and the PARP-1 inhibitor (BMN-673 10µM) was added to all buffers. Furthermore a sonication step was added to the pellet obtained from the membrane proteins, corresponding to the nuclear and cytoskeletal proteins, to better shear the DNA and removed DNA-bound proteins. The nuclear fraction obtained was diluted in CHAPS lysis buffer (40mM HEPES pH 7.5, 120 mM NaCl, 0.3% CHAPS, 1X complete protease inhibitors (Roche), 5µM BMN-673 and 1µM ADP-HPD).

4.4.4 Immunoprecipitation of PAR-binding proteins (PAR-IP) and Mass-spectrometry

Using at least 3 petri dishes (150 mm) of S-phase synchronized cells at 75-80% confluency, either irradiated with 5Gy or treated with 5µM BMN-673 for 1 hour, the cells were scraped in CHAPS lysis buffer immediately after irradiation. The extracts were pooled and sonicated for 30 seconds before incubating on ice for 15 minutes. The mix was rotated at 4°C for 30 minutes before centrifuging at 3000 RPM for 5 minutes to remove cellular debris and any insoluble material. The supernatant was incubated with 10H PAR antibody paired magnetic Dynabeads^{TM} for 2 hours at 4°C on rotation. The beads were washed, and the samples eluted from the beads using 75mM ammonium bicarbonate pH 8.0 and then treated for mass-spectrometry analysis. The samples were reduced with the addition of 10mM DTT for 20 minutes at room temperature and alkylated with 50mM iodoacetamide for 20 minutes at room temperature in the dark. The samples were then digested at 37°C with the addition of 1 µg of Trypsin/Lys-C mixture, this was halted by acidifying the samples with 2.5% TFA solution. The peptides were isolated on C18 tips according to the manufacturer's instructions and dried in a speed-vac evaporator.

4.4.5 Immunofluorescence

For RAD51, pRPA, phosphorylated DNA-PK and BRCA1 immunofluorescence studies, cells were either untreated or treated with 5Gy irradiation which is released for 1 hour and fixed with 4% paraformaldehyde in PBS for 25 minutes. For pRPA, prior to fixation the cells were subjected to *in situ* fractionation on ice for 10 min using sequential extraction with two different buffers. Pre-extraction buffer 1 (10 mM PIPES, pH 7.0, 300 mM sucrose, 100 mM NaCl, 3 mM $MgCl_2$ and 0.5% Triton-X100) and followed by pre-extraction buffer 2 (10 mM Tris pH 7.5, 10 mM NaCl, 3 mM $MgCl_2$, 1% Nonidet P-40 and 0.5% sodium deoxycholate). Then in all cases, cells were permeabilized with PBS containing 0.5% Triton X-100 for 15 min and washed three times with PBS. Following permeabilisation RAD51, pRPA and phospho DNA-PK experiments were treated with the EdU Click-it reaction to mark S-phase cells. This was done according to the protocol supplied by ThermoFisher. For these experiments, cells had been exposed to 10µM EdU for 15 minutes prior to fixation. The cells were blocked in PBS containing 10% FBS for

1 hour and incubated with the primary antibody (RAD51 1:1000, pRPA 1:500, phosphoDNA-pk 1:1000, BRCA1 1:300, Geminin 1:300) diluted in the blocking buffer for 2 hours at room temperature. Coverslips were washed three times with PBS before 1 hour incubation with the appropriate secondary antibody (1:1000) conjugated to a fluorophore again in blocking buffer. The coverslips were rinsed again twice with PBS, then incubated in (1:1000) PBS-DAPI solution for 5 minutes, then washed twice with PBS. Coverslips were mounted onto slides with prolong gold antifade reagent.

4.4.6 BrdU/ssDNA assays

Cells were pre-incubated in the presence of 10 μM BrdU (Sigma) for 16 hrs followed by a 3-hour incubation after irradiation at 10 Gy. Cells were subjected to *in situ* fractionation on ice for 10 min using sequential extraction with two different buffers. Pre-extraction buffer 1 (10 mM PIPES, pH 7.0, 300 mM sucrose, 100 mM NaCl, 3 mM $MgCl_2$ and 0.5% Triton-X100) and followed by pre-extraction buffer 2 (10 mM Tris pH 7.5, 10 mM NaCl, 3 mM $MgCl_2$, 1% Nonidet P-40 and 0.5% sodium deoxycholate). The coverslips were washed three time with PBS followed by fixation with 4% paraformaldehyde (w/v) for 15 min at room temperature. The coverslips were washed three times with PBS then treated with ice-cold methanol for 5 minutes at -20^{0}C. The coverslips were washed again three times with PBS followed by permeabilization in 0.5% Triton X-100 PBS for 5 min. Cells were blocked for 1 hour at room temperature with 3%BSA/PBS. Following blocking, the cells were incubated overnight at 4^{0}C with anti-BrdU antibody (1:1000) and anti-PCNA (1:1000) in 3%BSA/PBS at 4°C in a covered humid chamber. The following day unbound primary antibody was removed by washing the cells in PBS 3 times. The subsequent incubation with the appropriate secondary antibody (1:1000) conjugated to a fluorophore again in blocking buffer. was done at room temperature for 1 hour. Coverslips were then washed 3 times in PBS before staining with PBS-Dapi (1:1000) and mounted with prolong gold antifade reagent.

4.4.7 Recruitment to lazer-induced DNA damage sites

The evaluation of the recruitment kinetics of ZNF432 to DNA damage sites was performed. After overnight transfections with Effectene reagent (Qiagen), unsynchronized HEK 293 cells pEGFP-ZNF432 fusion proteins were incubated with

fresh medium containing 1 μg/ml of Hoechst 33342 for 15 min at 37°C. For the BMN-673 treated condition the cells were treated with 5μM BMN-673 for 1 hour prior to the Hoechst treatment. A 37°C pre-heated stage with 5% CO_2 perfusion was used for time-lapse analysis on a Zeiss LSM-510 META NLO laser-scanning confocal microscope (40X objective). Localized DNA damage was generated along a defined region across the nucleus of a single living cell by using a bi-photonic excitation of the Hoechst 33342 dye, generated with a near-infrared 750-nm titanium:sapphire laser line (Chameleon Ultra II, Coherent Inc.) The laser output was set to 1.5% with 5 iterations. For each cell, 10 images were collected with a 20 second interval. A Multi-Time macro developed in-house for AIM software v3.2 (Zeiss) was used for image acquisition. Background and photobleaching corrections were applied to each dataset. The average accumulation ± S.E.M of ZNF432 was plotted using a minimum of ten recruitment kinetic profiles from three independent experiments.

4.4.8 Laser-induced DNA damage

U20S WT and U20S PARP-1 -/- cells which transiently expressed pEGFP-ZNF432 were micro-irradiated along in a spot in signle nuclei using a 405 nm UV-laser coupled into a Leica TCS SP5 II confocal microscope driven by Leica LAS AF software. The settings were as follows: laser power output 100%, format 512 × 512 pixels, scan speed 100 Hz, scan iterations 5, mode bidirectional, zoom 2×. The transient expression was done by transfecting 800ng of the pEGFP-ZNF432 plasmid overnight with the Effectene transfection reagent (Qiagen) prior to microirradition. Images were taken every 1.3 seconds for 2.5 minutes. In the case of the BMN-673 treated cells, 5μM BMN-673 treatment occurred 1 hour prior to microirradition. The average accumulation ± S.E.M of ZNF432 was plotted using a minimum of ten recruitment kinetic profiles from three independent experiments.

4.4.9 GFP-TRAP Pulldown

Hela cells were transfected overnight with pEGFP or pEGFP-ZNF432 in a 10cm dish using Lipofectamine 2000, per the commercial guidelines. The following day the cells were irradiated with 10Gy and allowed to recover for 5 minutes prior to harvesting. The cells were harvested with the use of trypsin and pelleted through centrifugation. The cells

were lysed with 1ml of ice-cold lysis buffer (50mM Tris-HCL pH7.5, 150mM NaCl, 0.5%NP40, PMSF, Aprotinin, Leupeptin, NaF, Na2V04) and incubated on ice for 30 minutes. Using a bioreputor the cells were sonicated for 15 minutes with a 30 second on/off cycle. Subsequently they were centrifuged at 4°C for 30 minutes at max speed. The supernatant was added to 25µl of GFP beads and supplemented with benzonase and 2.5mM $MgCl_2$ and incubated at 4°C for 4 hour on rotation. The beads were spun down at 2500g for 2 minutes and washed with the lysis buffer three times, then the beads resuspended in Laemli buffer and western blotted.

4.4.10 Protein purification

ZNF432 was tagged at the N-terminus with GST and at the C-terminus with a His-tag. Sf9 insect cells (200 mL at 10^6 cells/ml) were infected with a GST-ZNF432-His baculovirus. At 48 hrs post-infection, cells were harvested by centrifugation and the pellet was frozen on dry ice. Cells were lysed in Buffer 1 (K_2HPO_4 (1M), KH_2PO_4 (1M), KCl (300Mm), 0.05% Triton-X-100, Aprotinin (1:500), leupeptin (1:200), DTT 1M, 1X complete protease inhibitors Roche) and homogenized by 20 passes through a Dounce homogenizer. Followed by 4x30sec on/off cycles of sonication on ice repeated twice. The cell lysate was incubated with 1 mM $MgCl_2$ and 2.5 U/ml benzonase nuclease at 4°C for 45 minutes followed by centrifugation at 35000 rpm for 45 minutes. The soluble cell lysate was incubated with 1 mL of GST- Sepharose beads for 90 min at 4°C with gentle rotation. The beads were washed twice with PBS300 (1x PBS (150mM NaCl), 150mM NaCl, 1mM DTT) followed by incubation with HSP buffer (PBS300, 5mM ATP and 15mM $MgCl_2$) for 1 hour at 4°C. Sepharose GST beads were washed twice with PBS500 (1x PBS (150mM NaCl, 350mM NaCl) and once with P5 buffer (50 mM $NaHPO_4$ pH 7.0, 500 mM NaCl, 10% glycerol, 0.05% Triton-X-100, 5 mM imidazole). Following washing the beads were incubated in P5 and Gultathione 25mM (pH between 7 and 8) to release the protein from the beads for 1 hour on rotation at 4°C. Both the beads and the glutathione elution were cleaved with PreScission protease (60 U/ml, GE Healthcare Life Sciences), overnight at 4°C in P5 buffer on rotation. The supernatant was then collected and completed to 10 mL with P5 before incubation with 400 µl of Talon beads for 1 hour at 4°C. The beads were washed with P30 (95% P5, 5% P500(500mM NaCl, 10% Glycerol, 0.05% Triton, 500mM Imidazole, 20mM Na_2HPO_4, 20mM NaH_2PO_4) pH 7) and transferred to an eppendorf. Proteins were eluted twice in one volume of beads with

200µl of P500 and dialyzed for 1 hour at 4°C in the storage buffer (20 mM Tris-HCl, pH 7.4, 200 mM NaCl, 10% glycerol, 1 mM DTT) and stored in aliquots at −80°C.

4.4.11 DNA-binding assays

The DNA binding reactions (10 µl) contained γ-^{32}P-labelled DNA oligonucleotides (100 nM) and the indicated concentrations of ZNF432 in MOPS binding buffer (25mM MOPS pH 7.0, 60mM KCL, 0.2% Tween, 2mM DTT, H_2O). The reaction mix was made up of the probe, 2ul 5x MOPS buffer, 40nM $CaCl_2$, up to 2µl of SB and H_2O. Reaction mixtures were incubated at 37°C for 5 min before adding the protein. The mix was then incubated with the protein for 30 minutes at 37°C and then protein–DNA complexes were fixed with 0.2% (v/v) glutaraldehyde for 20 min at 37°C. The reactions were subjected to electrophoresis at 150V for 1.5 hours at 4°C on an 8% TBE1X-acrylamide gel and γ-^{32}P-labeled DNA was visualized by autoradiography.

4.4.12 DNA resection assays

Assays were performed with PUC18 DNA linearized with *Kpn*I and then 3' labelled with [α-^{32}P] ATP and terminal deoxynucleotidyl transferase (NEB). The reactions were conducted using 50 nM of substrate in standard buffer (20 mM Na-HEPES pH 7.5, 0.1 mM DTT, 0.05% Triton X-100, 100 µg/ml BSA). Two millimolar ATP and 5 mM $MgCl_2$ were added to the reaction buffer immediately before reconstitution of the resection machineries. The reactions were initiated on ice by adding ZNF432 as indicated in the figure and transferred immediately to 37°C. In the experiment involving PAR (purified polymer from Marie-France Langelier & John M. Pascal), purified PAR was added to the reaction 5 minutes prior to the addition of ZNF432. After 5 minutes of ZNF432 incubation 6.5nM of purified EXO1 was incubated for 45 minutes at 37°C. Reactions were followed by proteinase K treatment for 1 hour at 37°C. Products were analyzed on a 1% native agarose gel. Gels were dried on DE81 paper (Whatman) and signals were detected by autoradiography. Densitometric analyses were performed using the FLA-5100 phosphor-imager (Fujifilm) and quantified using the Image Reader FLA-5000 v1.0 software.

4.4.13 Hoechst cell viability assay

3000 cells/100µl per well was plated in a 96-well plate, each condition was plated in triplicate and an extra condition of each cell line was plated to be read as the Day 0. After 6 hours 50µl of media including the desired concentration of BMN-673, with a constant concentration of DMSO. To read the plates, the cells are incubated with 50µl media containing Hoechst for 30 minutes and then read using the Cytation 5. One set of readings was done on untreated cells on Day 0, the rest of the plate was then read at 72 hours.

4.5 Figures and Legends

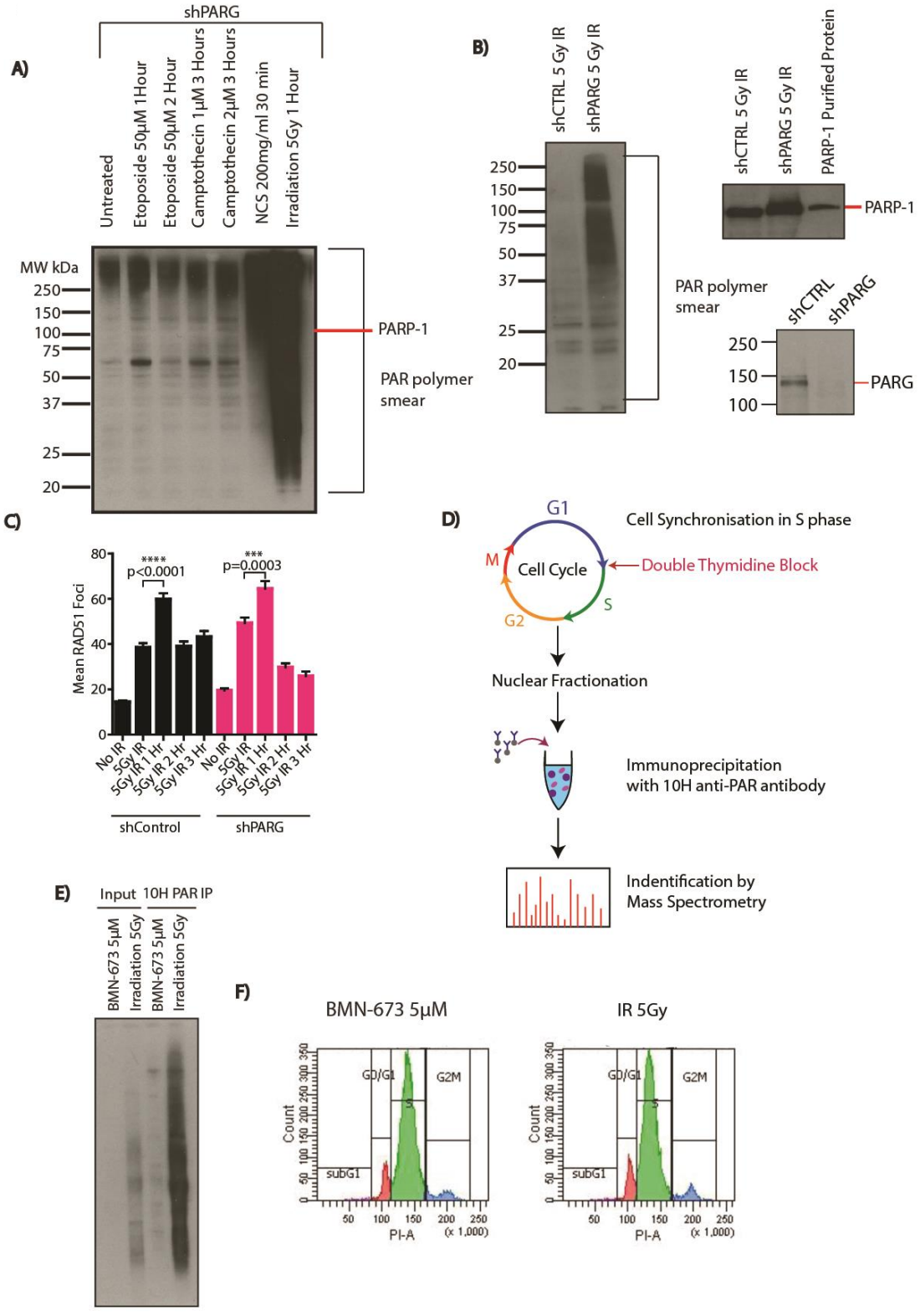

Figure 4.1: Immunoprecipitation of PAR in shPARG cells to uncover PAR interactors due to IR-induced DNA damage.

A) Western blot using the 96:10 antibody demonstrating the PAR accumulation following different damage conditions in shPARG hela cells. B) Western blots using the 96:10 to show base PAR levels in the shCTRL and shPARG cells, and the F1:23 antibody to observe PARP-1. The PARG antibody was used to confirm the PARG KO status of the cells. C) RAD51 foci formation time course post 5 Gy irradiation. D) Schematic of the experiment plan for IP:MS. E) Western blot against PAR using the 96:10 antibody on the input and IP samples (IP using the 10H antibody) which were sent for MS. F) FACs analysis of the cell cycle following the double thymidine block to synchronise the cells in S-phase.

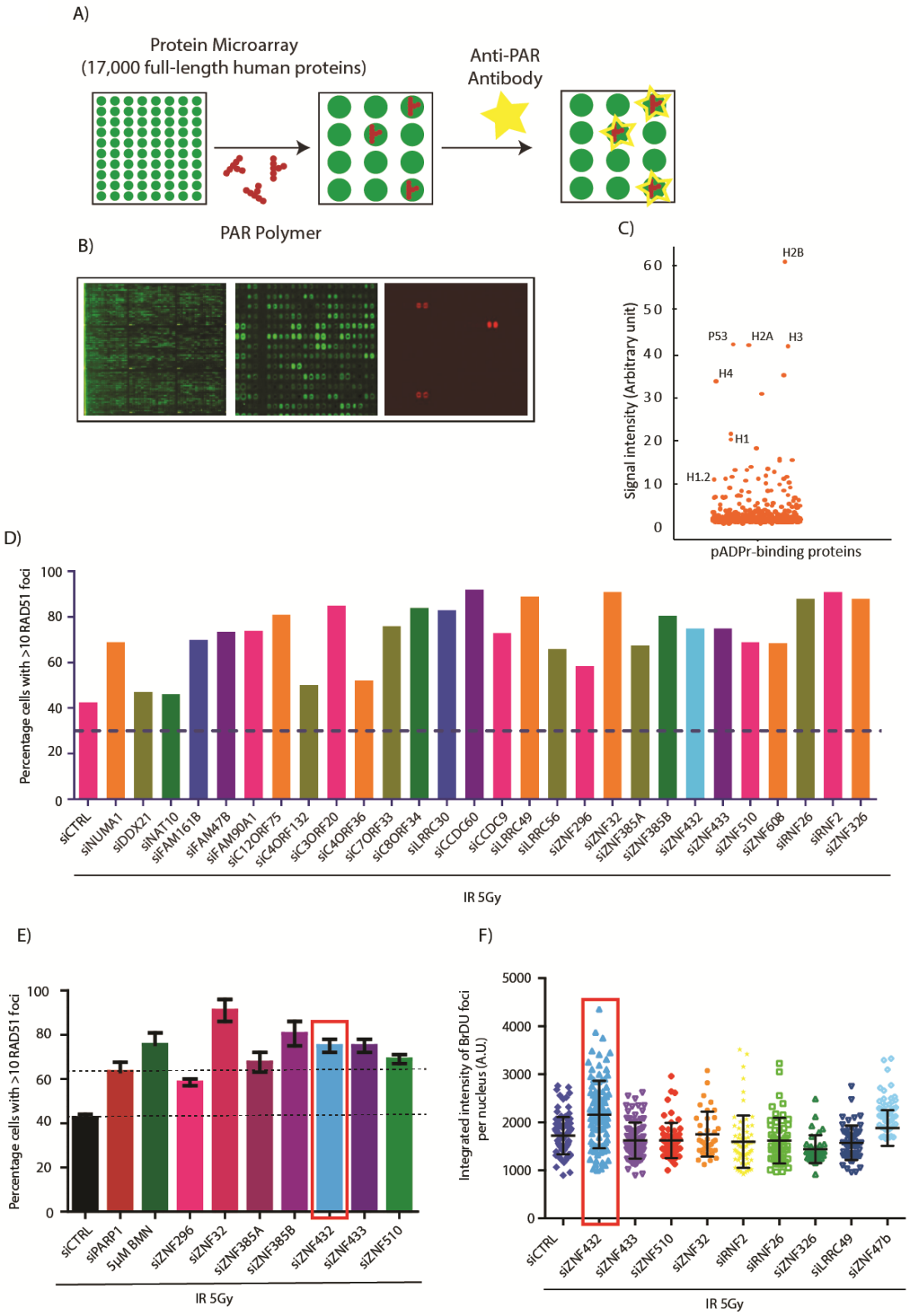

Figure 4.2: Identification of potential resection regulators from the PAR biding list provided by the Dawson Lab.

A) Schematic representation of the PAR microarray used to generate the PAR-binder data set. B) Photographs of the microarray, the red fluorescence indicating bound PAR. C) scatter of the 375 proteins identified through this method. D) The preliminary screen

graph showing percentage of cells with greater than RAD51 foci 1 hour post 5Gy irradiation n=1. E) Repeat graph showing percentage of cells with greater than RAD51 foci under the same conditions with the ZNF family proteins from the data set, with ZNF432 highlighted with a red box, n = 2. F) The BrdU foci formation graph 3 hours post 5Gy irradiation on the same ZNF proteins to identify those who modulate resection, with ZNF432 highlighted with a red box, n = 2.

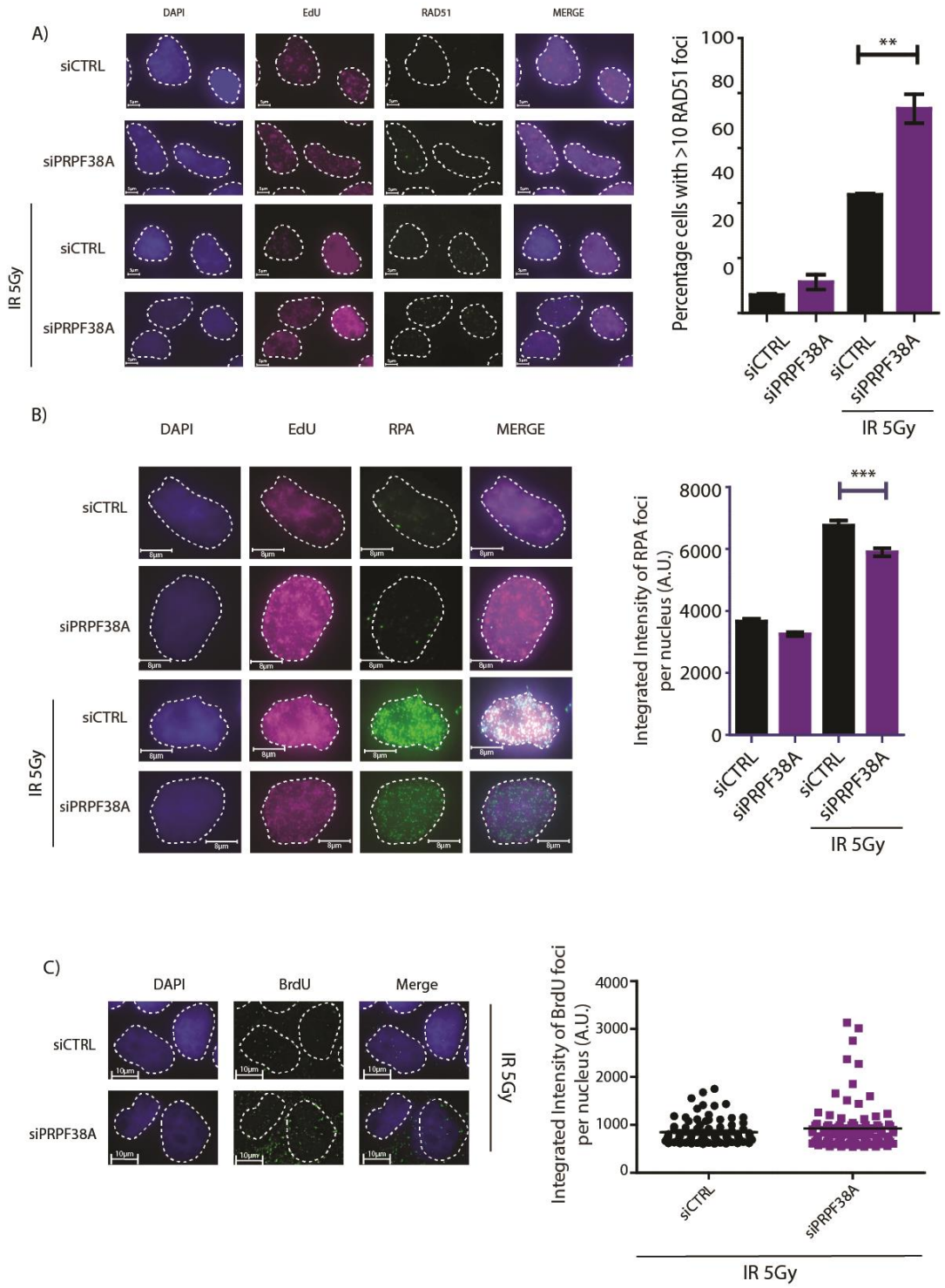

Figure 4.3 Exploration of the effect of PRPF38A knock down on RAD51, RPA, and BrdU foci.

A) Comparison of RAD51 foci formation with and without IR-induced damage in siCTRL and siPRPF38A cells. The cells were selected for S-phase using EdU click-it.

The graph shows the percentage of S-phase cells with greater than 10 foci(n=3). B) Intensity of phsopho-RPA foci in S-phase siCTRL and siPRPF38A with and without IR-induced damage (n=3). The cells were selected for S-phase using EdU click-it. C) Intensity of BrdU foci formation siCTRL and siPRPF38A 3 hours post IR-induced damage (n=3).

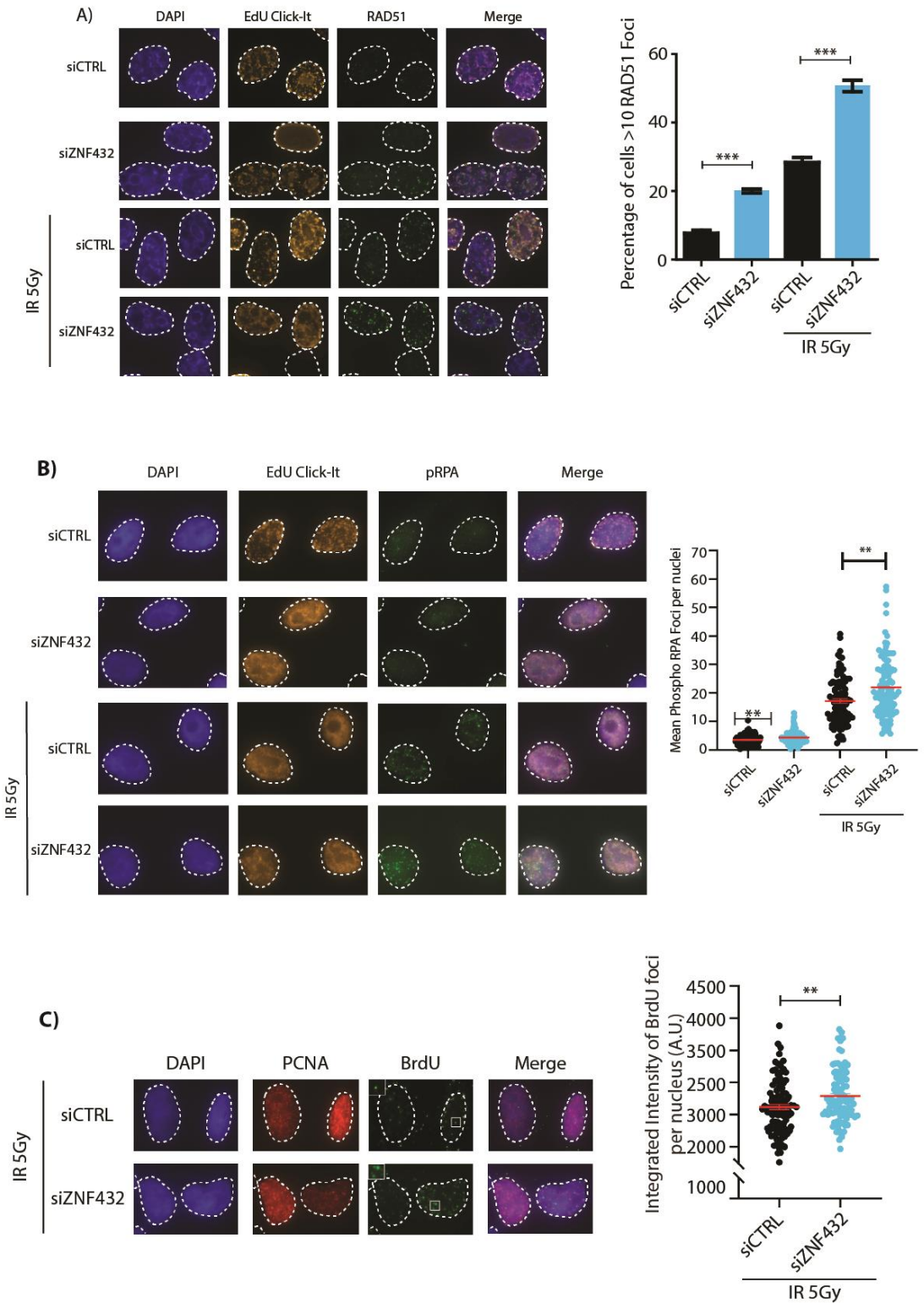

Figure 4.4 Exploration of the effect ZNF432 knock down on RAD51, RPA, and BrdU foci.

A) Comparison of RAD51 foci formation with and without IR-induced damage in siCTRL and siZNF432 cells. The cells were selected for S-phase using EdU click-it. The graph shows the percentage of S-phase cells with greater than 10 foci (n=3). B) Mean of phsopho-RPA foci per nuclei in S-phase siCTRL and siZNF432 with and without IR-induced damage(n=3). The cells were selected for S-phase using EdU click-it. C) Nuclear integrated intensity of BrdU foci in siCTRL and siZNF432 3 hours post IR-induced damage in S/G2-phase cells as labelled by PCNA (n=3).

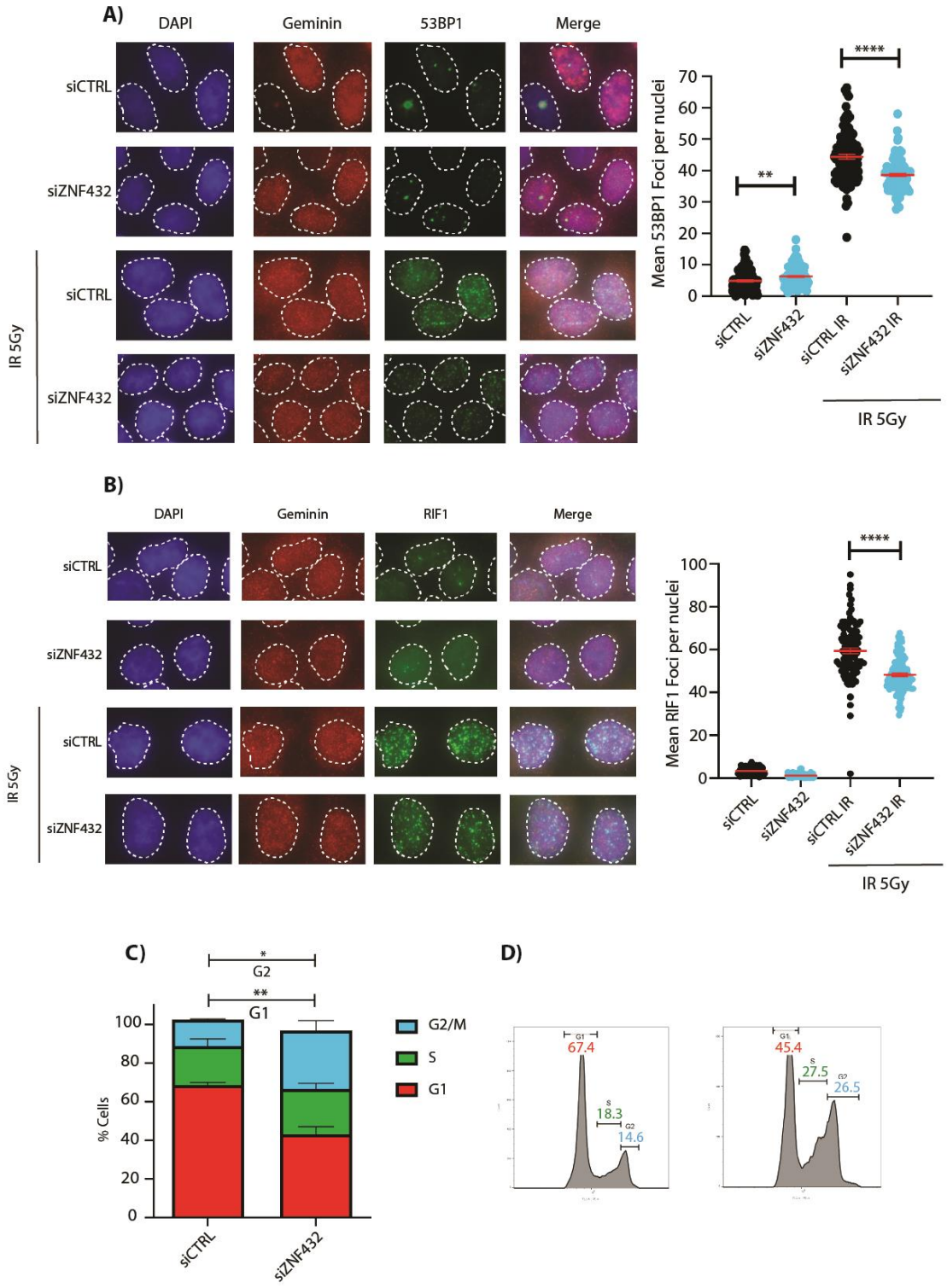

Figure 4.5 ZNF432 a modulator of DNA repair

A) Comparison of 53BP1 foci formation with and without IR-induced damage in siCTRL and siZNF432 cells (n=3). The cells were selected for S/G2-phase through the use of a Geminin antibody. B) Comparison of RIF1 foci formation with and with and without IR-

induced damage in siCTRL and siZNF432 cells(n=3). The cells were selected for S/G2-phase through the use of a Geminin antibody. C&D) FACs analysis of siCTRL and siZNF432 cells to determine cell cycle aberrations(n=3).

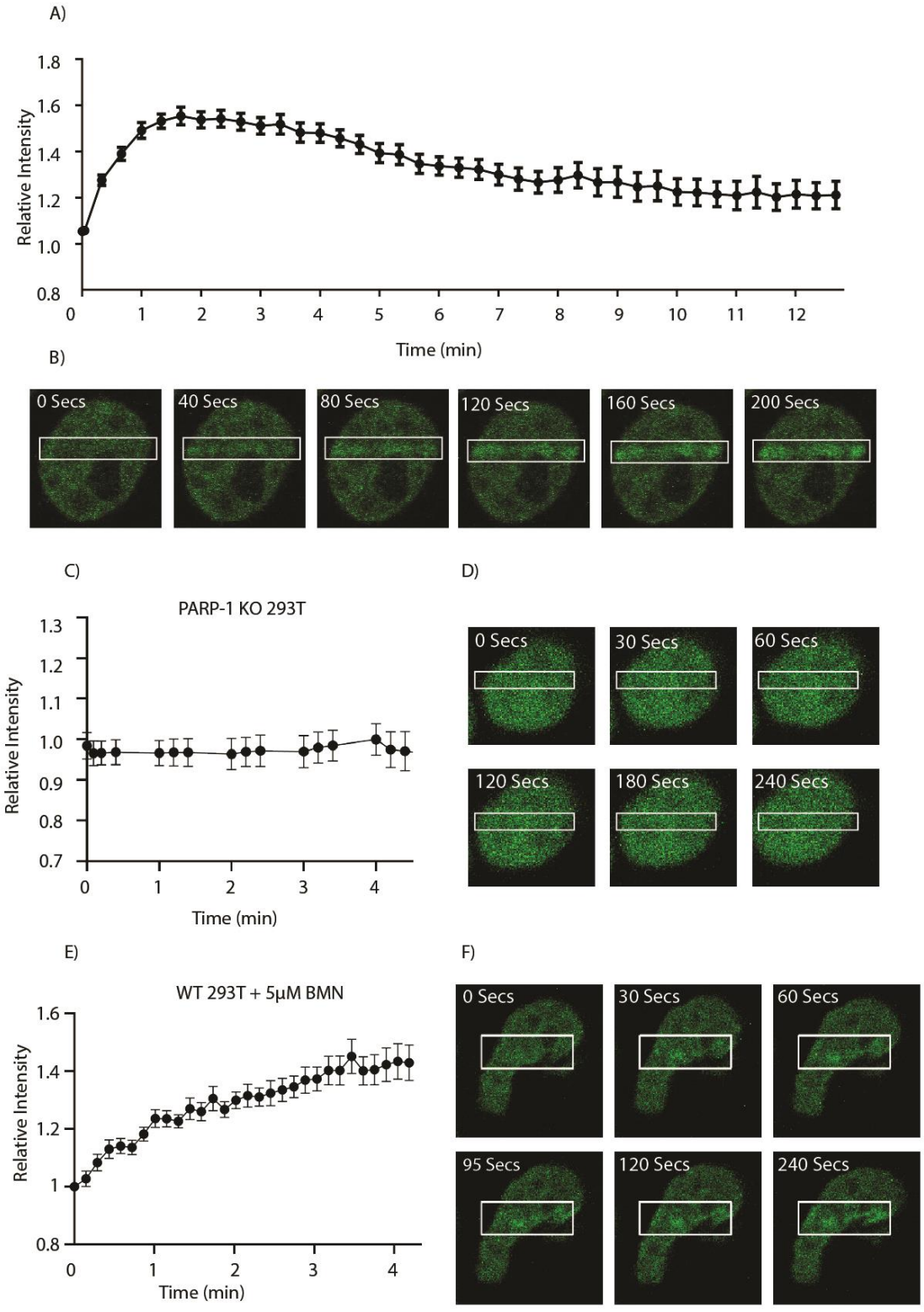

Figure 4.6 PARP-1 dependent recruitment of ZNF432 to damage sites.

A) Graph showing the recruitment and eventual disassociation of GFP-ZNF432 following laser-tract damage in 293T WT cells. B) Images showing the GFP-ZNF432 laser-tract

recruitment in 293T WT cells. C) Graph showing the loss of GFP-ZNF432 recruitment in 293T PARP-1 KO cells. D) Images showing the loss of GFP-ZNF432 recruitment in 293T PARP-1 KO cells. E) Graph showing the recruitment of GFP-ZNF432 following 1 hour pre-treatment with 5µM BMN-673. F) Images showing the recruitment of GFP-ZNF432 following 1 hour pre-treatment with 5µM BMN-673.

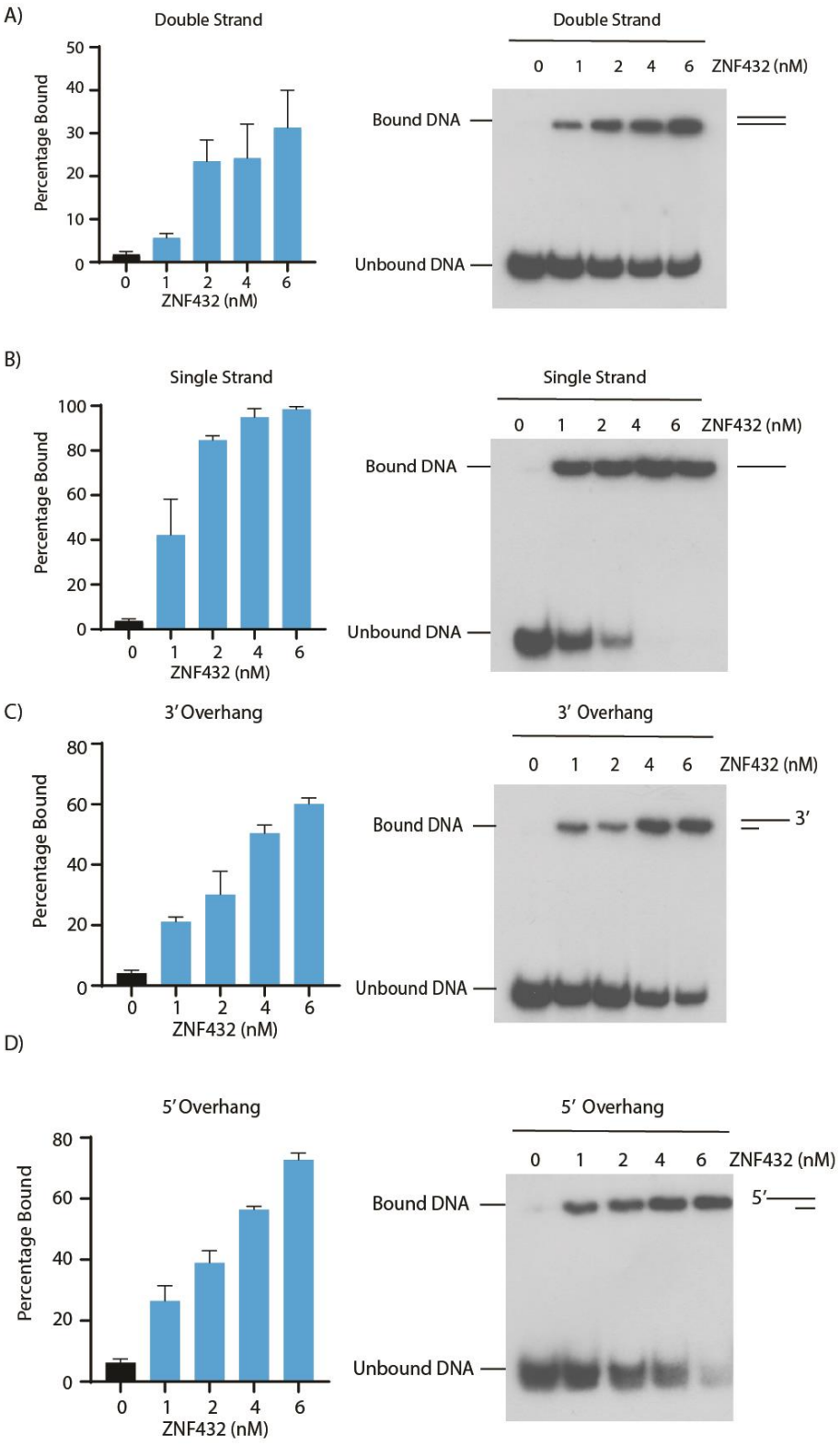

Figure 4.7: ZNF432 Binds DNA *in vitro*.

A-D) Bandshift assays demonstrating the binding capabilities of SF9 purified ZNF432 to γ-32P labelled DNA substrates; A) Single-strand DNA, B) Double-Strand DNA, C) 3' Overhang D) 5'Overhang (n=3).

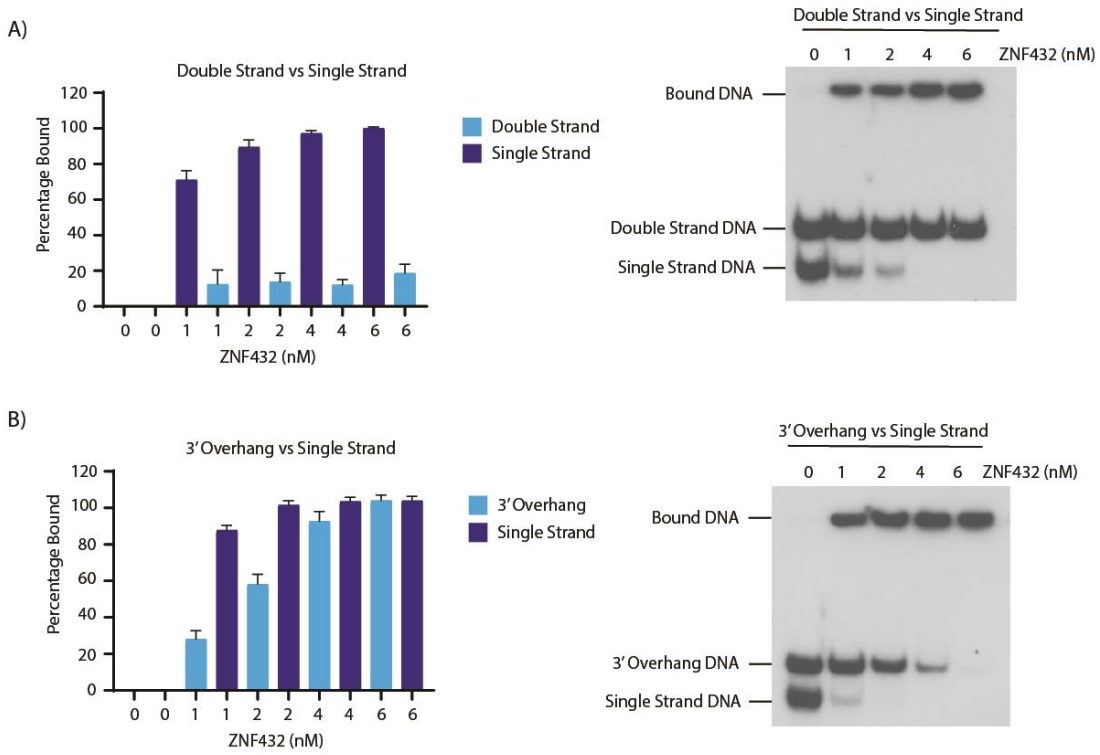

Figure 4.8 ZNF432 Preferentially binds single-strand DNA.

A&B) Competition binding bandshift assays using the single-strand probe in competition with either the double-strand or 3' overhang probes(n=3). All assays were done at 37ºC and with glutaraldehyde fixation prior to running on SDS-Acrylamide gels. A) Competition between single-strand DNA (dark blue) and double-strand DNA (light blue) (n=3). B) Competition between single-strand DNA (dark blue) and 3' overhang DNA (light blue) (n=3).

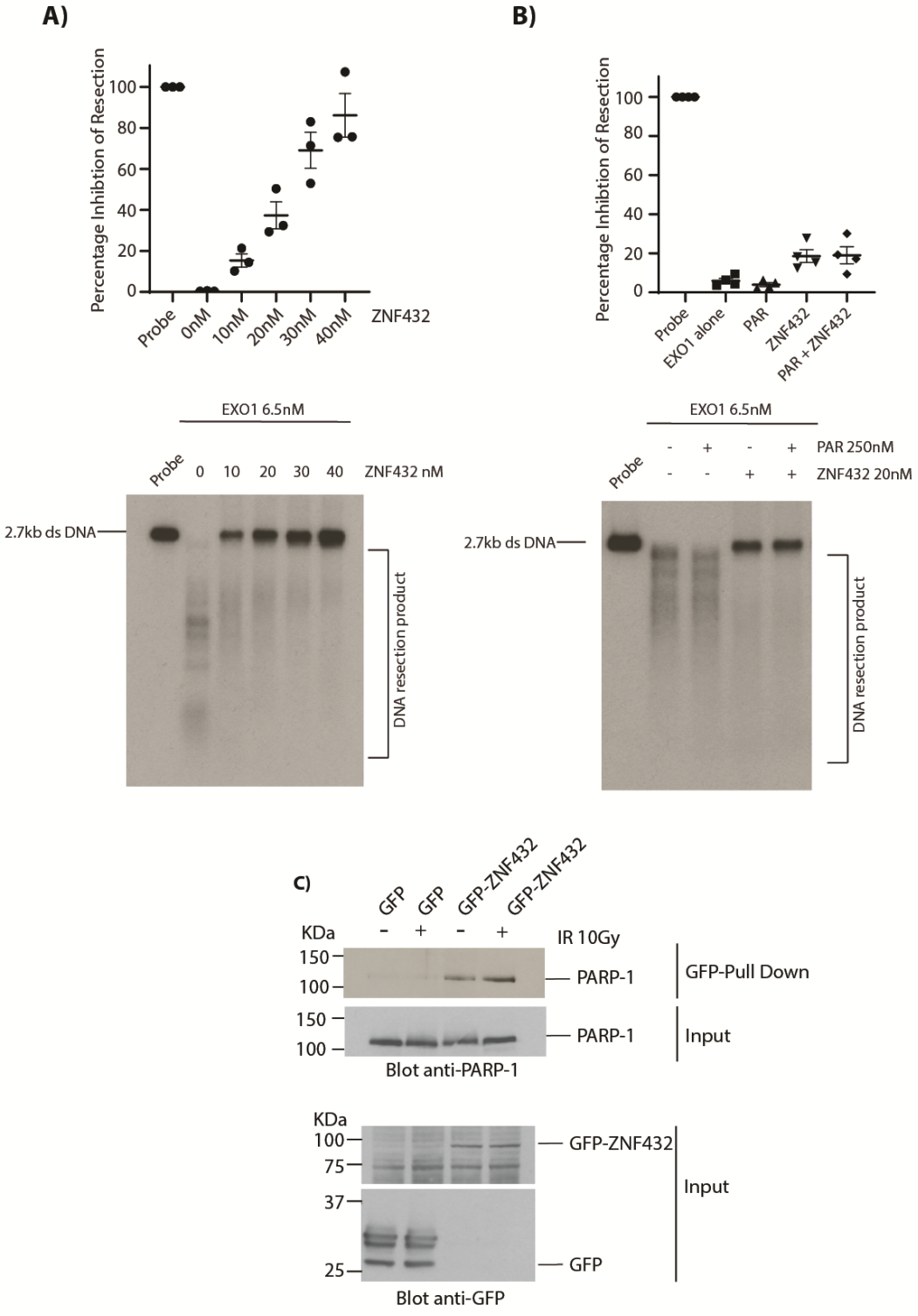

Figure 4.9 ZNF432 inhibits EXO1 resection and interacts directly with the resection regulator PARP-1.

A) *In vitro* resection assay using 2.7Kb double-strand α-^{32}P radio labelled DNA probes and SF9 purified EXO1 (6.5nM) and increasing concentrations of SF9 purified ZNF432

(0, 10, 20, 30 & 40nM) (n=3). B) *In vitro* resection assay using 2.7Kb double-strand α-^{32}P radio labelled DNA probes and SF9 purified EXO1 (6.5nM) and ZNF432 (20nM) with and without 250nM purified PAR (n=3). C) Western blot of GFP-Trap pull-down of PARP-1 from Hela cells transfected with either GFP or GFP-ZNF432 (F1:23 PARP-1 antibody and Roche GFP antibody) (n=3).

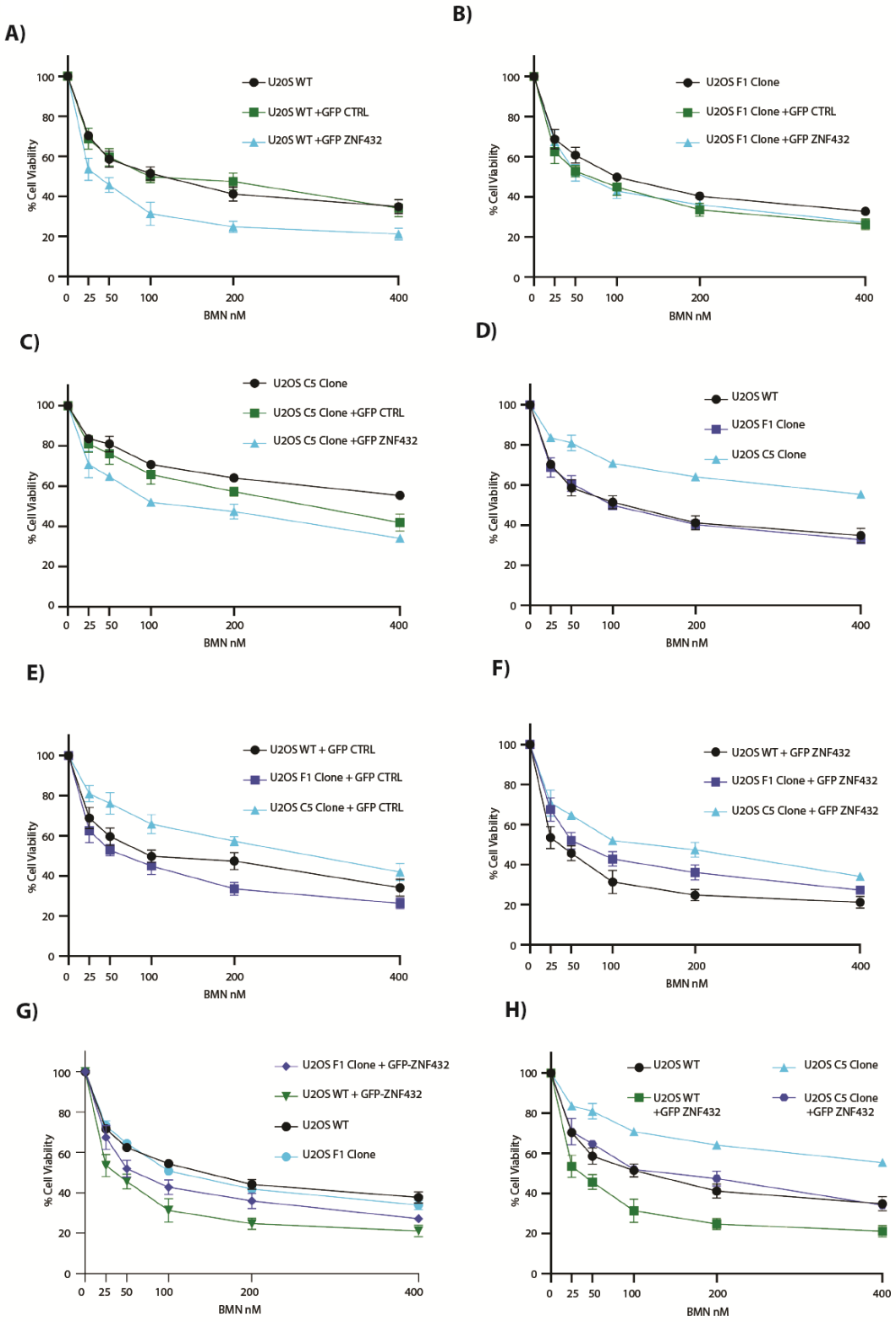

Figure 4.10 ZNF432 overexpression results in BMN-673 sensitivity and ZNF432 knock down leads to BMN-673 resistance which can be reduced by ZNF432 transfection.

A-G) Cell viability assay following BMN-673 treatment, concentrations 0, 25nM, 50nm, 100nm, 200nm and 400nm (n=3). A) U20S WT cell viability following 3 days of treatment with BMN-673. The cell line was either not transfected or transfected with GFP-CTRL or GFP-ZNF432. B) U20S ZNF432 KD clone F1 cell viability following 3 days of treatment with BMN-673. The cell line was either not transfected or transfected with GFP-CTRL or GFP-ZNF432. C) U20S ZNF432 KD clone C5 cell viability following 3 days of treatment with BMN-673. The cell line was either not transfected or transfected with GFP-CTRL or GFP-ZNF432. D) Comparison of the cell viability of all three cell lines without transfection. E) Comparison of the cell viability of all three cell lines with GFP-ZNF432. F) Comparison of the cell viability of the WT and F1 cell lines with and without GFP-ZNF432 transfection. G) Comparison of the cell viability of the WT and C5 cell lines with and without GFP-ZNF432 transfection.

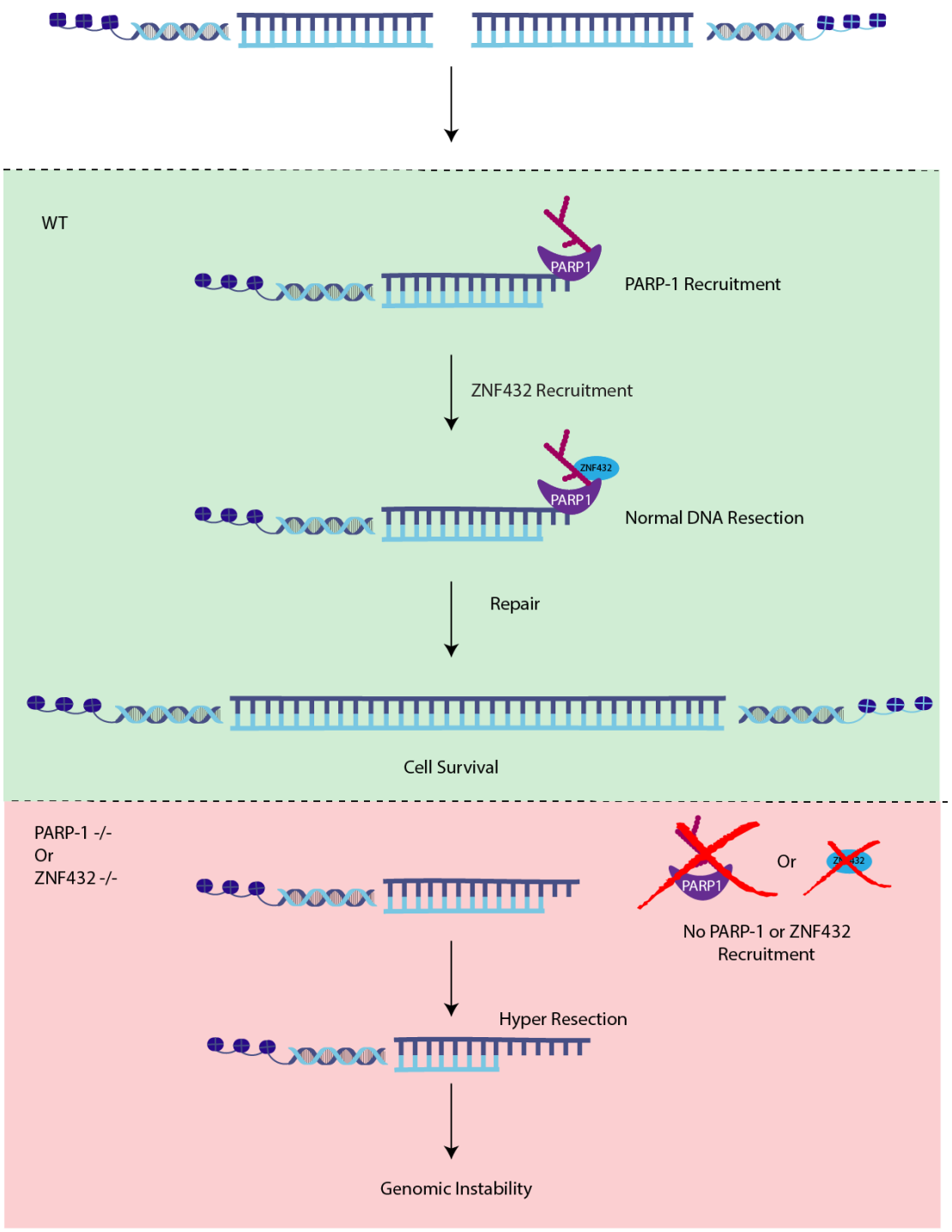

Figure 4.11 Model.

Schematic representation of our suggested model. In wild-type cells PARP-1 is recruited to the site of damage which then recruits ZNF432, together they antagonistically regulated resection. If, however PARP-1 is lost ZNF432 is no longer recruited and hyper-resection occurs leading to genomic instability. If ZNF432 is depleted we also see this hyper-resection phenotype, indicating that the mechanism for regulating resection requires both PARP-1 and ZNF432.

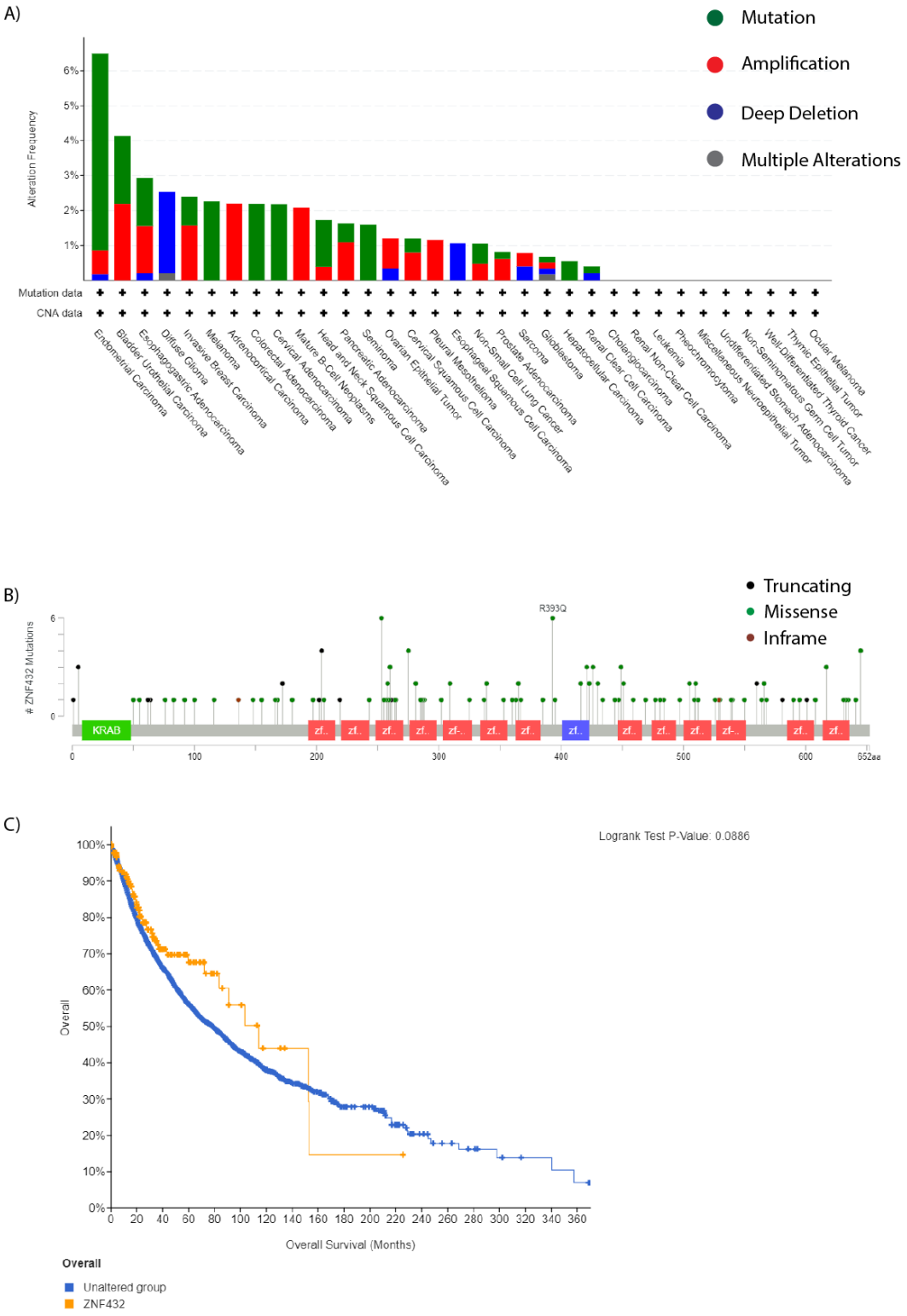

Figure 4.12 cBioPortal data for ZNF432.

A) cBioPortal graphs showing the ZNF432 mutation distribution among different cancer types. B) The location of identified ZNF432 mutations. C) Graph depicting the reduced survival rates for those with ZNF432 mutated cancers[496, 497].

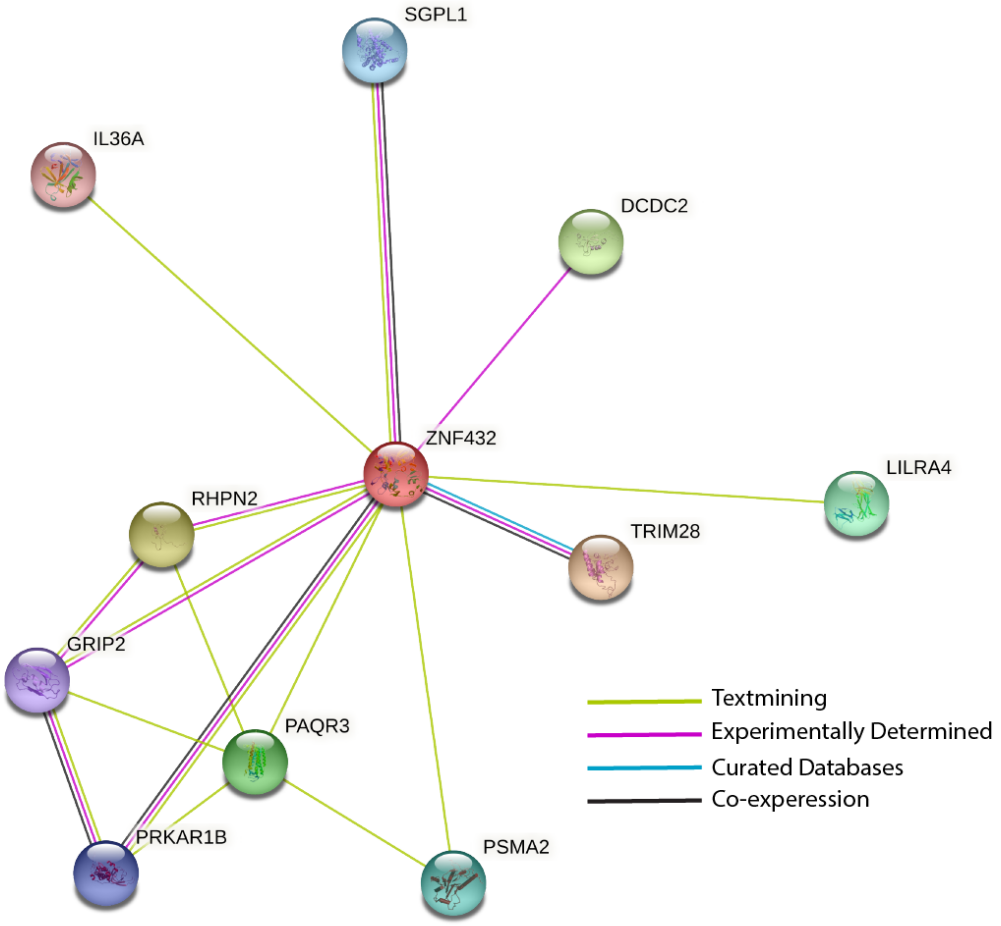

Figure 4.13 Protein network from string-db.

String-db network of the proposed ZNF432 interactors. STRING is a collated database of known and predicted protein interactions. These interactions are derived from genomic context predictions, high-throughput experiments, conserved co-expression, computerised text mining and previous knowledge databases. The interactions include both physical (direct) and functional (indirect) interactions. This can provide a base point when looking for interactions or to confirm identified interactors[498].

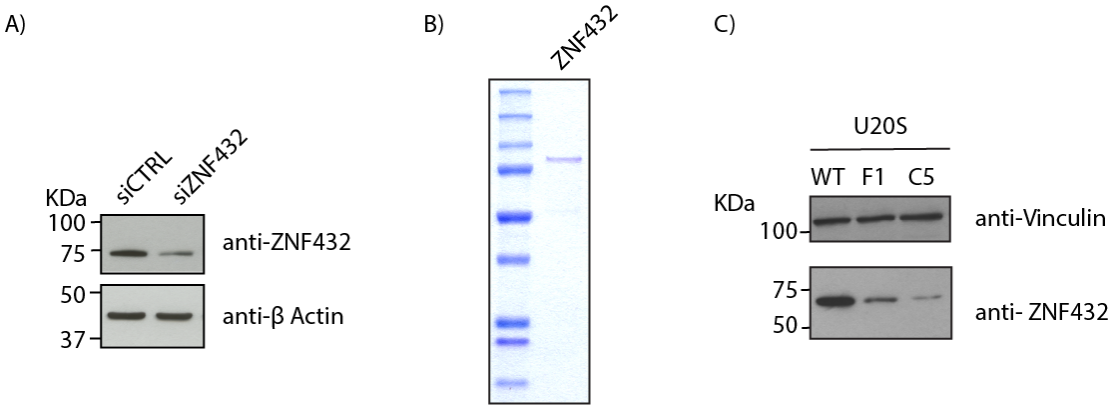

Figure 4.14 Supplemental Figure 1 RNAi-mediated knock-down of ZNF432 and purified ZNF432 from Sf9 cells.

A) Western blot against ZNF432 showing siRNA knock down efficiency. B) Coomassie staining of the Sf9 purified ZNF432. C) Western blot against ZNF432 showing the CRISPR knock down clones.

5.15

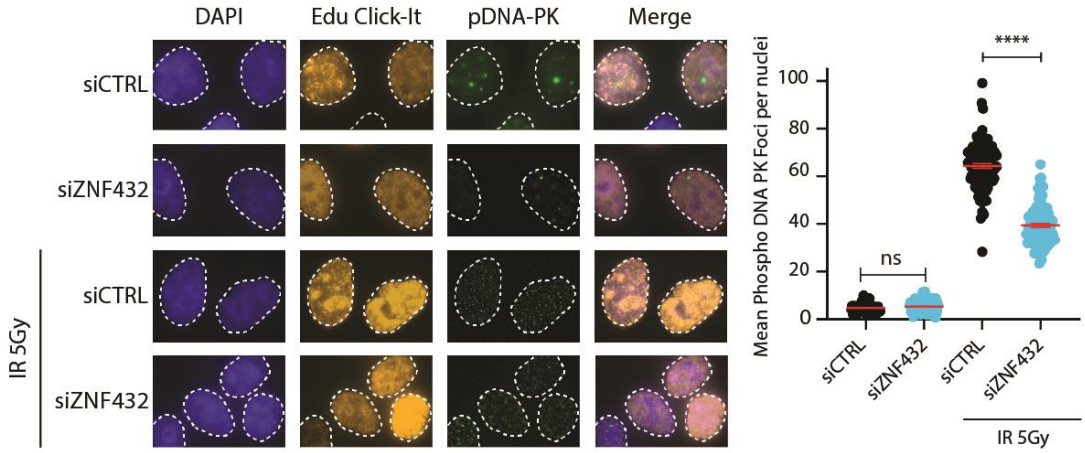

Figure 4.15 Supplemental Figure 2 ZNF432 knock down reduces phosphoDNA-PK Ser2056 foci in S-phase.

Comparison of phosphoDNA-PK Ser2056 foci formation with and without IR-induced damage in siCTRL and siZNF432 cells. The cells were selected for S-phase using EdU click-it. The graph shows the percentage of mean foci in S-phase cells(n=3).

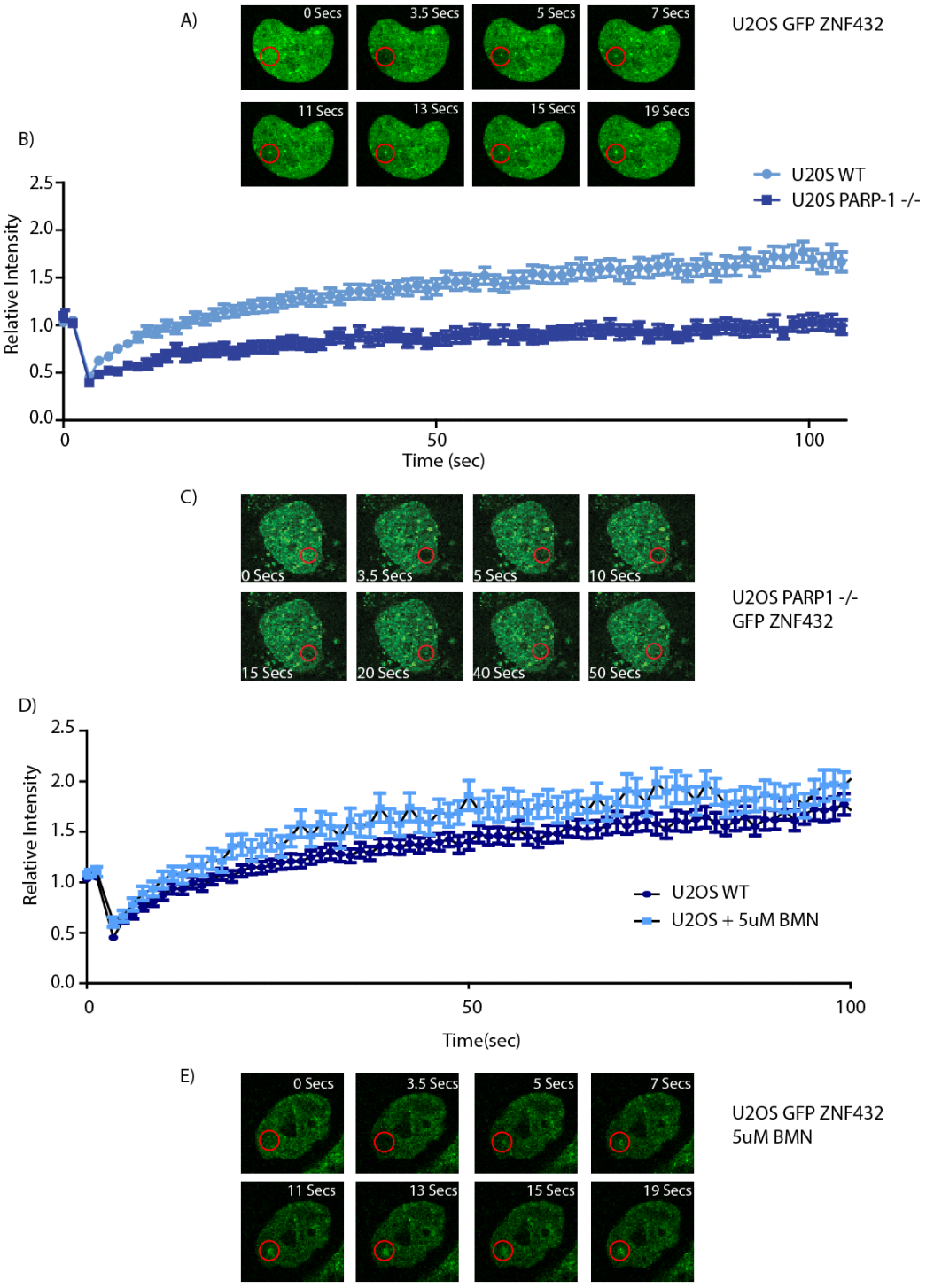

Figure 4.16 Supplemental Figure 3: ZNF432 is recruited to the site of DNA damage in a PARP-1 dependent manner.

A) Images showing the recruitment of GFP-ZNF432 in U2OS WT cells, the blast site is circled in red. B) Graph showing the recruitment of GFP-ZNF432 in U2OS WT and U2OS PARP-1 KO cells following a UV blast. C) Images showing the loss of recruitment of GFP-ZNF432 in U2OS PARP-1 KO cells, the blast site is circled in red. D) Recruitment of GFP-ZNF432 in U2OS WT cells with and without 1 hour pre-treatment with 5μM BMN-673 following a UV blast. E) Images

showing the recruitment of GFP-ZNF432 in U2OS WT cells pre-treated for 1 hour with 5µM BMN-673, the blast site is circled in red.

A)

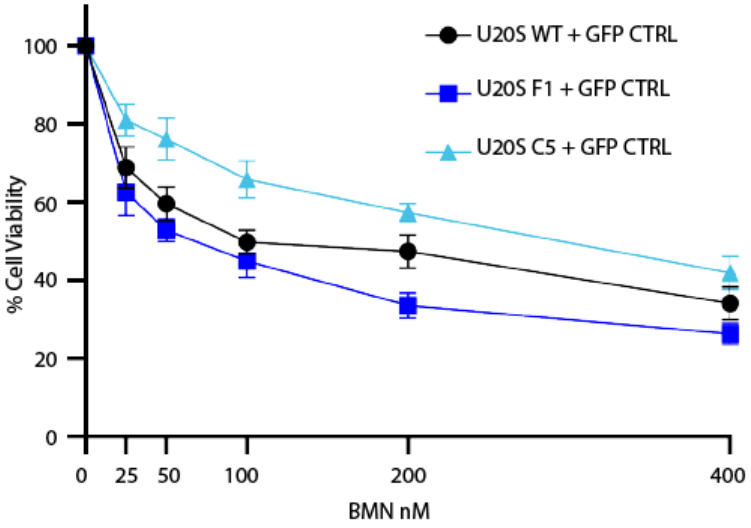

Figure 4.17 Supplemental Figure 4: Comparison of the cell viability of the CRISPR KD cell lines following GFP-CTRL transfection.

A) Comparison of the cell viability of all three cell lines with GFP-CTRL transfection following 3 days of treatment with BMN-673 concentrations ranging from 0 – 400nM.

Table 4.1 Supplemental Table 1 ZNF432 interactors without damage identified by MS.

WT Untreated	
Description	Gene
Histone H4	H4C1
Zinc finger protein 432	ZNF432
Histone H1.3	H1-3
Histone H2A type 2-A	H2AC18
Histone H3.2	H3C15
Histone H2B type 1-K	H2BC12
Transcription intermediary factor 1-beta (KAP-1)	TRIM28
Kinesin-like protein KIF20B	KIF20B
Tubulin beta chain	TUBB
Nucleolin	NCL
NEDD4-like E3 ubiquitin-protein ligase WWP2	WWP2

Dolichyl-diphosphooligosaccharide--protein glycosyltransferase subunit 1	RPN1
Nucleophosmin	NPM1
Ribonucleases P/MRP protein subunit POP1	POP1
Heterogeneous nuclear ribonucleoprotein M	HNRNPM
Heterogeneous nuclear ribonucleoprotein U	HNRNPU
ADP/ATP translocase 2	SLC25A5
Nucleolar RNA helicase 2	DDX21
Prohibitin-2	PHB2
Poly [ADP-ribose] polymerase 1	PARP1
Tubulin alpha-1B chain	TUBA1B
Isoleucine--tRNA ligase, cytoplasmic	IARS1
Titin	TTN
Heat shock cognate 71 kDa protein	HSPA8
RNA-binding protein 14	RBM14

Table 4.2 Supplemental Table 1 ZNF432 interactors identified with H2O2 damage by MS.

WT H2O2	
Description	Gene
Histone H4	H4C1
Histone H2A type 2-A	H2AC18
Histone H2B type 1-M	H2BC14
Histone H1.2	H1-2
Histone H3.3	H3-3A
Kinesin-like protein KIF2C	KIF2C
Zinc finger protein 432	ZNF432
ADP/ATP translocase 2	SLC25A5
Nucleolin	NCL
Tubulin beta chain	TUBB

Transcription intermediary factor 1-beta (KAP-1)	TRIM28
Nucleophosmin	NPM1
Prohibitin-2	PHB2
Nucleolar RNA helicase 2	DDX21
ATP synthase subunit beta, mitochondrial	ATP5F1B
ATP synthase subunit alpha, mitochondrial	ATP5F1A
Insulin-like growth factor 2 mRNA-binding protein 1	IGF2BP1
Poly [ADP-ribose] polymerase 1	PARP1
Glyceraldehyde-3-phosphate dehydrogenase	GAPDH
Heterogeneous nuclear ribonucleoprotein U	HNRNPU
Histone H2B type 2-E	H2BC21
ATP-dependent RNA helicase A	DHX9
Tubulin alpha-1B chain	TUBA1B
Isoleucine--tRNA ligase, cytoplasmic	IARS1
Voltage-dependent anion-selective channel protein 1	VDAC1

Final Discussion, Conclusions and Perspectives

The DNA damage response is a complex and carefully controlled network of proteins whose activity is essential for cell survival. Genomic instability as a result of repair defects is a highly competitive research field. Questions constantly arise from both fundamental and translational research groups into how and why these repair pathways function and in the case of cancers, dysregulate. In order to better understand these cancers and help in the identification of targets for chemical modulation, our laboratory investigates the fundamental mechanisms of DNA repair. My Ph.D. work has focused on the mechanism of homologous recombination, a pathway that is significantly affected in many cancers through the mutation of key repair proteins such as BRCA1 and BRCA2. Our interest in the pathway has stemmed largely due to the emergence of PARP inhibition as a tool in the field of cancer therapeutics.

Since the discovery of PARP-1 and the post-translational modification of PARylation in the 1960s, a vast and exciting field of study has been emerged. It is now acknowledged that PARP-1 and PARylation play pivotal roles in DNA repair processes. Though there has been some controversy as to the exact role, it is now generally accepted that PARP-1 and PAR play a part in multiple DNA repair pathways. Our interest has been centred around PARP-1 and PAR in DSB repair. We hope that in better understanding DSB repair new therapeutics can be developed or those already in production can be used more efficiently to treat cancer.

PARP inhibitors are one such therapy that has proven to be largely effective, though it is not fool proof[102, 136, 140, 150, 481]. Resistance to PARPi remains an important clinical issue that is under scrutiny[155, 171, 499]. Currently there are four PARPi which have been FDA approved; olaparib, rucaparib, talazoparib (BMN-673) and niraparib. Veliparib is currently in stage 3 trials and is expected to join the other PARPi on the market in the near future. While we are aware of how these inhibitors function chemically, there is still much that is unknown on why PARP inhibition is so useful in treating cancer. These inhibitors have been used in combination with radiation therapy, but are now being tested as monotherapies. For a time, it was believed that these inhibitors functioned solely by dampening alternate pathways, such as NHEJ, resulting in cell death in HR deficient

cells. While this is still possible, our group has now identified a role for PARP-1 in HR, which may explain how these PARPi are effective in non-HR deficient cells. One possible way to overcome PARPi resistance could be through combination of new therapies, combining PARPi and other drugs, or through the development of completely alternative targets that have similar phenotypes.

To properly understand how PARPi functions as an effective cancer therapeutic it is essential to understand the role of PARP-1 in DSB repair. By studying this mechanism, we can better understand the most favourable context to use PARPi and the mechanism for PARPi resistance. Furthermore, a clear understanding of the role of PARP-1 in DSB repair could provide insight to a key process that could be chemically altered in other ways than PARP inhibition and still produce a similar result, thus potentially negating PARPi resistance.

Hence, the major objective of my doctoral thesis has been in studying the role of PARP-1 in DSB repair by HR, and further, uncovering PARP-1 and PAR interactors that also play a role in this mechanism. This has involved the functional analysis of PARP-1 in HR to better determine its role, and the use of proteomics and microarray techniques to identify new members of the PAR interactome. The analysis of the PAR interactome has acted as a jumping-off point for the in-depth study of a previously unstudied zinc-finger protein: ZNF432. The subsequent section briefly summarises and discusses the results obtained from this study in relation to the current literature and the perspectives of this work.

PARP-1 a regulator of DNA end resection in HR

Since PARP-1 is recruited within milliseconds to DSBs, we envisioned that PARP-1 activation orchestrates the initial steps of DNA resection. PARP-1 interacts with DNA-PKcs/Ku70/Ku80[438] and mediates this effect through DNA end binding. Although Ku and PARP-1 have been found to compete for binding to DNA end *in vitro*[53]. Temporally, PARP-1 precedes Ku loading and its activity is required to load Ku onto DSB ends. This correlates well with the timing of PARP-1-mediated displacement of

histones[418], suggesting that PARP-1 activity is necessary to prepare chromatin for loading of Ku onto broken DSB ends.

We determined when PARP-1 is absent, neither PARP-1 nor Ku assemble to protect the DNA ends, as was observed when analysed by ChIP at nuclease-induced DSBs. Consequently, EXO1 has increased access to DSBs and with an accompanying decrease of RIF1 and 53BP1, leads to increased DNA processing. In line with this observation, using the ER-*Asi*SI system, the group of Tanya Paull has shown that siKu86 or Ku86 conditional-null HCT116 cells show an increase in DNA resection [433]. This observation fits into a model where both PARP-1 and Ku limit end resection, possibly by controlling the accumulation of the MRN complex[439] and CtIP, whereby loss of either PARP-1 or Ku binding results in over-resection. PARP-2 has recently been shown to promote DNA resection[122], but since BMN-673 inhibits PARP-2 also[441], it might not contribute to the over-resection phenotype observed in BMN-673 inhibited cells.

There are two predominant models for the synthetic lethality caused by PARPi: 1) loss of BER and SSB repair, 2) toxic lesions and stalled replication forks formed as a result of PARP trapping. The first hypothesis relies on PARP-1 being primarily associated with the BER and SSB repair pathways, something that has been contested due to the lack of increase in SSBs following PARPi. The same synthetic lethality was not seen when XRCC1, a key BER protein, was modulated[446, 447]. Hence, these observations raised the possibility that the effects of PARPi may be mediated through a mechanism distinct from BER. Consistent with this, Patel *et al*. have shown that deregulated NHEJ plays a major role in generating the genomic instability and cytotoxicity in HR-deficient cells treated with PARPi[447]. The second theory is one that is favoured, though recent work has suggested that this trapping effect is not as prolific as first believed. For example, BMN-673 one of the more severe “trappers” does not keep PARP-1 on the DNA though it does delay its dissociation[141]. As such it is possible that there is an alternative mechanism which leads to the synthetic lethal response. We sought to uncover the role of PARP-1 in HR in order to shed some light on this possible mechanism.

Our work has suggested that PARP-1 loss promotes HR through increased resection explaining the (i) increase of sister chromatid exchanges[442]; (ii) anti-recombinogenic function of PARP-1[444]; and (iii) increased HR repair by a BRCA1 PARylation

mutant[445]. This PARP-1 inhibition-induced HR correlates with our previous findings using ABT-888 [189], also mimicking the effect of another DNA resection inhibitor, HELB [176].

Conclusions

Our work in clarifying the mechanism of PARP-1's action in HR revealed it as a key regulator for the process of DNA end resection. Through the use of *in cellulo* BrdU, RPA staining and SMART analysis we observed that loss of PARP-1 results in hyper-resection. Providing an explanation for the reduced cell survival seen after irradiation in cells deficient of PARP-1 or treated with the PARPi BMN-673. With the use of purified proteins from Sf9 cells, we determined through *in vitro* biochemical methods that PARP-1 inhibits the DNA resection, in both EXO1 and DNA2 machinery contingents. Interestingly, through the use of DNA curtains, we saw that PARP-1 slides down the DNA and prevents the binding of EXO1 at the DNA ends. While loss of PARP-1 leads to hyper-resection it also results in the reduced accumulation of the HR suppressors 53BP1 and RIF1 and an increase in RAD51 accumulation, a marker for HR progression. The reduction in 53BP1 and RIF1 increases DNA accessibility to EXO1 thus allowing for the unchecked hyper resection of the DNA, as seen in PARP-1 knock down or inhibited conditions. This increased HR repair is seen in conjunction with an increase in sister chromatid exchanges.

This provides the background for our model (Figure 3.8), whereby loss of PARP-1 results in the loss of resection regulation from 53BP1 and RIF1, along with the loss of end protection provided by the binding of Ku70/80. Allowing for the uninhibited resection activity of EXO1 along the DNA ends. In the presence of PARPi, once again there is loss of the resection inhibition resulting from the 53BP1 and RIF1 decrease and loss of the protection provided by KU70/80. Although the displacement of PARP-1 is delayed by the inhibitor; it is not lost, leaving the ends open to unregulated resection. Our work has provided the data to support this hypothesis, and thus provides a potential answer for the cytotoxicity and synthetic lethality which is observed under varying genetic contexts, such as BRCA1 deficiencies. All together our data identifies DNA resection as a key process that is strongly affected by PARP-1 modulation. As such alterations in the expression or functionality of resections enzymes may need to be considered when treating with PARPi.

Future Perspectives

One of the limiting factors of this study was that while we tested PARP-1 mutants in our *in vitro* assays we did not make use of them in our *in cellulo* work. This could help in further clarifying the importance of the PARP-1 protein itself or/and PARylation. In our *in vitro* assay the catalytic mutant of PARP-1, PARP-1 E988K, maintained the ability to inhibit resection whereas the mutant lacking the zinc-fingers failed to. Using the PARP-1 KO cells transfected with PARP-1 E988K it would be possible to identify which DDR factors are affected by the presence of PARP-1 at break and those which require PARylation. The use of BMN-673 while inhibiting PARylation also alters the recruitment kinetics of PARP-1 and as such may affect other DDR proteins simply by remaining at the break site longer than intended. To make full use of this mutant the recruitment and disassociation kinetics would need to be determined, if they are different to the wild type PARP-1 then it could also skew the observed results. Pursuing this line of experimentation could provide some very valuable data in the separation of PARP-1 and PARylation functions.

Similarly, as the current PARP inhibitors target PARP-1, PARP-2 and PARP-3 there is always the possibility that the inhibition of PARP-2 or PARP-3 is having some effect on our assay which we are not aware of as the function is usually masked by PARP-1 activity. Understanding how PARP-2 and PARP-3 loss affects HR would provide a clearer understanding of how synthetic lethality with PARPi functions. Furthermore, clear understanding of how different PARPi affect PARP-2 and PARP-3 function may provide some insight into the different IC50s of these drugs; 1nM for Olaparib, 0.6nM for Talazoparib, 4nM for Niraprib and 1nM for Rucaparib[478]. The cytotoxicity resulting from PARPi treatment has been attributed primarily to interference with PARP-1, however that is not to say that inhibition of PARP-2 does not have an effect. PARP-2 is a complicated protein to study due to the redundancy shared with PARP-1. However, more and more is being uncovered about the importance of PARP-2 in a variety of cellular processes. For example, PARP-2 has been linked to the augmentation of resection contrary to the function of PARP-1 as an antagonistic regulator of resection. PARP-2 stops the accumulation of 53BP1 at DNA damage sites to allow for CtIP-dependent resection[122]. It has also been linked to the maintenance of heterochromatin, integrity of centromeres and telomeres, and acts as a cofactor to several transcription factors[500]. PARP-2 has also been found to act as a coactivator for the androgen receptor and contributes to the growth of androgen-dependant prostate cancer[501]. These findings

suggest that PARP-2 also plays an important role in DDR and in cancer progression, understanding how it acts in these pathways could open new avenues of treatment and identify cancers which could be better treated with PARP inhibition.

As we know PAR acts as a scaffold for other proteins, it is possible that in the plethora of PAR-binding proteins there are targets which greatly influence the resulting phenotypes of PARPi treatment. Considering the number of RNA processing factors that have been observed to interact with PAR it is distinctly possible that PAR plays a role in other pathways such as the resolution of R-Loops. Which if left unresolved can result in further damage, as demonstrated by the NFAT5 and PARP-1 interaction. Determining if any of these PAR producing PARPs are involved in such a process would be extremely valuable. Recent studies have shown that R-loops induce replicative stress in cancer cells[502]. As such if PAR plays a role in the resolution of these structures, inhibition could be detrimental particularly when combined with the knowledge that PARP-2 has been linked to stabilising replication forks.

Additionally, exploring PARG in this context could provide another target for chemical inhibition[503]. We showed in this work how important PARP-1 and its activity is as a regulator of DNA resection. As PARG is primarily responsible for the degradation of PAR in stands to reason that loss of this degradation similarly to loss of the production could have serious consequences. It is possible that PARG inhibition would have a similar effect as PARPi, as it is thought that PARP-1 disassociation is as a consequence of the length of the PAR chain. However, that does not mean that the now modified PARP-1 who still retains these PAR chains would not have other effects. We saw in our *in vitro* assay that in the context of EXO1 PAR formation did not change the inhibition of resection, it was however reduced in the case of DNA2 These are of course in *in vitro* assays with purified proteins. As such it is not recommended to make a final conclusion based on this alone, the cellular environment could change these results. It is possible that the loss of PAR degradation could have effects on the recruitment or binding of other DNA repair proteins. PARG inhibition could severely impact the NAD^+ levels of the cells, another aspect which would need to be studied and considered before they could be used as a potential treatment. Thus, separating the function of PARP-1 itself and the production PAR could provide a valuable source of information. In separating PARP-1 and PAR function we could better understand whether to treat with PARP inhibitors or

should they be approved PARG inhibitors. While PARG inhibitors represent another exciting avenue of study in the treatment of cancer, it is always a possibility that they will not prove to be a successful candidate for use in humans. One, such possible reason for this is Parthanatos, cell death as a result of excessive PAR, this however will need much more research before a conclusion can be made.

Regardless, more information on PARP-1 and PAR in DSB repair will only increase our ability to successfully target it in cancer therapy. However, aside from better understanding the mechanism of action of PARPi it is critical that we determine the causes for PARPi resistance and develop methods to circumvent this. Studying the other PARPs which may compensate for PARP-1 loss could help in answering these questions. There is also the possibility that other proteins which interact with PARP-1 or PAR may play a role in the resection mechanism and thus provide more answers for the functionality of PARPi and potential alternative targets for therapeutics.

Continuing our exploration of the function of PARP-1, it is important to identify all the players that are interacting with PARP-1 in DNA repair. This of course is a herculean task that will take many years to reach completion, however each individual interaction that we identify and characterise will chip away at the mystery that is PARP-1.

In order to continue to expose the mechanism by which PARP-1 regulates, we wish to determine if there are any other PAR interacting proteins involved in this process. This was the basis for the work shown in Chapter 4 and summarised below.

Global BrdU incorporation as a tool to measure *in cellulo* DNA resection

In Chapter 3, we share the advancements made in our *in cellulo* DNA resection assay used in chapters 2 and 4. This assay makes use of BrdU incorporation and cell marking to measures DNA resection *in cellulo* in an HR context. Prior to this paper the assay was done without cell marking, allowing for potential inclusion of G1 cells which were not using HR repair. Another alternative method for measuring DNA resection *in cellulo* through immunofluorescence is RPA staining. RPA foci formation can however be influenced by replication or the modulation of RPA recruitment or expression. One of

the limitations of this technique is due to the intensive pre-extraction, non-nuclear proteins are lost thus limiting the possible co-stainings. For example, for cell cycle marking neither Geminin nor Cyclin A will be visible following the pre-extraction. Furthermore, due to the small size of the foci and the background fluorescence it is as yet not possible to co-localise with other proteins to determine if they are present at the break sites. This however does not negate the benefit of this method in measuring DNA resection. It provides a tool to determine if a protein or treatment affects this first stage of HR repair. Providing an important insight into the function of the protein in question or the mechanism by which the treatment functions. As such it is a valuable technique in both fundamental DNA repair research and in the study of treatment mechanisms.

ZNF432 a PARP-1 dependant regulator of DNA resection

The role of PARP-1 in DSB repair has been somewhat contentious but in chapter 3 our group previously demonstrated its importance as an antagonistic regulator for DNA resection [467]. However, we hypothesized that there may be other proteins involved in this process in a PARP-1 or PAR-dependent manner. Thus, we searched for PARP-1 or PAR interactors which also influenced resection.

In this study, we show that PARP-1/PAR interactors are a rich source for identifying new DNA repair proteins. This was unsurprising as multiple proteomic studies have showed that the PARylome formed following DNA damage includes proteins involved in many processes, such as transcription, chromatin remodelling and importantly the DDR. For our attempt at MS we increased the probability of repair occurring via HR by synchronising our cells. From our two PAR data sets we uncovered two proteins of interest: a pre-RNA processing factor, PRPF38A and a zinc finger protein, ZNF432. Through the use of cell cycle markers to identify S/G2 phase we were able to restrict our results to cells capable of HR during the microscopy-based portion of our screening. While depletion of both proteins showed increased accumulation of RAD51 foci formation, a marker for HR, only ZNF432 showed an effect on resection as measured by the integrated nuclear BrdU intensity, which is a measure for DNA end resection *in cellulo*, the technique was described in Chapter 3.

Conclusions

Though initially PRPF38A, which was identified from an S-phase synchronised MS screen following irradiation, showed potential as a modulator of HR it had no role we could discern in resection. While this does not discount it as an interesting target for future studies, our goal was to further explore the process of resection and the role that PARP-1 plays in it. For this reason, we sought out other sources for PAR binding candidates and were fortunate to be given the dataset generated in the Dawson laboratory of Johns Hopkins (Figure 4.2). To initially narrow down the list of candidates we performed an siRNA screen on the selected candidates and monitored HR by using RAD51 foci formation. This allowed for the selection and testing of a smaller group of candidates with the BrdU assay, thus identifying any potential modulators of resection directly, preventing a repeat of the disappointment of PRPF38A.

As our goal was to further explore the mechanism for regulating resection, we focused our attentions on ZNF432. This was only candidate from the second screen which had an effect on both RAD51 and BrdU. According to cBioPortal analysis of the TCGA Research Network: https://www.cancer.gov/tcga, it has been found to be altered in many cancers, and that this alteration coincides with a reduced survival (Figure 4.12)[496, 497]. There have been some articles suggesting ZNF432 as a biomarker for cancer progression in both glioblastoma and prostate cancer[504, 505]. Aside from this, the only information on ZNF432 comes from several cDNA screens and screens linked to asthma[489, 506, 507].

The zinc-finger family of proteins are poorly studied with many having no known function, as was the case for ZNF432. They are however regularly pulled down in DNA break repair IP:MS experiments, thus suggesting that more ZnFs may play important roles in the DDR. We observed an increase in BrdU and RPA foci when ZNF432 was knocked down, thus indicating an increase in resection following the depletion of ZNF432. Furthermore, knock-down of ZNF432 led to a decrease in 53BP1 and RIF1 foci formation, both of which are HR suppressors. This is a similar phenotype to what we had observed in chapter 2 studying PARP-1. We also observed a reduction in phosphorylated DNA-PK S2056 foci, a marker for NHEJ. This in tandem with the cell cycle analysis showing a decrease in G1 and an increase in G2 phases of the cell cycle suggests a

preference for HR when ZNF432 is reduced. These observations confirmed that ZNF432 affects DNA repair.

Upon successful purification of this protein, we observed binding capabilities to double- and single-strand and 3' and 5' overhang substrates with a preference for single-strand DNA over that of double-strand DNA or 3' overhangs. Following this confirmation of DNA binding we showed evidence that ZNF432 has the ability to halt EXO1 resection *in vitro*. This supports my *in cellulo* data showing that ZNF432 is an inhibitor of resection. While identified from a PAR-binding data set, the presence of purified free PAR had no effect on the inhibition of EXO1 resection. This was also seen in the resection assay when PARP-1was incubated with free PAR contrasting to PAR generated by PARP-1 activated by NAD^+ in the assay, as demonstrated in chapter 2 [467]. As such this does not remove the possibility that PAR may have an effect on ZNF432 inhibition of EXO1 *in vivo*.

We found that ZNF432 is recruited to sites of damage by laser-tracks and UV-blast. It is done in a PARP-1 dependent manner, as it is lost in our 293T PARP-1 KO and U2OS PARP-1 KO cells. Curiously, this recruitment was not lost with PARP inhibition by BMN-673. This is likely as the recruitment of PARP-1 is not stopped by BMN-673 treatment, though it does affect the dissociation from the DNA[141]. This indicates that PAR may not be required for recruitment of ZNF432 to the sites of damage, though it may play a role in the kinetics of ZNF432 recruitment. Regardless, this does not mean that PARylation is not involved in the proper activity of ZNF432. Using GFP-binding beads we were able to confirm the interaction between ZNF432 and PARP-1. GFP-ZNF432 was capable of pulling down PARP-1 from whole cell extracts with and without irradiation damage. This was also confirmed through MS analysis of a GFP-ZNF432 pulldown.

We have now received Ubigene ZNF432 knock-out cell lines, which were shown to be edited genomically but were not knock-out at the protein level, they do show significant knock-down, however. Using these cells, we have tested cell viability following three days of BMN-673 treatment. We saw that significant knock-down of ZNF432 results in resistance to BMN-673 lethality, this suggests that ZNF432 and PARP-1 work together as these Ubigene cells are already deficient in this pathway and thus not sensitive to BMN-673. Interestingly overexpression of ZNF432 results in sensitivity to

BMN-673 treatment, possibly as a result of failed resection. Though we have not determined the reason for this sensitivity and resistance, these results already support the possibility of using ZNF432 levels as a biomarker to monitor the efficiency of PARPi treatments. As such it would suggest that in tumours expressing lower concentrations of ZNF432 that PARPi treatment would not be recommended. Conversely in high ZNF432 expressing tumours PARPi treatment should prove more successful.

Future Perspectives

As I terminate my Ph.D. studies, the exploration into the activity of ZNF432 in DSB repair shall continue. The following will focus on some of the areas that we will explore.

Throughout this study we have faced difficult challenges some in the form of tools that were lacking and others as a result of the protein itself. As a previously unstudied protein we had no frame of reference for its behaviour nor the quality of the few reagents available for its study, making the process somewhat slow and arduous. However, we hope to continue making progress in its study in the future, some our future plans are detailed below.

While we have explored the effects of ZNF432 siRNA knockdown on many DDR proteins, we need to validate these results with the CRISPR knockdown cells. Once repeated in the Ubigene cells, we will endeavour to explore other DDR proteins using immunofluorescence or fluorescent recruitment experiments to further elucidate the mechanism of action of ZNF432. Exploring the effect on other resection proteins such as MRE11, NBS1 or EXO1 could help in determining exactly which factors are affected by ZNF432 depletion. EXO1 is of particular interest, as in our *in vitro* resection assay we see inhibition of EXO1 resection by ZNF432. HDR assays such as the CRISPR-Clover-LMNA assay could be attempted in the KD cell lines. This assay relies on the transfection of CRISPR system which will induce a DSB, if repaired by HR it will produce green fluorescent cells. This was previously not possible with the siRNA due to the poor KD efficiency and the requirement for a double siRNA transfection. This would provide valuable information as to whether the HDR mediated repair is successful in these cells.

To further understand this protein, dividing ZNF432 into an N-terminal consisting of the KRAB domain and C-terminal comprised of the 16 zinc-fingers will allow us to test which structures of the protein or the protein as whole is important for both DNA binding and for the inhibitory effect on EXO1 mediated resection. Exploring the PAR binding affinity of both the whole protein and these fragments using surface plasmon resonance (SPR) or exploring the PAR levels using dot blots following ZNF432 pull-downs from cell lysates may provide valuable information as to whether PAR plays a role in ZNF432's activity or if it is purely PARP-1. Furthermore, determining specific PARylation sites on ZNF432 and mutating them to observe if there is any altered function would be a possible direction in determining the role of PAR in ZNF432 activity.

Moving forward from the cell viability results it would be exceptionally illuminating to repeat this *in vivo*. Using mice models to test the sensitivity and resistance to PARPi would confirm ZNF432 as a treatment biomarker. Whereby cancers with high levels of ZNF432 would be ideal candidates for PARPi treatment potentially as a monotherapy, conversely cancers with low levels of ZNF432 might be better served with alternative treatments. However, at this point this may prove incredibly difficult to test. We struggled for many months, using 4 different cell lines, multiple guides, and strategies to generate a CRISPR KO cell line. After more than 300 clones screened none of which were KO, we sought the expertise of a CRISPR editing company. After double the estimated time they were able to generate two knockdown clones in a single cell line. It is distinctly possible that a true ZNF432 KO is lethal on cells. As such I would not be surprised to learn that to generate an animal model that also has aberrant levels though not a complete KO of ZNF432 would be as difficult if not more so, Furthermore we have no current knowledge of if ZNF432 plays a role in development.

Another avenue of exploration would be to test if traditionally PARPi resistant cells can be sensitised through the augmentation of ZNF432 expression. For example, testing the cell viability of a BRCA1/DYNLL1 KO cell line which is PARPi resistant[177] with and without transfection of ZNF432 to see if the level of PARPi resistance is affected. Should this prove to be the case, addition of ZNF432 could present a solution for PARPi resistance in cancer treatment. The development of ZNF432 as a drug would no doubt take time and would require a much greater knowledge of the structure of the protein, which we do not currently have.

Aside from further exploring the importance of different aspects of ZNF432 structure on DSB repair, we are also interested in the possible interaction between ZNF432 and TRIM28 (KAP1)[487]. TRIM28 is known to participate in many different cellular processes, including proliferation, differentiation, senescence, pluripotency, and apoptosis[508-511]. TRIM28 is a member of the Tripartite Motif (TRIM) family of E3 ligases and is comprised of a RING-finger motif, two B-boxes, a leucine sipper coiled-coil region, a PxVxL pentapeptide region, a plant homeodomain finger and a bromodomain[508, 512-514]. The different domains within TIRM28 have been linked to various important roles, such as the interaction between TRIM28 and Heterochromatin Protein 1 (HP1) which is mediated by the PxVxL pentapeptide region. The PHD, bromodomain and PxVxL domains are thought to cooperatively form condensed heterochromatin which is characterized by low histone acetylation and high tri-methylation of Histone H3 lysine 9 (H3K9) and high HP1 binding[515-517]. The C-terminal of TRIM28 which contains the PHD and bromodomains, is involved in the recruitment of the Nucleosome Remodelling Deacetylase and the H3K9 specific methyltransferase SETDB1 in order to condense chromatin. The ring finger domain binds along with the two B-boxes and the leucine zipper is responsible for the interaction with the KRAB domain[518, 519]. It is this structural interaction which makes the interaction between ZNF432 and TRIM28 unsurprising.

While TRIM28 is involved in many processes, it is the relatively recent suggestion that it is involved in DSB repair that sparked our curiosity. TRIM28 has been shown to be recruited to DNA lesions and is phosphorylated by ATM and DNA-PK. Phosphorylation of TRIM28 S824 by ATM[520], which is found exclusively at damage sites, leads to the release of HP1 from chromatin and thus the relaxation of the DNA which allows for the assembly and activity or the repair machinery at DSBs[211, 513, 521-523]. In the absence of pTRIM28, heterochromatic DSB repairs stall[513, 524, 525]. Furthermore, deregulation of TRIM28 has been linked to different cancers. Knockdown of TRIM28 in breast and lung cancer cells lines results in increased proliferation. Higher expressions of TRIM28 in early-stage lung cancer has been linked to increased overall survival, though it has also been linked to pro metastatic cervical cancer. Also, upregulation has been observed in gastric cancer and is associated with a poor

prognosis[526-530]. Finally, deletion of TRIM28 has been seen to be embryonically lethal in mice which is indicative of its importance to health[531].

Clearly its involvement in cancer is complicated. Determining if TRIM28 is involved in the ZNF432 mediated resection regulation could provide some insight into these findings. Initially we wish to confirm the interaction between ZNF432 and TRIM28. Following this we will explore the recruitment of TRIM28 in our ZNF432 depleted cells. Further explorations into the involvement of TRIM28 in resection will be undertaken in the same manner as was done for ZNF432. Our hope is that, should TRIM28 have a role in resection it will further shed light onto the mechanism of PARP-1/ZNF432 resection regulation. Much is still to be determined in regard to how ZNF432 affects resection and what regulates ZNF432 itself, though it is likely it will take many years to fully uncover the mysteries of ZNF432.

Much is left to be discovered regarding ZNF432 and its role in HR, however we hope that the work done here will act as a foundation in the future study of this important player of the DDR. Aside from some of the discoveries I hope to still make before leaving the laboratory, there are many areas of ZNF432 that I look forward to seeing uncovered in the future by others. Studies in the structure of ZNF432 and *in vivo* studies will be essential if ZNF432 is to be considered as a treatment option for cancer. If the production of an inhibitor or supplement of ZNF432 is not the way forward for this protein, *in vivo* studies may prove its worth as a biomarker to identify the ideal treatment methods. This foundation will hopefully provide inspiration in the development and modulation of ZNF432 in the study and treatment of cancer. Furthermore, I hope it will encourage others to study the often-forgotten zinc-finger proteins. They provide a trove of candidates which likely play important roles in many different pathways. The study of ZNF432 has been riddled with challenges but in the process, we have uncovered a protein that I hope impact DNA repair-based cancer research positively.

References

1. Hoeijmakers, J.H., *DNA damage, aging, and cancer*. New England Journal of Medicine, 2009. **361**(15): p. 1475-1485.
2. Ganten, D. and K. Ruckpaul, *Encyclopedic reference of genomics and proteomics in molecular medicine*. Book. 2006: Springer-Verlag Berlin Heidelberg.
3. Cadet, J., E. Sage, and T. Douki, *Ultraviolet radiation-mediated damage to cellular DNA.* Mutation Research/Fundamental and Molecular Mechanisms of Mutagenesis, 2005. **571**(1-2): p. 3-17.
4. Kawanishi, S., et al., *Oxidative and nitrative DNA damage in animals and patients with inflammatory diseases in relation to inflammation-related carcinogenesis.* Biological chemistry, 2006. **387**(4): p. 365-372.
5. Krejci, L., et al., *Homologous recombination and its regulation.* Nucleic acids research, 2012. **40**(13): p. 5795-5818.
6. Jackson, A.L. and L.A. Loeb, *The contribution of endogenous sources of DNA damage to the multiple mutations in cancer.* Mutation Research/Fundamental and Molecular Mechanisms of Mutagenesis, 2001. **477**(1-2): p. 7-21.
7. De Bont, R. and N. Van Larebeke, *Endogenous DNA damage in humans: a review of quantitative data.* Mutagenesis, 2004. **19**(3): p. 169-185.
8. Tubbs, A. and A. Nussenzweig, *Endogenous DNA damage as a source of genomic instability in cancer.* Cell, 2017. **168**(4): p. 644-656.
9. Majidinia, M. and B. Yousefi, *DNA repair and damage pathways in breast cancer development and therapy.* DNA repair, 2017. **54**: p. 22-29.
10. Hanahan, D. and R.A. Weinberg, *The hallmarks of cancer.* cell, 2000. **100**(1): p. 57-70.
11. Bahman, F., et al., *Chapter 8 - Polymeric Micelles in Management of Lung Cancer*, in *Nanotechnology-Based Targeted Drug Delivery Systems for Lung Cancer*, P. Kesharwani, Editor. 2019, Academic Press. p. 193-216.
12. Maeda, H., *Pharmacological Uniqueness and Clinical Effects of Neocarzinostatin*, in *Neocarzinostatin: The Past, Present, and Future of an Anticancer Drug*, H. Maeda, K. Edo, and N. Ishida, Editors. 1997, Springer Japan: Tokyo. p. 205-226.
13. Wang, Y., et al., *The BRCA1-Δ11q alternative splice isoform bypasses germline mutations and promotes therapeutic resistance to PARP inhibition and cisplatin.* Cancer research, 2016. **76**(9): p. 2778-2790.
14. Sakai, W., et al., *Secondary mutations as a mechanism of cisplatin resistance in BRCA2-mutated cancers.* Nature, 2008. **451**(7182): p. 1116-1120.
15. Feldman, D., *DNA repair, by Errol C. Friedberg, WH Freeman, New York, 1984, 614 pp.* . Journal of Polymer Science: Polymer Letters Edition, 1985. **23**(11): p. 605-605.
16. Ciccia, A. and S.J. Elledge, *The DNA damage response: making it safe to play with knives.* Molecular cell, 2010. **40**(2): p. 179-204.
17. Hustedt, N. and D. Durocher, *The control of DNA repair by the cell cycle.* Nature cell biology, 2017. **19**(1): p. 1-9.
18. Lee, J.-H. and T.T. Paull, *ATM activation by DNA double-strand breaks through the Mre11-Rad50-Nbs1 complex.* Science, 2005. **308**(5721): p. 551-554.
19. Dart, D.A., et al., *Recruitment of the cell cycle checkpoint kinase ATR to chromatin during S-phase.* Journal of Biological Chemistry, 2004. **279**(16): p. 16433-16440.

20. Zou, L. and S.J. Elledge, *Sensing DNA damage through ATRIP recognition of RPA-ssDNA complexes.* Science, 2003. **300**(5625): p. 1542-1548.

21. Lupardus, P.J., et al., *A requirement for replication in activation of the ATR-dependent DNA damage checkpoint.* Genes & development, 2002. **16**(18): p. 2327-2332.

22. Lisby, M. and R. Rothstein, *Localization of checkpoint and repair proteins in eukaryotes.* Biochimie, 2005. **87**(7): p. 579-589.

23. Lukas, C., et al., *Mdc1 couples DNA double-strand break recognition by Nbs1 with its H2AX-dependent chromatin retention.* The EMBO journal, 2004. **23**(13): p. 2674-2683.

24. Haince, J.-F., et al., *PARP1-dependent kinetics of recruitment of MRE11 and NBS1 proteins to multiple DNA damage sites.* Journal of Biological Chemistry, 2008. **283**(2): p. 1197-1208.

25. Rogakou, E.P., et al., *DNA double-stranded breaks induce histone H2AX phosphorylation on serine 139.* Journal of biological chemistry, 1998. **273**(10): p. 5858-5868.

26. Iacovoni JS, C.P., Lassadi I, Nicolas E, Massip L, Trouche D, Legube G., *High-resolution profiling of gammaH2AX around DNA double strand breaks in the mammalian genome.* EMBO J., 2010. **29**(8): p. 1446-57.

27. Mah, L., A. El-Osta, and T. Karagiannis, *γH2AX: a sensitive molecular marker of DNA damage and repair.* Leukemia, 2010. **24**(4): p. 679-686.

28. Dickey, J.S., et al., *H2AX: functional roles and potential applications.* Chromosoma, 2009. **118**(6): p. 683-692.

29. Stucki, M., *Histone H2A. X Tyr142 phosphorylation: a novel sWItCH for apoptosis?* DNA repair, 2009. **8**(7): p. 873-876.

30. Harper, J.W. and S.J. Elledge, *The DNA damage response: ten years after.* Molecular cell, 2007. **28**(5): p. 739-745.

31. Luo, X. and W.L. Kraus, *On PAR with PARP: cellular stress signaling through poly (ADP-ribose) and PARP-1.* Genes & development, 2012. **26**(5): p. 417-432.

32. Doil, C., et al., *RNF168 binds and amplifies ubiquitin conjugates on damaged chromosomes to allow accumulation of repair proteins.* Cell, 2009. **136**(3): p. 435-446.

33. Huen, M.S., et al., *RNF8 transduces the DNA-damage signal via histone ubiquitylation and checkpoint protein assembly.* Cell, 2007. **131**(5): p. 901-914.

34. Kolas, N.K., et al., *Orchestration of the DNA-damage response by the RNF8 ubiquitin ligase.* Science, 2007. **318**(5856): p. 1637-1640.

35. Mailand, N., et al., *RNF8 ubiquitylates histones at DNA double-strand breaks and promotes assembly of repair proteins.* Cell, 2007. **131**(5): p. 887-900.

36. Stewart, G.S., et al., *The RIDDLE syndrome protein mediates a ubiquitin-dependent signaling cascade at sites of DNA damage.* Cell, 2009. **136**(3): p. 420-434.

37. Fradet-Turcotte, A., et al., *53BP1 is a reader of the DNA-damage-induced H2A Lys 15 ubiquitin mark.* Nature, 2013. **499**(7456): p. 50-54.

38. Watanabe, S., et al., *JMJD1C demethylates MDC1 to regulate the RNF8 and BRCA1–mediated chromatin response to DNA breaks.* Nature structural & molecular biology, 2013. **20**(12): p. 1425.

39. Chen, H., et al., *RNF8 promotes efficient DSB repair by inhibiting the pro-apoptotic activity of p53 through regulating the function of Tip60.* Cell proliferation, 2020. **53**(3): p. e12780-e12780.

40. Abraham, R.T., *PI 3-kinase related kinases:'big'players in stress-induced signaling pathways.* DNA repair, 2004. **3**(8-9): p. 883-887.

41. Bartek, J. and J. Lukas, *DNA damage checkpoints: from initiation to recovery or adaptation.* Current opinion in cell biology, 2007. **19**(2): p. 238-245.

42. Sulli, G., R. Di Micco, and F.d.A. di Fagagna, *Crosstalk between chromatin state and DNA damage response in cellular senescence and cancer.* Nature Reviews Cancer, 2012. **12**(10): p. 709-720.

43. Saldivar, J.C., et al., *An intrinsic S/G(2) checkpoint enforced by ATR.* Science (New York, N.Y.), 2018. **361**(6404): p. 806-810.

44. Choi, E.-H. and K.P. Kim, *E2F1 facilitates DNA break repair by localizing to break sites and enhancing the expression of homologous recombination factors.* Experimental & Molecular Medicine, 2019. **51**(9): p. 1-12.

45. Stevens, C., L. Smith, and N.B. La Thangue, *Chk2 activates E2F-1 in response to DNA damage.* Nat Cell Biol, 2003. **5**(5): p. 401-9.

46. Waterman, D.P., J.E. Haber, and M.B. Smolka, *Checkpoint Responses to DNA Double-Strand Breaks.* Annual Review of Biochemistry, 2020. **89**(1): p. 103-133.

47. Radhakrishnan, S.K., N. Jette, and S.P. Lees-Miller, *Non-homologous end joining: emerging themes and unanswered questions.* DNA repair, 2014. **17**: p. 2-8.

48. Al-Minawi, A.Z., N. Saleh-Gohari, and T. Helleday, *The ERCC1/XPF endonuclease is required for efficient single-strand annealing and gene conversion in mammalian cells.* Nucleic Acids Research, 2007. **36**(1): p. 1-9.

49. Zimmermann, M., et al., *53BP1 regulates DSB repair using Rif1 to control 5' end resection.* Science, 2013. **339**(6120): p. 700-704.

50. Ismail, I.H., et al., *The RNF138 E3 ligase displaces Ku to promote DNA end resection and regulate DNA repair pathway choice.* Nature cell biology, 2015. **17**(11): p. 1446-1457.

51. Lieber, M.R., *The mechanism of double-strand DNA break repair by the nonhomologous DNA end-joining pathway.* Annual review of biochemistry, 2010. **79**: p. 181-211.

52. Sugawara, N., G. Ira, and J.E. Haber, *DNA length dependence of the single-strand annealing pathway and the role of Saccharomyces cerevisiae RAD59 in double-strand break repair.* Molecular and cellular biology, 2000. **20**(14): p. 5300-5309.

53. Wang, M., *PARP-1 and Ku compete for repair of DNA double strand breaks by distinct NHEJ pathways.* Nucleic Acids Res., 2006. **34**(21): p. 6170–6182.

54. Ishida, N., et al., *Ubiquitylation of Ku80 by RNF126 promotes completion of nonhomologous end joining-mediated DNA repair.* Molecular and cellular biology, 2017. **37**(4): p. e00347-16.

55. Feng, L. and J. Chen, *The E3 ligase RNF8 regulates KU80 removal and NHEJ repair.* Nature structural & molecular biology, 2012. **19**(2): p. 201.

56. Marini, F., et al., *Regulation of DNA Double Strand Breaks Processing: Focus on Barriers.* Frontiers in Molecular Biosciences, 2019. **6**: p. 55.

57. Deshpande, R.A., et al., *DNA-dependent protein kinase promotes DNA end processing by MRN and CtIP.* Science advances, 2020. **6**(2): p. eaay0922.

58. Wang, J., et al., *PTIP associates with Artemis to dictate DNA repair pathway choice.* Genes & development, 2014. **28**(24): p. 2693-2698.

59. Grundy, G.J., et al., *APLF promotes the assembly and activity of non-homologous end joining protein complexes.* The EMBO journal, 2013. **32**(1): p. 112-125.

60. Hammel, M., et al., *An intrinsically disordered APLF links Ku, DNA-PKcs, and XRCC4-DNA ligase IV in an extended flexible non-homologous end joining complex.* Journal of Biological Chemistry, 2016. **291**(53): p. 26987-27006.

61. Rulten, S.L., *PARP-3 and APLF function together to accelerate nonhomologous end-joining.* Mol. Cell, 2011. **41**(1): p. 33-45.

62. Capp, J.-P., et al., *The DNA polymerase λ is required for the repair of non-compatible DNA double strand breaks by NHEJ in mammalian cells.* Nucleic acids research, 2006. **34**(10): p. 2998-3007.

63. Capp, J.-P., et al., *Involvement of DNA polymerase μ in the repair of a specific subset of DNA double-strand breaks in mammalian cells.* Nucleic acids research, 2007. **35**(11): p. 3551-3560.

64. Covo, S., L. Blanco, and Z. Livneh, *Lesion bypass by human DNA polymerase μ reveals a template-dependent, sequence-independent nucleotidyl transferase activity.* Journal of Biological Chemistry, 2004. **279**(2): p. 859-865.

65. Gu, J., et al., *Single-stranded DNA ligation and XLF-stimulated incompatible DNA end ligation by the XRCC4-DNA ligase IV complex: influence of terminal DNA sequence.* Nucleic acids research, 2007. **35**(17): p. 5755-5762.

66. Fell, V.L. and C. Schild-Poulter, *Ku regulates signaling to DNA damage response pathways through the Ku70 von Willebrand A domain.* Molecular and cellular biology, 2012. **32**(1): p. 76-87.

67. Taylor, R.M., C.J. Whitehouse, and K.W. Caldecott, *The DNA ligase III zinc finger stimulates binding to DNA secondary structure and promotes end joining.* Nucleic acids research, 2000. **28**(18): p. 3558-3563.

68. Villarreal, D.D., et al., *Microhomology directs diverse DNA break repair pathways and chromosomal translocations.* PLoS Genet, 2012. **8**(11): p. e1003026.

69. Ronato, D.A., et al., *Limiting the DNA Double-Strand Break Resectosome for Genome Protection.* Trends Biochem Sci, 2020. **45**(9): p. 779-793.

70. Shibata, A., et al., *DNA double-strand break repair pathway choice is directed by distinct MRE11 nuclease activities.* Molecular cell, 2014. **53**(1): p. 7-18.

71. Nimonkar, A.V., *BLM-DNA2-RPA-MRN and EXO1-BLM-RPA-MRN constitute two DNA end resection machineries for human DNA break repair.* Genes Dev., 2011. **25**(4): p. 350-362.

72. Anand, R., et al., *Phosphorylated CtIP Functions as a Co-factor of the MRE11-RAD50-NBS1 Endonuclease in DNA End Resection.* Molecular Cell, 2016. **64**(5): p. 940-950.

73. Yun, M.H. and K. Hiom, *CtIP-BRCA1 modulates the choice of DNA double-strand-break repair pathway throughout the cell cycle.* Nature, 2009. **459**: p. 460-463.

74. Nakamura, K., *Collaborative action of Brca1 and CtIP in elimination of covalent modifications from double-strand breaks to facilitate subsequent break repair.* PLoS Genet., 2010. **6**(1): p. e1000828.

75. Cruz-Garcia, A., A. Lopez-Saavedra, and P. Huertas, *BRCA1 accelerates CtIP-mediated DNA-end resection.* Cell Rep., 2014. **9**(2): p. 451-459.

76. Golub, E.I., et al., *Interaction of human rad51 recombination protein with single-stranded DNA binding protein, RPA.* Nucleic acids research, 1998. **26**(23): p. 5388-5393.

77. Stauffer, M.E. and W.J. Chazin, *Physical interaction between replication protein A and Rad51 promotes exchange on single-stranded DNA.* Journal of Biological Chemistry, 2004. **279**(24): p. 25638-25645.

78. Ma, C.J., et al., *Protein dynamics of human RPA and RAD51 on ssDNA during assembly and disassembly of the RAD51 filament.* Nucleic Acids Res, 2017. **45**(2): p. 749-761.

79. Zhao, W., et al., *BRCA1–BARD1 promotes RAD51-mediated homologous DNA pairing.* Nature, 2017. **550**(7676): p. 360-365.

80. Buisson, R., *Cooperation of breast cancer proteins PALB2 and piccolo BRCA2 in stimulating homologous recombination.* Nat. Struct. Mol. Biol., 2010. **17**(10): p. 1247-1254.

81. Roy, U. and E.C. Greene, *Demystifying the D-loop during DNA recombination.* Nature, 2020. **586**(7831): p. 677-678.

82. Sun, Y., et al., *Structural basis of homologous recombination.* Cellular and Molecular Life Sciences, 2020. **77**(1): p. 3-18.

83. Chambon, P., J.D. Weill, and P. Mandel, *Nicotinamide mononucleotide activation of new DNA-dependent polyadenylic acid synthesizing nuclear enzyme.* Biochem Biophys Res Commun, 1963. **11**: p. 39-43.

84. d'AMOURS, D., et al., *Poly (ADP-ribosyl) ation reactions in the regulation of nuclear functions.* Biochemical Journal, 1999. **342**(2): p. 249-268.

85. Kim, M.Y., T. Zhang, and W.L. Kraus, *Poly (ADP-ribosyl) ation by PARP-1:PAR-laying'NAD+ into a nuclear signal.* Genes & development, 2005. **19**(17): p. 1951-1967.

86. Hottiger, M.O., et al., *Toward a unified nomenclature for mammalian ADP-ribosyltransferases.* Trends in biochemical sciences, 2010. **35**(4): p. 208-219.

87. Langelier, M.-F., et al., *Structural basis for DNA damage–dependent poly (ADP-ribosyl) ation by human PARP-1.* Science, 2012. **336**(6082): p. 728-732.

88. Karras, G.I., et al., *The macro domain is an ADP-ribose binding module.* The EMBO journal, 2005. **24**(11): p. 1911-1920.

89. Amé, J.C., C. Spenlehauer, and G. de Murcia, *The PARP superfamily.* Bioessays, 2004. **26**(8): p. 882-893.

90. Vyas, S., et al., *Family-wide analysis of poly (ADP-ribose) polymerase activity.* Nature communications, 2014. **5**(1): p. 1-13.

91. Daugherty, M.D., et al., *Rapid Evolution of PARP Genes Suggests a Broad Role for ADP-Ribosylation in Host-Virus Conflicts.* PLOS Genetics, 2014. **10**(5): p. e1004403.

92. Langelier, M.F., et al., *Purification of human PARP-1 and PARP-1 domains from Escherichia coli for structural and biochemical analysis.* Methods Mol. Biol., 2011. **780**: p. 209-226.

93. Langelier, M.-F., et al., *Crystal structures of poly (ADP-ribose) polymerase-1 (PARP-1) zinc fingers bound to DNA structural and functional insights into DNA-dependent PARP-1 activity.* Journal of biological chemistry, 2011. **286**(12): p. 10690-10701.

94. Langelier, M.-F., et al., *NAD+ analog reveals PARP-1 substrate-blocking mechanism and allosteric communication from catalytic center to DNA-binding domains.* Nature communications, 2018. **9**: p. 844.

95. David, K.K., et al., *Parthanatos, a messenger of death.* Frontiers in bioscience (Landmark edition), 2009. **14**: p. 1116.

96. Gagné, J.-P., et al., *Quantitative site-specific ADP-ribosylation profiling of DNA-dependent PARPs.* DNA Repair, 2015. **30**: p. 68-79.

97. Ali, A.A., et al., *The zinc-finger domains of PARP1 cooperate to recognize DNA strand breaks.* Nature structural & molecular biology, 2012. **19**(7): p. 685.

98. Langelier, M.-F., et al., *A third zinc-binding domain of human poly (ADP-ribose) polymerase-1 coordinates DNA-dependent enzyme activation.* Journal of biological chemistry, 2008. **283**(7): p. 4105-4114.

99. Tao, Z., P. Gao, and H.-w. Liu, *Identification of the ADP-ribosylation sites in the PARP-1 automodification domain: analysis and implications.* Journal of the American Chemical Society, 2009. **131**(40): p. 14258-14260.

100. Langelier, M.-F. and J.M. Pascal, *PARP-1 mechanism for coupling DNA damage detection to poly (ADP-ribose) synthesis.* Current opinion in structural biology, 2013. **23**(1): p. 134-143.

101. Altmeyer, M., et al., *Molecular mechanism of poly (ADP-ribosyl) ation by PARP1 and identification of lysine residues as ADP-ribose acceptor sites.* Nucleic acids research, 2009. **37**(11): p. 3723-3738.

102. Rouleau, M., et al., *PARP inhibition: PARP1 and beyond.* Nature reviews cancer, 2010. **10**(4): p. 293-301.

103. Langelier, M.-F., A.A. Riccio, and J.M. Pascal, *PARP-2 and PARP-3 are selectively activated by 5' phosphorylated DNA breaks through an allosteric regulatory mechanism shared with PARP-1.* Nucleic acids research, 2014. **42**(12): p. 7762-7775.

104. Obaji, E., T. Haikarainen, and L. Lehtiö, *Characterization of the DNA dependent activation of human ARTD2/PARP2.* Scientific reports, 2016. **6**: p. 34487.

105. Obaji, E., T. Haikarainen, and L. Lehtiö, *Structural basis for DNA break recognition by ARTD2/PARP2.* Nucleic acids research, 2018. **46**(22): p. 12154-12165.

106. Riccio, A.A., G. Cingolani, and J.M. Pascal, *PARP-2 domain requirements for DNA damage-dependent activation and localization to sites of DNA damage.* Nucleic acids research, 2016. **44**(4): p. 1691-1702.

107. Huber, A., et al., *PARP-1, PARP-2 and ATM in the DNA damage response: functional synergy in mouse development.* DNA repair, 2004. **3**(8-9): p. 1103-1108.

108. Yélamos, J., V. Schreiber, and F. Dantzer, *Toward specific functions of poly (ADP-ribose) polymerase-2.* Trends in molecular medicine, 2008. **14**(4): p. 169-178.

109. Meder, V.S., et al., *PARP-1 and PARP-2 interact with nucleophosmin/B23 and accumulate in transcriptionally active nucleoli.* Journal of cell science, 2005. **118**(1): p. 211-222.

110. Léger, K., et al., *ARTD2 activity is stimulated by RNA.* Nucleic Acids Research, 2014. **42**(8): p. 5072-5082.

111. Kutuzov, M.M., et al., *Interaction of PARP-2 with AP site containing DNA.* Biochimie, 2015. **112**: p. 10-19.

112. Mortusewicz, O., et al., *Feedback-regulated poly (ADP-ribosyl) ation by PARP-1 is required for rapid response to DNA damage in living cells.* Nucleic acids research, 2007. **35**(22): p. 7665-7675.

113. Sukhanova, M.V., et al., *Single molecule detection of PARP1 and PARP2 interaction with DNA strand breaks and their poly (ADP-ribosyl) ation using high-resolution AFM imaging.* Nucleic acids research, 2016. **44**(6): p. e60.

114. De Murcia, J.M., et al., *Requirement of poly (ADP-ribose) polymerase in recovery from DNA damage in mice and in cells.* Proceedings of the National Academy of Sciences, 1997. **94**(14): p. 7303-7307.

115. Forsyth, N.R., W.E. Wright, and J.W. Shay, *Telomerase and differentiation in multicellular organisms: turn it off, turn it on, and turn it off again.* Differentiation: REVIEW ARTICLE, 2002. **69**(4-5): p. 188-197.

116. Masutani, M., et al., *The response of Parp knockout mice against DNA damaging agents.* Mutation Research/Reviews in Mutation Research, 2000. **462**(2-3): p. 159-166.

117. Wang, Z.-Q., et al., *PARP is important for genomic stability but dispensable in apoptosis.* Genes & development, 1997. **11**(18): p. 2347-2358.

118. de Murcia, J.M., et al., *Functional interaction between PARP-1 and PARP-2 in chromosome stability and embryonic development in mouse.* The EMBO journal, 2003. **22**(9): p. 2255-2263.

119. Farrés, J., et al., *Parp-2 is required to maintain hematopoiesis following sublethal γ-irradiation in mice.* Blood, The Journal of the American Society of Hematology, 2013. **122**(1): p. 44-54.

120. Schreiber, V., et al., *Poly (ADP-ribose) polymerase-2 (PARP-2) is required for efficient base excision DNA repair in association with PARP-1 and XRCC1*. Journal of Biological Chemistry, 2002. **277**(25): p. 23028-23036.

121. Fisher, A.E., et al., *Poly (ADP-ribose) polymerase 1 accelerates single-strand break repair in concert with poly (ADP-ribose) glycohydrolase.* Molecular and cellular biology, 2007. **27**(15): p. 5597-5605.

122. Fouquin, A., et al., *PARP2 controls double-strand break repair pathway choice by limiting 53BP1 accumulation at DNA damage sites and promoting end-resection.* Nucleic acids research, 2017. **45**(21): p. 12325-12339.

123. Althaus, F.R. and C. Richter, *Poly (ADP-ribose) biosynthesis*, in *ADP-ribosylation of Proteins*. 1987, Springer. p. 12-37.

124. Hassa, P.O., et al., *Nuclear ADP-ribosylation reactions in mammalian cells: where are we today and where are we going?* Microbiol. Mol. Biol. Rev., 2006. **70**(3): p. 789-829.

125. Kiehlbauch, C.C., et al., *High resolution fractionation and characterization of ADP-ribose polymers.* Analytical biochemistry, 1993. **208**(1): p. 26-34.

126. Liu, C., et al., *The role of poly ADP-ribosylation in the first wave of DNA damage response.* Nucleic Acids Res, 2017. **45**(14): p. 8129-8141.

127. Krishnakumar, R. and W.L. Kraus, *PARP-1 regulates chromatin structure and transcription through a KDM5B-dependent pathway.* Molecular cell, 2010. **39**(5): p. 736-749.

128. Gibbs-Seymour, I., et al., *HPF1/C4orf27 is a PARP-1-interacting protein that regulates PARP-1 ADP-ribosylation activity.* Molecular cell, 2016. **62**(3): p. 432-442.

129. Poirier, G.G., et al., *Poly (ADP-ribosyl) ation of polynucleosomes causes relaxation of chromatin structure.* Proceedings of the National Academy of Sciences, 1982. **79**(11): p. 3423-3427.

130. Timinszky, G., et al., *A macrodomain-containing histone rearranges chromatin upon sensing PARP1 activation.* Nature structural & molecular biology, 2009. **16**(9): p. 923.

131. Krishnakumar, R. and W.L. Kraus, *The PARP side of the nucleus: molecular actions, physiological outcomes, and clinical targets.* Molecular cell, 2010. **39**(1): p. 8-24.

132. Nguyen, D.-D., et al., *Roles of OB-Fold Proteins in Replication Stress.* Frontiers in Cell and Developmental Biology, 2020. **8**: p. 954.

133. Arcus, V.L., P.B. Rainey, and S.J. Turner, *The PIN-domain toxin-antitoxin array in mycobacteria.* Trends Microbiol, 2005. **13**(8): p. 360-5.

134. Min, W., et al., *Poly (ADP-ribose) binding to Chk1 at stalled replication forks is required for S-phase checkpoint activation.* Nature communications, 2013. **4**(1): p. 1-14.

135. Altmeyer, M., *Liquid demixing of intrinsically disordered proteins is seeded by poly(ADP-ribose).* Nat. Commun., 2015. **6**: p. 8088.

136. Garber, K., *PARP inhibitors bounce back.* 2013, Nature Publishing Group. p. 725-727.

137. Bryant, H.E., et al., *Specific killing of BRCA2-deficient tumours with inhibitors of poly (ADP-ribose) polymerase.* Nature, 2005. **434**(7035): p. 913-917.

138. Farmer, H., et al., *Targeting the DNA repair defect in BRCA mutant cells as a therapeutic strategy.* Nature, 2005. **434**(7035): p. 917-921.

139. Ferraris, D.V., *Evolution of poly (ADP-ribose) polymerase-1 (PARP-1) inhibitors. From concept to clinic.* Journal of medicinal chemistry, 2010. **53**(12): p. 4561-4584.

140. Murai, J., et al., *Trapping of PARP1 and PARP2 by clinical PARP inhibitors.* Cancer research, 2012. **72**(21): p. 5588-5599.

141. Shao, Z., et al., *Clinical PARP inhibitors do not abrogate PARP1 exchange at DNA damage sites in vivo.* Nucleic acids research, 2020. **48**(17): p. 9694-9709.

142. Zandarashvili, L., et al., *Structural basis for allosteric PARP-1 retention on DNA breaks.* Science (New York, N.Y.), 2020. **368**(6486): p. eaax6367.

143. Salmas, R.E., et al., *In silico investigation of PARP-1 catalytic domains in holo and apo states for the design of high-affinity PARP-1 inhibitors.* Journal of enzyme inhibition and medicinal chemistry, 2016. **31**(1): p. 112-120.

144. Li, J., et al., *In silico screening identifies a novel potential PARP1 inhibitor targeting synthetic lethality in cancer treatment.* International journal of molecular sciences, 2016. **17**(2): p. 258.

145. Hopkins, T.A., et al., *PARP1 trapping by PARP inhibitors drives cytotoxicity in both cancer cells and healthy bone marrow.* Molecular Cancer Research, 2019. **17**(2): p. 409-419.

146. Slade, D., et al., *The structure and catalytic mechanism of a poly (ADP-ribose) glycohydrolase.* Nature, 2011. **477**(7366): p. 616-620.

147. Thomas, H.D., et al., *Preclinical selection of a novel poly (ADP-ribose) polymerase inhibitor for clinical trial.* Molecular cancer therapeutics, 2007. **6**(3): p. 945-956.

148. Wahlberg, E., et al., *Family-wide chemical profiling and structural analysis of PARP and tankyrase inhibitors.* Nature biotechnology, 2012. **30**(3): p. 283-288.

149. Knezevic, C.E., et al., *Proteome-wide profiling of clinical PARP inhibitors reveals compound-specific secondary targets.* Cell chemical biology, 2016. **23**(12): p. 1490-1503.

150. Chan, C.Y., K.V. Tan, and B. Cornelissen, *PARP Inhibitors in Cancer Diagnosis and Therapy.* Clinical Cancer Research, 2020. **27**(6): p. 1585-1594.

151. Pathikonda, S., S.H. Cheng, and K.N. Yu, *Role of PARP1 regulation in radiation-induced rescue effect.* Journal of radiation research, 2020. **61**(3): p. 352-367.

152. Mansoori, B., et al., *The different mechanisms of cancer drug resistance: a brief review.* Advanced pharmaceutical bulletin, 2017. **7**(3): p. 339.

153. D'Andrea, A.D., *Mechanisms of PARP inhibitor sensitivity and resistance.* DNA repair, 2018. **71**: p. 172-176.

154. Hee Choi, Y. and A.-M. Yu, *ABC transporters in multidrug resistance and pharmacokinetics, and strategies for drug development.* Current pharmaceutical design, 2014. **20**(5): p. 793-807.

155. Barber, L.J., et al., *Secondary mutations in BRCA2 associated with clinical resistance to a PARP inhibitor.* The Journal of pathology, 2013. **229**(3): p. 422-429.

156. Norquist, B., et al., *Secondary somatic mutations restoring BRCA1/2 predict chemotherapy resistance in hereditary ovarian carcinomas.* Journal of clinical oncology, 2011. **29**(22): p. 3008.

157. Goodall, J., et al., *Circulating cell-free DNA to guide prostate cancer treatment with PARP inhibition.* Cancer discovery, 2017. **7**(9): p. 1006-1017.

158. Christie, E.L., et al., *Reversion of BRCA1/2 germline mutations detected in circulating tumor DNA from patients with high-grade serous ovarian cancer.* Journal of Clinical Oncology, 2017. **35**(12): p. 1274-1280.

159. Kondrashova, O., et al., *Secondary somatic mutations restoring RAD51C and RAD51D associated with acquired resistance to the PARP inhibitor rucaparib in high-grade ovarian carcinoma.* Cancer discovery, 2017. **7**(9): p. 984-998.

160. Pishvaian, M.J., et al., *BRCA2 secondary mutation-mediated resistance to platinum and PARP inhibitor-based therapy in pancreatic cancer.* British journal of cancer, 2017. **116**(8): p. 1021-1026.

161. Quigley, D., et al., *Analysis of circulating cell-free DNA identifies multiclonal heterogeneity of BRCA2 reversion mutations associated with resistance to PARP inhibitors.* Cancer discovery, 2017. **7**(9): p. 999-1005.

162. Lin, K.K., et al., *BRCA reversion mutations in circulating tumor DNA predict primary and acquired resistance to the PARP inhibitor rucaparib in high-grade ovarian carcinoma.* Cancer discovery, 2019. **9**(2): p. 210-219.

163. Weigelt, B., et al., *Diverse BRCA1 and BRCA2 reversion mutations in circulating cell-free DNA of therapy-resistant breast or ovarian cancer.* Clinical Cancer Research, 2017. **23**(21): p. 6708-6720.

164. Patch, A.-M., et al., *Whole–genome characterization of chemoresistant ovarian cancer*. Nature, 2015. **521**(7553): p. 489-494.

165. Drost, R., et al., *BRCA1 185delAG tumors may acquire therapy resistance through expression of RING-less BRCA1.* The Journal of clinical investigation, 2016. **126**(8): p. 2903-2918.

166. Bunting, S.F., et al., *53BP1 inhibits homologous recombination in Brca1-deficient cells by blocking resection of DNA breaks.* Cell, 2010. **141**(2): p. 243-254.

167. Callen, E., et al., *53BP1 mediates productive and mutagenic DNA repair through distinct phosphoprotein interactions.* Cell, 2013. **153**(6): p. 1266-1280.

168. Chapman, J.R., et al., *RIF1 is essential for 53BP1-dependent nonhomologous end joining and suppression of DNA double-strand break resection.* Molecular cell, 2013. **49**(5): p. 858-871.

169. Xu, G., et al., *REV7 counteracts DNA double-strand break resection and affects PARP inhibition.* Nature, 2015. **521**(7553): p. 541-544.

170. Barazas, M., et al., *The CST complex mediates end protection at double-strand breaks and promotes PARP inhibitor sensitivity in BRCA1-deficient cells.* Cell reports, 2018. **23**(7): p. 2107-2118.

171. Jaspers, J.E., et al., *Loss of 53BP1 causes PARP inhibitor resistance in Brca1-mutated mouse mammary tumors.* Cancer discovery, 2013. **3**(1): p. 68-81.

172. Gupta, R., et al., *DNA repair network analysis reveals shieldin as a key regulator of NHEJ and PARP inhibitor sensitivity.* Cell, 2018. **173**(4): p. 972-988. e23.

173. Ghezraoui, H., et al., *53BP1 cooperation with the REV7–shieldin complex underpins DNA structure-specific NHEJ.* Nature, 2018. **560**(7716): p. 122-127.

174. Noordermeer, S.M., et al., *The shieldin complex mediates 53BP1-dependent DNA repair.* Nature, 2018. **560**(7716): p. 117-121.

175. Escribano-Diaz, C. and D. Durocher, *DNA repair pathway choice—a PTIP of the hat to 53BP1.* EMBO reports, 2013. **14**(8): p. 665-666.

176. Tkáč, J., et al., *HELB is a feedback inhibitor of DNA end resection.* Molecular cell, 2016. **61**(3): p. 405-418.

177. He, Y.J., et al., *DYNLL1 binds to MRE11 to limit DNA end resection in BRCA1-deficient cells.* Nature, 2018. **563**(7732): p. 522-526.

178. Dev, H., et al., *Shieldin complex promotes DNA end-joining and counters homologous recombination in BRCA1-null cells.* Nature cell biology, 2018. **20**(8): p. 954-965.

179. Bouwman, P., et al., *53BP1 loss rescues BRCA1 deficiency and is associated with triple-negative and BRCA-mutated breast cancers.* Nature structural & molecular biology, 2010. **17**(6): p. 688.

180. Hengel, S.M., et al., *Tandem mass spectrometry investigation of ADP-ribosylated kemptide.* Journal of the American Society for Mass Spectrometry, 2009. **20**(3): p. 477-483.

181. Rosenthal, F., et al., *Optimization of LTQ-Orbitrap mass spectrometer parameters for the identification of ADP-ribosylation sites.* Journal of proteome research, 2015. **14**(9): p. 4072-4079.

182. Daniels, C.M., S.-E. Ong, and A.K. Leung, *Phosphoproteomic approach to characterize protein mono-and poly (ADP-ribosyl) ation sites from cells.* Journal of proteome research, 2014. **13**(8): p. 3510-3522.

183. Chapman, J.D., et al., *Mapping PARP-1 auto-ADP-ribosylation sites by liquid chromatography–tandem mass spectrometry.* Journal of proteome research, 2013. **12**(4): p. 1868-1880.

184. Gibson, B.A., et al., *Chemical genetic discovery of PARP targets reveals a role for PARP-1 in transcription elongation.* Science, 2016. **353**(6294): p. 45-50.

185. Zhen, Y., Y. Zhang, and Y. Yu, *A cell-line-specific atlas of PARP-mediated protein Asp/Glu-ADP-ribosylation in breast cancer.* Cell reports, 2017. **21**(8): p. 2326-2337.

186. Zhang, Y., et al., *Site-specific characterization of the Asp-and Glu-ADP-ribosylated proteome.* Nature methods, 2013. **10**(10): p. 981.

187. Gagné, J.-P., et al., *Hydrofluoric Acid-Based Derivatization Strategy To Profile PARP-1 ADP-Ribosylation by LC–MS/MS.* Journal of proteome research, 2018. **17**(7): p. 2542-2551.

188. Gagné, J.-P., et al., *Proteome-wide identification of poly(ADP-ribose) binding proteins and poly(ADP-ribose)-associated protein complexes.* Nucleic Acids Research, 2008. **36**(22): p. 6959-6976.

189. Krietsch, J., *PARP activation regulates the RNA-binding protein NONO in the DNA damage response to DNA double-strand breaks.* Nucleic Acids Res., 2012. **40**(20): p. 10287-10301.

190. Gagne, J.P., *Quantitative proteomics profiling of the poly(ADP-ribose)-related response to genotoxic stress.* Nucleic Acids Res., 2012. **40**(16): p. 7788-7805.

191. Dzieciatkowska, M., R. Hill, and K.C. Hansen, *GeLC-MS/MS analysis of complex protein mixtures.* Methods Mol Biol, 2014. **1156**: p. 53-66.

192. Wiese, S., et al., *Protein labeling by iTRAQ: a new tool for quantitative mass spectrometry in proteome research.* Proteomics, 2007. **7**(3): p. 340-50.

193. Ong, S.-E. and M. Mann, *A practical recipe for stable isotope labeling by amino acids in cell culture (SILAC).* Nature Protocols, 2006. **1**(6): p. 2650-2660.

194. Vivelo, C.A., et al., *ADPriboDB: The database of ADP-ribosylated proteins.* Nucleic Acids Research, 2016. **45**(D1): p. D204-D209.

195. Ayyappan, V., et al., *ADPriboDB 2.0: an updated database of ADP-ribosylated proteins.* Nucleic Acids Research, 2020. **49**(D1): p. D261-D265.

196. Klug, A., *The discovery of zinc fingers and their development for practical applications in gene regulation and genome manipulation.* Q Rev Biophys, 2010. **43**(1): p. 1-21.

197. Hudson, N.O. and B.A. Buck-Koehntop, *Zinc Finger Readers of Methylated DNA.* Molecules, 2018. **23**(10): p. 2555.

198. Laity, J.H., B.M. Lee, and P.E. Wright, *Zinc finger proteins: new insights into structural and functional diversity.* Current opinion in structural biology, 2001. **11**(1): p. 39-46.

199. Brown, R.S., *Zinc finger proteins: getting a grip on RNA.* Current opinion in structural biology, 2005. **15**(1): p. 94-98.

200. Brayer, K.J., S. Kulshreshtha, and D.J. Segal, *The protein-binding potential of C2H2 zinc finger domains.* Cell biochemistry and biophysics, 2008. **51**(1): p. 9-19.

201. Font, J. and J.P. Mackay, *Beyond DNA: zinc finger domains as RNA-binding modules*, in *Engineered Zinc Finger Proteins*. 2010, Springer. p. 479-491.

202. Matthews, J.M. and M. Sunde, *Zinc fingers--folds for many occasions.* IUBMB life, 2002. **54**(6): p. 351-355.

203. McCarty, A.S., et al., *Selective dimerization of a C2H2 zinc finger subfamily.* Molecular cell, 2003. **11**(2): p. 459-470.

204. Krishna, S.S., I. Majumdar, and N.V. Grishin, *Structural classification of zinc fingers: survey and summary.* Nucleic acids research, 2003. **31**(2): p. 532-550.

205. Ahel, I., et al., *Poly(ADP-ribose)-binding zinc finger motifs in DNA repair/checkpoint proteins.* Nature, 2008. **451**(7174): p. 81-85.

206. Macrae, C.J., et al., *APLF (C2orf13) facilitates nonhomologous end-joining and undergoes ATM-dependent hyperphosphorylation following ionizing radiation.* DNA repair, 2008. **7**(2): p. 292-302.

207. Yang, C., et al., *A20/TNFAIP3 regulates the DNA damage response and mediates tumor cell resistance to DNA-damaging therapy.* Cancer research, 2018. **78**(4): p. 1069-1082.

208. Juhász, S., et al., *ATRX promotes DNA repair synthesis and sister chromatid exchange during homologous recombination.* Molecular cell, 2018. **71**(1): p. 11-24. e7.

209. Clynes, D., D.R. Higgs, and R.J. Gibbons, *The chromatin remodeller ATRX: a repeat offender in human disease.* Trends in biochemical sciences, 2013. **38**(9): p. 461-466.

210. Vancurova, M., et al., *PML nuclear bodies are recruited to persistent DNA damage lesions in an RNF168-53BP1 dependent manner and contribute to DNA repair.* DNA repair, 2019. **78**: p. 114-127.

211. Ziv, Y., et al., *Chromatin relaxation in response to DNA double-strand breaks is modulated by a novel ATM-and KAP-1 dependent pathway.* Nature cell biology, 2006. **8**(8): p. 870-876.

212. Chang, H.R., et al., *The functional roles of PML nuclear bodies in genome maintenance*. Mutation Research/Fundamental and Molecular Mechanisms of Mutagenesis, 2018. **809**: p. 99-107.

213. Wu, S., et al., *A YY1–INO80 complex regulates genomic stability through homologous recombination–based repair.* Nature structural & molecular biology, 2007. **14**(12): p. 1165-1172.

214. Peng, M., et al., *BACH1 is a DNA repair protein supporting BRCA1 damage response.* Oncogene, 2006. **25**(15): p. 2245-2253.

215. Liu, X.-S., et al., *LRF maintains genome integrity by regulating the non-homologous end joining pathway of DNA repair.* Nature communications, 2015. **6**(1): p. 1-10.

216. Cantor, S.B., et al., *BACH1, a novel helicase-like protein, interacts directly with BRCA1 and contributes to its DNA repair function.* Cell, 2001. **105**(1): p. 149-160.

217. Li, J.S.Z., et al., *TZAP: A telomere-associated protein involved in telomere length control.* Science, 2017. **355**(6325): p. 638-641.

218. Izhar, L., et al., *A systematic analysis of factors localized to damaged chromatin reveals PARP-dependent recruitment of transcription factors.* Cell reports, 2015. **11**(9): p. 1486-1500.

219. Helfricht, A., et al., *Loss of ZBTB24 impairs nonhomologous end-joining and class-switch recombination in patients with ICF syndrome.* Journal of Experimental Medicine, 2020. **217**(11): p. e20191688.

220. Nicolai, S., et al., *ZNF281 is recruited on DNA breaks to facilitate DNA repair by non-homologous end joining.* Oncogene, 2020. **39**(4): p. 754-766.

221. Gong, Y., et al., *PHF11 promotes DSB resection, ATR signaling, and HR.* Genes & development, 2017. **31**(1): p. 46-58.

222. Nakajima, S., et al., *Ubiquitin-specific protease 5 is required for the efficient repair of DNA double-strand breaks.* PloS one, 2014. **9**(1): p. e84899.

223. Chen, G., et al., *ZNF830 mediates cancer chemoresistance through promoting homologous-recombination repair.* Nucleic acids research, 2018. **46**(3): p. 1266-1279.

224. Pommier, Y., et al., *Roles of eukaryotic topoisomerases in transcription, replication and genomic stability.* Nature reviews Molecular cell biology, 2016. **17**(11): p. 703.

225. Khoury-Haddad, H., et al., *PARP1-dependent recruitment of KDM4D histone demethylase to DNA damage sites promotes double-strand break repair.* Proceedings of the National Academy of Sciences, 2014. **111**(7): p. E728-E737.

226. Cao, L., et al., *ATM-mediated KDM2A phosphorylation is required for the DNA damage repair.* Oncogene, 2016. **35**(3): p. 301-313.

227. Gong, F., et al., *Histone demethylase KDM5A regulates the ZMYND8–NuRD chromatin remodeler to promote DNA repair.* Journal of Cell Biology, 2017. **216**(7): p. 1959-1974.

228. Bueno, M.T., et al., *Recruitment of lysine demethylase 2A to DNA double strand breaks and its interaction with 53BP1 ensures genome stability.* Oncotarget, 2018. **9**(22): p. 15915.

229. Leng, R.P., et al., *Pirh2, a p53-induced ubiquitin-protein ligase, promotes p53 degradation.* Cell, 2003. **112**(6): p. 779-791.

230. Xie, H.-Y., et al., *Dimerization of MORC2 through its C-terminal coiled-coil domain enhances chromatin dynamics and promotes DNA repair.* Cell Communication and Signaling, 2019. **17**(1): p. 1-11.

231. Pospiech, H., A.K. Rytkönen, and J.E. Syväoja, *The role of DNA polymerase activity in human non-homologous end joining.* Nucleic acids research, 2001. **29**(15): p. 3277-3288.

232. Nowsheen, S., et al., *L3MBTL2 orchestrates ubiquitin signalling by dictating the sequential recruitment of RNF8 and RNF168 after DNA damage.* Nature cell biology, 2018. **20**(4): p. 455-464.

233. Słabicki, M., et al., *A genome-scale DNA repair RNAi screen identifies SPG48 as a novel gene associated with hereditary spastic paraplegia.* PLoS Biol, 2010. **8**(6): p. e1000408.

234. Lovejoy, C.A., et al., *Functional genomic screens identify CINP as a genome maintenance protein.* Proceedings of the National Academy of Sciences, 2009. **106**(46): p. 19304-19309.

235. Latonen, L., et al., *Ultraviolet B radiation regulates cysteine-rich protein 1 in human keratinocytes.* Photodermatology, photoimmunology & photomedicine, 2010. **26**(2): p. 70-77.

236. Galanty, Y., et al., *Mammalian SUMO E3-ligases PIAS1 and PIAS4 promote responses to DNA double-strand breaks.* Nature, 2009. **462**(7275): p. 935-939.

237. Potts, P.R. and H. Yu, *Human MMS21/NSE2 is a SUMO ligase required for DNA repair.* Molecular and cellular biology, 2005. **25**(16): p. 7021-7032.

238. Leung, J.W., et al., *ZMYM3 regulates BRCA1 localization at damaged chromatin to promote DNA repair.* Genes & development, 2017. **31**(3): p. 260-274.

239. Gong, F., et al., *Screen identifies bromodomain protein ZMYND8 in chromatin recognition of transcription-associated DNA damage that promotes homologous recombination.* Genes & development, 2015. **29**(2): p. 197-211.

240. Chen, Y.-J., et al., *SMYD3 promotes homologous recombination via regulation of H3K4-mediated gene expression.* Scientific reports, 2017. **7**(1): p. 1-12.

241. Ray Chaudhuri, A. and A. Nussenzweig, *The multifaceted roles of PARP1 in DNA repair and chromatin remodelling.* Nat. Rev. Mol. Cell Biol., 2017. **18**: p. 610–621.

242. Liu, C., et al., *CHFR is important for the first wave of ubiquitination at DNA damage sites.* Nucleic acids research, 2013. **41**(3): p. 1698-1710.

243. Warmerdam, D.O., et al., *PHF6 promotes non-homologous end joining and G2 checkpoint recovery.* EMBO reports, 2020. **21**(1): p. e48460.

244. Liu, Z., et al., *Structural and functional insights into the human Börjeson-Forssman-Lehmann syndrome-associated protein PHF6.* Journal of Biological Chemistry, 2014. **289**(14): p. 10069-10083.

245. Lan, L., et al., *The ACF1 complex is required for DNA double-strand break repair in human cells.* Molecular cell, 2010. **40**(6): p. 976-987.

246. Huang, J., et al., *RAD18 transmits DNA damage signalling to elicit homologous recombination repair.* Nature cell biology, 2009. **11**(5): p. 592-603.

247. Ogi, T., et al., *Three DNA polymerases, recruited by different mechanisms, carry out NER repair synthesis in human cells.* Molecular cell, 2010. **37**(5): p. 714-727.

248. Ting, L., H. Jun, and C. Junjie, *RAD18 lives a double life: Its implication in DNA double-strand break repair.* DNA repair, 2010. **9**(12): p. 1241-1248.

249. Centore, R.C., et al., *Spartan/C1orf124, a reader of PCNA ubiquitylation and a regulator of UV-induced DNA damage response.* Molecular cell, 2012. **46**(5): p. 625-635.

250. Ali, M.A., et al., *RYBP is a K63-ubiquitin-chain-binding protein that inhibits homologous recombination repair.* Cell reports, 2018. **22**(2): p. 383-395.

251. Semlow, D.R., et al., *Replication-dependent unhooking of DNA interstrand cross-links by the NEIL3 glycosylase.* Cell, 2016. **167**(2): p. 498-511. e14.

252. Ciccia, A., et al., *Polyubiquitinated PCNA recruits the ZRANB3 translocase to maintain genomic integrity after replication stress.* Molecular cell, 2012. **47**(3): p. 396-409.

253. Densham, R.M., et al., *Human BRCA1–BARD1 ubiquitin ligase activity counteracts chromatin barriers to DNA resection.* Nature structural & molecular biology, 2016. **23**(7): p. 647-655.

254. Rona, G., et al., *PARP1-dependent recruitment of the FBXL10-RNF68-RNF2 ubiquitin ligase to sites of DNA damage controls H2A. Z loading.* Elife, 2018. **7**: p. e38771.

255. Lazzerini-Denchi, E. and A. Sfeir, *Stop pulling my strings—what telomeres taught us about the DNA damage response.* Nature reviews Molecular cell biology, 2016. **17**(6): p. 364.

256. Jackson, S.P. and D. Durocher, *Regulation of DNA damage responses by ubiquitin and SUMO.* Molecular cell, 2013. **49**(5): p. 795-807.

257. Huen, M.S., S.M. Sy, and J. Chen, *BRCA1 and its toolbox for the maintenance of genome integrity.* Nature reviews Molecular cell biology, 2010. **11**(2): p. 138-148.

258. Martín, V., et al., *Sws1 is a conserved regulator of homologous recombination in eukaryotic cells.* The EMBO journal, 2006. **25**(11): p. 2564-2574.

259. Liu, T., et al., *hSWS1· SWSAP1 is an evolutionarily conserved complex required for efficient homologous recombination repair.* Journal of Biological Chemistry, 2011. **286**(48): p. 41758-41766.

260. Ogiwara, H., et al., *Histone acetylation by CBP and p300 at double-strand break sites facilitates SWI/SNF chromatin remodeling and the recruitment of non-homologous end joining factors.* Oncogene, 2011. **30**(18): p. 2135-2146.

261. Rezaeian, A.-H., et al., *A hypoxia-responsive TRAF6–ATM–H2AX signalling axis promotes HIF1α activation, tumorigenesis and metastasis.* Nature cell biology, 2017. **19**(1): p. 38-51.

262. Mosbech, A., et al., *The deubiquitylating enzyme USP44 counteracts the DNA double-strand break response mediated by the RNF8 and RNF168 ubiquitin ligases.* Journal of Biological Chemistry, 2013. **288**(23): p. 16579-16587.

263. Shanbhag, N.M., et al., *ATM-dependent chromatin changes silence transcription in cis to DNA double-strand breaks.* Cell, 2010. **141**(6): p. 970-981.

264. Wang, Z., et al., *USP51 deubiquitylates H2AK13, 15ub and regulates DNA damage response.* Genes & development, 2016. **30**(8): p. 946-959.

265. Nicassio, F., et al., *Human USP3 is a chromatin modifier required for S phase progression and genome stability.* Current biology, 2007. **17**(22): p. 1972-1977.

266. Hu, R., et al., *Zinc finger protein 668 interacts with Tip60 to promote H2AX acetylation after DNA damage.* Cell Cycle, 2013. **12**(13): p. 2033-2041.

267. Danielsen, J.R., et al., *DNA damage–inducible SUMOylation of HERC2 promotes RNF8 binding via a novel SUMO-binding Zinc finger.* Journal of Cell Biology, 2012. **197**(2): p. 179-187.

268. Vilas, C.K., et al., *Caught with one's zinc fingers in the genome integrity cookie jar.* Trends in Genetics, 2018. **34**(4): p. 313-325.

269. Singh, J.K. and H. van Attikum, *DNA double-strand break repair: Putting zinc fingers on the sore spot*, in *Seminars in Cell & Developmental Biology*. 2020, Elsevier. p. 65-74.

270. Klug, A. and J. Schwabe, *Protein motifs 5. Zinc fingers.* The FASEB journal, 1995. **9**(8): p. 597-604.

271. Mackeh, R., et al., *C2H2-type zinc finger proteins: evolutionarily old and new partners of the nuclear hormone receptors.* Nuclear receptor signaling, 2018. **15**: p. 1550762918801071.

272. Gamsjaeger, R., et al., *Sticky fingers: zinc-fingers as protein-recognition motifs.* Trends in biochemical sciences, 2007. **32**(2): p. 63-70.

273. Collins, T., J.R. Stone, and A.J. Williams, *All in the family: the BTB/POZ, KRAB, and SCAN domains.* Mol Cell Biol, 2001. **21**(11): p. 3609-15.

274. Urrutia, R., *KRAB-containing zinc-finger repressor proteins.* Genome Biology, 2003. **4**(10): p. 231.

275. Emerson, R.O. and J.H. Thomas, *Adaptive Evolution in Zinc Finger Transcription Factors.* PLOS Genetics, 2009. **5**(1): p. e1000325.

276. Lehmann, W., et al., *ZEB1 turns into a transcriptional activator by interacting with YAP1 in aggressive cancer types.* Nat Commun, 2016. **7**: p. 10498.

277. Hwang, S.Y., et al., *CTCF cooperates with CtIP to drive homologous recombination repair of double-strand breaks.* Nucleic acids research, 2019. **47**(17): p. 9160-9179.

278. Hilmi, K., et al., *CTCF facilitates DNA double-strand break repair by enhancing homologous recombination repair.* Science advances, 2017. **3**(5): p. e1601898.

279. Lang, F., et al., *CTCF prevents genomic instability by promoting homologous recombination-directed DNA double-strand break repair.* Proceedings of the National Academy of Sciences, 2017. **114**(41): p. 10912-10917.

280. Gupte, R., Z. Liu, and W.L. Kraus, *PARPs and ADP-ribosylation: recent advances linking molecular functions to biological outcomes.* Genes & development, 2017. **31**(2): p. 101-126.

281. Palazzo, L., A. Mikoč, and I. Ahel, *ADP-ribosylation: new facets of an ancient modification.* The FEBS journal, 2017. **284**(18): p. 2932-2946.

282. Perina, D., et al., *Distribution of protein poly (ADP-ribosyl) ation systems across all domains of life.* DNA repair, 2014. **23**: p. 4-16.

283. Teloni, F. and M. Altmeyer, *Readers of poly (ADP-ribose): designed to be fit for purpose.* Nucleic acids research, 2015. **44**(3): p. 993-1006.

284. Deng, Q. and J.T. Barbieri, *Molecular mechanisms of the cytotoxicity of ADP-ribosylating toxins.* Annu. Rev. Microbiol., 2008. **62**: p. 271-288.

285. Cohen, M.S. and P. Chang, *Insights into the biogenesis, function, and regulation of ADP-ribosylation.* Nature chemical biology, 2018. **14**(3): p. 236.

286. Hatakeyama, K., et al., *Purification and characterization of poly (ADP-ribose) glycohydrolase. Different modes of action on large and small poly (ADP-ribose).* Journal of Biological Chemistry, 1986. **261**(32): p. 14902-14911.

287. Bütepage, M., et al., *Intracellular mono-ADP-ribosylation in signaling and disease.* Cells, 2015. **4**(4): p. 569-595.

288. Meyer, R.G., et al., *Human poly (ADP-ribose) glycohydrolase (PARG) gene and the common promoter sequence it shares with inner mitochondrial membrane translocase 23 (TIM23).* Gene, 2003. **314**: p. 181-190.

289. Meyer-Ficca, M.L., et al., *Human poly (ADP-ribose) glycohydrolase is expressed in alternative splice variants yielding isoforms that localize to different cell compartments.* Experimental cell research, 2004. **297**(2): p. 521-532.

290. Meyer-Ficca, M.L., et al., *Overexpression of poly (ADP-ribose) glycohydrolase (PARG) isoforms*. 2005, AACR. p. 420.

291. Davidovic, L., et al., *Importance of poly (ADP-ribose) glycohydrolase in the control of poly (ADP-ribose) metabolism.* Experimental cell research, 2001. **268**(1): p. 7-13.

292. Jean-Philippe Gagné, X.M., Pierre Gagné, Yves Labelle, Arnaud Droit, Mélissa Chevalier-Paré, Sylvie Bourassa, Darin McDonald, Michael J Hendzel, Claude Prigent, Guy G Poirier, *Proteomic investigation of phosphorylation sites in poly(ADP-ribose) polymerase-1 and poly(ADP-ribose) glycohydrolase*. Journal of proteome research, 2009. **8**(2): p. 1014-1029.

293. Botta, D. and M.K. Jacobson, *Identification of a regulatory segment of poly (ADP-ribose) glycohydrolase.* Biochemistry, 2010. **49**(35): p. 7674-7682.

294. Patel, C.N., et al., *Identification of three critical acidic residues of poly (ADP-ribose) glycohydrolase involved in catalysis: determining the PARG catalytic domain.* Biochemical Journal, 2005. **388**(2): p. 493-500.

295. Hassler, M., G. Jankevicius, and A.G. Ladurner, *PARG: a macrodomain in disguise.* Structure, 2011. **19**(10): p. 1351-1353.

296. Bonicalzi, M.E., et al., *Alteration of poly (ADP-ribose) glycohydrolase nucleocytoplasmic shuttling characteristics upon cleavage by apoptotic proteases.* Biology of the Cell, 2003. **95**(9): p. 635-644.

297. Winstall, E., et al., *Preferential perinuclear localization of poly (ADP-ribose) glycohydrolase*. Experimental cell research, 1999. **251**(2): p. 372-378.

298. Bonicalzi, M., et al., *Regulation of poly (ADP-ribose) metabolism by poly (ADP-ribose) glycohydrolase: where and when?* Cellular and molecular life sciences: CMLS, 2005. **62**(7-8): p. 739-750.

299. Niere, M., et al., *ADP-ribosylhydrolase 3 (ARH3), not poly (ADP-ribose) glycohydrolase (PARG) isoforms, is responsible for degradation of mitochondrial matrix-associated poly (ADP-ribose).* Journal of Biological Chemistry, 2012. **287**(20): p. 16088-16102.

300. Davies, G. and B. Henrissat, *Structures and mechanisms of glycosyl hydrolases.* Structure, 1995. **3**(9): p. 853-859.

301. Brochu, G., et al., *Mode of action of poly (ADP-ribose) glycohydrolase.* Biochimica et Biophysica Acta (BBA)-Gene Structure and Expression, 1994. **1219**(2): p. 342-350.

302. BRAUN, S.A., et al., *Endoglycosidic cleavage of branched polymers by poly (ADP-ribose) glycohydrolase.* European journal of biochemistry, 1994. **220**(2): p. 369-375.

303. Koh, D.W., et al., *Failure to degrade poly (ADP-ribose) causes increased sensitivity to cytotoxicity and early embryonic lethality.* Proceedings of the National Academy of Sciences, 2004. **101**(51): p. 17699-17704.

304. Cortes, U., et al., *Depletion of the 110-kilodalton isoform of poly (ADP-ribose) glycohydrolase increases sensitivity to genotoxic and endotoxic stress in mice.* Molecular and cellular biology, 2004. **24**(16): p. 7163-7178.

305. Min, W., et al., *Deletion of the nuclear isoform of poly (ADP-ribose) glycohydrolase (PARG) reveals its function in DNA repair, genomic stability and tumorigenesis.* Carcinogenesis, 2010. **31**(12): p. 2058-2065.

306. Illuzzi, G., et al., *PARG is dispensable for recovery from transient replicative stress but required to prevent detrimental accumulation of poly (ADP-ribose) upon prolonged replicative stress.* Nucleic acids research, 2014. **42**(12): p. 7776-7792.

307. Mortusewicz, O., et al., *PARG is recruited to DNA damage sites through poly (ADP-ribose)-and PCNA-dependent mechanisms.* Nucleic acids research, 2011. **39**(12): p. 5045-5056.

308. Kaufmann, T., et al., *A novel non-canonical PIP-box mediates PARG interaction with PCNA.* Nucleic acids research, 2017. **45**(16): p. 9741-9759.

309. Shirai, H., et al., *PARG dysfunction enhances DNA double strand break formation in S-phase after alkylation DNA damage and augments different cell death pathways.* Cell death & disease, 2013. **4**(6): p. e656-e656.

310. Chaudhuri, A.R., et al., *Poly (ADP-ribosyl) glycohydrolase prevents the accumulation of unusual replication structures during unperturbed S phase.* Molecular and cellular biology, 2015. **35**(5): p. 856-865.

311. Koh, D.W., V.L. Dawson, and T.M. Dawson, *The road to survival goes through PARG.* Cell Cycle, 2005. **4**(3): p. 397-399.

312. Galluzzi, L., et al., *Molecular mechanisms of cell death: recommendations of the Nomenclature Committee on Cell Death 2018.* Cell Death & Differentiation, 2018. **25**(3): p. 486-541.

313. Wang, Y., et al., *Poly (ADP-ribose)(PAR) binding to apoptosis-inducing factor is critical for PAR polymerase-1–dependent cell death (parthanatos).* Science signaling, 2011. **4**(167): p. ra20.

314. Yu, S.-W., et al., *Mediation of poly (ADP-ribose) polymerase-1-dependent cell death by apoptosis-inducing factor.* Science, 2002. **297**(5579): p. 259-263.

315. Fatokun, A.A., V.L. Dawson, and T.M. Dawson, *Parthanatos: mitochondrial-linked mechanisms and therapeutic opportunities.* British journal of pharmacology, 2014. **171**(8): p. 2000-2016.

316. Blenn, C., F.R. Althaus, and M. Malanga, *Poly (ADP-ribose) glycohydrolase silencing protects against H2O2-induced cell death.* Biochemical Journal, 2006. **396**(3): p. 419-429.

317. Yang, L., et al., *Tankyrase1-mediated poly (ADP-ribosyl) ation of TRF1 maintains cell survival after telomeric DNA damage.* Nucleic acids research, 2017. **45**(7): p. 3906-3921.

318. Sun, L., et al., *WRN is recruited to damaged telomeres via its RQC domain and tankyrase1-mediated poly-ADP-ribosylation of TRF1.* Nucleic acids research, 2017. **45**(7): p. 3844-3859.

319. Krueger, K.M. and J.T. Barbieri, *The family of bacterial ADP-ribosylating exotoxins.* Clinical Microbiology Reviews, 1995. **8**(1): p. 34-47.

320. Mashimo, M., J. Kato, and J. Moss, *Structure and function of the ARH family of ADP-ribosyl-acceptor hydrolases.* DNA repair, 2014. **23**: p. 88-94.

321. Leung, A.K., *PARPs.* Current Biology, 2017. **27**(23): p. R1256-R1258.

322. Oka, S., J. Kato, and J. Moss, *Identification and characterization of a mammalian 39-kDa poly (ADP-ribose) glycohydrolase.* Journal of Biological Chemistry, 2006. **281**(2): p. 705-713.

323. Laing, S., et al., *ADP-ribosylation of arginine.* Amino acids, 2011. **41**(2): p. 257-269.

324. Fontana, P., et al., *Serine ADP-ribosylation reversal by the hydrolase ARH3.* Elife, 2017. **6**: p. e28533.

325. Kato, J., et al., *Enhanced sensitivity to cholera toxin in ADP-ribosylarginine hydrolase-deficient mice*. Molecular and cellular biology, 2007. **27**(15): p. 5534-5543.

326. Kato, J., et al., *ADP-ribosylarginine hydrolase regulates cell proliferation and tumorigenesis.* Cancer research, 2011. **71**(15): p. 5327-5335.

327. Abplanalp, J., et al., *Proteomic analyses identify ARH3 as a serine mono-ADP-ribosylhydrolase.* Nature communications, 2017. **8**(1): p. 1-11.

328. Hanai, S., et al., *Loss of poly (ADP-ribose) glycohydrolase causes progressive neurodegeneration in Drosophila melanogaster.* Proceedings of the National Academy of Sciences, 2004. **101**(1): p. 82-86.

329. Mashimo, M., J. Kato, and J. Moss, *ADP-ribosyl-acceptor hydrolase 3 regulates poly (ADP-ribose) degradation and cell death during oxidative stress.* Proceedings of the National Academy of Sciences, 2013. **110**(47): p. 18964-18969.

330. Koch-Nolte, F., *Endogenous ADP-ribosylation*. Book. 2015: Springer.

331. Daniels, C.M., S.-E. Ong, and A.K. Leung, *The promise of proteomics for the study of ADP-ribosylation.* Molecular cell, 2015. **58**(6): p. 911-924.

332. Han, W., X. Li, and X. Fu, *The macro domain protein family: structure, functions, and their potential therapeutic implications.* Mutation Research/Reviews in Mutation Research, 2011. **727**(3): p. 86-103.

333. Sharifi, R., et al., *Deficiency of terminal ADP-ribose protein glycohydrolase TARG1/C6orf130 in neurodegenerative disease.* The EMBO journal, 2013. **32**(9): p. 1225-1237.

334. Bütepage, M., et al., *Nucleolar-nucleoplasmic shuttling of TARG1 and its control by DNA damage-induced poly-ADP-ribosylation and by nucleolar transcription.* Scientific reports, 2018. **8**(1): p. 1-17.

335. Barkauskaite, E., et al., *Visualization of poly (ADP-ribose) bound to PARG reveals inherent balance between exo-and endo-glycohydrolase activities.* Nature communications, 2013. **4**(1): p. 1-8.

336. Barkauskaite, E., G. Jankevicius, and I. Ahel, *Structures and mechanisms of enzymes employed in the synthesis and degradation of PARP-dependent protein ADP-ribosylation.* Molecular cell, 2015. **58**(6): p. 935-946.

337. Sakthianandeswaren, A., et al., *MACROD2 Haploinsufficiency Impairs Catalytic Activity of PARP1 and Promotes Chromosome Instability and Growth of Intestinal Tumors.* Cancer Discov, 2018. **8**(8): p. 988-1005.

338. Sakthianandeswaren, A., et al., *MACROD2 deletions cause impaired PARP1 activity and chromosome instability in colorectal cancer.* Oncotarget, 2018. **9**(69): p. 33056.

339. Reeder, R.H., et al., *Studies on the Polymer of Adenosine Diphosphate Ribose: II. CHARACTERIZATION OF THE POLYMER.* Journal of Biological Chemistry, 1967. **242**(13): p. 3172-3179.

340. Palazzo, L., et al., *Processing of protein ADP-ribosylation by Nudix hydrolases.* Biochemical Journal, 2015. **468**(2): p. 293-301.

341. Daniels, C.M., et al., *Nudix hydrolases degrade protein-conjugated ADP-ribose.* Scientific reports, 2015. **5**(1): p. 1-12.

342. Palazzo, L., et al., *ENPP 1 processes protein ADP-ribosylation in vitro.* The FEBS journal, 2016. **283**(18): p. 3371-3388.

343. Williams, J., J. Chambers, and J. Liehr, *Glutamyl ribose 5-phosphate storage disease. A hereditary defect in the degradation of poly (ADP-ribosylated) proteins.* Journal of Biological Chemistry, 1984. **259**(2): p. 1037-1042.

344. Shirato, M., et al., *Poly (etheno ADP-ribose) blocks poly (ADP-ribose) glycohydrolase activity.* Biochemical and biophysical research communications, 2007. **355**(2): p. 451-456.

345. Bessman, M.J., D.N. Frick, and S.F. O'Handley, *The MutT proteins or "Nudix" hydrolases, a family of versatile, widely distributed,"housecleaning" enzymes.* Journal of Biological Chemistry, 1996. **271**(41): p. 25059-25062.

346. Formentini, L., et al., *Poly (ADP-ribose) catabolism triggers AMP-dependent mitochondrial energy failure.* Journal of Biological Chemistry, 2009. **284**(26): p. 17668-17676.

347. Ethier, C., et al., *PARP-1 modulation of mTOR signaling in response to a DNA alkylating agent.* PloS one, 2012. **7**(10): p. e47978.

348. Wright, R.H., et al., *ADP-ribose–derived nuclear ATP synthesis by NUDIX5 is required for chromatin remodeling.* Science, 2016. **352**(6290): p. 1221-1225.

349. Ménard, L. and G.G. Poirier, *Rapid assay of poly (ADP-ribose) glycohydrolase.* Biochemistry and Cell Biology, 1987. **65**(7): p. 668-673.

350. Haince, J.-F., et al., *Dynamic relocation of poly (ADP-ribose) glycohydrolase isoforms during radiation-induced DNA damage.* Biochimica et Biophysica Acta (BBA)-Molecular Cell Research, 2006. **1763**(2): p. 226-237.

351. Wang, Z., et al., *Crystallographic and biochemical analysis of the mouse poly (ADP-ribose) glycohydrolase.* PLoS One, 2014. **9**(1): p. e86010.

352. Finch, K.E., et al., *Selective small molecule inhibition of poly (ADP-ribose) glycohydrolase (PARG).* ACS chemical biology, 2012. **7**(3): p. 563-570.

353. Falsig, J., et al., *Poly (ADP-ribose) glycohydrolase as a target for neuroprotective intervention: assessment of currently available pharmacological tools.* European journal of pharmacology, 2004. **497**(1): p. 7-16.

354. Putt, K.S. and P.J. Hergenrother, *A nonradiometric, high-throughput assay for poly (ADP-ribose) glycohydrolase (PARG): application to inhibitor identification and evaluation.* Analytical biochemistry, 2004. **333**(2): p. 256-264.

355. Miwa, M., et al., *Purification and properties of a glycohydrolase from calf thymus splitting ribose-ribose linkages of poly (adenosine diphosphate ribose).* Journal of Biological Chemistry, 1974. **249**(11): p. 3475-3482.

356. James, D.I., et al., *An assay to measure poly (ADP ribose) glycohydrolase (PARG) activity in cells.* F1000Research, 2016. **5**: p. 736.

357. Kawamitsu, H., et al., *Monoclonal antibodies to poly (adenosine diphosphate ribose) recognize different structures.* Biochemistry, 1984. **23**(16): p. 3771-3777.

358. Gibson, B.A., et al., *Generation and characterization of recombinant antibody-like ADP-ribose binding proteins.* Biochemistry, 2017. **56**(48): p. 6305-6316.

359. Rosenthal, F., et al., *Macrodomain-containing proteins are new mono-ADP-ribosylhydrolases.* Nature structural & molecular biology, 2013. **20**(4): p. 502.

360. Liu, Q., et al., *A general approach towards triazole-linked adenosine diphosphate ribosylated peptides and proteins.* Angewandte Chemie, 2018. **130**(6): p. 1675-1678.

361. Zhen, Y. and Y. Yu, *Proteomic analysis of the downstream signaling network of PARP1.* Biochemistry, 2018. **57**(4): p. 429-440.

362. Haag, F. and F. Buck, *Identification and analysis of ADP-ribosylated proteins.* Endogenous ADP-Ribosylation, 2014: p. 33-50.

363. Rosenthal, F. and M.O. Hottiger, *Identification of ADP-ribosylated peptides and ADP-ribose acceptor sites.* Front Biosci (Landmark Ed), 2014. **19**: p. 1041-1056.

364. Vivelo, C.A. and A.K. Leung, *Proteomics approaches to identify mono-(ADP-ribosyl) ated and poly (ADP-ribosyl) ated proteins.* Proteomics, 2015. **15**(2-3): p. 203-217.

365. Laing, S., et al., *Strategies for the identification of arginine ADP-ribosylation sites.* Journal of proteomics, 2011. **75**(1): p. 169-176.

366. Bonfiglio, J.J., T. Colby, and I. Matic, *Mass spectrometry for serine ADP-ribosylation? Think o-glycosylation!* Nucleic acids research, 2017. **45**(11): p. 6259-6264.

367. Kistemaker, H.A., et al., *Synthesis and macrodomain binding of mono-ADP-ribosylated peptides.* Angewandte Chemie, 2016. **128**(36): p. 10792-10796.

368. Lüscher, B., et al., *ADP-ribosylation, a multifaceted posttranslational modification involved in the control of cell physiology in health and disease.* Chemical reviews, 2018. **118**(3): p. 1092-1136.

369. Alvarez-Gonzalez, R. and F.R. Althaus, *Poly (ADP-ribose) catabolism in mammalian cells exposed to DNA-damaging agents.* Mutation Research/DNA Repair, 1989. **218**(2): p. 67-74.

370. Talhaoui, I., et al., *Poly (ADP-ribose) polymerases covalently modify strand break termini in DNA fragments in vitro.* Nucleic acids research, 2016. **44**(19): p. 9279-9295.

371. Zarkovic, G., et al., *Characterization of DNA ADP-ribosyltransferase activities of PARP2 and PARP3: new insights into DNA ADP-ribosylation.* Nucleic acids research, 2018. **46**(5): p. 2417-2431.

372. Munnur, D. and I. Ahel, *Reversible mono-ADP-ribosylation of DNA breaks*. 2017, Wiley Online Library. p. 4002-4016.

373. Ziegler, M., *ADP-ribosylation of DNA moving into focus.* FEBS journal, 2017. **284**(23): p. 3999-4001.

374. Agnew, T., et al., *MacroD1 is a promiscuous ADP-ribosyl hydrolase localized to mitochondria.* Frontiers in microbiology, 2018. **9**: p. 20.

375. Jacobson, E.L., D. Cervantes-Laurean, and M.K. Jacobson, *Glycation of proteins by ADP-ribose.* ADP-Ribosylation: Metabolic Effects and Regulatory Functions, 1994: p. 207-212.

376. Martello, R., et al., *Proteome-wide identification of the endogenous ADP-ribosylome of mammalian cells and tissue.* Nature communications, 2016. **7**(1): p. 1-13.

377. Desmarais, Y., et al., *Enzymological properties of poly (ADP-ribose) polymerase: characterization of automodification sites and NADase activity.* Biochimica et biophysica acta, 1991. **1078**(2): p. 179-186.

378. Clark, N.J., et al., *Alternative modes of binding of poly (ADP-ribose) polymerase 1 to free DNA and nucleosomes.* Journal of Biological Chemistry, 2012. **287**(39): p. 32430-32439.

379. Pic, E., J.-P. Gagné, and G.G. Poirier, *Mass spectrometry-based functional proteomics of poly (ADP-ribose) polymerase-1.* Expert review of proteomics, 2011. **8**(6): p. 759-774.

380. Berger, F., C. Lau, and M. Ziegler, *Regulation of poly (ADP-ribose) polymerase 1 activity by the phosphorylation state of the nuclear NAD biosynthetic enzyme NMN adenylyl transferase 1.* Proceedings of the National Academy of Sciences, 2007. **104**(10): p. 3765-3770.

381. Bonfiglio, J.J., et al., *Serine ADP-ribosylation depends on HPF1.* Molecular cell, 2017. **65**(5): p. 932-940. e6.

382. Leung, A.K., *SERious surprises for ADP-ribosylation Specificity: HPF1 switches PARP1 specificity to ser residues.* Molecular cell, 2017. **65**(5): p. 777-778.

383. Liu, Q., B.I. Florea, and D.V. Filippov, *ADP-ribosylation goes normal: serine as the major site of the modification.* Cell chemical biology, 2017. **24**(4): p. 431-432.

384. Palazzo, L., et al., *Serine is the major residue for ADP-ribosylation upon DNA damage.* Elife, 2018. **7**: p. e34334.

385. Leidecker, O., et al., *Serine is a new target residue for endogenous ADP-ribosylation on histones.* Nature chemical biology, 2016. **12**(12): p. 998-1000.

386. Leslie Pedrioli, D.M., et al., *Comprehensive ADP-ribosylome analysis identifies tyrosine as an ADP-ribose acceptor site.* EMBO Rep, 2018. **19**(8): p. e45310.

387. Sung, V.M.-H., *Mechanistic overview of ADP-ribosylation reactions.* Biochimie, 2015. **113**: p. 35-46.

388. Karch, K.R., et al., *The nucleosomal surface is the main target of histone ADP-ribosylation in response to DNA damage.* Molecular BioSystems, 2017. **13**(12): p. 2660-2671.

389. Thomassin, H., et al., *Poly (ADP-ribosyl) ation of chromatin in an in-vitro poly (ADP-ribose)-turnover system.* Biochimica et Biophysica Acta (BBA)-Molecular Cell Research, 1992. **1137**(2): p. 171-181.

390. Lagueux, J., et al., *Poly (ADP-ribose) catabolism in mammalian cells*, in *ADP-Ribosylation: Metabolic Effects and Regulatory Functions*. 1994, Springer. p. 45-52.

391. Menard, L., L. Thibault, and G.G. Poirier, *Reconstitution of an in vitro poly (ADP-ribose) turnover system.* Biochimica et Biophysica Acta (BBA)-Gene Structure and Expression, 1990. **1049**(1): p. 45-58.

392. Na, Z., et al., *A Small-Molecule Protein–Protein Interaction Inhibitor of PARP1 That Targets Its BRCT Domain.* Angewandte Chemie, 2015. **127**(8): p. 2545-2549.

393. Dawicki-McKenna, J.M., et al., *PARP-1 activation requires local unfolding of an autoinhibitory domain.* Molecular cell, 2015. **60**(5): p. 755-768.

394. Eustermann, S., et al., *Structural basis of detection and signaling of DNA single-strand breaks by human PARP-1*. Molecular cell, 2015. **60**(5): p. 742-754.

395. Pacheco-Rodriguez, G. and R. Alvarez-Gonzalez, *Measurement of poly (ADP-ribose) glycohydrolase activity by high resolution polyacrylamide gel electrophoresis: specific inhibition by histones and nuclear matrix proteins*, in *ADP-Ribosylation Reactions: From Bacterial Pathogenesis to Cancer*. 1999, Springer. p. 13-18.

396. Gaudreau, A., et al., *Poly (ADP-ribose) accessibility to poly (ADP-ribose) glycohydrolase activity on poly (ADP-ribosyl) ated nucleosomal proteins.* Biochemistry and Cell Biology, 1986. **64**(2): p. 146-153.

397. Jankevicius, G., et al., *A family of macrodomain proteins reverses cellular mono-ADP-ribosylation.* Nature structural & molecular biology, 2013. **20**(4): p. 508.

398. Minaga, T. and E. Kun, *Probable helical conformation of poly (ADP-ribose). The effect of cations on spectral properties.* Journal of Biological Chemistry, 1983. **258**(9): p. 5726-5730.

399. Tavassoli, M., M.H. Tavassoli, and S. Shall, *Effect of DNA intercalators on poly (ADP-ribose) glycohydrolase activity.* Biochimica et Biophysica Acta (BBA)-Protein Structure and Molecular Enzymology, 1985. **827**(3): p. 228-234.

400. Tsai, Y., et al., *Effects of chemically defined tannins on poly (ADP-ribose) glycohydrolase activity.* Biochemistry international, 1991. **24**(5): p. 889-897.

401. Formentini, L., et al., *Mono-galloyl glucose derivatives are potent poly (ADP-ribose) glycohydrolase (PARG) inhibitors and partially reduce PARP-1-dependent cell death.* British journal of pharmacology, 2008. **155**(8): p. 1235-1249.

402. Fathers, C., et al., *Inhibition of poly (ADP-ribose) glycohydrolase (PARG) specifically kills BRCA2-deficient tumor cells.* Cell cycle, 2012. **11**(5): p. 990-997.

403. Slama, J.T., et al., *Specific inhibition of poly (ADP-ribose) glycohydrolase by adenosine diphosphate (hydroxymethyl) pyrrolidinediol.* Journal of medicinal chemistry, 1995. **38**(2): p. 389-393.

404. Slama, J.T., N. Aboul-Ela, and M.K. Jacobson, *Mechanism of inhibition of poly (ADP-ribose) glycohydrolase by adenosine diphosphate (hydroxymethyl) pyrrolidinediol.* Journal of medicinal chemistry, 1995. **38**(21): p. 4332-4336.

405. Ramsinghani, S., et al., *Syntheses of photoactive analogues of adenosine diphosphate (hydroxymethyl) pyrrolidinediol and photoaffinity labeling of poly (ADP-ribose) glycohydrolase.* Biochemistry, 1998. **37**(21): p. 7801-7812.

406. Lu, X.-C.M., et al., *Post-treatment with a novel PARG inhibitor reduces infarct in cerebral ischemia in the rat.* Brain research, 2003. **978**(1-2): p. 99-103.

407. Tentori, L., et al., *Poly (ADP-ribose) glycohydrolase inhibitor as chemosensitiser of malignant melanoma for temozolomide.* European journal of cancer, 2005. **41**(18): p. 2948-2957.

408. James, D.I., et al., *First-in-class chemical probes against poly (ADP-ribose) glycohydrolase (PARG) inhibit DNA repair with differential pharmacology to olaparib.* ACS chemical biology, 2016. **11**(11): p. 3179-3190.

409. Gravells, P., et al., *Specific killing of DNA damage-response deficient cells with inhibitors of poly (ADP-ribose) glycohydrolase.* DNA repair, 2017. **52**: p. 81-91.

410. Gravells, P., et al., *Radiosensitization with an inhibitor of poly (ADP-ribose) glycohydrolase: a comparison with the PARP1/2/3 inhibitor olaparib.* DNA repair, 2018. **61**: p. 25-36.

411. Amé, J.-C., et al., *Radiation-induced mitotic catastrophe in PARG-deficient cells.* Journal of cell science, 2009. **122**(12): p. 1990-2002.

412. Shirai, H., et al., *Parg deficiency confers radio-sensitization through enhanced cell death in mouse ES cells exposed to various forms of ionizing radiation.* Biochemical and biophysical research communications, 2013. **435**(1): p. 100-106.

413. Chand, S.N., et al., *Posttranscriptional regulation of PARG mRNA by HuR facilitates DNA repair and resistance to PARP inhibitors.* Cancer research, 2017. **77**(18): p. 5011-5025.

414. Gogola, E., et al., *Selective loss of PARG restores PARylation and counteracts PARP inhibitor-mediated synthetic lethality.* Cancer cell, 2018. **33**(6): p. 1078-1093. e12.

415. Vilenchik, M.M. and A.G. Knudson, *Endogenous DNA double-strand breaks: production, fidelity of repair, and induction of cancer.* Proc. Natl Acad. Sci. USA, 2003. **100**(22): p. 12871-12876.

416. Jungmichel, S., *Proteome-wide identification of poly(ADP-Ribosyl)ation targets in different genotoxic stress responses.* Mol. Cell, 2013. **52**(2): p. 272-285.

417. Wacker, D.A., et al., *Regulation of chromatin structure and chromatin-dependent transcription by poly(ADP-ribose) polymerase-1: possible targets for drug-based therapies.* Subcell. Biochem., 2007. **41**: p. 45-69.

418. Strickfaden, H., *Poly(ADP-ribosyl)ation-dependent transient chromatin decondensation and histone displacement following laser microirradiation.* J. Biol. Chem., 2016. **291**(4): p. 1789-1802.

419. Krietsch, J., *Reprogramming cellular events by poly(ADP-ribose)-binding proteins.* Mol. Aspects Med., 2013. **34**(6): p. 1066-1087.

420. D'Amours, D., et al., *Gain-of-function of poly(ADP-ribose) polymerase-1 upon cleavage by apoptotic proteases: implications for apoptosis.* J. Cell Sci., 2001. **114**: p. 3771-3778.

421. Maya-Mendoza, A., *High speed of fork progression induces DNA replication stress and genomic instability.* Nature, 2018. **559**: p. 279-284.

422. Hanzlikova, H., *The importance of poly(ADP-ribose) polymerase as a sensor of unligated Okazaki fragments during DNA replication.* Mol. Cell, 2018. **71**: p. 319-331.

423. Zimmermann, M., *CRISPR screens identify genomic ribonucleotides as a source of PARP-trapping lesions.* Nature, 2018. **559**: p. 285-289.

424. Couto, C.A.M., *PARP regulates nonhomologous end joining through retention of Ku at double-strand breaks.* J. Cell Biol., 2011. **194**: p. 367-375.

425. Langelier, M.F., et al., *The Zn3 domain of human poly(ADP-ribose) polymerase-1 (PARP-1) functions in both DNA-dependent poly(ADP-ribose) synthesis activity and chromatin compaction.* J. Biol. Chem., 2010. **285**(24): p. 18877-18887.

426. Escribano-Diaz, C., *A cell cycle-dependent regulatory circuit composed of 53BP1-RIF1 and BRCA1-CtIP controls DNA repair pathway choice.* Mol. Cell, 2013. **49**(5): p. 872-883.

427. Isabelle, M., *Investigation of PARP-1, PARP-2, and PARG interactomes by affinity-purification mass spectrometry.* Proteome Sci., 2010. **8**: p. 22.

428. LaFargue, C.J., et al., *Exploring and comparing adverse events between PARP inhibitors.* Lancet Oncol., 2019. **20**(1): p. e15-28.

429. Drean, A., C.J. Lord, and A. Ashworth, *PARP inhibitor combination therapy.* Crit. Rev. Oncol. Hematol., 2016. **108**: p. 73-85.

430. Aleksandrov, R., *Protein dynamics in complex DNA lesions.* Mol. Cell, 2018. **69**(6): p. 1046-1061.

431. Nam, E.A., *Thr-1989 phosphorylation is a marker of active ataxia telangiectasia-mutated and Rad3-related (ATR) kinase.* J. Biol. Chem., 2011. **286**(33): p. 28707-28714.

432. Sartori, A.A., *Human CtIP promotes DNA end resection.* Nature, 2007. **450**: p. 509-514.

433. Zhou, Y., et al., *Quantitation of DNA double-strand break resection intermediates in human cells.* Nucleic Acids Res., 2014. **42**(3): p. e19.

434. Gallardo, I.F., *High-throughput universal DNA curtain arrays for single-molecule fluorescence imaging.* Langmuir, 2015. **31**(37): p. 10310-10317.

435. Schultz, N., et al., *Poly(ADP-ribose) polymerase (PARP-1) has a controlling role in homologous recombination.* Nucleic Acids Res., 2003. **31**(17): p. 4959-4964.

436. Mirman, Z., *53BP1-RIF1-shieldin counteracts DSB resection through CST- and Polalpha-dependent fill-in.* Nature, 2018. **560**: p. 112-116.

437. Findlay, S.t.e.v.e.n., et al., *SHLD2/FAM35A co-operates with REV7 to coordinate DNA double-strand break repair pathway choice.* The EMBO Journal, 2018. **37**(18): p. e100158.

438. Spagnolo, L., et al., *Visualization of a DNA-PK/PARP1 complex.* Nucleic Acids Res., 2012. **40**(9): p. 4168-4177.

439. Ying, S., F.C. Hamdy, and T. Helleday, *Mre11-dependent degradation of stalled DNA replication forks is prevented by BRCA2 and PARP1*. Cancer Res., 2012. **72**(11): p. 2814-2821.

440. Soni, A., *Inhibition of Parp1 by BMN673 effectively sensitizes cells to radiotherapy by upsetting the balance of repair pathways processing DNA double-strand breaks.* Mol. Cancer Ther., 2018. **17**(10): p. 2206-2216.

441. Shen, Y., et al., *BMN 673, a Novel and Highly Potent PARP1/2 Inhibitor for the Treatment of Human Cancers with DNA Repair Deficiency.* Clinical Cancer Research, 2013. **19**(18): p. 5003-5015.

442. Oikawa, A., et al., *Inhibitors of poly(adenosine diphosphate ribose) polymerase induce sister chromatid exchanges.* Biochem Biophys. Res. Commun., 1980. **97**(4): p. 1311-1316.

443. Hori, T., *High incidence of sister chromatid exchanges and chromatid interchanges in the conditions of lowered activity of poly(ADP-ribose)polymerase.* Biochem Biophys. Res. Commun., 1981. **102**(1): p. 38-45.

444. Morrison, C., *Genetic interaction between PARP and DNA-PK in V(D)J recombination and tumorigenesis.* Nat. Genet., 1997. **17**(4): p. 479-482.

445. Hu, Y., *PARP1-driven poly-ADP-ribosylation regulates BRCA1 function in homologous recombination-mediated DNA repair.* Cancer Discov., 2014. **4**(12): p. 1430-1447.

446. Gottipati, P., *Poly(ADP-ribose) polymerase is hyperactivated in homologous recombination-defective cells.* Cancer Res., 2010. **70**(13): p. 5389-5398.

447. Patel, A.G., J.N. Sarkaria, and S.H. Kaufmann, *Nonhomologous end joining drives poly(ADP-ribose) polymerase (PARP) inhibitor lethality in homologous recombination-deficient cells.* Proc. Natl Acad. Sci. USA, 2011. **108**(8): p. 3406-3411.

448. Mirza, M.R., *Niraparib maintenance therapy in platinum-sensitive, recurrent ovarian cancer.* New Engl. J. Med., 2016. **375**: p. 2154-2164.

449. Zou, L., D. Cortez, and S.J. Elledge, *Regulation of ATR substrate selection by Rad17-dependent loading of Rad9 complexes onto chromatin.* Genes Dev., 2002. **16**(2): p. 198-208.

450. Niraj, J., *The identification of FANCD2 DNA binding domains reveals nuclear localization sequences.* Nucleic Acids Res., 2017. **45**(14): p. 8341-8357.

451. Schonenberger, F., et al., *Discrimination of cell cycle phases in PCNA-immunolabeled cells.* BMC Bioinformatics, 2015. **16**: p. 180.

452. Dery, U., *A glycine-arginine domain in control of the human MRE11 DNA repair protein.* Mol. Cell. Biol., 2008. **28**(9): p. 3058-3069.

453. Herbert, A.D., A.M. Carr, and E. Hoffmann, *FindFoci: a focus detection algorithm with automated parameter training that closely matches human assignments, reduces human inconsistencies and increases speed of analysis.* PLoS ONE, 2014. **9**(12): p. e114749.

454. Yu, Z., *The MRE11 GAR motif regulates DNA double-strand break processing and ATR activation.* Cell Res., 2012. **22**(2): p. 305-320.

455. Henricksen, L.A., C.B. Umbricht, and M.S. Wold, *Recombinant replication protein A: expression, complex formation, and functional characterization.* J. Biol. Chem., 1994. **269**(15): p. 11121-11132.

456. Myler, L.R., *Single-molecule imaging reveals the mechanism of Exo1 regulation by single-stranded DNA binding proteins.* Proc. Natl Acad. Sci. USA, 2016. **113**(9): p. E1170-1179.

457. Efron, B.T., R. , *An Introduction to the Bootstrap (Chapman & Hall, London, 1993)*.

458. Mouw, K.W., et al., *DNA Damage and Repair Biomarkers of Immunotherapy Response.* Cancer Discov, 2017. **7**(7): p. 675-693.

459. Scully, R., et al., *DNA double-strand break repair-pathway choice in somatic mammalian cells.* Nat Rev Mol Cell Biol, 2019. **20**(11): p. 698-714.

460. Chang, H.H.Y., et al., *Non-homologous DNA end joining and alternative pathways to double-strand break repair.* Nat Rev Mol Cell Biol, 2017. **18**(8): p. 495-506.

461. Heyer, W.D., K.T. Ehmsen, and J. Liu, *Regulation of homologous recombination in eukaryotes.* Annu Rev Genet, 2010. **44**: p. 113-39.

462. Satoh, M.S. and T. Lindahl, *Role of poly(ADP-ribose) formation in DNA repair.* Nature, 1992. **356**(6367): p. 356-8.

463. Sugimura, K., et al., *PARP-1 ensures regulation of replication fork progression by homologous recombination on damaged DNA.* J Cell Biol, 2008. **183**(7): p. 1203-12.

464. Bryant, H.E., et al., *Specific killing of BRCA2-deficient tumours with inhibitors of poly(ADP-ribose) polymerase.* Nature, 2005. **434**(7035): p. 913-7.

465. Zhou, P., et al., *Recent advancements in PARP inhibitors-based targeted cancer therapy.* Precis Clin Med, 2020. **3**(3): p. 187-201.

466. Noordermeer, S.M. and H. van Attikum, *PARP Inhibitor Resistance: A Tug-of-War in BRCA-Mutated Cells.* Trends Cell Biol, 2019. **29**(10): p. 820-834.

467. Caron, M.C., et al., *Poly(ADP-ribose) polymerase-1 antagonizes DNA resection at double-strand breaks.* Nat Commun, 2019. **10**(1): p. 2954.

468. Zhou, Y., et al., *Quantitation of DNA double-strand break resection intermediates in human cells.* Nucleic Acids Res, 2014. **42**(3): p. e19.

469. Raderschall, E., E.I. Golub, and T. Haaf, *Nuclear foci of mammalian recombination proteins are located at single-stranded DNA regions formed after DNA damage.* Proceedings of the National Academy of Sciences, 1999. **96**(5): p. 1921-1926.

470. Huertas, P. and A. Cruz-García, *Single Molecule Analysis of Resection Tracks.* Methods Mol Biol, 2018. **1672**: p. 147-154.

471. O'Driscoll, M. and P.A. Jeggo, *The role of double-strand break repair — insights from human genetics.* Nature Reviews Genetics, 2006. **7**(1): p. 45-54.

472. Takata, M., et al., *Homologous recombination and non-homologous end-joining pathways of DNA double-strand break repair have overlapping roles in the maintenance of chromosomal integrity in vertebrate cells.* The EMBO journal, 1998. **17**(18): p. 5497-5508.

473. Wright, W.D., S.S. Shah, and W.-D. Heyer, *Homologous recombination and the repair of DNA double-strand breaks.* Journal of Biological Chemistry, 2018. **293**(27): p. 10524-10535.

474. Pandey, N. and B.E. Black, *Rapid Detection and Signaling of DNA Damage by PARP-1.* Trends Biochem Sci, 2021. **46**(9): p. 744-757.

475. Bian, L., et al., *MRE11-RAD50-NBS1 complex alterations and DNA damage response: implications for cancer treatment.* Molecular Cancer, 2019. **18**(1): p. 169.

476. Yuan, S.-S.F., et al., *BRCA2 is required for ionizing radiation-induced assembly of Rad51 complex in vivo.* Cancer research, 1999. **59**(15): p. 3547-3551.

477. Azarm, K. and S. Smith, *Nuclear PARPs and genome integrity.* Genes & development, 2020. **34**(5-6): p. 285-301.

478. Curtin, N.J. and C. Szabo, *Poly (ADP-ribose) polymerase inhibition: past, present and future.* Nature Reviews Drug Discovery, 2020. **19**(10): p. 711-736.

479. Konstantinopoulos, P.A., et al., *Olaparib and α-specific PI3K inhibitor alpelisib for patients with epithelial ovarian cancer: a dose-escalation and dose-expansion phase 1b trial.* The Lancet Oncology, 2019. **20**(4): p. 570-580.

480. Fong, P.C., et al., *Inhibition of poly (ADP-ribose) polymerase in tumors from BRCA mutation carriers.* New England Journal of Medicine, 2009. **361**(2): p. 123-134.

481. Rottenberg, S., et al., *High sensitivity of BRCA1-deficient mammary tumors to the PARP inhibitor AZD2281 alone and in combination with platinum drugs.* Proceedings of the National Academy of Sciences, 2008. **105**(44): p. 17079-17084.

482. Clements, K.E., et al., *Identification of regulators of poly-ADP-ribose polymerase inhibitor response through complementary CRISPR knockout and activation screens.* Nature communications, 2020. **11**(1): p. 1-14.

483. Pettitt, S.J., et al., *Genome-wide and high-density CRISPR-Cas9 screens identify point mutations in PARP1 causing PARP inhibitor resistance.* Nature communications, 2018. **9**(1): p. 1-14.

484. Edwards, S.L., et al., *Resistance to therapy caused by intragenic deletion in BRCA2.* Nature, 2008. **451**(7182): p. 1111-1115.

485. Arnoult, N., et al., *Regulation of DNA repair pathway choice in S and G2 phases by the NHEJ inhibitor CYREN.* Nature, 2017. **549**(7673): p. 548-552.

486. Gerhard, D.S., et al., *The status, quality, and expansion of the NIH full-length cDNA project: the Mammalian Gene Collection (MGC).* Genome Res, 2004. **14**(10b): p. 2121-7.

487. Huttlin, E.L., et al., *Architecture of the human interactome defines protein communities and disease networks.* Nature, 2017. **545**(7655): p. 505-509.

488. Strausberg, R.L., et al., *Generation and initial analysis of more than 15,000 full-length human and mouse cDNA sequences.* Proc Natl Acad Sci U S A, 2002. **99**(26): p. 16899-903.

489. Wu, A.C., et al., *Inhaled corticosteroid treatment modulates ZNF432 gene variant's effect on bronchodilator response in asthmatics.* J Allergy Clin Immunol, 2014. **133**(3): p. 723-8.e3.

490. Zhan, X. and D.M. Desiderio, *Nitroproteins from a human pituitary adenoma tissue discovered with a nitrotyrosine affinity column and tandem mass spectrometry.* Anal Biochem, 2006. **354**(2): p. 279-89.

491. Fasci, D., et al., *Histone Interaction Landscapes Visualized by Crosslinking Mass Spectrometry in Intact Cell Nuclei.* Mol Cell Proteomics, 2018. **17**(10): p. 2018-2033.

492. Gaudet, P., et al., *Phylogenetic-based propagation of functional annotations within the Gene Ontology consortium.* Brief Bioinform, 2011. **12**(5): p. 449-62.

493. Luck, K., et al., *A reference map of the human binary protein interactome.* Nature, 2020. **580**(7803): p. 402-408.

494. Kimura, K., et al., *Diversification of transcriptional modulation: large-scale identification and characterization of putative alternative promoters of human genes.* Genome Res, 2006. **16**(1): p. 55-65.

495. Nagase, T., et al., *Prediction of the coding sequences of unidentified human genes. XI. The complete sequences of 100 new cDNA clones from brain which code for large proteins in vitro.* DNA Res, 1998. **5**(5): p. 277-86.

496. Cerami, E., et al., *The cBio cancer genomics portal: an open platform for exploring multidimensional cancer genomics data.* Cancer Discov, 2012. **2**(5): p. 401-4.

497. Gao, J., et al., *Integrative analysis of complex cancer genomics and clinical profiles using the cBioPortal.* Sci Signal, 2013. **6**(269): p. pl1.

498. Szklarczyk, D., et al., *STRING v11: protein-protein association networks with increased coverage, supporting functional discovery in genome-wide experimental datasets.* Nucleic Acids Res, 2019. **47**(D1): p. D607-d613.

499. Li, H., et al., *PARP inhibitor resistance: the underlying mechanisms and clinical implications.* Molecular cancer, 2020. **19**(1): p. 1-16.

500. Szántó, M., et al., *Poly(ADP-ribose) polymerase-2: emerging transcriptional roles of a DNA-repair protein.* Cell Mol Life Sci, 2012. **69**(24): p. 4079-92.

501. Gui, B., et al., *Selective targeting of PARP-2 inhibits androgen receptor signaling and prostate cancer growth through disruption of FOXA1 function.* Proceedings of the National Academy of Sciences, 2019. **116**(29): p. 14573-14582.

502. Kotsantis, P., et al., *Increased global transcription activity as a mechanism of replication stress in cancer.* Nature communications, 2016. **7**(1): p. 1-13.

503. Pillay, N., et al., *DNA replication stress and emerging prospects for PARG inhibitors in ovarian cancer therapy.* Progress in Biophysics and Molecular Biology, 2021. **163**: p. 160-170.

504. Li, X. and Y. Meng, *SUMOylation Regulator-Related Molecules Can Be Used as Prognostic Biomarkers for Glioblastoma.* Front Cell Dev Biol, 2021. **9**: p. 658856.

505. Zhao, S., et al., *Novel transcription-induced fusion RNAs in prostate cancer.* Oncotarget, 2017. **8**(30): p. 49133-49143.

506. Boulet, L.-P. and P. Chanez, *Clinically relevant outcome measures for new therapies of asthma using pharmaceutical and biologic agents.* Current Opinion in Allergy and Clinical Immunology, 2015. **15**(3): p. 213-219.

507. Pouladi, N., et al., *Complex genetics of pulmonary diseases: lessons from genome-wide association studies and next-generation sequencing.* Translational Research, 2016. **168**: p. 22-39.

508. Iyengar, S., et al., *Functional analysis of KAP1 genomic recruitment.* Molecular and cellular biology, 2011. **31**(9): p. 1833-1847.

509. Santos, J. and J. Gil, *TRIM28/KAP1 regulates senescence.* Immunology letters, 2014. **162**(1): p. 281-289.

510. Bunch, H., et al., *Transcriptional elongation requires DNA break-induced signalling.* Nature communications, 2015. **6**(1): p. 1-12.

511. Bunch, H., *Role of genome guardian proteins in transcriptional elongation.* FEBS letters, 2016. **590**(8): p. 1064-1075.

512. Xiao, T.Z., et al., *MAGE I Transcription Factors Regulate KAP1 and KRAB Domain Zinc Finger Transcription Factor Mediated Gene Repression.* PLOS ONE, 2011. **6**(8): p. e23747.

513. Groner, A.C., et al., *KRAB-zinc finger proteins and KAP1 can mediate long-range transcriptional repression through heterochromatin spreading.* PLoS Genet, 2010. **6**(3): p. e1000869.

514. Cheng, C.-T., C.-Y. Kuo, and D.K. Ann, *KAPtain in charge of multiple missions: Emerging roles of KAP1.* World journal of biological chemistry, 2014. **5**(3): p. 308.

515. Schultz, D.C., J.R. Friedman, and F.J. Rauscher, 3rd, *Targeting histone deacetylase complexes via KRAB-zinc finger proteins: the PHD and bromodomains of KAP-1 form a cooperative unit that recruits a novel isoform of the Mi-2alpha subunit of NuRD.* Genes Dev, 2001. **15**(4): p. 428-43.

516. Ivanov, A.V., et al., *PHD domain-mediated E3 ligase activity directs intramolecular sumoylation of an adjacent bromodomain required for gene silencing.* Mol Cell, 2007. **28**(5): p. 823-37.

517. Aleksandrov, R., et al., *The Chromatin Response to Double-Strand DNA Breaks and Their Repair*. Cells, 2020. **9**(8): p. 1853.

518. Peng, H., et al., *Reconstitution of the KRAB-KAP-1 repressor complex: a model system for defining the molecular anatomy of RING-B box-coiled-coil domain-mediated protein-protein interactions.* J Mol Biol, 2000. **295**(5): p. 1139-62.

519. Friedman, J.R., et al., *KAP-1, a novel corepressor for the highly conserved KRAB repression domain.* Genes Dev, 1996. **10**(16): p. 2067-78.

520. Li, X., et al., *Role for KAP1 serine 824 phosphorylation and sumoylation/desumoylation switch in regulating KAP1-mediated transcriptional repression.* J Biol Chem, 2007. **282**(50): p. 36177-89.

521. Goodarzi, A.A., T. Kurka, and P.A. Jeggo, *KAP-1 phosphorylation regulates CHD3 nucleosome remodeling during the DNA double-strand break response.* Nature structural & molecular biology, 2011. **18**(7): p. 831.

522. Ayoub, N., et al., *HP1-β mobilization promotes chromatin changes that initiate the DNA damage response.* Nature, 2008. **453**(7195): p. 682-686.

523. Baldeyron, C., et al., *HP1α recruitment to DNA damage by p150CAF-1 promotes homologous recombination repair.* Journal of Cell Biology, 2011. **193**(1): p. 81-95.

524. Goodarzi, A.A., et al., *ATM signaling facilitates repair of DNA double-strand breaks associated with heterochromatin.* Molecular cell, 2008. **31**(2): p. 167-177.

525. Lemaître, C. and E. Soutoglou, *Double strand break (DSB) repair in heterochromatin and heterochromatin proteins in DSB repair.* DNA repair, 2014. **19**: p. 163-168.

526. Czerwińska, P., S. Mazurek, and M. Wiznerowicz, *The complexity of TRIM28 contribution to cancer.* Journal of biomedical science, 2017. **24**(1): p. 1-14.

527. Qi, Z.-X., et al., *TRIM28 as an independent prognostic marker plays critical roles in glioma progression.* Journal of neuro-oncology, 2016. **126**(1): p. 19-26.

528. Diets, I.J., et al., *TRIM28 haploinsufficiency predisposes to Wilms tumor.* International journal of cancer, 2019. **145**(4): p. 941-951.

529. Yokoe, T., et al., *KAP1 Is Associated With Peritoneal Carcinomatosis in Gastric Cancer.* Annals of Surgical Oncology, 2010. **17**(3): p. 821-828.

530. Addison, J.B., et al., *KAP1 promotes proliferation and metastatic progression of breast cancer cells.* Cancer Res, 2015. **75**(2): p. 344-55.

531. Herquel, B., et al., *Transcription cofactors TRIM24, TRIM28, and TRIM33 associate to form regulatory complexes that suppress murine hepatocellular carcinoma.* Proc Natl Acad Sci U S A, 2011. **108**(20): p. 8212-7.

Articles in Annex

During my PhD I was given opportunity to collaborate with an exceptional PhD student Dr. Suryasree Subramania from the laboratory of Dr. Marc-Étienne Huot on the article entitled "**SAM68 interaction with U1A modulates U1 snRNP recruitment and regulates *mTor* pre-mRNA splicing**". This work allowed me to expand my technical expertise into RNA and using radioactivity.

https://academic.oup.com/nar/article/47/8/4181/5320378

Also in the annex are PDF copies of the articles in Chapters 1, 2, and 3:

Emerging roles of eraser enzymes in the dynamic control of protein ADP-ribosylation–

https://www.nature.com/articles/s41467-019-08859-x

Poly (ADP-ribose) polymerase-1 antagonizes DNA resection at double-strand breaks –

https://www.nature.com/articles/s41467-019-10741-9

Assessment of Global DNA Double-Strand End Resection using BrdU-DNA Labeling coupled with Cell Cycle Discrimination Imaging –

https://www.jove.com/t/62553/assessment-global-dna-double-strand-end-resection-using-brdu-dna

Published online 15 February 2019

Nucleic Acids Research, 2019, Vol. 47, No. 8 4181–4197
doi: 10.1093/nar/gkz099

SAM68 interaction with U1A modulates U1 snRNP recruitment and regulates *mTor* pre-mRNA splicing

Suryasree Subramania[1,2], Laurence M. Gagné[1,2], Sébastien Campagne[3], Victoire Fort[1,2], Julia O'Sullivan[1,2], Karel Mocaer[1], Miki Feldmüller[3], Jean-Yves Masson[1,2], Frédéric H.T. Allain[3], Samer M. Hussein[1,2] and Marc-Étienne Huot[1,2,*]

[1]Centre de recherche du CHU de Québec-Université Laval (axe Oncologie), Québec, QC G1R 3S3, Canada, [2]CRCHU de Québec – Axe Oncologie, Québec, QC G1R 3S3, Canada and [3]Institute of Molecular Biology and Biophysics, Department of Biology, ETH Zurich, CH-8093 Zurich, Switzerland

Received November 17, 2017; Revised January 14, 2019; Editorial Decision February 04, 2019; Accepted February 05, 2019

ABSTRACT

Src associated in mitosis (SAM68) plays major roles in regulating RNA processing events, such as alternative splicing and mRNA translation, implicated in several developmental processes. It was previously shown that SAM68 regulates the alternative splicing of the mechanistic target of rapamycin (*mTor*), but the mechanism regulating this process remains elusive. Here, we report that SAM68 interacts with U1 small nuclear ribonucleoprotein (U1 snRNP) to promote splicing at the 5′ splice site in intron 5 of *mTor*. We also show that this direct interaction is mediated through U1A, a core-component of U1snRNP. SAM68 was found to bind the RRM1 domain of U1A through its C-terminal tyrosine rich region (YY domain). Deletion of the U1A-SAM68 interaction domain or mutation in SAM68-binding sites in intron 5 of *mTor* abrogates U1A recruitment and 5′ splice site recognition by the U1 snRNP, leading to premature intron 5 termination and polyadenylation. Taken together, our results provide the first mechanistic study by which SAM68 modulates alternative splicing decision, by affecting U1 snRNP recruitment at 5′ splice sites.

INTRODUCTION

Alternative splicing is a highly regulated event requiring an impressive amount of ribonucleoprotein complexes and associated factors (1,2). In this process, intervening sequences are excised out from nuclear pre-messenger RNA (pre-mRNA) by the macromolecular machinery called the spliceosome (3). The recognition of the 5′ splice sites by U1 small nuclear ribonucleoprotein (U1 snRNP) defines the initial stages of spliceosome assembly. U1 snRNP along with U2, U4, U5 and U6 snRNPs forms the major spliceosome, the core machinery that catalyzes splicing reactions in eukaryotes (4). Although core spliceosomal assembly and its catalytic activity are rather well defined, an increasing number of accessory spliceosomal proteins modulate its activity and specificity, thereby making alternative splicing a highly regulated process (5). The main challenge for efficient intron splicing is the recognition of the 5′ and 3′ splice sites. This is mainly achieved by U1 snRNP (6,7), U2 snRNP and U2AF (8,9). These spliceosome components drive the assembly of the formation of the early spliceosome called complex E (10,11). Now it is well known that regulatory factors can bind sequences neighboring the 5′ splice site to prevent or promote U1 snRNP binding (12). Increasing evidence highlight the importance of RNA-binding proteins in facilitating U1 snRNP recognition of 5′ splice sites and regulating alternative and constitutive splicing. These include FUS (13,14), SF2 (15,16), TIA-1 (17), RBM24 (18), hnRNPs (19,20) and SAM68 (21–24).

Src associated in mitosis of 68 kDa (SAM68), a 443-amino acid polypeptide, belongs to the signal transduction and activation of RNA family of RNA-binding proteins (RBPs) and was identified as a substrate of phosphorylation by c-SRC during mitosis and cellular transformation (25,26). SAM68 was shown to be able to bind mRNA (27), as well as DNA, upon its methylation (28). The multi-functionality of SAM68 can be rightly attributed to its modular organization. The RNA binding activity of SAM68 is confined to its highly conserved GSG (GRP33/SAM68/GLD-1) domain, comprising of hnRNP K homology (KH) domain flanked on its N terminus by 80 amino acids (NK) and its C-terminus of 30 amino acids (CK), respectively (29,30). It has been demonstrated by X-ray crystallography that the NK region is required for the RNA-dependent homodimerization of SAM68 (31). In addition, SAM68 has six proline rich sequences on either side of GSG domain along with a tyrosine rich C-terminus that were shown to be targeted by various signaling pathways (32–34). The tyrosine phosphorylation of SAM68 as well as its interaction with SH2 binding proteins has been shown to

*To whom correspondence should be addressed. Tel: +418 525 4444(Ext. 14552); Fax: +418 69 5439; Email: marc-etienne.huot@crchudequebec.ulaval.ca

impair its affinity for RNA (23,33). Thus, SAM68 is a versatile adaptor and nucleic acid docking protein whose activity is modulated by cell signaling.

SAM68 is known to bind single-stranded U/A-rich mRNA molecules, mainly through U(U/A)AA repeats (35). The RNA-binding activity of SAM68 was shown to be involved in various aspects of mRNA processing including alternative splicing (29). This was initially shown following ERK1/2 signaling pathway activation, which promoted a SAM68-induced inclusion of the variable exon5 in CD44 (24,33). SAM68 has been involved in the alternative splicing of mRNAs implicated in neurogenesis (36,37), adipogenesis (21,38–40), spermatogenesis (41,42) and epithelial-to-mesenchymal transition (43). SAM68 regulated alternative splicing was further highlighted with *SMN2* (44), *BCL-x* (22), *Cyclin D1* (22) and *mTor* (21) pre-mRNA transcripts. While the mechanisms underlying the splicing of SMN-2, BCL-x and Cyclin D1 are becoming clearer, the mechanism regulating SAM68-induced alternative splicing of *mTor* pre-mRNA remains elusive.

mTOR is a central regulator of cell homeostasis, growth, proliferation and survival (45). Its dysregulation occurs in many human diseases such as cancer, obesity, Type 2 diabetes and neurodegeneration (45,46). Hence, it is crucial to understand the mechanism of SAM68 regulated *mTor* pre-mRNA splicing. Using the *Sam68*$^{-/-}$ mouse as models, we had previously unveiled a novel role of SAM68 in driving alternative splicing of *mTor* pre-mRNA (21). We found that impairing SAM68 binding to its target elements found near the 5′ splice site of intron 5 decreases the expression of full-length *mTor* mRNA by increasing intron 5-induced premature termination leading to the production of a shorter mRNA termed $mTor_{i5}$, with no detectable protein product. The production of $mTor_{i5}$ is increased in *Sam68*$^{-/-}$ mouse tissues indicating that SAM68 mediates the balance between both isoforms. As a result, *Sam68*$^{-/-}$ mice have decreased mTOR protein levels and attenuated mTORC1 and mTORC2 activities. RNA-binding assays determined that SAM68 binds multiple U/A-rich sequences distributed throughout intron 5 and enhances splicing at the upstream exon/intron junction (21). These observations suggest that SAM68 has the ability to regulate an important *mTor* pre-mRNA alternative splicing checkpoint, though the underlying mechanism remains unknown.

Here, we investigated the mechanism by which SAM68 modulates *mTor* pre-mRNA splicing. First, we found that SAM68 was detected in the immunoprecipitates of the core components of U1 snRNP, namely U1A and U1–70K. Reciprocal immunoprecipitation with Flag-tagged SAM68 showed enrichment of U1 snRNP. Concomitantly, purified recombinant SAM68 can capture U1 snRNP through direct interaction with U1A. Domain mapping experiments revealed that the tyrosine rich C-terminal region of SAM68 (YY domain) was sufficient to interact with U1A. Using endogenous RNA immunoprecipitation assays, we found that SAM68 can recruit U1 snRNP to the 5′ splice site of *mTor* intron 5. Thus, these results provide the first mechanistic insight on how SAM68 regulates *mTor* pre-mRNA alternative splicing and could unveil a broader regulatory function of SAM68-mediated 5′ splice site recognition.

MATERIALS AND METHODS

Plasmid constructions

pGEX-6P3-*SAM68*-Flag and pGEX-6P3-*Sam68*-Flag were constructed by inserting full-length human and mouse *SAM68* coding sequence (cds) into pGEX-6P3 (GE Healthcare) with N-terminal GST tag, a PreScission protease cleavage site (see below 'Protein purification and GST pulldown' section) between GST and SAM68. Due to the high sequence homology between human and mouse *SAM68*, both constructs were produced using EcoRI-*SAM68*-F and NotI-*SAM68*-R. Flag tag was then inserted at the C-terminus of *SAM68* by annealing the oligos, SacI-Flag-F and SacI-Flag-R, and inserting the adaptor at SacI sites of the plasmid. pGEX-6P2-U1A-His was generated by inserting U1A cds, obtained by polymerase chain reaction (PCR) from HEK-293T total cDNA using EcoRI-U1A-F and SalI-U1A-R at EcoRI-SalI sites. cDNA was amplified from total RNA of HEK-293T using Superscript VILO Master mix (Invitrogen). pGEX-6P2-U1C-His was sub-cloned by PCR from pGEX-2TK-U1C using EcoRI-U1C-F and XhoI-U1C-R and inserted at EcoRI-XhoI sites. pGEX-6P2-U1–70K was sub-cloned by PCR from pINTO-NSA:hSNRNP70 using EcoRI-U1–70K-F and XhoI-U1–70K-R and inserted at EcoRI-XhoI sites. pcDNA-Flag-*SAM68* and pcDNA-Flag-*Sam68* were constructed by inserting corresponding cds, obtained by PCR from pGEX-6P3-*SAM68*-Flag and pGEX-6P3-*Sam68*-Flag using EcoRI- *SAM68*-F and NotI- *SAM68*-R at EcoRI-NotI sites.

pcDNA-Flag-$SAM68_{I184N}$ and pcDNA-Flag-$SAM68_{V229F}$ were generated by swapping the 679 bp, AgeI-XbaI fragment from pcDNA mCherry-$SAM68_{I184N}$ and pcDNA mCherry-$SAM68_{V229F}$, respectively, to pcDNA-Flag-*SAM68* WT. pcDNA-Flag-*SAM68*-Nter and pEGFP-*Sam68*-Nter were generated by deletion PCR with *SAM68*-F and *SAM68*-Nter-R primers using pcDNA-Flag-*SAM68* and pEGFP-*SAM68* as templates, respectively. pcDNA-Flag-*SAM68*-Cter was generated from pcDNA-Flag-*SAM68* by PCR using EcoRI-*SAM68*-Cter-F and NotI-*SAM68* Cter-R and cloning the amplicon at EcoRI-SalI sites of pEGFP-C1. pEGFP-C1-*SAM68*-C1 was obtained by deletion PCR using *SAM68*-F and *SAM68*-C1-R, respectively. pEGFP-*SAM68*-C2 to C5 were generated by cloning the PCR amplicons obtained using the reverse primer, SalI-*SAM68*-R and forward primers namely EcoRI-*SAM68*-C2, C3, C4, C5 at EcoRI-SalI sites of pEGFP-C1. pEGFP-*SAM68*-NLS was obtained by deletion PCR using EcoRI-*SAM68*-NLS-F and EcoRI-*SAM68*-NLS-R. pLKO-sh*SAM68* was generated by annealing and inserting the oligos, sh*SAM68*-F and sh*SAM68*-R, at AgeI-EcoRI restriction sites of pLKO.1 (Addgene plasmid #8453). Primer sequences and generated plasmid are listed in supplementary Table S1.

Antibodies, western blotting and immunoprecipitation

The following antibodies were used in this study: anti-Flag (1:2000, 2368S, Cell Signaling Technology), anti-U1–70K (1:1000, 05–1588, EMD-Millipore), anti-U1A (1:1000, ab55751, abcam), anti-U1C (1:1000, ab192028, Abcam),

anti-SAM68 (1:2000, AD-1, gift from Dr Stéphane Richard), anti-GAPDH (1:2000, MM-0163-P, Médimabs), anti-mTOR (1:1000, 2983S, Cell Signaling Technology), beta-actin (1:1000, 8457L, Cell Signaling Technology), anti-GFP (1:2000, ab290, Abcam) and anti-His (1:1000, 12698S, Cell Signaling Technology). Endogenous immunoprecipitation was done by immobilizing anti-U1–70K, anti-U1A or control IgG-Mouse (Santa Cruz Biotechnology, sc-2025) on Protein A/G PLUS-Agarose beads (Santa Cruz Biotechnology, #sc-2003). HEK-293T cells were harvested, lysed for 10 min at 4°C in 1× phosphate-buffered saline (PBS), pH 7.4, 1% Triton-X-100, 150 mM NaCl, RNaseA (10 mg/ml; Sigma, #R5503) and 1× protease inhibitor complete ethylenediaminetetraacetic acid (EDTA)-free (Roche). The cell lysates were sonicated five times for 30 s with a Bioruptor ultrasonic cell disruptor and centrifuged at high speed for 30 min at 4°C to remove cell debris. For endogenous immunoprecipitation, the respective antibodies conjugated to Protein-A/G PLUS-Agarose beads (Santa Cruz Biotechnology, sc-2003) were added to pre-cleared cell lysates. Following 1 h at 4°C, the beads were washed several times with lysis buffer and the immunoprecipitates were eluted with Laemmlli buffer. Flag-tagged proteins were immunoprecipitated with Flag-M2 affinity beads (Sigma, #A2220). GFP-tagged proteins were immunoprecipitated with homemade GFP-Trap-A beads.

RNA immunoprecipitation and RT-PCR

RNA from 50% of the Flag-*Sam68* and Flag-YFP immunoprecipitates was isolated using TRIzol™ Reagent (Invitrogen, #15596–018) and reverse transcribed using SuperScript™ VILO™ MasterMix (Invitrogen, #11755–050) or M-MuLV reverse transcriptase, according to the manufacturer's instructions. Extracted RNA was incubated with random hexamers, oligo-dT or gene-specific primer for first strand cDNA synthesis at 25°C for 10 min, 42°C for 1 h and 85°C for 5 min. One-fifth of the reaction product was amplified for U1snRNA transcript using U1snRNA-F and U1snRNA-R primers and GAPDH mRNA using GAPDH-F and GAPDH-R primers, respectively. Primer sequences are listed in Supplementary Table S1.

RNA-binding assay

Purified SAM68 or U1A (stored in 20 mM Tris–HCl, pH 7.4, 200 mM NaCl, 10% Glycerol, 1 mM dithiothreitol) was added at the indicated concentration to a mix containing 10 nM of ^{32}P-labeled U1 snRNA in 1× RNA binding buffer (50 mM Tris–Cl, pH 7.6, 200 mM potassium acetate, 5 mM $MgCl_2$, 2.5 mM dithiothreitol) supplemented with 0.25 µl of RNasin Ribonuclease Inhibitor. The mix was incubated at room temperature for 15 min, then complexes were fixed with 0.5% glutaraldehyde for 10 min at room temperature. The samples were loaded onto a 5.5% Tris/Borate/EDTA (TBE) 1× acrylamide (29:1) gel and run at 150 V for 2 h and 30 min at 4°C, dried onto DE81 filter paper, then visualized by autoradiography. Quantifications were performed on a FLA-5100 phosphorimager system (Fujifilm), and statistics were analyzed with Prism.

Protein purification and GST pulldown

Competent *Escherichia coli* BL21 DE3 Codon plus RP strain (Stratagene, Agilent technologies # 230255) were transformed with pGEX-6p3-*SAM68*-flag, pGEX-6p3-*Sam68*-flag, pGEX-6p3-*SAM68*-Nter, pGEX-6p3-Cter, pGEX6p2-U1A-His, pGEX6p2-U1–70k-His, pGEX6p2-U1C-His and empty vectors, namely pGEX6p3-flag and pGEX-6p2-His, respectively. Single colony of each construct was then grown in LB media at 37°C until desired density and then induced with 0.3 mM isopropyl B-D_l-thiogalactopyranoside (IPTG) at 30°C overnight. Bacterial pellets were collected and lysed with 50 mM Tris–Cl, pH 7.5, 1% Triton-X-100, 200 mM NaCl, 20% glycerol, 5 mM $MgCl_2$, 1 mM dithiothreitol (DTT) for 30 min, sonicated and centrifuged at 17 000 *g* for 30 min 4°C. GST fusion proteins were bound to 500 µl of washed and equilibrated Glutathione agarose beads (Sigma, #G4510). For GST-SAM68-flag, the GST-tag was removed by 20 units of PreScission Protease (2U/µl; GE Healthcare, #27-0843-01) at 4°C overnight in 50 mM Tris-HCl, pH 7.0, 150 mM NaCl, 1 mM EDTA, 1 mM DTT. Following this step, SAM68-flag was immunoprecipitated with flag-M2 affinity beads (Sigma, #A2220) for 1 h at 4°C, eluted with 9 µg of 3X FLAG® Peptide (4 mg/ml; Sigma, #F4799), and pooled elutes were dialyzed in 1× PBS, 200 mM NaCl, 0.05% Triton-X-100, 20% glycerol. Aliquots of the preparation were run on sodium dodecylsulphate-polyacrylamide gel electrophoresis (SDS-PAGE) and stained with Coomassie Brilliant Blue to validate preparation purity (Supplementary Figure S1).

For the NMR part of this study, GB1-hSAM68 (C2), GB1-U1A (1-282), U1A linkerRRM2 (156–282) and U1A RRM1 (1-126) were expressed under the control of lactose inducible promoters in *E-coli* BL21 DE3 at 37°C during 4 h in presence of 1 mM IPTG. To achieve isotope labeling, cells were grown in M9 minimal medium complemented with ^{15}N-NH_4Cl and/or ^{13}C-glucose. Bacterial pellets were re-suspended in buffer A (10 mM HEPES, pH 7.6, 500 mM NaCl, 0.5 M Urea, β-mercapto-ethanol 2.8 mM) in the presence of lysozyme and DNAse I (0.01 mg/ml each). Cells were lysed using a microfluidizer by five cycles at 15 000 psi and the lysates were clarified by centrifugation (30 000 *g*, 40 min). Proteins were then purified using Ni^{2+}-affinity chromatography and eluted with a gradient of imidazole. The C-terminal histidine tag of U1A RRM1 and U1A RRM2 were cleaved by thrombin (10 U/mg of purified protein, 6 h at room temperature in buffer A), while GB1-hSAM68 (C2) and GB1-U1A were kept as fusion proteins. All the proteins were further purified by size exclusion chromatography in 10 mM sodium phosphate, pH 6.8, NaCl 50 mM.

For GST pulldown, 300 ng of purified recombinant hSAM68-Flag was incubated with 150 ng of glutathione bound GST-tagged U1–70K-His, U1A-His, U1-C-His or with negative control GST-His in binding buffer (50 mM Tris, pH 7.5, 200 mM NaCl, 10% glycerol, 0.5% Triton-X-100, 10 mg/ml RNaseA), supplemented with 1× protease inhibitor complete EDTA-free (Roche). The reaction volume was made upto 300 µl in total and incubated for 1 h at 4°C. Beads were washed and bound proteins were resolved by SDS-PAGE and analyzed by western blot.

Biotinylated probes synthesis and RNP pulldown

Intron 5 baits with and without 5′ splice sites and either Wild-Type (WT) or Mutated (Mut) SAM68-binding sequence were cloned in pcDNA-Neo. The baits were *in vitro* transcribed from EcoRI linearized plasmids using T7-Hi-Scribe kit (Invitrogen) according to manufacturer's instructions. After DNaseI treatment, the reaction mixtures were column purified and 3′ end labeled with UTP-Biotin (Roche) with poly-U-polymerase according to manufacturer's instructions. Baits were immobilized on streptavidin agarose beads and were washed three times with binding buffer (20 mM HEPES, pH 7.9, 200 mM NaCl, 10% glycerol, 0.5% Triton-X-100, RNase inhibitor, 1× protease inhibitor). The beads were blocked with 100 μg/ml of bovine serum albumin for 30 min at 4°C and washed again in binding buffer. Immobilized baits were incubated with 1 μg of either purified SAM68-Flag or GST-Flag for 30 min at 4°C, then sh*SAM68* HEK-293T cell lysates were added for 1-h incubation at 4°C. Beads were washed in binding buffer and the retained proteins were eluted in Laemmli buffer, run on SDS-PAGE gels and blotted using Flag and U1A antibodies.

NMR spectroscopy

NMR data were recorded at 313 K using the 500 MHz Avance III or the 600 MHz Avance III (Bruker), both equipped with cryo-probe. Data were processed with Topspin (Bruker) and analyzed with CARA. Sequential assignment of hSAM68(C2) was deduced from the analysis of classical triple resonance experiments (3D HNCACB, 3D CACB(CO)NH, 3D HNCO and 3D HN(CA)CO). Uniformly ^{15}N labeled GB1-hSAM68 (C2) was titrated with unlabeled GB1-U1A, U1A RRM1 (1-126) or U1A linker-RRM2 (156–282) and the formation of the binary complexes was monitored by measuring 2D ^{15}N-^{1}H HSQC spectra after each addition. Reverse NMR titrations of uniformly ^{15}N labeled U1A versions by unlabeled GB1-SAM68 (C2) were performed using a similar strategy. Chemical shift perturbations were plotted onto the surface representation of the structure of the free form of the RRM1 of U1A (47).

In vitro Xrn-1 protection assay

XbaI linearized pcDNA 3.1-mTor minigene plasmid was used for *in vitro* transcription. Plasmid DNA templates were eliminated by DNaseI treatment followed by column purification of the RNA template. RNA templates were either used directly for 5′ Xrn-1 exonuclease assay or 3′ end labeled with poly-UTP-biotin using poly-U-polymerase and bound to streptavidin agarose beads. Streptavidin-bound RNA templates were incubated with WT MEFs cell extracts or Sam68$^{-/-}$ MEFs cell extracts supplemented with either *in vitro* purified GST-Flag or mSAM68-Flag for 30 min at 4°C in binding buffer (10 mM Tris–HCl, pH 7.9, 10 mM $MgCl_2$, 50 mM NaCl, 0.5% Triton-X-100, 1 mM DTT). 5′ monophosphate RNA templates were generated by treating with RNA 5′ pyrophosphohydrolase or RppH (5000 U/ml, New England Biolabs, M0356S) for 1 h at 37°C in reaction buffer (50 mM NaCl, 10 mM Tris–HCl, pH 7.9, 10 mM $MgCl_2$, 1 mM DTT). The 5′ monophosphate RNA transcripts were then treated with 1U of Xrn-1 (1000 U/ml, NEB, M0338L) for 1 h at 37°C in reaction buffer. The reaction was stopped by heating at 70°C for 10 min. cDNA was amplified using primer RRT and amplicon corresponding to full-length bait was produced using forward (FSS) and reverse (RSB) primers while mSAM68 protected amplicon was produced using forward (FSB) and reverse (RSB) primers.

RNA immunoprecipitation (RIP)

RNA immunoprecipitation (RIP) assays were performed using a modified CLIP protocol (48). Nuclear fraction was isolated and lysed in 1× PBS, pH 7.4, 150 mM NaCl, 1% Triton-X-100, 0.5% sodium deoxycholate, 0.1% SDS, protease inhibitor cocktail for 30 min on ice. The extracts were treated with DNase I (10 U/μl, Roche, Cat. No. 04716728001) and RNase A (10 mg/ml, Sigma, R-4875) for 1 h at 4°C under rotation. The samples were diluted in binding buffer (1× PBS, pH 7.4, 150 mM NaCl, 1% Triton-X-100) and supplemented with RNase inhibitor. Samples were precleared and 10% of were saved for inputs, while the rest were used for immunoprecipitation using anti-U1A antibody (Abcam, mab55751) or rabbit IgGs (Jackson Immuno Research, 011–000-003). The inputs and immunoprecipitated samples were treated with 50 μg Proteinase K for 30 min at 65°C. RNA was then isolated and used for RT-qPCR analyses that were performed using primers ei5-F and ei5-R for exon5–intron 5 junction, ei4-F and ei4-R for exon4–intron4 junction and ei37-F and ei37-R for exon37–intron37 junction.

In vivo splicing assays

Endogenous *mTor* transcript premature termination and polyadenylation in wild-type (WT) mouse embryonic fibroblasts (MEFs) and *Sam68*$^{-/-}$ MEFs were rescued using lentivirus-mediated transduction of mouse *Sam68(*WT) or mouse *Sam68*(ΔARM). Total RNA was extracted using TRIzol® reagent and digested with DNase I to get rid of contaminating genomic DNA. After column purification, cDNA was amplified by reverse transcription using oligo-dT and M-MuLV reverse transcriptase. The following pairs of primers were used F(e4) and R(i5) to amplify $mTor_{i5}$ and F(e4) and R(e6) to amplify $mTor_{Exon4-6}$. A portion of cell lysates were resolved in SDS-PAGE and blotted with mTOR, SAM68 and GAPDH antibodies.

mTor genomic fragment spanning from exon4 to exon6 with corresponding introns 4 and 5 was cloned in pcDNA Neo and referred to as $mTor_{Exon4-6}$ minigene, hereafter. sh*SAM68* HEK-293T cells were co-transfected with $mTor_{Exon4-6}$ minigene and either Flag-YFP, Flag-h*SAM68*-WT or Flag-h*SAM68*ΔARM. Forty-eight hours post-transfection, total RNA was extracted using Trizol® reagent and digested with DNase I to get rid of contaminating plasmid DNA. After column purification, cDNA was amplified by reverse transcription with random hexamers using Superscript VILO according to manufacturer's instructions. Cell lysates were resolved in SDS-PAGE and

blotted with Flag and β-actin antibodies. To identify splicing patterns derived from the reporter ($mTor_{Exon4-6}$ minigene), we used the following primers: F2; T7 Forward and R2; exon4 Reverse to amplify the total RNA produced from $mTor_{Exon4-6}$ minigene. F1; exon4 Forward and R1; intron 5 Reverse were used to amplify intron 5 retained minigene transcripts. Primer pairs GAPDH-F and GAPDH-R were used to amplify *GAPDH* mRNA. Primer sequences are listed in Supplementary Table S1.

RESULTS

SAM68 interacts with U1 snRNP

As aforementioned, mSAM68 depletion causes an increase in the rate of *mTor* intron 5-induced premature termination, resulting in the production of a non-translated smaller mRNA, termed $mTor_{i5}$ (21,40). Analysis of the intron 5 shows the presence of two stretches of high-affinity SAM68 U/A binding elements located near the upstream 5′ splice site, one of which is embedded in a cryptic polyadenylation signal (Figure 1A). This suggests that SAM68 association with these U/A rich sequences could facilitate 5′ splice site recognition and promote normal splicing of intron 5. Hence, we reasoned that SAM68 could be interacting with the U1 snRNP, the spliceosomal component that recognizes the 5′ splice site, and thus be a determining factor for early spliceosome assembly within *mTor* intron 5 (4). While the initial discovery was observed in mice, we reasoned that any SAM68–U1 interaction would also be observed in human cells, as human SAM68 (hSAM68) is almost identical to mouse SAM68 (mSAM68).

To validate if SAM68 could interact with U1 snRNP, flag-tagged hSAM68 (flag-hSAM68) was expressed in HEK-293T cells depleted of endogenous *SAM68* using lentiviral-shRNA targeting the 3'UTR of *SAM68* mRNA (sh*SAM68* HEK-293T) (Supplementary Figure S2A). Flag-tagged yellow fluorescent protein (flag-YFP) was used as negative control. Western blot analyses showed that the three core protein components of U1 snRNP, namely U1–70K, U1A and U1C, efficiently co-immunoprecipitated with Flag-hSAM68, while undetected in Flag-YFP controls (Figure 1B). RIP followed by RT-PCR using primers specific to U1 snRNA and GAPDH mRNA showed that U1 snRNA only co-immunoprecipitated in the presence of Flag-hSAM68, confirming that the U1 snRNP could be associated with hSAM68 (Figure 1B). This interaction was further validated endogenously, since U1 snRNP component U1A co-immunoprecipitated, with SAM68 (Supplementary Figure S2B). Concomitantly, hSAM68 was efficiently immunoprecipitated with endogenous U1–70K and U1A as compared to control immunoglobulin G (IgG) (Figure 1C and D).

Interaction of SAM68 with U1 snRNP is RNA independent

Given that SAM68 is an RNA-binding protein, we first assessed if the SAM68-U1 snRNP interaction was mediated through U1 snRNA. Sequence analyses showed the presence of a potential SAM68-binding site (AUAAUUU) upstream and partially within the Sm domain (49). We tested and compared the affinity of both Sam68 and U1A to the U1 snRNA. While SAM68 can indeed bind U1 snRNA, it showed minimal affinity for this RNA when compared to U1A, a *bona fide* U1 associated protein (Figure 1F and G). Considering that SAM68 has numerous preferential RNAs targets (21,27,50) and its low affinity for the U1 snRNA (Figure 1F), it would be highly unlikely that its association with the U1 snRNP is mediated by U1 snRNA.

To identify which protein component of the U1 snRNP mediates this interaction, recombinant hSAM68-Flag were incubated with cell extracts from sh*SAM68* HEK-293T cells in the presence or absence of RNase A. Treatment with RNAse A had no effect on SAM68 association with U1 snRNP core components even though total RNA was completely digested, suggesting that SAM68 captures U1 snRNP independent of RNA (Figure 2A). However, U1 snRNPs were previously shown to resist RNaseA treatment, due to a compacted conformation (51). Therefore, these results do not exclude the possibility that tight association between U1 snRNP and SAM68 could also protect RNA mediating their interaction from enzymatic digestion. To demonstrate that this interaction was indeed RNA independent, we transfected sh*SAM68* HEK-293T with an RNA-binding deficient mutant of SAM68 (*Flag-*$hSAM68_{I184N}$) (36,52). This mutant was still able to co-immunoprecipitate U1 snRNP, further confirming that this interaction is not mediated through RNA but through protein–protein interactions (Figure 2B). This result was corroborated with another RNA-binding deficient mutant of SAM68 (Flag-$hSAM68_{V229F}$) (23) (Supplementary Figure S2C).

SAM68 interact with the U1 snRNP component U1A

To identify which of the core components of U1 snRNP had more affinity for SAM68, we first performed a salt sensitivity test strategy previously shown to disrupt U1 core proteins from the U1 snRNA, therefore disrupting the complex (53). Flag pulldown of purified hSAM68-Flag incubated with sh*SAM68* HEK-293T cell lysate were washed with buffer containing increasing salt concentration. Residual association between U1 snRNP proteins and Sam68 was then detected by Western blot (Figure 2C). We found that only U1A remained bound to hSAM68-Flag at salt concentration exceeding 300–400 mM of NaCl, while both U1–70K and U1C dissociate from the complex at a concentration of 200–250 mM NaCl. This result suggested that the interaction between SAM68 and U1 snRNP may be mediated by U1A. To address this, we incubated purified recombinant GST tagged U1A-His, and as controls U1C-His and U1–70K-His with the aforementioned purified hSAM68-Flag. Using these *in vitro* purified proteins, we confirmed that only GST-U1A-His could efficiently pulldown hSAM68-Flag, while both GST-U1C-His and GST-U1–70K-His as well as the negative control (GST-His) failed to pull down hSAM68-Flag (Figure 2D). Furthermore, U1A-His was still bound to hSAM68-Flag in the presence of micrococcal nuclease (MNAse), a non-specific endo-exonuclease that degrades both DNA and RNA, further demonstrating a direct interaction between both proteins, which is not mediated by nucleic acids (Supplementary Figure S2D).

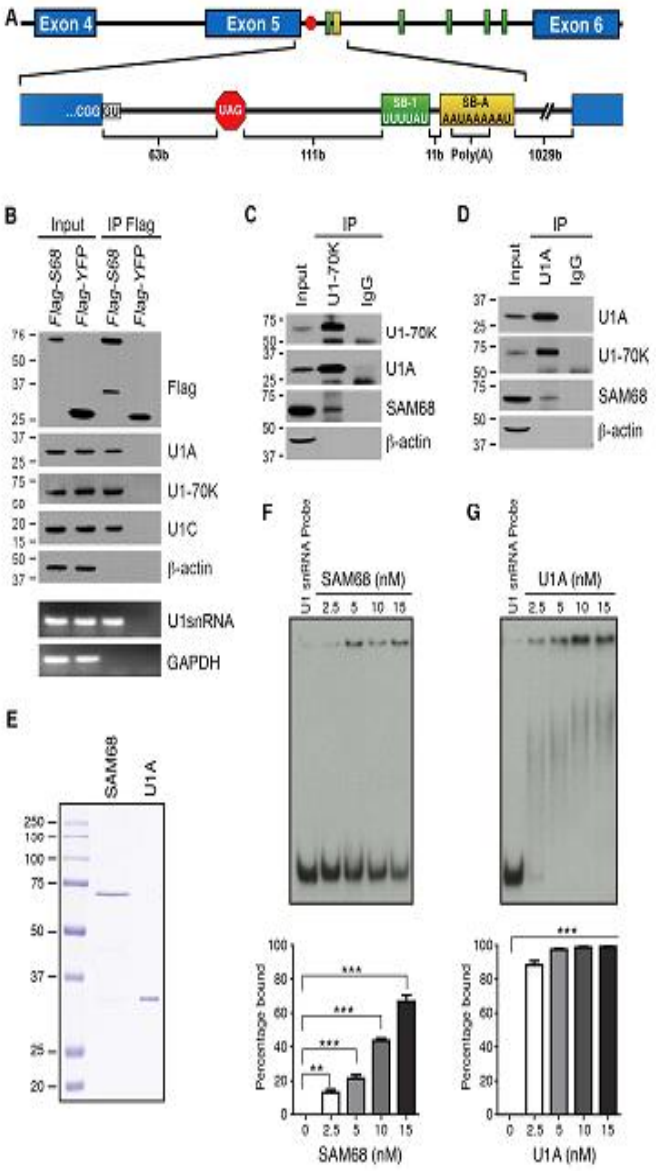

Figure 1. *In vivo* association of SAM68 with U1 snRNP. (A) Schematic representation of a portion of *mTor* pre-mRNA spanning from exon4 to exon6 (upper panel), with a close-up of the 5′ splice site and the subsequent SAM68-binding site (SB-1), as well as the cryptic polyadenylation signal that harbor SAM68-binding site (SB-A). (B) Co-immunoprecipitation of U1 snRNP with Flag-hSAM68. HEK-293T cells depleted of endogenous SAM68 (sh*SAM68* HEK-293T) were transiently transfected with Flag-hSAM68 or Flag-YFP (yellow-fluorescent protein), the latter serving as negative control. Flag-tagged proteins were immunoprecipitated using anti-Flag M2 agarose beads and immunoprecipitated proteins were detected with antibodies specific to U1–70K, U1A and U1C. β-Actin was used as negative control. Portion of the Flag-immunoprecipitates was used for RNA isolation and RT-PCR using U1 snRNA specific primers. GAPDH (glyceraldehyde 3-phosphate dehydrogenase) RNA was used as negative control of the RT-PCR made from the RNA immunoprecipitation. (C) Co-immunoprecipitation of endogenous hSAM68 with U1–70K. Immunoprecipitated proteins were detected with antibodies directed against SAM68 and U1–70K. β-Actin was used as negative control of immunoprecipitated proteins. (D) Co-immunoprecipitation of endogenous hSAM68 with U1A. Immunoprecipitated proteins were detected with antibodies directed against SAM68 and U1A. β-Actin was used as negative control of immunoprecipitated proteins. (E) Coomassie staining of purified human SAM68 and U1A. (F) RNA binding assay with purified SAM68 and labeled U1snRNA. Reactions contained 10 nM γ-p32 labeled U1snRNA in buffer with no protein (lane 1) or with purified SAM68 (lanes 2–5). Bottom panel: quantification from three independent binding experiments. Error bars represent the corresponding standard error. Unpaired two-tailed *t*-tests were used to compare the different concentrations of purified protein to the RNA only control. SAM68 *P*-values are 0.0014, 0.0005, <0.0001, <0.0001 in increasing order of SAM68 concentration. (G) RNA binding assay with purified U1A and labeled U1snRNA. Reactions contained 10 nM γ-p32 labeled U1snRNA in buffer with no protein (lane 1) or with purified U1A (lanes 2–5). Bottom panel: U1snRNA *P*-values = 0.0008, <0.0001, <0.0001, <0.0001 in increasing order of U1A concentration. ***P*-value < 0.005, ****P*-value < 0.001.

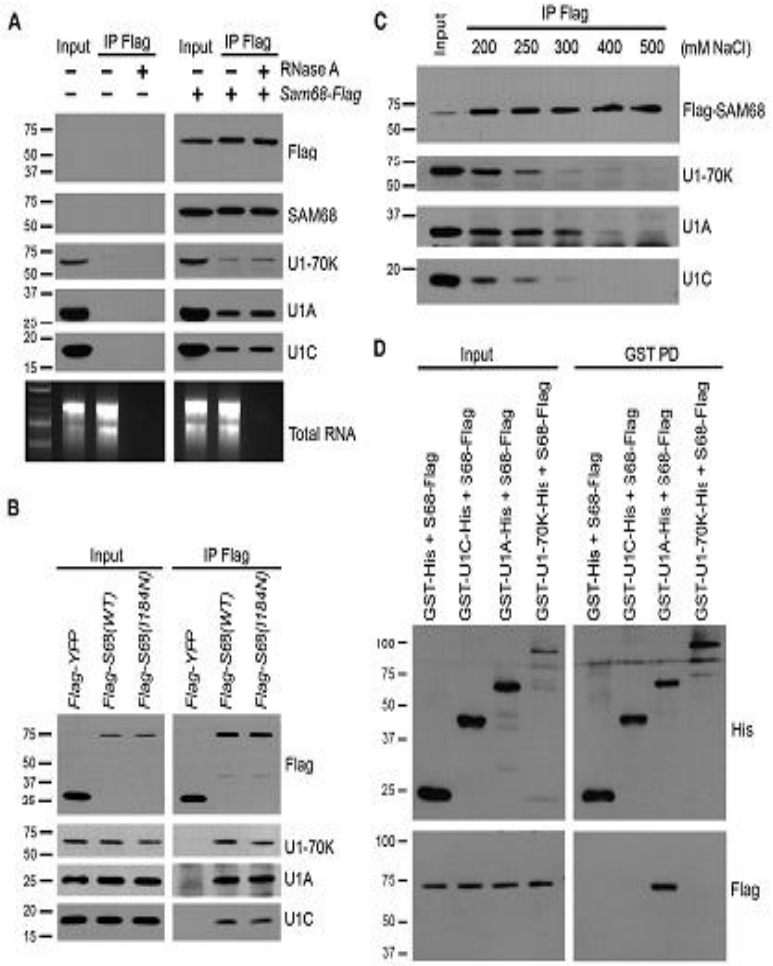

Figure 2. *In vitro* Purified SAM68 associated with U1 snRNP in an RNA-independent manner. (A) *In vitro* purified hSAM68-Flag was added to sh*SAM68* HEK-293T cell lysates for 1 h at 4°C, in the presence or absence of 50 μg/ml RNaseA. hSAM68-Flag and associated proteins were immunoprecipitated using Flag-M2 affinity beads and treated further with RNaseA at 37°C for 30 min. Bound proteins were eluted with Laemmli and immunoblotted with antibodies specific to U1–70K, U1A and U1C. To assess RNaseA treatment efficiency, total RNA from sh*SAM68* HEK-293T was treated with either Mock or RNaseA for 30 min at 37°C, and the remaining total RNA was assessed on agarose gel. (B) RNA-binding defective mutant hSAM68$_{I184N}$ interacts with U1 snRNP. sh*SAM68* HEK-293T were transiently transfected with Flag-hSAM68, Flag-hSAM68$_{I184N}$ and Flag-YFP (negative control). The Flag-tagged proteins were immunoprecipitated using anti-Flag M2 agarose beads and immunoblotted with antibodies directed against U1–70K, U1A and U1C. (C) Association of hSAM68-Flag with U1 snRNP withstands high salt washes. Purified *in vitro* produced hSAM68-Flag was added to cell lysates of sh*SAM68* HEK-293T for 1 h at 4°C. Flag-M2 affinity beads were added to the reaction and left for 1 h at 4°C. The washes were done, by increasing salt concentration, from 150 to 500 mM of NaCl. Bound proteins were eluted with Laemmli and immunoblotted with antibodies directed against U1–70K, U1A and U1C. (D) SAM68 interacts with U1A *in vitro*. About 300 ng of purified hSAM68-Flag was incubated with 100 ng of glutathione-agarose bound GST-U170k-His, GST-U1A-His, GST-U1C-His and GST-His. Following washes, the beads were washed five times in binding buffer and the bound proteins eluted with Laemmli and immunoblotted using anti-Flag or anti-His antibodies.

SAM68 interaction with U1A is mediated through its tyrosine-rich (YY) domain

Being an adaptor protein, SAM68 comprises many protein–protein interaction domains such as SH3 binding proline-rich motifs and SH2 binding tyrosine-rich domain (28). In order to determine which domain was responsible for the association with U1A, we first truncated hSAM68 in two fragments (Figure 3A). The first fragment (N-term) contains the RNA-binding domain of hSAM68, spans from amino acids 1–280 and comprises the KH domain and proline-rich motifs (P0-P2) and the hSAM68 nuclear-localization signal (NLS). The second fragment (C-term) spanning from amino acids 281–443 comprises proline-rich motifs (P3-P5), the tyrosine-rich domain (YY), the SH2-binding tyrosine residues and the hSAM68 NLS. Both fragments were Flag-tagged at their N-terminus (Supplementary Figure S3A). Both flag-tagged hSAM68 fragments (N- and C-term), along with positive control Flag-hSAM68 and

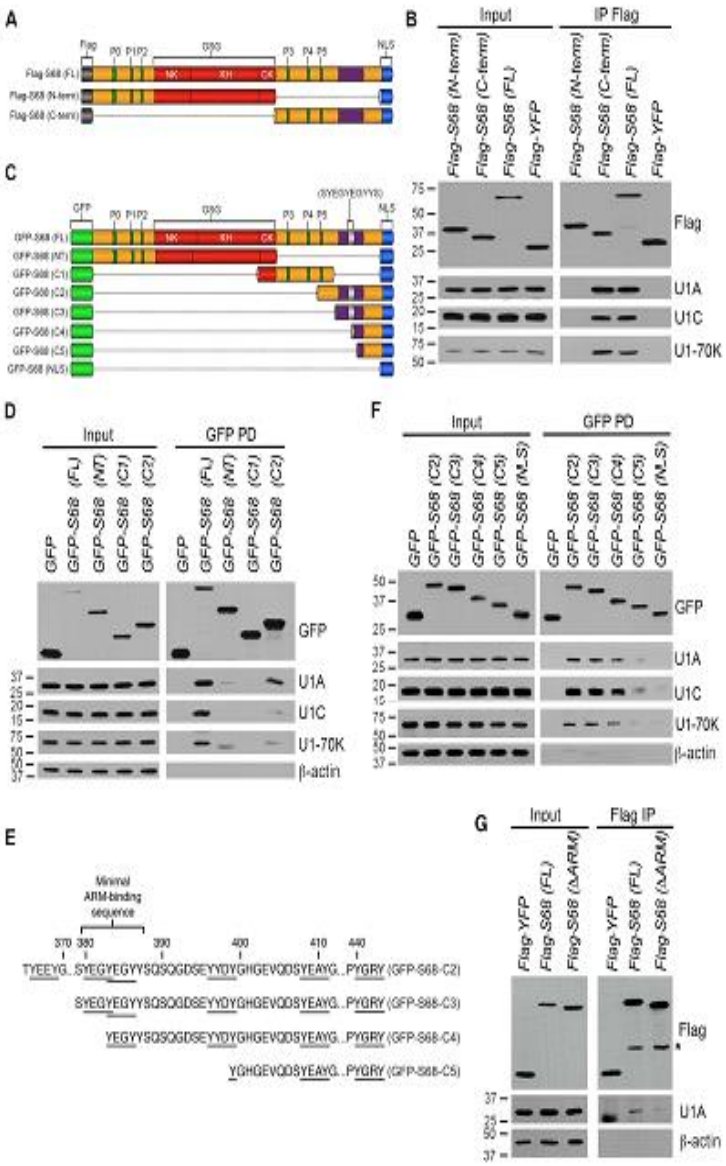

Figure 3. SAM68 interaction with U1A is mediated through its C-terminal portion. (A) Schematic representation of C-terminus (aa. 1–280) and N-terminus (aa.281–443) deletion domains of hSAM68 fused to flag. (B) sh*SAM68* HEK-293T cells were transiently transfected with Flag-*SAM68*(N-term), Flag-*SAM68*(C-term), Flag-*SAM68*(FL) and flag-YFP (negative control). Forty-eight hours post transfection, the flag-tagged proteins were immunoprecipitated using anti-flag M2 agarose beads and immunoblotted with antibodies specific to U1–70K, U1A and U1C. (C) Schematic representation of full-length SAM68, C-terminus deleted SAM68 (NT, aa. 1–280), C-terminus truncated to proline rich C1 (aa. 269–364) and tyrosine rich C2 (aa. 365–443), C3 (aa. 370–443), C4 (aa. 385–443), C5 (aa. 340–443) and NLS (aa. 430–443). Fragments were fused to GFP tag at their N-terminus and all fragments had SAM68 NLS at their C-terminus. (D) GFP-Trap-A pulldown of GFP-tagged proteins. sh*SAM68* HEK-293T cells were transiently transfected with *GFP*, *GFP-SAM68*(FL), *GFP- SAM68*(NT), *GFP- SAM68*(C1) and *GFP-SAM68*(C2). Forty-eight hours post transfection, cells were lysed and GFP-Trap-A beads were used to pull down GFP-tagged proteins, and their association with U1A was validated by western blot using specific antibodies. (E) Primary amino acid sequence of the various deletion constructs of SAM68 YY domain (GFP-hSAM68 C2 to C5). Underlined indicates YXXY motifs in the YY domain. Also highlighted is the minimal ARM-binding region. (F) GFP-Trap-A pulldown of GFP-tagged proteins. shSAM68 HEK-293T cells were transiently transfected with *GFP*, *GFP-SAM68*(C2), *GFP-SAM68*(C3), *GFP-SAM68*(C4), *GFP-SAM68*(C5) and *GFP-SAM68*(NLS). Forty-eight hours post transfection, cells were lysed and GFP-Trap-A beads were used to pull down GFP-tagged proteins, and their association with U1A was validated by western blot using specific antibodies. (G) U1A binds preferentially to the minimal ARM motif (YEGYEGY) within the YY domain of SAM68. Flag-hSAM68(FL) and Flag-hSAM68(ΔARM) were transiently transfected in sh*SAM68* HEK-293T cells. Forty-eight hours post transfection, cells were lysed and Flag-tagged proteins were immunoprecipitated using anti-flag M2 agarose beads, and U1A association was assessed using U1A antibody. ⋆: denotes an unspecific band.

negative control flag-YFP, were transfected in sh*SAM68* HEK-293T cells. Confocal images showed that while the N-terminal fragment remained largely cytoplasmic, it also partially localized to the nucleus, suggesting that the addition of the NLS allows efficient nuclear localization of the N-terminal fragment (Supplementary Figure S3A). Flag-tagged proteins were immunoprecipitated and immunoblotted with U1A antibody, while U1–70K and U1C antibodies were used as positive controls. As expected, full-length hSAM68 showed a strong association with U1 A (Figure 3B) as well as U1–70K and U1C, while they were not detected in Flag-YFP immunoprecipitates (negative control). The U1 snRNP components co-immunoprecipitated with the Flag-hSAM68 C-terminal fragment with as strong of an association as the full-length protein, but not the N-terminal fragment containing the KH RNA-binding domain (Figure 3B). While confocal immunofluorescence detection shows that the N-terminal fragment can also be located in nucleus due to the addition of the NLS (Supplementary Figure S3A), the partial cytoplasmic localization of this fragment could explain the decreased association with U1A. To assess this possibility, equal amounts of *in vitro* purified N-term and C-term fragments were immobilized and incubated with whole cell lysate taken from sh*SAM68* HEK-293T, validating our initial observation where U1A specifically binds the C-terminal fragment and not the N-terminal fragment (Supplementary Figure S3B). This result further corroborates our previous observation that the interaction is RNA-independent and implies that the SAM68 binds U1A through its C-terminal region.

To refine our mapping of the SAM68–U1A interaction, we truncated the C-terminal fragment of SAM68 into two smaller parts: GFP-hSAM68 (C1) and GFP-hSAM68 (C2) (Figure 3C). As the fragments were very short, we opted to clone them in frame with the larger, GFP-tag and performed a GFP-binding protein pulldown and as expected showed a strong nuclear localization by confocal imaging (Supplementary Figure S4A). Using these constructs, we found that like the full-length hSAM68, the C2 fragment of hSAM68 was associated with U1A, while the C1 fragment did not (Figure 3D). This initial interaction mapping suggests that the YXXY motif rich domain (YY domain) of SAM68, located in the C2 fragment (six YXXY motifs) but not C1, could be involved in the interaction with U1 snRNP. This domain consists of tyrosine-rich motifs involved in the association between SAM68 and the armadillo repeat domain (ARM) of the adenomatous polyposis coli (APC) protein (54,55). To assess the importance of this motif in the SAM68–U1A interaction, we further divided the GFP-hSAM68 (C2) domain in four different fragments with decreasing number of YXXY motifs (Figure 3E). GFP-hSAM68 fragment (C3) contains five YXXY motifs, (C4) has four, (C5) has two, while (NLS) has none. We found that the co-immunoprecipitation efficiency of U1A was directly dependent on the number of YXXY motifs, since the C4 fragment showed a slight decrease in association strength, while the C5 and the NLS fragments showed little or no association with U1A (Figure 3F). This change in association is unlikely to be related to mislocalization caused by the GFP moiety, since all the fragments showed a predominant nuclear localization (Supplementary Figure S4B).

Interestingly, there are six YXXY motifs within SAM68 YY domain, of which two successive YEGY motifs (SYEGYEGYYS) are defined as the minimal ARM interaction domain (54). Results obtained in Figure 3F suggested that losing this minimal motif could drastically affect the ability of SAM68 to bind U1A, like it was observed with APC. To validate this possibility, we proceeded with the deletion of this ten amino acid stretch (SYEGYEGYYS) within the Flag-hSAM68 (FL) construct. Similarly to what was observed with APC, deletion of the minimal ARM-binding motif (ΔARM) was enough to abrogate most of SAM68 association with U1A (Figure 3G), while it did not affect SAM68 affinity for its RNA target (Supplementary Figure S4C). Taken together, these results strongly indicate that SAM68 interaction with U1A is mediated through a specific sequence found in the YY domain (55).

SAM68 interact with U1A–RRM1 domain

To further confirm that SAM68 was directly interacting with U1A and to identify which part of both proteins interact, we used solution-state NMR spectroscopy. The hSAM68 (C2) fragment was isotopically labeled and resonances from backbone atoms were assigned using classical approaches. Analysis of the backbone chemical shifts revealed that in solution, the hSAM68 (C2) fragment adopts a random coil conformation without any secondary structure. Upon addition of unlabeled GB1-U1A, several resonances of the ^{15}N-labeled hSAM68 (C2) experienced chemical shift changes (Figure 4A) that were reproduced with U1A RRM1 (1–126) but not by the C-terminal part of U1A containing RRM2 (156–282). Reverse NMR titration performed with ^{15}N-labeled GB1-U1A revealed that upon addition of unlabeled GB1-hSAM68 (C2), the NMR signals from the RRM1 of U1A experienced strong line broadening and almost disappeared from the spectra (Supplementary Figure S5). However, when the ^{15}N-labeled U1A RRM1 (1–126) was titrated with unlabeled hSAM68 (C2), several signals of the U1A RRM1 shifted from their initial positions (Figure 4B). The chemical shift perturbations observed on the N-terminal part of U1-A reveal an interaction surface with the C-terminal part of hSAM68 located between the edge of β-sheet surface (β2), the C-terminal helix α3 and the interdomain linker (Figure 4C). In addition, the NMR titration of hSAM68 (C2) by unlabeled U1A shown that the NMR signals from the tyrosine-rich sequence (370–400) of SAM68 (C2) are the most affected and thus strongly support that U1A RRM1 interacts with this aromatic rich sequence of hSAM68 *in vitro* at G-Y-E/D triplets.

SAM68 recruits U1 snRNP to the 5′ splice site of *mTor* intron 5

We next sought to determine if SAM68, through its association to U1A, could serve as an adaptor protein mediating the interaction between *mTor* pre-mRNA and the U1 snRNP. More specifically, we assessed if this interaction is mediated through the simultaneous association of SAM68 with its binding motifs (SBs) found near the 5′ splice site of

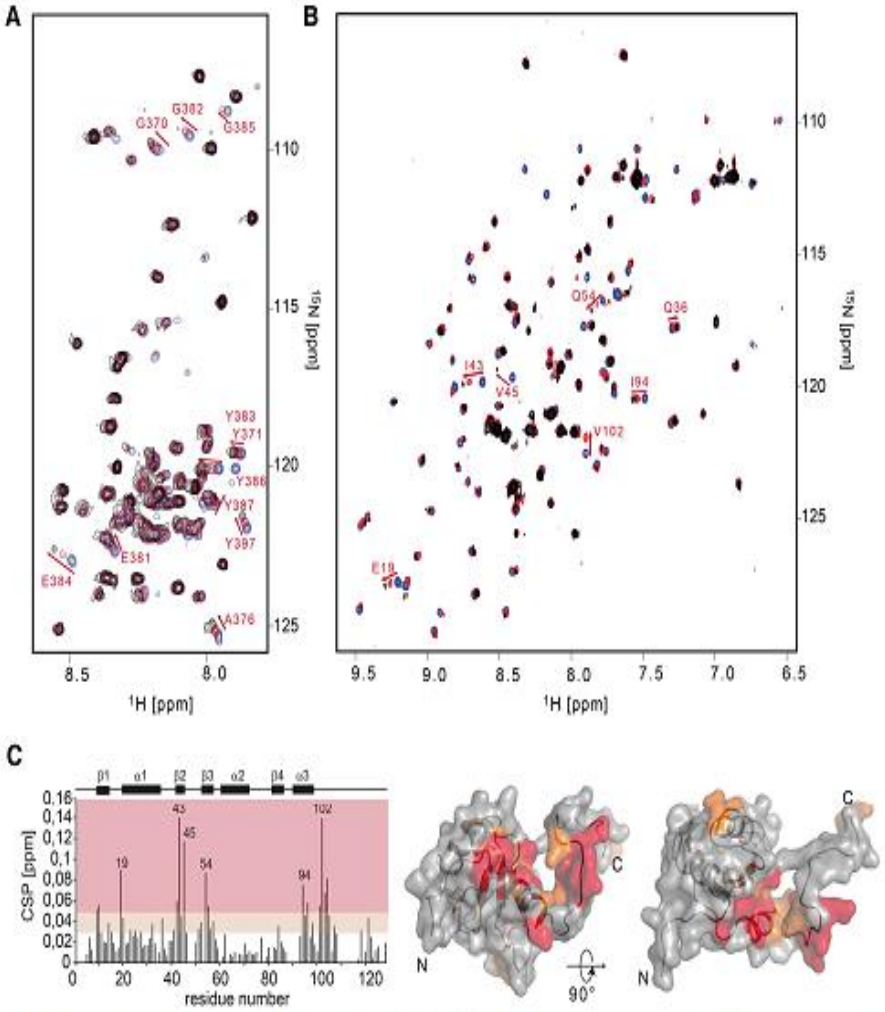

Figure 4. Tyrosine-rich (YY) domain of SAM68 mediates the interaction with U1 snRNP via YXXY repeated motif. (A) Overlay of the 2D ^{15}N-^{1}H HSQC spectra of GB1-hSAM68 (C2) recorded before and after the addition of unlabeled GB1-U1A. The spectra are colored according to the molar ratio hSAM68 (C2):U1A (1:0; 1:0.6 and 1:1.4 are colored in blue, red and black, respectively). Strongly perturbed signals are marked by red arrows and their assignment is indicated. (B) Overlay of the 2D ^{15}N-^{1}H HSQC spectra of U1A RRM1 recorded before and after the addition of unlabeled GB1-hSAM68 (C2). The spectra are colored according to the molar ratio U1A RRM1:hSAM68 (C2) (1:0; 1:0.6 and 1:1.4 are colored in blue, red and black, respectively). (C) Plot of the normalized chemical shift perturbations observed in panel (B) in function of the sequence of U1A RRM1. The chemical shift perturbations are then plotted onto the surface representation of the structure of the free form of the RRM1 of U1A (47). Amino acids that experienced chemical shift perturbation between 0.03 and 0.05 are colored in orange while the CSP higher than 0.05 are colored in red.

mTor intron 5 and with U1A. Indeed, while SAM68 binding sequence 1 (SB-1) does not correspond to the *bona fide* U/AAA consensus sequences identified by SELEX (35), it was previously shown that SAM68 binding to its target sequence closest to the 5′ splice site (SB-1) was essential for *mTor* normal splicing and expression during adipogenesis (21). Moreover, SB-1 shares a high level of homology to a specific SAM68 binding sequence identified in the β-actin mRNA (27). On the other hand, the SAM68 binding motif embedded within the cryptic poly(A) signal (SB-A) has the U/AAAA consensus sequences. Both SB-1 (UUUUAU) and SB-A (AUAAAAAU) were shown to be bound by mSAM68 *in vivo* (21). Interestingly, these two sequences are separated by only 11 nucleotides, which correspond to a bipartite pattern (UUUUAU-(n_{11})-AUAAAAAU), found to favor binding and homodimerization of GSG protein family, including SAM68 (56,57). As such, we reasoned that disrupting SAM68 binding to intron 5 by mutating both these sequences should drastically hinder U1 snRNP recruitment at the 5′ splice site of *mTor* intron 5 (Figure 5A).

To assess this, we *in vitro* transcribed different RNA baits using a minimal portion of the *mTor* minigene that

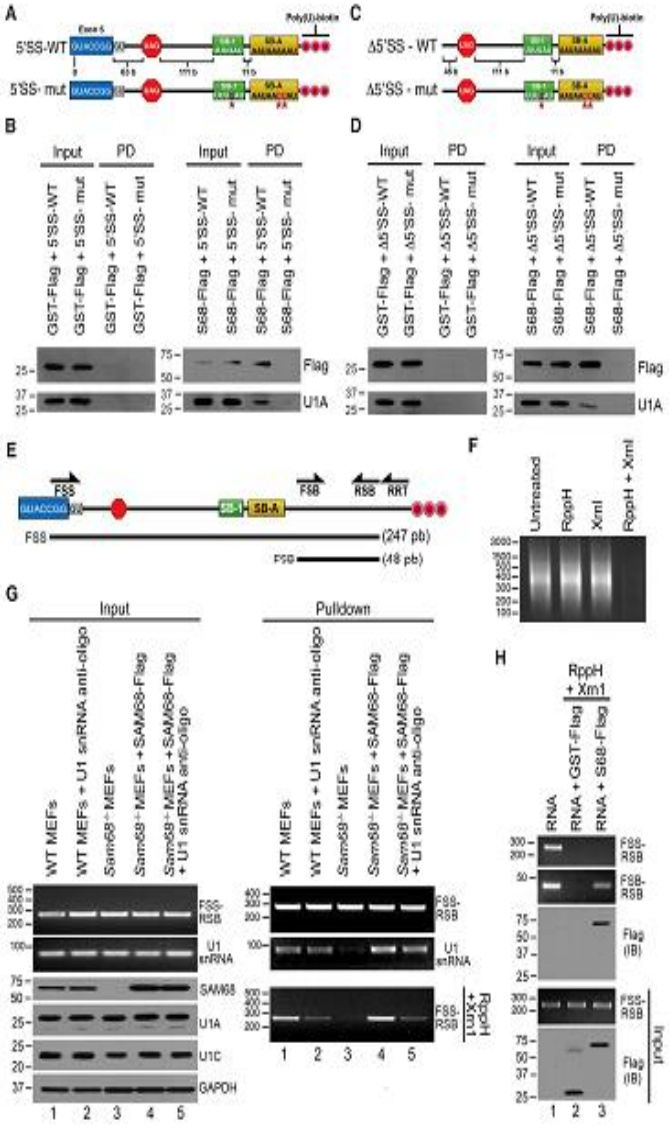

Figure 5. Both SAM68 and intronic enhancer sequences in *mTor* intron 5 are required for U1A recruitment to 5'SS *in vitro*. (A) Schematic representation of the various *in vitro* transcribed *mTor* minigene baits with the 5' splice site. As shown, the baits span from last 7 nucleotides of exon5 to the poly-adenylation signal in intron 5. WT refers to the wild-type intronic SAM68-binding sequences of SB-1 (UUUUAU) and SB-A (UAAAA), the latter is embedded in the cryptic poly-adenylation signal (AAUAAA). The 'mut' denotes the combined mutations of SB-1 (UUUUAU to UUUCAU) and SB-A (AAUAAAA to AAUAACC). (B) SAM68 recruits U1A to 5' splice site *in vitro*. Recombinant *in vitro* purified hSAM68-Flag was tested for its ability to recruit U1A to *mTor* intron 5 baits with either WT or mutated SAM68-binding sites. GST-Flag was used as negative control. (C) Schematic representation of the various *in vitro* transcribed *mTor* minigene baits that are deleted for the 5' splice site. As shown, the baits span 18 nucleotides downstream of the 5' splice site to the poly-adenylation signal of intron 5. WT refers to the wild-type intronic SAM68-binding sequences, SB-1 (UUUUAU) and SB-A (UAAAA). The 'mut' denotes the combined mutations of SB-1 (UUUUAU to UUUCAU) and SB-A (AAUAAAA to AAUAACC). (D) SAM68 recruits U1A in the absence of 5' splice site *in vitro*. Recombinant *in vitro* purified hSAM68-Flag was tested for its ability to recruit U1A to *mTor* intron 5 baits lacking 5'SSs with either WT or mutated SAM68-binding sites. GST-Flag was used as negative control. (E) Schematic representation of the *in vitro* transcribed mTor minigene bait and the primers used for the RppH/Xrn1 protection assays. (F) Assessment of the processivity of RppH and Xrn1 enzyme on the naked mRNA bait, showing that RppH treatment is necessary for Xrn1-mediated degradation of the mRNA bait. (G) RppH and Xrn1 protection assays *in vitro* produced mRNA bait incubated with either WT MEFs cell lysate (lane 1), *Sam68*$^{-/-}$ MEFs cell lysate (lane 2), *in vitro* produced mSAM68(WT) + *Sam68*$^{-/-}$ MEFs cell lysate (lane 3) or *in vitro* produced mSAM68(WT) + *Sam68*$^{-/-}$ MEFs cell lysate + U1 nRNAs antisense oligo (lane 4). U1snRNP components (U1A, U1C) and mSAM68 levels were assessed by western blot, while U1 snRNA levels was assessed by RT-PCR. GAPDH served as loading control for the western blot. (H) SAM68 protects the mTor RNA bait from Xrn1 degradation. Biotinylated RNA baits were incubated with buffer (lane 1), 100 ng of GST-Flag (lane 2) or 100 ng of mSAM68-Flag (lane 3) for 30 min on ice. Sam68 levels were assessed by western blotting using anti-Flag, while baits levels were measured by semi-quantitative RT-PCR using FSS-RSB primers for the full-length RNA and FSB-RSB for the SAM68 protected fragment.

span from the last 7 nucleic acid of exon5 to the cryptic polyadenylation signal at the intron 5 (Figure 5A). To determine if U1 snRNP recognition of the 5′ splice site was driven by SAM68, we mutated SAM68-binding sequence closest the 5′ splice site (SB-1), as well as the binding site embedded in the polyadenylation (SB-A) (Figure 5A). The 3′-end of the RNA baits were labeled with UTP-Biotin tails and immobilized on streptavidin-agarose beads. The baits were first incubated with *in vitro* purified hSAM68-Flag recombinant protein and then, sh*SAM68* HEK-293T cell extract was added to the mix. As observed in figure 5B, U1A was mostly detected on the baits harboring WT SAM68-binding sites, while its presence was greatly decreased on baits lacking the SAM68-binding sites. This suggests that not only SAM68 association with *mTor* intron 5 strengthen the 5′ splice site recognition by U1 snRNP, but also that SAM68 association could recruit U1 snRNP to the 5′ splice site of *mTor* intron 5 (Figure 5B). To assess this, we used RNA baits lacking the 5′ splice site (Δ5′SS) harboring either WT or mutated SB-1 and SB-A (Figure 5C). Surprisingly, we found that SAM68 was able to recruit the U1A even when the 5′ splice site was absent (Figure 5D).

While these results suggest a Sam68-dependent recruitment of U1A, it remains unclear whether U1 snRNP is only tethered to the RNA bait by a direct protein interaction with SAM68 or if there is an improved recognition by U1 snRNP to the 5′ splice site. To determine that, we incubated a mRNA bait produced *in vitro*, similar to the one used in the previous pulldown experiments (Figure 5E), which was incubated with different nuclear extracts and subjected to Xrn1, a 5′→3′ exoribonuclease (58). As shown in figure 5F, Xrn1 can efficiently degrade the RNA bait following treatment with RppH, an RNA 5′ pyrophosphohydrolase that removes pyrophosphate from the 5′ end of triphosphorylated RNA to leave a 5′ monophosphate RNA, the substrate of Xrn1 (59–61). To determine if SAM68 could recruit and enhance U1 snRNP 5′ splice site recognition, we incubated our bait with either WT MEFs cell lysate, Sam68$^{-/-}$ MEFs cell lysate or Sam68$^{-/-}$ MEFs cell lysate supplemented with an *in vitro* produced flag-tagged mSAM68 (Figure 5G). RNP complexes were pulled down using streptavidin agarose beads and treated with RppH prior to their digestion with Xrn1. Using specific primers (Figure 5E), we found that, in the presence of mSAM68 (from WT MEFs cell lysate or *in vitro* production), 5′ splice sites were highly protected from RppH/Xrn1, while the baits were completely degraded in the absence of mSAM68 (Figure 5G). Using *in vitro* produced mSAM68 and our RNA bait, we found that SAM68, by itself, could only partially protect the RNA downstream of the SAM68-binding site, while the 5′ end of the bait was completely degraded by Xrn1. This result indicates that Xrn1 accessibility at the 5′ end of our bait (5′ splice site of *mTor* intron 5) is efficiently impeded only by steric hindrance caused by the mSAM68–U1 snRNP complex. Hence, change in Xrn1 accessibility observed in Figure 5G suggests that recruitment and association of U1 snRNP is dependent on SAM68. This was further confirmed with a competing U1 snRNA antisense oligo directed against the RNA-binding site of U1 snRNP (Figure 5G, lanes 2 and 5). In both cases, the SAM68-induced U1 snRNP protection of the 5′ splice site was significantly reduced when the cell extracts were supplemented with the U1 snRNA antisense oligo in order to impair U1 snRNA hybridization with the 5′-splice site of the *mTor* RNA bait.

SAM68 recruitment of U1 snRNP is specific to endogenous *mTor* intron 5

To confirm that SAM68 binds to the endogenous intron 5 sequences of mTOR, we performed cross-linking immunoprecipitation (CLIP) on WT and *Sam68*$^{-/-}$ MEFs and assessed mSAM68 binding to different intron of mTOR pre-mRNA. mSAM68 specifically associated in intron 5 near the exon-intron junction in WT MEFs, while no binding was detected in two other introns (4 and 37), which lack mSAM68 binding sites (Supplementary Figure S6A). Furthermore, no signal was observed in the *Sam68*$^{-/-}$ background. To rescue mSAM68 binding, we performed SAM68 CLIP on *Sam68*$^{-/-}$ MEFs transfected with *mSam68(WT)*, *mSam68(ΔARM)* or *GFP* as a negative control. Enrichment of the intron 5 sequence was observed in MEFs expressing either the WT or ΔARM versions of mSAM68 but was undetectable at the other tested intron (Supplementary Figure S6B).

We then sought to determine if mSAM68 could recruit U1 snRNP on endogenous mTOR, as observed with *in vitro* synthesized baits. To address this, we performed RNA immunoprecipitation (RIP) of U1A and assessed U1 snRNP coverage of the different exon–intron junctions in both WT and *Sam68*$^{-/-}$ MEFs. No U1A signal was found at mTOR exon5–intron 5 junction (ei5) of *Sam68*$^{-/-}$ MEFs (Figure 6A), while U1A signal was easily detectable in WT MEFs, and in the other exon–intron junctions (ei4 and ei37) of both WT and *Sam68*$^{-/-}$ MEFs (Figure 6A). These results confirm that mSAM68 directly facilitates the recruitment of U1 snRNP to ei5, while not affecting other exon–intron junctions where there is no SAM68-binding site. Moreover, mSAM68 ability to recruit U1 snRNP was not shared with the mSAM68(ΔARM) mutant in a *Sam68*$^{-/-}$ MEF background, further suggesting that the recruitment of U1 snRNP to ei5 is indeed through SAM68 (Figure 6B). Accordingly, U1A immunoprecipitation in *Sam68*$^{-/-}$ MEFs expressing mSAM68(WT) or mSAM68(ΔARM) revealed that only the WT protein allowed the detection of ei5, and no change of U1 snRNP association was observed in other exon–intron junctions.

Taken together, these results confirm that SAM68 binding to its target intronic sequences is sufficient to recruit the U1 snRNP through U1A to the 5′ splice site of *mTor* intron 5 and thus facilitates its recognition and the stabilization of the U1 complex at the 5′ splice site.

SAM68 regulates *mTor* splicing through the recruitment of U1 snRNP

To determine the role of SAM68–U1snRNP interaction in the regulation of *mTor* intron 5 splicing endogenously, we performed *in vivo* splicing assay on *mTor* in WT or Sam68$^{-/-}$ MEFs, using a common forward primer and a splicing specific reverse primer (i5 versus e6) (Figure 7A). As expected, we observed a drastic decrease of $mTor_{4-6}$ amplicon upon *Sam68* inactivation, which was replaced

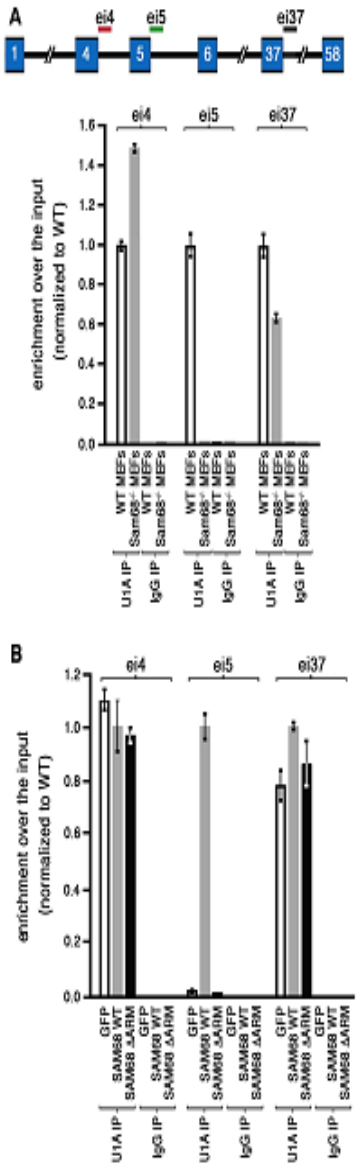

Figure 6. U1snRNP is recruited in a SAM68-dependent manner at the exon5–intron 5 junction (ei5) in *mTor* pre-mRNA. (A) RNA immunoprecipitation (RIP) assay of mSAM68 on *mTor* pre-mRNA. (Top) Schematic representation of *mTor* pre-mRNA showing location of amplicon used to detect U1 snRNP binding by RIP (ei4 in red, ei5 in green and ei37 in black). (Below) U1A-RIP was done from WT MEFs or *Sam68*$^{-/-}$ MEFs using anti-U1A or control IgG antibodies. Bound RNA was analyzed by RT-qPCR using the highlighted primers. Mean values are expressed as fold enrichment over input and normalized to WT signal. Error bars represent ± standard deviations of the means. (B) U1snRNP recruitment is restored at *mTor* EI5, in *Sam68*$^{-/-}$ MEFs expressing *mSam68(WT)* but not with *mSam68(ΔArm)*. U1A-RIP was done using anti-U1A or control IgG antibodies in *Sam68*$^{-/-}$ MEFs, *Sam68*$^{-/-}$ MEFs rescued with *mSam68(WT)* or *mSam68(ΔArm)*. Bound RNA was analyzed in triplicates by RT-qPCR using the highlighted primers. Mean values are expressed as fold enrichment over input and normalized to WT signals. Error bars represent ± standard deviations of the means.

by a robust increase of the $mTor_{i5}$ transcript (Figure 7B), confirming our previous observation that *Sam68* depletion leads to increased intron 5-induced termination (21). To rescue Sam68 depletion splicing effects, *Sam68*$^{-/-}$ MEFs were transduced with either *Sam68(WT)* or *Sam68(ΔARM)*. Total RNA was isolated 48 h post transfection and analyzed by semi-quantitative RT-PCR. As expected, upon expression of mSAM68(WT), there was a significant decrease in intron 5-induced premature termination and polyadenylation (Figure 7B). On the other hand, cells that expressed mSAM68(ΔARM) were unable to rescue the splicing defect. This result confirms that reduced association with U1A leads to U1 snRNP recruitment impairments and thus, *mTor* intron 5 proper splicing. While robust level of intron 5 detection was still observed in cells expressing mSAM68(ΔARM), levels were lower than vector control (Figure 7B). This partial decrease in intron 5-induced termination is assumingly provoked by the remaining hSAM68(ΔARM)–U1A interaction, as observed in Figure 4C. As proposed in our previous work using the 3T3-L1 cell lines, this SAM68 splicing defect was also associated with decreased *mTor* expression level in MEFs. Indeed, mTOR protein level was highly decreased in *Sam68*$^{-/-}$ MEFs and *Sam68*$^{-/-}$ MEFs expressing mSAM68(ΔARM), when compared to WT MEFs or *Sam68*$^{-/-}$ MEFs expressing mSAM68(WT) (Supplementary Figure S7).

These results were also observed in an *in vivo* splicing assays using the *mTor* minigene, a plasmid that drives the expression of the 2.3 kb genomic fragment spanning from exon4 to exon6 of mouse *mTor* (Supplementary Figure S7A). Indeed, hSAM68-depleted HEK-293T cells co-transfected with the minigene and either Flag-YFP, Flag-hSAM68(WT) or Flag-hSAM68(ΔARM) showed similar results that Flag-hSAM68(WT) was able to revert the increased $mTor_{i5}$ / $mTor_{tot}$ ratio, while the Flag-hSAM68(ΔARM) behaved like Flag-YFP (Supplementary Figure S6B).

DISCUSSION

The KH domain RNA-binding protein, SAM68, regulates splicing of *mTor* as well as the ribosomal S6 kinase *(Rps6kb1)* transcripts in pre-adipocytes (21,39). In turn, pre-adipocytes of *Sam68*$^{-/-}$ mice do not differentiate to adipocytes due to defective mTOR signaling. Our data show that SAM68 modulates *mTor* splicing by binding to specific regulatory elements found in intron 5 (SB-1 and SB-A), of which SB-A overlaps with the poly-adenylation signal (AAUAAA). This led us to postulate that these AU-rich *cis*-acting elements were intronic splicing enhancers to which SAM68 bound with great affinity to modulate the recruitment of U1 snRNP at the upstream 5′ splice site.

In this study, we report that SAM68 functionally interacts with U1 snRNP, the spliceosomal component that recognizes 5′ splice sites (10). While SAM68 can bind with low affinity to the U1 snRNA *in vitro*, it is highly unlikely that it will happen *in vivo*. Furthermore, the potential AU-rich SAM68 binding motif found in the U1 snRNA is located in the Sm site, which is rapidly masked by the Sm protein ring during U1 snRNP assembly (49,62). Rather, we found that SAM68 interacts directly with U1A, the stem–

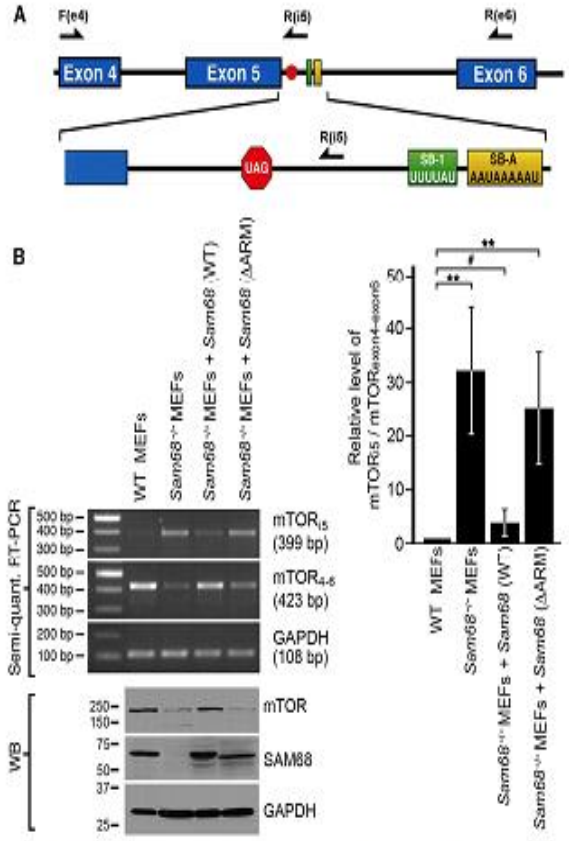

Figure 7. SAM68 deletion of 'ARM binding region' shows decrease in U1A binding. (A) Schematic of the pcDNA $mTor_{4-6}$ minigene, comprising the *mTor* genomic fragment from exon4 to exon6. (B) (Left panel) *Sam68*$^{-/-}$ MEFs cells were infected with *Sam68*(WT) or *Sam68*(ΔARM) and compared to uninfected *Sam68*$^{-/-}$ MEFs or WT MEFs. Total RNA was extracted in each cell lines and semi-quantitative RT-PCRs were performed using endogenous *mTor* specific primers. Forward (Fe4) and Reverse (Re6) were used to quantify *mTor* transcripts that were spliced normally ($mTor_{4-6}$), while Forward (Fe4) and Reverse (Ri5) were used to quantify intron 5 including *mTor* transcripts ($mTor_{i5}$). *Gapdh* was used to normalize the values obtained. Total protein was also extracted and run on 10% SDS-PAGE and blotted with SAM68, U1A and GAPDH antibodies. (Right panel) Quantification of intron 5-induced termination over normally spliced mRNA based on three independent experiments using endogenous *mTor* specific primers. **P-value ≤ 0.05 and # = non-significant (two-tailed t-test).

loop II binding protein of U1 snRNA. This SAM68–U1A interaction was shown to be resistant to RNaseA treatment and RNA-binding defective mutant versions of SAM68 bearing point mutations in the KH domain; $SAM68_{V229F}$ (23) and $SAM68_{I184N}$ (36,52) could still bind U1A and the U1snRNP. Domain mapping studies showed that U1A binds to the 'minimal ARM binding region of SAM68 and that deleting this region (379–389 aa) in SAM68(WT) was sufficient to impair U1A association. This region located within SAM68 YY domain was initially identified to regulate T-cell factor 1 splicing by binding the armadillo repeat (ARM) domain of Adenomatous polyposis coli (APC) (54,55). Hence, our results confirmed that SAM68 can directly interact with U1A, making it the only identified protein interactor of this U1 snRNP core protein to date. NMR spectroscopy also confirmed that this protein–protein interaction is mediated through the tyrosine-rich 'ARM-binding domain' of SAM68 and the RRM1 domain of U1A. Conversely, we observed that deleting the ARM domain of SAM68 greatly impaired its association with U1A, resulting in increased intron 5 inclusion. Residual splicing activity could still be observed, which might be due to the remaining YXXY motifs in SAM68(ΔARM) that may act as weak surrogate binding sites in the absence of the ARM motif.

Results obtained with synthetized RNA baits suggest that mSAM68 initiate U1 snRNP recruitment, which then allows the recognition of the sub-optimal splice site. Hence, the presence of mSAM68 increases the recognition rate of the 5′ splice site of *mTor* intron 5, by increasing U1 snRNP stoichiometry close to the splice site. This was further confirmed by the endogenous mSAM68 CLIP, the U1A RNA immunoprecipitation assays and the *mTor* splicing disparity observed using either the *mTor* $minigene_{exon4-6}$ or the endogenous *mTor*. These findings highlight the importance of intronic enhancer mediated binding of SAM68, subsequent recruitment of U1snRNP via U1A and the resultant

splicing of *mTor* intron 5. This is strikingly similar to the mechanism by which other RNA-binding proteins, such as TIA1 and RBM24, modulate 5′ splice site recognition of Drosophila male specific lethal (msl) gene and inhibitor of κ light polypeptide gene enhancer in B cells, kinase complex-associated protein (IKBKAP) gene in familial dysautonomia (FD) by interacting with U1snRNP (17,63). Indeed, both of these RNA-binding proteins were shown to promote splicing of pre-mRNA's containing sub-optimal splicing signals by interacting with components of U1 snRNP. While TIA1 interacts with U1C and SAM68 with U1A, both act as intronic splicing enhancers by binding sequences close to the 5′ splice sites, thus facilitating U1 snRNP recruitment.

As shown here, SAM68 seems to initiate spliceosome assembly at the 5′ splice site of *mTor* intron 5, through the recruitment the U1 snRNP. This is mainly achieved when SAM68 binds specific sequence within the 5′ portion of mTor intron 5, mainly the bipartite sequences designated as SB-1 and SB-A. While these two sequences are clearly involved in U1 snRNP recruitment, the role of the downstream SAM68-binding sites found throughout intron 5 remains to be defined. One main hypothesis could be that SAM68 regulates early steps of spliceosome assembly (e.g. complex E formation) in specific introns. This seems to be in line with the observation that SAM68 binds U2AF65, a subunit of the U2AF complex known to initiate 3′ splice site recognition (64). Moreover SAM68 binding to U2AF65 increased its efficiency. As SAM68 homodimerizes through its association with RNA, it is also possible that multiple binding sites favor its dimerization, thus decreasing the gap between the 5′ and the 3′ splice site, which would again facilitate early spliceosome assembly.

It has been recently reported that introns with weak 5′ splice sites are susceptible to premature cleavage and polyadenylation events in the absence of U1 snRNP binding and RNA-binding proteins are required for U1 snRNP occupancy at such sites (65). Indeed, morpholino oligonucleotides interfering with U1 snRNA binding causes premature cleavage and polyadenylation in numerous pre-mRNAs at cryptic polyA sites in introns and this occurs near the start of the transcripts (66). This mechanism seems to involve core protein components of the U1 snRNP, since both U1–70K and U1A were reported to inhibit polyadenylation by mediating a direct interaction with poly-A-polymerase (67,68). This U1-mediated inhibition of polyadenylation even led to the characterization of a Polyadenylation inhibitory Elements (69). Concomitantly, SAM68 has also recently been reported to regulate 3′ end processing of *Aldh1a3* pre-mRNA, a mechanism that is required to maintain glycolytic metabolism and self-renewal of mouse neural progenitor cells (37). While our results show that mSAM68 recruits U1 snRNP to the 5′ splice site of *mTor* intron 5 and increases the rate of intron 5 excision, it also seems to cooperate in masking cryptic polyadenylation sites, a process that is known to be mediated by U1 snRNP (66,70). Indeed, SAM68 alone (without U1 snRNP) is unable to modulate alternative intronic polyadenylation usage, since SAM68(ΔARM) can bind the poly(A) signal as efficiently as the WT version, but still allows polyadenylation of the $mTor_{I5}$ transcript. Hence, these results suggest that 5′ splice site recognition by the SAM68–U1 snRNP complex precludes intronic cryptic polyadenylation usage, while allowing proper excision of *mTor* intron 5. This also suggest that SAM68 could also be involved in the modulation of the previously described U1-dependent modulation of alternative poly(A) usage (37,66,70,71).

Our findings illustrate the first mechanistic evidence showing that SAM68 recruits U1 snRNP via direct interaction with U1A to upstream 5′ splice site, while it binds AU-rich regulatory sequences in *mTor* intron 5, through its RNA-binding KH domain. This is subsequently mediated through its tyrosine-rich 'ARM-binding domain', and in turn enhances splicing of intron 5, while SAM68 depletion inhibits U1 snRNP recruitment and promotes premature intron 5-induced termination and polyadenylation. Although the regulatory mechanism of this interaction remains elusive, the presence of numerous tyrosine residues located within the 'YY region' of SAM68 suggest that phosphorylation might be involved. Indeed, SAM68 tyrosine phosphorylation was shown to negatively affect its ability to bind RNA (31,33,34), and its splicing functions (i.e. *Bcl-X*, *CD-44* and *Cyclin D1*) (22,23,33).

In the future, the global identification of mRNA targets regulated by this SAM68-dependent alternative splicing should allow us to better understand these possible regulatory mechanisms and determine how a binding site situated 174-nt downstream of the 5′ splice site can modulate its recognition by the U1 snRNP. Indeed, it would be interesting to assess if other alternatively spliced mRNAs targeted by SAM68 could be differentially regulated through distance changes between SAM68-binding sites and the 5′ splice site during cellular processes such as development or cancer. Moreover, determining how the SAM68–U1A interaction is modulated by distance constraints, secondary structures or associated proteins to regulate not only *mTor*, but also a specific sub-class of mRNA, remains to be investigated.

SUPPLEMENTARY DATA

Supplementary Data are available at NAR Online.

ACKNOWLEDGEMENTS

We thank Dr Stéphane Richard, Dr Roberto Bonasio and Dr Philip Leder for sharing reagents. We thank Dr Rachid Mazroui and Dr Martin Simard for critical reading of the manuscript. We are grateful to Yan Coulombe and Maripier Hainse for technical assistance. We thank Jonathan Bergeman and Carl St-Pierre from the Cell Imaging Unit of the Centre de recherche du CHU de Québec-Université Laval for their technical assistance.

FUNDING

Fonds de Recherche du Québec - Santé (FRQ-S) (to M.-E., S.M.H., J.-Y.M.); Bourse de la Fondation du CHU de Québec (to J.O's. and V.F.); Natural Sciences and Engineering Research Council of Canada (NSERC) [402880-2012 to M.-E.H.; 2016-05847 to S.M.H.], NCCR RNA and Disease of the Swiss National Foundation (to F.H.T.A.); Canadian

Institutes of Health Research (to J.-Y.M.). Funding for open access charge: Natural Sciences and Engineering Research Council of Canada (NSERC) [402880-2012 to M.-E.H.].
Conflict of interest statement. None declared.

REFERENCES

1. Wahl,M.C., Will,C.L. and Luhrmann,R. (2009) The spliceosome: design principles of a dynamic RNP machine. *Cell*, **136**, 701–718.
2. Faustino,N.A. and Cooper,T.A. (2003) Pre-mRNA splicing and human disease. *Genes Dev.*, **17**, 419–437.
3. Matera,A.G. and Wang,Z. (2014) A day in the life of the spliceosome. *Nat. Rev. Mol. Cell Biol.*, **15**, 108–121.
4. Papasaikas,P. and Valcarcel,J. (2016) The Spliceosome: the ultimate RNA chaperone and sculptor. *Trends Biochem. Sci.*, **41**, 33–45.
5. Baralle,F.E. and Giudice,J. (2017) Alternative splicing as a regulator of development and tissue identity. *Nat. Rev. Mol. Cell Biol.*, **18**, 437–451.
6. Chabot,B. and Steitz,J.A. (1987) Recognition of mutant and cryptic 5′ splice sites by the U1 small nuclear ribonucleoprotein in vitro. *Mol. Cell. Biol.*, **7**, 698–707.
7. Mount,S.M., Pettersson,I., Hinterberger,M., Karmas,A. and Steitz,J.A. (1983) The U1 small nuclear RNA-protein complex selectively binds a 5′ splice site in vitro. *Cell*, **33**, 509–518.
8. Alibert,C., Tazi,J., Temsamani,J., Jeanteur,P., Brunel,C. and Cathala,G. (1990) Interplay between U2 snRNP and 3′ splice factor(s) for branch point selection on human beta-globin pre-mRNA. *Nucleic Acids Res.*, **18**, 235–245.
9. Ruskin,B., Zamore,P.D. and Green,M.R. (1988) A factor, U2AF, is required for U2 snRNP binding and splicing complex assembly. *Cell*, **52**, 207–219.
10. Shao,W., Kim,H.S., Cao,Y., Xu,Y.Z. and Query,C.C. (2012) A U1-U2 snRNP interaction network during intron definition. *Mol. Cell. Biol.*, **32**, 470–478.
11. Jurica,M.S. and Moore,M.J. (2003) Pre-mRNA splicing: awash in a sea of proteins. *Mol. Cell*, **12**, 5–14.
12. Roca,X., Krainer,A.R. and Eperon,I.C. (2013) Pick one, but be quick: 5′ splice sites and the problems of too many choices. *Genes Dev.*, **27**, 129–144.
13. Sun,S., Ling,S.C., Qiu,J., Albuquerque,C.P., Zhou,Y., Tokunaga,S., Li,H., Qiu,H., Bui,A., Yeo,G.W. *et al.* (2015) ALS-causative mutations in FUS/TLS confer gain and loss of function by altered association with SMN and U1-snRNP. *Nat. Commun.*, **6**, 6171.
14. Rogelj,B., Easton,L.E., Bogu,G.K., Stanton,L.W., Rot,G., Curk,T., Zupan,B., Sugimoto,Y., Modic,M., Haberman,N. *et al.* (2012) Widespread binding of FUS along nascent RNA regulates alternative splicing in the brain. *Sci. Rep.*, **2**, 603.
15. Mayeda,A. and Krainer,A.R. (1992) Regulation of alternative pre-mRNA splicing by hnRNP A1 and splicing factor SF2. *Cell*, **68**, 365–375.
16. Krainer,A.R., Conway,G.C. and Kozak,D. (1990) The essential pre-mRNA splicing factor SF2 influences 5′ splice site selection by activating proximal sites. *Cell*, **62**, 35–42.
17. Forch,P., Puig,O., Martinez,C., Seraphin,B. and Valcarcel,J. (2002) The splicing regulator TIA-1 interacts with U1-C to promote U1 snRNP recruitment to 5′ splice sites. *EMBO J.*, **21**, 6882–6892.
18. Ohe,K., Yoshida,M., Nakano-Kobayashi,A., Hosokawa,M., Sako,Y., Sakuma,M., Okuno,Y., Usui,T., Ninomiya,K., Nojima,T. *et al.* (2017) RBM24 promotes U1 snRNP recognition of the mutated 5′ splice site in the IKBKAP gene of familial dysautonomia. *RNA*, **23**, 1393–1403.
19. Geuens,T., Bouhy,D. and Timmerman,V. (2016) The hnRNP family: insights into their role in health and disease. *Hum. Genet.*, **135**, 851–867.
20. Mayeda,A., Munroe,S.H., Caceres,J.F. and Krainer,A.R. (1994) Function of conserved domains of hnRNP A1 and other hnRNP A/B proteins. *EMBO J.*, **13**, 5483–5495.
21. Huot,M.E., Vogel,G., Zabarauskas,A., Ngo,C.T., Coulombe-Huntington,J., Majewski,J. and Richard,S. (2012) The Sam68 STAR RNA-binding protein regulates mTOR alternative splicing during adipogenesis. *Mol. Cell*, **46**, 187–199.
22. Paronetto,M.P., Cappellari,M., Busa,R., Pedrotti,S., Vitali,R., Comstock,C., Hyslop,T., Knudsen,K.E. and Sette,C. (2010) Alternative splicing of the cyclin D1 proto-oncogene is regulated by the RNA-binding protein Sam68. *Cancer Res.*, **70**, 229–239.
23. Paronetto,M.P., Achsel,T., Massiello,A., Chalfant,C.E. and Sette,C. (2007) The RNA-binding protein Sam68 modulates the alternative splicing of Bcl-x. *J. Cell Biol.*, **176**, 929–939.
24. Matter,N., Herrlich,P. and Konig,H. (2002) Signal-dependent regulation of splicing via phosphorylation of Sam68. *Nature*, **420**, 691–695.
25. Bielli,P., Busa,R., Paronetto,M.P. and Sette,C. (2011) The RNA-binding protein Sam68 is a multifunctional player in human cancer. *Endocr. Relat. Cancer*, **18**, R91–R102.
26. Taylor,S.J., Anafi,M., Pawson,T. and Shalloway,D. (1995) Functional interaction between c-Src and its mitotic target, Sam 68. *J. Biol. Chem.*, **270**, 10120–10124.
27. Itoh,M., Haga,I., Li,Q.H. and Fujisawa,J. (2002) Identification of cellular mRNA targets for RNA-binding protein Sam68. *Nucleic Acids Res.*, **30**, 5452–5464.
28. Chen,T., Damaj,B.B., Herrera,C., Lasko,P. and Richard,S. (1997) Self-association of the single-KH-domain family members Sam68, GRP33, GLD-1, and Qk1: role of the KH domain. *Mol. Cell. Biol.*, **17**, 5707–5718.
29. Frisone,P., Pradella,D., Di Matteo,A., Belloni,E., Ghigna,C. and Paronetto,M.P. (2015) SAM68: Signal transduction and RNA metabolism in human cancer. *Biomed. Res. Int.*, **2015**, 528954.
30. Lukong,K.E. and Richard,S. (2003) Sam68, the KH domain-containing superSTAR. *Biochim. Biophys. Acta*, **1653**, 73–86.
31. Meyer,N.H., Tripsianes,K., Vincendeau,M., Madl,T., Kateb,F., Brack-Werner,R. and Sattler,M. (2010) Structural basis for homodimerization of the Src-associated during mitosis, 68-kDa protein (Sam68) Qua1 domain. *J. Biol. Chem.*, **285**, 28893–28901.
32. Perez-Perez,A., Sanchez-Jimenez,F., Vilarino-Garcia,T., de la Cruz,L., Virizuela,J.A. and Sanchez-Margalet,V. (2016) Sam68 mediates the activation of insulin and leptin signalling in breast cancer cells. *PLoS One*, **11**, e0158218.
33. Huot,M.E., Brown,C.M., Lamarche-Vane,N. and Richard,S. (2009) An adaptor role for cytoplasmic Sam68 in modulating Src activity during cell polarization. *Mol. Cell. Biol.*, **29**, 1933–1943.
34. Lukong,K.E., Larocque,D., Tyner,A.L. and Richard,S. (2005) Tyrosine phosphorylation of sam68 by breast tumor kinase regulates intranuclear localization and cell cycle progression. *J. Biol. Chem.*, **280**, 38639–38647.
35. Lin,Q., Taylor,S.J. and Shalloway,D. (1997) Specificity and determinants of Sam68 RNA binding. Implications for the biological function of K homology domains. *J. Biol. Chem.*, **272**, 27274–27280.
36. Chawla,G., Lin,C.H., Han,A., Shiue,L., Ares,M. Jr and Black,D.L. (2009) Sam68 regulates a set of alternatively spliced exons during neurogenesis. *Mol. Cell. Biol.*, **29**, 201–213.
37. La Rosa,P., Bielli,P., Compagnucci,C., Cesari,E., Volpe,E., Farioli Vecchioli,S. and Sette,C. (2016) Sam68 promotes self-renewal and glycolytic metabolism in mouse neural progenitor cells by modulating Aldh1a3 pre-mRNA 3′-end processing. *Elife*, **5**, e20750.
38. Li,N., Hebert,S., Song,J., Kleinman,C.L. and Richard,S. (2017) Transcriptome profiling in preadipocytes identifies long noncoding RNAs as Sam68 targets. *Oncotarget*, **8**, 81994–82005.
39. Song,J. and Richard,S. (2015) Sam68 regulates S6K1 alternative splicing during adipogenesis. *Mol. Cell. Biol.*, **35**, 1926–1939.
40. Huot,M.E. and Richard,S. (2012) Stay lean without dieting: Lose Sam68. *Adipocyte*, **1**, 246–249.
41. Paronetto,M.P., Messina,V., Bianchi,E., Barchi,M., Vogel,G., Moretti,C., Palombi,F., Stefanini,M., Geremia,R., Richard,S. *et al.* (2009) Sam68 regulates translation of target mRNAs in male germ cells, necessary for mouse spermatogenesis. *J. Cell. Biol.*, **185**, 235–249.
42. Venables,J.P., Vernet,C., Chew,S.L., Elliott,D.J., Cowmeadow,R.B., Wu,J., Cooke,H.J., Artzt,K. and Eperon,I.C. (1999) T-STAR/ETOILE: a novel relative of SAM68 that interacts with an RNA-binding protein implicated in spermatogenesis. *Hum. Mol. Genet.*, **8**, 959–969.
43. Valacca,C., Bonomi,S., Buratti,E., Pedrotti,S., Baralle,F.E., Sette,C., Ghigna,C. and Biamonti,G. (2010) Sam68 regulates EMT through alternative splicing-activated nonsense-mediated mRNA decay of the SF2/ASF proto-oncogene. *J. Cell. Biol.*, **191**, 87–99.
44. Pedrotti,S., Bielli,P., Paronetto,M.P., Ciccosanti,F., Fimia,G.M., Stamm,S., Manley,J.L. and Sette,C. (2010) The splicing regulator

Sam68 binds to a novel exonic splicing silencer and functions in SMN2 alternative splicing in spinal muscular atrophy. *EMBO J.*, **29**, 1235–1247.
45. Laplante,M. and Sabatini,D.M. (2012) mTOR signaling in growth control and disease. *Cell*, **149**, 274–293.
46. Johnson,S.C., Rabinovitch,P.S. and Kaeberlein,M. (2013) mTOR is a key modulator of ageing and age-related disease. *Nature*, **493**, 338–345.
47. Avis,J.M., Allain,F.H., Howe,P.W., Varani,G., Nagai,K. and Neuhaus,D. (1996) Solution structure of the N-terminal RNP domain of U1A protein: the role of C-terminal residues in structure stability and RNA binding. *J. Mol. Biol.*, **257**, 398–411.
48. Pagliarini,V., Pelosi,L., Bustamante,M.B., Nobili,A., Berardinelli,M.G., D'Amelio,M., Musaro,A. and Sette,C. (2015) SAM68 is a physiological regulator of SMN2 splicing in spinal muscular atrophy. *J. Cell. Biol.*, **211**, 77–90.
49. Stark,H., Dube,P., Luhrmann,R. and Kastner,B. (2001) Arrangement of RNA and proteins in the spliceosomal U1 small nuclear ribonucleoprotein particle. *Nature*, **409**, 539–542.
50. Consortium,E.P. (2012) An integrated encyclopedia of DNA elements in the human genome. *Nature*, **489**, 57–74.
51. Savarese,F., Chae,O.W., Trowitzsch,S., Weber,G., Kastner,B., Akira,S., Wagner,H., Schmid,R.M., Bauer,S. and Krug,A. (2006) U1 small nuclear ribonucleoprotein immune complexes induce type I interferon in plasmacytoid dendritic cells through TLR7. *Blood*, **107**, 3229–3234.
52. De Boulle,K., Verkerk,A.J., Reyniers,E., Vits,L., Hendrickx,J., Van Roy,B., Van den Bos,F., de Graaff,E., Oostra,B.A. and Willems,P.J. (1993) A point mutation in the FMR-1 gene associated with fragile X mental retardation. *Nat. Genet.*, **3**, 31–35.
53. Satoh,M., Richards,H.B., Hamilton,K.J. and Reeves,W.H. (1997) Human anti-nuclear ribonucleoprotein antigen autoimmune sera contain a novel subset of autoantibodies that stabilizes the molecular interaction of U1RNP-C protein with the Sm core proteins. *J. Immunol.*, **158**, 5017–5025.
54. Zhang,Z., Akyildiz,S., Xiao,Y., Gai,Z., An,Y., Behrens,J. and Wu,G. (2015) Structures of the APC-ARM domain in complexes with discrete Amer1/WTX fragments reveal that it uses a consensus mode to recognize its binding partners. *Cell. Discov.*, **1**, 15016.
55. Morishita,E.C., Murayama,K., Kato-Murayama,M., Ishizuka-Katsura,Y., Tomabechi,Y., Hayashi,T., Terada,T., Handa,N., Shirouzu,M., Akiyama,T. *et al.* (2011) Crystal structures of the armadillo repeat domain of adenomatous polyposis coli and its complex with the tyrosine-rich domain of Sam68. *Structure*, **19**, 1496–1508.
56. Feracci,M., Foot,J.N., Grellscheid,S.N., Danilenko,M., Stehle,R., Gonchar,O., Kang,H.S., Dalgliesh,C., Meyer,N.H., Liu,Y. *et al.* (2016) Structural basis of RNA recognition and dimerization by the STAR proteins T-STAR and Sam68. *Nat. Commun.*, **7**, 10355.
57. Galarneau,A. and Richard,S. (2009) The STAR RNA binding proteins GLD-1, QKI, SAM68 and SLM-2 bind bipartite RNA motifs. *BMC Mol. Biol.*, **10**, 47.
58. Nagarajan,V.K., Jones,C.I., Newbury,S.F. and Green,P.J. (2013) XRN 5′→3′ exoribonucleases: structure, mechanisms and functions. *Biochim. Biophys. Acta*, **1829**, 590–603.
59. Chapman,E.G., Moon,S.L., Wilusz,J. and Kieft,J.S. (2014) RNA structures that resist degradation by Xrn1 produce a pathogenic Dengue virus RNA. *Elife*, **3**, e01892.
60. Braun,J.E., Truffault,V., Boland,A., Huntzinger,E., Chang,C.T., Haas,G., Weichenrieder,O., Coles,M. and Izaurralde,E. (2012) A direct interaction between DCP1 and XRN1 couples mRNA decapping to 5′ exonucleolytic degradation. *Nat. Struct. Mol. Biol.*, **19**, 1324–1331.
61. Jinek,M., Coyle,S.M. and Doudna,J.A. (2011) Coupled 5′ nucleotide recognition and processivity in Xrn1-mediated mRNA decay. *Mol. Cell*, **41**, 600–608.
62. Raker,V.A., Hartmuth,K., Kastner,B. and Luhrmann,R. (1999) Spliceosomal U snRNP core assembly: Sm proteins assemble onto an Sm site RNA nonanucleotide in a specific and thermodynamically stable manner. *Mol. Cell. Biol.*, **19**, 6554–6565.
63. Ohe,K., Yoshida,M., Nakano-Kobayashi,A., Hosokawa,M., Sako,Y., Sakuma,M., Okuno,Y., Usui,T., Ninomiya,K., Nojima,T. *et al.* (2017) RBM24 promotes U1 snRNP recognition of the mutated 5′ splice site in the IKBKAP gene of familial dysautonomia. *RNA*, **23**, 1393–1403.
64. Tisserant,A. and Konig,H. (2008) Signal-regulated Pre-mRNA occupancy by the general splicing factor U2AF. *PLoS One*, **3**, e1418.
65. Tian,B., Pan,Z. and Lee,J.Y. (2007) Widespread mRNA polyadenylation events in introns indicate dynamic interplay between polyadenylation and splicing. *Genome Res.*, **17**, 156–165.
66. Kaida,D., Berg,M.G., Younis,I., Kasim,M., Singh,L.N., Wan,L. and Dreyfuss,G. (2010) U1 snRNP protects pre-mRNAs from premature cleavage and polyadenylation. *Nature*, **468**, 664–668.
67. Gunderson,S.I., Polycarpou-Schwarz,M. and Mattaj,I.W. (1998) U1 snRNP inhibits pre-mRNA polyadenylation through a direct interaction between U1 70K and poly(A) polymerase. *Mol. Cell*, **1**, 255–264.
68. Gunderson,S.I., Beyer,K., Martin,G., Keller,W., Boelens,W.C. and Mattaj,L.W. (1994) The human U1A snRNP protein regulates polyadenylation via a direct interaction with poly(A) polymerase. *Cell*, **76**, 531–541.
69. Klein Gunnewiek,J.M., Hussein,R.I., van Aarssen,Y., Palacios,D., de Jong,R., van Venrooij,W.J. and Gunderson,S.I. (2000) Fourteen residues of the U1 snRNP-specific U1A protein are required for homodimerization, cooperative RNA binding, and inhibition of polyadenylation. *Mol. Cell. Biol.*, **20**, 2209–2217.
70. Berg,M.G., Singh,L.N., Younis,I., Liu,Q., Pinto,A.M., Kaida,D., Zhang,Z., Cho,S., Sherrill-Mix,S., Wan,L. *et al.* (2012) U1 snRNP determines mRNA length and regulates isoform expression. *Cell*, **150**, 53–64.
71. Workman,E., Veith,A. and Battle,D.J. (2014) U1A regulates 3′ processing of the survival motor neuron mRNA. *J. Biol. Chem.*, **289**, 3703–3712.

nature COMMUNICATIONS

REVIEW ARTICLE

https://doi.org/10.1038/s41467-019-08859-x OPEN

Emerging roles of eraser enzymes in the dynamic control of protein ADP-ribosylation

Julia O'Sullivan[1,2], Maria Tedim Ferreira[1,2,3], Jean-Philippe Gagné[2,3], Ajit K. Sharma[4], Michael J. Hendzel[4,5], Jean-Yves Masson[1,2,6] & Guy G. Poirier[2,3,6]

Protein ADP-ribosylation is essential for the regulation of several cellular pathways, enabling dynamic responses to diverse pathophysiological conditions. It is modulated through a dynamic interplay between ADP-ribose readers, writers and erasers. While ADP-ribose synthesis has been studied and reviewed extensively, ADP-ribose processing by erasing enzymes has received comparably less attention. However, major progress in the mass spectrometric identification of ADP-ribosylated residues and the biochemical characterization of ADP-ribose erasers has substantially expanded our knowledge of ADP-ribosylation dynamics. Herein, we describe recent insights into the biology of ADP-ribose erasers and discuss the intricately orchestrated cellular processes to switch off ADP-ribose-dependent mechanisms.

Reversible post-translational modifications (PTMs) contribute to the dynamic regulation of the proteome through a diversified repertoire of functions. Protein ADP-ribosylation has emerged as a complex, dynamic, and reversible PTM system within which fundamental components work antagonistically to fine tune and tightly regulate protein behavior[1]. Similar to other transient biological processes, the ADP-ribosylation turnover relies on synthesis and degradation mechanisms[2,3]. The enzymes that perform these functions can essentially be described as writers and erasers, a nomenclature borrowed from the classification of proteins involved in epigenetic regulation. ADP-ribose writers are collectively referred to as ADP-ribose transferases (ARTs), a family of proteins with mono- or poly(ADP-ribose) transferase activities. These enzymes, especially the promising drug target poly(ADP-ribose) polymerase-1 (PARP-1), have been intensely studied by the ADP-ribosylation community for many years. More recently, attention has shifted towards the biological roles of ADP-ribose erasers, stimulated by the identification of a variety of ADP-ribose degrading enzymes with different substrate specificities. These recent findings have profoundly changed the prevailing view that ADP-ribose erasing depends almost solely on poly(ADP-ribose) glycohydrolase (PARG) activity.

[1] Genome Stability Laboratory, Centre de Recherche du Centre Hospitalier Universitaire de Québec-Université Laval, HDQ Pavilion, Oncology Division, Québec G1R 2J6, Canada. [2] Département de Biologie Moléculaire, Biochimie Médicale et Pathologie, Faculté de Médecine, Université Laval, Québec G1V 0A6, Canada. [3] Centre de Recherche du Centre Hospitalier Universitaire de Québec-Université Laval, CHUL Pavilion, Oncology division, Québec G1V 4G2, Canada. [4] Department of Oncology, Faculty of Medicine and Dentistry, University of Alberta, Edmonton T6G 1Z2, Canada. [5] Department of Cell Biology, Faculty of Medicine and Dentistry, University of Alberta, Edmonton T6G 2H7, Canada. [6] Centre de Recherche sur le Cancer de l'Université Laval, Québec G1R 3S3, Canada. These authors contributed equally: Julia O'Sullivan, Maria Tedim Ferreira. Correspondence and requests for materials should be addressed to M. J.H. (email: mhendzel@ualberta.ca) or to J.-Y.M. (email: Jean-Yves.Masson@crchudequebec.ulaval.ca) or to G.G.P. (email: Guy.Poirier@crchudequebec.ulaval.ca)

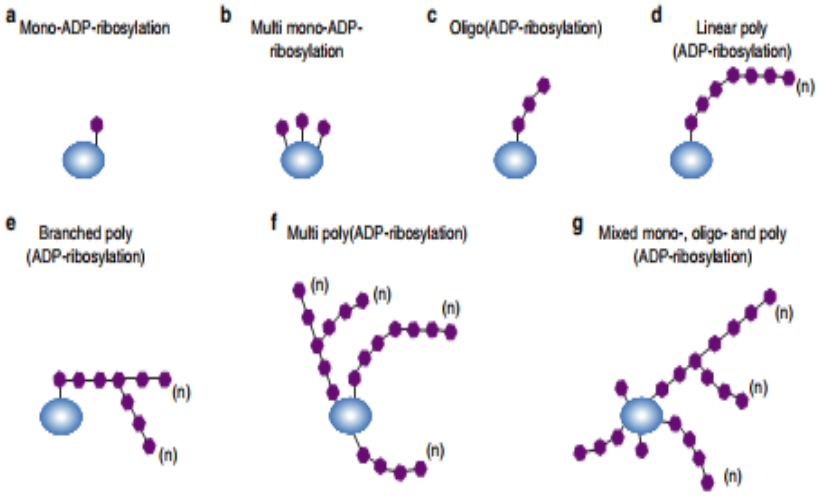

Fig. 1 Possible patterns of ADP-ribosylation on target proteins. **a** Mono-ADP-ribosylation; a single ADP-ribose molecule is attached to the protein. **b** Multi mono-ADP-ribosylation; multiple single ADP-ribose units are bound along the protein. **c** Oligo(ADP-ribosylation); short linear chains of ADP-ribose are transferred to the protein. **d** Linear poly(ADP-ribosylation); ADP-ribose moieties forming a long linear chain up to 200 units in length. **e** Branched poly (ADP-ribosylation); complex molecules composed of large and branched polymers of ADP-ribose. **f** Multi poly(ADP-ribosylation); multiple PAR chains either linear or branched on the same protein. **g** Mixed ADP-ribosylation; a mixture of the previously described ADP-ribose patterns on the same protein, generated either by the combined action of MAR- and PAR transferases or by the degradative action of erasers

ADP-ribosylation—in its strictest sense—refers to the enzymatic addition of an ADP-ribose molecule to a target substrate. The transferrable ADP-ribosyl units are typically derived from NAD^+ through the cleavage of the nicotinamide-ribosyl bond. Therefore, ADP-ribosylation reactions generally depend on NADase activity. A fundamental distinction exists between mono-ADP-ribosylation (MARylation), i.e., the transfer of a single ADP-ribose monomer, and poly(ADP-ribosylation) (PARylation), which involves the biosynthesis of elongated ADP-ribose polymers (Fig. 1). PAR polymers form nucleic acid-like polyanion structures that can serve as a docking site for a variety of reader domains (reviewed in ref. [4]). MARylation can impact protein activity, stability, substrate specificity, folding, or localization. For instance, substrates of the bacterial MAR transferases can undergo substantial structural rearrangements that profoundly modify host cell physiology and promote cellular intoxication[5]. The functional divergence between MARylating and PARylating enzymes is consistent with a biological system that involves multiple layers of antagonizing activities. This concept is supported by a rapidly expanding repertoire of ADP-ribose-degrading enzymes, suggesting that MAR and PAR modifications are continuously transferred to, and removed from, substrates by an antagonizing set of enzymes.

This review will first focus on PARG and the more recently characterized enzymes that can reverse ADP-ribosylation. Subsequently, we will discuss the biochemical methods used to detect ADP-ribosylation turnover, and expand on the regulation of ADP-ribosylation through combinatorial selective erasing mechanisms. We will conclude by discussing the therapeutic target potential of ADP-ribose erasers, focusing on the use of PARG inhibitors in synthetic lethal approaches against cancer.

Enzymes involved in the removal of ADP-ribosylation

Recent advances in defining ADP-ribose metabolism suggest that the balance between ADP-ribose writers and erasers is crucial for the coordination of multiple cellular response pathways[6]. This view is supported by the identification of a growing number of proteins implicated in writing, reading, and erasing the ADP-ribosylation modifications. Although a synthesis and degradation duality is inherent to transient PTMs, specialized erasers might occupy different catalytic niches to provide a functional and temporal reversibility of the reaction and for the recycling of ADP-ribosylated substrates. The inability of PARG—the main dePARylating enzyme—to remove MARylation marks[7,8], and its limited processivity on short PAR polymers, leaves room for the involvement of other erasers (Table 1). A complete reversal of MARylation is performed in human cells by amino-acid-specific ADP-ribose-acceptor hydrolases, such as the macrodomain-containing proteins MacroD1 and MacroD2, the terminal ADP-ribose protein glycohydrolase 1 (TARG1), and the ADP-ribose hydrolase (ARH) family members ARH1 and ARH3. Moreover, several phosphodiesterases have been shown to possess ADP-ribose processing activity. In this section, we provide an overview of these different ADP-ribose erasing enzymes.

Poly(ADP-ribose) glycohydrolase (PARG). Although a role of MARylation in response to genotoxic stress has become better established recently (reviewed in ref. [9]), only PARylation occurs in conjunction with a substantial decrease of intracellular NAD^+ concentrations when extensive DNA damage is encountered. Globally, PARylation processes account for a large proportion of the ART activity in cells. Therefore, dePARylation can be viewed as the predominant erasing activity.

PARG is the major dePARylating enzyme, and is primarily responsible for hydrolyzing the glycosidic linkages between ADP-ribose units of PAR polymers to generate free ADP-ribose monomers. Only a single *PARG* gene has been identified in mammals and its sequence is highly conserved[10]. *PARG* homologs are detected in a wide range of eukaryotes with the exception of budding yeast. The human *PARG* gene encodes for multiple variants produced by alternative splicing of a unique mRNA[11,12]. The characterization of *PARG* expression products and the apparent molecular weight heterogeneity of PARG have been reviewed elsewhere[13]. PARG is a modular protein with a four domain architecture[10] (Fig. 2). Domain A spans exons 1–3 and forms a predicted N-terminal intrinsically disordered

Table 1 Human ADP-ribose erasers

Eraser	Classification	Substrate	Targeted bond	ADP-ribosylation reversal	Protein adduct	Amino acid selectivity	References
PARG	Macrodomain	PAR	O-glycosidic	Partial	ADP-ribose	Linkage-independent	23,80
MacroD1	Macrodomain	MAR	Carboxyl ester	Complete	None	D/E	84
MacroD2	Macrodomain	MAR	Carboxyl ester	Complete	None	D/E	84
TARG1	Macrodomain	MAR/PAR	Carboxyl ester	Complete	None	D/E	58
ARH1	ARH fold	MAR	N-glycosidic	Complete	None	R	48
ARH3	ARH fold	MAR/PAR	O-glycosidic	Complete	None	S	46,48
NUDT9	NUDIX	PAR	Phosphodiester	Partial	Phosphoribose	Linkage-independent	65
NUDT16	NUDIX	MAR/PAR	Phosphodiester	Partial	Phosphoribose	Linkage-independent	65,66
ENPP1	ENPP (PDNP)	MAR/PAR	Phosphodiester	Partial	Phosphoribose	Linkage-independent	67

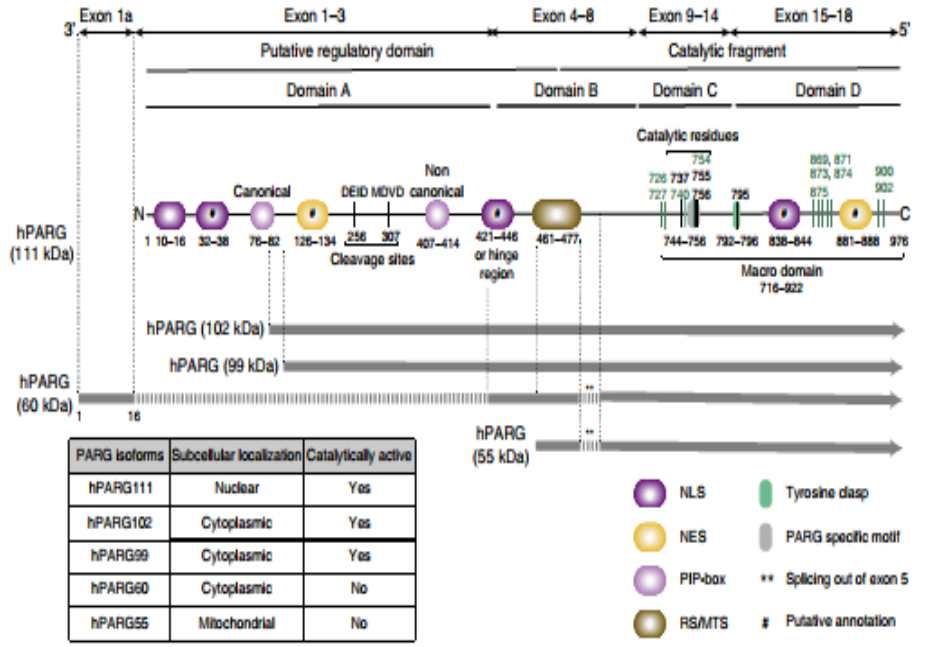

PARG isoforms	Subcellular localization	Catalytically active
hPARG111	Nuclear	Yes
hPARG102	Cytoplasmic	Yes
hPARG99	Cytoplasmic	Yes
hPARG60	Cytoplasmic	No
hPARG55	Mitochondrial	No

Fig. 2 Schematic representation of human PARG and its isoforms. Human PARG originates from a 3198 bp mRNA sequence with a single 2931 bp open reading frame (ORF). The ORF contains 18 exons and encodes a protein of 976 amino acids with a molecular weight of 111.1 kDa. This mRNA undergoes alternative splicing to produce different PARG isoforms. Five human PARG transcripts have been identified. Full-length human PARG (hPARG111) contains an N-terminal regulatory domain and a C-terminal catalytic domain that is essentially a macrodomain fold. hPARG102 and hPARG99 are translated from the start codons located in exon 2 and exon 3, respectively. hPARG60 results from alternative splicing that connects exon 1a, exon 4, and exons 6–18. Because of the usage of a facultative exon (exon 1a), hPARG60 has an alternative N-terminal protein sequence of 16 amino acids that is unique to this isoform. hPARG55 is produced from the initiation of translation at the start codon located in exon 4. Exon 5 is spliced out in both hPARG60 and hPARG55 isoforms. PARG can be sub-classified into four different domains. Domain A, which includes exons 1–3, forms the majority of the putative regulatory domain. This region contains two caspase-3 cleavage sites at amino acid position 256 (DEID) and 307 (MDVD). An uncharacterized nuclear localization signal (NLS) overlaps with a hinge region between the putative regulatory domain and the catalytic fragment. Furthermore, PARG comprises domain B (exons 4–8), domain C (exons 9–15) and domain D (exons 15–18). The latter two domains form the base of the macrodomain fold and contain the catalytic pocket and ligand binding sites. The catalytic residues (Asp737, Glu755, and Glu756) and Tyr795, which interacts with PARG inhibitor ADP-HPD are indicated as black lines. Residues colored in green have been implicated in the binding of ADP-ribose. Furthermore, colored boxes denote PARG-specific motif (GGG-X_{6-8}-QEE), regulatory segment/mitochondrial targeting sequence (RS/MTS), Tyrosine Clasp structural motif, PCNA-interacting protein (PIP) motif, and nuclear export signal (NES)

regulatory domain[14]. Domain B (exons 4–8) connects the N-terminal region to the catalytic domain through a hinge region[11] and contains a regulatory segment[15]. Domain C (exons 9–14) contains the catalytic active site and the PARG signature motif[16]. Domains C and the C-terminal domain D (exons 15–18) form the PARG macrodomain[7,17]. A number of nuclear export signals (NES) and nuclear localization signals (NLS) are distributed throughout the PARG sequence.

The expression of a variety of *PARG* splice variants with different localizations enables functional specialization[11,18]. In human cells, major isoforms include a full length 111 kDa PARG enzyme and splice variants that generate proteins of 102 and 99 kDa (Fig. 2). While full length PARG is mostly nuclear and accounts for a minor fraction of global cellular activity, the smaller isoforms localize primarily to the cytoplasm with a perinuclear distribution, and seem to be responsible for most of

the PAR processing activity[19]. Therefore, nuclear and cytoplasmic compartmentalization, and the shuttling of PARG isoforms between the nucleus and cytoplasm have been proposed as a mechanism to regulate cellular PAR levels[18,20]. PARG mRNA also undergoes additional alternative splicing that generates small isoforms of 55 and 60 kDa. Both hPARG55 and hPARG60 isoforms have been found to be catalytically inactive due to the absence of exon 5-encoded amino-acids[21] (Fig. 2). Therefore, these small human PARG isoforms are not involved in general PAR turnover in cells.

Human PARG is a constitutively active, low abundance enzyme that possesses both exoglycosidase and endoglycosidase activities. PARG mainly functions as an exoglycosidase, sequentially digesting glycosidic linkages from the protein-distal end of the polymer similar to carbohydrate glycosyl hydrolases[22]. This processivity improves the catalytic activity of PARG but is strongly chain-length dependent[23]. On the other hand, it has been estimated that ~20% of PARG depolymerization activity can be accounted for by in-chain endoglycosidic degradation[24]. The fact that PARG has two mechanisms of action with different degradation kinetic parameters and PAR structure-affinity might be an overlooked characteristic in the complex and intricate interplay between ADP-ribose readers and erasers, as will be discussed further below.

The importance of the catalytic activity of PARG became clear with the observation that *PARG*$^{-/-}$ mice were embryonic lethal[25] and that PARG-depleted cells are hypersensitive to genotoxic insults[26,27]. This is accompanied by PAR accumulation and early apoptosis, suggesting that efficient PARG-mediated PAR turnover is required for the recovery from DNA damage. PARG has also been shown to be necessary to prevent massive PAR production upon prolonged replicative stress[28]. Schreiber and colleagues demonstrated that PARG deficiency delays cellular recovery from persistent replication stress, triggered by prolonged hydroxyurea treatment[28]. These blocked cells display high PAR levels, which negatively impacts RPA foci formation and its association with single-stranded DNA (ssDNA). The prevention of RPA loading eventually leads to increasing areas of uncovered ssDNA, which then transform into DNA double-strand breaks (DSBs), resulting in the formation of more PAR. Ultimately, this amplification loop promotes apoptosis and/or necrotic cell death in proliferating cell populations. These observations are in agreement with the finding that PARG localizes to replication foci throughout S-phase and interacts with the replication protein PCNA[29,30]. Furthermore, they complement an earlier report that PARG-deficient cells treated with DNA alkylating agents have an increase in S-phase arrest together with high levels of the DSB marker γH2AX[31]. Correspondingly, the Lopes group showed that PARG inactivation affects the progression of all replication forks and alters the molecular architecture of a significant fraction of replication intermediates[32]. These results provided mechanistic insight into the essential role of PARG in cell growth and development, in line with the observed embryonic lethality of *PARG*$^{-/-}$ mice[33].

Another important role of PARG during the DNA damage response is to maintain stable levels of PAR and to recycle highly automodified PARP-1. The stabilization of PAR levels is crucial for protecting the cell against parthanatos, a caspase-independent PAR-mediated type of cell death[34]. Parthanatos is triggered by the release of the apoptosis-inducing factor (AIF) from the mitochondria to the nucleus[35,36]. Once translocated to the chromatin environment, AIF leads to large-scale DNA fragmentation and chromatin condensation, which is followed by cell death[37]. Depletion of PARG has been shown to be protective against oxidative stress-induced parthanatos by preventing the release of AIF from the mitochondria[38].

Lastly, PARG has also been implicated in telomere maintenance. PARG is capable of negatively regulating the access to telomeric DNA by reversing ADP-ribosylation of the telomeric-specific protein TRF1, contributing to the regulation of telomere repair and replication[39,40]. Overall, these examples show that the dynamic equilibria established between PARP-1 and PARG activities, and therefore PAR levels, are key for controlling cell fate, suggesting that PAR erasers are as important as PAR writers for cellular homeostasis.

ADP-ribose hydrolases (ARHs). ADP-ribose conjugation was first described as a PTM catalyzed by bacterial ADP-ribosylating exotoxins (bAREs)[41]. Bacterial MAR transferases (MARTs) have related genes in humans whose extracellular expression makes them irrelevant or inoperative with respect to intracellular ADP-ribose-mediated pathways[42]. In human cells, intracellular protein MARylation is performed by members of the ADP-ribosyl transferases diphtheria toxin-like proteins (ARTDs). Formerly classified as PARPs[43], the 17 members of the ARTD family in human were renamed according to a systematic nomenclature that better reflects their structural features and catalytic properties[44]. There are currently 11 members of the human ARTD family characterized as MARTs, typically renamed after the type of ADP-ribose molecule (i.e., MAR) they transfer onto themselves or target substrates[45,46].

The ADP-ribose hydrolase (ARH) family consists of three related proteins[47]. While ARH2 substrates are yet to be discovered, ARH1 is a highly active ADP-ribosyl-arginine hydrolase[48] and ARH3 is an ADP-ribosyl-serine hydrolase[49] (Table 1 and Fig. 3). Mice that lack ARH1 are more sensitive to cholera toxin[50] and tumor-prone, having increased incidences of adenocarcinoma, lymphoma, and metastases[51]. ARH3-deficient mouse embryonic fibroblasts show increased steady-state abundance of serine-ADP-ribosylation in vivo[52] and DNA damage-induced serine-ADP-ribosylation is efficiently reversed by ARH3[49]. In contrast to ARH1, ARH3 also possesses activity toward the O-glycosidic bond of PAR, similar to the exoglycosidic activity of PARG[42]. However, ARH3 does not rescue *Drosophila* or mouse genetic knockouts of PARG from cell death or PAR accumulation[25,53], suggesting that it cannot compensate for the loss of PARG. Owing to its abundance in the cytoplasm, ARH3 participates in a second stage of PAR hydrolysis following the release of free PAR polymer branches by other erasers. This may help lower the cytoplasmic PAR levels, ultimately preventing mitochondria-dependant apoptotic pathways such as parthanatos[54].

While ARHs only erase arginine- and serine-MARylation and macrodomain-containing enzymes specifically target aspartate- and glutamate-MARylation (see next section), ARTDs have been shown to mediate ADP-ribosylation on a wide range of amino-acid residues[55,56] This apparent discrepancy will be discussed later on in this article.

Macrodomain-containing ADP-ribose erasers. The macrodomain fold is an evolutionarily conserved, compact globular-shaped structure of ~25 kDa present throughout all of the biological kingdoms[57]. It can be found as a stand-alone module or integrated into multi-domain proteins. The macrodomain was the first characterized ADP-ribose-binding module. It can bind terminal ADP-ribose structures with nanomolar affinity[58]. There is functional diversity related to structural variation in the macrodomain protein family. A subgroup of macrodomains lacks the ability to bind ADP-ribose while others acquired glycosidic activity involved in ADP-ribosylation reversal[4]. There are ten human macrodomain-coding genes: the histone H2A variants

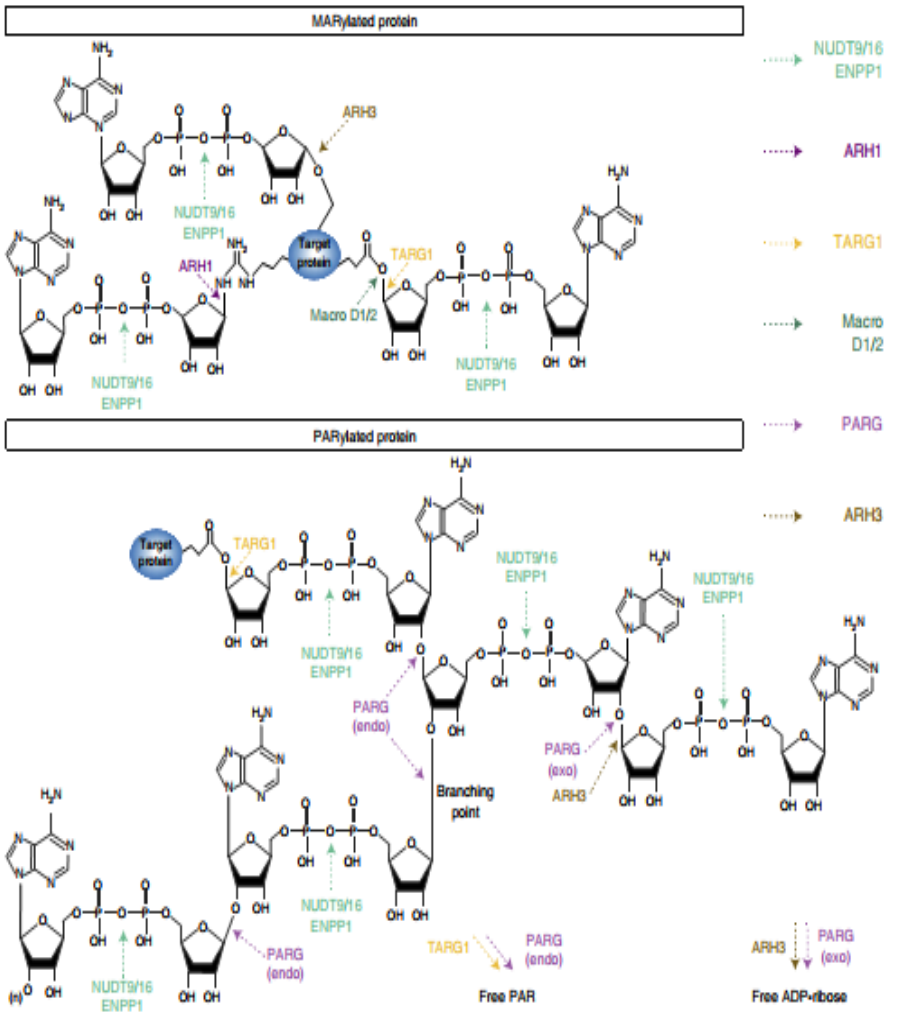

Fig. 3 Reversal of protein ADP-ribosylation by MAR and PAR erasers. The diagrams represent MARylated (upper panel) and PARylated proteins (lower panel) with bond-specific chemical cleavage sites for each eraser. A subgroup of erasers that comprises MacroD1, MacroD2, and ARH1 are MAR-specific erasers involved in the removal of single ADP-ribose adducts. MacroD1 and MacroD2 are macrodomain-containing enzymes that release ADP-ribose from ADP-ribosylated acidic residues (aspartate and glutamate). ARH1 is currently the only known MAR hydrolase that specifically removes MAR from arginine residues. A second subgroup that includes TARG1, ARH3, NUDT9, NUDT16, and ENPP1 can target both MAR and PAR modifications. The TARG1 macroprotein hydrolyzes glutamate-ADP-ribose bonds and releases ADP-ribose from MARylated proteins. TARG1 has also the unique ability to remove entire PAR chains from acidic residues of PARylated proteins. ARH3 is limited to exoglycosidic activity toward PAR chains and releases free ADP-ribose. In addition, it possesses MAR hydrolase activity specifically targeting the O-linked ADP-ribosylation. NUDT9 and NUDT16 have nucleoside diphosphate-linked moiety-X (NUDIX) domains, which cleave pyrophosphate bonds and release phospho-ribosyl-AMP from PAR chains or AMP from MARylated proteins as major reaction products. ENPP1 is a pyrophosphatase lacking a NUDIX domain but with the capability of digesting PAR and MAR modifications similar to NUDIX enzymes. PARG is the main PAR-degrading enzyme but shows no activity towards MARylated proteins. Human PARG is unable to cleave the proximal ADP-ribose groups from a modified protein but possesses exo- and endoglycosidic activities to hydrolyze the glycosidic bonds between ribose units of PAR. The exoglycosidic activity of PARG generates free ADP-ribose from the processive degradation of PAR from the distal to the proximal end while its in-chain cleavage activity (endoglycosidic) produces protein-free PAR. The endoglycosidic degradation of PAR by of PARG is also responsible for the hydrolysis of the branching points formed when non-adenine riboses are linked together (branching point)

Macro H2A.1 and Macro H2A.2; MacroD1, D2, and D3; TARG1; the chromodomain-helicase-DNA-binding protein 1-like (CHD1L) and the macrodomain-containing ARTDs 7-8-9 (formerly named PARPs 15-14-9). Among these, MacroD1, MacroD2, and TARG1 were classified as ADP-ribose erasers because of their ADP-ribose hydrolase activities. MacroD1 and MacroD2 cleave the chemical link between MAR and an acceptor protein while TARG1 presents the unique capability of cleaving both MARylated and PARylated side chains of aspartate and glutamate residues[59] (Fig. 3).

The role of TARG1 in PAR turnover remains elusive but a PARylation-dependent relocation of TARG1 to the nucleoplasm has been observed[60] in addition to its recruitment to DNA lesions in a PAR-dependent fashion[59]. The catalytic domain of TARG1 is different from PARG but resembles the OGG1 DNA glycosylase[59] and directly targets the carboxyl ester ADP-ribose linkages

to remove the modification from its substrate. The ability of TARG1 to remove whole PAR chains from the substrate most proximal attachment point is unique among the known erasers, adding another putative regulatory layer to PAR cellular functions. For years, only PARG was known to generate protein-free ADP-ribose polymers as a consequence of its endoglycosidic activity[23] (Fig. 3), which becomes the major mode of action when robust PARP activation (i.e., strong genotoxic insults) leads to the synthesis of large and branched PAR[61]. Although this idea has not been fully evaluated, TARG1-mediated production of protein-free PAR might be involved in parthanatos[59].

Similarly to TARG1, the mono-ADP-ribose hydrolase activities of MacroD1 and MacroD2 are also selectively directed toward ester bonds established by ADP-ribosylated aspartate and glutamate residues, although with different catalytic modes (reviewed in ref. [62]). Current experimental data suggest that ester-type ADP-ribose bonds in protein substrates are specific targets of the macrodomain erasers. This activity could play a regulatory role in vivo as MacroD2, for example, has been implicated in the recycling of automodified PARP-1[63]. The removal of the autoinhibitory MAR moieties from PARP-1 by MacroD2 has been suggested to explain the accumulation of MARylated PARP-1 in the context of MacroD2 gene deletion in human colorectal cancer cells[64]. The underlying MacroD2-dependent PARP-1 recycling model proposed by Sakthianandeswaren et al. involves a biphasic erasing of PARP-1 automodification, which implicates PARG as the primary PAR trimming enzyme responsible for the generation of MAR adducts that can subsequently be targeted by MacroD2[64].

As mentioned above, PARG is a member of the macrodomain eraser family, although there is no similarity between the amino-acid sequence of PARG and other macrodomain-containing proteins. However, there is a close structural and evolutionary relationship between macrodomains and PARG[17], and its catalytic center is essentially a macrodomain fold[7,17].

Phosphodiester ADP-ribose hydrolases. Homopolymers of PAR are composed of successive ADP-ribose moieties linked together by alternating phosphodiester and O-glycosidic linkages (Fig. 3). The phosphodiester bond is also central to the ADP-ribose monomer itself as it links the adenosine structure to the ribose. The activity of snake venom phosphodiesterases was instrumental in the elucidation of PAR structure in the early studies of PAR-ylation, as it was used to determine chain length and PAR branching frequency[65]. Only recently, a role of phosphodiesterases in the reversal of ADP-ribosylation has been proposed, following the discovery of a group of ADP-ribose processing phosphodiesterases that includes NUDIX (nucleoside diphosphates linked to moiety-X) superfamily members NUDT9 and NUDT16 as well as ectonucleotide pyrophosphatase/phosphodiesterase 1 (ENPP1)[66–68]. These erasers target the phosphodiester bound in ADP-ribose moieties. Therefore, their activity is independent of the type of ADP-ribose linkage established with the substrate protein. However, these enzymes should be classified as partial erasers since they leave a phosphoribose remnant attached to the target protein (Fig. 3 and Table 1). It is still unclear whether these phosphoribose remnants are correlated with specific biological outcomes but a pathological accumulation of phosphoribose on glutamate residues has been described[69]. Furthermore, the phosphodiesterase-catalyzed removal of the distal adenine in PAR ploymers through cleavage of the terminal AMP likely prevents digestion by PARG, as it was observed with etheno-PAR, a derivatized PAR with modified adenine moieties[70].

In vivo, NUDIX hydrolases seem to fulfil 'housekeeping' functions, facilitating the detoxification of potentially deleterious endogenous metabolites[71]. Furthermore, they have been proposed to be involved in replenishing the cellular AMP pool from ADP-ribose monomer products of PARG/ARH3-mediated PAR depolymerization. This metabolic response is consistent with the AMP-dependent mitochondrial energy failure observed following DNA damage and PARP-1 activation[72]. The accumulation of PAR-derived AMP has also been implicated in the modulation of mTOR signalling through AMPK activation[73]. These examples show that ADP-ribose erasing reactions can have diverse effects on metabolism by generating free ADP-ribose monomers and related molecules such as AMP.

Interestingly, the hydrolase activity of a third NUDIX, NUDT5, diverges from the other ADP-ribose-processing NUDIX hydrolases because it cannot hydrolyze protein-conjugated ADP-ribose. However, NUDT5 generates ATP from free ADP-ribose and pyrophosphate in a recycling-like process to quickly replenish nuclear ATP levels[74]. While NUDT5 cannot be classified as an ADP-ribose eraser per se because of its inability to remove protein ADP-ribosylation, it certainly deserves attention as it can influence the level of energetic substrates following PAR catabolism.

The extracellular ENPP1 phosphodiesterase, which lacks a NUDIX and a macrodomain, is yet to be characterized regarding its involvement in ADP-ribose processing. ENPP1 shows considerable phosphodiesterase activity in vitro against MAR and PAR, exceeding that observed for NUDT16 in a cell-free system[68]. The high conversion rate of ADP-ribosylation modifications to phosphoribose adducts by ENPP1 has been suggested as a key feature for the generation of phosphoribose signatures for analysis by liquid chromatography-mass spectrometry (LC-MS)[68].

Detection and evaluation of MAR and PAR erasing activities

The emergence of a variety of new players that modulate ADP-ribose catabolism underscore the urgent need for methods capable of rapidly measuring erasing activities. Historically, most assays were developed to measure the disappearance of PAR as a consequence of PARG glycosidic activity. Usually based on residual PAR precipitation assays, these methods give rise to inconsistencies when monitoring PARG activity[75]. Based on this observation, a thin-layer chromatography (TLC)-based strategy coupled to a radiolabed PAR substrate was developed to monitor ADP-ribose accumulation rather than substrate disappearance[75]. This TLC method has been used successfully to measure PARG activity in cell extracts and tissues[76], characterize site-directed mutants[77] and to evaluate the inhibitory strength of small molecules[78,79]. Later, the conversion of the reaction product, the monomeric ADP-ribose, into a quantifiable fluorophore has been reported as a nonradiometric and high-throughput assay for PARG activity[80].

TLC assays are inadequate to demonstrate the contribution of individual PARG isoforms or additional PAR-degrading enzymes to global PAR erasing activity in cells. In this respect, PAR zymograms were developed to detect alternative catabolic activity against PAR in complex samples. Zymograms are essentially composed of radiolabeled automodified PARP-1 co-polymerized with a polyacrylamide gel. Following renaturation, digested regions can be visualized on the autoradiogram. Although protein renaturation and in-gel activity constraints the applicability of this strategy, zymography proved to be an effective and sensitive method to detect PAR hydrolysis by PARG[75]. However, no significant additional PAR erasing activity has been detected in most cell extracts using this approach, contributing to the long held

belief that PARG was solely responsible for mediating PAR degradation in cells.

Consistent measurements of PARG activity under standardized conditions are hindered by the absence of a well-defined substrate (i.e., of defined length and branching frequency). Additionally, none of the above-mentioned methods is sufficiently accurate to discriminate between the exo- and endoglycosidic activities of PARG. A number of assays have been designed to specifically monitor the endoglycosidic activity of PARG in protein-bound and protein-free polymer populations, but the most widely used methods are based on the analysis of PAR reaction products on high-resolution DNA sequencing gels[24] and by HPLC[23,81]. Despite being experimentally challenging, HPLC analysis of PARG degradation products following digestion with snake venom phosphodiesterase (svPDE) remains the method of choice to determine the relative contribution of both PARG glycosidic activities to PAR erasing. In this assay, the exoglycosidic activity allows PARG to attack PAR polymers at the protein-distal chain end to release ADP-ribose units, which are subsequently converted to AMP by cleaving the phophodiester bond with snake venom phosphodiesterase. The endoglycosidic actvity of PARG generates additional chain termini that release supplementary AMP upon double digestion with svPDE, which can be measured to estimate the relative endo/exo activities[23].

A more recently developed alternative to measure PARG endoglycosidic activity is based on the detection of ADP-ribose oligomers by LC-MS[61]. In this approach, PAR termini are protected with an inactive bacterial PARG^{E115Q} mutant that blocks exoglycosidic cleavage. When human PARG is added to the blocked PAR substrate, only endoglycosidic cleavage can occur. The accumulation of PAR fragments (ADP-ribose oligomers) is detected by LC-MS in the form of specific mass-to-charge ratios and correlated to the endoglycosidic activity of PARG[61]. Although exo- and endoglycosidic mechanisms are essential for efficient dePARylation, it is common to reflect PARG activity in a single value that integrates both activities based on commercially available chemiluminescence- and colorimetric-based detection systems. These assays are suitable for high-throughput screening of PARG inhibitors in addition to antibody-based detection methods[82]. However, immunological detection of PAR is prone to underestimating the presence of residual ADP-ribose oligomers for which the antibodies generally possess low affinity[83]. The recent development of antibody-like MAR- and PAR-binding reagents should prove beneficial to the evaluation of PARG inhibition in cells[84].

Given the increasingly important role of MAR erasers, a number of approaches have also been developed to facilitate the detection of MAR hydrolase activities. One of the most effective approaches is to use the auto-MARylated PARP-1^{E988Q} mutant as a substrate for MARylation erasers. This PARP-1 mutant is significantly more active than other MARTs and thus represents a robust approach to generate a MARylated substrate. *Bona fide* MARTs such as PARP-10/ARTD10 also have been used as MARylated substrates[49,59,67,68,85]. Furthermore, the oligo(ADP-ribosyl)ated PARP of *H. aurantiacus* was employed as an intermediate length substrate for ADP-ribose erasing assays[66]. Reaction products are generally resolved by SDS-PAGE or TLC. These approaches provide valuable substrate models for ADP-ribosylation erasing studies but may not reflect the diversity and wide range of ADP-ribose polymer species, which could explain the persisting confusion regarding the linkage selectivity of MAR hydrolases. While some MARTs such as PARP-10/ARTD10 appear to be MARylated exclusively on acidic residues[85], it is less clear which types of ADP-ribose–protein linkages exist in other MARTs and PARP-1^{E988Q}. A panel of linkage-specific substrates would be necessary to assess the diversity of MARylation reversal. For example, ADP-ribosylated actin by the arginine-specific ADP-ribosyltransferase CDTa provides a defined substrate for arginine-mediated ADP-ribosylation studies while the threonine-specific transferase TccC3 mono-ADP-ribosylates threonine residues of the same substrate[85].

It should be kept in mind that the amino-acid sequence surrounding the ADP-ribosylation site is unknown in these substrates and might influence the recognition by the eraser. Similarly, MARylated substrates, such as histones, may carry additional PTM decorations that could also tune the binding affinity of the erasing enzyme. The development of synthetic peptides with site-specific ADP-ribosylations will be particularly useful for dissecting the substrate specificity of ADP-ribose erasers[86]. *Trans*-ADP-ribosylation of synthetic peptides with PARP-1^{E988Q} has been demonstrated by MS analysis but the actual yield of peptide MARylation is probably too low for subsequent biochemical analysis, even after affinity purification[87]. Alternatively, peptide microarrays containing several ADP-ribosylated residues in a variety of sequence contexts may allow profiling of the recognition and processing specificity of MARylation erasers.

ADP-ribose linkage selectivity of erasers

An intrinsic characteristic of ADP-ribosylation is the molecular heterogeneity and complexity of the reaction product transferred to target substrates. Therefore, ADP-ribosylation needs to be viewed in a length- and site-dependent manner. The site-specific length of PAR polymers is difficult to test experimentally and further studies are needed to characterize the length diversity of PARylated substrates. More progress has been made with regard to determining ADP-ribosylation sites within proteins. The site-specific localization of ADP-ribosylation modifications could be mapped in a system-wide manner in several recent MS-based proteomics studies. Notably, these methods are significantly more challenging and difficult to implement than standard MS-based approaches that only aim for protein identification[56,88–92].

A survey of the current literature indicates that all chemically reactive amino acids (i.e., excluding those with hydrophobic side chains) may be targeted by ADP-ribosylation under physiological conditions[45,93]. The biological significance of differential ADP-ribosylation site usage is unknown but ADP-ribose–protein linkages appear to be processed by erasers with rigid selectivity (Table 1). For instance, ARH1 hydrolyzes N-linked MARylated arginines[42], the macrodomain-containing proteins are specific for the carboxyl ester bond formed with the side chains of aspartate and glutamate residues[85] while ARH3 hydrolyzes O-linked MARylated serines[52]. Although only limited information is available, a modulation of ADP-ribose recognition has been reported for MAR erasers, suggesting that the local amino acid sequence environment influences ADP-ribosylation erasability[52,94].

The different susceptibility of each type of ADP-ribosylation to degradation by the erasers suggests that the stability of ADP-ribosylation in cells may vary depending on the type of linkages. For example, the absence of a specific enzyme to erase ketoamine-linked ADP-ribose from lysine residues has been hypothesized to be involved in the long-term maintenance of histone epigenetic marks[95]. Furthermore, PAR polymer populations with different half-lives, depending on their length and complexity, have been reported[23,96]. This suggests that recognition and processing of multi-site and multi-structural ADP-ribosylation involves complex coordination of the erasers. However, current atlases of ADP-ribosylation signatures, notwithstanding their importance, from human cancer cells provide little information regarding the occupancy rate of different ADP-ribosylation modifications.

At the moment, it is unclear how multiple ADP-ribosylation linkages can be read and transformed into meaningful signalling information.

The termini of a DNA strand break can also be reversibly modified by covalent PARylation in vitro[97–100], and the ADP-ribose ester bonds of MARylated, phosphorylated double-stranded DNA can be hydrolyzed by MacroD1[101]. PARP-3-mediated MARylation of DNA can also be erased by MacroD2, TARG1, PARG, and ARH3[99]. For DNA MARylation reversal, MacroD1, MacroD2, and TARG1 target the same type of ester bonds (Table 1), while ARH3 activity likely targets the O-glycosidic ribose-ribose bond. Moreover, PARG can efficiently remove MAR moieties attached to DNA phosphate residues - in contrast to its activity on protein substrates[98,99]. This observation emphasizes the importance of exploring the substrate specificity of erasers, which might not be as rigid as initially thought. The role of DNA ADP-ribosylation in the repair mechanisms that maintain the integrity of genomic DNA remains elusive but represents a new dimension in ADP-ribosylation dynamics.

The identification of ADP-ribosylated substrates is undergoing rapid expansion owing to the development of high-sensitivity mass spectrometers. The functional significance of most ADP-ribosylation that occurs on a variety of amino-acid targets is not yet understood. Some of these modifications might be generated nonenzymatically when a biomolecule encounters a reactive metabolite such as ADP-ribose. The formation of ketoamine glycation conjugates on histones lysine and arginine amino acids, in the presence of ADP-ribose, has been documented[102]. This phenomenon might be explained by the local accumulation of ADP-ribose, as a result of PAR hydrolysis by PARG in vitro during sample preparation for MS analysis[56]. However, artefactual glycation by free ADP-ribose released by PARG on lysine and arginine residues was not observed in cell extracts supplemented with free PAR chains and PARG[103]. Alternatively, the accumulation of free ADP-ribose within a confined area might arise from a side reaction based on PARP-1's abortive NADase activity[104]. Following PARP-1 automodification, NAD^+ hydrolysis becomes a major component of PARP-1 activity, which releases ADP-ribose that can react with glycation-prone amino groups of proteins or other biomolecules. Therefore, caution is recommended in interpreting results based on the identification of rare, low abundant or atypical ADP-ribosylation modifications.

A model for cellular PARylation dynamics

The existence of a continuum of ADP-ribose polymer lengths in cells coupled to a variety of amino acid linkages suggests that various erasing modes act together to drive the ADP-ribosylation cycle. PARG possesses the highest level of PAR chain degradation activity. However, its inability to remove the proximal ADP-ribose moiety from proteins illustrates that a complete reversal of ADP-ribosylation likely requires an orchestrated cellular response involving both MAR and PAR erasers[61]. Substrates that would have undergone fast, but partial, trimming of their PARylation modifications by PARG could then be processed by a group of specialized erasers. The rapid initial degradation process likely depends on the synergistic endo/exo dePARylation activity of PARG, considering that endoglycosidic PARG activity also releases protein-bound PAR polymers and predominates in the earliest phases of the degradation process[24].

At the same time, the interplay between ADP-ribosylation writers and erasers could regulate the temporal order of the signalling response to PARP-1 activation. For example, the dynamics of ADP-ribosylation reversal strongly depend on the type of PAR polymer synthesized. Large and complex polymers generated during the DNA damage response are short-lived and transient with half-lives of few seconds while the constitutive fraction of PAR is degradation-resistant for hours[96]. Collectively, these observations suggest that ADP-ribosylation erasing may be described as a multistep processing cascade with specific kinetics depending on the physiological context (Fig. 4).

Our understanding of ADP-ribosylation has been substantially advanced by the identification of histone PARylation factor 1 (HPF1) as a regulator of both histone ADP-ribosylation and PARP-1 automodification. This finding demonstrated that a PARP-1-interacting factor can modulate PARP-1's PARylation activity, switching it to O-linked ADP-ribosylation[105]. In contrast, most previous reports showed that PARP-1 activity is modulated by a variety of DNA lesions[106], post-translational modifications[107] or NAD^+ availability[108]. The observed HPF1-dependent serine-ADP-ribosylation of PARP-1, histones and chromatin-interacting factors as well as accumulating evidence that serine residues are the preferred ADP-ribosylation targets upon DNA damage induction[109–113] suggest that serine-ADP-ribosylation predominates. This challenges the current model, in which protein ADP-ribosylation is primarily localized to aspartate, glutamate, lysine and arginine residues with cell type- and tissue context-dependent stoichiometries. However, it would be premature to conclude that DNA-dependent PARPs are uniquely engaged in O-glycosidic linkages with serine and, as recently demonstrated, tyrosine residues[114] in all HPF1-expressing cells and that all other amino acid linkages are in vitro artifacts. For instance, large-scale proteomics studies provided convincing and robust evidence of site-specific glutamate and aspartate ADP-ribosylation[88,115,116].

As discussed above, HPF1 appears to switch PARP-1 ADP-ribosyltransferase activity toward O-linked ADP-ribosylation. This observation implies that PARP-1-interacting proteins can have profound impact on the PARP-1 enzymatic mechanism. In the case of HPF1, the switch from a carboxyl ester ADP-ribosylation chemistry on acidic glutamate and aspartate amino acids to O-linked ADP-ribosylation of neutral serine residues may be explained by an HPF1-dependent reconfiguration of PARP-1 active site[110,117]. HPF1 accumulates at DNA lesions in a PARP-1-dependent but PAR-independent manner[105]. Considering that PARP-1 relocation to DNA damage sites precedes HPF1 recruitment, PARP-1 could be involved in the glutamate and aspartate ADP-ribosylation of the nucleosomal surface[118] before switching its catalytic activity toward serine residues as HPF1 accumulates locally. This may indicate a regulatory mechanism with several overlapping waves of linkage-specific ADP-ribosylation (Fig. 4).

The modulation of PARP-1 activity can also be observed in polymer turnover systems that recapitulate PAR metabolism. In these systems, the addition of PARG shifts the ADP-ribose transferase activity of PARP-1 from automodification to histone modification[23,119–121]. Similarly, HPF1 promotes histone ADP-ribosylation and limits PARP-1 hyper-automodification[105]. These results motivate the identification of additional modulators of PARP-1 activity. They also suggest that PARP-1 intramolecular conformational changes may be transmitted via protein-protein interactions. This mechanism is exploited to provide an alternative to common PARP-1 inhibition by antagonizing NAD^+ binding at the catalytic site[122]. Besides, a network of allosteric communications is known to connect damage recognition to catalytic domain remodelling in order to activate PARP-1[123–127]. The fact that PARP-1 activity depends on protein conformational flexibility is illustrated by the identification of a PARP-1 inhibitor that promotes the formation of a complex specifically through PARP-1 BRCT domain[122]. Although the BRCT domain itself is dispensable for PARP-1 activity[127], the rigidity of the cross-linked

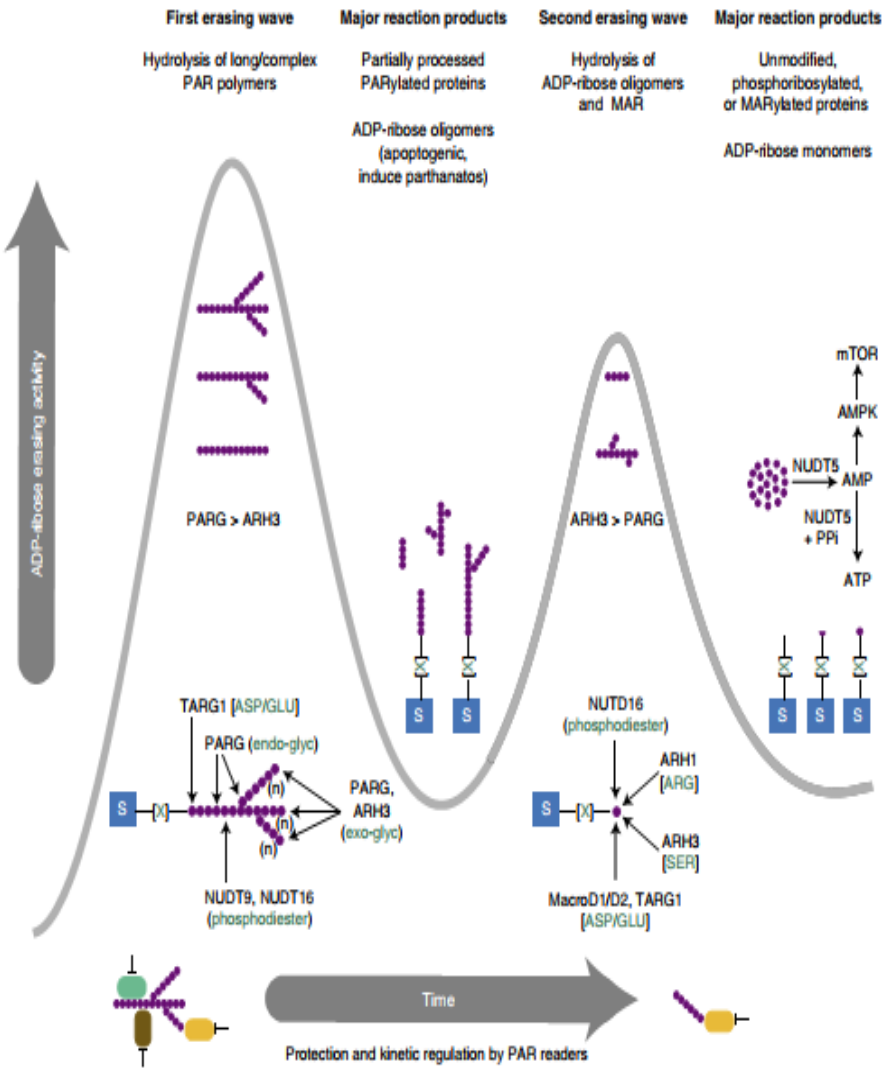

Fig. 4 The dynamic mechanism of ADP-ribosylation reversal. ARTDs consume NAD+ and transfer ADP-ribose moieties onto target substrates (blue boxes) on different amino acids side chains (green [X]). These proteins can have a variety of different ADP-ribosylation modification patterns, as described in Fig. 1. In the context of severe genotoxic insult, complex PAR polymers composed of large and branched molecules are synthesized by ARTD1 and ARTD2 (PARP-1 and PARP-2). These polymers are rapidly recognized and processed by a variety of erasers in a biphasic mode. At the same time, a variety of PAR readers can bind PAR and regulate the kinetics of the erasing process. In the first phase of the ADP-ribosylation reversal, PARG activity predominates and presumably exceeds ARH3 activity since PARG possesses high affinity for complex polymers and a very rapid and processive exoglycosidic activity toward ribose-ribose linkages. The dePARylation process is enhanced by the unique ability of PARG to cleave in-chain ribose-ribose linkages and branching points owing to its endoglycosidic activity. In addition, TARG1 can contribute to protein dePARylation by detaching entire PAR chains through cleavage of the proximal protein–ribose linkage. As PAR polymers are rapidly shortened by the combined endo- and exoglycosidic activities of PARG, the dePARylation activity drops and partially trimmed apoptogenic ADP-ribose oligomers accumulate. These small PAR fragments induce a second erasing wave in which rate and processivity of PARG is markedly decreased while ARH3 activity becomes dominant. The residual PARG activity and ARH3-catalyzed PAR hydrolysis generate MARylated proteins, which are further degraded by amino acid-specific MAR hydrolases and NUDIX phosphodiesterases. These waves of ADP-ribosylation erasing generate unmodified, phosphoribosylated, and MARylated proteins as well as free ADP-ribose. The latter might be deleterious for the cells and thus recycled by NUDT5 to quickly replenish ATP levels or converted to AMP which activates the AMP kinase (AMPK) and the mTOR signalling pathway

PARP-1 BRCT/small-molecule inhibitor product presumably blocks allosteric communications and the propagation of the activation signal to the active site. We can only speculate how additional effectors might rearrange the PARP-1 active site pocket to enable the formation of alternative ADP-ribosylation linkages. Notwithstanding, different PARP-1 ADP-ribosylation activities within the same pathway further support the notion that cells must produce diverse, specialized erasers.

Non-covalent interactions are thought to play an important regulatory role in ADP-ribose catabolism. For example, a marked inhibition of PARG activity is observed when free PAR is associated with histones or nuclear matrix proteins, most likely

through protection of ADP-ribose polymers from PARG-mediated degradation[128]. Alternatively, ADP-ribose polymers that are non-covalently bound to different acceptor proteins may be differentially accessible to PARG[96,129]. Such competition between PAR and MAR-binding proteins (i.e., readers) and erasers adds an additional layer of complexity as PAR readers might influence the kinetics of degradation of polymers and MAR production.

The regulatory model of sequential erasing waves shown in Fig. 4 can be illustrated by the bimodal recruitment kinetics of MacroD2 to sites of laser-induced DNA damage[130]. Following a rapid relocation of MacroD2 in a PARP-1-dependent initial phase, a second slower phase is observed, presumably as a consequence of the accumulation of MARylated species generated through PARG activity. This two-step mechanism reveals that ADP-ribosylation reversal provides a temporal ordering to orchestrate MAR/PAR-regulated pathways. More generally, the different states of ADP-ribosylation and the proteins responding to them may help to sequence and coordinate related reactions and eventually decide cell fate (Fig. 4). Since the loss of the eraser can have consequences other than removing the writer, it is likely that the ADP-ribsolyation intermediates are exploited to activate reactions rather than to simply terminate the actions of the writers.

Synthetic lethal strategies with PARG inhibitors

Fueled by the success of PARP inhibition (PARPi) as a therapeutic strategy for the treatment of many cancers, the field is now exploring the therapeutic potential of PARG inhibition (PARGi). Probably inspired by the postulated nucleic acid-like helical conformation of PAR[131], Tavassoli and colleagues reported that DNA intercalators can form a complex with PAR and protect it from PARG hydrolysis[132]. These homopolynucleotide intercalators (e.g., ethacridine) were the first class of compounds used to inhibit PARG. However, the influence of DNA intercalators on PARG activity is primarily indirect by restricting access of substrates rather than through direct interaction with PARG. Later, naturally occurring polyphenolic compounds such as the tannins were found to inhibit PARG activity[133]. In particular, Gallotannin[134] was shown to inhibit PARG and to be synthetic lethal to BRCA2-deficient tumors[135]. However, the utility of this compound was subsequently called into question as it exhibits nonspecific effects and is essentially cell membrane impermeable[79].

Despite its lack of cell permeability, one of the most widely used and best characterized PARG inhibitors is adenosine diphosphate hydroxymethyl pyrrolidinediol (ADP-HPD)[136,137]. Photoincorporation studies with analogues of ADP-HPD showed that the high molecular weight and branched PAR bind PARG at a different sites than short, linear polymers and ADP-HPD[138]. This is consistent with the identification of a secondary substrate binding site on PARG, hypothesized to be involved in its processive behavior[77]. These results indicate that small-molecule inhibitors of PARG might have different effects on PAR processing by modulating its ratio of exo/endoglycosidic activities.

To overcome cellular permeability issues with PARG inhibitors, a new generation of compounds was developed by Hergenrother and colleagues[78]. Rhodamine-based PARG inhibitors (RBPIs) proved to be potent and selective PARG inhibitors since they do not inhibit ARH3 as does ADP-HPD[78]. However, these compounds exhibited only low micromolar inhibitory activity against PARG. Other non-tannin inhibitors such as the GPI 1552 were reported to protect against neuronal damage[139] and potentiate temolozomide anti-metastatic activity in brain tumours[140]. A careful reexamination of the actual evidence for PARG inhibition leads to the conclusion that GPI 1552 was inadequate for a pharmacological evaluation of PARG[79].

More recently, using the cell permeable PARGi PDD00017273[141], Bryant and colleagues demonstrated that PARGi treatment selectively kills BRCA1-, BRCA2-, PALB2-, FAM175A/ABRAXAS-, and BARD1-depleted cells in the absence of any exogenous DNA damaging agents. The underlying mechanism for this synthetic lethality is that PARGi provokes replication forks stalling and a reduction of DNA double-strand break repair via homologous recombination (HR). An alternative explanation is that inhibition of PARG might cause irreversible PAR association with several proteins needed to complete HR[142]. Importantly, PARGi does not phenocopy PARPi. PARGi induces a rapid increase in IR-induced activation of DNA-PK and impairs normal mitotic progression. This suggests that PARG has different effects on activation of DNA damage repair pathways following ionizing radiation, consistent with the notion that blocking PAR removal has a different consequence to inhibiting PAR addition[143].

Genetic studies have suggested PARG inhibitors as chemosensitizing agents. PARG-deficient cells display centrosome amplification and accumulate aberrant mitotic figures, which induced either polyploidy or cell death by mitotic catastrophe[144]. ES cells derived from knock-out PARG mice showed enhanced sensitivity towards γ-irradiation and other forms of ionizing radiation[145]. More recently it was shown that PARG suppression potentiates the toxicity of radiation therapy in BRCA-deficient cells[142] and that PDD00017273 radiosensitizes MCF-7 cells[143].

PARG protein expression can be regulated by the stabilization of its mRNA by the RNA-binding protein HuR[146]. In pancreatic ductal adenocarcinomas (PDA) cells, genetic deletion of HuR enhances PARPi sensitivity. In this context, the PARPi-induced toxicity is attributable to downregulation of PARG expression. The inhibition of HuR can also re-sensitize PDA cells to PARPi, suggesting that the loss of PARG activity could enhance the clinical effectiveness of PARP inhibitors[146]. In contrast, Gogola and colleagues have shown that PARPi-resistance can be mediated by PARG downregulation[147]. The loss of PARG activity in BRCA2-deficient tumours treated with potent PARP-1 inhibitors is sufficient to restore PAR formation and rescue PARP-1 downstream signaling. PARG depletion indeed occurs in triple-negative breast cancers and serous ovarian cancers. When treatment-naive TNBC biopsies from women eligible for PARPi treatment were analyzed for PARG expression, lack of PARG occurred in some areas of the tumours[147]. This suggests that these tumour sections can become de facto resistant to PARPi treatment. Further studies are needed to clarify the role of PARG and the accumulation of PAR polymers that survived erasing in a dynamic system that has undergone profound alterations. Differences in genetic backgrounds can certainly account for contradictory results (e.g., DNA damage response-proficient vs -deficient cells) but the nature of PAR itself (either free or protein-bound) might also be an important and significant clue to interpret these results. Although there is a bright future for PARG inhibitors, so far they are only effective at relatively high doses in contrast to PARP-1 inhibitors characterized with half maximal inhibitory concentration in the low nanomolar range. In addition, the fact that PARG activity can be regulated at multiple levels with respect to PAR length and branching patterns poses a particular challenge.

Concluding remarks and future challenges

In this review, we have provided an overview of the dynamic and reversible processes that regulate ADP-ribosylation. Determining the contribution of each regulator in this delicate equilibrium

represents a daunting challenge. Experimental dissection of these processes are complicated by the heterogeneous nature of ADP-ribosylation, which needs to be addressed by the development of specialized analytical methods.

Substantial progress has been made to understand the mechanisms that contribute to ADP-ribosylation reversal, yet several obstacles need to be overcome: (1) Sensitive and reproducible methods to monitor physiological MAR and PAR levels in cells are difficult to implement; (2) better methods are needed to evaluate site-specific PAR chain length distribution in ADP-ribosylated substrates; (3) measuring kinetics and performance of erasers are precluded by the lack of standardized and defined substrates; (4) the ADP-ribosylation conjugation chemistry and linkage selectivity of erasers need to be further clarified; (5) enzyme-specific targets and interactors, especially for the MARTs and ARHs, remain largely unknown; (6) the modulatory effect of many ADP-ribose readers, which have multiple binding sites for the same ligand is largely unresolved; (7) the biological relevance of site-specific ADP-ribosylation events is often difficult to determine.

Despite these obstacles and intricacies, the machinery responsible for the processing of ADP-ribose is now beginning to be revealed. A more detailed understanding of the interplay between ADP-ribosylation writers, readers and erasers, at a molecular level, will be required to correlate these dynamics with cellular responses and translate them into clinical applications.

Received: 30 July 2018 Accepted: 2 February 2019
Published online: 12 March 2019

References

1. Gupte, R., Liu, Z. & Kraus, W. L. PARPs and ADP-ribosylation: recent advances linking molecular functions to biological outcomes. *Genes Dev.* 31, 101–126 (2017).
A comprehensive review that describes the current concepts of ARTD biology with a focus on new technologies to detect and study ADP-ribosylation.
2. Palazzo, L., Mikoc, A. & Ahel, I. ADP-ribosylation: new facets of an ancient modification. *FEBS. J.* 284, 2932–2946 (2017).
3. Perina, D. et al. Distribution of protein poly(ADP-ribosyl)ation systems across all domains of life. *DNA Repair (Amst.)* 23, 4–16 (2014).
4. Teloni, F. & Altmeyer, M. Readers of poly(ADP-ribose): designed to be fit for purpose. *Nucleic Acids Res.* 44, 993–1006 (2016).
5. Deng, Q. & Barbieri, J. T. Molecular mechanisms of the cytotoxicity of ADP-ribosylating toxins. *Annu. Rev. Microbiol.* 62, 271–288 (2008).
6. Cohen, M. S. & Chang, P. Insights into the biogenesis, function, and regulation of ADP-ribosylation. *Nat. Chem. Biol.* 14, 236–243 (2018).
7. Slade, D. et al. The structure and catalytic mechanism of a poly(ADP-ribose) glycohydrolase. *Nature* 477, 616–620 (2011).
8. Hatakeyama, K., Nemoto, Y., Ueda, K. & Hayaishi, O. Purification and characterization of poly(ADP-ribose) glycohydrolase. Different modes of action on large and small poly(ADP-ribose). *J. Biol. Chem.* 261, 14902–14911 (1986).
9. Butepage, M., Eckei, L., Verheugd, P. & Luscher, B. Intracellular mono-ADP-ribosylation in signaling and disease. *Cells* 4, 569–595 (2015).
10. Meyer, R. G., Meyer-Ficca, M. L., Jacobson, E. L. & Jacobson, M. K. Human poly(ADP-ribose) glycohydrolase (PARG) gene and the common promoter sequence it shares with inner mitochondrial membrane translocase 23 (TIM23). *Gene* 314, 181–190 (2003).
11. Meyer-Ficca, M. L., Meyer, R. G., Coyle, D. L., Jacobson, E. L. & Jacobson, M. K. Human poly(ADP-ribose) glycohydrolase is expressed in alternative splice variants yielding isoforms that localize to different cell compartments. *Exp. Cell Res.* 297, 521–532 (2004).
12. Meyer-Ficca, M. L., Meyer, R. G., Jacobson, E. L. & Jacobson, M. K. Overexpression of poly(ADP-ribose) glycohydrolase (PARG) isoforms. *Cancer Res.* 65, 420 LP–420420 (2005).
13. Davidovic, L., Vodenicharov, M., Affar, E. B. & Poirier, G. G. Importance of poly(ADP-ribose) glycohydrolase in the control of poly(ADP-ribose) metabolism. *Exp. Cell Res.* 268, 7–13 (2001).
14. Gagne, J. P. et al. Proteomic investigation of phosphorylation sites in poly (ADP-ribose) polymerase-1 and poly(ADP-ribose) glycohydrolase. *J. Proteome Res.* 8, 1014–1029 (2009).
15. Botta, D. & Jacobson, M. K. Identification of a regulatory segment of poly (ADP-ribose) glycohydrolase. *Biochemistry* 49, 7674–7682 (2010).
16. Patel, C. N., Koh, D. W., Jacobson, M. K. & Oliveira, M. A. Identification of three critical acidic residues of poly(ADP-ribose) glycohydrolase involved in catalysis: determining the PARG catalytic domain. *Biochem. J.* 388, 493–500 (2005).
17. Hassler, M., Jankevicius, G. & Ladurner, A. G. PARG: a macrodomain in disguise. *Structure* 19, 1351–1353 (2011).
18. Bonicalzi, M. E., Vodenicharov, M., Coulombe, M., Gagne, J. P. & Poirier, G. G. Alteration of poly(ADP-ribose) glycohydrolase nucleocytoplasmic shuttling characteristics upon cleavage by apoptotic proteases. *Biol. Cell* 95, 635–644 (2003).
19. Winstall, E. et al. Preferential perinuclear localization of poly(ADP-ribose) glycohydrolase. *Exp. Cell Res.* 251, 372–378 (1999).
20. Bonicalzi, M. E., Haince, J. F., Droit, A. & Poirier, G. G. Regulation of poly (ADP-ribose) metabolism by poly(ADP-ribose) glycohydrolase: where and when? *Cell. Mol. Life Sci.* 62, 739–750 (2005).
21. Niere, M. et al. ADP-ribosylhydrolase 3 (ARH3), not poly(ADP-ribose) glycohydrolase (PARG) isoforms, is responsible for degradation of mitochondrial matrix-associated poly(ADP-ribose). *J. Biol. Chem.* 287, 16088–16102 (2012).
This paper provides conclusive evidence regarding the nature of PARG isoforms expressed in human cells, their erasing activities and their subcellular localizations.
22. Davies, G. & Henrissat, B. Structures and mechanisms of glycosyl hydrolases. *Structure* 3, 853–859 (1995).
23. Brochu, G. et al. Mode of action of poly(ADP-ribose) glycohydrolase. *Biochim. Biophys. Acta* 1219, 342–350 (1994).
In this study, the authors provide a formal demonstration of the endoglycosidic activity of human PARG that has been suggested in previous reports.
24. Braun, S. A., Panzeter, P. L., Collinge, M. A. & Althaus, F. R. Endoglycosidic cleavage of branched polymers by poly(ADP-ribose) glycohydrolase. *Eur. J. Biochem.* 220, 369–375 (1994).
25. Koh, D. W. et al. Failure to degrade poly(ADP-ribose) causes increased sensitivity to cytotoxicity and early embryonic lethality. *Proc. Natl Acad. Sci. USA* 101, 17699–17704 (2004).
26. Cortes, U. et al. Depletion of the 110-kilodalton isoform of poly(ADP-ribose) glycohydrolase increases sensitivity to genotoxic and endotoxic stress in mice. *Mol. Cell Biol.* 24, 7163–7178 (2004).
27. Min, W., Cortes, U., Herceg, Z., Tong, W. M. & Wang, Z. Q. Deletion of the nuclear isoform of poly(ADP-ribose) glycohydrolase (PARG) reveals its function in DNA repair, genomic stability and tumorigenesis. *Carcinogenesis* 31, 2058–2065 (2010).
28. Illuzzi, G. et al. PARG is dispensable for recovery from transient replicative stress but required to prevent detrimental accumulation of poly (ADP-ribose) upon prolonged replicative stress. *Nucleic Acids Res.* 42, 7776–7792 (2014).
29. Mortusewicz, O., Fouquerel, E., Ame, J. C., Leonhardt, H. & Schreiber, V. PARG is recruited to DNA damage sites through poly(ADP-ribose)- and PCNA-dependent mechanisms. *Nucleic Acids Res.* 39, 5045–5056 (2011).
30. Kaufmann, T. et al. A novel non-canonical PIP-box mediates PARG interaction with PCNA. *Nucleic Acids Res.* 45, 9741–9759 (2017).
31. Shirai, H. et al. PARG dysfunction enhances DNA double strand break formation in S-phase after alkylation DNA damage and augments different cell death pathways. *Cell Death Dis.* 4, e656 (2013).
32. Ray Chaudhuri, A., Ahuja, A. K., Herrador, R. & Lopes, M. Poly(ADP-ribosyl) glycohydrolase prevents the accumulation of unusual replication structures during unperturbed S phase. *Mol. Cell Biol.* 35, 856–865 (2015).
33. Koh, D. W., Dawson, V. L. & Dawson, T. M. The road to survival goes through PARG. *Cell Cycle* 4, 397–399 (2005).
34. Galluzzi, L. et al. Molecular mechanisms of cell death: recommendations of the Nomenclature Committee on Cell Death 2018. *Cell Death Differ.* 25, 486–541 (2018).
35. Wang, Y. et al. Poly(ADP-ribose) (PAR) binding to apoptosis-inducing factor is critical for PAR polymerase-1-dependent cell death (parthanatos). *Sci. Signal.* 4, ra20 (2011).
36. Yu, S. W. et al. Mediation of poly(ADP-ribose) polymerase-1-dependent cell death by apoptosis-inducing factor. *Science* 297, 259–263 (2002).
This is the first in a series of studies characterizing PAR as a cell death signal that induces release of AIF, elucidating the basis of the parthanatos cell death pathway.
37. Fatokun, A. A., Dawson, V. L. & Dawson, T. M. Parthanatos: mitochondrial-linked mechanisms and therapeutic opportunities. *Br. J. Pharmacol.* 171, 2000–2016 (2014).

38. Benn, C., Althaus, F. R. & Malanga, M. Poly(ADP-ribose) glycohydrolase silencing protects against H2O2-induced cell death. *Biochem. J.* 396, 419–429 (2006).
39. Yang, L. et al. Tankyrase1-mediated poly(ADP-ribosyl)ation of TRF1 maintains cell survival after telomeric DNA damage. *Nucleic Acids Res.* 45, 3906–3921 (2017).
40. Sun, L. et al. WRN is recruited to damaged telomeres via its RQC domain and tankyrase1-mediated poly-ADP-ribosylation of TRF1. *Nucleic Acids Res.* 45, 3844–3859 (2017).
41. Krueger, K. M. & Barbieri, J. T. The family of bacterial ADP-ribosylating exotoxins. *Clin. Microbiol. Rev.* 8, 34–47 (1995).
42. Mashimo, M., Kato, J. & Moss, J. Structure and function of the ARH family of ADP-ribosyl-acceptor hydrolases. *DNA Repair (Amst.)* 23, 88–94 (2014).
43. Ame, J. C., Spenlehauer, C. & de Murcia, G. The PARP superfamily. *Bioessays* 26, 882–893 (2004).
44. Hottiger, M. O., Hassa, P. O., Luscher, B., Schuler, H. & Koch-Nolte, F. Toward a unified nomenclature for mammalian ADP-ribosyltransferases. *Trends Biochem. Sci.* 35, 208–219 (2010).
45. Leung, A. K. L. PARPs. *Curr. Biol.* 27, R1256–R1258 (2017).
46. Vyas, S. et al. Family-wide analysis of poly(ADP-ribose) polymerase activity. *Nat. Commun.* 5, 4426 (2014).
Based on in vitro automodification assays, this family-wide analysis of ARTDs shows that most ARTDs are MARTs and presents one of the most comprehensive lists of ARTDs MARylation sites identified by MS.
47. Oka, S., Kato, J. & Moss, J. Identification and characterization of a mammalian 39-kDa poly(ADP-ribose) glycohydrolase. *J. Biol. Chem.* 281, 705–713 (2006).
48. Laing, S., Unger, M., Koch-Nolte, F. & Haag, F. ADP-ribosylation of arginine. *Amino Acids* 41, 257–269 (2011).
49. Fontana, P. et al. Serine ADP-ribosylation reversal by the hydrolase ARH3. *eLife* 6, e28533 (2017).
50. Kato, J., Zhu, J., Liu, C. & Moss, J. Enhanced Sensitivity to Cholera Toxin in ADP-Ribosylarginine Hydrolase-Deficient Mice. *Mol. Cell Biol.* 27, 5534–5543 (2007).
51. Kato, J. et al. ADP-ribosylarginine hydrolase regulates cell proliferation and tumorigenesis. *Cancer Res.* 71, 5327–5335 (2011).
52. Abplanalp, J. et al. Proteomic analyses identify ARH3 as a serine mono-ADP-ribosylhydrolase. *Nat. Commun.* 8, 2055 (2017).
53. Hanai, S. et al. Loss of poly(ADP-ribose) glycohydrolase causes progressive neurodegeneration in Drosophila melanogaster. *Proc. Natl Acad. Sci. USA* 101, 82–86 (2004).
54. Mashimo, M., Kato, J. & Moss, J. ADP-ribosyl-acceptor hydrolase 3 regulates poly (ADP-ribose) degradation and cell death during oxidative stress. *Proc. Natl Acad. Sci. USA* 110, 18964–18969 (2013).
55. Koch-Nolte F. *Endogenous ADP-Ribosylation* (Springer International Publishing, Switzerland, 2015).
56. Daniels, C. M., Ong, S. E. & Leung, A. K. The promise of proteomics for the study of ADP-ribosylation. *Mol. Cell* 58, 911–924 (2015).
57. Han, W., Li, X. & Fu, X. The macro domain protein family: structure, functions, and their potential therapeutic implications. *Mutat. Res.* 727, 86–103 (2011).
58. Karras, G. I. et al. The macro domain is an ADP-ribose binding module. *EMBO J.* 24, 1911–1920 (2005).
59. Sharifi, R. et al. Deficiency of terminal ADP-ribose protein glycohydrolase TARG1/C6orf130 in neurodegenerative disease. *EMBO J.* 32, 1225–1237 (2013).
This paper describes the identification of TARG1 as a novel ADP-ribose eraser, revealing its ability to remove entire PAR chains from a substrate protein in addition to its MAR hydrolase activity.
60. Butepage, M. et al. Nucleolar-nucleoplasmic shuttling of TARG1 and its control by DNA damage-induced poly-ADP-ribosylation and by nucleolar transcription. *Sci. Rep.* 8, 6748 (2018).
61. Barkauskaite, E. et al. Visualization of poly(ADP-ribose) bound to PARG reveals inherent balance between exo- and endo-glycohydrolase activities. *Nat. Commun.* 4, 2164 (2013).
62. Barkauskaite, E., Jankevicius, G. & Ahel, I. Structures and mechanisms of enzymes employed in the synthesis and degradation of PARP-dependent protein ADP-ribosylation. *Mol. Cell* 58, 935–946 (2015).
63. Sakthianandeswaren, A. et al. MACROD2 haploinsufficiency impairs catalytic activity of PARP1 and promotes chromosome instability and growth of intestinal tumors. *Cancer Discov.* 8, 988–1005 (2018).
64. Sakthianandeswaren, A., Parsons, M. J., Mouradov, D. & Sieber, O. M. MACROD2 deletions cause impaired PARP1 activity and chromosome instability in colorectal cancer. *Oncotarget* 9, 33056–33058 (2018).
65. Reeder, R. H., Ueda, K., Honjo, T., Nishizuka, Y. & Hayaishi, O. Studies on the polymer of adenosine diphosphate ribose. II. *Charact. Polym. J. Biol. Chem.* 242, 3172–3179 (1967).
66. Palazzo, L. et al. Processing of protein ADP-ribosylation by Nudix hydrolases. *Biochem. J.* 468, 293–301 (2015).
This is the first demonstration of ADP-ribosylation processing by the NUDIX family of enzymes.
67. Daniels, C. M., Thirawatananond, P., Ong, S. E., Gabelli, S. B. & Leung, A. K. Nudix hydrolases degrade protein-conjugated ADP-ribose. *Sci. Rep.* 5, 18271 (2015).
This paper demonstrates the use of NUDIX enzymes to generate phosphoribose signatures for site-specific identification of ADP-ribosylation sites by MS.
68. Palazzo, L. et al. ENPP1 processes protein ADP-ribosylation in vitro. *FEBS J.* 283, 3371–3388 (2016).
This study describes the characterization of ENPP1 as the first mammalian enzyme without a NUDIX domain that generates phosphoribose remnants as a consequence of its phosphodiesterase activity against ADP-ribosylated proteins.
69. Williams, J. C., Chambers, J. P. & Liehr, J. G. Glutamyl ribose 5-phosphate storage disease. A hereditary defect in the degradation of poly(ADP-ribosylated) proteins. *J. Biol. Chem.* 259, 1037–1042 (1984).
70. Shirato, M. et al. Poly(etheno ADP-ribose) blocks poly(ADP-ribose) glycohydrolase activity. *Biochem. Biophys. Res. Commun.* 355, 451–456 (2007).
71. Bessman, M. J., Frick, D. N. & O'Handley, S. F. The MutT proteins or "Nudix" hydrolases, a family of versatile, widely distributed, "housecleaning" enzymes. *J. Biol. Chem.* 271, 25059–25062 (1996).
72. Formentini, L. et al. Poly(ADP-ribose) catabolism triggers AMP-dependent mitochondrial energy failure. *J. Biol. Chem.* 284, 17668–17676 (2009).
73. Ethier, C., Tardif, M., Arul, L. & Poirier, G. G. PARP-1 modulation of mTOR signaling in response to a DNA alkylating agent. *PLoS One* 7, e47978 (2012).
74. Wright, R. H. et al. ADP-ribose-derived nuclear ATP synthesis by NUDIX5 is required for chromatin remodeling. *Science* 352, 1221–1225 (2016).
75. Menard, L. & Poirier, G. G. Rapid assay of poly(ADP-ribose) glycohydrolase. *Biochem. Cell Biol.* 65, 668–673 (1987).
76. Haince, J. F., Ouellet, M. E., McDonald, D., Hendzel, M. J. & Poirier, G. G. Dynamic relocation of poly(ADP-ribose) glycohydrolase isoforms during radiation-induced DNA damage. *Biochim. Biophys. Acta* 1763, 226–237 (2006).
77. Wang, Z., Gagne, J. P., Poirier, G. G. & Xu, W. Crystallographic and biochemical analysis of the mouse poly(ADP-ribose) glycohydrolase. *PLoS One* 9, e86010 (2014).
78. Finch, K. E., Knezevic, C. E., Nottbohm, A. C., Partlow, K. C. & Hergenrother, P. J. Selective small molecule inhibition of poly(ADP-ribose) glycohydrolase (PARG). *ACS Chem. Biol.* 7, 563–570 (2012).
79. Falsig, J. et al. Poly(ADP-ribose) glycohydrolase as a target for neuroprotective intervention: assessment of currently available pharmacological tools. *Eur. J. Pharmacol.* 497, 7–16 (2004).
80. Putt, K. S. & Hergenrother, P. J. A nonradiometric, high-throughput assay for poly(ADP-ribose) glycohydrolase (PARG): application to inhibitor identification and evaluation. *Anal. Biochem.* 333, 256–264 (2004).
81. Miwa, M., Tanaka, M., Matsushima, T. & Sugimura, T. Purification and properties of glycohydrolase from calf thymus splitting ribose-ribose linkages of poly(adenosine diphosphate ribose). *J. Biol. Chem.* 249, 3475–3482 (1974).
82. James, D. I. et al. An assay to measure poly(ADP ribose) glycohydrolase (PARG) activity in cells. *F1000Res.* 5, 736 (2016).
83. Kawamitsu, H. et al. Monoclonal antibodies to poly(adenosine diphosphate ribose) recognize different structures. *Biochemistry* 23, 3771–3777 (1984).
84. Gibson, B. A., Conrad, L. B., Huang, D. & Kraus, W. L. Generation and characterization of recombinant antibody-like ADP-Ribose binding proteins. *Biochemistry* 56, 6305–6316 (2017).
85. Rosenthal, F. et al. Macrodomain-containing proteins are new mono-ADP-ribosylhydrolases. *Nat. Struct. Mol. Biol.* 20, 502–507 (2013).
This article and ref. 129 were published back-to-back, demonstrating the MAR hydrolase activity of macrodomain-containing proteins and their role in ADP-ribosylation reversal.
86. Liu, Q. et al. A general approach towards triazole-linked adenosine diphosphate ribosylated peptides and proteins. *Angew. Chem. Int. Ed. Engl.* 57, 1659–1662 (2018).
87. Tao, Z., Gao, P. & Liu, H. W. Identification of the ADP-ribosylation sites in the PARP-1 automodification domain: analysis and implications. *J. Am. Chem. Soc.* 131, 14258–14260 (2009).
This method paper opens the door to further exploration of the ADP-ribosylation PTM by MS and establishes the first MS-based map of PARP-1 automodification sites.
88. Zhen, Y. & Yu, Y. Proteomic analysis of the downstream signaling network of PARP1. *Biochemistry* 57, 429–440 (2018).
89. Haag, F. & Buck, F. Identification and analysis of ADP-ribosylated proteins. *Curr. Top. Microbiol. Immunol.* 384, 33–50 (2015).

90. Rosenthal, F. & Hottiger, M. O. Identification of ADP-ribosylated peptides and ADP-ribose acceptor sites. *Front. Biosci. (Landmark Ed.)* 19, 1041–1056 (2014).
91. Vivelo, C. A. & Leung, A. K. Proteomics approaches to identify mono-(ADP-ribosyl)ated and poly(ADP-ribosyl)ated proteins. *Proteomics* 15, 203–217 (2015).
92. Laing, S., Koch-Nolte, F., Haag, F. & Buck, F. Strategies for the identification of arginine ADP-ribosylation sites. *J. Proteom.* 75, 169–176 (2011).
93. Bonfiglio, J. J., Colby, T. & Matic, I. Mass spectrometry for serine ADP-ribosylation? Think o-glycosylation! *Nucleic Acids Res.* 45, 6259–6264 (2017).
94. Kistemaker, H. A. et al. Synthesis and macrodomain binding of Mono-ADP-ribosylated peptides. *Angew. Chem. Int. Ed. Engl.* 55, 10634–10638 (2016).
95. Luscher, B. et al. ADP-ribosylation, a multifaceted posttranslational modification involved in the control of cell physiology in health and disease. *Chem. Rev.* 118, 1092–1136 (2018).
96. Alvarez-Gonzalez, R. & Althaus, F. R. Poly(ADP-ribose) catabolism in mammalian cells exposed to DNA-damaging agents. *Mutat. Res.* 218, 67–74 (1989).
97. Talhaoui, I. et al. Poly(ADP-ribose) polymerases covalently modify strand break termini in DNA fragments in vitro. *Nucleic Acids Res.* 44, 9279–9295 (2016).
98. Zarkovic, G. et al. Characterization of DNA ADP-ribosyltransferase activities of PARP2 and PARP3: new insights into DNA ADP-ribosylation. *Nucleic Acids Res.* 46, 2417–2431 (2018).
99. Munnur, D. & Ahel, I. Reversible mono-ADP-ribosylation of DNA breaks. *FEBS J.* 284, 4002–4016 (2017).
100. Dolle, C. & Ziegler, M. ADP-ribosylation of DNA moving into focus. *FEBS J.* 284, 3999–4001 (2017).
101. Agnew, T. et al. MacroD1 is a promiscuous ADP-ribosyl hydrolase localized to mitochondria. *Front. Microbiol.* 9, 20 (2018).
102. Jacobson, E. L., Cervantes-Laurean, D. & Jacobson, M. K. Glycation of proteins by ADP-ribose. *Mol. Cell Biochem.* 138, 207–212 (1994).
103. Martello, R. et al. Proteome-wide identification of the endogenous ADP-ribosylome of mammalian cells and tissue. *Nat. Commun.* 7, 12917 (2016).
104. Desmarais, Y., Menard, L., Lagueux, J. & Poirier, G. G. Enzymological properties of poly(ADP-ribose)polymerase: characterization of automodification sites and NADase activity. *Biochim. Biophys. Acta* 1078, 179–186 (1991).
105. Gibbs-Seymour, I., Fontana, P., Rack, J. G. M. & Ahel, I. HPF1/C4orf27 is a PARP-1-interacting protein that regulates PARP-1 ADP-ribosylation activity. *Mol. Cell* 62, 432–442 (2016).
106. Clark, N. J., Kramer, M., Muthurajan, U. M. & Luger, K. Alternative modes of binding of poly(ADP-ribose) polymerase 1 to free DNA and nucleosomes. *J. Biol. Chem.* 287, 32430–32439 (2012).
107. Pic, E., Gagne, J. P. & Poirier, G. G. Mass spectrometry-based functional proteomics of poly(ADP-ribose) polymerase-1. *Expert Rev. Proteom.* 8, 759–774 (2011).
108. Berger, F., Lau, C. & Ziegler, M. Regulation of poly(ADP-ribose) polymerase 1 activity by the phosphorylation state of the nuclear NAD biosynthetic enzyme NMN adenylyl transferase 1. *Proc. Natl Acad. Sci. USA* 104, 3765–3770 (2007).
109. Bonfiglio, J. J. et al. Serine ADP-ribosylation depends on HPF1. *Mol. Cell* 65, 932–940 e936 (2017).
Following their assignment of ADP-ribosylation modification to histones serine residues via O-glycosidic linkages, Matic's lab here reports that serine ADP-ribosylation is strictly dependent on the presence of HPF1 as a cofactor to PARP-1.
110. Leung, A. K. Serious surprises for ADP-ribosylation specificity: HPF1 switches PARP1 specificity to ser residues. *Mol. Cell* 65, 777–778 (2017).
111. Liu, Q., Florea, B. I. & Filippov, D. V. ADP-ribosylation goes normal: serine as the major site of the modification. *Cell Chem. Biol.* 24, 431–432 (2017).
112. Palazzo, L. et al. Serine is the major residue for ADP-ribosylation upon DNA damage. *eLife* 7, e34334 (2018).
113. Leidecker, O. et al. Serine is a new target residue for endogenous ADP-ribosylation on histones. *Nat. Chem. Biol.* 12, 998–1000 (2016).
This paper demonstrates physiological ADP-ribosylation on serine amino acid side-chains through a O-linked glycosidic chemical bond.
114. Leslie Pedrioli, D. M. et al. Comprehensive ADP-ribosylome analysis identifies tyrosine as an ADP-ribose acceptor site. *EMBO Rep.* 19, e45310 (2018).
115. Zhen, Y., Zhang, Y. & Yu, Y. A cell-line-specific atlas of PARP-mediated protein Asp/Glu-ADP-ribosylation in breast cancer. *Cell Rep.* 21, 2326–2337 (2017).
116. Zhang, Y., Wang, J., Ding, M. & Yu, Y. Site-specific characterization of the Asp- and Glu-ADP-ribosylated proteome. *Nat. Methods* 10, 981–984 (2013).
This paper describes a major advance in large-scale MS-based analysis of protein ADP-ribosylation, demonstrating the identification of site-specific ADP-ribosylation in complex protein samples based on hydroxylamine treatment.
117. Sung, V. M. Mechanistic overview of ADP-ribosylation reactions. *Biochimie* 113, 35–46 (2015).
118. Karch, K. R., Langelier, M. F., Pascal, J. M. & Garcia, B. A. The nucleosomal surface is the main target of histone ADP-ribosylation in response to DNA damage. *Mol. Biosyst.* 13, 2660–2671 (2017).
119. Thomassin, H., Menard, L., Hengartner, C., Kirkland, J. B. & Poirier, G. G. Poly(ADP-ribosyl)ation of chromatin in an in-vitro poly(ADP-ribose)-turnover system. *Biochim. Biophys. Acta* 1137, 171–181 (1992).
120. Lagueux, J. et al. Poly(ADP-ribose) catabolism in mammalian cells. *Mol. Cell Biochem.* 138, 45–52 (1994).
121. Menard, L., Thibault, L. & Poirier, G. G. Reconstitution of an in vitro poly (ADP-ribose) turnover system. *Biochim. Biophys. Acta* 1049, 45–58 (1990).
122. Na, Z. et al. A small-molecule protein-protein interaction inhibitor of PARP1 that targets its BRCT domain. *Angew. Chem. Int. Ed. Engl.* 54, 2515–2519 (2015).
123. Langelier, M. F., Zandarashvili, L., Aguiar, P. M., Black, B. E. & Pascal, J. M. NAD(+) analog reveals PARP-1 substrate-blocking mechanism and allosteric communication from catalytic center to DNA-binding domains. *Nat. Commun.* 9, 844 (2018).
124. Dawicki-McKenna, J. M. et al. PARP-1 activation requires local unfolding of an autoinhibitory domain. *Mol. Cell* 60, 755–768 (2015).
125. Eustermann, S. et al. Structural basis of detection and signaling of DNA single-strand breaks by human PARP-1. *Mol. Cell* 60, 742–754 (2015).
126. Langelier, M. F. & Pascal, J. M. PARP-1 mechanism for coupling DNA damage detection to poly(ADP-ribose) synthesis. *Curr. Opin. Struct. Biol.* 23, 134–143 (2013).
127. Langelier, M. F., Planck, J. L., Roy, S. & Pascal, J. M. Structural basis for DNA damage-dependent poly(ADP-ribosyl)ation by human PARP-1. *Science* 336, 728–732 (2012).
128. Pacheco-Rodriguez, G. & Alvarez-Gonzalez, R. Measurement of poly(ADP-ribose) glycohydrolase activity by high resolution polyacrylamide gel electrophoresis: specific inhibition by histones and nuclear matrix proteins. *Mol. Cell Biochem.* 193, 13–18 (1999).
129. Gaudreau, A., Menard, L., de Murcia, G. & Poirier, G. G. Poly(ADP-ribose) accessibility to poly(ADP-ribose) glycohydrolase activity on poly(ADP-ribosyl)ated nucleosomal proteins. *Biochem. Cell Biol.* 64, 146–153 (1986).
130. Jankevicius, G. et al. A family of macrodomain proteins reverses cellular mono-ADP-ribosylation. *Nat. Struct. Mol. Biol.* 20, 508–514 (2013).
131. Minaga, T. & Kun, E. Probable helical conformation of poly(ADP-ribose). The effect of cations on spectral properties. *J. Biol. Chem.* 258, 5726–5730 (1983).
132. Tavassoli, M., Tavassoli, M. H. & Shall, S. Effect of DNA intercalators on poly (ADP-ribose) glycohydrolase activity. *Biochim. Biophys. Acta* 827, 228–234 (1985).
133. Tsai, Y. J. et al. Effects of chemically defined tannins on poly (ADP-ribose) glycohydrolase activity. *Biochem. Int.* 24, 889–897 (1991).
134. Formentini, L. et al. Mono-galloyl glucose derivatives are potent poly(ADP-ribose) glycohydrolase (PARG) inhibitors and partially reduce PARP-1-dependent cell death. *Br. J. Pharmacol.* 155, 1235–1249 (2008).
135. Fathers, C., Drayton, R. M., Solovieva, S. & Bryant, H. E. Inhibition of poly (ADP-ribose) glycohydrolase (PARG) specifically kills BRCA2-deficient tumor cells. *Cell Cycle* 11, 990–997 (2012).
This study demonstrates that HR-deficient cells are sensitive to PARG inhibition and - although the applied gallotannin compound is of low potency against PARG - paves the way for further evaluations of the synthetic lethal relationship between PARG and DNA damage response-associated factors.
136. Slama, J. T. et al. Specific inhibition of poly(ADP-ribose) glycohydrolase by adenosine diphosphate (hydroxymethyl)pyrrolidinediol. *J. Med. Chem.* 38, 389–393 (1995).
137. Slama, J. T., Aboul-Ela, N. & Jacobson, M. K. Mechanism of inhibition of poly (ADP-ribose) glycohydrolase by adenosine diphosphate (hydroxymethyl) pyrrolidinediol. *J. Med. Chem.* 38, 4332–4336 (1995).
138. Ramsinghani, S. et al. Syntheses of photoactive analogues of adenosine diphosphate (hydroxymethyl)pyrrolidinediol and photoaffinity labeling of poly(ADP-ribose) glycohydrolase. *Biochemistry* 37, 7801–7812 (1998).
139. Lu, X. C. et al. Post-treatment with a novel PARG inhibitor reduces infarct in cerebral ischemia in the rat. *Brain Res.* 978, 99–103 (2003).
140. Tentori, L. et al. Poly(ADP-ribose) glycohydrolase inhibitor as chemosensitiser of malignant melanoma for temozolomide. *Eur. J. Cancer* 41, 2948–2957 (2005).
141. James, D. I. et al. First-in-class chemical probes against poly(ADP-ribose) glycohydrolase (PARG) inhibit DNA repair with differential pharmacology to olaparib. *ACS Chem. Biol.* 11, 3179–3190 (2016).
142. Gravells, P., Grant, E., Smith, K. M., James, D. I. & Bryant, H. E. Specific killing of DNA damage-response deficient cells with inhibitors of poly(ADP-ribose) glycohydrolase. *DNA Repair (Amst.)* 52, 81–91 (2017).
143. Gravells, P. et al. Radiosensitization with an inhibitor of poly(ADP-ribose) glycohydrolase: a comparison with the PARP1/2/3 inhibitor olaparib. *DNA Repair (Amst.)* 61, 25–36 (2018).

This study shows that, in addition to BRCA2, mutations in other HR-associated proteins can be synthetic lethal with PARG inhibition, which may be a promising approach to treat HR-deficient tumors.
144. Ame, J. C. et al. Radiation-induced mitotic catastrophe in PARG-deficient cells. *J. Cell Sci.* 122, 1990–2002 (2009).
145. Shirai, H. et al. Parg deficiency confers radio-sensitization through enhanced cell death in mouse ES cells exposed to various forms of ionizing radiation. *Biochem. Biophys. Res. Commun.* 435, 100–106 (2013).
146. Chand, S. N. et al. Posttranscriptional regulation of PARG mRNA by HuR facilitates DNA repair and resistance to PARP inhibitors. *Cancer Res.* 77, 5011–5025 (2017).
147. Gogola, E. et al. Selective loss of PARG restores PARylation and counteracts PARP inhibitor-mediated synthetic lethality. *Cancer Cell* 33, 1078–1093 e1012 (2018).
This paper establishes a clear connection between PARG downregulation and the resistance to PARP inhibition, showing that PARG depletion restores PARylation upon treatment with PARP inhibitors.

Acknowledgements

This work was supported by Canadian Institutes of Health Research (CIHR).

Author contributions

All authors contributed to the final manuscript.

Additional information

Competing interests: The authors declare no competing interests.

nature COMMUNICATIONS

ARTICLE

https://doi.org/10.1038/s41467-019-10741-9 OPEN

Poly(ADP-ribose) polymerase-1 antagonizes DNA resection at double-strand breaks

Marie-Christine Caron[1,2,7], Ajit K. Sharma[3,7], Julia O'Sullivan[1,2], Logan R. Myler[4], Maria Tedim Ferreira[2,5], Amélie Rodrigue[1,2], Yan Coulombe[1,2], Chantal Ethier[2,5], Jean-Philippe Gagné[2,5], Marie-France Langelier[6], John M. Pascal[6], Ilya J. Finkelstein[4], Michael J. Hendzel[3], Guy G. Poirier[2,5] & Jean-Yves Masson[1,2]

PARP-1 is rapidly recruited and activated by DNA double-strand breaks (DSBs). Upon activation, PARP-1 synthesizes a structurally complex polymer composed of ADP-ribose units that facilitates local chromatin relaxation and the recruitment of DNA repair factors. Here, we identify a function for PARP-1 in DNA DSB resection. Remarkably, inhibition of PARP-1 leads to hyperresected DNA DSBs. We show that loss of PARP-1 and hyperresection are associated with loss of Ku, 53BP1 and RIF1 resection inhibitors from the break site. DNA curtains analysis show that EXO1-mediated resection is blocked by PARP-1. Furthermore, PARP-1 abrogation leads to increased DNA resection tracks and an increase of homologous recombination in cellulo. Our results, therefore, place PARP-1 activation as a critical early event for DNA DSB repair activation and regulation of resection. Hence, our work has direct implications for the clinical use and effectiveness of PARP inhibition, which is prescribed for the treatment of various malignancies.

[1] Genome Stability Laboratory, CHU de Québec Research Center, HDQ Pavilion, Oncology Division, 9 McMahon, Québec City, QC G1R 3S3, Canada. [2] Department of Molecular Biology, Medical Biochemistry and Pathology, Laval University Cancer Research Center, Québec City, QC G1V 0A6, Canada. [3] Department of Oncology, Faculty of Medicine and Dentistry, University of Alberta, 11560 University Avenue, Edmonton, AL T6G 1Z2, Canada. [4] Department of Molecular Biosciences, University of Texas at Austin, Austin, TX 78712, USA. [5] CHU de Québec Research Center, CHUL Pavilion, Oncology Division, 2705 Boulevard Laurier, Québec City, QC G1V 4G2, Canada. [6] Biochemistry and Molecular Medicine, Université de Montréal, 2900 Boulevard Edouard-Montpetit, Pavillon Roger-Gaudry, Montréal, QC H3T 1J4, Canada. [7] These authors contributed equally: Marie-Christine Caron, Ajit Sharma. Correspondence and requests for materials should be addressed to M.J.H. (email: mhendzel@ualberta.ca) or to G.G.P. (email: guy.poirier@crchudequebec.ulaval.ca) or to J.-Y.M. (email: Jean-Yves.Masson@crchudequebec.ulaval.ca)

Each day, the eukaryotic genome is confronted with up to 50 endogenous DNA double-strand breaks (DSBs)[1]. These are extremely hazardous for a cell, because if left unrepaired, DSBs can have pathological consequences, such as cell death, or drive cells to genomic instability and tumor development. The cellular response to DNA damage involves an intricate network of enzymes responsible for sensing, signaling, and repairing damaged DNA, as well as the regulation of cell cycle checkpoints that collectively maintain genomic integrity[2].

Poly(ADP-ribose) polymerase-1 (PARP-1) is an abundant and ubiquitous nuclear protein that uses NAD^+ to synthesize a multibranched polyanion composed of ADP-ribose moieties, giving rise to poly(ADP-ribose) (PAR), onto itself or a variety of target proteins. Protein ADP-ribosylation permits the transfer of the ADP-ribose moiety from NAD^+ to the side chain of several amino acids[3–5]. Predominant biological processes targeted by PARylation include RNA splicing, processing, and maturation, DNA replication, and transcription as well as the DNA damage response (DDR)[3,6,7]. PARP-1 acts as a highly sensitive sensor for DNA damage and rapidly produces PAR at newly generated DNA DSBs. This promotes local chromatin relaxation due to its negative charge[8] and histone displacement[9], as well as facilitating the recruitment of repair factors, such as MRE11[10]. Several PAR-binding modules orchestrate the relocation of DDR-associated factors in addition to the accumulation of intrinsically disordered proteins through an intracellular liquid demixing mechanism[11,12]. PARP-1 is responsible for 80–90% of the global PAR synthesis following DNA strand breakage[13]. The dynamic turnover of PAR within seconds to minutes is executed by poly (ADP-ribose) glycohydrolase, the main PAR-degrading enzyme, which possesses both endoglycosidic and exoglycosidic activities, thereby enabling a new round of DNA damage signaling[14]. More recently, it has been shown that PARP-1 inhibition increases the speed of fork elongation and does not cause fork stalling, which is in contrast to the accepted model in which inhibitors of PARP induce fork stalling and collapse[15]. It was also recently shown that PARP-1 is a sensor of unligated Okazaki fragments during DNA replication[16] and cells deficient in ribonucleotide excision repair are sensitized to PARP inhibition[17].

PARP-1 is the best-characterized member of the diphtheria toxin-like ADP-ribosyl transferases (ARTDs) family of proteins. Among the 17 ARTDs members, only PARP-1, PARP-2, and PARP-3 are activated by DNA strand breaks[18–20]. De Murcia and colleagues provided the first evidence implicating PARP-1 in DNA repair by demonstrating that PARP-1-deficient mice are highly sensitive to γ-irradiation[21]. PARP-1 plays a critical role in DSB sensing and we have shown that PARP-1 recruitment and activation occur within 100 ms after introduction of DSBs. This makes PARP-1 activation one of the earliest and most critical events in the sensing of DSBs. Consistent with this, PARP-1 activity increases the rate of recruitment of the MRE11-RAD50-NBS1 (MRN) complex[10] and stimulates Ku binding in Dictyostelium[22]. Structural analyses of PARP-1 have shown that PARP-1 binds DSBs. It does so through interactions with its zinc fingers and a WGR domain[23–25].

In mammalian cells, most DSBs are repaired using long homologous sequences (homologous recombination (HR)), microhomology-mediated end joining, or no homology end joining (NHEJ). A key event that controls the DSB repair pathway choice is DNA end resection, which is characterized by 5′ to 3′ degradation of one strand at each side of the break. HR is initiated by CtBP-interacting protein (CtIP), a key molecular switch that controls DNA end resection and interacts with BRCA1. Although BRCA1 is a CtIP-interacting protein, there are conflicting reports on the roles of BRCA1 in DNA resection. While an early report found that disrupting the CtIP–BRCA1 interaction in DT40 cells diminished DNA-end resection[26], a later report showed that CtIP mutated at Ser332, which is required for interaction with BRCA1, is competent for RPA and Rad51 assembly, indicating that resection is proficient in this background[27]. More recently, the CtIP–BRCA1 complex was found not to be essential for DNA end resection but rather modulated its speed[28]. The resection process is controlled by two core resection machineries in human cells: BLM–DNA2–RPA–MRN and EXO1–BLM–RPA–MRN[29]. DNA resection is also negatively regulated by the HELB helicase in an RPA-dependent manner[30] and by 53BP1 and RIF1 proteins[31,32].

Many years ago, we demonstrated that MRE11 and NBS1, which are core components of the early DSB sensing complex MRN, are recruited in a PARP-1-dependent manner to laser-induced DNA damage tracks. MRE11 was further shown to interact non-covalently with PAR via its intrinsically disordered glycine- and arginine-rich region, an interaction that modulates the resection functions of MRE11[10]. We have previously shown that PARP-1 can interact with Ku70 and Ku80[33] and PARP-1 activity is necessary for Ku binding in Dictyostelium through PAR binding by Ku70[22]. Importantly, PARP-1 activation precedes the recruitment of both the MRN and the Ku complex, previously recognized as the primary DSB sensors that recruit signaling proteins at DSB sites. Because the Ku complex and MRN bind PAR, PARylation may serve to guide and concentrate the Ku and MRN complexes at DSBs to facilitate their loading. As MRN is the initiator of DNA resection while the Ku complex inhibits end resection, we set out to determine whether PARP-1 could affect DNA resection.

The hypersensitivity of HR-deficient cancers to PARP inhibitors (PARPi) provided a conceptual basis for synthetic lethality. PARPi are currently being tested in over 200 clinical studies, with at least 50 trials in phase III (www.clinicaltrials.gov). Because of their specific mechanism of action, PARPi show a low toxicity profile[34]. PARPi has proven to be of significant clinical benefit, even for patients without HR deficiencies. Defining how PARP-1-dependent DNA processing functions mechanistically will help identify genetic markers of sensitivity and resistance to guide PARPi therapy by identifying patients most likely to respond to either single agent or combination therapy through cytotoxic or radiation chemopotentiation[35]. Here, we identify PARP-1 as a critical regulator of DNA end resection of DSBs. We show that PARP-1 recruitment protects DNA ends from nucleolytic degradation and inhibition of PARP-1 leads to hyper-resected DNA double-strand breaks. Our data provide an alternative mechanism by which PARPi function in the presence of irradiation (IR).

Results

Recruitment of PARP-1 and PARP-2 at laser-induced DNA breaks. We initially scrutinized the recruitment kinetics of PARP-1 to laser-induced DNA damage. Consistent with previous findings[36,37], we observed that PARP-1 is recruited rapidly to laser-induced DNA damage tracks within milliseconds (Supplementary Fig. 1). The dynamics of PARP-1 recruitment under normal conditions was compared with the dynamics observed under PARP inhibition with BMN 673 (Talazoparib). The initial rapid accumulation of PARP-1 at sites of damage was followed by a steady reduction over the next 10 min, while in the presence of BMN 673, PARP-1 is lost from the damage site more slowly, possibly due to trapping at DSBs[38]. Similar to PARP-1, PARP-2 retention at laser-induced DNA lesions is normally transient, with a slow decline after an initial maxima at approximately 2 min post damage. However, in cells exposed to BMN 673, an initial rapid accumulation is observed, but rather than decline, there persists a slowly increasing accumulation of PARP-2 over the 10 min experiment (Supplementary Fig. 2). Because the

ultrafast recruitment of PARP-1 at DNA lesions precedes and primes the accumulation of other DNA damage repair factors, including the MRN complex, and because PARylation is a determining factor for their local accumulation, we reasoned that PARylation-dependent events might also affect DSB repair pathway choice through DNA end resection.

Effect of PARPi on DNA end resection. We used two different methods to determine whether PARP-1 itself or its catalytic activation influences DNA resection. First, we used a bromodeoxyuridine (BrdU)-based assay for visualizing the single-stranded DNA (ssDNA) product of resection. Second, we measured the accumulation of replication protein A (RPA). RPA is an essential trimeric protein complex that binds to ssDNA in eukaryotic cells. It is recruited to sites of DNA damage when regions of ssDNA are exposed. Hence, it serves as a readout for resection and for ongoing HR. Thus the amount of RPA that accumulates at each site should reflect the amount of ssDNA. Remarkably, both PARP-1 inhibition by BMN 673 or small interfering RNA (siRNA)-mediated PARP-1 silencing led to a substantial increase in the generation of ssDNA as measured by BrdU intensity in U2OS or HeLa cells (Fig. 1a, c). This was further confirmed using CRISPR/Cas9-mediated knockout of PARP-1 in 293T cells (Supplementary Fig. 3A, B). We quantified this data by measuring the total amount of BrdU (or RPA) in each focus. The summed intensity values for each individual focus reveals a greater than two-fold increase in the average amount of ssDNA generated per DSB (focus) when PARP-1 is inhibited by BMN 673 or silenced by siRNA. Consistent with an accumulation of RPA foci following pharmacological inhibition of PARP-1 or PARP-1 knockdown (Fig. 1b, d, Supplementary Fig. 3C), we observed an overall increase of chromatin-bound and phosphorylated RPA (Fig. 1e). Microirradiation experiments also showed enhanced recruitment of GFP-RPA1, GFP-RPA2, or GFP-RPA3 in S-phase cells following pharmacological inhibition of PARP-1 (Fig. 1f, Supplementary Fig. 3E, F). It is well known that the activation of the ATR kinase following perturbations in S-phase relies on a complex mechanism involving ATR recruitment to RPA-coated ssDNA. Consistent with an increase in RPA recruitment in PARP-1 knockdown cells, the activation of ATR was enhanced as judged by using anti-ATR Thr-1989 as a proximal marker of ATR activation[39] (Supplementary Fig. 3G).

To rule out the possibility that PARP-1 plays an indirect role that promotes the accumulation of ssDNA, we repeated the BrdU-based assay with a knockdown of CtIP, which is expected to suppress DNA resection at DSBs[40]. The simultaneous knockdown of PARP-1 and CtIP completely suppressed the accumulation of ssDNA, implying that knockdown of PARP-1 affects the DSB resection process and does not promote a resection-independent accumulation of ssDNA (Fig. 1g, Supplementary Fig. 4A, B). CtIP foci formation was also increased in PARP-1 knockdown cells (Supplementary Fig. 4C, D). The accumulation of ssDNA was not observed in DNA Ligase IV knockdown cells, suggesting that cells compromised in later stages of NHEJ do not share this phenotype (Supplementary Fig. 4E). Since we are monitoring DNA resection products 3 h after IR, we ascertained that the above results were not a consequence of an accumulation of cells in S/G2 (Supplementary Fig. 5A, B). In addition to the intensity, the number of BrdU or RPA foci per nucleus were increased in BMN 673-treated U2OS cells or PARP-1-silenced HeLa cells compared to controls (Supplementary Fig. 5C–F). Treatment with another PARPi, Veliparib, caused also an enhancement of BrdU or RPA intensity per nucleus (Supplementary Fig. 6A, B).

To quantify ssDNA at the sites of DSBs, we used the ER-*Asi*SI system in which the restriction enzyme *Asi*SI is fused to the estrogen receptor hormone-binding domain. Upon treatment with 4-hydroxytamoxifen (4-OHT), the *Asi*SI nuclease translocates to the nucleus and generates up to 150 DSBs at sequence-specific sites[41,42]. In this system, the presence of DSB resection will lead to the generation of ssDNA that cannot be cleaved by the duplex DNA-specific endonuclease *Bsr*GI before PCR. In the absence of DNA resection, the remaining double-stranded DNA (dsDNA) will be cleaved, therefore yielding no PCR products (Fig. 2a). Thus the system can be used to distinguish between ssDNA and dsDNA. Interestingly, PARP-1 depletion or inhibition by BMN 673 (Fig. 2b) led to a ~30% increase in DNA resection compared to the control at two different sites (Fig. 2c). Similarly, PARP-1 inhibition led to a ~3–6-fold increase in bound RPA2 to processed DSBs (Fig. 2d). Altogether, these results show that PARP-1 limits DNA processing in cellulo.

PARP-1 knockdown cells show decreased 53BP1 and RIF1 foci. The mechanism underlying PARP-1-regulated DNA resection was investigated further. We monitored the accumulation of the resection inhibitors 53BP1 and RIF1 in G1 cells (Fig. 3a, b) depleted of PARP-1. Interestingly, PARP-1 inhibition led to a decrease of 53BP1 and RIF1 foci following etoposide treatment (average number of foci = 46 in the control and 28 in PARP-1 knockdown for 53BP1, and average number of foci = 27 in the control and 11 in PARP-1 knockdown for RIF1). These results were corroborated by chromatin immunoprecipitation (ChIP) analysis using cells stably expressing mCherry-*Lac*I-*Fok*I at an integrated reporter transgene (U2OS-DSB-reporter system (Fig. 3c)), which showed a drastic reduction of 53BP1 (Fig. 3d) or RIF1 accumulation (Fig. 3e) on two different DSBs in PARP-1 knockdown or BMN 673-treated cells.

PARP-1 blocks DNA resection by MRN-RPA-BLM-EXO1-DNA2. The above data suggest that PARP-1 may be able to directly suppress the activity of DNA resection enzymes. We further examined whether purified PARP proteins (Fig. 4a) could block DNA resection in vitro. We monitored DNA resection of a 3′-end-labeled dsDNA (2.7 kb) via the two main DNA resection machineries MRN-RPA-BLM-EXO1 or MRN-RPA-BLM-DNA2. In the absence of PARPs, the MRN-RPA-BLM-EXO1 assembly resected ~75% of the 2.7 kb substrate (Fig. 4b). When the reaction was supplemented with PARP-1, a concentration-dependent inhibition was observed. At 50 nM PARP-1, only 10% of the DNA could be resected within the 60 min incubation time, without NAD or at a NAD concentration that still supports DNA binding. As specificity controls, we also performed similar reactions with PARP-2 and PARP-3. Importantly, PARP-2 and PARP-3 enzymes did not inhibit MRN-RPA-BLM-EXO1-mediated DNA degradation. PARP-1 also blocked the MRN-RPA-BLM-DNA2 complex and PARP-1-mediated inhibition was retained with the catalytic mutant E988K but abolished when a PARP-1 fragment devoid of its zinc fingers (PARP-1 216-1014) was used (Fig. 4c, Supplementary Fig. 6C). PARP-1 216-1014 has been reported to have a severely decreased affinity (250-fold less) for DNA lesions compared to wild-type (WT) PARP-1[23]. PARP-1 blocked the resection complexes at 5 and 30 μM concentration of NAD^+, where PARP-1 undergoes only moderate PAR automodification (Supplementary Fig. 6D, E) and remains bound to DNA (Fig. 4b–d, Supplementary Fig. 6F, G). In contrast, the higher NAD^+ concentration of 250 μM NAD^+, where PAR automodification releases PARP-1 from DNA, prevented PARP-1 inhibition of resection (Fig. 4e, Supplementary Fig. 6F, G). Since even low levels of PAR alone could sequester protein components

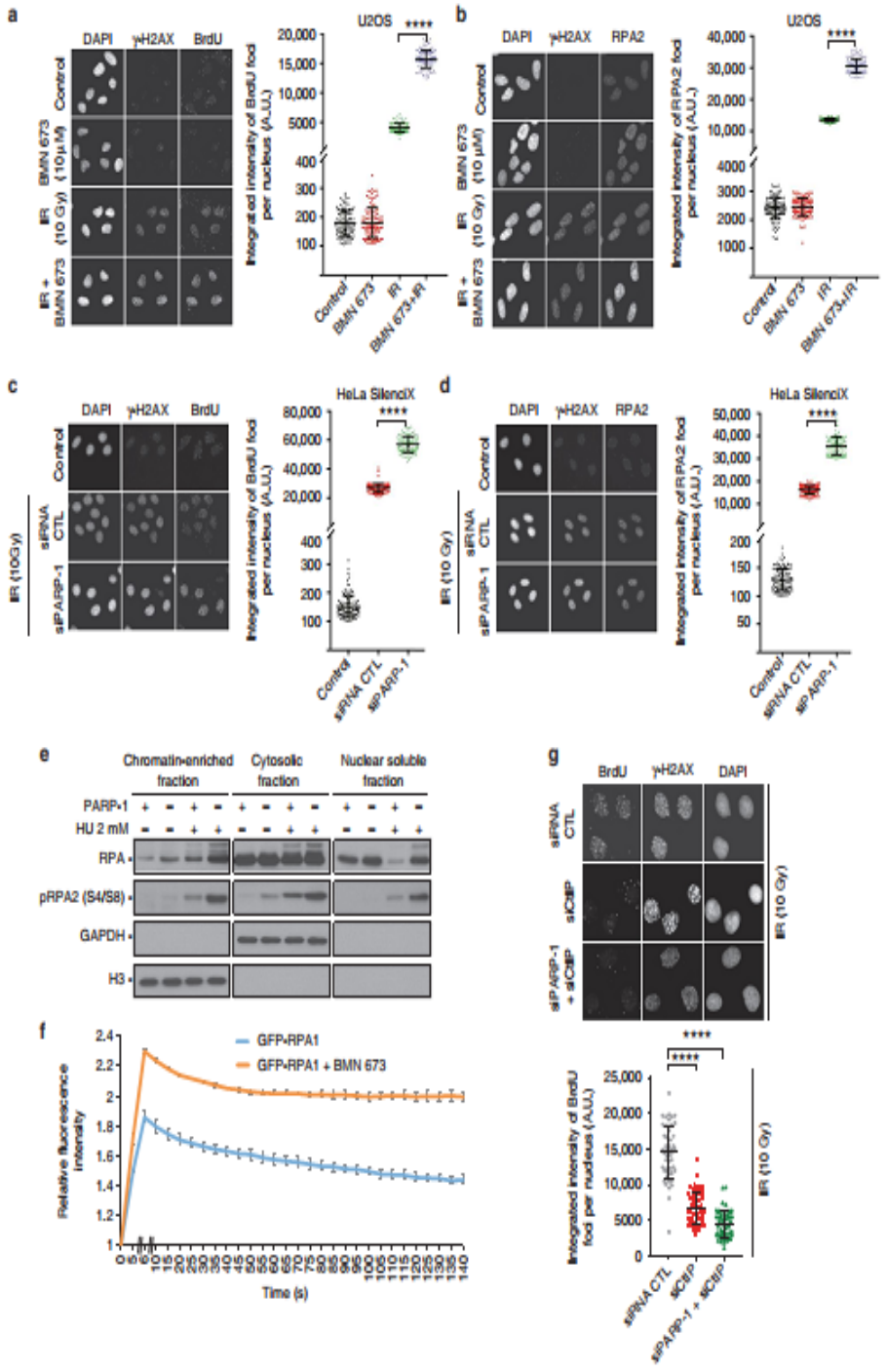

of the resection reaction leading to suppression of DNA resection, we performed reactions with protein-free PAR (Fig. 4f). This failed to inhibit DNA resection. These results show that PARP-1 but not PARP-2, PARP-3, or PAR can robustly inhibit DNA resection through a direct DNA-binding mechanism.

We used a high-throughput single-molecule DNA curtain assay to directly observe how PARP-1 inhibits EXO1 processing of substrate DNA. Arrays of DNA molecules (48.5 kb, derived from λ-phage) were assembled on the surface of a microfluidic flowcell coated with a surface-passivating fluid lipid bilayer[43]. The DNA substrate was linked to the bilayer via a biotin–streptavidin linkage. Fluorescently labeled PARP-1 was injected into the flowcell and visualized using total internal reflection fluorescence microscopy on thousands of DNA molecules for high-throughput

Fig. 1 Poly(ADP-ribose) polymerase-1 (PARP-1) regulates DNA end resection and chromatin accumulation of replication protein A (RPA). U2OS cells mock treated, treated with BMN 673, irradiated (10 Gy), or irradiated (10 Gy) in combination with BMN 673 were subjected to immunofluorescence against γ-H2AX, bromodeoxyuridine (BrdU) (**a**), or RPA2 foci formation (**b**). HeLa SilenciX cells underexpressing PARP-1 by siRNA-mediated gene knockdown were subjected to immunofluorescence against γ-H2AX, BrdU (**c**) or RPA2 foci formation after irradiation (10 Gy, 3 h release) (**d**). In panels **a**–**d**, the data show the mean ± s.d. (Mann–Whitney *U* test). **e** HEK293T wild type or CRISPR-PARP-1 were treated with 2 mM hydroxyurea for 16 h, fractionated into chromatin enriched, nuclear soluble and cytoplasmic fractions. **f** GFP-RPA1 recruitment in the absence (blue line) or presence of BMN 673 (orange line). The peak of intensity was at 6 s. Data show the mean ± s.e.m. **g** knockdown of CtIP suppresses the accumulation of single-stranded DNA in HeLa SilenciX PARP-1 knockdown cells after irradiation (10 Gy, 3 h release). The data show the mean ± s.d. $^{****}p \leq 0.0001$ (Mann–Whitney *U* test). Source data are provided as a source data file

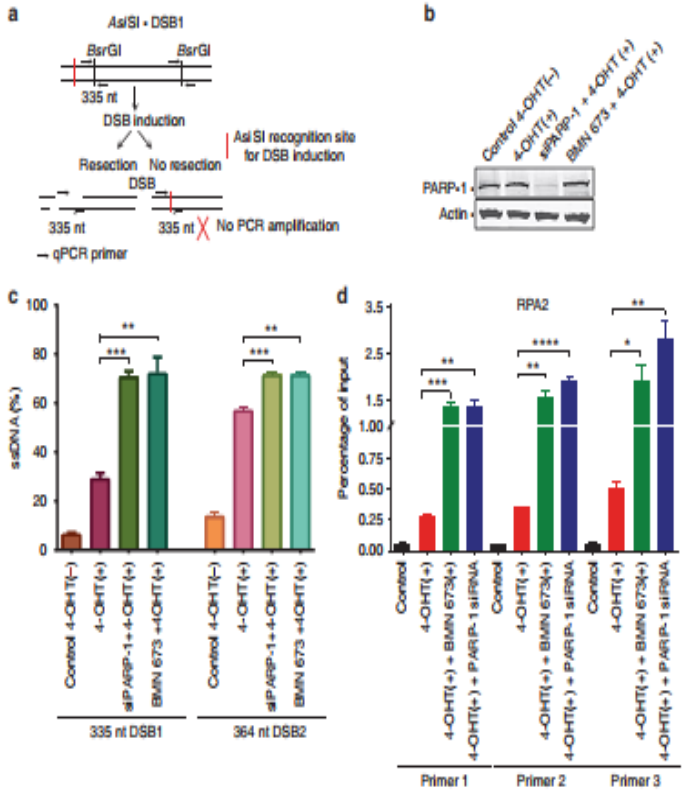

Fig. 2 Measurement of double-strand break (DSB) resection in ER-AsiSI U2OS cells knocked down for poly(ADP-ribose) polymerase-1 (PARP-1) or treated with a PARP inhibitor. **a** Quantitative polymerase chain reaction (qPCR) primers and probes for measurement of DSB resection at two *AsiSI* sites. **b** ER-AsiSI U2OS cells were knocked down for PARP-1 or treated with BMN 673 for 1 h, followed by induction with 300 nM 4-hydroxytamoxifen for 3 h. **c** Quantitation of the percentage of DNA resection. Error bars represent mean ± s.e.m. $^{**}p \leq 0.01$, $^{***}p \leq 0.001$ (Mann–Whitney *U* test). **d** Chromatin immunoprecipitation-qPCR was performed with antibody against RPA2 in the ER-AsiSI U2OS cells. DSBs were induced at 48–72 h after siRNA transfection or after 1 h BMN 673 treatment. Immunoprecipitated chromatin samples were analyzed by qPCR using specific primer pairs located at Chr 1: chr1_89231183, Chr 6: chr6_90404906, and Chr 21: distal region of chr21_21292316. Error bars represent mean ± s.e.m. $^{*}p \leq 0.05$, $^{**}p \leq 0.01$, $^{***}p \leq 0.001$, $^{****}p \leq 0.0001$, (Mann–Whitney *U* test). Source data are provided as a source data file

data collection and analysis (Fig. 5a). Nearly all PARP-1 molecules were bound to the end of the DNA. This conclusion is based on the observation that turning off buffer flow led to the coordinated retraction of both the DNA and associated PARP-1 molecules to the diffusion barrier (Fig. 5b, c). Most PARP-1 molecules localized to the DNA end via binding internally and sliding along the DNA in the direction of buffer flow (88% of PARP-1 molecules, $N = 109/124$). This indicates that PARP-1 is able to diffuse along the DNA and one-dimensional (1D) diffusion may represent a mechanism by which PARP-1 quickly associates with DNA ends or other DNA lesions. In conditions where PARP-1 was pre-bound to the end of DNA molecules (Fig. 5d, magenta in right panel), a second PARP-1 molecule (Fig. 5d, green in right panel) bound upstream and slid along the DNA to co-localize at the DNA end. Consequently, the red and green traces can be seen to merge in the kymograph (Fig. 5d). Pre-bound PARP-1 blocked DNA resection by preventing EXO1 loading onto the DNA end (Fig. 5e–g). This suggests that PARP-1 may physically occlude the end of DNA. In contrast, end-bound PARP-2 did not block EXO1 loading and DNA resection.

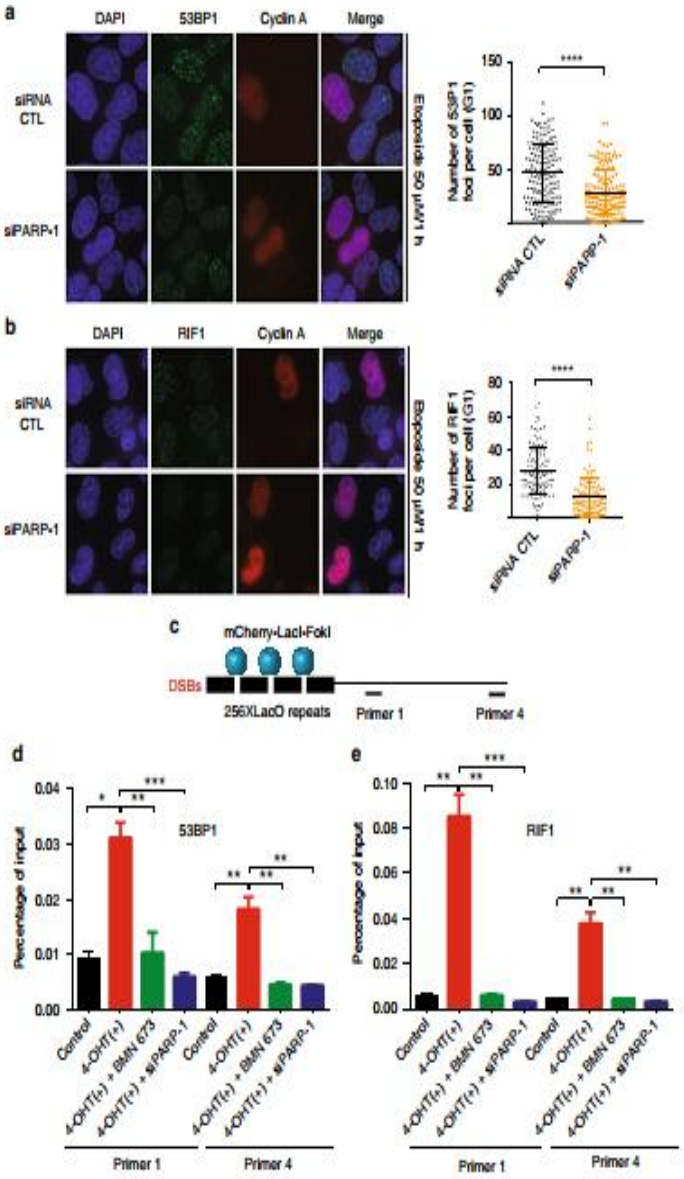

Fig. 3 Poly(ADP-ribose) polymerase-1 (PARP-1) inhibition reduces the accumulation of 53BP1 and RIF1 foci. **a** Etoposide-treated HeLa cells were either transfected with an small interfering RNA (siRNA) control or PARP-1 siRNA and subjected to immunofluorescence staining against 53BP1 or Cyclin A. The mean foci count was 46.05 for siRNA CTL and 28.42 for siPARP-1. Data show the mean ± s.d. $^{****}p \leq 0.0001$ (Mann–Whitney *U* test). **b** Etoposide-treated HeLa cells were either transfected with a control siRNA or PARP-1 siRNA and subjected to immunofluorescence staining against RIF1 or Cyclin A. The mean foci count was 27.52 for siRNA CTL and 11.68 for siPARP-1. Data show the mean ± s.d. $^{****}p \leq 0.0001$ (Mann–Whitney *U* test). **c** Cartoon of the U2OS-DSB-reporter with inducible DSB generation by mCherry-*Lac*I-FokI. Chromatin immunoprecipitation (ChIP)–quantitative polymerase chain reaction (qPCR) primer sets are shown as p1–p4. ChIP of 53BP1 (**d**) or RIF1 (**e**) from the fixed chromatin of U2OS-DSB reporter cells stably expressing mCherry-*Lac*I-FokI construct and treated with both 0.5 mM Shield-1 (1:500 dilution) and 1 mM 4-hydroxytamoxifen (4-OHT) for 1 h in order to generate DSBs. The ChIP–qPCR primer sets are labeled as primer 1 and primer 4. Data in **d**–**e** show the mean ± s.e.m. $^{*}p \leq 0.05$, $^{**}p \leq 0.01$, $^{***}p \leq 0.001$ (Mann–Whitney *U* test). Source data are provided as a source data file

Consistent with this, microirradiation experiments showed enhanced accumulation of GFP-EXO1 in PARP-1-deficient cells at laser-induced DNA damage sites (Fig. 5h) and phosphorylated EXO1 accumulated more in the absence of PARP-1 (Supplementary Fig. 7A). Altogether, our results show that PARP-1 counteracts DNA resection in vitro, likely by occluding the free DNA ends from the EXO1 or DNA2 resection machineries.

PARP-1 is required for efficient loading of the Ku complex. Another mechanism whereby PARP-1 could inhibit end resection

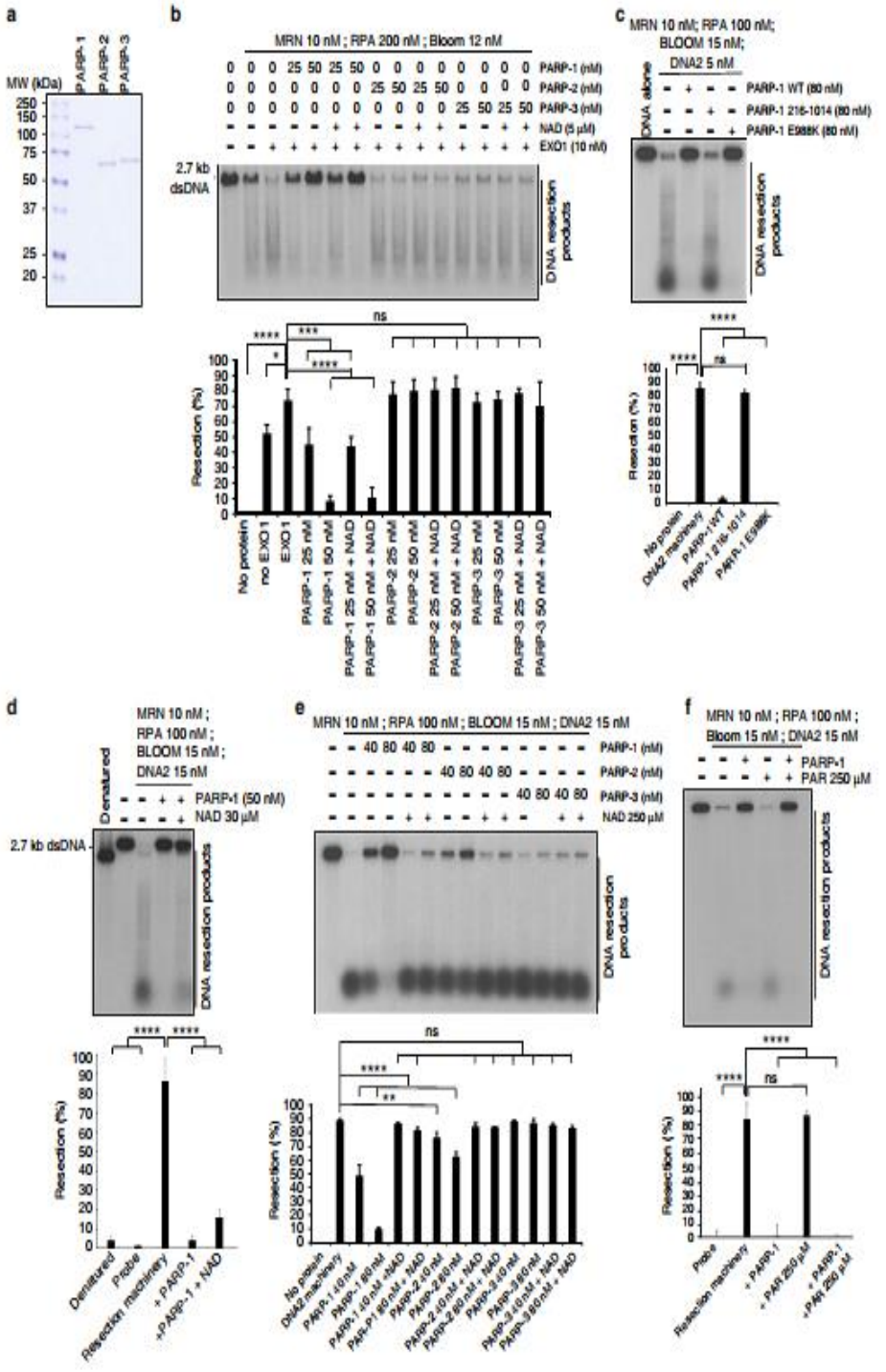

is through regulation of the association of the Ku complex with DNA ends. Consequently, we performed laser microirradiation experiments to determine whether Ku80-GFP recruitment to sites of DNA damage is sensitive to PARPis (Fig. 6a, b). We found that the recruitment of Ku80-GFP was almost completely inhibited in cells treated with PARPi but robustly recruited in control cells. We next tested PARP-1-deficient cells and found that they also fail to efficiently recruit Ku80-GFP to sites of DNA damage (Fig. 6c, d). In order to determine the influence of PARP activity on the association of Ku80 with DNA ends, we performed ChIP experiments in the presence or absence of PARP-1 or PARPi (Fig. 6e) and in the presence of RNAse to avoid indirect binding through

Fig. 4 Poly(ADP-ribose) polymerase-1 (PARP-1) limits DNA end resection in vitro. **a** Sodium dodecyl sulfate-polyacrylamide gel electrophoresis of purified human PARP-1, PARP-2, and PARP-3. **b** The indicated PARP proteins were incubated with the MRN-RPA-BLM-EXO1 machinery in the absence or presence of NAD (5 μM). The resection products were detected by autoradiography after agarose gel electrophoresis. Bottom: quantification of the results. **c** The PARP-1 DNA-binding mutant PARP-1 216-1014 fails to inhibit DNA resection. Bottom: quantification of the results. **d** DNA end resection by the MRN-RPA-BLM-DNA2 machinery is decreased in the absence or presence of NAD (30 μM). **e** The indicated PARP proteins were incubated with the MRN-BLM-RPA-DNA2 machinery in the absence or presence of NAD (250 μM). **f** The addition of purified PAR (250 μM) alone does not block DNA resection by MRN-BLM-RPA-DNA2. PARP-1 was used at 87 nM. Error bars in **b**–**f** indicate s.d. from three independent experiments. $^{*}p \le 0.05$, $^{**}p \le 0.01$, $^{***}p \le 0.001$, $^{****}p \le 0.0001$ (ordinary one-way analysis of variance). Source data are provided as a source data file

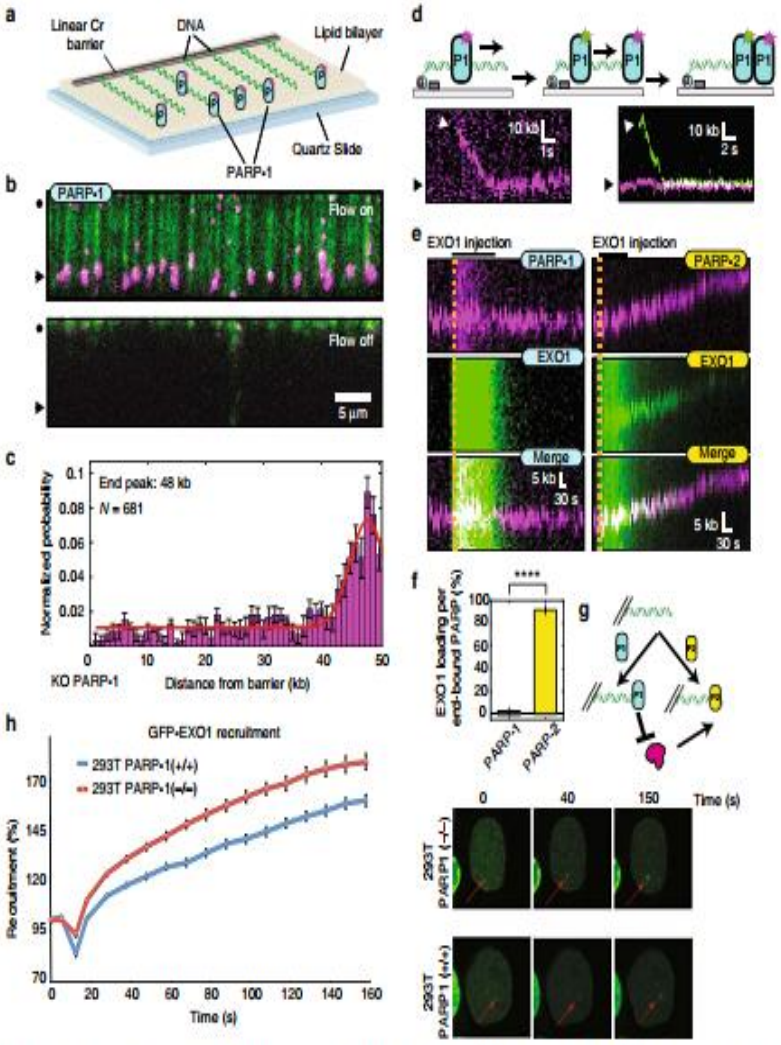

Fig. 5 Poly(ADP-ribose) polymerase-1 (PARP-1) slides to accumulate at ends and prevent EXO1 binding. **a** Illustration of the DNA curtain assay with fluorescent PARP-1 (blue ovals). **b** Fluorescent PARP-1 (magenta) binding to DNA curtains in the presence (top) or absence (bottom) of buffer flow. Black circles indicate the diffusion barrier and arrows indicate the DNA ends. After PARP-1 was loaded, the DNA was stained with the fluorescent intercalating dye YoYo-1. **c** Histogram of the positions of 681 individual PARP-1 molecules along the length of the DNA substrate. Error bars were calculated by bootstrapping the data[74] and indicate a 70% confidence interval. **d** Illustration (top) and kymograph (bottom) of two differently labeled PARP-1 (P1) molecules binding to the DNA end. PARP-1 reached the end by buffer flow-assisted one-dimensional sliding 88% of the time ($N = 109/124$). **e** Representative kymographs of EXO1 resection of DNA pre-bound with PARP-1 (left) or PARP-2 (right). **f** Quantification of EXO1 loading events per DNA end bound by PARP-1 (left; 2.4 ± 3.4%; $N = 42$ PARP-1 molecules) or PARP-2 (right; 91.8 ± 4.1%; $N = 65$ PARP-2 molecules). Error bars represent mean ± s.e.m. $^{****}p \le 0.0001$, (Student's t test). **g** Model for PARP-1 inhibition of EXO1. P2 refers to PARP-2. YoYo-1 was omitted from all experiments described in **c**–**f**. **h** Recruitment of GFP-EXO1 at laser-induced double-strand breaks in HEK293T wild-type or PARP-1−/− cells. Source data are provided as a source data file

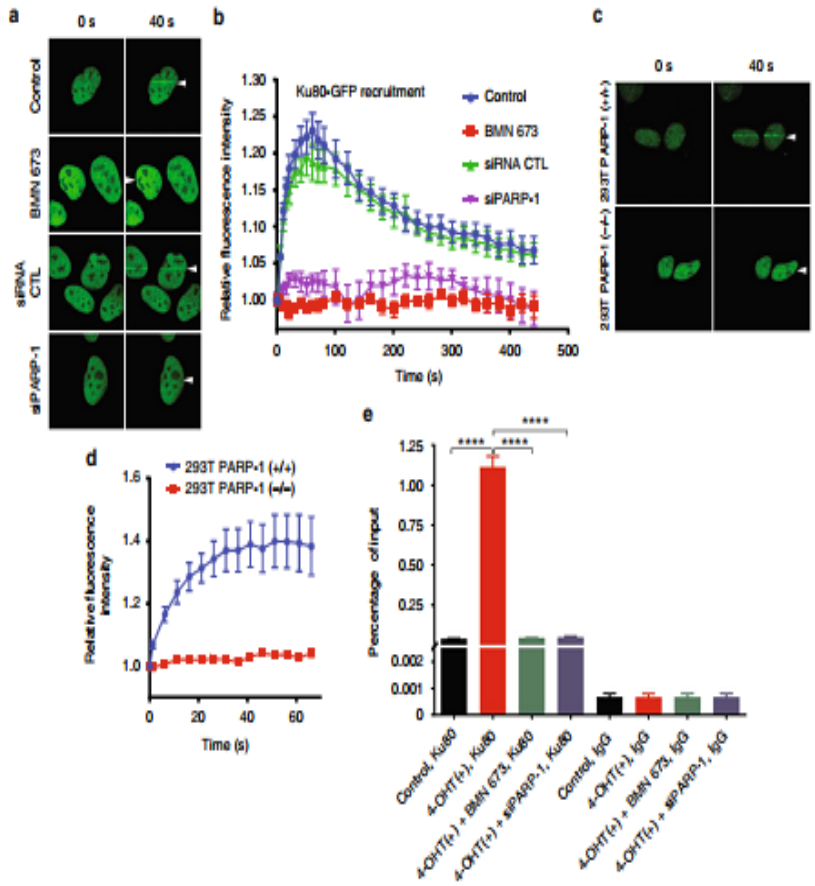

Fig. 6 Poly(ADP-ribose) polymerase-1 (PARP-1) knockdown or pharmacological inhibitor affects Ku80 recruitment on double-strand breaks. **a** U2OS cells stably expressing the Ku80-GFP were mock treated, treated with BMN 673, or silenced with PARP-1 siRNA and subjected to laser microirradiation-track studies. **b** Quantification of the relative fluorescence intensity of Ku80-GFP over time. Error bars represent mean with s.e.m. **c** Recruitment of Ku80-GFP in PARP-1-deficient CRISPR 293T cells is severely affected. **d** Quantification of the relative fluorescence intensity of Ku80-GFP over time. Error bars represent mean with s.e.m. **e** AsiS1-ER-U2OS reporter cells were cultured and treated with 4-hydroxytamoxifen (300 nM) for 1 h. Soluble chromatin fractions were prepared and subjected to immunoprecipitation against IgG control and Ku80-specific antibody. Immunoprecipitated chromatins fractions were analyzed by quantitative polymerase chain reaction using specific primer pairs: chr1_89231183. Error bars represent mean ± s.e.m. ****$p \leq 0.0001$ (Mann–Whitney *U* test). Source data are provided as a source data file

RNA. We find that Ku association with the DSB is dependent on both PARP-1 and PARP-1 activity. Consequently, in addition to acting as a direct inhibitor of DNA end resection, PARP-1 also inhibits end resection by promoting Ku loading onto the DSB. To assess this further on other NHEJ components, we monitored phospho-DNA-PKcs foci formation in PARP-1 U2OS CRISPR/Cas9-mediated knockout cells. Consistent with our previous studies showing a decrease of NHEJ in cellulo following ABT-888 treatment[44], a decrease of phosphorylated DNA-PKcs foci was observed (Supplementary Fig. 7B). A Ku80 knockdown in HEK 293T cells leads to enhanced EXO1 recruitment (Supplementary Fig. 7C), suggesting that the recruitment of Ku80 by PARP-1 is a critical event for regulating EXO1-mediated DNA resection.

Increased resection tracks and HR in PARP-1-deficient cells. Next, we measured DNA resection in cellulo using a high-resolution technique to see whether PARP-1 inhibition would lead to increased resection in different genetic contexts. The single-molecule analysis of resection tracks (SMART) assays is a very sensitive technique that can detect DNA resection upon IR, while almost no fibers can be detected without DNA damage[28]. It has been reported that BRCA1 is important to control the speed of DNA resection[28] and that inhibition of 53BP1 in BRCA1-deficient cells rescue these cells through enhanced DNA resection[45]. Hence, our data predict that the DSB-induced over-resection phenotype would not appear in BRCA1-deficient cells when challenged with the PARP-1 inhibitor BMN 673. However, the DNA resection machinery is intact in BRCA2-deficient cells, because BRCA2 acts later in HR, and we should observe this over-resection phenotype under the same conditions. First, SMART assays revealed that PARP-1-deficient cells have longer resection tracks after IR treatment (Fig. 7a) and are IR sensitive in survival assays (Fig. 7b). When cells were treated with BMN 673 and IR, BRCA1 knockdown led to a decrease of BrdU accumulation, which could be partially rescued by 53BP1 knockdown (Supplementary Fig. 8A, B, D). SMART assays also recapitulated these results (Supplementary Figs. 8C, D and 9A). Conversely, BRCA2

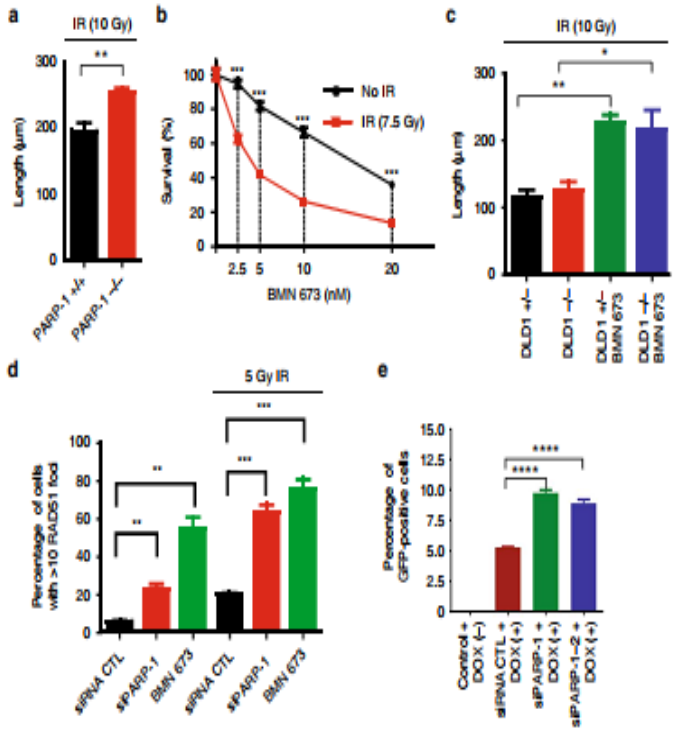

Fig. 7 Single-molecule analysis of resection tracks (SMART) analysis and effect of poly(ADP-ribose) polymerase-1 (PARP-1) on homologous recombination. **a** SMART of PARP-1-deficient mouse embryonic fibroblasts (MEFs). MEFs were treated with 10 Gy irradiation (IR). Error bars represent mean ± s.e.m. **b** Treatment of HeLa cells with BMN 673 results in IR sensitivity. Error bars represent mean with s.e.m. **c** SMART of BRCA2-proficient (DLD1 BRCA2 (+/−)) and BRCA2-deficient cells (DLD1 BRCA2 (−/−)) either mock treated of treated with BMN 673 (5 µM) were irradiated (10 Gy). Error bars represent Mean with s.e.m. **d** Attenuation of PARP-1 increases RAD51 foci in cellulo. Error bars represent mean ± s.e.m. **e** Homologous recombination is increased in PARP-1 knockdown cells. Error bar represents mean ± s.d. $^{*}p \leq 0.05$, $^{**}p \leq 0.01$, $^{***}p \leq 0.001$, $^{****}p \leq 0.0001$ (Mann–Whitney *U* test). Source data are provided as a source data file

knockdown or DLD1 BRCA2 (−/−) cells showed a similar increase of BrdU staining (Supplementary Fig. 8A, B) or DSB resection tracks following treatment with BMN 673 (Fig. 7c) compared to the controls. These results show that PARP-1 inhibition-mediated over-resection of DSBs is achieved when cells have an effective DNA resection machinery.

Based on these results, we hypothesize that PARP-1 plays an important regulatory role in the DNA damage response by influencing DNA resection and consequently DNA repair. HR depends heavily on the extent of DNA resection. To address whether PARP-1 influences HR, we monitored RAD51 foci formation following γ-irradiation (Fig. 7d). In agreement with previous findings with an older generation of PARP-1 inhibitors[46], we observed that the percentage of cells harboring >10 RAD51 foci was increased in HEK 293T cells subjected to CRISPR/Cas9-mediated knockout of PARP-1 (Supplementary Fig. 9B, C) or in cells treated with a siRNA targeting PARP-1 or exposed to PARP-1 inhibition (Fig. 7d). In addition, using a doxycycline (Dox)-inducible I-SceI/DRGFP cell line, HR was increased with PARP-1 knockdown (Fig. 7e), BMN 673, or ABT 888-treated cells (Supplementary Fig. 9D). Collectively, these results show that PARP-1 negatively regulates HR in cellulo.

Discussion

In this study, we show evidence that PARP-1 antagonizes the activity of the MRN-RPA-BLM-EXO1 and MRN-RPA-BLM-DNA2 machineries for DNA DSB repair. Interestingly, PARP-1 mediates this effect through DNA end binding and promoting Ku80 loading. Furthermore, loss of PARP-1 leads to a decrease in the accumulation of HR suppressors 53BP1 and RIF1 at DSBs, which in turn increases the DNA accessibility to EXO1 resulting in excessive degradation of DNA lesions. Such an effect can be obtained with either PARP-1 knockdown or pharmacological inhibition of PARP-1 activity. Thus mammalian cells have evolved several distinct regulatory systems that limit ssDNA overhang formation. First, a PARP-1-dependent mechanism influencing the Ku heterodimer and the 53BP1 pathway, and second, HELB that limits end resection in an RPA-dependent manner[30]. Recent studies have shown that DYNLL1[47] and the Shieldin complex[48–50] can also counteract DNA resection.

PARP-1 is an abundant nuclear chromatin-associated protein, well characterized for its high DNA damage-sensing ability. Once encountering free DNA ends, PARP-1 is catalytically activated and generates large amounts of PAR, which can function as a scaffold for the recruitment of a variety of DNA repair proteins[12]. It has been proposed that the local accumulation of PAR at DNA damage sites promotes liquid demixing, a phase separation event leading to compartmentalization of repair foci[12]. PAR polymers not only provide a loading platform for DDR-associated proteins and repair factors but also reprograms their functions through spatial and temporal interactions with their PAR reading motifs[12,44]. We envision that PARP-1 activation orchestrates the initial steps of DNA resection, granting access to the resection machineries. PARP-1 interacts

with DNA-PKcs/Ku70/Ku80[51] and mediates this effect through DNA end binding and recruitment of the Ku complex to DNA ends. Although Ku and PARP-1 have been found to compete for binding to DNA end in vitro[52], temporally, PARP-1 precedes Ku loading and its activity is required to load Ku onto DSB ends. This correlates well with the timing of PARP-1-mediated displacement of histones[9], suggesting that PARP-1 activity is necessary to prepare chromatin for loading of Ku onto broken DSB ends. When PARP-1 is absent, neither PARP-1 nor Ku assemble to protect the DNA ends when analyzed by ChIP at nuclease-induced DSBs. Consequently, EXO1 has higher access to DSBs, and with a concomitant decrease of RIF1 and 53BP1, this leads to excessive DNA processing. In line with this observation, using the ER-*Asi*SI system, the group of Tanya Paull has shown that siKu86 or Ku86 conditional HCT116 cells show increased DNA resection[42]. This enhanced DNA resection has been observed in PARP-1 knockdown and PARP-1 knockout using SMART analysis, RPA staining as a surrogate marker of ssDNA accumulation, and native anti-BrdU staining. It is important to note that this excess of ssDNA is dependent on CtIP thereby confirming that the ssDNA detected is generated by DNA end resection. In a similar manner, we also observed excessive DSB processing in Veliparib- or BMN 673-treated cells. Initially, BMN 673 delays the displacement of PARP-1 on DSBs but does not prevent displacement, which reaches completion over a 10 min time frame following laser-induced DNA damage. At that point, it will no longer protect DSB ends, leading to a similar phenotype as a complete deletion of PARP-1 (Model in Fig. 8).

Using purified proteins, we also show that PARP-1 directly blocks both the EXO1 and DNA2 end resection machineries. Specifically, PARP-1 is able to slide to the end of DNA. This suggests a search mode employing 1D diffusion, which should stimulate the rate of recognition of newly formed DNA ends relative to three-dimensional diffusion mechanisms. Using single-molecule microscopy, we determined that PARP-1, but not PARP-2, prevents the binding of EXO1 to DNA ends. The structural differences that allow PARP-1 but not PARP-2 or PARP-3 to inhibit end resection would be interesting to determine, given that PARP-1 physically occludes DNA ends from recognition by EXO1. The regulatory zinc finger domains that are unique to PARP-1 are likely to be key to this specificity of function. Our data suggest that, even prior to Ku loading, which strongly prevents the loading of EXO1, PARP-1 acts to block the end resection machinery. This observation fits into a model where both PARP-1 and Ku limit end resection, possibly by controlling the accumulation of the MRN complex[53] and CtIP and that loss of either PARP-1 or Ku binding results in over-resection. We propose that this mechanism is conserved in pluricellular organisms, as the Iliakis group report that Chinese hamster ovary (CHO) Hamster cells treated with BMN 673 also have elevated DNA processing as measured by RPA foci[54]. PARP-2 has recently been shown to promote DNA resection[55], but since BMN 673 inhibits PARP-2[56], it might not contribute to the over-resection phenotype observed in BMN673-inhibited cells.

Our work provides a conceptual framework to explain many observations reported in previous studies detailing the effects of PARP inhibition in a variety of contexts involving DNA

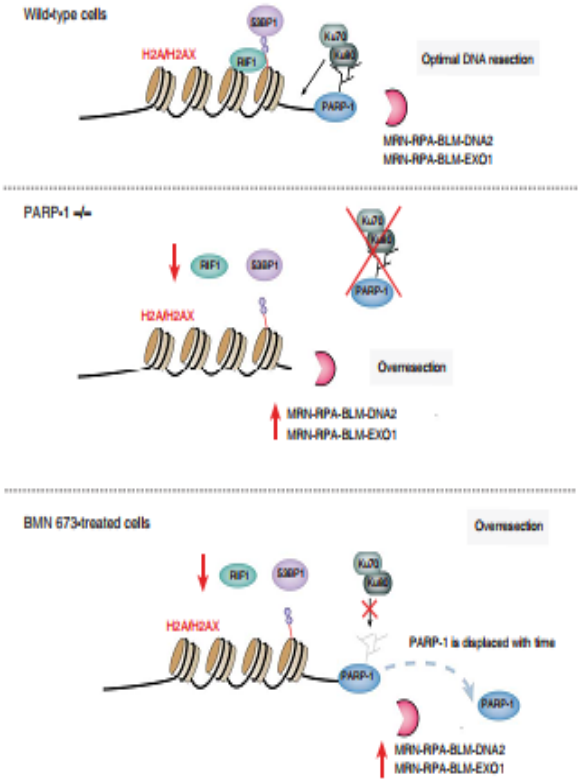

Fig. 8 Model. Following DNA damage, poly(ADP-ribose) polymerase-1 inhibition leads to a decrease of Ku80-end protection, RIF1 and 53BP1 foci formation, and increased DNA resection. Details are given in the text

recombination transactions. Since the early 1980s, PARP-1 has been proposed to carry out an antirecombinogenic function. The group of Oikawa et al. first described a positive correlation between PARPis (benzamide and *m*-aminobenzamide) and induction of sister-chromatid exchanges (SCEs) in CHO-K1 cells[57]. Hori demonstrated that reduced NAD as well as inhibition of PARP-1 (using 3-aminobenzamide) lead to a significant increase in SCEs in CHO cells[58]. Morrison et al. using PARP-1$^{-/-}$ mice, provided evidence of PARP-1 functions in maintaining genomic stability by demonstrating that PARP-1 is an anti-recombinogenic factor that inhibits ligation between the DNA termini exposed during (V(D)J) recombination[59]. More recently, it was shown that PARP-1 PARylates BRCA1, and short- and long-track gene conversions, as well as chromosome aberrations after DNA damage, were increased by a BRCA1 PARylation mutant. In addition, treatment with olaparib also led to an enhancement of both types of HR frequencies[60]. Altogether, our data suggest that loss of PARP-1 facilitates HR, through enhanced DNA resection accounting for the (i) increase of sister chromatid exchanges[57]; (ii) anti-recombinogenic function of PARP-1[59]; and (iii) increased HR repair by a BRCA1 PARylation mutant[60]. PARP-1 inhibition-induced HR is in accordance with our previous findings with another PARPi, ABT-888, which remained unexplained at the time[44]. It also mimics the effect of a HELB knockdown, another DNA resection inhibitor[30].

One of the first models proposed to explain the antitumor effects of PARPis in HR-deficient cells was based on the functions of PARP-1 in BER. This model postulated that catalytic inhibition of PARP-1 results in the accumulation of single-strand breaks that could not be repaired in HR-deficient cells. Two observations challenged this model. First, it was not possible to demonstrate increased single-strand breaks after PARP inhibition[61], and synthetic lethality was not achieved when XRCC1, a key BER protein, was downregulated in BRCA2-deficient cells[62]. Hence, these observations raised the possibility that the effects of PARPis may be mediated through a mechanism distinct from BER. Consistent with this, Patel et al. have shown that deregulated NHEJ plays a major role in generating the genomic instability and cytotoxicity in HR-deficient cells treated with PARPis[62].

We suggest that the observed synthetic lethality and cytotoxicity in different genetic contexts can be related to aberrant DNA resection as consequence of PARP-1 inhibition and DNA damage. Under these conditions, this phenotype will only be attained if DSBs are created and the DNA resection machinery is functional. This conclusion is highlighted by SMART analysis or BrdU staining of BRCA1- and BRCA2-deficient cells. Recent phase III studies have shown that PARPi activity extends beyond BRCA-related cancers for ovarian cancers devoid of known *BRCA* mutations, especially when platinum sensitivity and high-grade serous histology are present[63]. We propose that this effect could be due to misregulation of DNA resection. There are several ongoing clinical trials combining PARP-1 inhibitors with radiation therapy for which our study provides mechanistic insights into the tumor-killing activity observed in the clinic. Collectively, our results highlight that the functionality of DNA resection enzymes in response to DNA damage may be an important criterion to consider for the cell's ability to survive BMN 673 in the presence of DNA damage during clinical interventions in breast/ovarian cancer and other solid tumors.

Methods

Cell lines, cell culture, drugs, and DNA constructs. Mouse embryonic fibroblasts proficient for PARP-1 (WT), or deficient for PARP-1 (PARP-1 (−/−)) were cultured in Dulbecco's modified Eagle's medium (DMEM) supplemented with 10% fetal bovine serum (FBS) (Hyclone-ThermoFisher Scientific, Ottawa, Canada). U2OS, HeLa, and HeLa PARP-1 SilenciX control (Tebu-bio) were cultured in DMEM with 10% FBS. PARP-1 HeLa SilenciX is a cell line engineered to stably knock down PARP-1 via RNA interference. Cells were maintained under hygromycin B selection (250 µg/mL; Invitrogen). U2OS-PARP-1 (−/−) cells were cultured in DMEM supplemented with 10% FBS and 2 µg/mL puromycin. U2OS cells stably expressing GFP-RPA2 were maintained in DMEM through continuous G418 selection (500 µg/mL; Invitrogen). The ER-AsiSI U2OS cell line was maintained in phenol red-free DMEM media supplemented with 10% charcoal-stripped FBS (Sigma) and 1 µg/mL puromycin. In order to induce DNA damage, AsiSI U2OS cells were treated with 300 nM 4-OHT for 3 h. U2OS cells stably expressing an mCherry-LacI-FokI construct containing an integrated reporter transgene were maintained in DMEM by puromycin (2 µg/mL) and hygromycin B (100 µg/mL) selection. To induce DNA DSBs, cell lines were treated with both 0.5 mM Shield-1 and 1 mM 4-OHT for 1 h. Human embryonic kidney 293 cells (HEK 293), HEK 293T, or HEK 293T-PARP-1 (−/−) cells were cultured in DMEM supplemented with 10% FBS.

Generation of PARP-1 CRISPR/Cas9. U2OS cells were transfected with the appropriate guide RNA against PARP-1, cloned in a pSpCas9(BB)-2A-Puro (PX459) V2.0. The sgDNA sequence (5′-CGATGCCTATTACTGCACTG -3′) was cloned at the *Bbs*I site into pSpCas9(BB)-2A-Puro (PX459) V2.0 (Addgene plasmid ID: 62988). The positive clone was confirmed by restriction enzyme digestion (*Bbs*I and *Age*I) of purified plasmids to check for insertion and further confirmed by Sanger sequencing. Twenty-four hours later, the transfected cells were selected in medium containing 2 µg/mL puromycin and then subcloned into 96-well plates. Once at sufficient cell density, the subclones were analyzed for the presence of the target protein by western blotting (PARP-1).

Cell fractionation. Cell fractionation was carried out as described in ref. [64] with slight modifications. Briefly, 3×10^6 HEK293T or CRISPR PARP-1 (−/−) cells per condition were collected and resuspended in 200 µL of buffer A (10 mM HEPES pH 8.0, 10 mM KCl, 1.5 mM $MgCl_2$, 0.34 M sucrose, 10 % glycerol, 1 mM dithiothreitol (DTT), 1 mM phenylmethanesulfonylfluoride (PMSF), 0.1 % Triton-X-100, 10 mM NaF, 1 mM Na_3VO_4, supplemented with protease inhibitors) and kept for 5 min on ice. The soluble cytoplasmic fraction (S1) was separated from the nuclei (P2) by centrifugation for 4 min at 1300 × *g* at 4 °C. The nuclear fraction P2 was washed twice with 300 µL buffer A, then resuspended in 200 µL buffer B (3 mM EDTA, 0.2 mM EGTA, 1 mM DTT, 1 mM PMSF, 10 mM NaF, 1 mM Na_3VO_4, and protease inhibitors) and kept for 30 min on ice. The insoluble chromatin fraction (P3) was separated from nuclear soluble proteins (S3) by centrifugation for 4 min at 1700 × *g* at 4 °C and washed three times with solution B. S1 was cleared of insoluble proteins by centrifugation at 14,000 × *g* for 15 min at 4 °C and the supernatant (S2) was kept for analysis. Cell fractions were subsequently analyzed by western blotting.

Antibodies, reagents, resources, and siRNAs. The antibodies used in this study as well as the working dilutions are listed in Supplementary Table 1. Key reagents or resources are listed in Supplementary Table 2. siRNAs are listed in Supplementary Table 3.

Western blot analysis. Total cell lysates were prepared by lysing cells in RIPA buffer (25 mM Tris–HCl, 125 mM NaCl, 1% Nonidet-P-40, 0.5% sodium deoxycholate, 0.1% sodium dodecyl sulfate (SDS), and a complete protease inhibitor cocktail (Roche)). Equal amounts of total protein were separated by SDS-polyacrylamide gel electrophoresis and then transferred to polyvinylidene difluoride membrane (BioRad) and immunoblotted with antibodies (Supplementary Table 1). When secondary antibodies conjugated with infrared-specific dyes (either Alexa Fluor 680 or Alexa Fluor 750) were used, fluorescence was imaged on the Odyssey Infrared Imaging system (LiCor Biosciences).

Transfection and siRNA. Transient siRNA transfections were carried out with Lipofectamine RNAiMax (Invitrogen) or Oligofectamine (Thermo Fisher Scientific) and analyses were performed 48–72 h after siRNA transfection. The siRNAs used in this study can be found in Supplementary Table 3.

Immunofluorescence staining. The effect of PARP-1 knockdown on IR-induced DNA end-resection was analyzed by immunofluorescence staining against RPA2 and BrdU. For RPA2 immunodetection, cells were pre-extracted with RPA buffer (25 mM HEPES pH 7.9, 300 mM sucrose, 50 mM NaCl, 1 mM EDTA, 3 mM $MgCl_2$, and 0.5% Triton X-100) for 5 min on ice before being fixed at the indicated incubation time points after IR. This method removes nucleoplasmic signal and helps in the detection of foci. Cells were washed two times with phosphate-buffered saline (PBS) followed by fixation with 4% paraformaldehyde (w/v) in PBS for 15 min at room temperature. After two washes with PBS, cells were permeabilized in 0.5% Triton X-100 in PBS for 5 min. Cells were co-stained with primary antibodies against γ-H2AX (Active motif) and RPA2 (Abcam) in PBS for 1 h at room temperature. After three washes with PBS, cells were stained with goat anti-rabbit Alexa Fluor 488 and anti-mouse Cy3 secondary antibody (Molecular Probes, 1:400) in PBS for 30 min at room temperature.

CtIP and Geminin immunofluorescence was performed as reported previously[65]. For RIF1, 53BP1, and cyclin A immunofluorescence staining, cells were either untreated or treated with 50 μM etoposide for 1 h and fixed with 4% paraformaldehyde in PBS for 15 min. Then cells were washed with TBS and fixed with cold methanol (−20 °C) for 5 min and permeabilized with PBS containing 0.2% Triton X-100 for 5 min and washed three times 5 min with TBS. The cells were quenched with 0.1% sodium borohydride for 5 min, washed once with TBS, blocked in PBS containing 10% goat serum and 1% bovine serum albumin (BSA) for 1 h, and incubated with the primary antibody diluted in PBS 1% BSA for 2 h at room temperature. Coverslips were washed three times for 10 min with TBS before 1-h incubation with the appropriate secondary antibody conjugated to a fluorophore. Cells were rinsed again three times for 10 min with TBS. Coverslips were mounted onto slides with ProLong Gold (Thermo Fisher Scientific) antifade mountant with 4′,6-diamidino-2-phenylindole (DAPI) (Life technologies).

For RAD51 and phosphoDNA-PKcs(S2056) immunostaining, cells were either untreated or treated with 5 Gy IR, released for 1 h, and fixed with 4% paraformaldehyde in PBS for 25 min. Next, cells were permeabilized with PBS containing 0.5% Triton X-100 (PBS-T) for 15 min and washed three times with PBS 1×. The cells were blocked in PBS containing 10% FBS for 1 h and incubated with the primary antibody (RAD51: 1:1000 or phosphoDNA-PKcs(S2056): 1:500) diluted in the blocking buffer for 2 h at room temperature. Coverslips were washed three times with PBS before 1-h incubation with the appropriate secondary antibody (1:1000) conjugated to a fluorophore again in blocking buffer. Cells were rinsed twice with PBS 1×, then incubated in (1:1000) PBS-DAPI solution for 5 min, and then washed twice with PBS 1×. Coverslips were mounted onto slides with ProLong Gold antifade mountant.

Recruitment of RPA and EXO1 to laser-induced DNA damage sites. The evaluation of the recruitment kinetics of RPA to DNA damage sites was performed essentially as described[6] with the exception of the following modifications. After overnight transfections with Effectene reagent (Qiagen), unsynchronized HEK 293 cells expressing the indicated RPA subunit fused to green fluorescent protein (GFP) and mCherry-PCNA fusion protein were incubated with fresh medium containing 1 μg/mL of Hoechst 33342 for 15 min at 37 °C and treated with 5 μM of PARPi BMN 673 (20 mM stock solution prepared in dimethyl sulfoxide (DMSO), Selleckchem) 1 h prior to microirradiation and recruitment analysis. A 37 °C pre-heated stage with 5% CO_2 perfusion was used for time-lapse analysis on a Zeiss LSM-510 META NLO laser-scanning confocal microscope (×40 objective). Localized DNA damage was generated along a defined region across the nucleus of a single living cell by using a bi-photonic excitation of the Hoechst 33342 dye, generated with a near-infrared 750-nm titanium:sapphire laser line (Chameleon Ultra II, Coherent Inc.) The laser output was set to 1.5% with 5 iterations. For each cell, 30 images were collected with a 5 sec interval. A Multi-Time macro developed in-house for the AIM software v3.2 (Zeiss) was used for image acquisition. Background and photobleaching corrections were applied to each dataset as described[10]. The average accumulation ± s.e.m. of RPA was plotted using a minimum of ten recruitment kinetic profiles per each RPA construct from three independent experiments. Only S-phase-positive PCNA (proliferating cell nuclear antigen) cells were chosen for recruitment[66]. Recruitment of GFP-EXO1 to laser-induced DSBs was performed as reported previously[67].

Recruitment of Ku80 to laser-induced DNA damage sites. For Ku80 laser microirradiation experiments, a 1-μm diameter band of damage was introduced across the width of the nucleus. Background was determined based on measuring the fluorescence intensity outside of the cells (i.e., in regions containing only the growth medium). Fluorescence loss due to photobleaching that takes place during acquisition is removed by normalizing the total nuclear fluorescence to remain constant throughout the experiment. The fluorescence intensity of the damaged region was then monitored over time after correcting for background and fluorescence loss. The distribution of recruited protein can deviate from the initial band for two reasons. First, the distribution of chromatin determines whether or not the full width and full diameter of the band are sites of DNA damage. Second, as we have previously published, there is a decondensation of the damaged chromatin that causes the band to expand in width beyond the boundary of the original damaged area. Consequently, measurements restricted to the 1-μm wide band where the laser microirradiation took place will slightly underestimate the extent of recruitment and chromatin-bound proteins that are unaffected will commonly show a very slight decrease in fluorescence intensity within the region.

BrdU/ssDNA assays. Cells were pre-incubated in the presence of 10 μM BrdU (Sigma) for 16 h followed by a 3-h incubation after IR at 10 Gy. Cells were subjected to in situ fractionation on ice for 10 min using sequential extraction with two different buffers. Pre-extraction buffer 1 (10 mM PIPES, pH 7.0, 300 mM sucrose, 100 mM NaCl, 3 mM $MgCl_2$, and 0.5% Triton-X100) and followed by pre-extraction buffer 2 (10 mM Tris pH 7.5, 10 mM NaCl, 3 mM $MgCl_2$, 1% Nonidet P-40, and 0.5% sodium deoxycholate). Cells were washed three time with PBS followed by fixation with 4% paraformaldehyde (w/v) for 15 min at room temperature. Cells were washed with PBS and permeabilized in 0.5% Triton X-100 in PBS for 5 min. Cells were incubated overnight at 4 °C with anti-BrdU antibody under non-denaturing conditions. In these native conditions, the anti-BrdU antibody only has access to its epitope in ssDNA. Unbound primary antibody was removed by washing in PBS at room temperature followed by incubation with the anti-mouse Cy3 secondary antibody for 30 min at room temperature. Slides were then washed for four times in PBS before mounting with Vectashield mounting medium (Vector Laboratories) containing DAPI. BrdU foci were observed by using an upright fluorescence microscope (Zeiss AxioImager.Z1) with a Plan Neofluar 1.3 N. A. ×40 oil immersion objective. Image analysis was carried out by the ImageJ software (version 1.51k). The integrated intensity of individual BrdU foci and RPA2 foci were quantified by using GDSC ImageJ Find Foci plugins[68].

ChIP assays. The effect of PARP-1 knockdown and PARP inhibition on RPA2, 53BP1, and RIF1 recruitment to a sequence-defined DSB site was determined quantitatively by ChIP followed by quantitative polymerase chain reaction (qPCR). Cells were crosslinked with 1% (v/v) formaldehyde for 10 min and then glycine was added to a final concentration of 125 mM for 5 min to stop the crosslinking reaction. Cells were lysed in lysis buffer (25 mM HEPES pH 7.9, 300 mM sucrose, 50 mM NaCl, 1 mM EDTA, 3 mM $MgCl_2$, and 0.5% Triton X-100) and nuclei were isolated. Nuclear fractions were resuspended in sonication buffer (50 mM HEPES pH 7.9, 140 mM NaCl, 1 mM EDTA, 1% Triton X-100, 0.1% sodium deoxycholate, 1% SDS, 1× protease inhibitor cocktail, and 1× phosphatase inhibitor cocktail (Roche)) for 10 min on ice and sonicated to obtain approximately 200–500-bp chromatin fragments using a Bioruptor (Diagenode). Chromatin fragments were precleared with magnetic Dynabeads protein G (Life Technologies) for 1 h and incubated with pre-bound antibody–Dynabeads protein G overnight at 4 °C. Beads were washed once in low-salt buffer (20 mM Tris, pH 8.1, 2 mM EDTA, 50 mM NaCl, 1% Triton X- 100, and 0.1% SDS), once in high-salt buffer (20 mM Tris, pH 8.1, 2 mM EDTA, 500 mM NaCl, 1% Triton X-100, and 0.1% SDS), once in LiCl buffer (10 mM Tris, pH 8.0, 1 mM EDTA, 0.25 mM LiCl, 1% Nonidet P-40, and 1% deoxycholic acid), and twice in TE buffer (10 mM Tris-HCl, pH 8.0, and 1 mM EDTA). Washed beads were eluted twice with 100 μL of elution buffer (1% SDS and 0.1 M $NaHCO_3$) and crosslinks were reversed by overnight incubation at 65 °C in 0.1 mg/mL RNase A, 0.3 M NaCl, and 0.2 mg/mL proteinase K. The DNA samples were purified with Qiaquick PCR columns (Qiagen). qPCR was carried out on an Applied Biosystem 7900 HT Fast instrument using the SYBR Green detection system. The results of the quantitative ChIP assays are the mean with s.e.m. of qPCR reactions from three independent experiments and primers used are listed in Supplementary Tables 4 and 5.

ER-AsiSI resection assay. The percentage of resection adjacent to a specific DSB1 (Chr 1: 89231183) was measured as described[42] with some modifications. The primer pairs for "DSB1" and "DSB2" are across *Bsr*GI and *Bam*H1 restriction sites, respectively. Briefly, ER-*Asi*SI U2OS cells were treated with 300 nM of 4-OHT (Sigma) for 3 h to allow the nuclear translocation of *Asi*SI and the induction of DSBs. Cells were collected and genomic DNA was extracted and digested with *Bsr*GI or *Bam*H1 enzymes or mock digested overnight at 37 °C. Digested or mock-digested samples were used as a template for qPCR performed using SYBR Green master mix. Primers used are listed in Supplementary Table 6[42]. For each sample, a ΔCt was calculated by subtracting the Ct value of the mock-digested sample from the Ct value of the digested sample.

Protein purification. PARP-1, PARP-2, and PARP-3 were purified according to standard procedures[69,70]. BLM was tagged at the N-terminus with GST and at the C-terminus with His_{10} and purified as described for PALB2[70]. MRE11-RAD50-NBS1 was purified according to an established protocol[71]. RPA was purified as described[72]. Human EXO1[38] or biotinylated EXO1 for single-molecule experiments was purified as described[73]. For recombinant DNA2 protein purification, Sf9 insect cells (1 L at 10^6 cells/mL) were infected with a GST-DNA2-FLAG baculovirus. At 48 h post-infection, cells were harvested by centrifugation and the pellet was frozen on dry ice. Cells were lysed in Buffer 1 (1× PBS containing 150 mM NaCl, 1 mM EDTA, 0.05% Triton X-100, 1 mM DTT, and protease inhibitors) and homogenized by 20 passes through a Dounce homogenizer (pestle A). The cell lysate was incubated with 1 mM $MgCl_2$ and 2.5 U/ml. benzonase nuclease at 4 °C for 1 h followed by centrifugation at 93,753 × *g* for 1 h. The soluble cell lysate was incubated with 1 mL of GST-Sepharose beads for 90 min at 4 °C with gentle rotation. The beads were washed twice with buffer 1 followed by incubation with buffer 2 (Buffer 1 with 5 mM ATP, 15 mM $MgCl_2$) for 1 h at 4 °C. Sepharose GST beads were washed twice with buffer 1 supplemented with 200 mM NaCl and once with P5 buffer (50 mM $NaHPO_4$ pH 7.0, 500 mM NaCl, 10% glycerol, 0.05% Triton-X-100, 5 mM imidazole) followed by cleavage with PreScission protease (60 U/mL, GE Healthcare Life Sciences), overnight at 4 °C in P5 buffer. The supernatant was then collected and completed to 10 mL with Flag-binding buffer (50 mM Tris–HCl pH 7.5, 150 mM NaCl, 1 mM EDTA, 10% glycerol, 0.025% Triton X-100) before incubation with 600 μL of M2 anti-Flag affinity gel (Invitrogen) for 1 h at 4 °C. The beads were washed twice with washing buffer (Flag-binding buffer supplemented with 100 mM NaCl). After two additional washes with Flag Elution buffer (50 mM Tris–HCl pH 7.5, 150 mM NaCl, 0.025% Triton X-100, and 10% glycerol), proteins were eluted twice in one volume of beads with Flag Elution buffer and 500 μg/mL of 3×-Flag peptide for 45 min at 4 °C. Proteins

were then dialyzed in the storage buffer (20 mM Tris-HCl, pH 7.4, 200 mM NaCl, 10% glycerol, 1 mM DTT) and stored in aliquots at −80 °C.

DNA resection assays. Assays were performed with pUC19 DNA linearized with *Kpn*I and then 3′ labeled with [α-^{32}P] ATP and terminal deoxytransferase (NEB). For the DNA2 resection machinery, reactions were conducted using 50 nM of substrate in standard buffer (20 mM Na-HEPES pH 7.5, 0.1 mM DTT, 0.05% Triton X-100, 100 µg/mL BSA). Two millimolar ATP and 5 mM $MgCl_2$ were added to the reaction buffer immediately before reconstitution of the resection machineries. The reactions were initiated on ice by adding either NAD, PARP-1, PARP-2 or PARP-3 as indicated in the figure and transferred immediately to 37 °C. After 5 min, the order of addition and incubation of the respective protein components were: MRN (10 nM, 5 min), RPA (100 nM, 5 min), BLM (15 nM, 3 min) and DNA2 (15 nM, 45 min). For the EXO1 resection machinery, reactions were conducted using resection buffer (25 mM MOPS pH 7, 60 mM KCl, 1% Tween 20, 2 mM DTT, 5 mM MgCl2, 2 mM ATP) and the same proteins and time of incubation as mentioned above except for EXO1 at a concentration of 10 nM instead of DNA2. Reactions were followed by proteinase K treatment for 30 min at 37 °C. Products were analyzed on a 1% native agarose gel. Gels were dried on DE81 paper (Whatman) and signals were detected by autoradiography. Densitometric analyses were performed using the FLA-5100 phosphorimager (Fujifilm) and quantified using the Image Reader FLA-5000 v1.0 software.

DNA-binding assays. The DNA-binding reactions (10 µL) contained ^{32}P-labeled DNA oligonucleotides (100 nM) and the indicated concentrations of PARP-1 and NAD in resection buffer (20 mM Na-HEPES pH 7.5, 0.1 mM DTT, 0.05% Triton X-100, 100 µg/mL BSA, 5 mM $MgCl_2$, 2 mM ATP). Reaction mixtures were incubated at 37 °C for 10 min and then protein–DNA complexes were fixed with 0.2% (v/v) glutaraldehyde for 15 min. The reactions were subjected to electrophoresis on an 8% 1×-TBE-acrylamide gel and ^{32}P-labeled DNA was visualized by autoradiography. Sequences of the oligonucleotides are found in Supplementary Table 7.

Single-molecule imaging and DNA curtains. Single-molecule DNA curtain data were collected at 37 °C using a Nikon Ti-E microscope in a prism-TIRF configuration. Data were collected with a 200-ms exposure through a ×60 water-immersion objective (1.2 NA, Nikon), a 500-nm long-pass (Chroma), and a 638-nm dichroic beam splitter (Chroma) for two-channel detection through two EMCCD cameras (Andor iXon DU897, cooled to −80 °C). Histograms of PARP-1-binding preference on DNA were acquired by fitting a two-dimensional Gaussian to each individual molecule and finding the center of the fit relative to the barrier position using a custom-written FIJI script (available upon request). A Gaussian curve with a constant offset was fit to the largest peak of the histogram using a custom script written in MATLAB (available upon request). The constant offset in the fitting accounts for molecules that bind nonspecifically along the length of the DNA substrate. The center of the fit is reported in the corresponding figure panel.

For DNA curtains, microscope slides with microfabricated chromium barriers were encased in a microfluidic flowcell and passivated with a fluid lipid bilayer. DNA molecules (λ, 48.5 kb) with biotinylated ends were bound to a subset of the lipids via a biotin–streptavidin interaction. The flowcells were attached by nanoports to a syringe pump-controlled microfluidics system.

λ–DNA substrates for DNA curtains were purchased from NEB and annealed with two oligonucleotides: IF7: (5′-[p]AGG TCG CCG CCC[Biotin]- 3′) and LM3: (5′- [p]GGG CGG CGA CCT TTT TTT TTT TTT TTT TTT TTT TTT TTT TTT TTT TTT TTT TTT TTT TTT TTT TTT TTT TTT TTT TTT TTT TTT TTT TTT TTT -3′). This generated a substrate that had a biotin for attaching to the flowcell surface on one side and a 78-nt 3′ overhang on the other side, which was suitable for Exo1 loading. For visualizing the DNA, YoYo-1 was injected into the flowcell with a glucose oxidase/catalase mixture.

To perform PARP-1 labeling, 300 nM mouse anti-6xHis antibody (Clontech) was pre-incubated with 400 nM anti-mouse secondary QDots (Invitrogen, 605 or 705 depending on labeling strategy) in a 5 µL volume for 10 min on ice. PARP-1 or PARP-2 were incubated with the antibody mixture for another 10 min on ice and diluted to a final volume of 200 µL (6.25 nM PARP, 7.5 nM anti-His antibody, 10 nM QDots; final concentrations). PARP-1 or PARP-2 were injected onto the microscope flowcell at 200 µL/min in loading buffer (40 mM Tris-HCl pH 8, 200 µg/mL BSA, 2 mM DTT, 2 mM $MgCl_2$). After binding, the flowcell was switched to EXO1 resection buffer (40 nM Tris-HCl pH 8, 60 mM NaCl, 200 µg/mL BSA, 2 mM DTT, 2 mM MgCl2, 1 mM ATP) for subsequent EXO1 loading.

EXO1 loading was performed by pre-incubating 100 nM Streptavidin QDots 605 with 80 nM EXO1-biotin in 10 µL EXO1 loading buffer (40 mM Tris-HCl pH 8, 60 mM NaCl, 200 µg/mL BSA, 2 mM DTT, 2 mM MgCl2, 1 mM ATP) on ice for 10 min. Then the mixture was diluted to a final volume of 200 µL in EXO1 loading buffer plus free biotin (4 nM EXO1, 5 nM QDots) and injected onto DNA curtains at 200 µL/min. To prevent dye-induced changes in protein–DNA interactions, YoYo-1 was omitted in experiments involving PARP-1/EXO1 and PARP-2/EXO1.

Single-molecule analysis of resection tracks. The indicated cell lines or siRNA transfected cells were incubated with 10 µM BrdU for 48 h. After 48 h, the cells were treated with 5 µM BMN 673 for 1 h before IR (10 Gy and released for 1 h). Cells were harvested and counted, 1×10^5 cells per condition were spun down, and resuspended in the resuspension buffer from the FiberPrep DNA Extraction Kit (Genomic Vision). Agarose plugs and DNA solutions were made according to the FiberPrep DNA extraction Kit. Using the FiberComb (Genomic Vision), the DNA was stretched onto a Combicoverslip. The cover slips were baked for 2 h at 60 °C, then incubated in primary antibody (1:100 anti-BrdU) in 5% PBS–BSA for 2 h at 37 °C. The coverslips were washed with PBS-T 3 times for 3 min with shaking and incubated for 1 h in the appropriate secondary antibody (1:200) conjugated to a fluorophore in a humidified chamber at 37 °C. The slides were washed with PBS-T 3 times for 3 min. If needed, YOYO™-1 Iodide staining (1:1000) was performed for 10 min. The slides were washed with ddH_2O for 1 min. The DNA is then dehydrated by submerging it for 1 min in 70%, 90%, and 100% ethanol sequentially and visualized on a DMI6000B microscope. Fiber length was evaluated by Image J analysis (version 1.51k).

Survival assays. Cells were seeded in triplicates into a Corning 3603 black-sided clear bottom 96-well microplate at a density of 2000 cells per well. Once attached, the media was changed to include the desired concentration of BMN 673. One hour after BMN 673 treatment, the plate was irradiated with 7.5 Gy. The plates were incubated for 120 h. The nuclei were stained with Hoechst 33342 (Invitrogen) at 10 µg/mL in media for 30 min at 37 °C. Images of entire wells were acquired at ×4 with a Cytation 5 Cell Imaging Multi-Mode Reader followed by quantification of Hoechst-stained nuclei with the Gen5 Data Analysis Software v3.03 (BioTek Instruments). Cell viability was expressed as the percentage of survival in BMN673-treated cells relative to vehicle (DMSO)-treated cells.

HR in cellulo reporter assays. Dox-inducible I-SceI/DRGFP cell line (TRI-DR-U2OS) was treated without/with 10 µg/mL Dox and BMN 673 (1 µM) or ABT-888 (5 µM) and incubated for 48 h. HR efficiencies were analyzed by flow cytometry after 48-h incubation. HR efficiency was expressed as the percentage of GFP-positive cells. Samples were analyzed in triplicate. Values are expressed as mean and s.e.m.

Statistical analyses. All data are representative of three or more independent experiments. Prism ver 6.0 was used to do the statistical analyses.

Reporting summary. Further information on research design is available in the Nature Research Reporting Summary linked to this article.

Data availability

The source data and uncropped gel pictures underlying Figs. 1A–G, 2B–D, 3A, B, D, E, 4A–F, 5C, F, H, 6B, D, E, and 7A–E and Supplementary Figs. 1A, B, 2A, B, 3A–G, 4A, B, D, E, 5A–F, 6A–G, 7A–C, 8B–D, and 9B–D are provided as a source data file. Data of this study are available from the authors upon reasonable request.

Received: 23 September 2018 Accepted: 29 May 2019
Published online: 04 July 2019

References

1. Vilenchik, M. M. & Knudson, A. G. Endogenous DNA double-strand breaks: production, fidelity of repair, and induction of cancer. *Proc. Natl Acad. Sci. USA* 100, 12871–12876 (2003).
2. Ciccia, A. & Elledge, S. J. The DNA damage response: making it safe to play with knives. *Mol. Cell* 40, 179–204 (2010).
3. Jungmichel, S. et al. Proteome-wide identification of poly(ADP-Ribosyl)ation targets in different genotoxic stress responses. *Mol. Cell* 52, 272–285 (2013).
4. Zhang, Y., Wang, J., Ding, M. & Yu, Y. Site-specific characterization of the Asp- and Glu-ADP-ribosylated proteome. *Nat. Methods* 10, 981–984 (2013).
5. Gagne, J. P. et al. Quantitative site-specific ADP-ribosylation profiling of DNA-dependent PARPs. *DNA Repair (Amst.)* 30, 68–79 (2015).
6. Gagne, J. P. et al. Quantitative proteomics profiling of the poly(ADP-ribose)-related response to genotoxic stress. *Nucleic Acids Res.* 40, 7788–7805 (2012).
7. Gibson, B. A. et al. Chemical genetic discovery of PARP targets reveals a role for PARP-1 in transcription elongation. *Science* 353, 45–50 (2016).
8. Wacker, D. A., Frizzell, K. M., Zhang, T. & Kraus, W. L. Regulation of chromatin structure and chromatin-dependent transcription by poly(ADP-ribose) polymerase-1: possible targets for drug-based therapies. *Subcell. Biochem.* 41, 45–69 (2007).
9. Strickfaden, H. et al. Poly(ADP-ribosyl)ation-dependent transient chromatin decondensation and histone displacement following laser microirradiation. *J. Biol. Chem.* 291, 1789–1802 (2016).
10. Haince, J. F. et al. PARP1-dependent kinetics of recruitment of MRE11 and NBS1 proteins to multiple DNA damage sites. *J. Biol. Chem.* 283, 1197–1208 (2008).
11. Krietsch, J. et al. Reprogramming cellular events by poly(ADP-ribose)-binding proteins. *Mol. Aspects Med.* 34, 1066–1087 (2013).

12. Altmeyer, M. et al. Liquid demixing of intrinsically disordered proteins is seeded by poly(ADP-ribose). *Nat. Commun.* 6, 8088 (2015).
13. D'Amours, D., Sallmann, F. R., Dixit, V. M. & Poirier, G. G. Gain-of-function of poly(ADP-ribose) polymerase-1 upon cleavage by apoptotic proteases: implications for apoptosis. *J. Cell Sci.* 114, 3771–3778 (2001).
14. Slade, D. et al. The structure and catalytic mechanism of a poly(ADP-ribose) glycohydrolase. *Nature* 477, 616–620 (2011).
15. Maya-Mendoza, A. et al. High speed of fork progression induces DNA replication stress and genomic instability. *Nature* 559, 279–284 (2018).
16. Hanzlikova, H. et al. The importance of poly(ADP-ribose) polymerase as a sensor of unligated Okazaki fragments during DNA replication. *Mol. Cell* 71, 319–331 e313 (2018).
17. Zimmermann, M. et al. CRISPR screens identify genomic ribonucleotides as a source of PARP-trapping lesions. *Nature* 559, 285–289 (2018).
18. Ame, J. C., Spenlehauer, C. & de Murcia, G. The PARP superfamily. *Bioessays* 26, 882–893 (2004).
19. Ray Chaudhuri, A. & Nussenzweig, A. The multifaceted roles of PARP1 in DNA repair and chromatin remodelling. *Nat. Rev. Mol. Cell Biol.* 18, 610–621 (2017).
20. Rulten, S. L. et al. PARP-3 and APLF function together to accelerate nonhomologous end-joining. *Mol. Cell* 41, 33–45 (2011).
21. De Murcia, J. M. et al. Requirement of poly(ADP-ribose) polymerase in recovery from DNA damage in mice and in cells. *Proc. Natl Acad. Sci. USA* 94, 7303–7307 (1997).
22. Couto, C. A.-M. et al. PARP regulates nonhomologous end joining through retention of Ku at double-strand breaks. *J. Cell Biol.* 194, 367–375 (2011).
23. Langelier, M. F., Planck, J. L., Roy, S. & Pascal, J. M. Crystal structures of poly (ADP-ribose) polymerase-1 (PARP-1) zinc fingers bound to DNA: structural and functional insights into DNA-dependent PARP-1 activity. *J. Biol. Chem.* 286, 10690–10701 (2011).
24. Langelier, M. F., Ruhl, D. D., Planck, J. L., Kraus, W. L. & Pascal, J. M. The Zn3 domain of human poly(ADP-ribose) polymerase-1 (PARP-1) functions in both DNA-dependent poly(ADP-ribose) synthesis activity and chromatin compaction. *J. Biol. Chem.* 285, 18877–18887 (2010).
25. Langelier, M. F., Zandarashvili, L., Aguiar, P. M., Black, B. E. & Pascal, J. M. NAD(+) analog reveals PARP-1 substrate-blocking mechanism and allosteric communication from catalytic center to DNA-binding domains. *Nat. Commun.* 9, 844 (2018).
26. Yun, M. H. & Hiom, K. CtIP-BRCA1 modulates the choice of DNA double-strand-break repair pathway throughout the cell cycle. *Nature* 459, 460–463 (2009).
27. Nakamura, K. et al. Collaborative action of Brca1 and CtIP in elimination of covalent modifications from double-strand breaks to facilitate subsequent break repair. *PLoS Genet.* 6, e1000828 (2010).
28. Cruz-Garcia, A., Lopez-Saavedra, A. & Huertas, P. BRCA1 accelerates CtIP-mediated DNA-end resection. *Cell Rep.* 9, 451–459 (2014).
29. Nimonkar, A. V. et al. BLM-DNA2-RPA-MRN and EXO1-BLM-RPA-MRN constitute two DNA end resection machineries for human DNA break repair. *Genes Dev.* 25, 350–362 (2011).
30. Tkac, J. et al. HELB is a feedback inhibitor of DNA end resection. *Mol. Cell* 61, 405–418 (2016).
31. Zimmermann, M., Lottersberger, F., Buonomo, S. B., Sfeir, A. & de Lange, T. 53BP1 regulates DSB repair using Rif1 to control 5′ end resection. *Science* 339, 700–704 (2013).
32. Escribano-Diaz, C. et al. A cell cycle-dependent regulatory circuit composed of 53BP1-RIF1 and BRCA1-CtIP controls DNA repair pathway choice. *Mol. Cell* 49, 872–883 (2013).
33. Isabelle, M. et al. Investigation of PARP-1, PARP-2, and PARG interactomes by affinity-purification mass spectrometry. *Proteome Sci.* 8, 22 (2010).
34. LaFargue, C. J., Dal Molin, G. Z., Sood, A. K. & Coleman, R. L. Exploring and comparing adverse events between PARP inhibitors. *Lancet Oncol.* 20, e15–e28 (2019).
35. Drean, A., Lord, C. J. & Ashworth, A. PARP inhibitor combination therapy. *Crit. Rev. Oncol. Hematol.* 108, 73–85 (2016).
36. Mortusewicz, O., Ame, J. C., Schreiber, V. & Leonhardt, H. Feedback-regulated poly(ADP-ribosyl)ation by PARP-1 is required for rapid response to DNA damage in living cells. *Nucleic Acids Res.* 35, 7665–7675 (2007).
37. Aleksandrov, R. et al. Protein dynamics in complex DNA lesions. *Mol. Cell* 69, 1046–1061 e1045 (2018).
38. Murai, J. et al. Trapping of PARP1 and PARP2 by clinical PARP inhibitors. *Cancer Res.* 72, 5588–5599 (2012).
39. Nam, E. A. et al. Thr-1989 phosphorylation is a marker of active ataxia telangiectasia-mutated and Rad3-related (ATR) kinase. *J. Biol. Chem.* 286, 28707–28714 (2011).
40. Sartori, A. A. et al. Human CtIP promotes DNA end resection. *Nature* 450, 509–514 (2007).
41. Iacovoni, J. S. et al. High-resolution profiling of gammaH2AX around DNA double strand breaks in the mammalian genome. *EMBO J.* 29, 1446–1457 (2010).
42. Zhou, Y., Caron, P., Legube, G. & Paull, T. T. Quantitation of DNA double-strand break resection intermediates in human cells. *Nucleic Acids Res.* 42, e19 (2014).
43. Gallardo, I. F. et al. High-throughput universal DNA curtain arrays for single-molecule fluorescence imaging. *Langmuir* 31, 10310–10317 (2015).
44. Krietsch, J. et al. PARP activation regulates the RNA-binding protein NONO in the DNA damage response to DNA double-strand breaks. *Nucleic Acids Res.* 40, 10287–10301 (2012).
45. Bunting et al. 53BP1 inhibits homologous recombination in Brca1-deficient cells by blocking resection of DNA breaks. *Cell* 141, 243–254 (2010).
46. Schultz, N., Lopez, E., Saleh-Gohari, N. & Helleday, T. Poly(ADP-ribose) polymerase (PARP-1) has a controlling role in homologous recombination. *Nucleic Acids Res.* 31, 4959–4964 (2003).
47. He, Y. J. et al. DYNLL1 binds to MRE11 to limit DNA end resection in BRCA1-deficient cells. *Nature* 563, 522–526 (2018).
48. Noordermeer, S. M. et al. The shieldin complex mediates 53BP1-dependent DNA repair. *Nature* 560, 117–121 (2018).
49. Mirman, Z. et al. 53BP1-RIF1-shieldin counteracts DSB resection through CST- and Polalpha-dependent fill-in. *Nature* 560, 112–116 (2018).
50. Findlay, S. et al. SHLD2/FAM35A co-operates with REV7 to coordinate DNA double-strand break repair pathway choice. *EMBO J.* 37, e100158 (2018).
51. Spagnolo, L., Barbeau, J., Curtin, N. J., Morris, E. P. & Pearl, L. H. Visualization of a DNA-PK/PARP1 complex. *Nucleic Acids Res.* 40, 4168–4177 (2012).
52. Wang, M. et al. PARP-1 and Ku compete for repair of DNA double strand breaks by distinct NHEJ pathways. *Nucleic Acids Res.* 34, 6170–6182 (2006).
53. Ying, S., Hamdy, F. C. & Helleday, T. Mre11-dependent degradation of stalled DNA replication forks is prevented by BRCA2 and PARP1. *Cancer Res.* 72, 2814–2821 (2012).
54. Soni, A. et al. Inhibition of Parp1 by BMN673 effectively sensitizes cells to radiotherapy by upsetting the balance of repair pathways processing DNA double-strand breaks. *Mol. Cancer Ther.* 17, 2206–2216 (2018).
55. Fouquin, A. et al. PARP2 controls double-strand break repair pathway choice by limiting 53BP1 accumulation at DNA damage sites and promoting end-resection. *Nucleic Acids Res.* 45, 12325–12339 (2017).
56. Shen, Y. et al. BMN 673, a novel and highly potent PARP1/2 inhibitor for the treatment of human cancers with DNA repair deficiency. *Clin. Cancer Res.* 19, 5003–5015 (2013).
57. Ohkawa, A., Tohda, H., Kanai, M., Miwa, M. & Sugimura, T. Inhibitors of poly (adenosine diphosphate ribose) polymerase induce sister chromatid exchanges. *Biochem Biophys. Res. Commun.* 97, 1311–1316 (1980).
58. Hori, T. High incidence of sister chromatid exchanges and chromatid interchanges in the conditions of lowered activity of poly(ADP-ribose) polymerase. *Biochem Biophys. Res. Commun.* 102, 38–45 (1981).
59. Morrison, C. et al. Genetic interaction between PARP and DNA-PK in V(D)J recombination and tumorigenesis. *Nat. Genet.* 17, 479–482 (1997).
60. Hu, Y. et al. PARP1-driven poly-ADP-ribosylation regulates BRCA1 function in homologous recombination-mediated DNA repair. *Cancer Discov.* 4, 1430–1447 (2014).
61. Gottipati, P. et al. Poly(ADP-ribose) polymerase is hyperactivated in homologous recombination-defective cells. *Cancer Res.* 70, 5389–5398 (2010).
62. Patel, A. G., Sarkaria, J. N. & Kaufmann, S. H. Nonhomologous end joining drives poly(ADP-ribose) polymerase (PARP) inhibitor lethality in homologous recombination-deficient cells. *Proc. Natl Acad. Sci. USA* 108, 3406–3411 (2011).
63. Mirza, M. R. et al. Niraparib maintenance therapy in platinum-sensitive, recurrent ovarian cancer. *New Engl. J. Med.* 375, 2154–2164 (2016).
64. Zou, L., Cortez, D. & Elledge, S. J. Regulation of ATR substrate selection by Rad17-dependent loading of Rad9 complexes onto chromatin. *Genes Dev.* 16, 198–208 (2002).
65. Niraj, J. et al. The identification of FANCD2 DNA binding domains reveals nuclear localization sequences. *Nucleic Acids Res.* 45, 8341–8357 (2017).
66. Schonenberger, F., Deutzmann, A., Ferrando-May, E. & Merhof, D. Discrimination of cell cycle phases in PCNA-immunolabeled cells. *BMC Bioinformatics* 16, 180 (2015).
67. Dery, U. et al. A glycine-arginine domain in control of the human MRE11 DNA repair protein. *Mol. Cell. Biol.* 28, 3058–3069 (2008).
68. Herbert, A. D., Carr, A. M. & Hoffmann, E. FindFoci: a focus detection algorithm with automated parameter training that closely matches human assignments, reduces human inconsistencies and increases speed of analysis. *PLoS ONE* 9, e114749 (2014).
69. Langelier, M. F., Planck, J. L., Servent, K. M. & Pascal, J. M. Purification of human PARP-1 and PARP-1 domains from *Escherichia coli* for structural and biochemical analysis. *Methods Mol. Biol.* 780, 209–226 (2011).
70. Buisson, R. et al. Cooperation of breast cancer proteins PALB2 and piccolo BRCA2 in stimulating homologous recombination. *Nat. Struct. Mol. Biol.* 17, 1247–1254 (2010).

71. Yu, Z. et al. The MRE11 GAR motif regulates DNA double-strand break processing and ATR activation. *Cell Res.* 22, 305–320 (2012).
72. Henricksen, L. A., Umbricht, C. B. & Wold, M. S. Recombinant replication protein A: expression, complex formation, and functional characterization. *J. Biol. Chem.* 269, 11121–11132 (1994).
73. Myler, L. R. et al. Single-molecule imaging reveals the mechanism of Exo1 regulation by single-stranded DNA binding proteins. *Proc. Natl Acad. Sci. USA* 113, E1170–E1179 (2016).
74. Efron, B. & Tibshirani, R. *An Introduction to the Bootstrap* (Chapman & Hall, London, 1993).

Acknowledgements

We would like to thank members of the Hendzel, Masson, and Poirier laboratories and Stéphane Richard, Michal Zimmerman, and Amélie Fradet-Turcotte for comments and suggestions. We also acknowledge Pablo Huertas for advice in performing SMART, Hilmar Strickfaden for assistance in data quantification, Philipp Oberdoerffer (National Cancer Institute, USA) for the kind gift of TSI-DR-GFP U2OS reporter cells, Dr Gaëlle Legube (University of Toulouse, France) for the ER-AsiSI U2OS cell line, Roger Greenberg (University of Pennsylvania, USA) for U2OS cells stably expressing mCherry-LacI-FokI construct, Scott Kern and Fumiko Esashi for DLD1 BRCA2+/− and DLD1 BRCA2−/− cells, and Jana Krietsch for generating the CRISPR HEK293T PARP-1 (−/−) cells. L.R.M. is supported by the National Cancer Institute of the National Institutes of Health (F99CA212452). This research was supported by the National Institute of General Medical Sciences of the National Institutes of Health (R01GM120554 to L.J.F.); the National Cancer Institute of the National Institutes of Health (P01CA092584 to L.J.F.); CPRIT (R1214 to L.J.F.); the Welch Foundation (F-1808 to L.J.F.); the CIHR (BMA342854 to J.M.P.); and a CIHR grant to M.H., J.-Y.M., and G.P. (MOP-311036). L.J.F. is a CPRIT Scholar in Cancer Research, J.O. was a recipient of a CRCHU de Quebec scholarship, and J.-Y.M. is a FRQS research chair in Genome Stability.

Author contributions

L.J.F., G.G.P., M.H., and J.-Y.M. conceived the studies. M.-C.C., A.S., L.R.M., J.O., M.T.F., A.R., Y.C., C.E., and J.-P.G. designed and carried out the experiments. M.-F.L. and J.M.P. provided purified proteins. M.H. and J.-Y.M. wrote the original draft and all authors edited the manuscript.

Additional information

Supplementary Information accompanies this paper at https://doi.org/10.1038/s41467-019-10741-9.

Competing interests: The authors declare no competing interests.

Reprints and permission information is available online at http://npg.nature.com/reprintsandpermissions/

Peer review information: *Nature Communications* thanks Michael Huen and other anonymous reviewer(s) for their contribution to the peer review of this work.

Publisher's note: Springer Nature remains neutral with regard to jurisdictional claims in published maps and institutional affiliations.

SUPPLEMENTARY INFORMATION

Poly(ADP-ribose) polymerase-1 antagonizes DNA resection at double-strand breaks

Caron, Sharma et al.

Supplementary Table 1. List of antibodies used in this study

REAGENTS	SOURCE	DILUTION USED	IDENTIFIER
Antibodies			
PARP-1	Abcam	1:4000 (WB)	ab194586
PARP-1 (C2-10)	Homemade	1:5000 (WB)	This study
PARP-2	Abcam	1:4000 (WB)	ab176330
β-Actin	Sigma	1:10000 (WB)	A5316
RIF1	Bethyl	3µl each sample (CHIP)	A300-569A
53BP1	Novus	3µl each sample (CHIP)	NB100-304
RPA2	Abcam	3µl each sample (CHIP)	ab76420
RPA2	Calbiochem	1:1000 (WB)	NA18
RPA2 S4/S8	Novus	1:1000 (WB)	NBP1-23017
BrdU	GE healthcare	1:750 (IF)	RPN202
Cyclin A	BD Biosciences	1:300 (IF)	611264
RPA2	Abcam	1:2000 (IF)	ab2175
γ-H2AX	Active motif	1:2000 (IF)	39117
BRCA1	Millipore	1:1000 (WB)	07-434
BRCA2	Millipore	1:250 (WB)	OP95
53BP1	Novus	1:2000 (WB)	NB100-304
53BP1	Novus	1:500 (IF)	NB100-304
Histone H3	Abcam	1:10 000 (WB)	Ab1791
GAPDH	Fitzgerald	1:20 000 (WB)	10R-G109A
Alpha-tubulin (DM1A)	Abcam	1:100 000 (WB)	Ab7291
RIF1	Bethyl	1:400 (IF)	A300-569A
CtIP	Active Motif	1:400 (IF)	61141
CtIP	Active Motif	1:3000 (WB)	61141
Geminin	Proteintech	1:300 (IF)	10802-1-AP
Alexa Fluor 488 goat anti-rabbit	Molecular probes	1:800 (IF)	A11008
Alexa Fluor 488 goat anti-mouse	Molecular probes	1:1000 (IF)	A11001

Alexa 568 goat anti-mouse	Molecular probes	1:800 (IF)	A11004
Alexa 568 goat anti-rabbit	Molecular probes	1:800 (IF)	A11011
Ku80	Cell Signalling	1:3000 (WB)	2180S
DNA Ligase IV	Abcam	1:3000 (WB)	ab193353
His tag	Clontech		631212
GFP	Abcam	1:8000 (WB)	Ab290
Alexa488 goat anti-rabbit	Life technology	1:400 (IF)	A11034
Mouse Cy3 goat anti-mouse	Jackson ImmunoResearch	1:400 (IF)	115-165-146
RAD51	Cedarlane Labs	1:1000 (IF)	70-001
QDot 605 streptavidin conjugate	Thermo Fisher Scientific	5 nM (final working concentration)	Q10101MP
QDot 605 anti-mouse conjugate	Thermo Fisher Scientific	10 nM (final working concentration)	Q11001MP
QDot 705 anti-mouse conjugate	Thermo Fisher Scientific	10 nM (final working concentration)	Q11062MP
YOYO™-1 Iodide	Thermo Fisher Scientific	1 nM (final working concentration)	Y3601
Anti-BrdU	GE Healthcare	1:100 (SMART)	RPN202
YOYO™-1 Iodide	Invitrogen	1:1000 (SMART)	Y3601
DNA PKcs(phospho S2056)	Abcam	1:500 (IF)	Ab18192
pADPr (10H)	Tulip Biolabs	1:5000 (WB)	1020
pATR(Thr1989)	Genetex	1:1000 (WB)	GTX128145
Vinculin	Sigma	1:100 000 (WB)	V9131
Phospho-EXO1	Homemade	1:1000 (WB)	Kum Kum Khanna https://doi.org/10.1093/nar/gkp1164

Supplementary Table 2. Reagents or resources used in this study

REAGENT or RESOURCE	SOURCE	IDENTIFIER
Chemicals, Peptides, and Recombinant Proteins		
Proteinase K	Sigma	P2308-100MG
Bromodeoxyuridine (BrdU)	Sigma	B5002
BMN 673	MedChem Express	HY-16106
Veliparib	MedChemExpress	HY-10129
Pre-stained Protein ladder	Frogga Bio	PM008-0500F
RNAiMAX	Invitrogen	13778-075
Oligofectamine	Thermo Fisher Scientific	12252011
Effectene	Qiagen	301425
BSA	Sigma	A7906
Fetal Bovine serum	Gibco	12483-020
Charcoal striped Serum	Sigma	F6765-100ML
Trypsin	Sigma	T4049-500ML
Hygromycin B	invitrogen	10687010
Shield1	TaKaRa	632189
Puromycin	Sigma	P9620-10ML
4-Hydroxytamoxifen (4-OHT)	Sigma	H7904-5MG
BsrG1	NEB	R0575S
BamH1-HF	NEB	R3136S
Bright Green 2x qPCR MasterMix-ROX	abm	MasterMix-R
DMEM high glucose	Fisher scientific	10063542
G418-Geneticin	Gibco	11811-031
Dynabeads Protein G	Invitrogen	10003D
Engraved Combicoverslips	Genomic Vision	COV-002-RUO

[α-32P] ATP	Perkin Elmer	NEG512H250UC
[γ-32P] ATP	Perkin Elmer	BLU002H250UC
NAD	Sigma	N0632
Terminal Transferase	NEB	M0315S
ProLong® Gold Antifade Mountant	Invitrogen Life Technology	P-36930
Critical Commercial Assays		
FiberPrep® (DNA Extraction Kit)	Genomic Vision	EXTR-001
Click-iT EdU Alexa Fluor™ 488 Imaging Kit	Thermo Fisher Scientific	C10337
Experimental Models: Cell Lines		
PARP-1 HeLa SilenciX	Tebu-bio	01-00019
Control Hela SilenciX	Tebu-bio	01-00001
U2OS	ATCC	HTB-96
U2OS CRISPR PARP-1(-/-)	This study	N/A
HeLa	ATCC	CCL-2
HEK 293T	ATCC	CRL-11268
HEK 293T CRISPR PARP-1 (-/-)	This study	N/A
ER-AsiSI U2OS	Gaëlle Legube	N/A
TRI-DR-U2OS	Philipp Oberdoerffer	N/A
DLD1 (BRCA2 +/-)	Scott Kern	N/A
DLD1 (BRCA2 -/-)	Scott Kern	N/A
HEK 293	ATCC	CRL-1573
U2OS-RPA2-GFP(stable)	This study	N/A
U2OS-DSB reporter cell line (Fok1 system)	Roger A Greenberg	N/A
Sf9	ThermoFisher	B82501
U2OS-Ku80-GFP(stable)	This study	N/A
MEFs PARP1 +/+	This study	N/A

MEFs PARP1-/-	This study	N/A
Oligonucleotides		
siRNA sequences	This paper	Table S3
qPCR primer sequences used in ER-*AsiSI* CHIP experiment	This paper	Table S4
qPCR primer sequences used in U2OS-DSB-reporter locus (FoK1) CHIP experiment.	This paper	Table S5
qPCR primer sequences used in ER-AsiSI resection assay	This paper	Table S6
Sequences of the oligonucleotides used for the bandshift assay	This paper	Table S7
Recombinant DNA		
Plasmid: pEGFP-C1-FLAG-Ku80	Addgene	Plasmid#46958
Plasmid: RPA1-GFP	This paper	N/A
Plasmid: RPA2-GFP	This paper	N/A
Plasmid: RPA3-GFP	This paper	N/A
Plasmid : GFP-EXO1	This paper	N/A
Plasmid : mCherry-PCNA	Schonenberger et al.	N/A
Software and Algorithms		
Prism	GraphPad	Ver-6
Image J	Image J	V1.51k
GDSC ImageJ (Find Foci plugins)	Herbert et al., 2014	http://www.sussex.ac.uk/gdsc/intranet/microscopy/imagej/gdsc_plugins.
Image Reader FLA-5000	FLA-5100 phosphorimager Software	V1.0
Gen5 Data Analysis Software v3.03	Gen5 Data Analysis Software	v3.03

Supplementary Table 3. List of siRNAs used in the study.

Target protein	siRNA name	Sequence 5′-3′
None	siRNA control	GGG AUA CCU AGA CGU UCU ATT dTdT
None	siRNA control	UUCGAACGUGUCACGUCAAdTdT
PARP-1	siPARP-1	AAG AUA GAG CGU GAA GGC GAA dTdT
PARP-1	siPARP-1-2	AAG AGC GAU GCC UAU UAC UGC dTdT
CtiP	CtiP	GGGAACAGCAGAAAGTCCTTCATGA
Ku80	siKu80	SASI_Hs01_00099411 (NM_021141, Sigma)
DNA Ligase IV	siDNA ligase IV	L-004254-00-0005 (Dharmacon)
53BP1	Si53BP1	GGACUCCAGUGUUGUCAUU dTdT
BRCA1	siBRCA1	CAGCAGUUUAUUACUCACUAA dTdT
BRCA2	siBRCA2	GAAGAAUGCAGGUUUAAUAUU dTdT
KU80	siKU80	GCGAGUAACCAGCUCAUAAUU

Supplementary Table 4: qPCR primer sequences used in ER-*Asi*SI CHIP experiment.

Name	Sequence 5′-3′
chr1_89231183: FW	GATTGGCTATGGGTGTGGAC
chr1_89231183: REV	CATCCTTGCAAACCAGTCCT
chr6_90404906: FW	TGCCGGTCTCCTAGAAGTTG
chr6_90404906: REV	GCGCTTGATTTCCCTGAGT

chr21_21292316:FW	TGGCTGGAACTGCTTTCTTT
chr21_21292316:REV	GGTGAGTGAATGAGCTGCAA

Supplementary Table 5: qPCR primer sequences used in U2OS-DSB-reporter locus (FoK1) CHIP experiment.

Name	Sequence 5′-3′
p1: FW	GGAAGATGTCCCTTGTATCACCAT
p1: Rev	TGGTTGTCAACAGAGTAGAAAGTGAA
p4: FW	CCACCTGACGTCTAAGAAACCAT
p4: REV	GATCCCTCGAGGACGAAAGG

Supplementary Table 6: qPCR primer sequences used in ER-AsiSI resection assay.

Name	Sequence 5′-3′
DSB-335 FW	GAATCGGATGTATGCGACTGATC'
DSB-335 REV	TTCCAAAGTTATTCCAACCCGAT
No DSB FW	ATTGGGTATCTGCGTCTAGTGAGG
No DSB Rev	GACTCAATTACATCCCTGCAGCT
DSB2-364 FW	CCAGCAGTAAAGGGGAGACAGA
DSB2-364 REV	CTGTTCAATCGTCTGCCCTTC

Across DSB1 Primer FW	GATGTGGCCAGGGATTGG
Across DSB1 Primer REV	CACTCAAGCCCAACCCGT

Supplementary Table 7: Sequences of the oligonucleotides used for the EMSA assays.

Name	Sequence 5′-3′
JYM696	GGGCGAATTGGGCCCGACGTCGCATGCTCCTCTAGACTCGAGGAA TTCGGTACCCCCGGGTTCGAAATCGATAAGCTTACAGTCTCCATTTAA AGGACAAG
JYM698	CTTGTCCTTTAAATGGAGACTGTAAGCTTATCGATTTCGAACCCGGG GTACCGAATTCCTCGAGTCTAGAGGAGCATGCGACGTCGGGCCCAA TTCGCCC

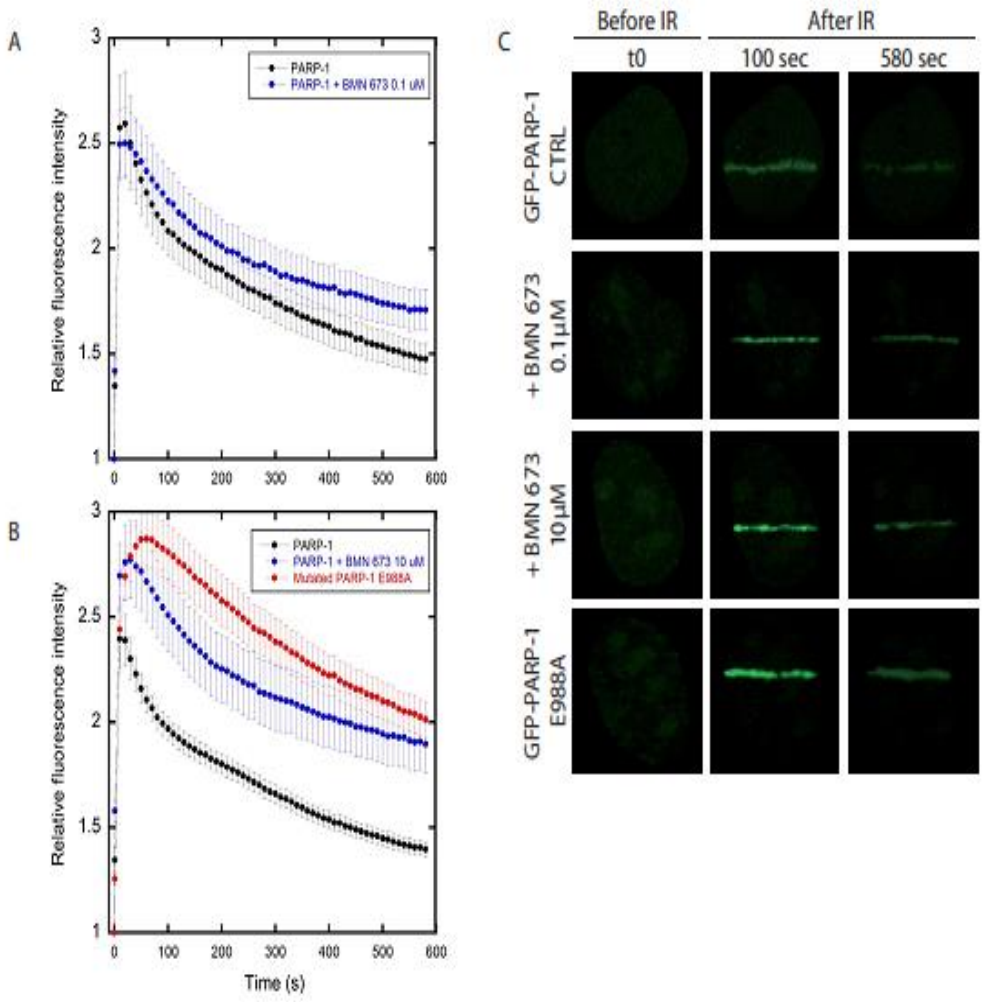

Supplementary Figure 1. Recruitment of PARP-1 at laser-induced DNA breaks. The recruitment dynamics of PARP-1 under normal conditions was compared with the dynamics observed following PARP inhibition. The recruitment kinetics was obtained by plotting the relative fluorescence intensity of GFP-PARP-1 at the damage site as a function of time. (A) Accumulation of PARP-1 in normal conditions or in presence of 0.1µM BMN 673. (B) Accumulation of PARP-1 in normal conditions, in presence of 10µM BMN 673, and of polymerization mutant (E988A). (C) Representative images of local accumulation of GFP-PARP-1 at laser-induced DNA damage sites. Experiments were repeated three times and the average of at least 8 cells from a representative experiment was used to generate the graphs. Two-way analysis of variance followed by Tukey pairwise comparisons shows no significant differences between PARP-1 and PARP-1 + BMN 673 0.1µM but significant differences in time between PARP-1 and PARP-1 + BMN 673 10µM ($P < 0.02$) and between PARP-1 and mutated PARP-1 E988A ($P < 0.01$) (from 20 to 580 seconds). Data show the mean ± s.d. (Tukey test).

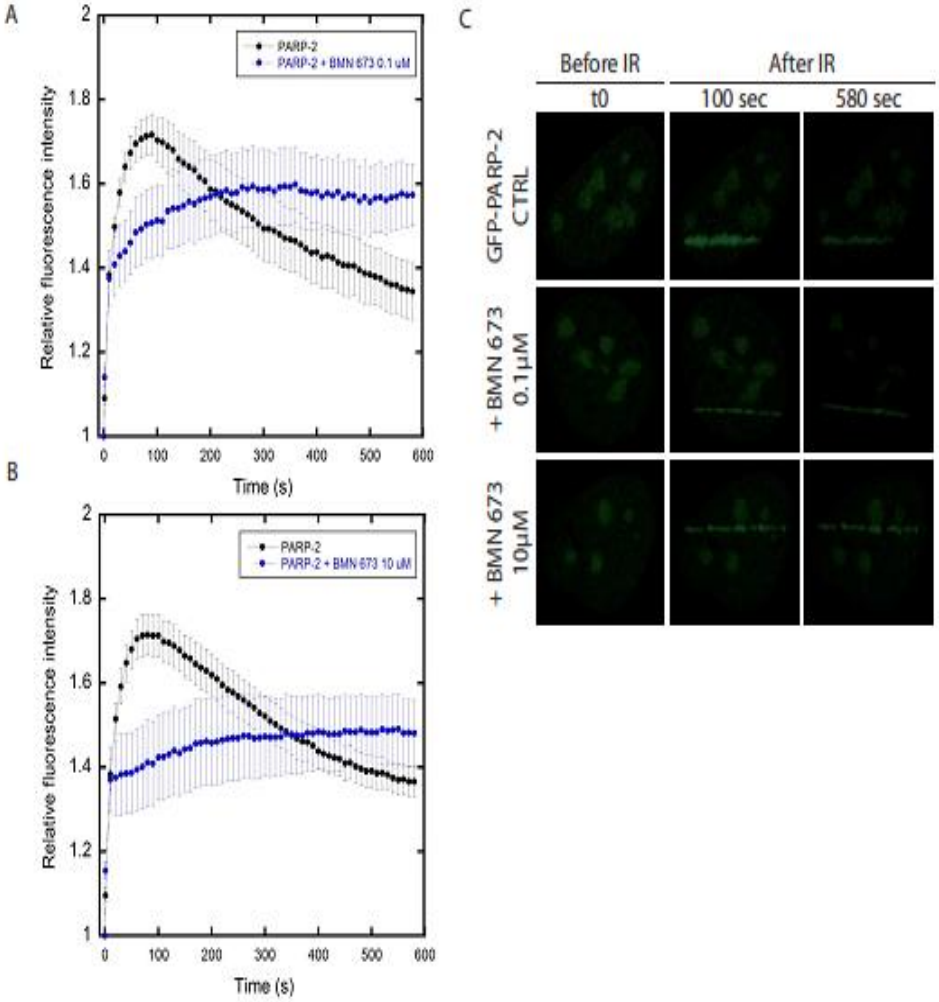

Supplementary Figure 2. Recruitment of PARP-2 at laser induced DNA breaks. The recruitment dynamics of PARP-2 under normal conditions was compared with the dynamics observed following PARP inhibition. The recruitment kinetics was obtained by plotting the relative fluorescence intensity of GFP-PARP-2 at the damage site as a function of time. Accumulation of PARP-2 in normal conditions or in presence of (A) 0.1µM BMN 673 and (B) 10µM BMN 673. (C) Representative images of local accumulation of GFP-PARP-2 at laser-induced DNA damage sites. Experiments were repeated three times and the average of at least 8 cells from a representative experiment was used to generate the graphs. Error bars represent the SEM. By two-way ANOVA, we observed a significant difference between PARP-2 and PARP-2 + BMN 673 0.1µM ($P < 0.002$) and between PARP-2 and PARP-2 + BMN 673 10µM ($P < 0.001$) over time. Data show the mean ± s.d. (Tukey test).

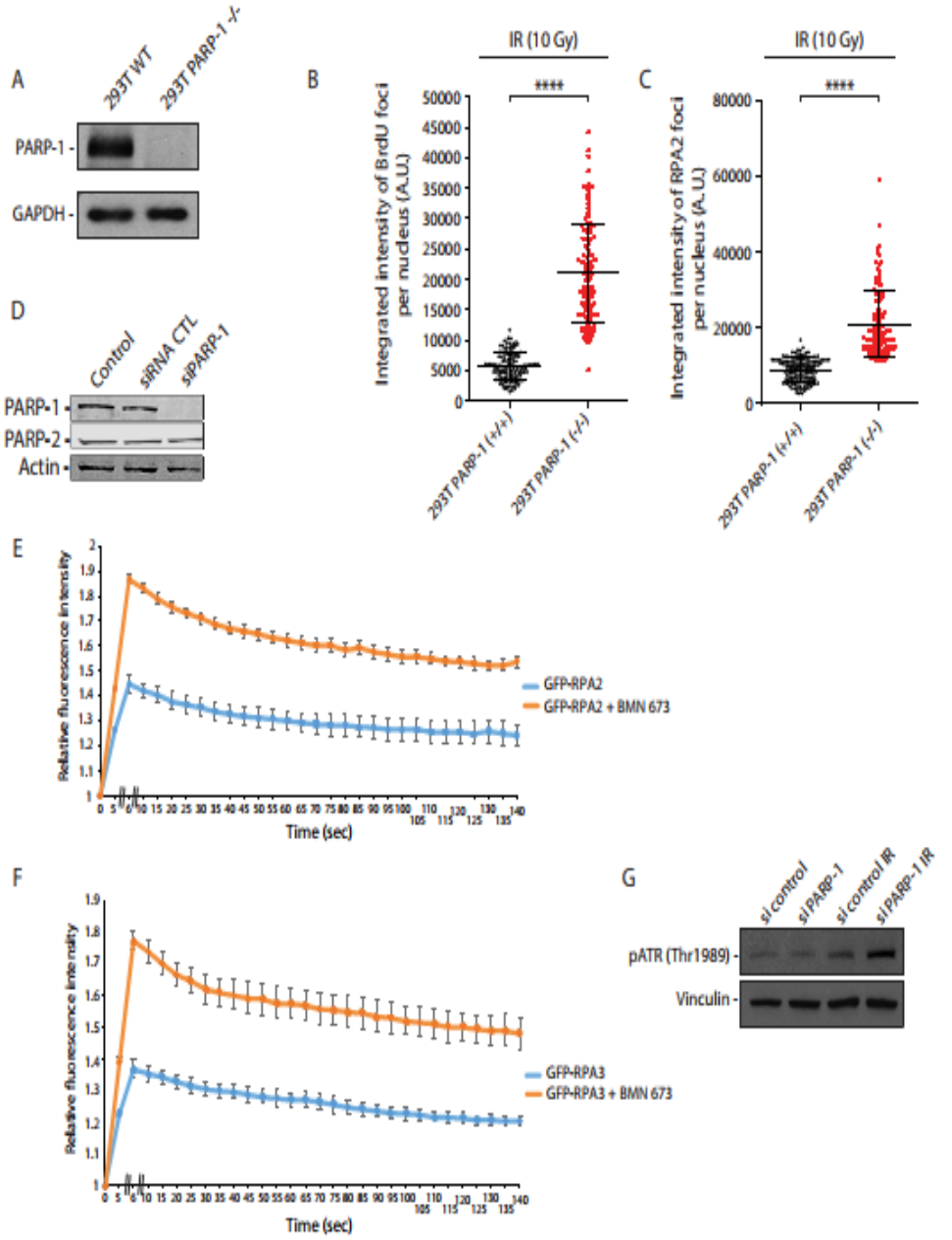

Supplementary Figure 3. (A) Western blotting to validate the absence of PARP-1 in CRISPR 293T PARP-1 (-/-) compared to the 293T PARP-1 (+/+) control. CRISPR 293T PARP-1 (+/+) or 293T PARP-1 (-/-) cells were subjected to immunofluorescence against BrdU (B) or RPA2 (C) after irradiation (10Gy, 3 hrs release). Data in panels B-C show the mean ± s.d. **** $p \leq 0.0001$, (Mann-Whitney U-test). (D) PARP-1 knockdown efficiency monitored by western blotting. The recruitment of GFP-RPA2 (E) or GFP-RPA3 (F) is accelerated by PARP inhibition at laser-induced DNA breaks. HEK293 cells were co-transfected with mCherry-PCNA and RPA subunit 2 or 3. Cells in S-phase, co-expressing mCherry and GFP, were micro-irradiated using 750-nm two-photon laser beam, and the accumulation of RPA at the sites of DNA damage was monitored on a Zeiss LSM 510 NLO laser scanning confocal microscope. The peak of intensity was at 6 seconds. Data show the mean ± s.e.m. (G) ATR is over-activated in the PARP-1 knockdown cells (after 5Gy irradiation and 90 min release).

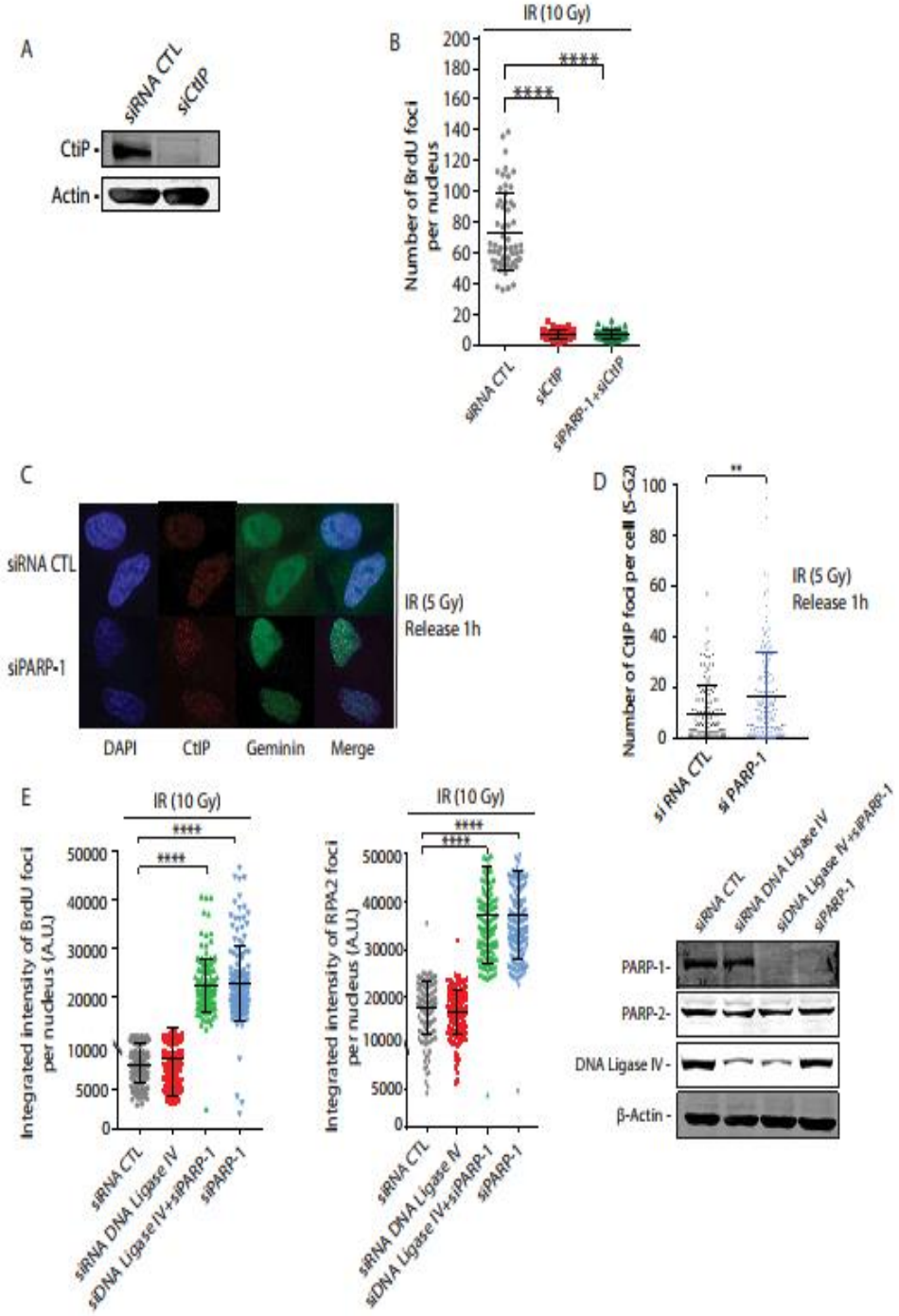

Supplementary Figure 4. (A) Western blotting to monitor CtIP knockdown efficiency. (B) Quantification of the number of BrdU foci in the indicated knockdowns in HeLa SilenciX following irradiation (10 Gy 3hr release). Data show the mean ± s.d. **** $p \leq 0.0001$, (Mann-Whitney U-test).

(C) CtIP foci formation is increased in PARP-1 knockdown cells. (D) Quantification of the results. Data show the mean ± s.d. ** $p \leq 0.01$, (Mann-Whitney U-test).

(E) The indicated knockdown in HeLa SilenciX control or PARP-1 HeLa SilenciX cells were subjected to immunofluorescence against BrdU (left panel) or RPA2 (middle panel) following irradiation (10 Gy, 3 hr release). (Right). Data show the mean ± s.d. **** $p \leq 0.0001$ (Mann-Whitney U-test). Western blotting to validate siRNA knockdowns of DNA ligase IV or/and PARP-1.

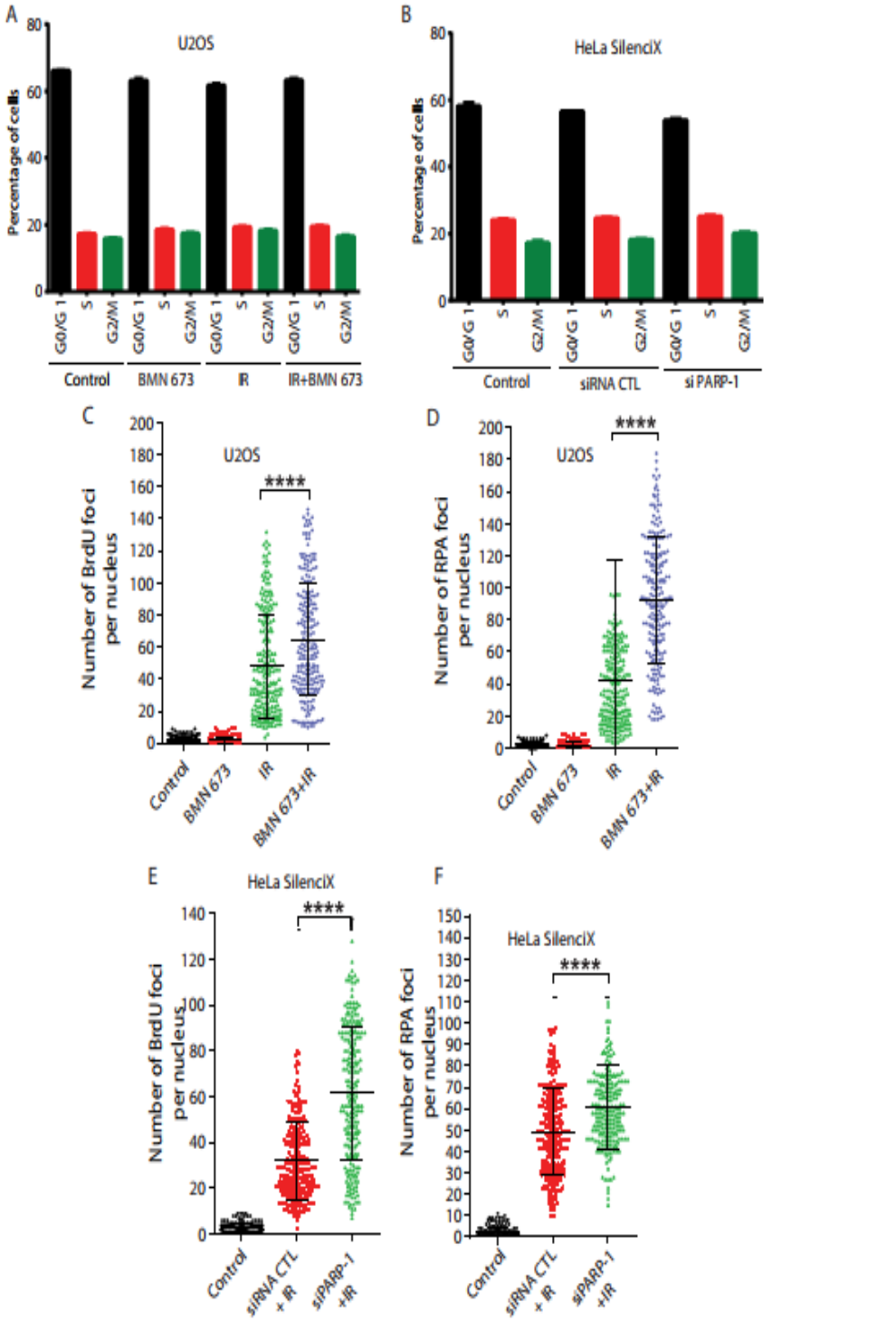

Supplementary Figure 5. (A-B) FACS analysis to monitor the distribution of the indicated cells in each cell cycle phase for the BrdU/RPA analysis (3 hours release from the indicated treatments). Data show the mean ± s.e.m.
U2OS cells either mock treated, treated with BMN 673, irradiated (10 Gy), or irradiated (10 Gy) in combination with BMN 673, were subjected to immunofluorescence against BrdU (C) or RPA2 foci formation (D). The graph represent the number of BrdU/RPA focus per nucleus. HeLa SilenciX cells underexpressing PARP-1 by siRNA-mediated gene knockdown were subjected to immunofluorescence against BrdU (E) or RPA2 foci formation (F).
The graph represent the number of BrdU/RPA focus per nucleus. Data in panels C-F show the mean ± s.d.
**** $p \leq 0.0001$, (Mann-Whitney, U-test).

Caron, Sharma et al. Supplementary Figures

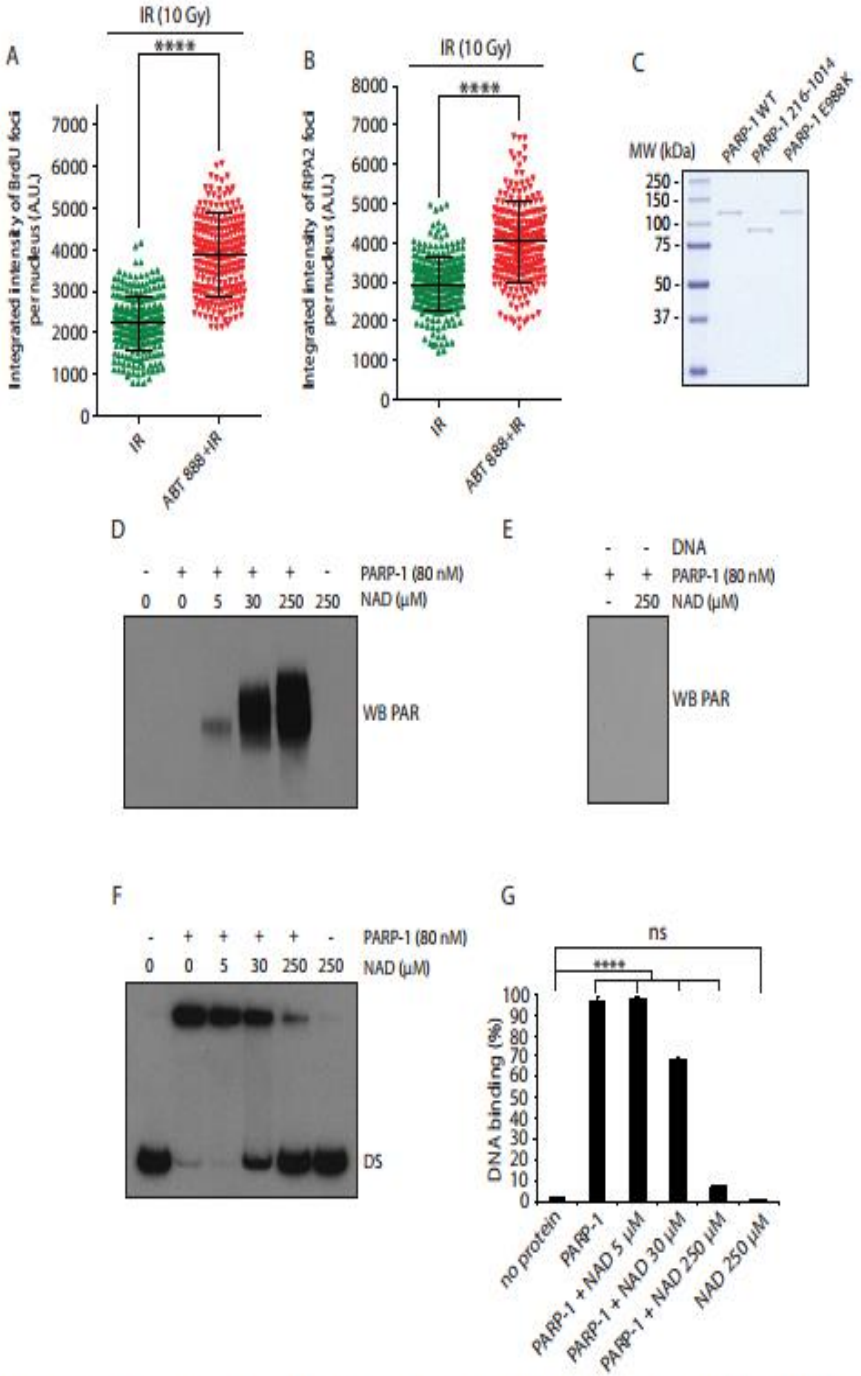

Supplementary Figure 6. U2OS cells were either irradiated (10 Gy), or irradiated (10 Gy) in combination with Veliparib (5 μM), and subjected to immunofluorescence against BrdU (A) or RPA2 foci formation (B). The graph represents the intensity of BrdU/RPA focus per nucleus after 3 hrs recovery. Data in A-B show the mean ± s.d. ****p<0.0001, (Mann-Whitney U-test). (C) SDS-PAGE of purified PARP-1 WT, PARP-1 DNA binding mutant 216-1014, and PARP-1 E988K. (D) PARP-1 was incubated in the resection buffer in the absence or presence of different concentrations of NAD and with 100 nM of dsDNA for 10 minutes at 37°C. PARP-1 activation was then visualized by western blotting using a pADPr antibody. (E) The same reactions were performed as mentioned in (D) without DNA. (F) DNA binding activity of PARP-1 to the dsDNA substrate in the presence or absence of different concentrations of NAD. (G) DNA binding quantifications. Data show the mean ± s.d. ****p<0.0001, (Ordinary one-way Anova).

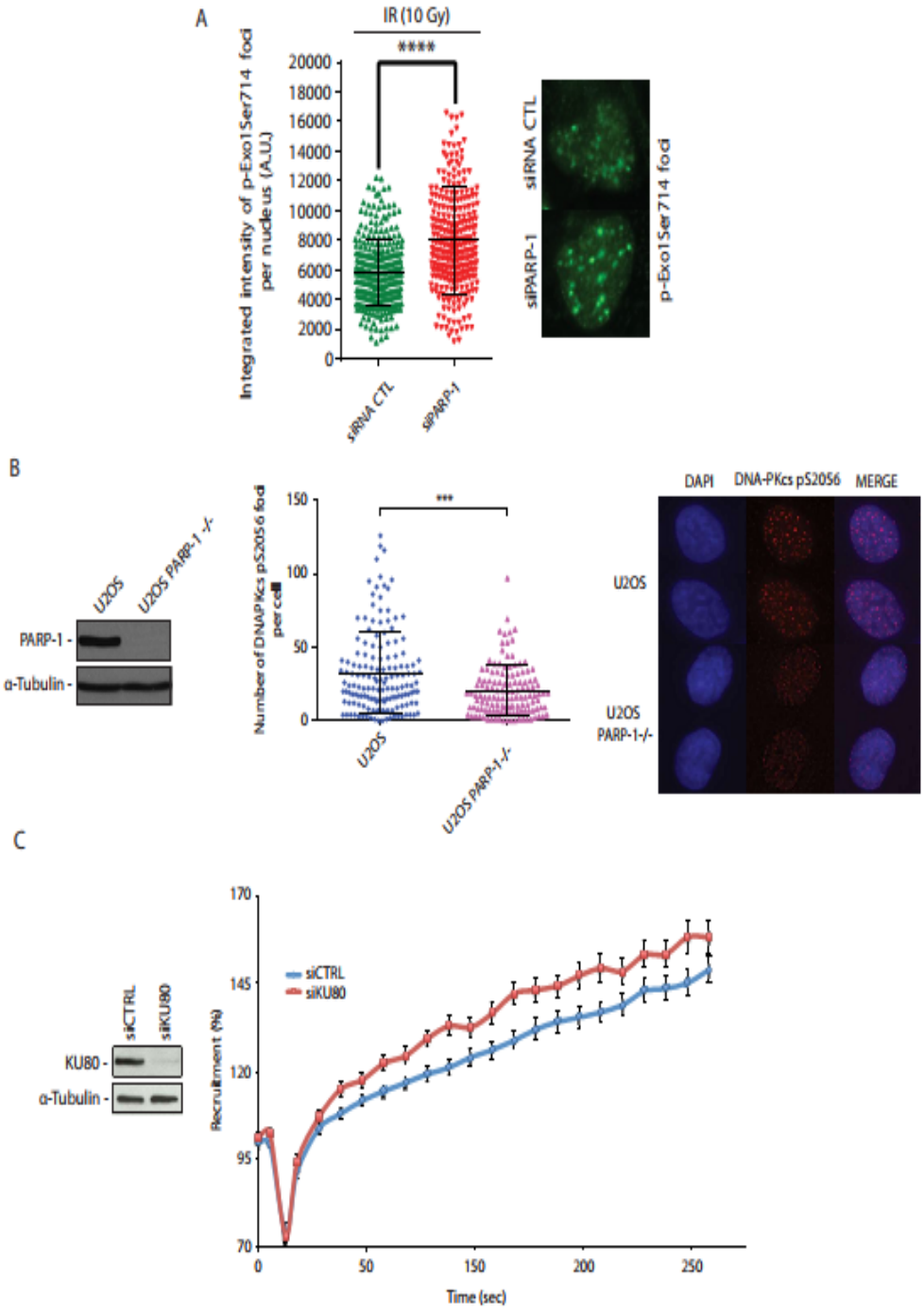

Supplementary Figure 7. (A) Quantification of EXO1 phospho-Ser 714 foci in U2OS cells knockdown for PARP-1 after irradiation (10 Gy, 3 hours release). A representative immunofluorescence picture is shown of the right. The graph represents the integrated intensity of EXO1phospho-Ser 714 foci per nucleus. Data show the mean ± s.d. **** $p \leq 0.0001$, (Mann-Whitney U-test). (B) Quantification of DNA-PKcs pS2056 foci in U2OS cells knockout for PARP-1 (left) after irradiation (5 Gy, 1 hour release). Data show the mean ± s.d. *** $p \leq 0.001$, (Mann-Whitney U-test). A representative immunofluorescence picture is shown (right).
(C) Left. Western blotting to monitor the knockdown efficiency of Ku80 in HeLa cells. Right. Recruitment of GFP-EXO1 in Ku80 knockdown cells. Data show the mean ± s.e.m.

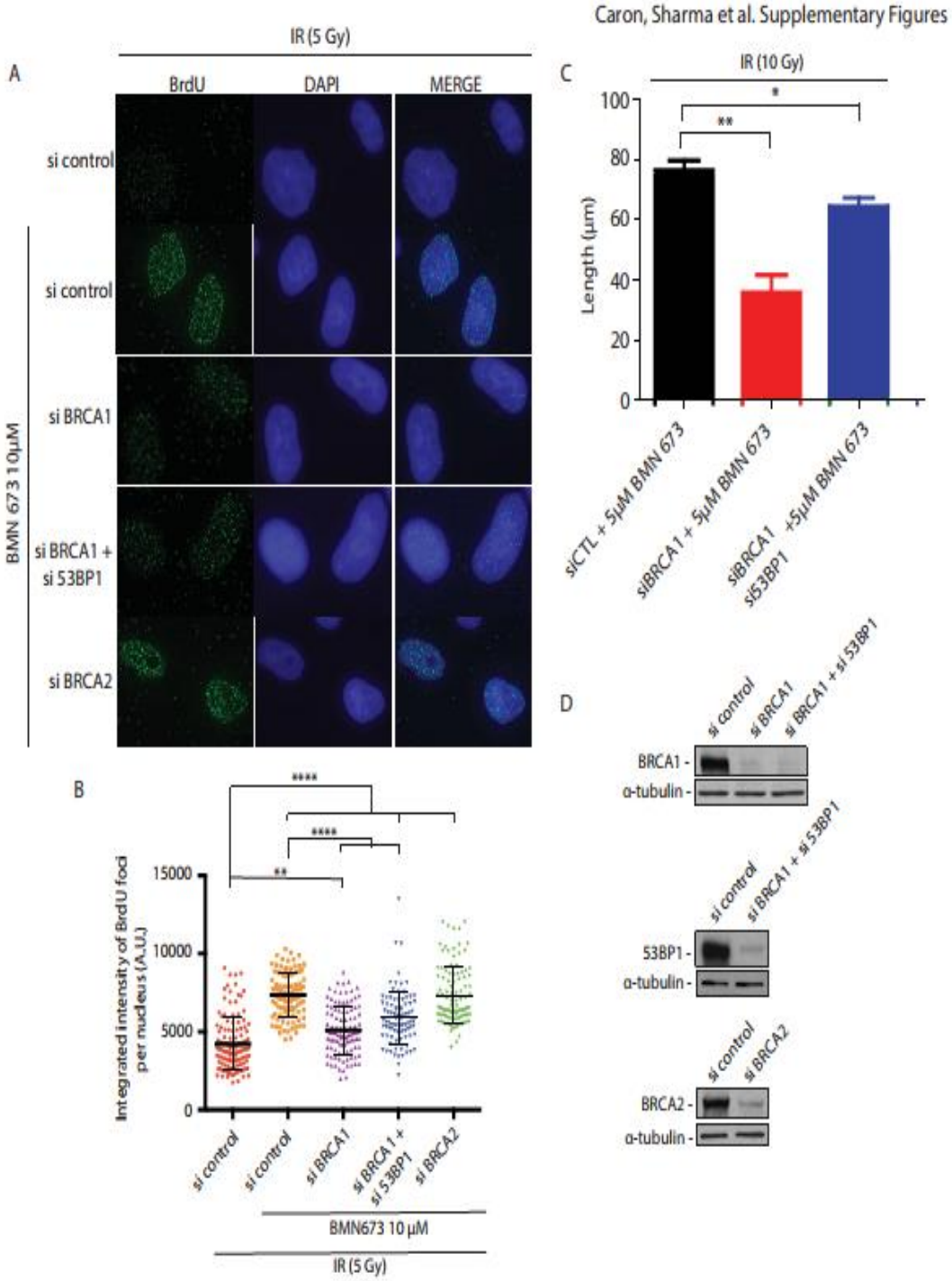

Supplementary Figure 8. (A) In contrast to siRNA inhibition of BRCA2, BRCA1 knockdown decreases single-strand DNA accumulation after irradiation as detected by BrdU staining following irradiation (5 Gy) and BMN 673 treatment.
(B) Quantification of the results by integrated intensity of BrdU foci per nucleus. Data show the mean ± s.d. ** $p \leq 0.01$, **** $p \leq 0.0001$, (Kruskal-Wallis).
(C) SMART assay. HeLa cells were transfected with the indicated siRNAs followed by irradiation (10 Gy) and treatment with BMN 673. 200 fibers were counted in triplicate. Data show the mean ± s.e.m. * $p \leq 0.05$; ** $p \leq 0.01$, (Mann-Whitney).
(D) Western blotting to monitor the knockdown efficiency of BRCA1, 53BP1, BRCA2 knockdown.

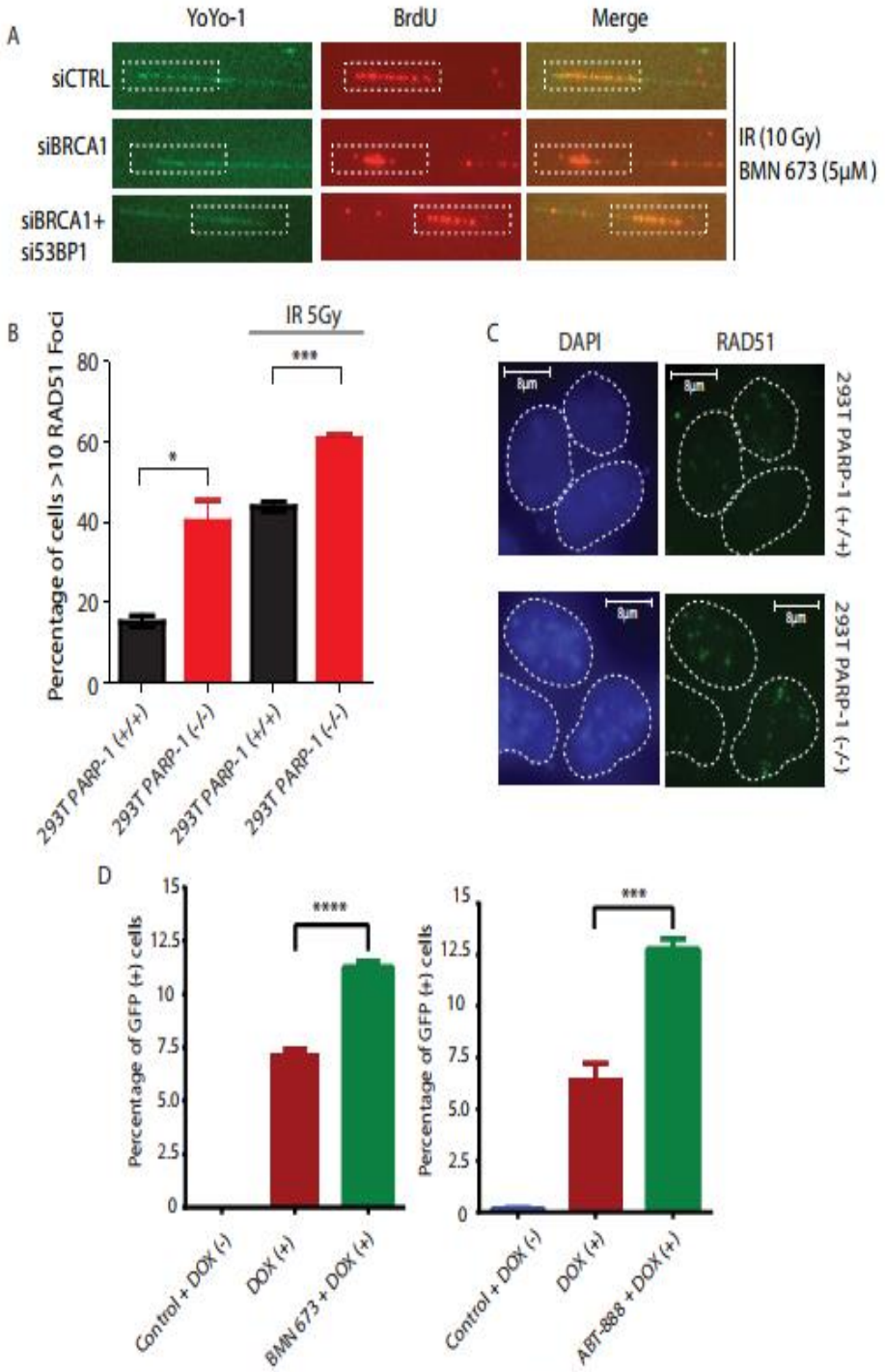

Supplementary Figure 9. (A) Representative pictures of SMART assay samples. DNA tracks were stained with YoYo-1 and an anti-BrdU. The merge picture represent the overlay between the green and red channels. The BrdU signal could not be detected without irradiation.
(B) RAD51 foci formation in CRISPR HEK293T cells proficient and deficient for PARP-1 without or with 5 Gy irradiation. The percentage of cells with more than 10 RAD51 foci were scored. (C) Typical example of RAD51 foci in both CRISPR HEK293T PARP-1 (+/+) and CRISPR HEK293T PARP-1 (-/-) after IR (5 Gy). (D) In cellulo homologous recombination is increased in BMN 673 (left) or ABT-888 (right) treated cells. Data in panels B and D show the mean ± s.e.m. * $p \leq 0.05$, *** $p \leq 0.001$, **** $p \leq 0.0001$ (Mann-Whitney, U-test).

jove

Assessment of Global DNA Double-Strand End Resection using BrdU-DNA Labeling coupled with Cell Cycle Discrimination Imaging

Julia O'Sullivan[*1,2], Sofiane Y. Mersaoui[*1,2], Guy Poirier[2,3], Jean-Yves Masson[1,2]

[1] Oncology Division, Genome Stability Laboratory, CHU de Québec Research Center, HDQ Pavilion [2] Department of Molecular Biology, Medical Biochemistry, and Pathology, Laval University Cancer Research Center [3] Oncology Division, CHU de Québec Research Center, CHUL Pavilion

[*] These authors contributed equally

Corresponding Authors

Guy Poirier
guy.poirier@crchudequebec.ulaval.ca

Jean-Yves Masson
Jean-Yves.Masson@crchudequebec.ulaval.ca

Citation

O'Sullivan, J., Mersaoui, S.Y., Poirier, G., Masson, J.Y. Assessment of Global DNA Double-Strand End Resection using BrdU-DNA Labeling coupled with Cell Cycle Discrimination Imaging. *J. Vis. Exp.* (170), e62553, doi:10.3791/62553 (2021).

Date Published

April 28, 2021

DOI

10.3791/62553

URL

jove.com/video/62553

Abstract

The study of the DNA damage response (DDR) is a complex and essential field, which has only become more important due to the use of DDR-targeting drugs for cancer treatment. These targets are poly(ADP-ribose) polymerases (PARPs), which initiate various forms of DNA repair. Inhibiting these enzymes using PARP inhibitors (PARPi) achieves synthetic lethality by conferring a therapeutic vulnerability in homologous recombination (HR)-deficient cells due to mutations in breast cancer type 1 (BRCA1), BRCA2, or partner and localizer of BRCA2 (PALB2).

Cells treated with PARPi accumulate DNA double-strand breaks (DSBs). These breaks are processed by the DNA end resection machinery, leading to the formation of single-stranded (ss) DNA and subsequent DNA repair. In a BRCA1-deficient context, reinvigorating DNA resection through mutations in DNA resection inhibitors, such as 53BP1 and DYNLL1, causes PARPi resistance. Therefore, being able to monitor DNA resection *in cellulo* is critical for a clearer understanding of the DNA repair pathways and the development of new strategies to overcome PARPi resistance. Immunofluorescence (IF)-based techniques allow for monitoring of global DNA resection after DNA damage. This strategy requires long-pulse genomic DNA labeling with 5-bromo-2′-deoxyuridine (BrdU). Following DNA damage and DNA end resection, the resulting single-stranded DNA is specifically detected by an anti-BrdU antibody under native conditions. Moreover, DNA resection can also be studied using cell cycle markers to differentiate between various phases of the cell cycle. Cells in the S/G2 phase allow the study of end resection within HR, whereas G1 cells can be used to study non-homologous end joining (NHEJ). A detailed protocol for this IF method coupled to cell cycle discrimination is described in this paper.

Introduction

Modulation of DNA repair factors is an ever-evolving method for cancer therapy, particularly in DNA DSB repair-deficient tumor environments. The inhibition of specific repair factors is one of the ingenious strategies used to sensitize cancer cells to DNA-damaging agents. Decades of research led to the identification of various mutations of DNA repair genes as biomarkers for therapeutic strategy choices[1]. Consequently, the DNA repair field has become a hub for drug development to ensure a wide range of treatments, empowering the personalized medicine concept.

DSBs are repaired by two main pathways: NHEJ and HR[2]. The NHEJ pathway is error-prone, rapidly ligating the two DNA ends with little to no DNA end-processing and involving the protein kinase (DNA-PKcs), the Ku70/80 complex, 53BP1, and RIF1 proteins[3]. In contrast, HR is a faithful mechanism initiated by BRCA1[4]. An essential step in HR repair is the DNA-end resection process, which is the degradation of the broken ends leading to single-stranded (ss) DNA with 3'-OH ends. BRCA1 facilitates the recruitment of the downstream proteins that form the resectosome MRN/RPA/BLM/DNA2/EXO1, which are involved in the 5' to 3' DNA resection[5].

The initial end-resection is accomplished through the endonuclease activity of MRE11, allowing for further processing by the DNA2 and EXO1 nucleases. The generated ssDNA overhangs are quickly coated by Replication Protein A (RPA) to protect them from further processing. Subsequently, BRCA2, PALB2, and BRCA1 engage to mediate the displacement of RPA and the assembly of the RAD51 nucleofilament required for homology-directed repair mechanism. A fine balance between the usage of NHEJ and HR is necessary for the optimal maintenance of genomic integrity. The pathway choice depends on the cell cycle phase. HR is preferentially used during the S to G2 phases wherein DNA resection is at the highest level, and the sister chromatids are available to ensure proper repair.

Poly (ADP-ribose) polymerase 1 (PARP-1) is one of the earliest proteins recruited to the DSB. It regulates both resection activity and the assembly of downstream effectors involved in the NHEJ[5,6]. PARP-1 is also required for DNA single-stranded break repair during replication[7,8]. Due to its important role in DNA repair, PARP inhibitors (PARPi) are used as cancer therapies. In several HR-deficient cancers, PARPi treatment leads to a synthetic lethal response due to the incapacity of HR-deficient cells to repair the accumulated damage via an alternative pathway[9,10]. There are currently four FDA approved PARPi: Olaparib, Rucaparib, Niriparib, and Talazoparib (also called BMN 673), which are used for various breast and ovarian cancer treatments[11]. However, PARPi resistance is common, and one potential cause arises through the reacquisition of HR proficiency[12]. Loss or inhibition of PARP-1 in the presence of irradiation dysregulates the resectosome machinery, leading to the accumulation of longer ssDNA tracts[13]. Therefore, an in-depth study of DNA resection *in vivo* is critical for a clearer understanding of the DNA repair pathways and the subsequent development of new strategies to treat cancer and to overcome PARPi resistance.

There have been several methods employed to detect DNA resection events[5]. One such method is the classical IF-based technique allowing for indirect staining and visualization of the resected DNA after stress-induced DSB by using an

anti-RPA antibody. Labelling genomic DNA with 5-bromo-2'-deoxyuridine (BrdU) and detecting only ssDNA is a direct measurement of DNA resection events. It circumvents the monitoring of RPA, which is involved in multiple cellular processes such as DNA replication. In the method described here, cells incubated with BrdU for a single cell cycle allow BrdU to be incorporated into one strand of the replicating cellular DNA. Following resection, IF staining is performed under conditions allowing wherein BrdU detection only in the ssDNA form, with the use of an anti-BrdU antibody. This antibody can only access exposed BrdU nucleotides and will not detect those integrated into double-stranded DNA. Using fluorescence microscopy, the resected DNA can be visualized in the form of punctate BrdU/ssDNA foci. The nuclear intensity of these foci can be used as a readout to quantify resection following DNA damage. This paper describes step-by-step the processes of this method, which can be applied to most mammalian cell lines. This method should be of broad utility as a simple way of monitoring DNA end resection *in cellulo*, as a proof of concept.

Protocol

1. Cell culture, treatments, and coverslip preparation

NOTE: All cell plating, transfections, and treatments, aside from irradiation, should take place under a sterile cell-culture hood.

1. Day 1
    1. In a 6-well plate, place a single coverslip in each well for as many conditions as needed. Plate ~150,000 HeLa cells for transfection or drug treatment, as desired.

        NOTE: If transfecting, it is recommended to do a reverse transfection at the time of plating, or it is possible to do a forward transfection several hours after plating to allow for adherence. A reverse transfection is accomplished by adding the transfection mix to the coverslip before the cells are added; thus, transfection begins before the cells start adhering. A forward transfection, by contrast, is the addition of the transfection mix post-adherence to the surface usually on the following day. However, it is possible to do this on the same day, provided enough time is given for the cells to adhere.

    2. For this method, use 4 wells: Well 1: siRNA control (termed siCTRL); Well 2: siRNA against PARP-1 (siPARP-1); Well 3: untreated; Well 4: Cells to be treated with 5 µM BMN673 1 h prior to irradiation.

        NOTE: In this protocol, all the tests were conducted under irradiated conditions (see section 1.3).

    3. Incubate the cells at 37 °C in a 5% CO_2 humidified incubator overnight, although the transfection protocol allows for up to 3 days of incubation. The incubation time prior to BrdU treatment will depend on the siRNA transfection efficiency. If there is no transfection, incubation for 16 h is sufficient to allow for adherence to the coverslip and some cell growth.

        NOTE: Incubator conditions can be changed according to the cell line used.

2. Day 2
    1. Add BrdU at a final concentration of 10 µM in the appropriate culturing media, and incubate for 16 h (one cell cycle).

NOTE: The BrdU solution is prepared in dimethylsulfoxide; the stock solution used is 10 mM and is stored in aliquots at -20 °C.

3. Day 3

1. Irradiate the plates with a total dose of 5 Gy of X-ray irradiation (vary the dose of irradiation depending on the irradiator type, for example, small animal irradiators vs. benchtop irradiators). See the **Table of Materials** for the brand and model of irradiator used.
2. Return the plates to the incubator, and release the cells for 3 h.
3. During the 3 h incubation period, prepare the two buffers, A and B, and 4% paraformaldehyde (PFA) in 1x phosphate-buffered saline (PBS).

   NOTE: Buffers A and B and the sucrose should be prepared fresh the day of fixation, using fresh sucrose solution to prevent contamination.

   1. Prepare buffer A (Pre-Extraction Buffer), according to the order (30 mL) described in **Table 1**.

      NOTE: The 1M sucrose should be prepared the day of use to prevent contamination.

   2. Prepare buffer B (Cytoskeleton Stripping Buffer) according to the order described in **Table 1** (30 mL).

      NOTE: Buffer B must be prepared in the cited order to prevent precipitation of Tween-20 and sodium deoxycholate solution.

   3. Prepare 4% PFA, 2 mL per condition (10 mL), under a chemical hood (**Table 1**).

2. Pre-extraction and fixation

NOTE: All pre-extraction and fixation are performed with the coverslips remaining in the tissue culture plate on ice or at 4 °C; the coverslip is only lifted in the last step of mounting (see discussion).

1. Pre-extraction

   1. Aspirate the medium, carefully wash the cells twice with 1x PBS, and remove the PBS. Add 2 mL of Pre-extraction Buffer A and immediately incubate at 4 °C for 10 min.

      NOTE: It is important that incubation time in buffer A is not extended. Extended incubation in the pre-extraction buffers will result in an increased number of detached cells from the coverslip. Alternatively, instead of incubation at 4°C, incubation can be done on ice.

   2. Remove Buffer A through aspiration.

      NOTE: Do not wash the coverslips after removing buffer A. Proceed to the next step.

   3. Add 2 mL of Cytoskeleton Stripping Buffer B and immediately incubate at 4 °C for 10 min. Carefully aspirate Buffer B, and carefully wash the cells once with 1x PBS. Carefully aspirate the 1x PBS.

2. Fixation

   1. Fix the cells by adding 2 mL of 4% PFA under the chemical hood.

      NOTE: PFA is toxic and must be manipulated under a chemical hood.

   2. Incubate the cells at room temperature for 20 min. Wash the coverslips twice with 1x PBS, and aspirate the excess.

3. Cover the coverslips with 100% cold methanol, and incubate the coverslips at -20 °C for 5 min. Wash twice with 1x PBS.

   NOTE: The protocol can be paused here. The coverslips can be stored at 4 °C in 1x PBS and the plate wrapped in aluminum foil if necessary. The cells should not be kept more than 5 days before continuing the IF protocol.

3. Permeabilization

1. Incubate the cells with 2 mL of 1x PBS containing 0.5% Triton X-100 at room temperature for 15 min. Wash the coverslips three times with 2 mL of 1x PBS.

4. Immunostaining

1. Blocking step
   1. Prepare enough fresh blocking buffer (3% BSA in 1x PBS) to use 2 mL per coverslip.

      NOTE: Prepare an extra 5mL of blocking buffer to make the antibody solutions.

   2. Add 2 mL of blocking buffer to each well and incubate at room temperature for 1 h.
2. Primary antibody incubation
   1. Prepare the primary antibody solution in fresh blocking buffer: BrdU RPN202 1:1000 and proliferating cell nuclear antigen (PCNA) 1:500, 100 µL per coverslip.

      NOTE: To preserve the antibody, a smaller volume can be used, 75-100 µL for a 22 x 22 mm coverslip, 50-75 µL for an 18 x 18 mm coverslip.

   2. On each coverslip, add 100 µL of primary antibody solution. Cover the coverslips with a square of parafilm using tweezers, and carefully position the parafilm to not create bubbles.
   3. Cover the plate in aluminum foil, and incubate the primary antibody overnight at 4 °C in a humidified chamber.
   4. Remove the parafilm squares, and wash the coverslips three times with 2 mL of sterile 1x PBS.
3. Secondary antibody incubation
   1. Prepare enough secondary antibody solution in fresh blocking buffer: anti-mouse 488 fluorescent secondary A11011 (for BrdU) dilution 1:800 and anti-rabbit 568 fluorescent secondary A11011 (for PCNA) dilution 1:800.

      NOTE: The colors used can be changed to suit the experimental needs. The specific brand used can be found in the **Table of Materials**.

   2. Add on each coverslip 100 µL of secondary antibody solution, cover the coverslips with a square of parafilm using tweezers, and carefully position the parafilm without bubbles.
   3. Incubate the secondary antibody at room temperature for 1 h with the plate covered in aluminum foil.
   4. Wash the coverslips three times with 2 mL of 1x PBS.
4. Nuclear staining
   1. Prepare a volume of 2 mL per coverslip of 1x PBS containing 4',6-diamidino-2-phenylindole (DAPI) at a final concentration of 1 µg/mL (1:1000).
   2. Add on each coverslip 2 mL of the DAPI solution. Incubate the coverslips at room temperature for 10

min with the plate covered in aluminum foil. Wash the coverslips twice with 1x PBS.

3. Cover the coverslips with 1x PBS, and use either a needle or fine tweezers to lift the coverslip from the bottom of the well.Carefully blot the off the excess liquid by tapping one edge gently on a paper towel.
   NOTE: Be careful not to drop the slide or allow the flat surface with the adherent cells to touch the paper.
4. Mount the coverslips on slides using 10-20 µL of IF-specific mounting media.

5. Image acquisition and analysis

NOTE: Image acquisition can be done on several types of fluorescent microscopes. An epifluorescence microscope with a 63x oil objective was used; see the **Table of Materials** for the brand and model. Z-stacks are not required, although they may be of use depending on the cell line and level of mitochondrial staining.

1. Image analysis
   1. For each image, create multiple tiff files; merge all planes, but keep the color channels separate. Import these files into Cell Profiler (The Broad Institute https://cellprofiler.org/home) and analyze using the Speckle Counting pipeline (**Supplemental Video 1**).
   2. Upload the images (**Supplemental Figure S1A**).
      1. To begin creating the project, load the speckle counting pipeline into the program and the images to be analyzed in the provided area.
      2. Use the **NamesAndTypes** module to assign a meaningful name to each image by which other modules will refer to it-C01: Representing BrdU Channel; C02: Representing PCNA Channel; C03: Representing DAPI Channel.
         NOTE: These identifiers will depend on the microscope; there should be an identifier in the file name to distinguish between the channels.
   3. Identify which file will be used to identify the nuclei and name it (change this name as required) (see **Supplemental Figure S1B** and **Supplemental Figure S1C**).
      1. Select the diameter of the object between 50 and 300 pixel units, which is the acceptable size range for nuclei, but change the value to fit the nuclei in the image.
         NOTE: It may be that 50 is too large a value and prevents smaller nuclei from being identified; likewise, 300 may allow for large groupings of nuclei to be counted as 1.
      2. Discard objects outside of the diameter range to ensure only those that match the criteria will be counted.
      3. Discard objects touching borders to remove cells that may only be partially in the field.
      4. Apply the threshold to fit the specific images. Note the following settings as an example. Change the thresholding correction factor based on how stringent the thresholding strategy will be. Other settings include threshold strategy: Global; thresholding method: Otsu; two class or three class thresholding: Two class; threshold smoothing scale: 1; threshold smoothing factor: 1; lower and upper bounds on threshold: 0.0 and 1.0; method to distinguish clumped objects: Shape; and method to

draw dividing lines between clumped objects: Propagate.

NOTE: For each parameter, cell profiler provides complementary definitions and available possibility for the variable setting.

4. Identify the primary object to identify the foci (**Supplemental Figure S2A**).
    1. Use the following settings: select the input image: Maskedgreen; named the primary object to be identified: BrdUFoci; typical diameter of the object: 1-15; discard the object outside the diameter range: Yes; discard the object touching the border of the image : No; threshold strategy: Adaptative; thresholding method: Otsu; two class or three class thresholding: Three class; threshold smoothing scale: 1; threshold smoothing factor: 3; and size of smoothing filter: 4.
5. Measure intensity (**Supplemental Figure S2B**).
    1. Select the image to be measured: OrigGreen.
    2. Click on **Add another image**. Select the image to be measured: PCNA. Select objects to measure: Nuclei.

    NOTE: This will be used to measure the BrdU and PCNA intensity-the final data that will be graphed.

Representative Results

In this protocol, the bromodeoxyuridine (BrdU)-based assay was used to quantitatively measure the resection response of HeLa cells to irradiation-induced damage. The generated ssDNA tracks are visualized as distinct foci after immunofluorescence staining (**Figure 1A**). The identified foci were then quantified and expressed as the total integrated intensity of the BrdU staining in the nuclei (**Figure 1B**, **Supplemental Figure S1**, **Supplemental Figure S2**, and **Supplemental Figure S3**). It is possible to measure the foci number or mean foci intensity, although this can be less reliable than the total nuclear intensity, largely in part to the variable size of the BrdU foci.

To differentiate between the short-range resection as a result of NHEJ and the long-range resection of HR, co-staining was performed using an anti-PCNA antibody to identify cells going through S-phase (**Figure 1** and **Supplemental Figure S4**). PCNA constitutes the DNA clamp that acts as a processivity factor for DNA polymerase and is essential for replication. PCNA is prominent in the nucleus and reaches maximal expression during the S-phase of the cell cycle. Hence, in early S-phase, the PCNA signal is low and has a granular distribution. In contrast, in late S-phase, the PCNA staining is quite strong (**Figure 1A**). When first analyzing the PCNA (S-phase) signal, the nuclei must be identified and the PCNA intensity measured.

The resulting values are then plotted as a scatter plot to best determine the cut-off intensity to discriminate between the PCNA-positive and PCNA-negative nuclei (**Supplemental Figure S4A**). The PCNA-negative results will then be removed from the data set to allow for the BrdU intensity-based analysis because of the low BrdU signal regardless of the condition (**Supplemental Figure S4B**). In these experimental conditions, the PCNA-negative nuclei harbor a basal integrated intensity of BrdU foci of 900 arbitrary units (A.U.). However, this value reaches 1800 A.U. in PCNA-positive nuclei (**Figure 1B**). This represents a 100% increase in the amount of the integrated signal of the BrdU foci. Increase in BrdU intensity can be then correlated to an

increase in DNA resection, which is more pronounced and efficient when cells go through S and G2 phases and are irradiated.

In this protocol, to demonstrate an increase in DNA resection after irradiation (5 Gy), PARP-1 activity was modulated either through the loss of PARP-1 using an siRNA knockdown condition or after potent inhibition of PARP-1 using Talazoparib (BMN673) (**Figure 2** and **Supplemental Figure S5**). The amounts of resected DNA in each condition were then quantified after IF (**Figure 2B**). In unperturbed condition (siCTRL), the integrated intensity of BrdU foci per nucleus is approximately 1500 A.U. in the PCNA-positive nuclei (**Figure 2A,B**). After an efficient knockdown of PARP-1 using an siRNA (**Figure 2C**), a significant increase in the intensity of the BrdU foci to approximately 1900 A.U. was observed, which corresponds to 26% increase in intensity ($p < 0.0001$). Similarly, after inhibition of PARP-1 using BMN673 (5 µM final concentration), the intensity of foci increased from approximately 1750 to 2500 A.U. corresponding to 43% increase of the foci intensity ($p < 0.0001$). Thus, loss of PARP-1 dysregulates DNA resection as reported previously[13].

It is important to remember that BMN-673 both inhibits the activity of PARP-1 and traps it in DNA, and the effect of this treatment is much more detrimental to the cell, resulting in the greater increase of BrdU intensity than in siRNA-treated cells. The slight difference in untreated and siCTRL intensities demonstrates how any treatment, such as siRNA transfection, may affect the response and output of an assay. It can further demonstrate the importance of using the proper controls for each condition.

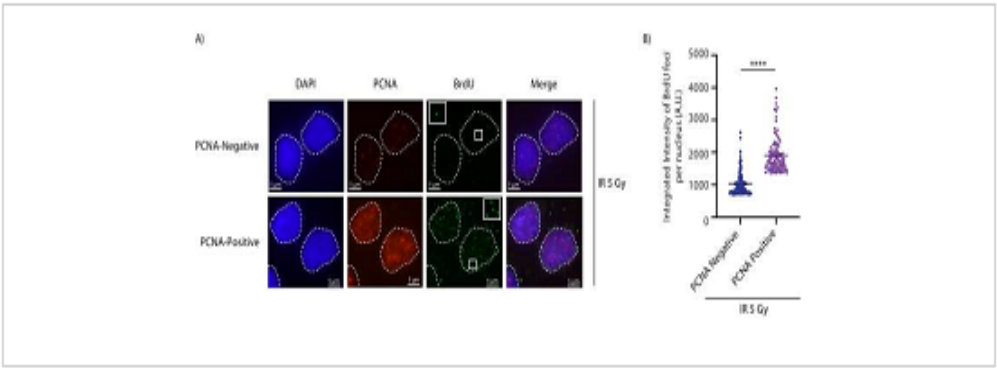

Figure 1: BrdU foci formation is more prone to occur in PCNA-positive cells than in replicating cells. (A) Representative images of BrdU foci formation and PCNA staining following 5 Gy irradiation and 3 h release. A zoomed-in square showing marked BrdU foci is present in the corner of each BrdU image. Scale bars = 5 µm. (**B**) Quantification of the BrdU nuclear intensity in untreated (without BMN-673) HeLa cells. The data show the mean ± s.e.m (Mann-Whitney *U*-test). Abbreviations: BrdU = 5-bromo-2'-deoxyuridine; PCNA = proliferating cell nuclear antigen; IR = irradiation; DAPI = 4',6-diamidino-2-phenylindole; A.U. = arbitrary units; s.e.m. = standard error of the mean. Please click here to view a larger version of this figure.

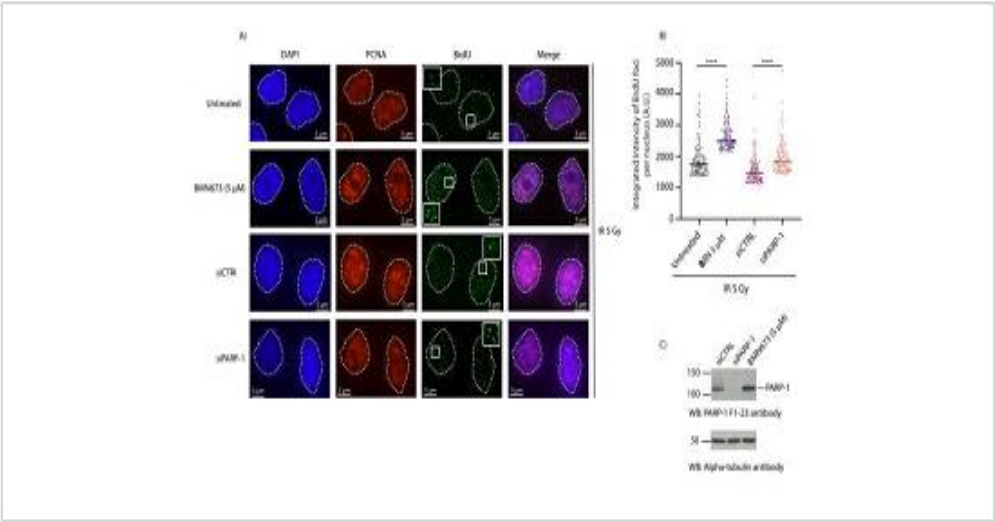

Figure 2: Poly(ADP-ribose) polymerase-1 knockdown or inhibition results in increased BrdU foci formation in replicating cells. (**A**) Representative images of BrdU foci formation and PCNA staining in untreated HeLa cells, treated with 5 μM BMN-673, siCTRL, and siPARP-1, followed by 5 Gy irradiation and 3 h release. A zoomed-in square showing marked BrdU foci is present in the corner of each BrdU image. Scale bars = 5 μm. (**B**) Quantification of the BrdU nuclear intensity in untreated HeLa cells, treated with 5 μM BMN-673, siCTRL, and siPARP-1 followed by 5 Gy irradiation, the data show the mean ± s.e.m (Mann-Whitney *U*-test). (**C**) Western blot to validate the siRNA knockdown of *PARP-1*. The F1-23 PARP-1 antibody recognizes automodified PARP-1 resulting in the smeared appearance of the siCTRL band and the solid appearance of the catalytically inhibited PARP-1 in BMN-673-treated samples. Abbreviations: PARP-1 = poly(ADP-ribose) polymerase 1; BrdU = 5-bromo-2'-deoxyuridine; PCNA = proliferating cell nuclear antigen; IR = irradiation; DAPI = 4',6-diamidino-2-phenylindole; A.U. = arbitrary units; siCTRL = siRNA control; siPARP-1 = siRNA to knock down *PARP-1*; s.e.m. = standard error of the mean. Please click here to view a larger version of this figure.

Buffer A (Pre-Extraction Buffer) 30 mL		
Reagent	**Volume**	**Final Concentration**
H_2O	18 mL	
PIPES (pH 7, 500 mM)	600 µL	10 mM
NaCl (4 M)	750 µL	100 mM
$MgCl_2$ (1 M)	90 µL	3 mM
EGTA (500 mM)	60 µL	1 mM
Trition X-100 (10%)	1.5 mL	0.50%
Sucrose (1 M)	9 mL	300 mM

Buffer B (Cytoskeleton Stripping Buffer) 30 mL		
Reagent	**Volume**	**Final Concentration**
H_2O	25.035 mL	
Tris pH 7.5 (1 M)	300 µL	10 mM
NaCl (4 M)	75 µL	10 mM
$MgCl_2$ (1 M)	90 µL	3 mM
Tween20 (10%)	3 mL	1%
10% Sodium Deoxycholcate	1.5 mL	0.50%

Reagent	**Volume**
16% PFA	2.5 mL
PBS 1x	7.5 mL

Table 1.

Supplemental Figure S1: Visual representation of the Cell Profiler Software and Speckle counting pipeline part 1. (**A**) Screenshot shows the window used to identify the different channel files of the images to be analyzed. These shots show the cell profiler interface. (**B**) Screenshot of the Identify Primary Objects menu to identify the Nuclei.

The highlighted values are the commonly altered values to best identify nuclei. Abbreviations: BrdU = 5-bromo-2′-deoxyuridine; DAPI = 4',6-diamidino-2-phenylindole. Please click here to download this File.

Supplemental Figure S2: Visual representation of the Cell Profiler Software and Speckle counting pipeline part 2. (**A**) Screenshot of the Identify Primary Objects menu to identify the BrdU foci within the nuclei. (**B**) Screenshot of Measure Object Intensity menu to measure the BrdU and PCNA nuclear intensity. Abbreviations: BrdU = 5-bromo-2′-deoxyuridine; PCNA = proliferating cell nuclear antigen. Please click here to download this File.

Supplemental Figure S3: Visual representation of the Cell Profiler Software and Speckle counting pipeline part 3. (**A**) Representation of the nuclei identification by cell profiler following optimization. (**B**) Representation of the BrdU foci identification. (**C**) Screenshot is a zoom-in on one cell within the initial window. Please click here to download this File.

Supplemental Figure S4: Scatter plot of PCNA-positive and PCNA-negative cells. (**A**) An example of a PCNA scatter plot used to distinguish PCNA-positive from PCNA-negative cells. The PCNA intensity from a single condition was plotted and the distinction between the two populations identified. The green highlights the PCNA-positive cells, the red represents the PCNA-negative cells. This is done for each individual experiment and condition. (**B**) Quantification of the BrdU nuclear intensity in PCNA-negative untreated HeLa cells, treated with 5 µM BMN-673, siCTRL, and siPARP-1; the data show the mean ± s.e.m (Mann-Whitney *U*-test). Abbreviations: PARP-1 = poly(ADP-ribose) polymerase 1; BrdU = 5-bromo-2′-deoxyuridine; IR = irradiation; PCNA = proliferating cell nuclear antigen; A.U. = arbitrary units; siCTRL = siRNA control; siPARP-1 = siRNA to knock down *PARP-1*; s.e.m. = standard error of the mean. Please click here to download this File.

Supplemental Figure S5: BrdU signal without irradiation. (**A**) Representative images of BrdU foci formation and PCNA staining without irradiation. Scale bars = 5 µm. A zoomed-in square showing marked BrdU foci is present in the corner of each BrdU image. (**B**) Quantification of the BrdU nuclear intensity in PCNA-positive untreated Hela cells, treated with 5 µM BMN-673, siCTRL, and siPARP-1; the data show the mean ± s.e.m (Mann-Whitney *U*-test). (**C**) Quantification of the BrdU nuclear intensity in PCNA-negative untreated HeLa cells, treated with 5 µM BMN-673, siCTRL, and siPARP-1; the data show the mean ± s.e.m (Mann-Whitney *U*-test). Abbreviations: PARP-1 = poly(ADP-ribose) polymerase 1; BrdU = 5-bromo-2′-deoxyuridine; PCNA = proliferating cell nuclear antigen; IR = irradiation; DAPI = 4',6-diamidino-2-phenylindole; A.U. = arbitrary units; siCTRL = siRNA control; siPARP-1 = siRNA to knock down *PARP-1*; s.e.m. = standard error of the mean. Please click here to download this File.

Supplemental Video 1: Use of Cell Profiler and the Speckle Counting pipeline to analyze BrdU staining for the measurement of DNA resection. This video demonstrates the use of Cell Profiler and the Speckle counting pipeline. It shows how to import and analyze images with this tool specifically for this protocol.*Abbreviation: BrdU* =5-bromo-2′-deoxyuridine. Please click here to download this Video.

Discussion

This paper describes a method that makes use of IF staining to measure variations in DNA resection *in cellulo*. The current standard for observing an effect on DNA resection is through RPA staining; however, this is an indirect method that may be influenced by DNA replication. Previously, another BrdU incorporation-based DNA resection IF technique has been described for classifying the resulting intensities in BrdU-positive and BrdU-negative cells. This method allowed for cells that are not undergoing HR to be counted as positive due to background or mitochondrial staining resulting in a high BrdU intensity[14,15,16]. The primary novelty of the method described in this paper is the addition of PCNA staining, which allows for selectivity for S and G2 phases of the cell cycle, ensuring that the resulting BrdU signal is due to resection and thus, to homology-directed repair.

The critical step in this protocol is the pre-extraction; without this, the BrdU foci will not be visible, and if done incorrectly, the cells will detach completely. Incorrectly prepared buffers will result in incomplete pre-extraction, such as partial cytoskeletal removal or increased background signal. It is very important to respect the duration of incubation with the pre-extraction buffers, increased duration in the buffers can result in the cells detaching from the coverslip. Importantly, if this protocol is performed with poorly adherent cells, pre-treat the coverslips with polylysine to reduce cell detachment during pre-extraction. Subsequently, without methanol fixation, the PCNA signal will not be visible.

Another important variable in this protocol is the blocking buffer: incompatible blocking buffers will result in loss of BrdU signal. For example, 10% fetal bovine serum in 1x PBS blocking buffer will function when not combined with methanol fixation; however, when combined with methanol fixation as required for the PCNA staining, the BrdU signal is considerably reduced. It is possible other blocking agents and methods will work with this protocol; 3% BSA in 1x PBS provided the best results. A final essential component to this technique is the use of a DNA damage source; without this, there will be little to no nuclear BrdU signal (**Supplemental Figure S5**). Experience has shown that irradiation is an excellent source of damage for this method. However, if there is no access to an irradiator, radiomimetic drugs such as neocarzinostatin can be used instead.

Cell profiler is a useful and versatile tool that allows easy and consistent analysis of the images produced in this technique. The settings can be customized for both the size of the objects identified and the threshold at which it does so (**Supplemental Video 1**). As the nuclear intensity of the BrdU staining is the desired readout, the key customization is in the identification of the nuclei from the DAPI files. The analysis of the images from each condition must be done separately as the results are obtained in the form of a single csv file containing cell and image numbers, but not condition names. To determine if the analysis conditions are appropriate, use the **Start test mode** feature, and make sure the eye icon is open in the desired steps. Close this icon when running the actual analysis as it will result in pop-up windows and slow down the program. In the **Start test mode**, users can go back and forth, altering the settings as needed to properly identify first the nuclei and then the BrdU foci.

Once satisfied with the resulting identification, use the same settings for each condition within the same experiment; this may require the acquisition of a test image for each condition prior to analyzing the whole batch to ensure that the settings comply with each condition. It is important to note that, depending on image acquisition, there may be

variability in the Cell profiler settings between users and between software versions. Hence, it is essential to go through the testing stage to determine the ideal parameters for specific experiments. When preparing to graph the results, the PCNA (S phase)-positive cells must be identified. To do this, the PCNA intensity is measured, in the same fashion as the BrdU intensity, and the resulting values plotted as a scatter plot to best visualize the cut-off intensity value for PCNA-positive cells. The PCNA-negative results will then be removed from the data set to allow for the BrdU intensity graphing. The provided supplementary figures show screenshots from the program highlighting the most optimized settings (**Supplemental Figure S1**, **Supplemental Figure S2**, and **Supplemental Figure S3**).

A possible modification to the protocol is the PCNA antibody used; two different PCNA antibodies were successfully tested, the one listed here and another which is no longer in production-a rat monoclonal antibody (Bulldog Bio PCA16D10). Finally, users should cover the coverslips with parafilm during antibody incubation. It is not strictly necessary, although a significantly larger volume of antibody solution would be required to cover the coverslip entirely without this. Another method is to place a sheet of parafilm surrounding a glass plate, place drops of the antibody solution onto the parafilm, and carefully place the coverslip cell-side down onto the drop of antibody solution. This glass plate can then be placed in a humid chamber at 4 °C overnight for primary incubation and in the dark at room temperature for secondary incubation. This method is completely functional although it does significantly increase the time of handling the coverslips and as a result, increases the probability of dropping or breaking the coverslip.

An alternative method to measure resection is through the use of the DNA-combing SMART method; while this technique provides very clear results, it is much more complicated, requires more time, and is more expensive[17]. The SMART method requires the extraction of the DNA without damaging it, followed by stretching this DNA onto coverslips to be followed by an IF. The BrdU IF method, by comparison, is both simple and cost-effective, not requiring a greater investment than the cost of the antibody. This method provides an initial way to measure resection that is more accurate than simply measuring RPA foci formation, which can be related to its effects on many cellular functions. However, RPA is phosphorylated on specific residues during resection as part of the DNA damage response.

Single-molecule imaging recently revealed phosphorylated RPA (pRPA) as a negative resection regulator[18]. Hence, in the long term, this method could be made even more precise by coupling PCNA/phosphorylated RPA staining with BrdU imaging with the use of appropriate antibodies and optimized staining conditions. However, the method presented provides a representation of resection that is observed independently from the proteins involved in the resection process, thus negating bias that can occur from changes in their signal in response to the treatment. This technique provides not only a method to determine if a protein is involved in resection, but also to determine if cell death resulting from drug treatment is related to hypo/hyper-resection. This information can be beneficial in understanding not only the mechanistic aspects of DNA repair, but also the biological mechanism underlying the drug-induced cell death.

Disclosures

The authors have nothing to disclose.

Acknowledgments

We thank Marie-Christine Caron for outstanding technical advice. This work is supported by funding from Canadian Institutes of Health Research J.Y.M (CIHR FDN-388879). J.-Y.M. holds a Tier 1 Canada Research Chair in DNA Repair and Cancer Therapeutics. J.O'S is an FRQS PhD student fellow, and S.Y.M is a FRQS postdoctoral fellow.

References

1. Mouw, K. W., Goldberg, M. S., Konstantinopoulos, P. A., D'Andrea, A. D. DNA damage and repair biomarkers of immunotherapy response. *Cancer Discovery.* **7** (7), 675-693 (2017).
2. Scully, R., Panday, A., Elango, R., Willis, N. A. DNA double-strand break repair-pathway choice in somatic mammalian cells. *Nature Reviews Molecular Cell Biology.* **20** (11), 698-714 (2019).
3. Chang, H. H. Y., Pannunzio, N. R., Adachi, N., Lieber, M. R. Non-homologous DNA end joining and alternative pathways to double-strand break repair. *Nature Reviews Molecular Cell Biology.* **18** (8), 495-506 (2017).
4. Heyer, W. D., Ehmsen, K. T., Liu, J. Regulation of homologous recombination in eukaryotes. *Annual Review of Genetics.* **44**, 113-139 (2010).
5. Ronato, D. A. et al. Limiting the DNA double-strand break resectosome for genome protection. *Trends in Biochemical Science.* **45** (9), 779-.793 (2020).
6. Hu, Y. et al. PARP1-driven poly-ADP-ribosylation regulates BRCA1 function in homologous recombination-mediated DNA repair. *Cancer Discovery.* **4** (12), 1430-1447 (2014).
7. Satoh, M. S., Lindahl, T. Role of poly(ADP-ribose) formation in DNA repair. *Nature.* **356** (6367), 356-358 (1992).
8. Sugimura, K., Takebayashi, S., Taguchi, H., Takeda, S., Okumura, K. PARP-1 ensures regulation of replication fork progression by homologous recombination on damaged DNA. *Journal of Cell Biology.* **183** (7), 1203-1212 (2008).
9. Bryant, H. E. et al. Specific killing of BRCA2-deficient tumours with inhibitors of poly(ADP-ribose) polymerase. *Nature.* **434** (7035), 913-917 (2005).
10. Farmer, H. et al. Targeting the DNA repair defect in BRCA mutant cells as a therapeutic strategy. *Nature.* **434** (7035), 917-921 (2005).
11. Zhou, P., Wang, J., Mishail, D., Wang, C. Y. Recent advancements in PARP inhibitors-based targeted cancer therapy. *Precision Clinical Medicine.* **3** (3), 187-201 (2020).
12. Noordermeer, S. M., van Attikum, H. PARP inhibitor resistance: a tug-of-war in BRCA-mutated cells. *Trends in Cell Biology.* **29** (10), 820-834 (2019).
13. Caron, M. C. et al. Poly(ADP-ribose) polymerase-1 antagonizes DNA resection at double-strand breaks. *Nature Communications.* **10** (1), 2954 (2019).
14. Zhou, Y., Caron, P., Legube, G., Paull, T. T. Quantitation of DNA double-strand break resection intermediates in human cells. *Nucleic Acids Research.* **42** (3), e19 (2014).
15. Raderschall, E., Golub, E. I., & Haaf, T. Nuclear foci of mammalian recombination proteins are located at single-stranded DNA regions formed after DNA damage. *Proceedings of the National Academy of Sciences of the United States of America.* **96** (5), 1921-1926 (1999).

16. Sartori, A. A. et al. Human CtIP promotes DNA end resection. *Nature*. **450** (7169), 509-514 (2007).

17. Huertas, P., Cruz-García, A. Single molecule analysis of resection tracks. *Methods in Molecular Biology*. **1672**, 147-154 (2018).

18. Soniat, M. M., Myler, L. R., Kuo, H.-C., Paull, T. T., Finkelstein, I. J. RPA phosphorylation inhibits DNA resection. *Molecular Cell*. **75** (1), 145-153.e145 (2019).